NASA CR-151950

PRELIMINARY SIMULATION OF AN ADVANCED, HINGELESS ROTOR XV-15 TILT-ROTOR AIRCRAFT

M. A. McVeigh

December 1976

Prepared Under Contract NAS 2-8048

for

National Aeronautics and Space Administration

Ames Research Center

by

BOEING VERTOL COMPANY
A DIVISION OF THE BOEING COMPANY
P. O. BOX 16858
PHILADELPHIA, PENNSYLVANIA 19142

D210-11161-1

NASA CR-151950

REV LTR

THE **BOEING** COMPANY

VERTOL DIVISION · PHILADELPHIA, PENNSYLVANIA

CODE IDENT. NO. 77272

NUMBER D210-11161-1

TITLE PRELIMINARY SIMULATION OF AN ADVANCED, HINGELESS ROTOR XV-15 TILT-ROTOR AIRCRAFT

ORIGINAL RELEASE DATE ______. FOR THE RELEASE DATE OF SUBSEQUENT REVISIONS, SEE THE REVISION SHEET. FOR LIMITATIONS IMPOSED ON THE DISTRIBUTION AND USE OF INFORMATION CONTAINED IN THIS DOCUMENT, SEE THE LIMITATIONS SHEET.

MODEL ______ CONTRACT NAS 2-8048

ISSUE NO. ______ ISSUED TO: ______

PREPARED BY M A McVeigh — M. A. McVeigh DATE 7th March 77

APPROVED BY HR Alexander for JPM — J. P. Magee DATE 7th March 77

APPROVED BY HR Alexander — H. R. Alexander DATE 7th March 77

APPROVED BY [illegible] — W. C. Boehm DATE [illegible]

SHEET i

FORM 46280 (6/68)

LIMITATIONS

This document is controlled by Research and Development - 7040

All revisions to this document shall be approved by the above noted organization prior to release.

ACTIVE SHEET RECORD

SHEET NUMBER	REV LTR	ADDED SHEETS: SHEET NUMBER	REV LTR	ADDED SHEETS: SHEET NUMBER	REV LTR	SHEET NUMBER	REV LTR	ADDED SHEETS: SHEET NUMBER	REV LTR	ADDED SHEETS: SHEET NUMBER	REV LTR
i						xL					
iii						xLi					
iv						xLii					
v						xLiii					
vi						xLiv					
vii						xLv					
viii						xLvi					
ix						xLvii					
x						xLviii					
xi						xLix					
xiii						L					
xv						Li					
xvii						Lii					
xviii						Liii					
xix						Liv					
xx						Lv					
xxi						Lvi					
xxii						Lvii					
xxiii						Lviii					
xxiv						Lix					
xxv						Lx					
xxvi						Lxi					
xxvii						Lxii					
xxviii						Lxiii					
xxix						Lxiv					
xxx						1-1					
xxxi						1-2					
xxxii						2-1					
xxxiii						2-2					
xxxiv						2-3					
xxxv						2-4					
xxxvii						2-5					
xxix						2-6					
XL						2-7					
XLi						2-8					
XLii						2-9					
XLiii						3-1					
						3-2					

FORM 46283 (7/67)

ACTIVE SHEET RECORD

SHEET NUMBER	REV LTR	ADDED SHEETS: SHEET NUMBER	REV LTR	ADDED SHEETS: SHEET NUMBER	REV LTR	SHEET NUMBER	REV LTR	ADDED SHEETS: SHEET NUMBER	REV LTR	ADDED SHEETS: SHEET NUMBER	REV LTR
3-3						5-17					
3-4						5-18					
3-5						5-19					
3-6						5-20					
3-7						5-21					
3-8						5-22					
3-9						5-23					
3-10						5-24					
3-11						5-25					
3-12						5-26					
4-1						5-27					
4-2						5-28					
4-3						5-29					
4-4						5-30					
4-5						5-31					
4-6						5-32					
4-7						5-33					
4-8						5-34					
4-9						5-35					
4-10						5-36					
4-11						6-1					
4-12						6-2					
4-13						6-3					
5-1						6-4					
5-2						7-1					
5-3						8-1					
5-4						8-2					
5-5						9-1					
5-6						9-2					
5-7						9-3					
5-8						10-1					
5-9						10-2					
5-10											
5-11											
5-12											
5-13											
5-14											
5-15											
5-16											

ACTIVE SHEET RECORD

SHEET NUMBER	REV LTR	ADDED SHEETS SHEET NUMBER	REV LTR	SHEET NUMBER	REV LTR	SHEET NUMBER	REV LTR	ADDED SHEETS SHEET NUMBER	REV LTR	SHEET NUMBER	REV LTR
10-3						11-41					
10-4						11-42					
10-5						11-43					
						11-44					
11-1						11-45					
11-2						11-46					
11-3						11-47					
11-4						11-48					
11-5						11-49					
11-6						11-50					
11-7						11-51					
11-8						11-52					
11-9						11-53					
11-10						11-54					
11-11						11-55					
11-12						11-56					
11-13						11-57					
11-14						11-58					
11-15						11-59					
11-16						11-60					
11-17						11-61					
11-18						11-62					
11-19						11-63					
11-20						11-64					
11-21						11-65					
11-22						11-66					
11-23						11-67					
11-24						11-68					
11-25						11-69					
11-26						11-70					
11-27						11-71					
11-28						11-72					
11-29						11-73					
11-30						11-74					
11-31						11-75					
11-32						11-76					
11-33						11-77					
11-34						11-78					
11-35						11-79					
11-36						11-80					
11-37						11-81					
11-38						11-82					
11-39						11-83					
11-40						11-84					
						11-85					

FORM 46283 (7/67)

ACTIVE SHEET RECORD

SHEET NUMBER	REV LTR	ADDED SHEETS				SHEET NUMBER	REV LTR	ADDED SHEETS			
		SHEET NUMBER	REV LTR	SHEET NUMBER	REV LTR			SHEET NUMBER	REV LTR	SHEET NUMBER	REV LTR
11-86						12-23					
11-87						12-24					
11-88						12-25					
11-89						12-26					
11-90						12-27					
11-91						12-28					
11-92						12-29					
11-93						12-30					
11-94						12-31					
11-95											
11-96											
11-97											
11-98						13-1					
11-99						13-2					
11-100						13-3					
11-101						13-4					
11-102						13-5					
11-103						13-6					
11-104						13-7					
11-105						13-8					
11-106						13-9					
						13-10					
						13-11					
12-1						13-12					
12-2						13-13					
12-3						13-14					
12-4						13-15					
12-5											
12-6											
12-7											
12-8						14-1					
12-9						14-2					
12-10											
12-11											
12-12						15-1					
12-13											
12-14											
12-15											
12-16						A-1					
12-17						A-2					
12-18						A-3					
12-19						A-4					
12-20						A-5					
12-21						A-6					
12-22						A-7					

FORM 46283 (7/67)

ACTIVE SHEET RECORD

SHEET NUMBER	REV LTR	ADDED SHEETS: SHEET NUMBER	REV LTR	ADDED SHEETS: SHEET NUMBER	REV LTR
A-8					
B-1					
B-2					
B-3					
B-4					
C-1					
C-2					
C-3					
C-4					
C-5					
C-6					
C-7					
C-8					
C-9					
C-10					
D-1					
D-2					
D-3					
D-4					
E-1					
E-2					
E-3					
E-4					
E-5					
E-6					
E-7					
E-8					
E-9					
E-10					
E-11					
E-12					
E-13					
E-14					
E-15					
E-16					
E-17					
E-18					

SHEET NUMBER	REV LTR	ADDED SHEETS: SHEET NUMBER	REV LTR	ADDED SHEETS: SHEET NUMBER	REV LTR
E-19					
E-20					
E-21					
E-22					
E-23					
E-24					
E-25					
E-26					
E-27					
E-28					
E-29					
E-30					
E-31					
E-32					
E-33					
E-34					
E-35					
E-36					
E-37					
E-38					
E-39					
E-40					
E-41					
E-42					
E-43					
E-44					
E-45					
E-46					
E-47					
E-48					
E-49					
E-50					
E-51					
E-52					
E-53					
E-54					
E-55					
E-56					
E-57					
E-58					
E-59					
E-60					
E-61					
E-62					
E-63					

FORM 46283 (7/67)

ACTIVE SHEET RECORD

SHEET NUMBER	REV LTR	ADDED SHEETS SHEET NUMBER	REV LTR	SHEET NUMBER	REV LTR
E-64					
E-65					
E-66					
E-67					
E-68					
E-69					
E-70					
E-71					
E-72					
E-73					
E-74					
E-75					
E-76					
F-1					
F-2					
F-3					
F-4					
F-5					
F-6					
F-7					
F-8					
F-9					
F-10					
F-11					
F-12					
F-13					
F-14					
F-15					
F-16					
F-17					
F-18					
F-19					
F-20					
F-21					
F-22					
F-23					
F-24					
F-25					
F-26					
F-27					
F-28					
F-29					
F-30					

SHEET NUMBER	REV LTR	ADDED SHEETS SHEET NUMBER	REV LTR	SHEET NUMBER	REV LTR
F-31					
F-32					
F-33					
F-34					
F-35					
F-36					
F-37					
F-38					
F-39					
G-1					
G-2					
G-3					
G-4					
G-5					
G-6					
G-7					
G-8					
G-9					
G-10					
G-11					
G-12					
G-13					
G-14					
G-15					
G-16					
G-17					
G-18					
G-19					
G-20					
G-21					
G-22					
G-23					
H-1					
H-2					
H-3					
H-4					
H-5					
H-6					
H-7					
H-8					

REVISIONS

LTR	DESCRIPTION	DATE	APPROVAL

FORM 46282 (12/65)

FOREWORD

This report was prepared by the Boeing Vertol Company for the National Aeronautics and Space Administration, Ames Research Center, under Contract NAS2-8048-4R. The contract was administered by NASA. Mr. Richard J. Abbott was the Contract Administrator; Messrs. M. A. Shovlin and T. Galloway were the Technical Monitors. The Boeing Vertol Project Manager was Mr. Harold Alexander and the Project Engineer was Mr. Michael A. McVeigh.

ABSTRACT

Results of a preliminary simulation of an Advanced Hingeless Rotor XV-15 Aircraft are presented. A simulation mathematical model was used to study the control and handling qualities of the NASA/Army XV-15 Tilt Rotor Aircraft with Boeing Hingeless rotors. The mathematical simulation model is described and the results obtained using the model are presented. A piloted evaluation was conducted and the pilot's comments on the aircraft handling qualities are detailed.

SUMMARY

A simulation model was developed in order to study the performance and control requirements of the NASA/Army XV-15 tilt rotor aircraft equipped with Boeing 26-foot diameter hingeless rotors in place of the existing 25-foot diameter gimballed rotors. Using the model, a piloted simulation was conducted to determine the handling qualities of the aircraft in hover, transition and airplane flight.

The mathematical model of the hingeless rotor XV-15 (HRXV-15) comprises the basic 6 degree-of-freedom equations of motion (extended to account for a moving center of gravity), airframe and rotor aerodynamics, including interference effects, a representation of the engine performance and dynamic response, and a model of the flight control and thrust management system.

The aerodynamics of the airframe, i.e., wings, tails, fuselage, is based on data furnished by NASA. The forces and moments generated by the large hingeless rotors are calculated explicitly using a set of equations derived from an analysis of full-scale and model-scale wind tunnel test data.

The mathematical model of the airframe was validated by comparing the airframe forces and moments with those obtained from an existing NASA simulation model of the current gimballed rotor XV-15 aircraft. The math model of the hingeless rotors was validated by a series of correlations with test data.

The validated simulation model was used to determine the schedules and phasing of the primary aircraft controls. In particular, the feasibility of scheduling rotor cyclic with stick position for the purpose of minimizing blade loads was established. The initial results show that a reasonably wide transition corridor can be provided that is essentially free of blade load limitations over an adequate maneuver range.

The results of the piloted simulation indicate that the aircraft has good overall flying qualities, SAS on and off. The piloted investigation was conducted without cyclic-on-the-stick installed. It is intended to evaluate pilots opinion of this feature during subsequent studies.

It is recommended that the math model be upgraded to reflect newly-acquired rotor data and that autorotation and systems failure studies be conducted.

TABLE OF CONTENTS

TABLE OF CONTENTS (CONT'D)

LIST OF ILLUSTRATIONS

LIST OF ILLUSTRATIONS (CONTINUED)

LIST OF ILLUSTRATIONS (CONTINUED)

LIST OF ILLUSTRATIONS (CONTINUED)

LIST OF ILLUSTRATIONS (CONTINUED)

LIST OF ILLUSTRATIONS (CONTINUED)

LIST OF ILLUSTRATIONS (CONTINUED)

LIST OF ILLUSTRATIONS (CONTINUED)

LIST OF ILLUSTRATIONS (CONTINUED)

LIST OF ILLUSTRATIONS (CONTINUED)

LIST OF ILLUSTRATIONS (CONTINUED)

LIST OF ILLUSTRATIONS (CONTINUED)

LIST OF ILLUSTRATIONS (CONTINUED)

LIST OF ILLUSTRATIONS (CONTINUED)

LIST OF ILLUSTRATIONS (CONTINUED)

LIST OF ILLUSTRATIONS (CONTINUED)

LIST OF ILLUSTRATIONS (CONTINUED)

LIST OF TABLES

LIST OF SYMBOLS

Symbol	Definition	Units
A	Rotor disc area (per rotor)	ft^2
AR	Aspect ratio, b^2/S	ND
A_{1c}	Lateral cyclic angle in rotor wind axes	deg
A'_{1c}	Lateral cyclic angle in swashplate axes	deg
A''_{1c}	Lateral cyclic angle in swashplate axes resolved through swashplate phase angle	deg
$\bar{a}$	Speed of sound or acceleration	ft/sec or ft/sec^2
a	Acceleration	ft/sec^2
(a_g/a)	Ratio of lift-curve slope in ground effect to lift-curve slope out of ground effect	ND
$a_o \rightarrow a_{32}$	Coefficients in wing lift and drag equations	--
B_G	Percent brake pedal deflection	ND
B.L.	Aircraft butt line	in.
B_{1c}	Longitudinal cyclic angle in rotor wind axes	deg
B'_{1c}	Longitudinal cyclic angle in swash-plate axes	deg
B''_{1c}	Longitudinal cyclic angle in swash-plate axes resolved through swash-plate phase angle	deg
b	Span of lifting surface (wing, tail, etc)	ft
c	Chord	ft
C_D	Drag coefficient, $\frac{D}{qS}$	ND

Symbol	Definition	Units
C_{D_O}	Drag coefficient at zero lift	ND
ΔC_D	Drag coefficient increment	ND
C_{DS}	Drag coefficient referred to rotor slipstream dynamic pressure, D/q_sS	ND
C_L	Lift coefficient, L/qS	ND
C_{L_O}	Average lift coefficient	ND
ΔC_L	Lift coefficient increment	ND
C_{L_S}	Lift coefficient referred to rotor slipstream dynamic pressure, L/q_sS	ND
C_{L_α}	Lift-curve slope	1/rad
C_{L_δ}	Lift increment due to flap deflection	1/deg
$C_{\mathcal{L}}$	Rolling moment coefficient, $\mathcal{L}/q\ bS$	ND
$C_{\mathcal{L}_S}$	Rolling moment coefficient referred to rotor slipstream dynamic pressure, $\mathcal{L}/q_sbS$	ND
C_M	Pitching moment coefficient, M/qSc	ND
C_{M_O}	Wing pitching moment coefficient as a function of flap deflection; pitching moment coefficient of fuselage or nacelles at zero angle of attack	ND
ΔC_M	Pitching moment coefficient increment	ND
C_{M_S}	Pitching moment coefficient referred to rotor slipstream dynamic pressure, M/q_sSc	
C_{M_δ}	Change in wing/body pitching moment coefficient as a function of flaperon deflection	ND
C_N	Yawing moment coefficient, N/qSb	ND
C_{N_O}	Yawing moment coefficient of fuselage or nacelles at zero angle of attack	ND

Symbol	Definition	Units
C_{N_S}	Yawing moment coefficient referred to rotor slipstream dynamic pressure, $N/q_S Sb$	ND
C_{NF}	Rotor normal force coefficient, $NF/\rho\pi\Omega^2R^4$	ND
C_{NF_O}	Rotor normal force coefficient with zero cyclic pitch	ND
C_P	Rotor power coefficient, $\frac{550RHP}{\rho\pi\Omega^3R^5}$	ND
C_{P_O}	Rotor power coefficient with zero cyclic pitch	ND
C_{PM}	Rotor hub pitching moment coefficient, $PM/\rho\pi\Omega^2R^5$	ND
C_{PM_O}	Rotor hub pitching moment coefficient with zero cyclic pitch	ND
C_{SF}	Rotor side force coefficient, $SF/\rho\pi\Omega^2R^4$	ND
C_{SF_O}	Rotor side force coefficient with zero cyclic pitch	ND
C_T	Rotor thrust coefficient, $T/\rho\pi\Omega^2R^4$	ND
C_{T_O}	Rotor thrust coefficient with zero cyclic pitch	ND
C_{T_S}	Rotor thrust coefficient referred to rotor slipstream dynamic pressure, $T/q_S A$	ND
C_Y	Side force coefficient, Y/qS	ND
C_{YM}	Rotor yawing moment coefficient, $\rho\pi\Omega^2R^5$	ND
C_{YM_O}	Rotor yawing moment coefficient with zero cyclic pitch	ND
C_{Y_α}	Lift-curve slope of vertical tail	1/rad
C_O	Coefficient of equation that defines pitching moment coefficient as a function of flap deflection	ND

Symbol	Definition	Units
C_1	Coefficient of equation that defines pitching moment coefficient as a function of flap deflection	1/rad
C_2	Coefficient of equation that defines pitching moment coefficient as a function of flap deflection	$1/rad^2$
D	Rotor diameter	ft
(D/T)	Aircraft download-to-thrust ratio	ND
$D_{NF_{1\to5}}$	Coefficients in the equation for the change in normal force coefficient with lateral cyclic angle	1/deg
$D_{PM_{1\to6}}$	Coefficients in the equation for the change in hub pitching moment coefficient with lateral cyclic angle	1/deg
$D_{SF_{1\to5}}$	Coefficients in the equation for the change in side force coefficient with lateral cyclic angle	1/deg
D_{ST_n}	Damping coefficients of the landing gear oleo struts	lb/ft/sec
$D_{YM_{1\to6}}$	Coefficients in the equation for the change in hub yawing moment coefficient with lateral cyclic angle	1/deg
dC_{NF}/dA_{1c}	Change in normal force coefficient with lateral cyclic angle	1/deg
dC_{NF}/dB_{1c}	Change in normal force coefficient with longitudinal cyclic angle	1/deg
dC_{PM}/dA_{1c}	Change in hub pitching moment coefficient with lateral cyclic angle	1/deg
dC_{PM}/dB_{1c}	Change in hub pitching moment coefficient with longitudinal cyclic angle	1/deg
dC_{PM}/dQ	Change in hub pitching moment coefficient with pitch rate	1/rad/sec
dC_{SF}/dA_{1c}	Change in side force coefficient with lateral cyclic angle	1/deg

Symbol	Definition	Units
dC_{SF}/dB_{1c}	Change in side force coefficient with longitudinal cyclic angle	1/deg
dC_{YM}/dA_{1c}	Change in hub yawing moment coefficient with lateral cyclic angle	1/deg
dC_{YM}/dB_{1c}	Change in hub yawing moment coefficient with longitudinal cyclic angle	1/deg
dC_{YM}/dR	Change in hub yawing moment coefficient with yaw rate	1/rad/sec
dC_M/dC_L	Change in wing pitching moment with lift coefficient	ND
$d\sigma/d\beta$	Change in fuselage sidewash angle with sideslip angle	ND
EI	Product of modulus of elasticity and moment of inertia	$lb\text{-}in^2$
EI_O	Product of modulus of elasticity and moment of inertia at wing root	$lb\text{-}in^2$
$E_{NF_{1\rightarrow5}}$	Coefficients in the equation for the change in normal force coefficient with longitudinal cyclic angle	1/deg
$E_{PM_{1\rightarrow6}}$	Coefficients in the equation for the change in hub pitching moment coefficient with longitudinal cyclic angle	1/deg
$E_{SF_{1\rightarrow5}}$	Coefficients in the equation for the change in side force coefficient with longitudinal cyclic angle	1/deg
$E_{YM_{1\rightarrow6}}$	Coefficients in the equation for the change in hub yawing moment coefficient with longitudinal cyclic angle	1/deg
E_{HT}, E_{VT}	Oswald efficiency of horizontal or vertical tail	ND
F	Generalized force or force on nacelle	lb
FPR	Lateral-directional SAS function	--
FR1	Lateral-directional SAS function	--
$F\phi$	Lateral-directional SAS function	--

Symbol	Definition	Units
$F\phi 1$	Lateral-directional SAS function	--
$F\phi 2$	Lateral-directional SAS function	--
$F\psi 1$	Lateral-directional SAS function	--
$F\psi 2$	Lateral-directional SAS function	--
F_a	Aerodynamic force on nacelle	lb
F_{gzn}	Landing gear oleo strut vertical force	lb
F_{sn}	Landing gear oleo strut lateral force	lb
F_x	Longitudinal generalized force	lb
F_y	Lateral generalized force	lb
F_z	Vertical generalized force	lb
$F_{\mu n}$	Landing gear oleo strut longitudinal force	lb
f_{NF}	Multiplier on rotor normal force	ND
f_P	Multiplier on rotor power	ND
f_{PM}	Multiplier on rotor hub pitching moment	ND
f_Q	Multiplier on rotor torque	ND
f_{SF}	Multiplier on rotor side force	ND
f_T	Multiplier on rotor thrust	ND
f_{YM}	Multiplier on rotor hub yawing moment	ND
G	Generalized moment	ft-lb
GEF	Ground effect factor	ND
G_{G1}	Governor gain	deg/sec/rad/sec
G_{G2}	Governor gain	deg/sec/rad/sec
G_{G3}	Governor gain	deg/sec/deg

Symbol	Definition	Units
G_p	Lateral directional SAS gain	in/rad/sec
G_{prl}	Lateral directional SAS gain	in/rad/sec
$G_{p\delta_s}$	Lateral directional SAS gain	in/in
G_q	Longitudinal SAS gain	deg/rad/sec
G_r	Lateral directional SAS gain	in/rad/sec
G_{r2}	Lateral directional SAS gain	in/rad/sec
$G_{r_{\delta r}}$	Lateral directional SAS gain	in/rad/sec
$G_{\beta p}$	Lateral directional SAS gain	in/rad
$G_{\beta r}$	Lateral directional SAS gain	in/rad
$G_{\beta\delta r}$	Lateral directional SAS gain	in/in
$G_{\delta B1}$	Longitudinal SAS gain	deg/in
$G_{\delta B2}$	Longitudinal SAS gain	deg/in
$G_{\delta TH}$	Governor throttle gain	deg/in
G_θ	Longitudinal SAS gain	deg/rad/sec
G_ϕ	Lateral directional SAS gain	in/rad/sec
G_ψ	Lateral directional SAS gain	in/in
$G_{\psi\delta r}$	Lateral directional SAS gain	in/in
g	Gravitational constant	ft/sec^2
H	Height	ft
HP	Horsepower	--
$H'_{w'FUEL}$	Horizontal distance between wing mass element center of gravity and fuel center of gravity	ft
$H'_{w'NF}$	Horizontal distance between wing mass element center of gravity and fixed nacelle center of gravity	ft
$H'_{w'w}$	Horizontal distance between wing mass element center of gravity and fixed nacelle center of gravity	ft

Symbol	Definition	Units
h	Height or angular momentum	ft or lb-ft-sec
h_{CG}^{N}	Angular momentum of nacelle about aircraft center of gravity	lb-ft-sec
h_F	Distance from wing pivot plane to fuselage mass element center of gravity	ft
h_P	Height of pivot above wing chord line or angular momentum of nacelle about the pivot	ft
h_T	Landing gear oleo strut deflection during ground contact	ft
h_W	Distance from wing pivot plane to wing mass element center of gravity	ft
h_O	Angular momentum of an element of mass about its own center of gravity	lb-ft-sec
h_1	Wing vertical bending deflection	ft
h/D	Rotor hub height to rotor diameter ratio	ND
h_θ	Distance from aircraft center of gravity to bottom of right main gear following a positive pitch rotation	ft
h_ϕ	Distance from aircraft center of gravity to bottom of right main gear following a positive roll	ft
I	Mass moment of inertia	slug-ft^2
I_{xx}	Vehicle mass roll moment of inertia about center of gravity	slug-ft^2
I_{xx_O}	Mass roll moment of inertia of aircraft components about their own center of gravity	slug-ft^2
$I_{xx}^{(F)}$	Mass roll moment of inertia of fuselage mass element about its center of gravity	slug-ft^2

Symbol	Definition	Units
$I_{xx}^{(W)}$	Mass roll moment of inertia of wing mass element about its center of gravity	slug-ft^2
I'_{xx}	Mass roll moment of inertia of the tilting portion of each nacelle about its center of gravity	slug-ft^2
I_{yy}	Vehicle mass pitch moment of inertia about center of gravity	slug-ft^2
I_{yy_o}	Mass pitch moment of inertia of aircraft components about their centers of gravity	slug-ft^2
$I_{yy}^{(F)}$	Mass pitch moment of inertia of fuselage mass element about its center of gravity	slug-ft^2
$I_{yy}^{(W)}$	Mass pitch moment of inertia of wing mass element about its center of gravity	slug-ft^2
I'_{yy}	Mass pitch moment of inertia of the tilting portion of each nacelle about its center of gravity	slug-ft^2
I_{xz}	Vehicle mass product of inertia about center of gravity	slug-ft^2
I_{xz_o}	Mass product of inertia of aircraft components about their own centers of gravity	slug-ft^2
$I_{xz}^{(F)}$	Mass product of inertia of fuselage mass element about its center of gravity	slug-ft^2
$I_{xz}^{(W)}$	Mass product of inertia of wing mass element about its center of gravity	slug-ft^2
I'_{xz}	Mass product of inertia of the tilting portion of each nacelle about its center of gravity	slug-ft^2
I_{zz}	Vehicle mass yaw moment of inertia about center of gravity	slug-ft^2
I_{zz_o}	Mass yaw moment of inertia of aircraft components about their own centers of gravity	slug-ft^2

Symbol	Definition	Units
$I_{zz}^{(F)}$	Mass yaw moment of inertia of fuselage mass element about its center of gravity	slug-ft^2
$I_{zz}^{(W)}$	Mass yaw moment of inertia of wing mass element about its center of gravity	slug-ft^2
I'_{zz}	Mass yaw moment of inertia of the tilting portion of <u>each</u> nacelle about its center of gravity	slug-ft^2
i	Incidence angle	deg or rad
$\hat{\underline{i}}$	Unit vector in i direction	
J_{xx}	Dummy inertia, $I_{zz}-I_{yy}$	slug-ft^2
J_{yy}	Dummy inertia, $I_{xx}-I_{zz}$	slug-ft^2
J_{zz}	Dummy inertia, $I_{yy}-I_{xx}$	slug-ft^2
$\hat{\underline{j}}$	Unit vector in j direction	--
K'_A	Wing slipstream correction factor	ND
$\frac{K_{D1}}{T} \rightarrow \frac{K_{D4}}{T}$	Coefficients of curve fit equation for wing download as a function of rotor height/diameter ratio	ND
$\frac{K_{M1}}{T} \rightarrow \frac{K_{M4}}{T}$	Coefficients of curve fit equation for wing pitching moment as a function of rotor height/diameter ratio	ND
$K_{\mathcal{L}}$	Multiplier on slipstream rolling moment coefficient	ND
K_{n}	Miltiplier on slipstream yawing moment coefficient	ND
K_{ST_n}	Landing gear spring constants	lb/ft
$K_{W1} \rightarrow K_{W10}$	Coefficients for wing bending equations	--
K_{δ_B}	Multiplier on longitudinal cyclic pitch available from longitudinal stick	in/in

Symbol	Definition	Units
K_{δ_e}	Ratio between longitudinal stick motion and elevator deflection	deg/in
K_{δ_R}	Multiplier on longitudinal cyclic pitch available from pedal displacement	in/in
$K\delta_{RUD}$	Ratio between pedal and rudder deflection	deg/in
$K_{\delta s}$	Multiplier on longitudinal cyclic pitch and differential collective available from lateral stick	in/in
$K_{\delta 's}$	Lateral cyclic pitch/degree of differential collective pitch	deg/deg
K_θ	Wing stiffness in torsion	ft-lb/rad
K_o	Coefficient of fuselage drag coefficient equation to account for drag due to sideslip	$1/rad^3$
K_1	Coefficient in fuselage drag coefficient equation	$1/rad^2$
K_2	Coefficient in fuselage drag coefficient equation	1/rad
K_3	Coefficient in fuselage lift coefficient equation	1/rad
K_4	Coefficient in fuselage lift coefficient equation	$1/rad^2$
K_5	Coefficient in fuselage pitching moment coefficient equation	1/rad
K_6	Coefficient in fuselage pitching moment coefficient equation	$1/rad^2$
K_7	Coefficient in fuselage side force coefficient equation	1/rad
K_8	Coefficient in fuselage side force coefficient equation	1/rad
K_9	Coefficient in fuselage yawing moment coefficient equation	1/rad

Symbol	Definition	Units
K_{10}	Coefficient in fuselage yawing moment coefficient equation	$1/rad^2$
K_{20}	Wing/body interference effects on $C_{\ell\beta}$	1/rad
K_{21}	Wing planform effects on $C_{\ell\beta}$	1/rad
K_{22}	Wing planform and lift effects on C_{N_β}	1/rad
K_{30}	Coefficient in nacelle drag coefficient equation	1/rad
K_{31}	Coefficient in nacelle drag coefficient equation	$1/rad^2$
K_{32}	Coefficient in nacelle lift coefficient equation	1/rad
K_{34}	Coefficient in nacelle pitching moment coefficient equation	1/rad
K_{35}	Coefficient in nacelle pitching moment coefficient equation	$1/rad^2$
K_{36}	Coefficient in nacelle side force coefficient equation	1/rad
K_{37}	Coefficient in nacelle side force coefficient equation	$1/rad^2$
K_{38}	Coefficient in nacelle yawing moment coefficient equation	1/rad
K_{39}	Coefficient in nacelle yawing moment coefficient equation	$1/rad^2$
K_{40}	Coefficient in nacelle yawing moment coefficient equation	1/rad
K_{41}	Coefficient in nacelle yawing moment coefficient equation	$1/rad^2$
K_{42}	Coefficient in fuselage lift coefficient equation	ND
$\underline{\hat{k}}$	Unit vector in k direction	--
L_s	Nacelle shaft length from pivot to spinner	ft

Symbol	Definition	Units
$\mathcal{L}$	Rolling moment	ft-lb
ℓ	Distance from nacelle pivot to nacelle center of gravity	ft
ℓ'	Horizontal distance from nacelle pivot to aircraft component center of gravity positive - positive forward from pivot	ft
ℓ_{AC}	Horizontal distance from horizontal tail quarter chord to wing aero-dynamic center	ft
ℓ_F	Horizontal distance from pivot to center of gravity of fuselage mass element	ft
ℓ_0	Wing root lift/foot	lb/ft
ℓ_{PA}	Horizontal distance from pivot to center of gravity of pilots' station - positive forward from pivot	ft
ℓ_W	Horizontal distance from pivot to wing mass element center of gravity	
M	Pitching moment	ft-lb
m	Pitching moment, or aircraft mass	ft-lb or slugs
M/T	Pitching moment/rotor thrust	ft-lb/lb
m_f	Mass of fuselage structure	slugs
m_N	Mass of one nacelle	slugs
m_W	Mass of wing	slugs
N	Yawing moment	ft-lb
NF	Rotor normal force	lb
N_I	Engine gas generator speed	rev/min
N_1 IND	Engine gas generator indicator	--
N_I^*	Engine gas generator speed at sea level standard, static conditions	rev/min

Symbol	Definition	Units
$N_{1\theta}$ IND	Referred engine gas generator speed indicator	--
N_{II}	Engine power turbine speed	rev/min
N^*_{II}	Engine power turbine speed at sea level standard static conditions	rev/min
P	Body axes roll rate	rad/sec
PC	Horizontal distance from wing leading edge to pivot location	ft
P^N	Nacelle axes roll rate	rad/sec
P^R	Nacelle wind axes roll rate	rad/sec
p	Body axes roll rate	rad/sec
Q	Body axes pitch rate or rotor torque	rad/sec or lb-ft
Q_{IND}	Torque indicator	ND
Q_{MAX}	Maximum engine torque available	lb-ft
Q^N	Nacelle axes pitch rate	rad/sec
Q^R	Nacelle wind axes pitch rate	rad/sec
Q^*	Engine torque at sea level standard static condition	lb-ft
q	Body axes pitch rate or freestream dynamic pressure	rad/sec or lb/ft^2
q_s	Dynamic pressure of rotor slipstream	lb/ft^2
R	Body axes yaw rate or rotor resultant force or rotor radius	rad/sec or lb or ft
RHP	Rotor horsepower	--
R^N	Nacelle axes yaw rate	rad/sec
R^R	Nacelle wind axes yaw rate	rad/sec
r	Body axes yaw rate	rad/sec
$\underline{r}$	Radius vector	--

Symbol	Definition	Units
r_n	Landing gear tire radius	ft
S	Surface area	ft^2
SF	Rotor side force	lb
SHP	Shaft horsepower	--
SHP*	Engine shaft horsepower at sea level standard static conditions	--
T	Rotor thrust	lb
TEA	Engine referred turbine inlet temperature	deg
(T_{IGE}/T_{OGE})	Ratio of the rotor thrust in ground effect to the thrust out of ground effect	--
$T_1 \rightarrow T_3$	Coefficients of curve fit equations for rotor/rotor interference	ND
t	Time	sec
U	Body axes longitudinal component of velocity at aircraft center of gravity or rotor hub, wing, horizontal and vertical tail velocities referred to rotor shaft and local surface chord axes, respectively	ft/sec
U'	Body axes longitudinal component of velocity at rotor hub and wing aero-dynamic center	ft/sec
U_{PA}	Body axes longitudinal component of velocity at pilot's station	ft/sec
V	Total velocity	ft/sec
V_t	Rotor tip speed	ft/sec
V'	Resultant flow through rotor disc	ft/sec
V_*	Non-dimensional rotor forward velocity	ND
$\underline{V}$	Total velocity vector	ft/sec

Symbol	Definition	Units
V	Body axes lateral component of velocity at aircraft center of gravity or rotor hub wing, horizontal and vertical tail velocities referred to rotor shaft and local surface chord axes, respectively	ft/sec
V'	Body axes lateral component of velocity at rotor hub and wing aerodynamic center	ft/sec
v_i	Rotor induced velocity	ft/sec
V_{PA}	Body axes lateral component of velocity at pilot's station	ft/sec
V_*	Non-dimensional rotor induced velocity	ND
W.L.	Fuselage water line position	in.
W'	Weight of aircraft components	lb
WDTIND	Fuel flow indicator	--
W	Body axes vertical component of velocity at aircraft center of gravity or rotor, hub, wing, horizontal and vertical tail velocities referred to rotor shaft and local surface chord axes, respectively	ft/sec
W'	Body axes vertical component of velocity at rotor hub and wing aerodynamic center	ft/sec
W_{PA}	Body axes vertical component of velocity at pilot's station	ft/sec
$X_{subscript}$	Longitudinal distance, measured positive forward from nacelle pivot along body axes	ft
$\Delta X_{subscript}$	Longitudinal force, measured positive forward along body axes	lb
X_{aero}	Total longitudinal aerodynamic force at center of gravity measured positive forward along body axes	lb

Symbol	Definition	Units
$X^{sprscript}_{subscript}$	Longitudinal force, measured positive forward along body axes	lb
$\dot{X}_{North}$	Longitudinal ground track velocity	ft/sec
$Y_{subscript}$	Lateral distance, measured positive along right wing along body axes	ft
$\Delta Y_{subscript}$	Lateral force, measured positive along right wing in body axes	lb
Y_{aero}	Total lateral aerodynamic force at center of gravity measured positive along right wing in body axes	lb
$Y^{sprscript}_{subscript}$	Lateral force, measured positive along right wing in body axes	lb
$\dot{Y}_{East}$	Lateral ground track velocity	ft/sec
$Z_{subscript}$	Vertical distance, measured positive down nacelle pivot along body axes	ft
$\Delta Z_{subscript}$	Vertical force, measured positive down along body axes	lb
Z_{aero}	Total vertical aerodynamic force at center of gravity, measured positive down along body axes	lb
$Z^{sprscript}_{subscript}$	Vertical force, measured positive down along body axes	lb
$\dot{Z}_{down}$	Vertical ground track velocity	ft/sec
z	Vertical distance from nacelle pivot to center of gravity of aircraft component, positive down from nacelle pivot along body axes	ft
α	Angle of attack	rad
β	Angle of sideslip	rad
$\Delta'_{w'fuel}$	Vertical distance between wing fuel center of gravity and wing mass element center of gravity	ft

Symbol	Definition	Units
$\Delta'_{w'fuel}$	Vertical distance between fixed nacelle center of gravity and wing mass element center of gravity	ft
$\Delta'_{w'w}$	Vertical distance between wing center of gravity and wing mass element center of gravity	ft
δ	Control element (surface or stick) angular or linear displacement	deg or in.
δ'_{c}	Vertical distance between cargo center of gravity and fuselage mass element center of gravity	ft
δ'_{CR}	Vertical distance between crew center of gravity and fuselage mass element center of gravity	ft
$\delta'_{F'}$	Vertical distance between fuselage center of gravity and fuselage mass element center of gravity	ft
δ'_{HT}	Vertical distance between horizontal tail center of gravity and fuselage mass element center of gravity	ft
δ_{STEER}	Nose wheel steering angle, positive right	deg
δ'_{VT}	Vertical distance between vertical tail center of gravity and fuselage mass element center of gravity	ft
ε	Wing or rotor downwash angle	rad
ε_{O}	Wing downwash angle at zero wing angle of attack	rad
ε_{iLR}	Rotor/rotor interference angle, left rotor on right rotor	rad
ε_{iRL}	Rotor/rotor interference angle, right rotor on left rotor	rad
ε_{W}	Wing on rotor interference	rad
ζ	Rotor sideslip angle or damping ratio	rad or ND
$\zeta_{w1} \rightarrow \zeta_{w4}$	Wing damping ratio	ND

Symbol	Definition	Units
$H'_{W',fuel}$	Horizontal distance between wing fuel center of gravity and wing mass element center of gravity	ft
$H'_{W',NF}$	Horizontal distance between fixed nacelle center of gravity and wing mass element center of gravity	ft
$H'_{W',W}$	Horizontal distance between wing center of gravity and wing mass element center of gravity	ft
η'_{C}	Horizontal distance between cargo center of gravity and fuselage mass element center of gravity	ft
η'_{CR}	Horizontal distance between crew center of gravity and fuselage mass element center of gravity	ft
η'_{F}	Horizontal distance between fuselage center of gravity and fuselage mass element center of gravity	ft
η_{HT}	Horizontal tail efficiency	ND
η'_{HT}	Horizontal distance between horizontal tail center of gravity and fuselage mass element center of gravity	lb
η_{VT}	Vertical tail efficiency factor	ND
η'_{VT}	Horizontal distance between vertical tail center of gravity and fuselage mass element center of gravity	ft
η_{TR}	Transmission efficiency	ND
θ	Aircraft pitch or Euler angle or temperature ratio	rad or ND
θ_{t}	Wing twist angle	rad
$\theta_{.75}$	Rotor collective pitch angle at three-quarter radius	deg
λ	Angle between the rotor shaft and a line drawn through the nacelle center of gravity from the pivot	rad

Symbol	Definition	Units
μ	Rotor advance ratio = $V/\Omega R$	ND
μ_s	Tire sliding coefficient of friction when sliding sidewards (for concrete)	ND
μ_o	Tire rolling coefficient of friction (for concrete)	ND
μ_1	Coefficient of rolling friction for brakes	ND
$\xi_{R1} \rightarrow \xi_{R4}$	Terms in wing immersed area calculation	--
ρ	Ambient air density	slug/ft^3
σ	Fuselage sidewash angle	rad
σ_h	Ambient density ratio	ND
τ	Angle between freestream velocity and rotor resultant force	rad
τ_D	Engine response time constant	sec
τ_E	Engine response time·constant	sec
τ_{HT}	Horizontal tail effectiveness	ND
τ_{LAS}	Load alleviation system time constant	sec
τ_{VT}	Vertical tail effectiveness	ND
τ_p	Lateral directional SAS time constant	sec
τ_r	Lateral directional SAS time constant	sec
τ_ϕ	Lateral directional SAS time constant	sec
$\tau_{\phi\delta s}$	Lateral directional SAS time constant	sec
τ_ψ	Lateral directional SAS time constant	sec
$\tau_{\psi\delta r}$	Lateral directional SAS time constant	sec
τ_1	Rotor thrust response time constant	sec
τ_2	Rotor thrust response time constant	sec
ϕ	Aircraft roll angle or Euler angle	rad

Symbol	Definition	Units
ϕ_p	Rotor swashplate phase angle	rad
$\phi_1 \rightarrow \phi_5$	Functions in wing vertical bending equations	--
χ	Rotor wake skew angle	rad
ψ	Aircraft yaw angle or Euler angle	rad
Ω	Rotor or engine rotational speed	rad/sec
$\underline{\Omega}$	Angular velocity vector	rad/sec
ω	Natural frequency	rad/sec
$\omega_{w1} \rightarrow \omega_{w3}$	Wing natural frequencies	rad/sec

Subscripts

A	Available
AC	Aerodynamic center
ACT	Actuator
AERO	Aerodynamic force
a	Aileron
B	Longitudinal stick
c	Cargo
CG	Center of gravity
CR	Crew
C/4	Quarter chord
DUM	Dummy variable
E	Engine
EFF	Effective
e	Elevator or effective
F	Fuselage
FAC	Fuselage aerodynamic center
FUEL	Fuel in wing
$FUEL_{CG}$	Fuel center of gravity
FUS	Fuselage
F'	Fuselage minus landing gear
f	Flap
GLAS	Load alleviation system
GYRO	Gyroscopic
g	Ground or gust
HL	Left rotor hub

Subscripts

HR	Right rotor hub
HT	Horizontal tail
HTCG	Horizontal tail center of gravity
IGE	In ground effect
i	Immersed
L	Left wing or rotor
LAS	Load alleviation system
LE	Left engine
LG	Landing gear
L-L	Rotor lead-lag
LN	Left nacelle
LR	Left rotor
LRH	Left rotor hub
LT	Left wing tip
LW	Left wing
LW_O	Left wing referred to freestream
MAX	Maximum
N	Nacelle or natural frequency
NF	Fixed portion of nacelle
NFCG	Fixed portion of nacelle center of gravity
NL	Left nacelle
NR	Right nacelle
NT	Tilting portion of nacelle
n	Landing gear index, n=1 left gear, n=2 right gear, n=3 nose gear
OGE	Out of ground effect

Subscripts

P	Power, nacelle pivot, or rotor polar moment of inertia
POWER	Power
PA	Pilot station
R	Right wing, rotor or rudder pedal
RE	Right engine
REQ	Required
RIGID	Rigid
RN	Right nacelle
RR	Right rotor
RRH	Right rotor hub
RT	Right wing tip
RUD	Rudder
RW	Right wing
RW_O	Right wing referred to freestream
S	Rotor shaft, side, or lateral stick
SP	Spoiler
STALL	Stall
T	Tail, total or wing tip
TH	Throttle
VT	Vertical tail
VTCG	Vertical tail center of gravity
W	Wing
WAC	Wing aerodynamic center
WCG	Wing center of gravity
x	Along the longitudinal axis, positive forward

Subscripts

y	Along the lateral body axis, positive out right wing
z	Along the vertical body axis, positive down
$\_$	Denotes a vector quantity

Superscripts

(c)	Refers to cargo or payload weight
(CR)	Refers to aircraft crew weight
F	Fuselage
F'	Fuselage less landing gear
HT	Horizontal tail
(HT)	Refers to horizontal tail weight component
IGE	In ground effect
LW	Left wing
N	Nacelle
NL	Left wing tip at pivot
NR	Right wing tip at pivot
RW	Right wing
T	Total of horizontal and vertical tail
VT	Vertical tail
(VT)	Refers to vertical tail weight component
W	Wing
(W'_{FUEL})	Refers to wing fuel weight
(W_f')	Refers to fuselage weight component
(W'_{NF})	Refers to weight of fixed portion of nacelle
(W'_W)	Refers to wing weight component

Superscripts

"	Denotes an interim calculation or coefficient in local wind axes
'''	Denotes an interim calculation
‾	Denotes average value
*	Denotes interim calculation or calculation in freestream wind axes
'	Denotes an interim calculation
+	Denotes an interim calculation
^	Denotes a unit vector

1.0 INTRODUCTION

1.0 INTRODUCTION

1.1 Background

The work reported in this document was undertaken as part of a more extensive program which has as its objective the flight test demonstration of a NASA-Army XV-15 Tilt Rotor Research Aircraft which will be modified by replacing the current gimballed rotor with a larger diameter hingeless rotor fabricated from advanced composite materials. The current NASA-Army tilt rotor research aircraft project is aimed at verifying the feasibility of the tilt-rotor concept through investigation of the performance, stability and handling qualities of the XV-15 tilt rotor. This aircraft utilizes 25 foot gimballed rotors constructed of bonded aluminum honeycomb and stainless steel. Replacement of these rotors by advanced-technology fiberglass/composite hingeless rotors of larger diameter, combined with an advanced integrated fly-by-wire control system, will further enhance the flying qualities, performance, maneuverability and rotor system fatigue life of the XV-15.

1.2 Objectives

The objectives of the subject program were (a) to develop a parametric simulation model of the HRXV-15, (b) to use the model to conduct engineering studies to define acceptable preliminary ranges of primary and secondary control schedules as functions of the flight parameters, (c) to conduct engineering evaluation of performance, flying qualities and structural loads, and (d) to have a Boeing-Vertol pilot conduct a simulated flight test evaluation of the aircraft.

All of these objectives have been fully met and are reported in the paragraphs which follow.

1.3 Mathematical Modelling Approach

A full force mathematical representation of the aircraft is used rather than a linearized derivative representation. This is considered necessary because of the degree of non-linearity in the behavior of the forces acting on the aircraft in transition. For example, the rotor forces are functions of higher powers of flight parameters such as α, μ and C_T, and aerodynamic interference effects between rotor and empennage are significantly non-linear. XV-15 data for airframe aerodynamics, c.g. ranges, stick and pedal travels were used, but no constraints were placed on the design of thrust management, rotor control or stability and control augmentation systems. Some difference in detailed requirements are to be expected and in addition, there are fewer constraints in achieving an ideal design when a fly-by-wire capability is envisioned.

1.4 Mathematical Model Development

The general format and architecture of earlier tilt rotor simulation models developed at Boeing Vertol was retained where possible for the subject activity. This required a conversion of the basic airframe aerodynamics provided by NASA for the XV-15 to a form compatible with Boeing Vertol usage. In addition, the H-tail configuration of the XV-15 required that the approach to rotor-empennage interference be changed to one using an extensive data bank of aerodynamic interactions.

An advance on previous practice was the use of rotor data based on full scale and model scale results and represented by a set of equations giving the rotor hub forces and moments, and blade loads as functions of the flight parameters. This represents a significant improvement over earlier practice, which used a data bank and time consuming look-up approach.

1.5 Nacelle Configuration

In the subject simulation the entire wing tip package, including the engines is assumed to tilt in the same manner as the XV-15. In the HRXV-15 the engine may be retained in a horizontal position while the rotor and drive train tilts. However, since this question was not resolved when the simulation effort was initiated, it was decided to retain the XV-15 nacelle configuration. The issues involved in this decision are not related to flying qualities, but have more to do with operational qualities such as the effect of jet efflux on the landing surface and the general accessibility of nacelle components for maintenance. Thus the conclusions reached in the present simulation activity will be valid whether or not the engine tilts along with the remainder of the nacelle.

1.6 Status of Current Simulation

The subject simulation and design investigation is a preliminary effort indicating generally acceptable flying qualities and performance for a tilt rotor aircraft of the same general configuration as the XV-15, but using 26-foot diameter hingeless soft in-plane rotor in place of the gimballed 25-foot diameter rotors currently installed. It is desirable that this simulation should be updated as more detailed design work on the compatibility of the Boeing rotor system with the XV-15 proceeds under NASA Contract NAS2-9015. Two areas are identified where continued activity is considered desirable. First the rotor force and moment mathematical model should be upgraded to reflect more fully the comprehensive data acquired on test during Contract NAS2-9015. Second, the definition of primary control system schedules can be further refined to provide additional speed and maneuvering capability through transition. This topic is discussed in detail in Appendix G.

2.0 DESCRIPTION OF A/C

2.0 DESCRIPTION OF AIRCRAFT

The hingeless rotor XV-15 Tilt Rotor Aircraft combines the NASA-Army XV-15 airframe and engines with a Boeing 7.92 meter (26 feet) diameter fiberglass hingeless rotor system and fly-by-wire controls. Figure 2.1 presents an artist's impression of the HRXV-15. The figure shows the aircraft with fixed engines although the present simulation was conducted with tilting engines as on the current XV-15. Figure 2.2 gives the general arrangement of the HRXV-15. Design gross weight is 5896 kg (13000 lb) and maximum weight is 6803 kg (15000 lb).

2.1 Component Data

With the exception of the rotors, data on the aircraft was obtained from Reference 1 and 2.

2.1.1 Rotors

The HRXV-15 uses Boeing-developed 26 foot diameter, hingeless, soft in-plane rotors of fiberglass composite construction. The hingeless rotor concept simplifies the design of the hub and upper controls compared to a gimballed or articulated system. This design simplicity yields high reliability, safety and low maintenance. These improvements derive from the reduction in the number of parts and bearings required in the rotor hub.

The large control hub moments and in-plane forces generated by cyclic control provides the capability for good pitch and yaw control of the aircraft at low speeds. This control power also enables the aircraft to be trimmed over a large center-of-gravity range.

Each rotor is three-bladed of solidity 0.1154. Twist, thickness and airfoil section characteristics are presented in Figure 2.3. The rotor hover and cruise performance together with its dynamic and structural integrity have been successfully demonstrated in full-scale wind tunnel tests.

2.1.2 Power Plant

The XV-15 is powered by 2 cross-shafted front-drive, free-turbine Lycoming LTC1K-4K (T53-L-13B) engines. The engine performance figures used in this simulation are detailed in Section 7.0.

2.1.3 Wing

The untwisted high wing is swept forward 6.5° at the leading edge and possesses 2° positive dihedral. The forward sweep was introduced to accommodate the high blade flapping angle experienced with the current gimballed rotor arrangement. This forward sweep is not required when hingeless rotors are utilized because of the modest blade flapping developed. In the present simulation the sweep is included, however.

The wing root and tip airfoil sections are NACA 64A223. The control surfaces consist of flaps and flaperons, the flaperons being connected to the flap controls so that they droop as the flaps are lowered. Figure 2.4 shows the relationship between aileron setting and flap setting.

2.1.4 Horizontal and Vertical Tails

The horizontal and vertical stabilizers form a H-tail configuration. The vertical fins are located at the extremities of the horizontal tail. The horizontal tail has a 30 percent chord plain elevator and the vertical fins a 25 percent chord rudder. The horizontal tail incidence is ground adjustable. The nominal setting is zero degrees.

2.1.5 Configuration Dimensions

Table 2.1 presents a summary of the HRXV-15 dimensions, areas and other pertinent data.

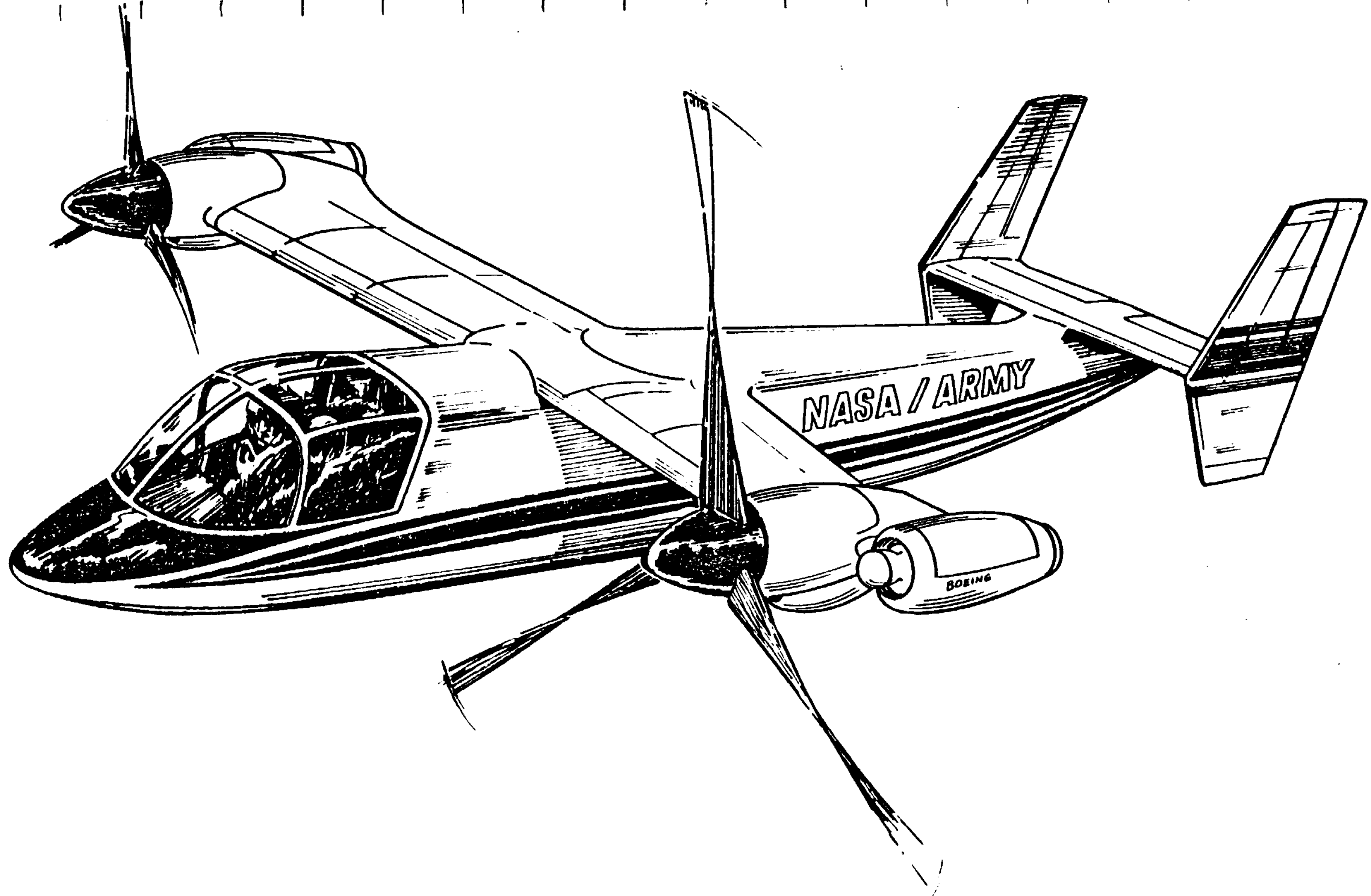

Figure 2.1. Artist's Concept of a Boeing Fixed Engine Hingeless Rotor Nacelle Design on the XV-15 Airframe

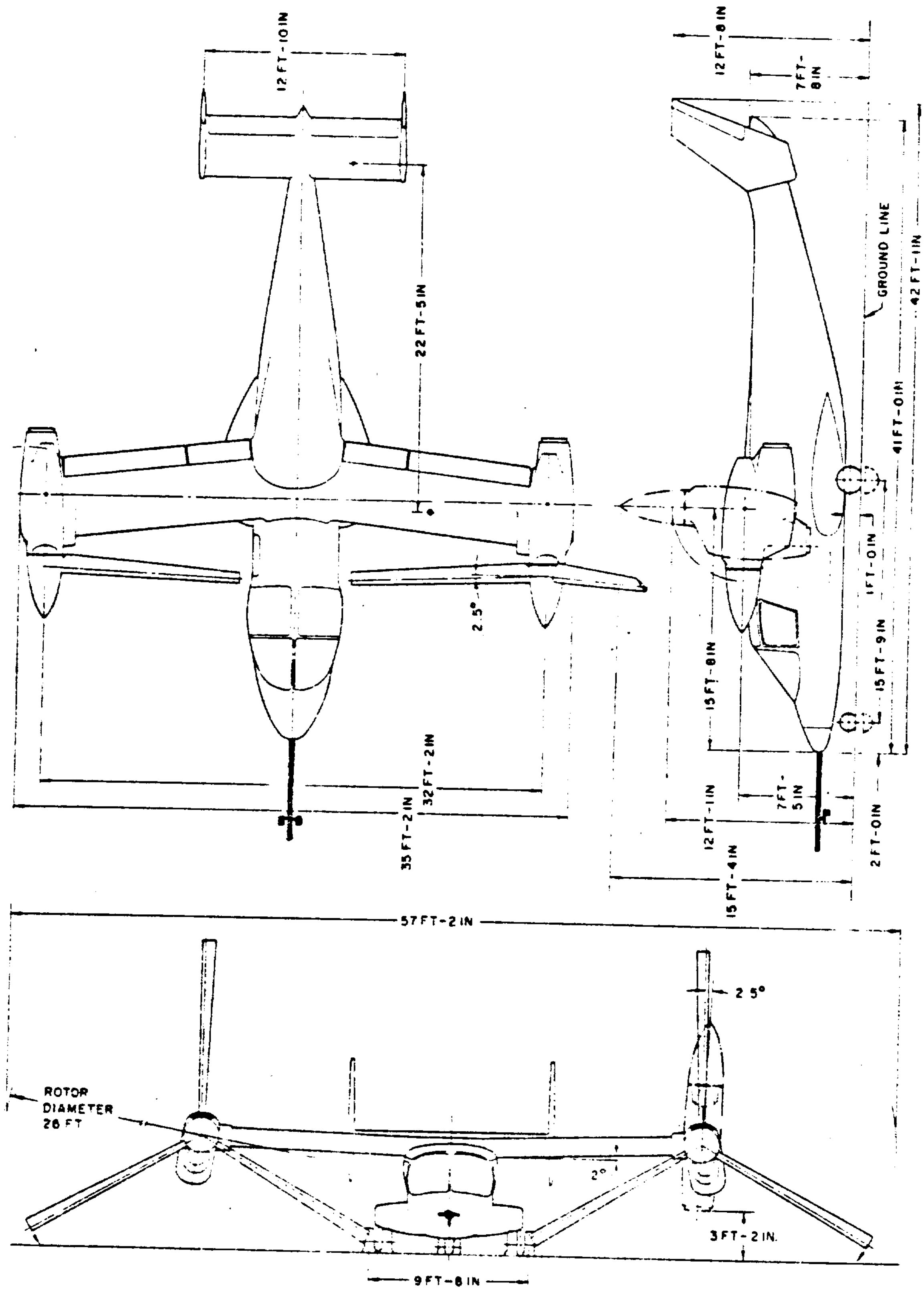

Figure 2.2. General Arrangement, Hingeless Rotor XV-15 Research Aircraft (Reproduced from Reference 2)

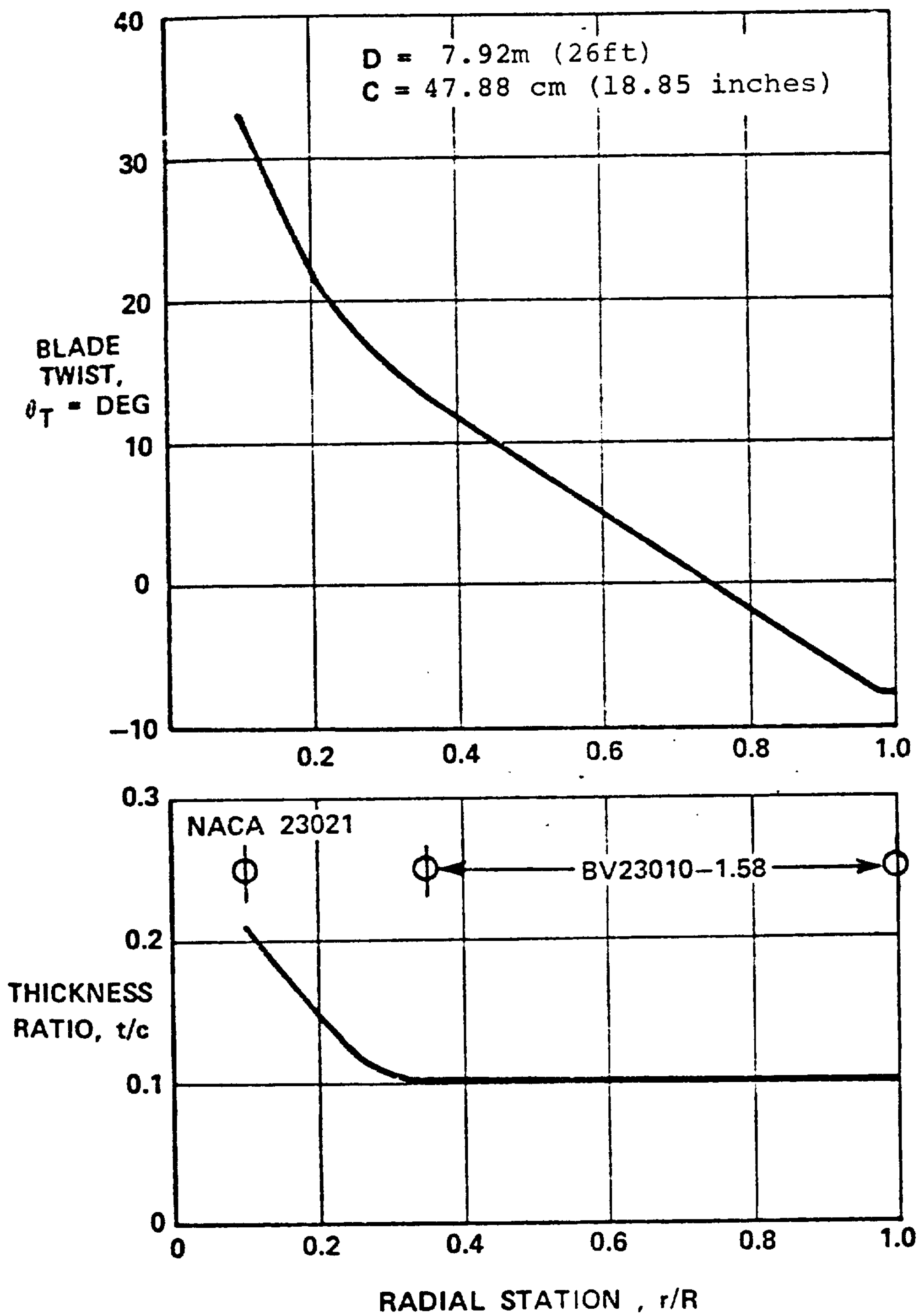

Figure 2.3 Rotor Blade Twist and Thickness Characteristics

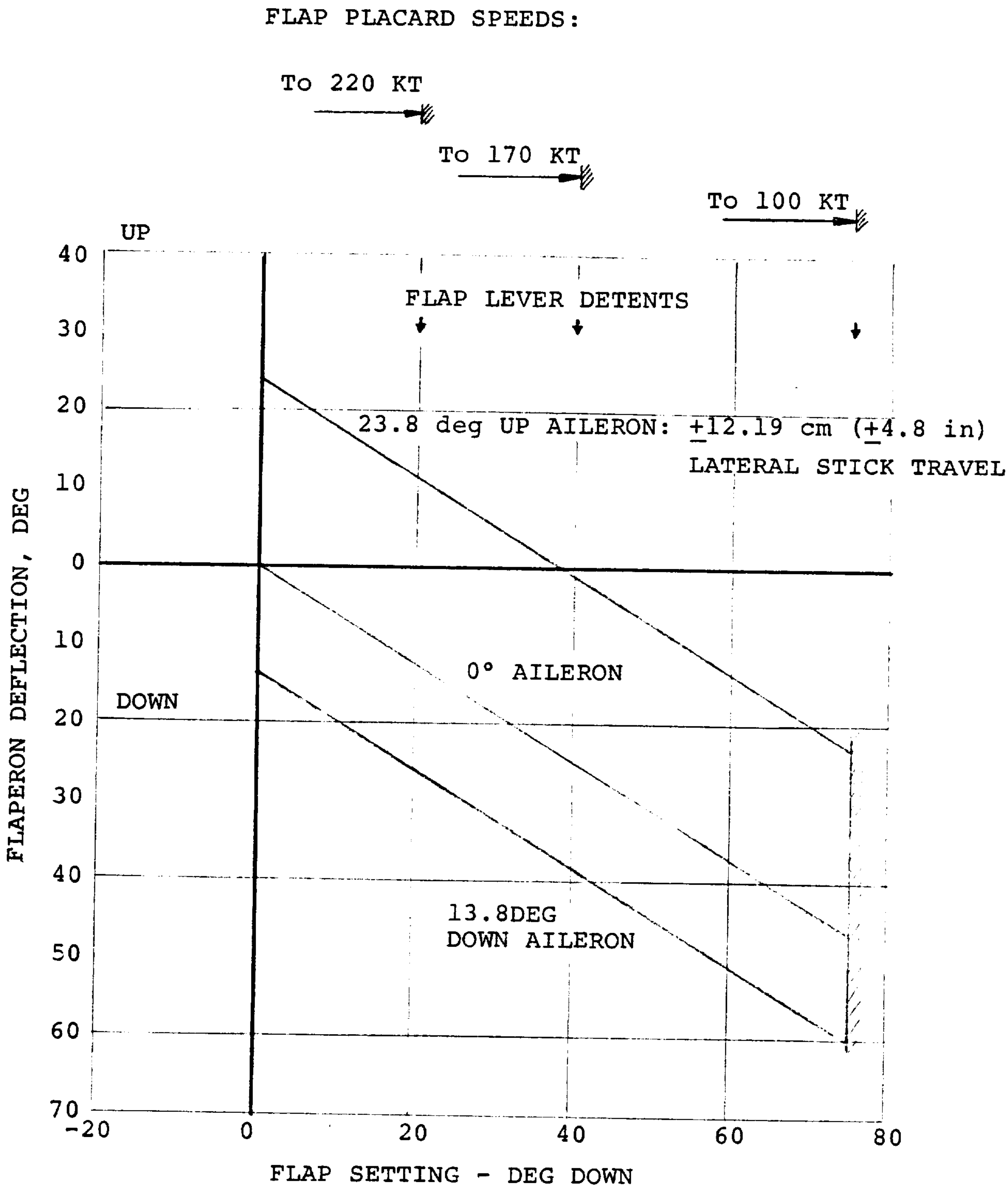

Figure 2.4 Flaperon Deflection with Flap Position

TABLE 2.1

HINGELESS ROTOR XV-15 TILT ROTOR - DIMENSIONAL DATA

WING		
Area (Reference)		$16.815 m^2$ ($181 ft^2$)
Span (Between Rotor ℄)		9.81 m (32.17 ft)
Chord		1.6 m (5.25 ft)
Aspect Ratio		5.72
Sweep		6.5 degree fwd.
Center of Pressure:		
	S.L.	7.396 m (291.17 in)
	B.L.	±2.604 m (102.5 in)
	W.L.	2.435 m (95.85 in)
ROTORS		
No. of Blades per Rotor		3
Diameter		7.925 m (26.0 ft)
Disc Area per Rotor		$49.325 m^2$ ($530.93 ft^2$)
Solidity		0.1154
Direction of Rotation (Airplane)		UP INBOARD
Rotor Speed		
Nacelles 90 deg (HOVER)		57.7 rad/sec (551 rpm)
0 deg (AIRPLANE)		40.4 rad/sec (386 rpm)
Polar Moment of Inertia		$764.8 kg.m^2$ (564 slug ft^2
Location of Shaft	S.L.	7.26 m (300.0 in)
Pivot Points	B.L.	±4.902 m (193.0 in)
	W.L.	2.54 m (100.0 in)
Distance from Hub to Pivot Point		1.423 m (4.667 ft)

TABLE 2.1 (continued)

NACELLES		
Center of Gravity (Nacelle at 90 deg)	S.L.	7.409 m (291.7 in)
	B.L.	±4.902 m (193.0 in)
	W.L.	3.0 m (118.0 in)
Mass per Nacelle		903.95 kg (61.94 slugs)
Nacelle Inertias	I_x	113.38 $kg.m^2$ (81.4 slugs ft^2)
	I_y	584.4 $kg.m^2$ (431.0slugs ft^2)
	I_z	515.3 $kg.m^2$ (380.0slugs ft^2)
Distance from C.G. to Pivot Point		0.503 m (1.65 ft)
Angular Depression of C.G. below Hub-to-Pivot Line		0.432 rad (24.75 deg)
Distance of Tail Pipe ℄ below Pivot		54.42 cm (23 ins)
FUSELAGE		
Center of Pressure	S.L.	7.442 m (293.0 in)
	B.L.	0.0
	W.L.	2.134 m (84.0 in)
PILOT STATION COORDINATES		
Eye Level	S.L.	5.311 m (209.1 in)
	B.L.	0.419 m (16.5 in)
	W.L.	2.083 m (82.0 in)
Seat	S.L.	5.467 m (215.25 in)
	B.L.	0.419 m (16.5 in)
	W.L.	1.283 m (50.5 in)

TABLE 2.1 (continued)

HORIZONTAL TAIL			
Area			4.668 m^2 (50.25 ft^2)
Span			3.911 m^2 (12.83 ft)
Chord			1.195 m (3.92 ft)
Aspect Ratio			3.276
Center of Pressure		S.L.	14.224 m (560.0 in)
		B.L.	0.0
		W.L.	2.616 m (103.0 in)
VERTICAL TAILS (ONE PANEL)			
Area			2.346 m^2 (25.25 ft^2)
Span			2.341 m (7.68 ft)
Chord			1.135 m (3.725 ft)
Center of Pressure		S.L.	14.479 m (570.02 in)
		B.L.	$\pm$1.956 m (77.0 in)
		W.L.	2.939 m (115.69 in)
LANDING GEAR			
Coordinates of Gear Down		S.L.	8.28 m (326.0 in)
	Main	B.L.	$\pm$1.302 m (51.25 in)
		W.L.	0.483 m (19.0 in)
		S.L.	3.531 m (139.0 in)
	Nose	B.L.	0.0
		W.L.	0.411 m (16.2 in)
Tyre Radii	Main		26.1 cm (10.26 in)
	Nose		16.5 cm (6.48 in)

3.0 EQUATIONS OF MOTION

3.0 EQUATIONS OF MOTION

This section presents the derivation of the airframe equations of motion and the simplifications that were made in order to obtain the final equations as presented in Appendix E. The treatment accounts for all six rigid-body degrees-of-freedom including the effects of the tilting nacelles and rotors. The principal features of the derivation are:

- Assumption of X-Z plane of symmetry
- The basic equations are derived about the instantaneous center of gravity of the aircraft since the center of gravity is strongly dependent on nacelle incidence.
- Rotor and engine gyroscopic terms are included.
- The wing elastic degrees of freedom do not couple inertially. The coupling occurs only through the aerodynamic terms.
- Wing aeroelastic effects are not included in the center of gravity calculations.

3.1 AXES SYSTEM

A set of right-handed orthogonal axes OXYZ is placed at the center of mass of the aircraft and is fixed in the aircraft such that OX lies in the lateral plane of symmetry and is positive forward parallel to the fuselage water line zero. The remaining axes are placed as shown in Figure 3.1.

The orientation of the aircraft is defined with respect to a set of earth-fixed axes C X'Y'Z'. With the axes OXYZ initially parallel to C X'Y'Z', the aircraft is yawed to the right about O through an angle ψ, then pitched up about OZ through the angle θ, and finally rolled right about OX through the angle ϕ.

If $\underline{V}$ and $\underline{\Omega}$ are the aircraft velocity and angular velocity vectors relative to the earth-fixed axes, the projections of these vectors on the moving axes are U, V, and W for the components along OX, OY, and OZ, and P, Q, and R for the angular velocity components.

Thus,

$$\underline{V} = U\underline{i} + V\underline{j} + W\underline{k} \tag{3.1}$$

$$\underline{\Omega} = P\underline{i} + Q\underline{j} + R\underline{k} \tag{3.2}$$

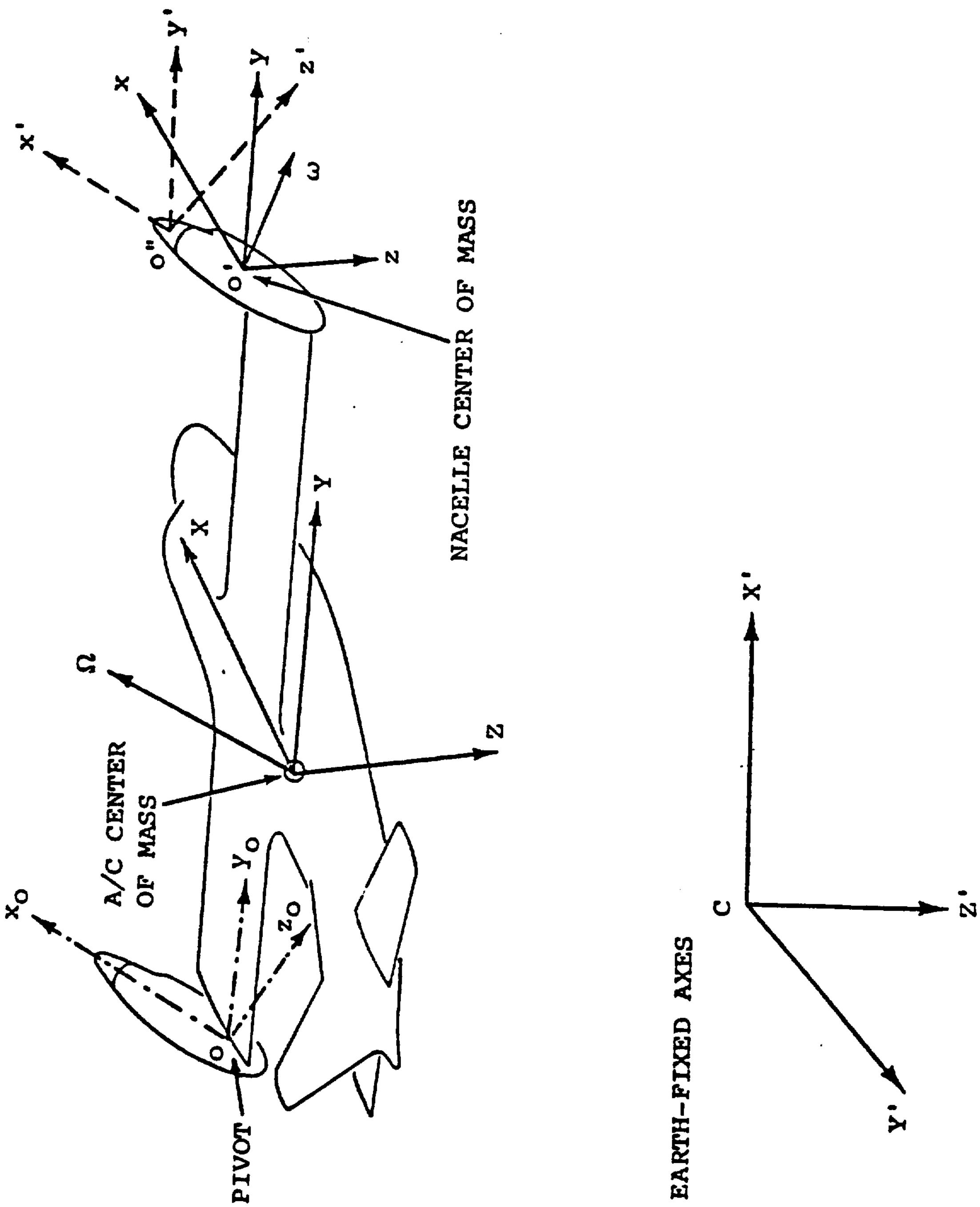

Figure 3.1 *Axes Systems*

where the unit vectors $\underline{i}$, $\underline{j}$, and $\underline{k}$ lie along OX, OY, and OZ.

3.2 AIRCRAFT GROUND TRACK

The components of $\underline{V}$ relative to the earth-fixed axes are obtained in terms of U, V, W and ψ, θ, ϕ as, (See Reference 2),

$$
\begin{aligned}
\frac{dX'}{dt} &= U\cos\theta\cos\psi + V(\sin\phi\sin\theta\cos\psi - \cos\phi\sin\psi) \\
&\quad + W(\cos\phi\sin\theta\cos\psi + \sin\theta\sin\psi) \\
\frac{dY'}{dt} &= U\cos\theta\sin\psi + V(\sin\phi\sin\theta\sin\psi + \cos\phi\cos\psi) \\
&\quad + W(\cos\phi\sin\theta\sin\psi - \sin\phi\cos\psi) \\
\frac{dZ'}{dt} &= -U\sin\theta + V\sin\phi\cos\theta + W\cos\phi\cos\theta
\end{aligned}
\tag{3.3}
$$

Integration of these equations gives the aircraft ground track. A further relationship may be obtained between the rate of change of the Euler angles (ψ, θ, ϕ) and the components of the angular velocity in the moving axes system, viz,

$$
\begin{aligned}
\dot{\psi} &= (R\cos\phi + Q\sin\phi)\sec\theta \\
\dot{\theta} &= Q\cos\phi - R\sin\phi \\
\dot{\phi} &= P + \dot{\psi}\sin\theta
\end{aligned}
\tag{3.4}
$$

3.3 FORCE EQUATION

The total external force, $\underline{F}$, acting at the aircraft center of mass is given by

$$\underline{F} = \frac{d}{dt}(m\underline{V}) = m\left[\frac{\delta \underline{V}}{\delta t} + \underline{\Omega} \times \underline{V}\right] \tag{3.5}$$

where m is the mass of the aircraft and $\frac{\delta \underline{V}}{\delta t}$ is the rate of change of $\underline{V}$ with respect to the moving reference frame OXYZ, i.e.

$$\frac{\delta \underline{V}}{\delta t} = \dot{U}\,\hat{\underline{i}} + \dot{V}\hat{\underline{j}} + \dot{W}\hat{\underline{k}} \tag{3.6}$$

If $\underline{F}$ has components F_x, F_y, and F_z along the respective axes then

$$\underline{F} = F_x \hat{\underline{i}} + F_y \hat{\underline{j}} + F_z \hat{\underline{k}} = m\left\{\dot{U}\,\hat{\underline{i}} + \dot{V}\hat{\underline{j}} + \dot{W}\hat{\underline{k}} + \begin{vmatrix} \hat{i} & \hat{j} & \hat{k} \\ P & Q & R \\ U & V & W \end{vmatrix}\right\}$$

thus

$$\begin{aligned} F_x &= m\ (\dot{U} + QW - RV) \\ F_y &= m\ (\dot{V} + RU - PW) \\ F_z &= m\ (\dot{W} + PV - QU) \end{aligned} \qquad (3.7)$$

The forces F_x, F_y and F_z are given by

$$\begin{aligned} F_x &= X_{AERO} - mg \sin\theta \\ F_y &= Y_{AERO} + mg \sin\phi \cos\theta \\ F_z &= Z_{AERO} + mg \cos\phi \cos\theta \end{aligned} \qquad (3.8)$$

Where X_{AERO}, etc., are the components of the total aerodynamic force acting at the aircraft center of mass.

Substituting equations (3.5) in equations (3.7), the following equations are obtained for the aircraft accelerations,

$$\begin{aligned} \dot{U} &= \frac{X_{AERO}}{m} - g \sin\theta - QW + RV \\ \dot{V} &= \frac{Y_{AERO}}{m} + g \cos\theta \sin\phi - RU + PW \\ \dot{W} &= \frac{Z_{AERO}}{m} + g \cos\theta \cos\phi + QU - PV \end{aligned} \qquad (3.9)$$

3.4 MOMENT EQUATION

The derivation of the equations for the total moment acting about the aircraft center of mass is complicated by the fact that the center of mass changes position due to the tilting nacelles. Thus the centers of gravity of the principal aircraft component masses of the wings (m_W), fuselage (including tails) (m_f), and nacelles (m_N), move with respect to the reference axes OXYZ placed at the instantaneous overall center of gravity of the aircraft. The equation of motion for such a mass element will first be obtained and the total moment found by adding the contributions of all the elements.

3.5 EQUATION OF MOTION FOR A MASS ELEMENT

With reference to Figure (3.1) O'xyz is a right-handed set of axes placed at the center of gravity of the representative mass. The axes are parallel to the set OXYZ. The mass, m, rotates about its own center of gravity with angular velocity $\underline{\omega}$ which, in general, differs from $\underline{\Omega}$ the angular velocity of the aircraft. If $\underline{r}$ is the radius vector from O to O' then the velocity of the center of mass of the element is

$$\underline{V} = \frac{\delta \underline{r}}{\delta t} + \underline{\Omega} \times \underline{r} \tag{3.10}$$

The angular momentum of this mass about O is

$$\underline{h} = m\,(\underline{r} \times \underline{V}) + \underline{h}o \tag{3.11}$$

where $\underline{h}o$ is the angular momentum of m about its own center of mass and is given by

$$\underline{h}o = \bar{I}\,\underline{\omega}$$

where

$$\bar{I} = \begin{bmatrix} I_{xx} & -I_{xy} & -I_{xz} \\ -I_{yx} & I_{yy} & -I_{yz} \\ -I_{zx} & -I_{zy} & I_{zz} \end{bmatrix} \tag{3.13}$$

and I_{xx}, etc., are the moments and products of inertia of the mass about O'xyz.

The total moment, $\underline{G}$, about the aircraft center of mass is given by

$$\underline{G} = \frac{d\underline{h}}{dt} = \frac{\delta \underline{h}}{\delta t} + \underline{\Omega} \times \underline{h}$$

Using equations (3.10), (3.11), and (3.12) in (3.14), the moment becomes

$$\underline{G} = m\left[\frac{\delta \underline{r}}{\delta t} \times \left(\frac{\delta \underline{r}}{\delta t} + \underline{\Omega} \times \underline{r}\right) + \underline{r} \times \frac{\delta}{\delta t}\left(\frac{\delta \underline{r}}{\delta t} + \underline{\Omega} \times \underline{r}\right)\right] + \frac{\delta}{\delta t}(\bar{I}\underline{\omega})$$
$$+ m\,\underline{\Omega} \times \left[\underline{r} \times \left(\frac{\delta \underline{r}}{\delta t} + \underline{\Omega} \times \underline{r}\right)\right] + \underline{\Omega} \times (\bar{I}\underline{\omega}) \tag{3.15}$$

which reduces to

$$\underline{G} = 2m\underline{\Omega}\left(\underline{r}\cdot\frac{\delta \underline{r}}{\delta t}\right) + m\underline{r} \times \frac{\delta^2 \underline{r}}{\delta t^2} + m\frac{\delta \underline{\Omega}}{\delta t}(\underline{r}\cdot\underline{r}) - m\underline{r}\left(\underline{r}\cdot\frac{\delta \underline{\Omega}}{\delta t}\right) \tag{3.16}$$
$$-2m\frac{\delta \underline{r}}{\delta t}(\underline{\Omega}\cdot\underline{r}) - m(\underline{r}\cdot\underline{\Omega})(\underline{\Omega}\times\underline{r}) + \bar{I}\frac{\delta \underline{\omega}}{\delta t} + \underline{\Omega}\times\left(\bar{I}\,\underline{\omega}\right)$$

The only masses that possess angular velocities different from that of the aircraft are the nacelles, which are free to pitch about O' with angular rate $\dot{i} = \frac{di_N}{dt}$. Thus $\underline{\omega}$ may be written generally as

$$\underline{\omega} = P\hat{\underline{i}} + (Q + \dot{i}_N)\,\hat{\underline{j}} + R\,\hat{\underline{k}} \tag{3.17}$$

Now, with $\underline{r} = X\hat{\underline{i}} + Y\hat{\underline{j}} + Z\hat{\underline{k}}$, where X, Y, and Z are the instantaneous coordinates of the individual mass center relative to the aircraft mass center, the various terms of equation (3.16) are, in component form,

$$\underline{r}\cdot\frac{\delta \underline{r}}{\delta t} = X\dot{X} + Y\dot{Y} + Z\dot{Z}$$

$$\underline{r} \times \frac{\delta^2 \underline{r}}{\delta t^2} = (Y\ddot{Z} - Z\ddot{Y})\hat{\underline{i}} - (X\ddot{Z} - Z\ddot{X})\hat{\underline{j}} + (X\ddot{Y} - Y\ddot{X})\hat{\underline{k}}$$

$$\frac{\delta \underline{\Omega}}{\delta t}(\underline{r}\cdot\underline{r}) = (X^2 + Y^2 + Z^2)(\dot{P}\hat{\underline{i}} + \dot{Q}\hat{\underline{j}} + \dot{R}\hat{\underline{k}}) \tag{3.18}$$

$$\underline{r}\cdot\frac{\delta \underline{\Omega}}{\delta t} = X\dot{P} + Y\dot{Q} + Z\dot{R}$$

$$\underline{\Omega}\cdot\underline{r} = XP + YQ + ZR$$

$$(\underline{r}\cdot\underline{\Omega})(\underline{\Omega}\times\underline{r}) = (XP+YQ+XR)\left[(QZ-RY)\hat{\underline{i}} - (PZ-RX)\hat{\underline{j}} + (PY-XQ)\hat{\underline{k}}\right]$$

$$\bar{I}\frac{\delta \underline{\omega}}{\delta t} = (I_{xx}\dot{P} - I_{xz}\dot{R})\hat{\underline{i}} + I_{yy}(\dot{Q} + \ddot{i}_N)\hat{\underline{j}} + (I_{zz}\dot{R} - I_{xz}\dot{P})\hat{\underline{k}}$$

$$\underline{\Omega}\times(\bar{I}\underline{\omega}) = (QR\,I_{zz} - QPI_{xz} - RQI_{yy} - R\dot{i}_N I_{yy})\hat{\underline{i}}$$
$$-(PR\,I_{zz} - P^2 I_{xz} - PR\,I_{xx} + R^2 I_{xz})\hat{\underline{j}}$$
$$+(QR\,I_{xz} + PQI_{yy} + P\dot{i}_N I_{yy} - PQ\,I_{xx})\hat{\underline{k}}$$

where, in the last two terms, the products of inertia I_{xy} and I_{yz} are zero from symmetry considerations.

Substituting the above relations into equation (3.16) and noting that $\dot{Y}$ and $\ddot{Y}$ are always zero (no lateral motion of the individual masses) the following expressions are obtained for the components of the moment $\underline{G} = \Delta L\underline{i} + \Delta M\underline{j} + \Delta N\underline{k}$:

$$\Delta L = \dot{P}[I_{xx} + m(Y^2 + Z^2)] - (\dot{R}+PQ)[I_{xz} + m\,XZ]$$
$$+ RQ[I_{zz}-I_{yy}+m(Y^2-Z^2)] + m\,YZ(R^2-Q^2) - I_{yy}R\,\dot{i}_N$$
$$+ m\,(Y\ddot{Z}-2\dot{X}YR - 2\dot{X}ZR + 2Z\dot{Z}P - XY\,(\dot{Q} - PR))$$

$$\Delta M = \dot{Q}\,[I_{yy}+m(X^2+Z^2)] - (R^2-P^2)[I_{xz} + mXZ] \tag{3.19}$$
$$+ PR\,[I_{xx}-I_{zz} + m(Z^2-X^2)] + I_{yy}\ddot{i}_N$$
$$+ m\,[\ddot{X}Z-X\ddot{Z} + 2Q(Z\dot{Z}+X\dot{X})-XY\,(\dot{P}+RQ)+YZ(PQ-\dot{R})]$$

$$\Delta N = \dot{R}\,[I_{zz}+m(X^2+Y^2)] - (\dot{P}-RQ)\,[I_{xz}+m\,XZ] \tag{3.20}$$
$$+ PQ\,[I_{yy}-I_{xx} + m(X^2-Y^2)] + I_{yy}P\,\dot{i}_N$$
$$+ m\,[2X\dot{X}R - Y\ddot{X} - 2XZP - 2Y\dot{Z}Q - YZ\,(\dot{Q}+PR)+XY(Q^2-P^2)]$$

Summing the rolling moment equation:

$$L = I_{xx}\dot{P}-I_{xz}\,(\dot{R}+PQ) + (I_{zz}-I_{yy})RQ$$
$$+ m_N(R^2-Q^2)(Z_{NR}-Z_{NL})Y_N + m_N\Big\{Y_N(\ddot{Z}_{NR}-\ddot{Z}_{NL})$$
$$-2Q(\dot{X}_{NR}-\dot{X}_{NL})Y_N-2R(\dot{X}_{NR}Z_{NR} + \dot{X}_{NL}Z_{NL}) + 2P(\dot{Z}_{NR}Z_{NR} + \tag{3.21}$$
$$\dot{Z}_{NL}Z_{NL})-(\dot{Q}-PR)(X_{NR}-X_{NL})\,Y_N\Big\}+ 2m_fZ_f(P\dot{Z}_f -$$
$$R\dot{X}_f) + 2m_wZ_w(P\dot{Z}_w - R\ddot{X}_w)-R\,I^N_{yy}\,(\dot{i}_{NL} + \dot{i}_{NR})$$

where I_{XX}, I_{XZ}, I_{ZZ}, and I_{YY} are the inertias of the aircraft about its center of gravity, and the subscripts f, w, NL and NR stand for fuselage, wing, left nacelle and right nacelle. The remaining symbols are defined in the List of Symbols. Similar expressions are obtained for the pitching moment and yawing moment. In the interests of brevity the remainder of the discussion will be limited to equation (3.21).

Evaluation of the terms of the rolling moment equation indicate that this equation may be simplified considerably without a significant change in accuracy. For example, terms containing $(\dot{X}_{NR}-\dot{X}_{NL})$ may be dropped because $\dot{X}_{NR}$ is normally identical to

$\dot{X}_{NL}$, i.e. the nacelles are raised or lowered together at the same rate. Equation (3.21) may thus be written

$$L=I_{XX}\dot{P}-I_{XZ}(\dot{R}+PQ) + (I_{ZZ}-I_{YY})RQ + m_N Y_N(\ddot{Z}_{NR}-\ddot{Z}_{NL}) \qquad (3.22)$$

where the last term has been retained in consideration of the high differential nacelle accelerations encountered during hover maneuvers.

From the relationships presented in Appendix C the last term of Equation (3.22) may be rewritten as

$$\begin{aligned}-\ell m_N Y_N [\ddot{i}_{NR} \cos (i_{NR}-\lambda) + \dot{i}_{NL}^2 \sin (i_{NL}-\lambda) \\ -\dot{i}_{NR}^2 \sin (i_{NR}-\lambda) - \ddot{i}_{NL} \cos (i_{NL}-\lambda)]\end{aligned} \qquad (3.23)$$

which may be approximated to

$$-\ell m_N Y_N [\ddot{i}_{NR} \cos (i_{NR}-\lambda) - \ddot{i}_{NL} \cos (i_{NL}-\lambda)] \qquad (3.24)$$

since the nacelle rates appear as squared terms.

Similar treatment of the pitching moment and yawing moment equations results in the following final form of the moment equations.

$$\begin{aligned}
L_{AERO} &= I_{XX}\dot{P}-I_{XZ}(\dot{R}+PQ) + (I_{ZZ}-I_{YY})RQ \\
&\quad -\ell m_N Y_N [\ddot{i}_{NR} \cos (i_{NR}-\lambda) - \ddot{i}_{NL} \cos (i_{NL}-\lambda)] \\
M_{AERO} &= I_{YY}\dot{Q} - I_{XZ}(R^2-P^2) + (I_{XX}-I_{ZZ})PR \\
&\quad + \ddot{i}_{NR} \left\{I^N_{YY_o} + \ell m_N [X_R \cos (i_{NR}-\lambda) - Z_R \sin (i_{NR}-\lambda)]\right\} \\
&\quad + \ddot{i}_{NL} \left\{I^N_{YY_o} + \ell m_N [X_L \cos (i_{NL}-\lambda) - Z_L \sin (i_{NL}-\lambda)]\right\} \\
N_{AERO} &= I_{ZZ}\dot{R}-I_{XZ}(\dot{P}-RQ) + (I_{YY}-I_{XX})PQ \\
&\quad + \ell m_N Y_N [\ddot{i}_{NR} \sin (i_{NR}-\lambda) - \ddot{i}_{NL} \sin (i_{NL}-\lambda)]
\end{aligned} \qquad (3.25)$$

where the moments L_{AERO}, M_{AERO}, and N_{AERO} represent the sum of the aerodynamic moments and rotor/engine gyroscopic moments about the aircraft center of mass. $I^N_{YY_o}$ is the nacelle pitch inertia referred to the nacelle-fixed axes system described in Appendix C. Equations for the aircraft inertias are also presented in that Appendix.

3.6 EQUATIONS OF MOTION FOR NACELLES

The equation of motion for a nacelle is required in order to obtain the moment exerted by the nacelle on the wing tip at the pivot. This moment is then used in the equations for wing twist.

The angular momentum of a nacelle about its pivot point is given by

$$\underline{h}_p = (\underline{r}-\underline{r}_p) \times m_N\underline{V} + \underline{h}_{O_N}$$

$$= m_n (\underline{r}\times\underline{V}) + \underline{h}_o - m_n\underline{r}_p \times \underline{V} \tag{3.26}$$

where $\underline{r}$ is the radius vector from aircraft c.g. to nacelle c.g.

$\underline{V}$ is the velocity of the nacelle c.g.

$\underline{h}_{O_N}$ is the angular momentum of the nacelle about its own c.g.

m_N is the nacelle mass

and $\underline{r}_p$ is the radius vector from aircraft c.g. to nacelle pivot

The term $m_n (\underline{r}\times\underline{V}) + \underline{h}_{O_N}$ is the angular momentum of the nacelle about the aircraft c.g. ($= \underline{h}^N_{CG}$).

i.e. $\underline{h}_p = \underline{h}^N_{CG} - m_N(\underline{r}_p \times \underline{V})$

The moment about the pivot is

$$\underline{G}_p = \frac{d\underline{h}_p}{dt} = \frac{d\underline{h}_N}{dt} - m_n \frac{d}{dt} (\underline{r}_p \times \underline{V}) = \underline{G}^N_{CG} - \Delta\underline{G} \tag{3.27}$$

Since the quantity $\underline{G}^N_{cg}$ has already been obtained (equations (3.18), (3.19), and (3.20)), only the remaining term needs to be evaluated.

$$\Delta\underline{G} = m_N \frac{d}{dt} (\underline{r}_p\times\underline{V}) = m_N\left\{\frac{\delta\underline{r}_p}{\delta t} \times \underline{V} + \underline{r}_p \times \frac{\delta\underline{V}}{\delta t} + \underline{\Omega}(\underline{r}_p \times \underline{V})\right\}$$

$$= m_N \left\{\frac{\delta\underline{r}_p}{\delta t} \times\left(\frac{\delta\underline{r}}{\delta t} + \underline{\Omega}\times\underline{r}\right) + \underline{r}_p \times \frac{\delta}{\delta t} \left(\frac{\delta\underline{r}}{\delta t} + \underline{\Omega}\times\underline{r}\right) + \underline{\Omega} \times \left[\underline{r}_p \times\left(\frac{\delta\underline{r}}{\delta t} + \underline{\Omega} \times \underline{r}\right)\right]\right\} \tag{3.28}$$

Expansion of these terms results in the following expression

$$\Delta \underline{G} = m_N\left\{\frac{\delta \underline{r}_p}{\delta t} \times \frac{\delta \underline{r}}{\delta t} + \underline{\Omega}\left(\underline{r}\cdot\frac{\delta \underline{r}_p}{\delta t}\right) - \underline{r}\left(\frac{\delta \underline{r}_p}{\delta t}\cdot\underline{\Omega}\right) + \underline{r}_p \times \frac{\delta^2 \underline{r}}{\delta t^2} + \frac{\delta \Omega}{\delta t}(\underline{r}\cdot\underline{r}_p)\right.$$
$$- \underline{r}\left(\underline{r}_p\cdot\frac{\delta \Omega}{\delta t}\right) + \underline{\Omega}\left(\frac{\delta \underline{r}}{\delta t}\cdot\underline{r}_p\right) - 2\frac{\delta \underline{r}}{\delta t}(\underline{r}_p\cdot\underline{\Omega}) \tag{3.29}$$
$$\left. + \underline{r}_p\left(\frac{\delta \underline{r}}{\delta t}\cdot\underline{\Omega}\right) - (\underline{r}_p\cdot\underline{\Omega})(\underline{\Omega}\times\underline{r})\right\}$$

We require only the $\underline{j}$ component of this vector in order to obtain the nacelle pivot pitching moment.

The components of the vectors $\underline{r}_p$, $\underline{r}$ and $\underline{\Omega}$ are

$$\underline{r}_p = X_p\hat{\underline{i}} + Y_N\hat{\underline{j}} + Z_p\hat{\underline{k}} = - X_{CG}\hat{\underline{i}} + Y_N\hat{\underline{j}} - Z_{CG}\hat{\underline{k}}$$

$$\underline{r} = X_N\hat{\underline{i}} + Y_N\hat{\underline{j}} + Z_N\hat{\underline{k}}$$

$$\underline{\Omega} = P\hat{\underline{i}} + Q\hat{\underline{j}} + R\hat{\underline{k}}$$

Noting that the $\underline{j}$ components of $\frac{\delta \underline{r}_p}{\delta t}$, $\frac{\delta \underline{r}}{\delta t}$ are zero (since Y_N is a constant), the above expression yields

$$\Delta M = m_N\left\{\ddot{X}_N Z_{CG} - \ddot{Z}_N X_{CG} + \dot{Z}_{CG}\dot{X}_N + \dot{Z}_N\dot{X}_{CG} + PQ\, Y_N Z_N \right.$$
$$\left. - RQ\, X_N Y_N\right\} \tag{3.30}$$

Combining this equation with Equation (3.19) and using the transformations given in Appendix C, the final equation for the right-hand nacelle pivot actuator pitching moment becomes, after some simplification,

$$M_{NR} = -\ddot{i}_{NR}\left[I^N_{YY_o} + \ell^2 m_N\left(1-\frac{m_N}{m}\right)\right] - \ell^2 m_N\left(1-\frac{m_N}{m}\right)\left[\dot{Q} - PR\cos 2(i_{NR}-\lambda)\right.$$
$$\left. + (R^2-P^2)\sin(i_{NR}-\lambda)\,\mathrm{Cos}\,(i_{NR}-\lambda)\right] - (R^2-P^2)\, I^N_{ZZ_o}\sin i_{NR}\cos i_{NR}$$
$$- I_{YY_o}\dot{Q} + \ell\frac{m_N}{m}\left[X_{AERO}\sin(i_{NR}-\lambda) + Z_{AERO}\cos(i_{NR}-\lambda)\right]$$
$$- \ell m_N Y_N\left\{(\dot{R}-PQ)\sin(i_{NR}-\lambda) - (\dot{P}+RQ)\cos(i_{NR}-\lambda)\right\}$$
$$+ M_{NR_{AERO}} \tag{3.31}$$

where $M_{NR_{AERO}}$ includes the moment resulting from nacelle aerodynamic loads and the rotor gyroscopic moments. The terms X_{AERO} and Z_{AERO} are, respectively, the total aircraft aerodynamic X and Z forces.

The corresponding equation for the left nacelle actuator moment is obtained by substituting $-Y_N = Y_N$ and changing the R subscript to L.

3.7 DETERMINATION OF ROTOR GYROSCOPIC MOMENTS

The gyroscopic moments are most readily obtained as follows. A set of axes O"x'y'z' is taken at the rotor hub (rotor c.g.) parallel to the nacelle-fixed set of axes $Ox_oy_oz_o$. Associated with each axis are the corresponding unit vectors $\underline{i}'$ $\underline{j}'$ and $\underline{k}'$. The angular velocity of the rotor with respect to these axes is the vector

$$\underline{\omega} = \Omega_R \underline{i}' \tag{3.32}$$

where Ω_R is the rotor rotational speed.

The angular momentum of the rotor with respect to its c.g. is

$$\underline{h}_o = \bar{I}_R \underline{\omega}$$

where $\bar{\underline{I}}_R$ is the inertia matrix $\begin{bmatrix} I_{R_{x'}} & & \\ & I_{R_{y'}} & \\ & & I_{R_{z'}} \end{bmatrix}$

the off-diagonal terms being zero since the axes O"x'y'z' are principal axes of inertia of the rotor and hub.

In component form the angular momentum of the rotor is

$$\underline{h}_o = I_{R_{y'}} \Omega_R \hat{\underline{i}}' = I_R \Omega_R \hat{\underline{i}}' \tag{3.34}$$

With respect to the inertial axes OYXZ, the components of $\underline{h}_o$ are

$$\underline{h}_o = I_R \Omega_R \cos i_N \hat{\underline{i}} - I_R \Omega_R \sin i_N \hat{\underline{k}} \tag{3.35}$$

The hub moment is therefore given by

$$\underline{G}_{HUB} = \frac{d\underline{h}_o}{\delta t} = \frac{\delta \underline{h}_o}{\delta t} + \underline{\Omega} \times \underline{h}_o \tag{3.36}$$

where $$\underline{\Omega} = P\hat{\underline{i}} + Q\hat{\underline{j}} + R\hat{\underline{k}} \tag{3.37}$$

Substitution of equations (3.35) and (3.37) into equation (3.36) results in the following equations for the rotor gyroscopic moments.

$$L_{gyro} = I_R\dot{\Omega}_R \cos i_N - I_R\Omega_R (\dot{i}_N+Q) \sin i_N \qquad (3.38)$$

$$M_{gyro} = I_R P\Omega_R \sin i_N + I_R R\Omega_R \cos i_N \qquad (3.39)$$

$$N_{gyro} = -I_R\dot{\Omega}_R \sin i_N - I_R\Omega_R (\dot{i}_N+Q) \cos i_N \qquad (3.40)$$

The above terms appear in the Computer Representation (Appendix E) as additions to the rotor aerodynamic forces and moments.

4.0 AIRFRAME AERODYNAMICS

4.0 AIRFRAME AERODYNAMICS

This section discusses the mathematical equations and representations of the aerodynamic data for wings, tails and fuselage. The rotor aerodynamics is presented in Section 5. The airframe aerodynamic data was extracted from Reference 1, supplied under the contract. In this reference the aerodynamic data is generally presented as tables which are suited to the interpolation approach used in that simulation model. However, the Boeing tilt rotor simulation model was originally structured to accept equations for the aerodynamic forces and moments rather than to perform table look-ups. A restructuring of the Boeing simulation math model into a table look-up format was considered and rejected because of the adverse impact on cost, schedule and time-frame. Therefore, the aerodynamic data was analyzed and expressed in the form of equations for the various component forces and moments. For the most part, the resulting equations yield results that are in sufficient agreement with the data. In some areas, notably rotor-on-tail interference, it was not possible to use a simple mathematical expression for the data and a table look-up format was utilized.

The representation of the aerodynamics used in the present simulation is given in detail in Appendix E and the values of the coefficients used in the equations are listed in Appendix F. The aerodynamics equations are written in local wind axes. All equations for lift, drag, pitching moment, etc., of the aircraft components are written to cover the complete range of angle of attack and sideslip from 0° through +180°.

4.1 Fuselage

The equations used to represent the lift, drag and pitching moment of the fuselage are:

$$C_{DF} = (C_{DOF} + K1|\alpha_F| + K2\alpha_F^2)\cos^2\beta_F + K_O C_{DOF}|1-\cos(.18\beta_F)| + \Delta C_{D_{LG}}(1 - \ell^{-t/t_G}) \qquad (4.1)$$

$$C_{LF} = (K_{42} + K_3\,\alpha_F')\cos^2\beta_F - K_4\sin^3|\beta_F| \qquad (4.2)$$

$$C_{YF} = K_7\,\beta_F' + K_8\,\beta_F'\,|\beta_F'| \qquad (4.3)$$

$$C_{\mathcal{L}F} = K_{13}\,\beta_F' \qquad (4.4)$$

$$C_{MF} = [-.11 + .36\sin(6.6 + 3.3\,\alpha_F^O)]\cos^2\beta_F + K_5\,|\beta_F'| + \Delta C_{M_{LG}}(1 - \ell^{-t/t_G}) \qquad (4.5)$$

$$C_{NF} = C_{NOF} + K_9\,\beta_F' + K_{10}\,\beta_F'|\beta_F'| \qquad (4.6)$$

where α_F, β_F are the angles of attack and sideslip of the fuselage

$$\alpha_F' = \sin \alpha_F \cos \alpha_F \qquad (4.7)$$

$$\beta_F' = \sin \beta_F \cos \beta_F \qquad (4.8)$$

t_G is the extend/retract time constant for the landing gear and the coefficients are based on the reference wing area and chord.

Correlation of these equations with the data of Reference 1 is presented in Figures 4.1 through 4.3.

4.2 Wing-Nacelles

The aerodynamic forces and moments on the complete wing-nacelle combination are obtained by first considering the wing to be rigid and uninfluenced by the rotor slipstream. Forces are next obtained assuming the wing to be wholly-immersed in the slipstream. A simple method is then used to obtain the forces for the partly-immersed wing.

Power-off data on the wing-nacelle lift, drag and pitching moment, as a function of nacelle angle and flap position, were obtained from Reference 1. This data was linearized to suit the existing math model structure. At angles of attack beyond stall the lift, drag and pitching moment equations are extended to $\pm 90°$ to provide a representation of wing operating conditions at low transition speeds. Figures 4.5, 4.6 and 4.7 show the results of the linearized representation compared with the data.

4.2.1 Rotor Slipstream Interference

The method used to compute the slipstream affects was developed at Boeing and gives acceptable agreement with wind tunnel test data for a wide range of configurations.

The method uses momentum theory to find the speed and direction of the full-contracted slipstream in the neighborhood of the wing. From this, the effective angle of attack of the wing in slipstream is calculated and the forces computed from the power-off data at this angle of attack assuming the entire wing to be immersed.

At the angle of attack of the wing outside the slipstream, the wing forces and moments are obtained from the power-off data. These forces are then scaled by the ratio of unimmersed to total wing areas to yield approximately the forces acting on the immersed wing. The sum of the approximations to immersed and unimmersed wing forces is now formed and is then multiplied by a correction factor to obtain the final forces. The immersed wing area is calculated as described in Appendix D.

The following is an outline of the method

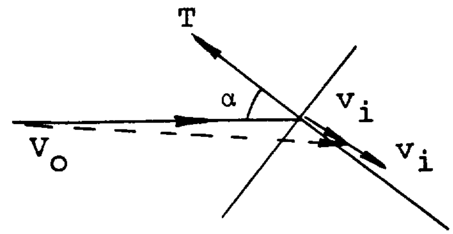

The sketch represents a thrusting rotor at angle of attack α. The induced velocity at the disc, v_i, is obtained by solving the following quartic equation:

$$v_*^4 + 2V_*v_*^3 \cos\alpha + v_*^2V_*^2 = 1 \qquad (4.9)$$

where $$v_* = v_i/\sqrt{T/2\rho A} \qquad (4.10)$$

$$V_* = V_o/\sqrt{T/2\rho A} \qquad (4.11)$$

The resultant angle of attack of the wing in the slipstream is calculated as

$$\alpha_{ss} = \mathrm{Tan}^{-1}\left[\frac{W-2v_i \sin(i_N - i_w)}{U+2v_i \cos(i_N - i_w)}\right] \qquad (4.12)$$

and $\varepsilon = \alpha_w - \alpha_{ss}$ is formed.

The aspect ratio of the immersed portion of the wing is calculated as

$$AR_i = \frac{S_i}{c^2} \qquad (4.13)$$

where S_i is the immersed area and c is the wing chord. Let C_L^* be lift on the wing that would exist if no slipstream were present, and C_L'' the lift that would exist if the wing were wholly immersed. Then the resultant lift is

$$C_{L_S} = K_A' \left[\frac{S_i}{S}(C_L'' \cos\varepsilon - C_D'' \sin\varepsilon) + q/qs\,[1-\frac{S_i}{S}]\,C_L^*\right] \qquad (4.14)$$

where the factor K'_A is a correction factor to account for the fact that the lift-sharing between immersed and unimmersed portions is not simply proportional to the respective areas. From a consideration of mass flows the factor K'_A can be shown to be

$$K'_A = \frac{V_* + (C_{L_{\alpha_i}}/C_{L_\alpha})\ v_*}{V_* + v_*} \tag{4.15}$$

where
$$\frac{C_{L_{\alpha i}}}{C_{L_\alpha}} = \frac{\pi}{\pi + C_{L_{\alpha_w}}\ [1/AR_i - 1/AR]} \tag{4.16}$$

Similarly the drag and pitching moments for the wing in the slipstream are

$$C_{D_S} = K'_A \left\{ \frac{S_i}{S}(C_L''\ \text{Sin}\ \varepsilon + C_D''\ \text{Cos}\ \varepsilon) + C_D^*\ \left(1 - \frac{S_i}{S}\right) \frac{q}{qs} \right\} \tag{4.17}$$

$$C_{M_S} = K'_A \left\{ \frac{S_i}{S}\ C_M'' + C_M^*\ \left(1 - \frac{S_i}{S}\right) \frac{q}{qs} \right\} \tag{4.18}$$

This procedure is carried out for the left and right wing panels and the forces used to compute rolling and yawing moments.

4.2 Horizontal Tail

The horizontal tail lift and drag coefficients are obtained from a linear representation of the data of Reference 1.

$$C_{L_{HT}} = C_{L_\alpha}\ \alpha_{e_{HT}} + C_{L_{H\beta}}\ \beta \tag{4.19}$$

where $\alpha_{e_{HT}}$ is the effective horizontal tail angle of attack and $C_{L_{H\beta}}\beta$ accounts for the slight reduction in tail effectiveness that occurs with sideslip. The effective horizontal tail angle of attack is

$$\alpha_{e_{HT}} = i_{HT} + \text{Tan}^{-1}\ (W'_{HT}/U'_{HT}) - \varepsilon + \tau_{HT}\ \delta_e \tag{4.20}$$

where δ_e is the elevator angle

τ_{HT} is the elevator effectiveness

ε is the wing-on-tail downwash angle

and W'_{HT} , U'_{HT} are obtained from

$$W'_{HT} = W_{HT} - v_{iHT} \operatorname{Sin} i_N \tag{4.21}$$

$$U'_{HT} = U_{HT} + v_{iHT} \operatorname{Cos} i_N \tag{4.22}$$

where v_{iHT} is the rotor-on-tail downwash velocity. This velocity is a function of the rotor induced velocity, sideslip angle, fuselage angle of attack, nacelle angle and airspeed. No simple equation represents the variation of v_{iHT} and it is, therefore, obtained from tables.

The wing downwash angle, ε, is a function of nacelle angle and flap deflection. The math model representation is

$$\varepsilon = \varepsilon_o + \frac{d\varepsilon}{d\alpha} (\alpha_w - \ell_{AC} \dot{W}/U^2) (1\text{-GEF}) \sqrt{1-M^2} \tag{4.23}$$

where $\varepsilon_o = f_4(i_N, \delta)$

$\frac{d\varepsilon}{d\alpha} = f_5(i_N, \delta)$

$\bar{\alpha}_W$ is the wing mean angle of attack

ℓ_{AC} is the distance from tail c/4 to wing c/4

GEF is the ground effect factor

and $\sqrt{1-M^2}$ is a correction for Mach number. The data of Reference 1 was curve fitted to yield equations for ε_o and $d\varepsilon/d\alpha$:

$$\varepsilon_o = f_4 (\bar{i}_N, \delta) = 2.55 - .0303 \bar{i}_N + 4.56\text{x}10^{-4} i_N^2 + .0673\delta - 3.609\text{x}10^{-4}\delta^2$$

$$\frac{d\varepsilon}{d\alpha} = f_5(\bar{i}_N, \delta) = 0.317 + .00078\bar{i}_N + 1.008\text{x}10^{-3}|\delta| - 5.567\text{x}10^{-6}\delta^2$$

$$\begin{aligned} \text{FOR } \alpha_W &> 16°,\ \varepsilon = \varepsilon_{@16}\,(1-(\alpha-16)/12) \\ \alpha_W &< -16°,\ \varepsilon = \varepsilon_{@-16}(1+(\alpha+16)/12) \\ |\alpha_W| &> 28°\ \ \varepsilon = 0 \end{aligned} \tag{4.24}$$

Figure 4.4 shows the results of equations 4.24 compared with the data of Reference 1.

4.3 Vertical Tails

The left and right vertical tails are treated separately. The rotor-on-tail interference velocity is calculated from

$$v_{iVT} = \frac{v_{iHT}}{\bar{v}_i} \bar{v}_i \tag{4.25}$$

where v_{iHT} is the rotor-on-tail downwash velocity and $\bar{v}_i$ is the mean induced velocity at the rotor discs. This velocity is then resolved into components chordwise and spanwise at the vertical tail

$$U_{iVT} = v_{iVT} \text{ Cos } i_N \tag{4.26}$$

$$W_{iVT} = v_{iVT} \text{ Sin } i_N \tag{4.27}$$

These components are then added to the inertial velocity components and the resultant vertical tail angles of attack calculated. The vertical tail lift and drag are then computed from a linearized representation of the data of Reference 1.

4.3 Ground Effects

The effects of operating near the ground on the wing and tail aerodynamics are represented in the model. The proximity of the ground increases the wing and tail lift-curve slopes and reduces the wing-on-tail downwash. The change in lift-curve slopes of the wing and tails with distance from the ground was obtained from Reference 3 directly. The change in downwash was computed from

$$\frac{\Delta\varepsilon}{\varepsilon} = \frac{b^2 + 4\ (h-H)^2}{b^2 + 4\ (h+H)^2} \tag{4.28}$$

where b is the wing of span

h is the tail root quarter chord height above the ground

and H is the wing root quarter chord height above the ground.

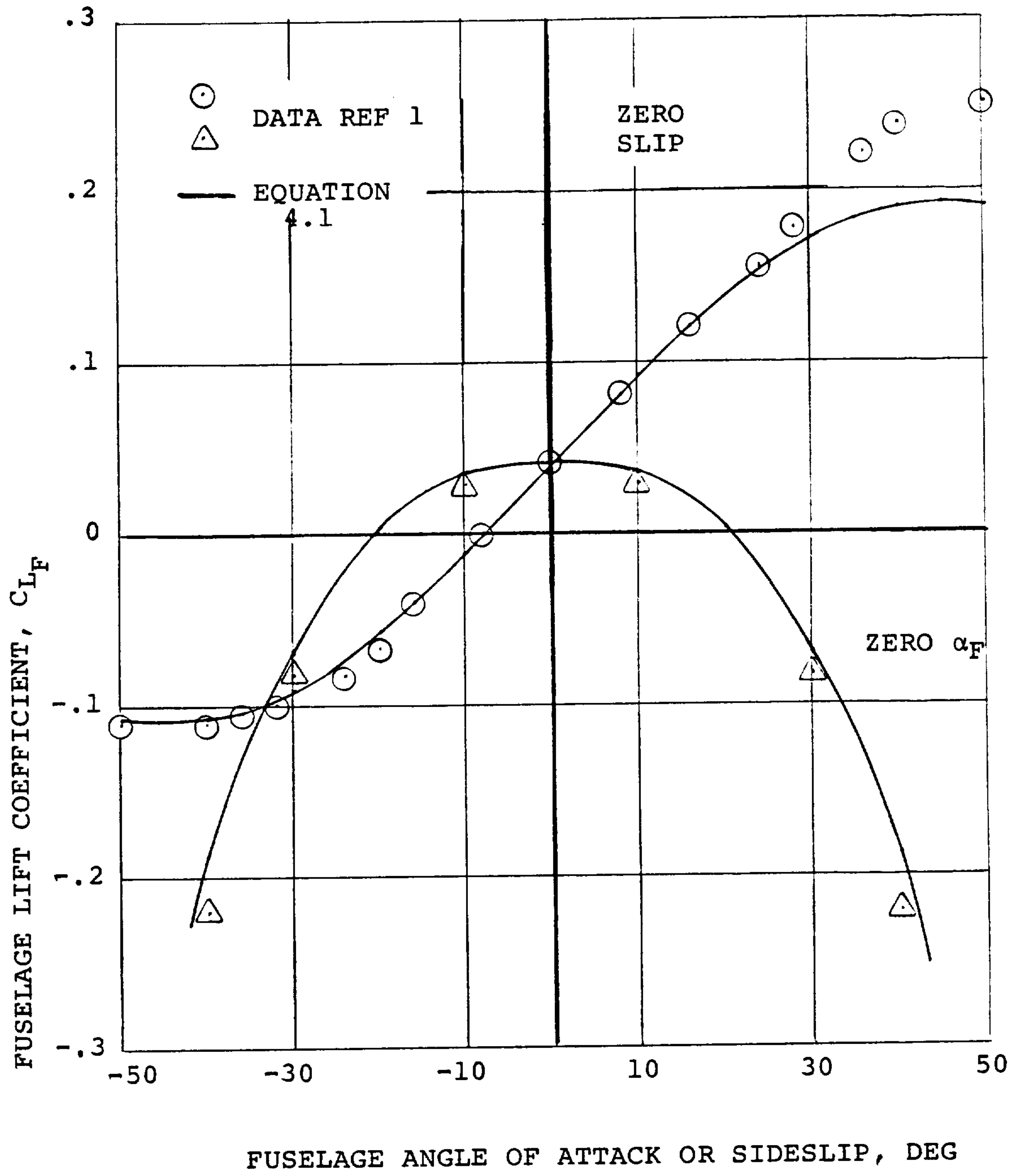

Figure 4.1 Correlation of Fuselage Lift

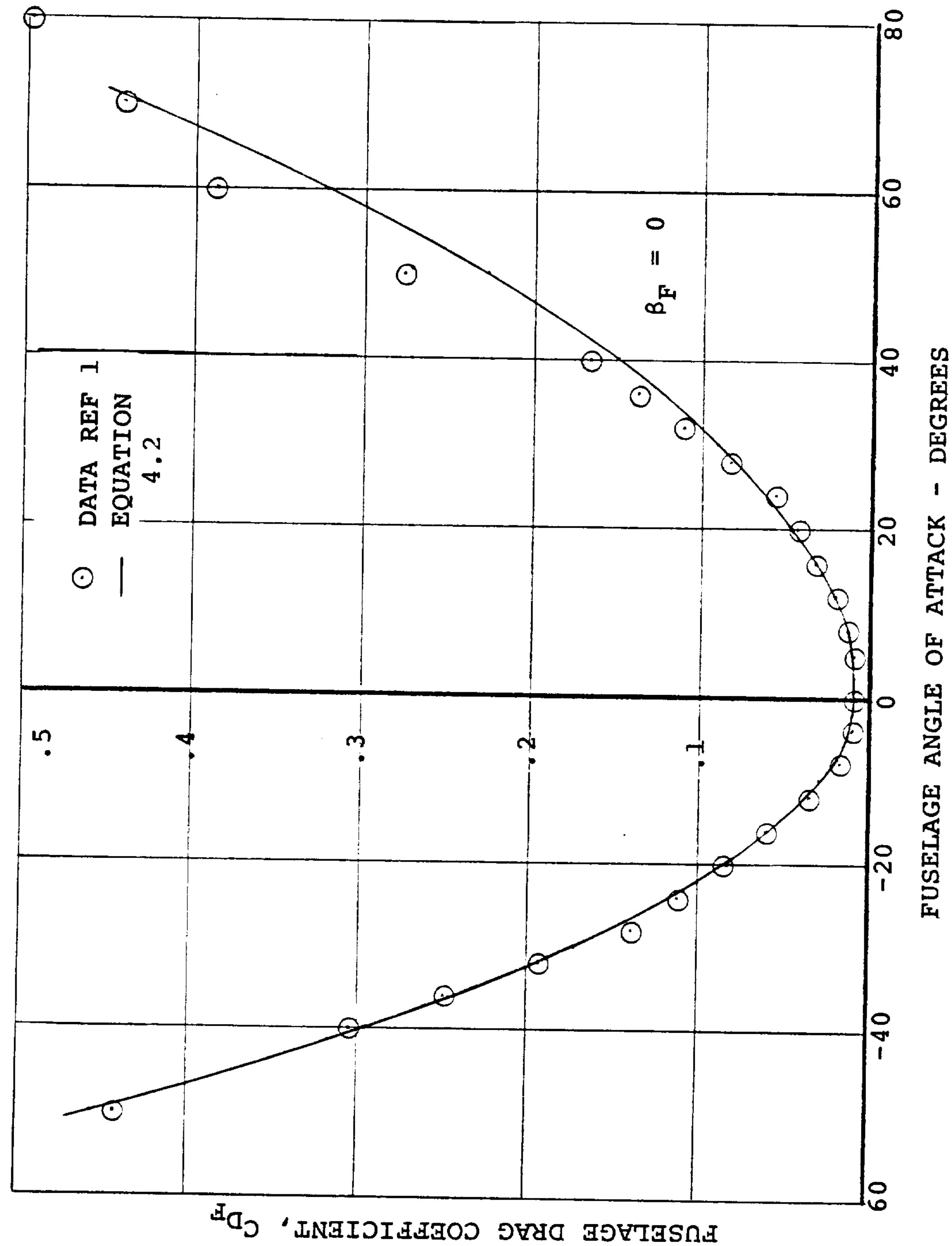

Figure 4.2 Correlation of Fuselage Drag

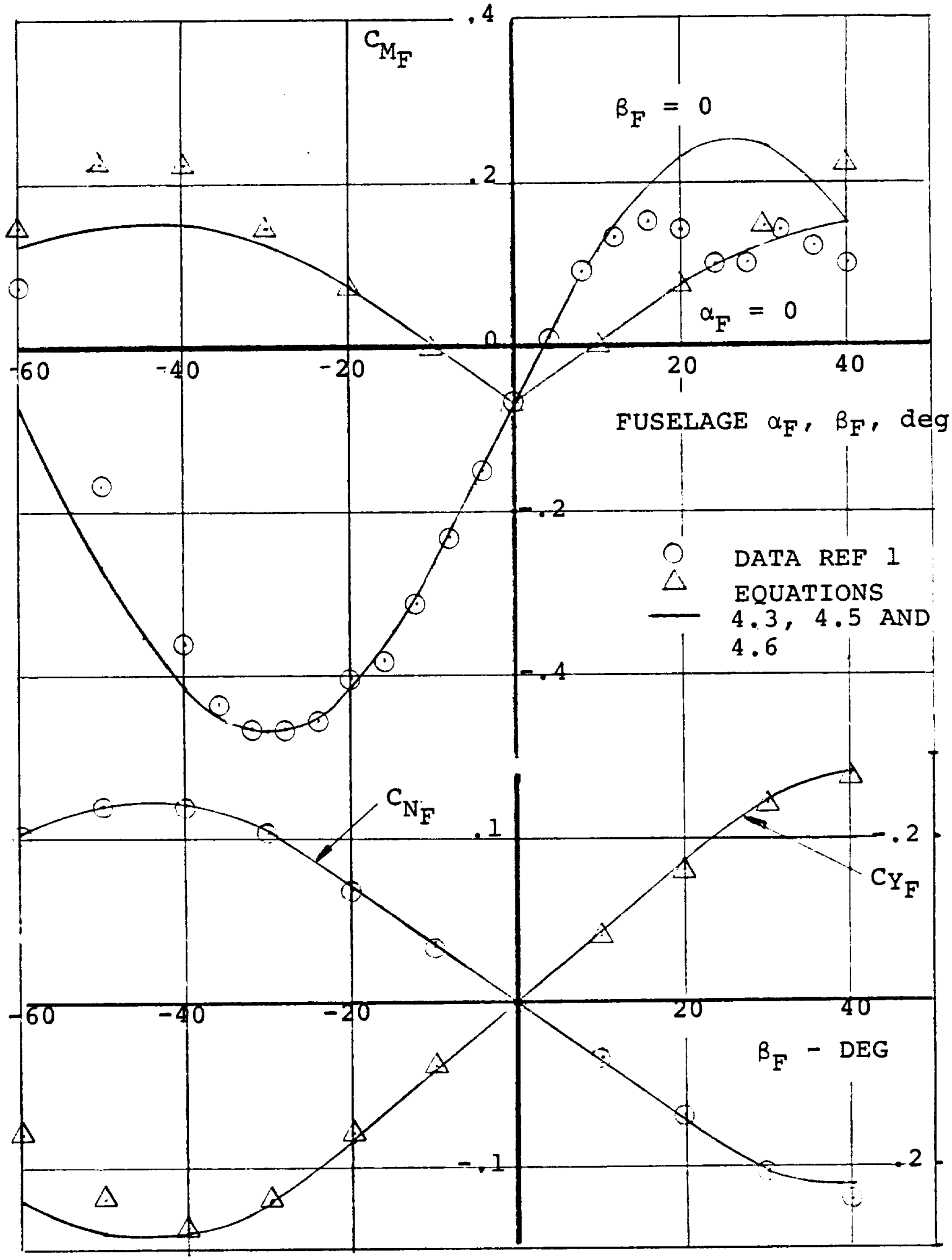

Figure 4.3 Correlation of Fuselage Pitching Moment, Yawing Moment and Side Force Data

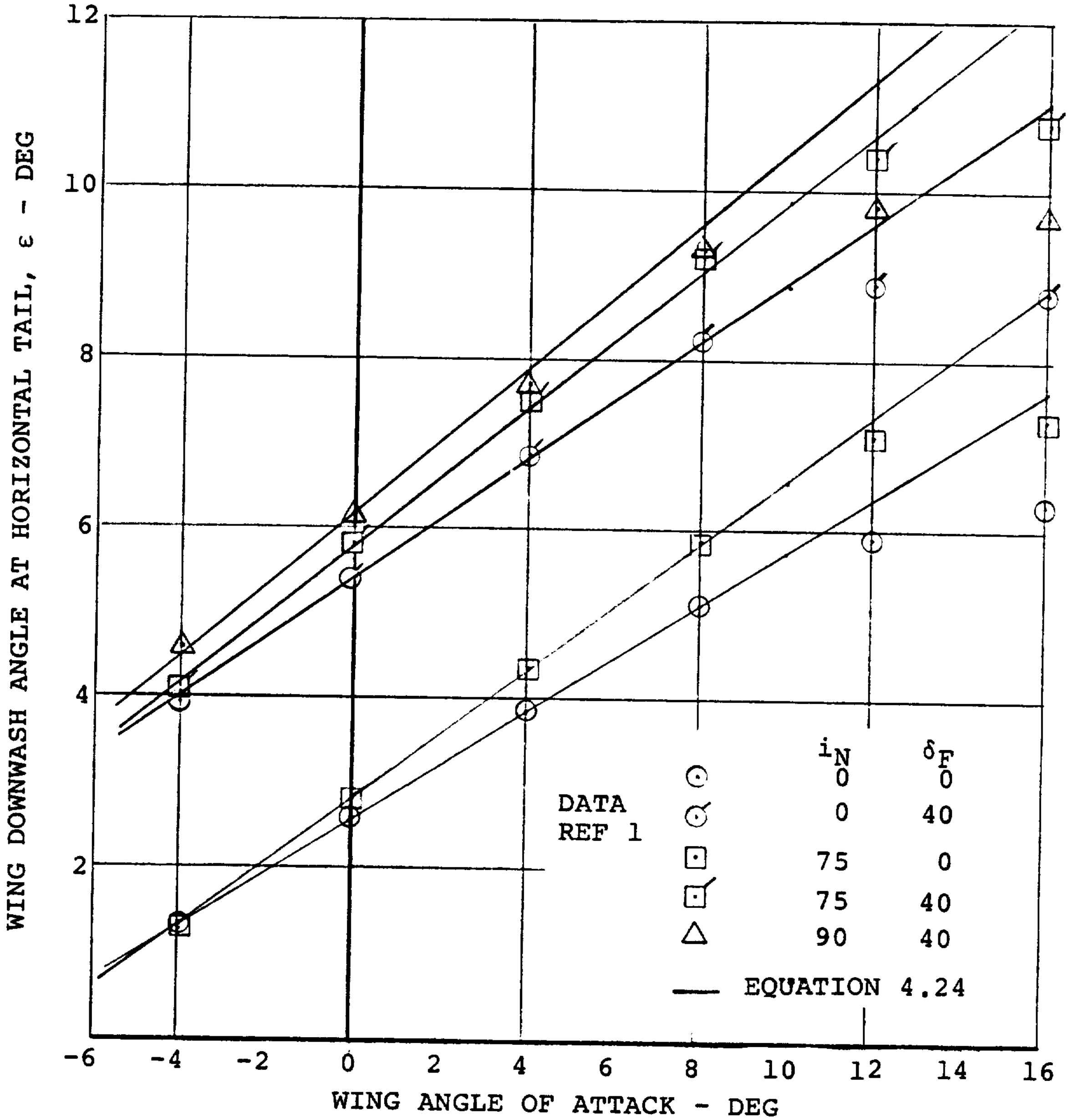

Figure 4.4 Correlation of Wing Downwash

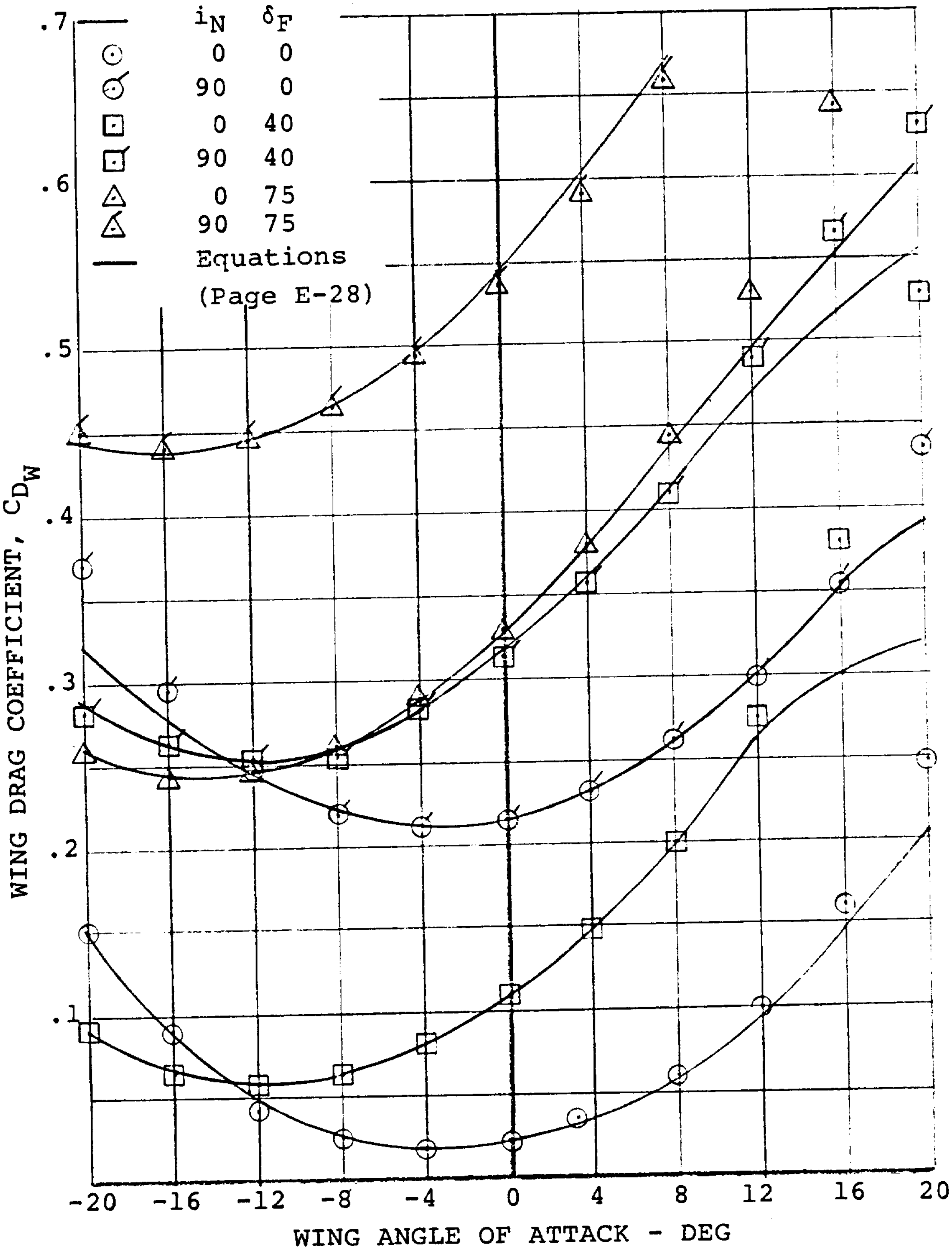

Figure 4.5 Correlation of Wing-Nacelle Drag

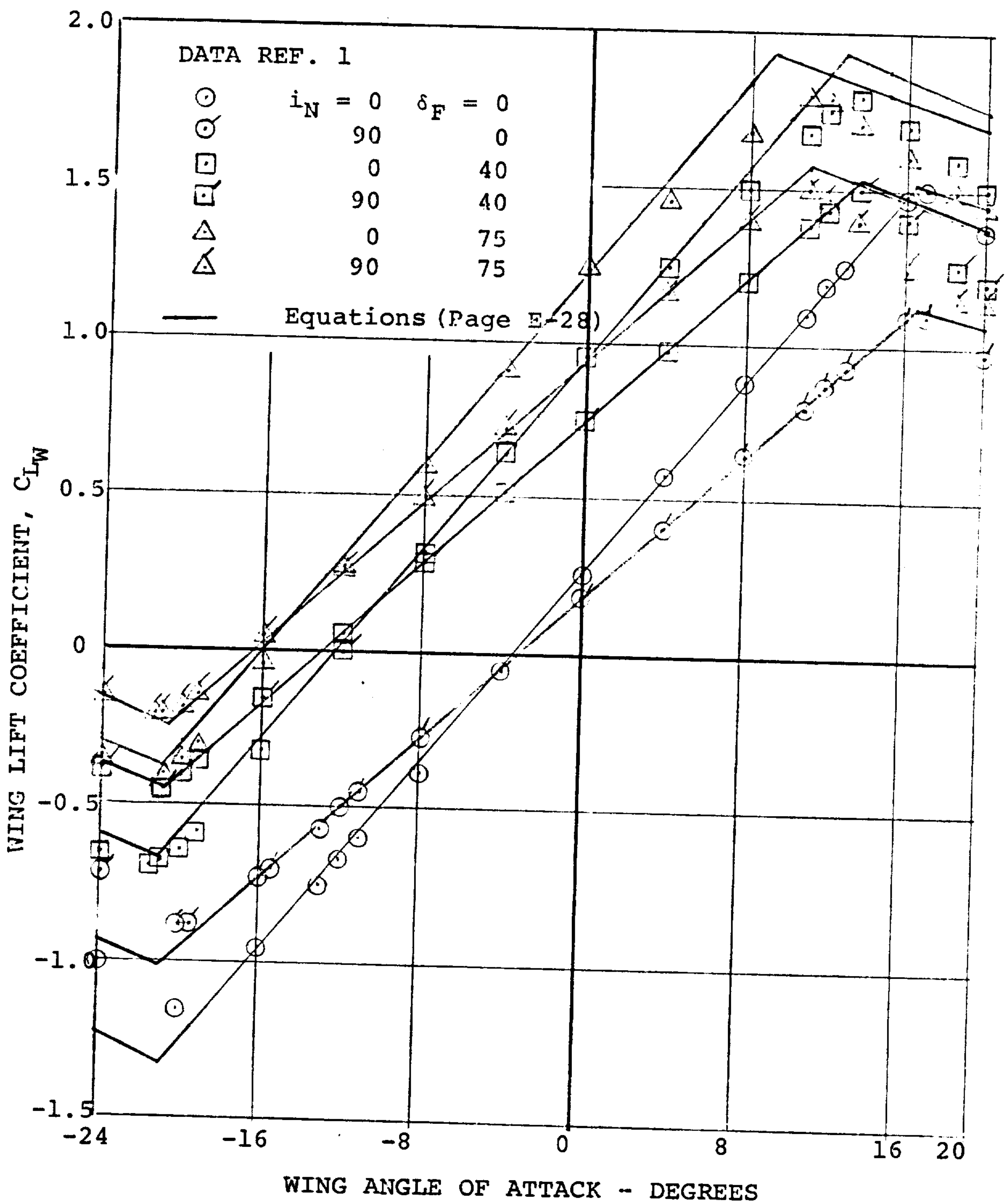

Figure 4.6. Correlation of Wing-Nacelle Lift

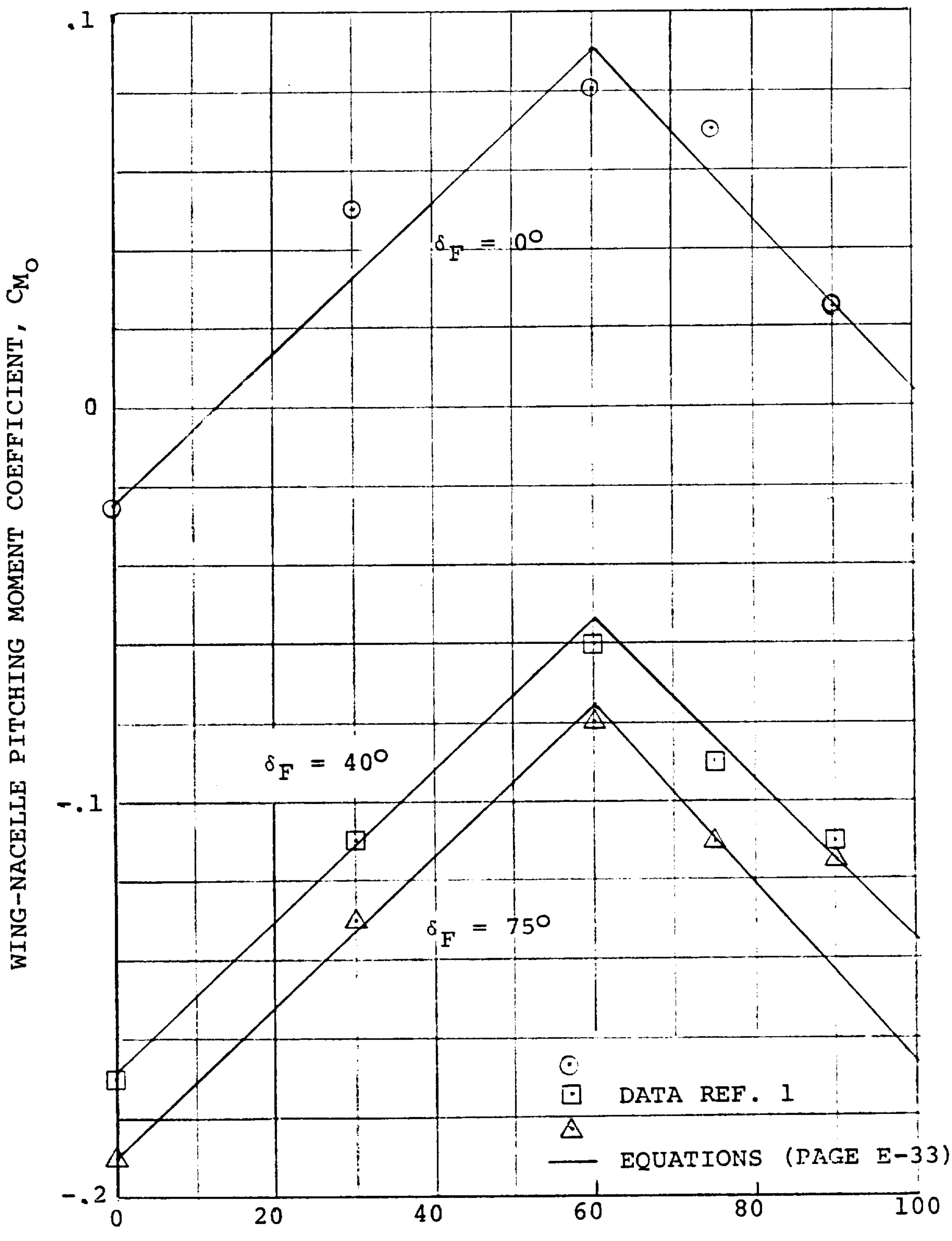

Figure 4.7. Correlation of Wing-Nacelle Pitching Moment

5.0 ROTOR AERODYNAMICS

5.0 ROTOR AERODYNAMICS

The mathematical representation of the forces and moments generated by the 26-foot hingeless rotors is presented. The forces and moments are expressed in equation form as functions of the nondimensional flight parameters e.g. μ, α, C_T. The equations were obtained from a regression analysis of full-scale wind tunnel test data. Where test data was not available, for example at high cruise speeds, supplementary data was obtained by calculation.

The resulting equations permit the rapid computation of thrust, power, normal force, side force and pitching moment in real time. Without the equations, the only alternative would be a large table look-up and interpolation procedure that would adversely affect simulation time-frame. Calculation of the forces and moments by rotor performance programs on-line in real-time is not feasible because of the complexity required to treat flap-lag coupling of soft-in-plane hingeless rotors.

The accuracy of the equations is demonstrated by a series of correlations with test data presented in Figures 5.2 through 5.17. Agreement is acceptable for preliminary simulation.

5.1 Sign Convention

The sign convention for rotor forces and moments is defined in Figure 5.1, which shows the rotors under combined pitch ($\alpha_{T.L.} = i_N + \alpha_F$) and sideslip β. The resultant rotor angle of attack is given by

$$\alpha_R = \cos^{-1} (\cos \alpha_{T.L.} \cos \beta)$$

and the rotor disc "sideslip" angle is

$$\zeta_H = \mathrm{Tan}^{-1}\left[\frac{\mathrm{Tan}\ \beta}{\mathrm{Sin}\ \alpha_{T.L.}}\right]$$

The resulting rotor forces and moments are defined with respect to the plane containing the resultant rotor angle of attack e.g. normal force lies in this plane while rotor side force is perpendicular to it.

5.2 Isolated Rotor Aerodynamics

The equations used to represent the isolated rotor aerodynamics are presented below. The equations are used to compute the rotor wind-axes forces which are then resolved through the rotor sideslip angle into nacelle axes and hence transferred to aircraft body axes for use in the equations of motion.

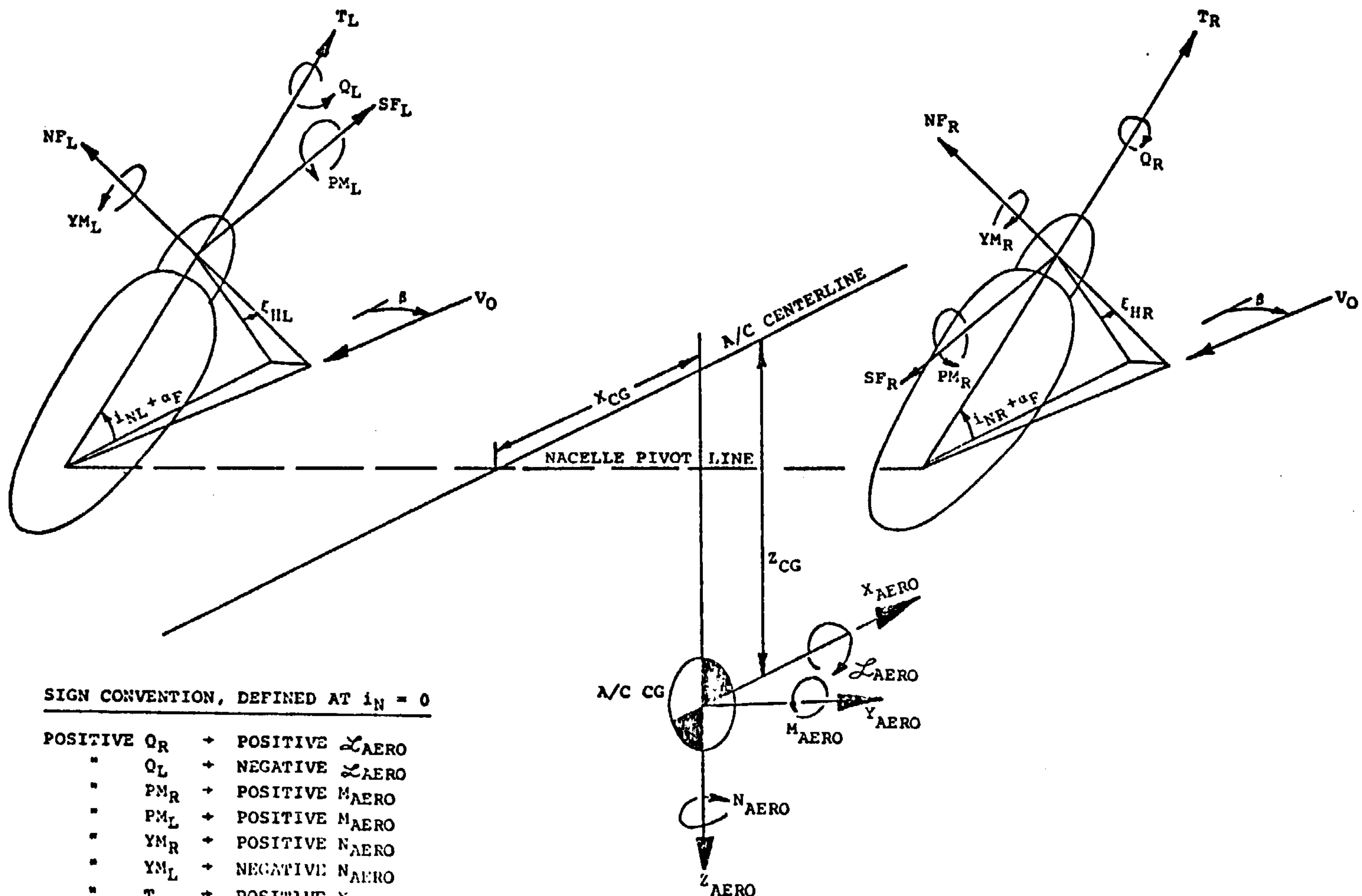

SIGN CONVENTION, DEFINED AT $i_N = 0$

POSITIVE	Q_R	→	POSITIVE $\mathcal{L}_{AERO}$
"	Q_L	→	NEGATIVE $\mathcal{L}_{AERO}$
"	PM_R	→	POSITIVE M_{AERO}
"	PM_L	→	POSITIVE M_{AERO}
"	YM_R	→	POSITIVE N_{AERO}
"	YM_L	→	NEGATIVE N_{AERO}
"	$T_{L'R}$	→	POSITIVE X_{AERO} (CRUISE)
"	NF_L	→	NEGATIVE Z_{AERO}
"	NF_R	→	NEGATIVE Z_{AERO}
"	SF_R	→	NEGATIVE Y_{AERO}
"	SF_L	→	POSITIVE Y_{AERO}

FIGURE 5.1 ROTOR FORCE AND MOMENT SIGN CONVENTIONS

5.2.1 Thrust Vs θ_{75}

The thrust produced by the rotor at any flight condition is obtained from the following equations

$$\phi = \theta_{75} - \tan^{-1}\left[\frac{\mu \cos \alpha}{0.75}\right] - 6.3015\mu + 5.5816\mu^2 - 8\,\mu \sin \alpha + 1.8 \quad (1)$$

and C_T is given by

$$C_T = 0.000679\,\phi + 0.000015\,\phi^2 + 0.0022\,\mu\phi + 0.000211\,\mu^2\phi \quad (2)$$

5.2.2 Thrust Vs Power

Once thrust has been established the power coefficient is given by

$$C_P = .00015 + .795\,C_T^{3/2} + \mu(.00005+.000843\mu + .910\,C_T) + \mu\,[\,0.00674-.0146\mu - (3.4-8\mu)C_T]\,\frac{|\alpha^\circ|}{180} + [(.08756-2.18\mu)\,C_T - .00043488]\,\mu \sin \alpha \quad (3)$$

5.2.3 Normal Force

Normal force is obtained as the sum of three terms

$$C_{NF} = F(\mu,\alpha,C_T) + \frac{\partial C_{NF}}{\partial A_1}\,A_1 + \frac{\partial C_{NF}}{\partial B_1}\,B_1 \quad (4)$$

where the cyclic pitch derivatives are functions of α, μ, and C_T.

In performing the analysis the cyclic derivatives were first defined as:

$$\frac{\partial C_{NF}}{\partial A_1} = 0.00002175 + 0.0014483\mu^2 - 0.0000734\mu - 0.0006\mu \sin 2\alpha + 0.00425\,C_T \quad (5)$$

and

$$\frac{\partial C_{NF}}{\partial B_1} = 0.0000425 - 0.0010492\mu - 0.0017028\mu^2 + 0.0017892\mu \sin \alpha - 0.0245\,C_T \quad (6)$$

The following expressions may be used to calculate normal force with zero cyclic pitch.

For $0 \leq \mu \leq 0.6$

$$C_{NF} = C_{NF_1} = 0.089\mu^3 \sin 2\alpha + [0.172753\mu C_T + 73.444\,\mu\, C_T^{\,2}\ (1-\mu)]K \quad 0 \leq \mu \leq 0.6 \tag{7}$$

where $K = \sin\alpha$ for $\alpha > 20°$

and $K = \sin\alpha(10-0.45\alpha°)$ for $0 \leq \alpha \leq 20$

For $0.6 < \mu$

$$C_{NF} = (C_{NF_1})(1-0.8(\mu-0.6)) \tag{8}$$

5.2.4 Side Force

Side force is defined in a similar manner to normal force

$$C_{SF} = F(\mu,\ C_T,\ \alpha) + \frac{\partial C_{SF}}{\partial A_1} A_1 + \frac{\partial C_{SF}}{\partial B_1} B_1 \tag{9}$$

where the cyclic derivatives are given by:

$$\frac{\partial C_{SF}}{\partial A_1} = -0.0000425 + 0.0010492\mu + 0.0017028\mu^2 + 0.0245\ C_T - 0.001735\ \mu \sin\alpha \tag{10}$$

and

$$\frac{\partial C_{SF}}{\partial B_1} = 0.00002175 + 0.0014483\mu^2 - 0.0000734\mu + 0.00425\ C_T - 0.00067758\ \mu \sin 2\alpha \tag{11}$$

The side force at zero cyclic is given by the following equations:

$$C_{SF} = 0.00566\ \mu \sin\alpha - 0.0037249\ \mu\ (\alpha_{RAD})^2 + 0.016\ \mu \sin\alpha\ C_T(90-\psi°) + 2.830\ \mu^3 \sin\alpha\ C_T \tag{12}$$

where $$\psi° = \tan\left[\frac{\mu-\mu_i \cos\alpha}{\mu_i \sin\alpha}\right] \tag{13}$$

and $$\mu_i = \left\{\left[(\mu^4 + C_T^{\,2})^{1/2} - \mu^2\right] /2\right\}^{1/2} \tag{14}$$

If $\alpha > \pi/2;\ \alpha = \pi-\alpha$

5.2.5 Hub Pitching Moment

Pitching moment is computed in the same manner as normal force and side force.

$$C_{PM} = F(\alpha,\ \mu,\ RPM,\ C_T) + \frac{\partial C_{PM}}{\partial A_1} A_1 + \frac{\partial C_{PM}}{\partial B_1} B_1 + \frac{\partial C_{PM}}{\partial Q} Q \qquad (15)$$

where the cyclic pitch derivatives are functions of α, μ, RPM and C_T.

$$\begin{aligned}\frac{\partial C_{PM}}{\partial A_1} &= 0.0002094 + 0.00111967\mu \\ &- 0.00072556\mu^2 - 0.00000764\mu\ (RPM-386) \\ &+ 0.00036524 \sin 2\alpha + 0.0020\ C_T\end{aligned} \qquad (16)$$

and

$$\begin{aligned}\frac{\partial C_{PM}}{\partial B_1} &= -0.000111245 + 0.0000729\mu \\ &+0.0004375\mu^2 - 0.0025\ C_T \\ &-0.00000713\mu\ (RPM-386) \\ &+0.00063045\mu \sin\alpha\end{aligned} \qquad (17)$$

$$\begin{aligned}F = C_{PM_O} &= 0.012857\ \mu \sin\alpha - 0.014163\mu^2 \sin\alpha \\ &+ 0.0036344\ \mu \sin 2\alpha - 0.0074613\mu \sin\alpha \frac{RPM}{386} \\ &+ \frac{\partial C_{PM}}{\partial C_T}\end{aligned} \qquad (18)$$

$$\begin{aligned}\frac{\partial C_{PM}}{\partial C_T} &= \mu(-.393141\text{x}10^{-2} + .201377\text{x}10^{-2}\alpha \\ &\quad -.220903 \text{ x } 10^{-4}\alpha^2) \\ &\quad + \mu^2(.120036 + .634542\text{x}10^{-2}\alpha + .799823\text{ x}10^{-3}\alpha^2) \\ &\quad + \mu^3(-.141322 - .170706 \text{ x } 10^{-1}\alpha - .61104\text{x}10^{-3}\alpha^2)\end{aligned} \qquad (19)$$

5.2.6 Hub Yawing Moment

The yawing moment derivatives due to cyclic pitch are similar to the pitching moment derivatives and are given by

$$\frac{\partial C_{YM}}{\partial A_1} = -0.000111245 + 0.0000792\ \mu \tag{20}$$

$$0.0004375\ \mu^2 - 0.0025\ C_T$$

$$-0.00000713\ \mu\ (RPM-386)$$

$$+0.0005\ \mu \sin\alpha$$

and

$$\frac{\partial C_{YM}}{\partial B_1} = -0.0002094\ -0.00111967\ \mu$$

$$+0.00072556\ \mu^2 + 0.00000764\ \mu\ (RPM-386) \tag{21}$$

$$-0.002\ C_T - 0.0004702\ \mu \sin 2\alpha$$

The yaw moment at zero cyclic pitch is given by the following equations

for $0 \leq \mu \leq 0.37$

$$C_{YM} = (0.023736\ \mu - 0.0010)\mu \sin\alpha - 1.6\ \mu^2\ C_T \sin\alpha \tag{22}$$

$$+\left[0.00816 - 0.003366\ \mu - 0.006303\left[\frac{RPM}{386} - 1\right]\right]\left(\frac{RPM}{386} - 1\right)\mu \sin\alpha$$

and for $\mu > 0.37$

$$C_{YM} = (0.02476 - 0.19798\ (\mu - 0.7024)^2) \sin\alpha \tag{23}$$

$$-1.6\ \mu^2\ C_T \sin\alpha + \mu\left[.00816 - .003366\mu - .006303\left[\frac{RPM}{386} - 1\right]\left(\frac{RPM}{386} - 1\right)\right]$$

5.2.7 Pitching Moment due to Pitch Rate

$$-1000\ \frac{dC_{PM}}{dQ} = 1.5 + \mu \qquad 0 \leq \mu \leq .2$$

$$= 0.25 + 7.26\ \mu \qquad .2 < \mu \leq .39$$

$$= 4.1681 - 2.79\ \mu \qquad \mu > .39$$

5.2.8 Yawing Moment due to Yaw Rate

$$\frac{dC_{YM}}{dR} = -\ \frac{dC_{PM}}{dQ}$$

5.3 Rotor/Rotor Interference

A procedure for calculating rotor-on-rotor interference effects is included in the mathematical model. Rotor-on-rotor interference arises during sideward flight at low airspeeds with the rotors up and, to a lesser extent, during slipped flight in the transition configurations. The basis for the method is as follows.

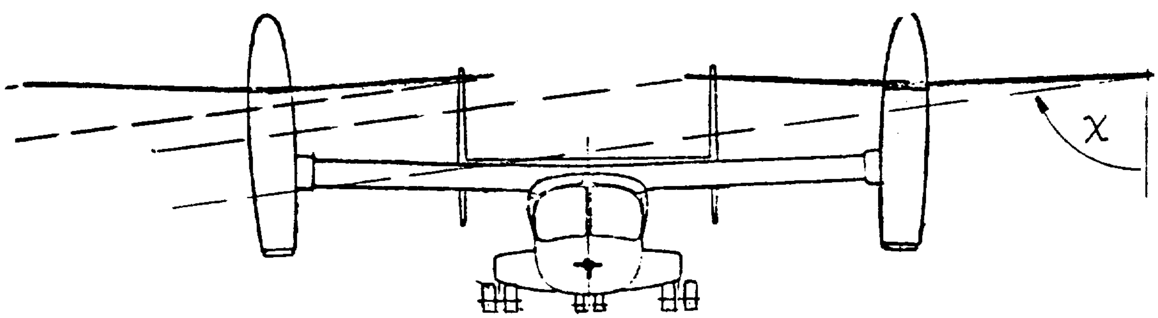

The above sketch depicts the tilt rotor aircraft flying sidewards at low speed. The wake of the upwind rotor interferes with the inflow to the downwind rotor producing a change in this rotor's forces and moments.

Reference 5 presents calculated values of the normal component of the induced velocity near a rotor having a triangular disc loading, for different wake skew angles, χ. This data was used to compute an interference velocity at the downwind rotor. The resulting rotor angle of attack was used in the calculation of the forces and moments. The rotor/rotor interference effect is washed out with nacelle angle and sideslip angle so that there is no interference at the high end of transition and in cruise. The equations used to calculate interference are presented in Appendix E under the rotor/rotor interference section.

5.4 Accuracy of the Rotor Equations

Figures 5.2 through 5.17 present correlations of the predictions of the rotor equations with test data obtained from full-scale tests conducted in the Ames 40'x80' wind tunnel and reported in Reference 4. While the correlation appears reasonable, the data on which it is based is limited in scope.

In order to broaden the data base, tests were recently conducted on a 1/4.622 Froude scale Boeing tilt rotor model under NASA Contract NAS2-9015. This test generated sufficient experimental data to define the hingeless rotor characteristics over the entire range of flight speeds expected of the XV-15 aircraft. Unfortunately the results were not available in time to update the rotor math model equations. This step is, however, being proposed in the near future.

Nevertheless, some of the elements of the test data have been correlated with the 40'x80' full-scale data and with the math model equations in order to check the fidelity of the existing equations and to assess scale effects between the sets of tests.

Figures 5.18 through 5.20 present rotor normal force due to A_1 cyclic pitch. The derivative is overpredicted by the math model in hover, but improves at 45, 100 and 140 knots over the operational range of angle of attack. Figures 5.21 through 5.23 show the normal force response to B_1 cyclic. The effect is underpredicted at hover, 45 knots, and 100 knots at high nacelle angles. At 140 knots a greement is satisfactory. In the cruise mode at zero angle of attack the math model equations fit the data reasonably well.

The effect of B_1 cyclic on pitching moment is presented in Figures 5.24 through 5.26. The math model equations generally underpredict the effect at all speeds, the error increasing with rotor angle of attack.

The above discussion is intended to show that the rotor representation employed in the current simulation is reasonably adequate for a preliminary assessment of the flying qualities and performance of the hingeless rotor XV-15. It also serves to emphasize the need for a thorough revision of the analytical representation based on the more extensive data now available.

Additional wind tunnel testing is also required to define the performance of the rotor at low power levels and in steep helicopter descents, and in autorotation. At present the rotor performance in these modes is obtained from the rotor equations which are based on test data that do not include these regions.

5.5 Wing-on-Rotor Upwash

The presence of a lifting wing generates an upwash field at the rotor disc plane which changes the rotor forces. This effect is evident from Figure 5.27 which shows the derivative of normal force with angle of attack and the derivative of side force with yaw angle. For an isolated rotor these derivatives would be identical. The equations used in the simulation math model contain this effect implicitly. However, more analysis is required to account for wing upwash in an explicit manner that will permit treatment of the effects of changes in flap setting on the wing lift and hence the upwash field at the rotors.

5.6 Blade Loads and Aircraft Flight Boundaries

The success of the tilt rotor aircraft concept depends to a large extent on the ability of the designer to provide a simple, reliable control system that will ensure adequate control effectiveness while maintaining low alternating loads on fatigue-critical elements. In the controls design phase it is essential therefore that a means exists for estimating alternating loads on these elements. The most important fatigue-sensitive elements are the rotors whose loads tolerance defines the safety, maneuverability, and flight boundaries of the aircraft.

In order to design the control system for the hingeless rotor XV-15, an equation was developed to calculate blade loads. This equation and the impact of blade loads on the aircraft control system design is discussed in Appendix G.

5.7 Ground Effect

The effects of operating near the ground on the rotors are included in this model. Ground effects on the rotor are difficult to predict analytically, especially in forward flight. Wind tunnel test data for the Boeing Model 160 powered model, Reference 6, was plotted as a thrust ratio versus effective rotor height/diameter ratio, for two rotor advance ratios. This data, shown in Figure 5.28 was curve fitted and linearly interpolated for advance ratio.

The equation for the effective rotor height to diameter ratio $(h/D)_{EFF}$ was derived by dividing the rotor hub height by $[\sin(\theta+i_N)\cos\phi]$. This yields the rotor height along the shaft. For the cruise condition the hub height is infinite, $(h/D)_{EFF}$ is infinite and the augmentation ratio due to ground effect is unity.

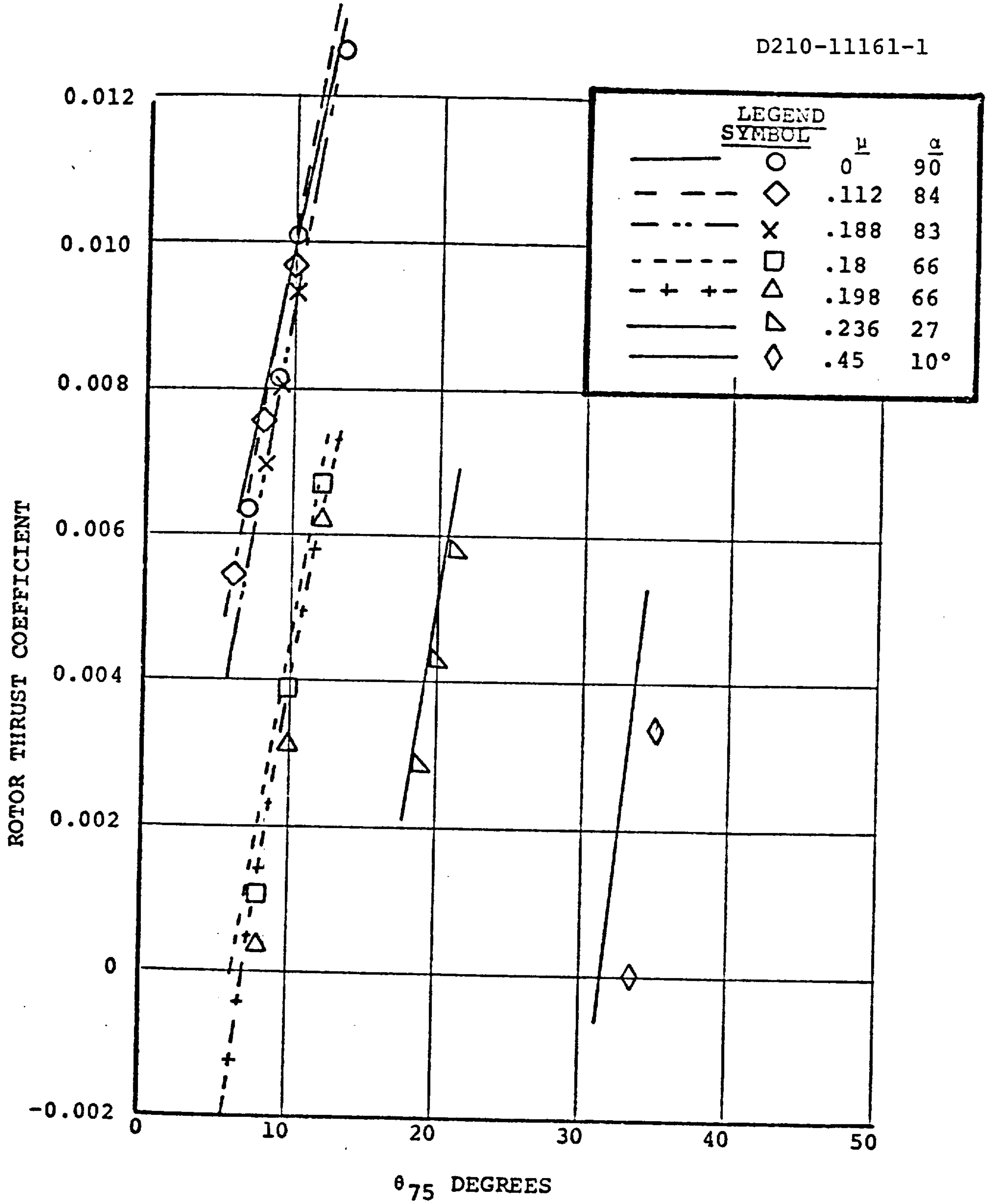

FIGURE 5.2 COMPARISON OF MATH MODEL VALUES OF THRUST COEFFICIENT WITH FULL SCALE TEST DATA

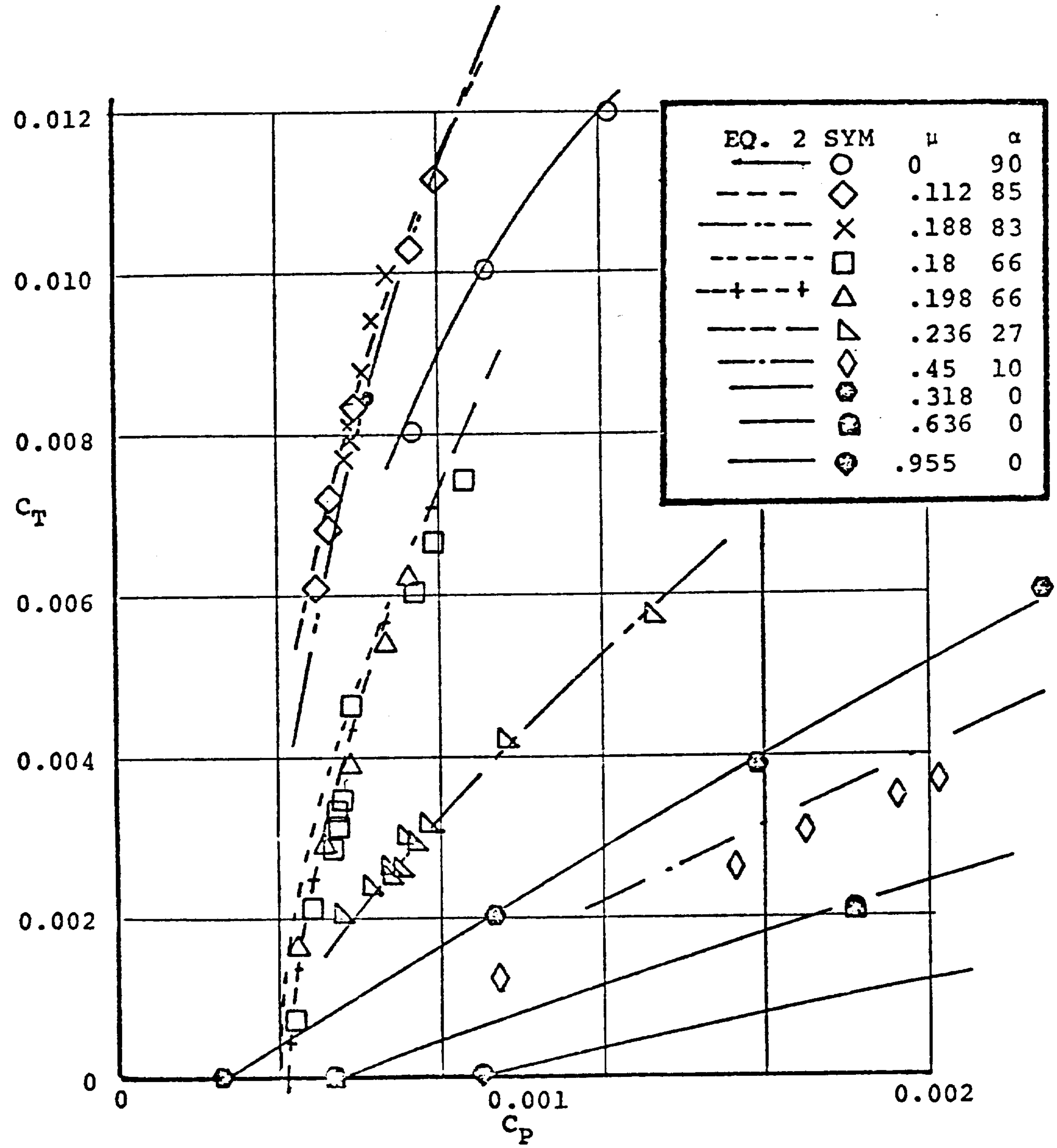

FIGURE 5.3 COMPARISON OF MATH MODEL COEFFICIENTS OF THRUST VERSUS POWER WITH FULL SCALE TEST DATA

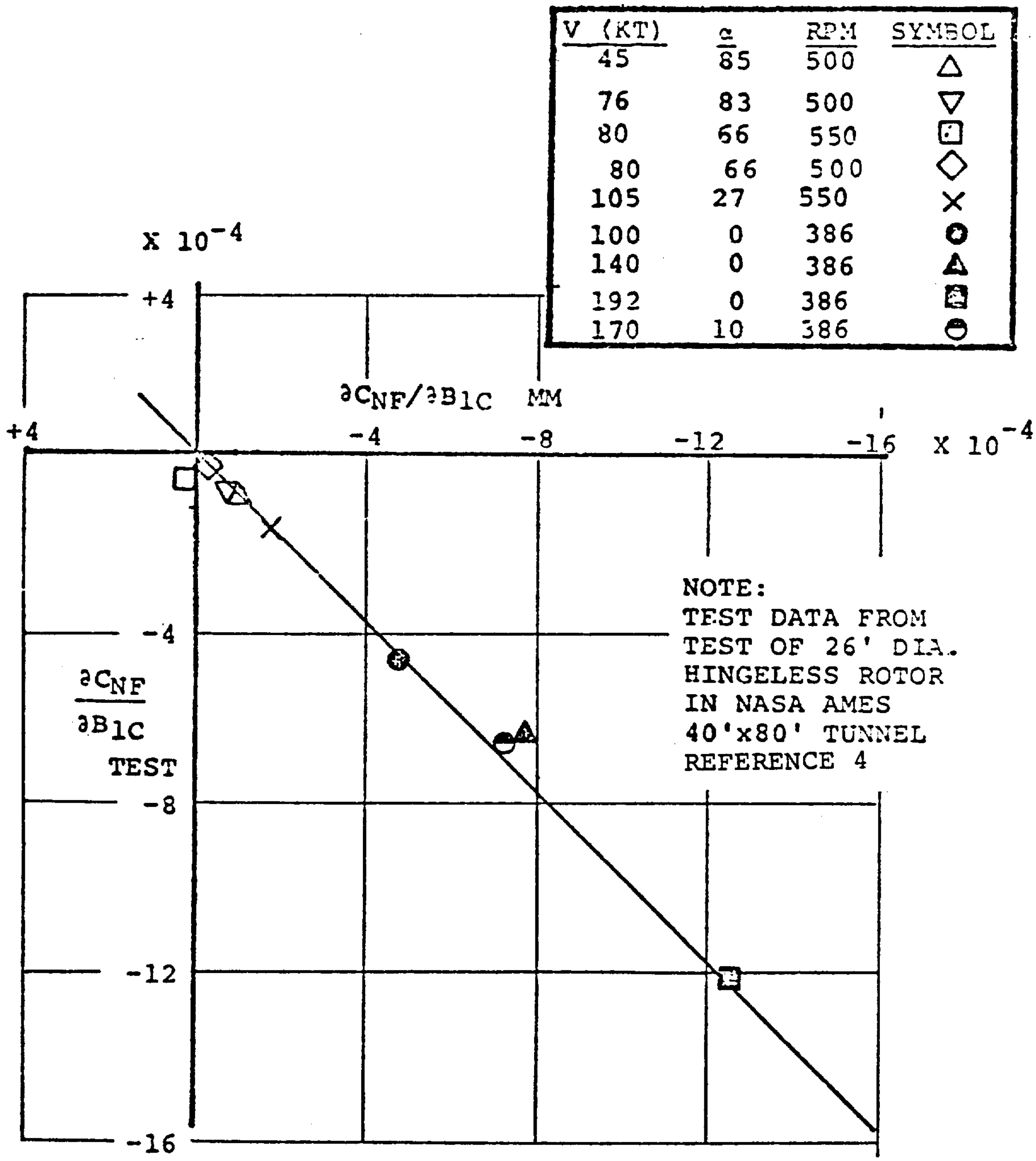

FIGURE 5.4 CORRELATION OF MATH MODEL REPRESENTATION OF $\partial C_{NF}/\partial B_{1C}$ WITH FULL SCALE TEST DATA

V (KT)	α	RPM	SYMBOL
45	85	500	△
76	83	500	▽
80	66	550	⊡
80	66	500	◇
105	27	550	×
100	0	386	●
140	0	386	▲
192	0	386	■
170	10	386	◒

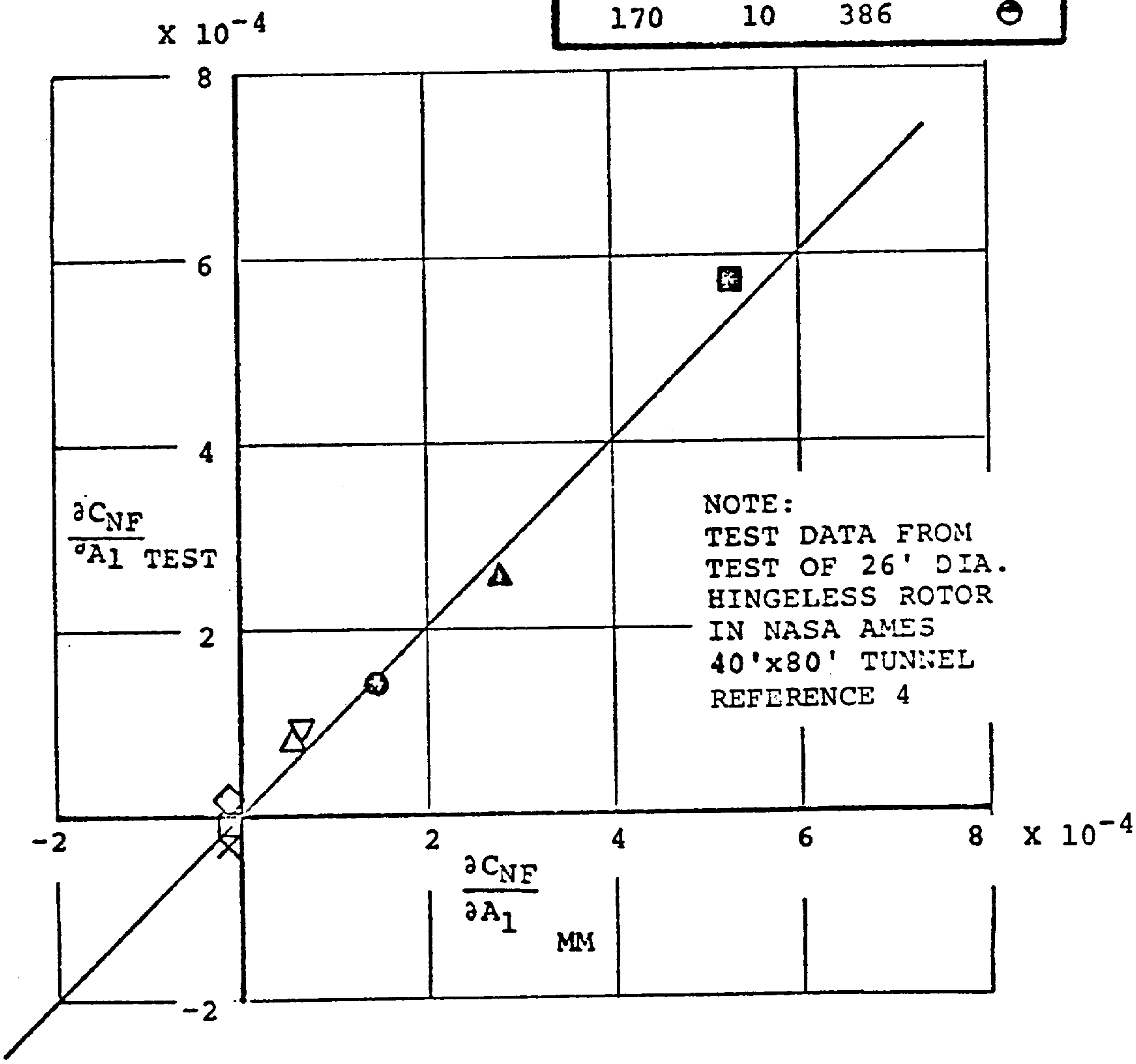

FIGURE 5.5 CORRELATION OF MATH MODEL $\partial C_{NF}/\partial A_1$ REPRESENTATION WITH FULL SCALE TEST DATA

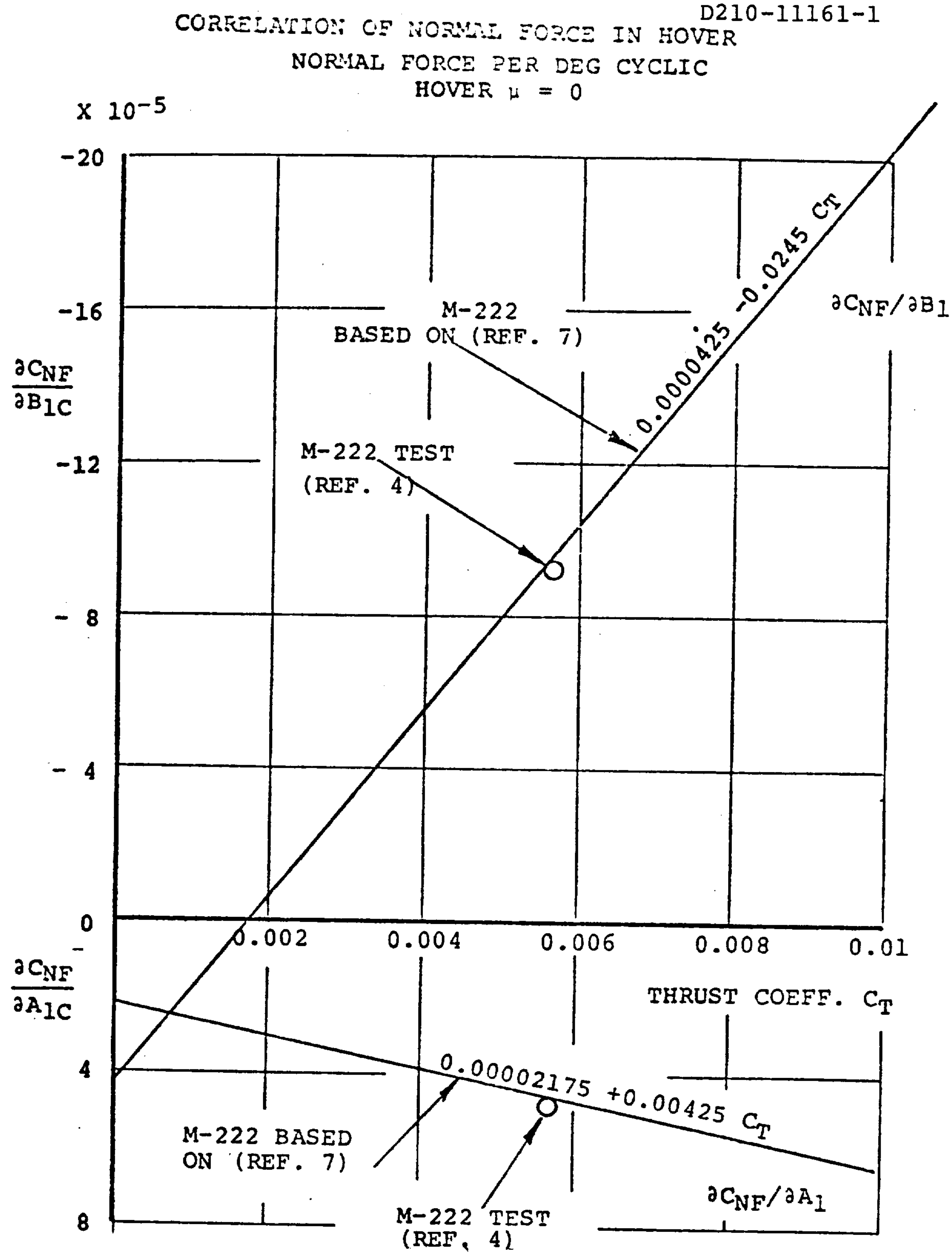

FIGURE 5.6 COMPARISON OF MATH MODEL VALUES OF $\partial C_{NF}/\partial A_{1C}$ IN HOVER WITH FULL SCALE TEST DATA

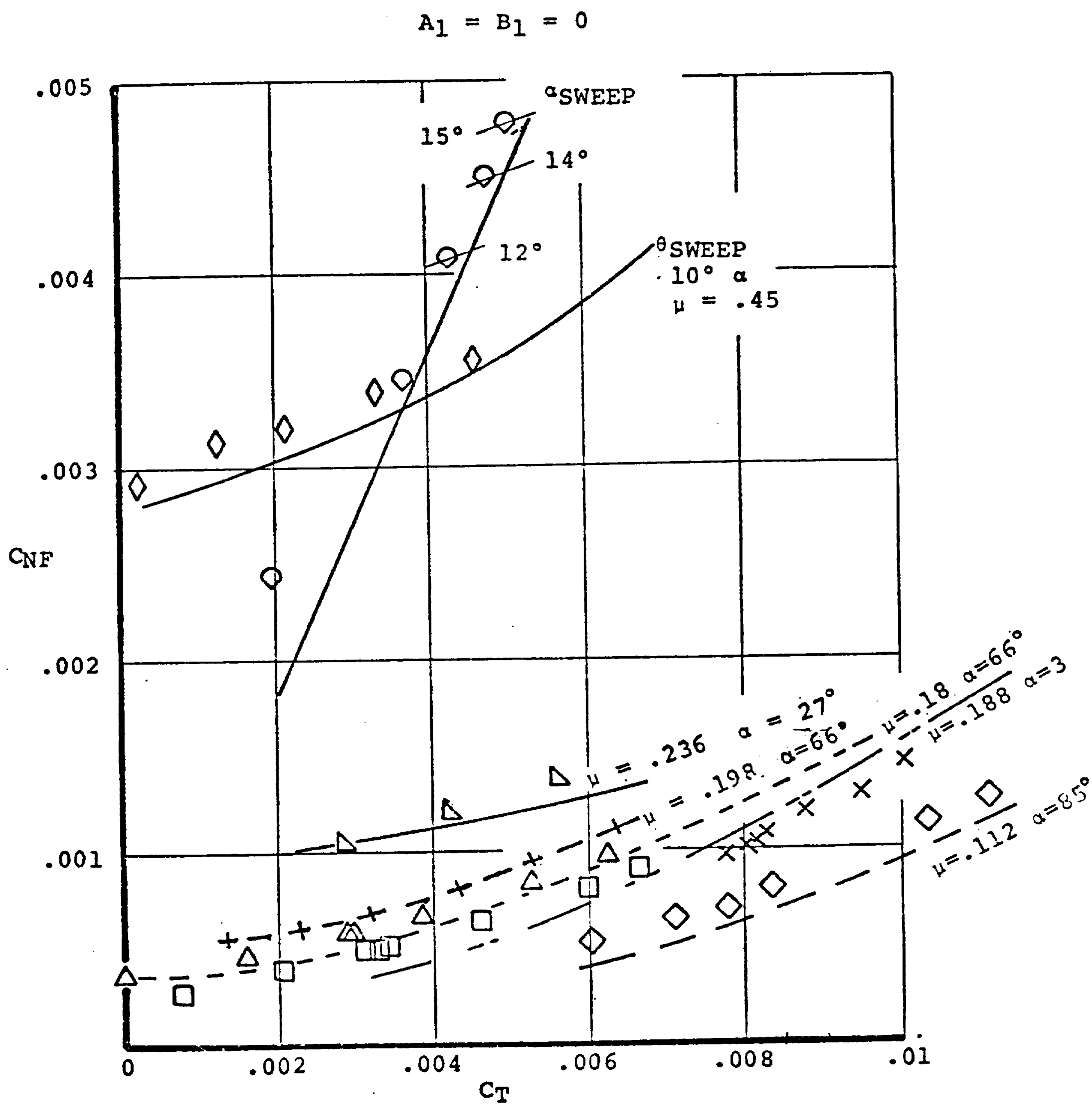

FIGURE 5.7 COMPARISON OF MATH MODEL SENSITIVITIES OF NORMAL FORCE COEFFICIENT WITH RESPECT TO THRUST COEFFICIENT AND FULL SCALE TEST DATA

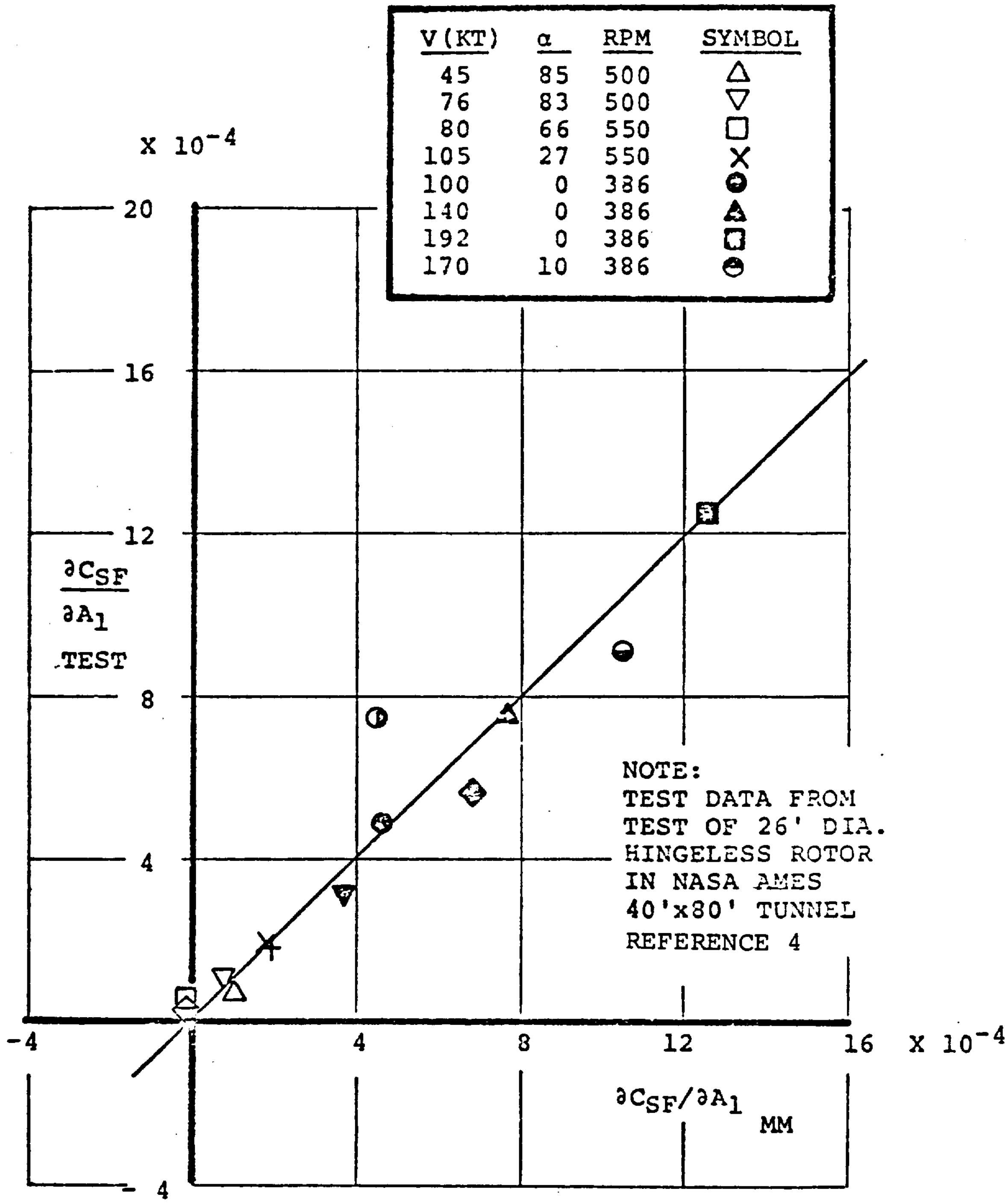

FIGURE 5.8 CORRELATION OF MATH MODEL REPRESENTATION OF $\partial C_{SF}/\partial A_1$ WITH FULL SCALE TEST DATA

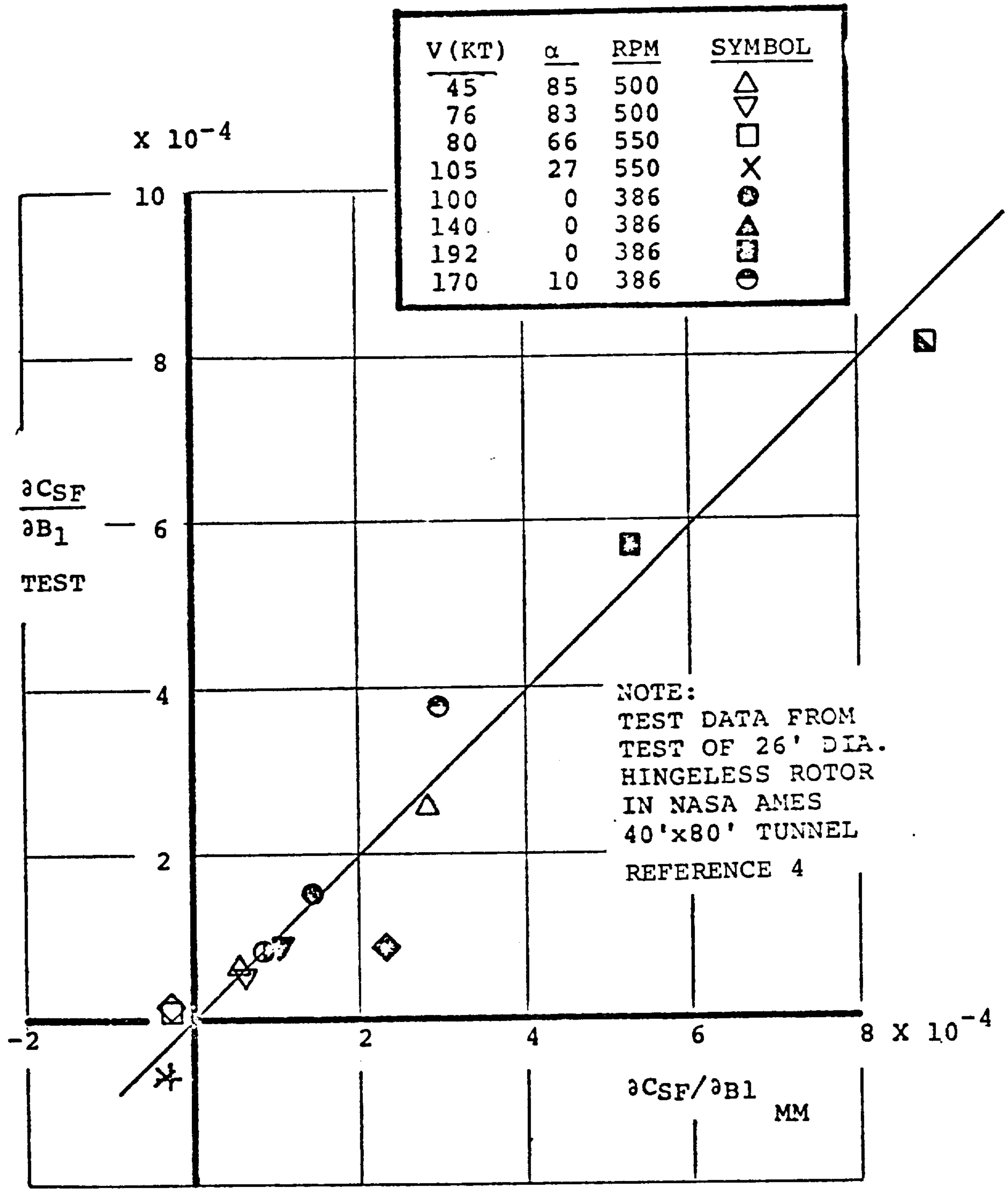

FIGURE 5.9 CORRELATION OF MATH MODEL REPRESENTATION OF $\partial C_{SF}/\partial B_1$ WITH FULL SCALE TEST DATA

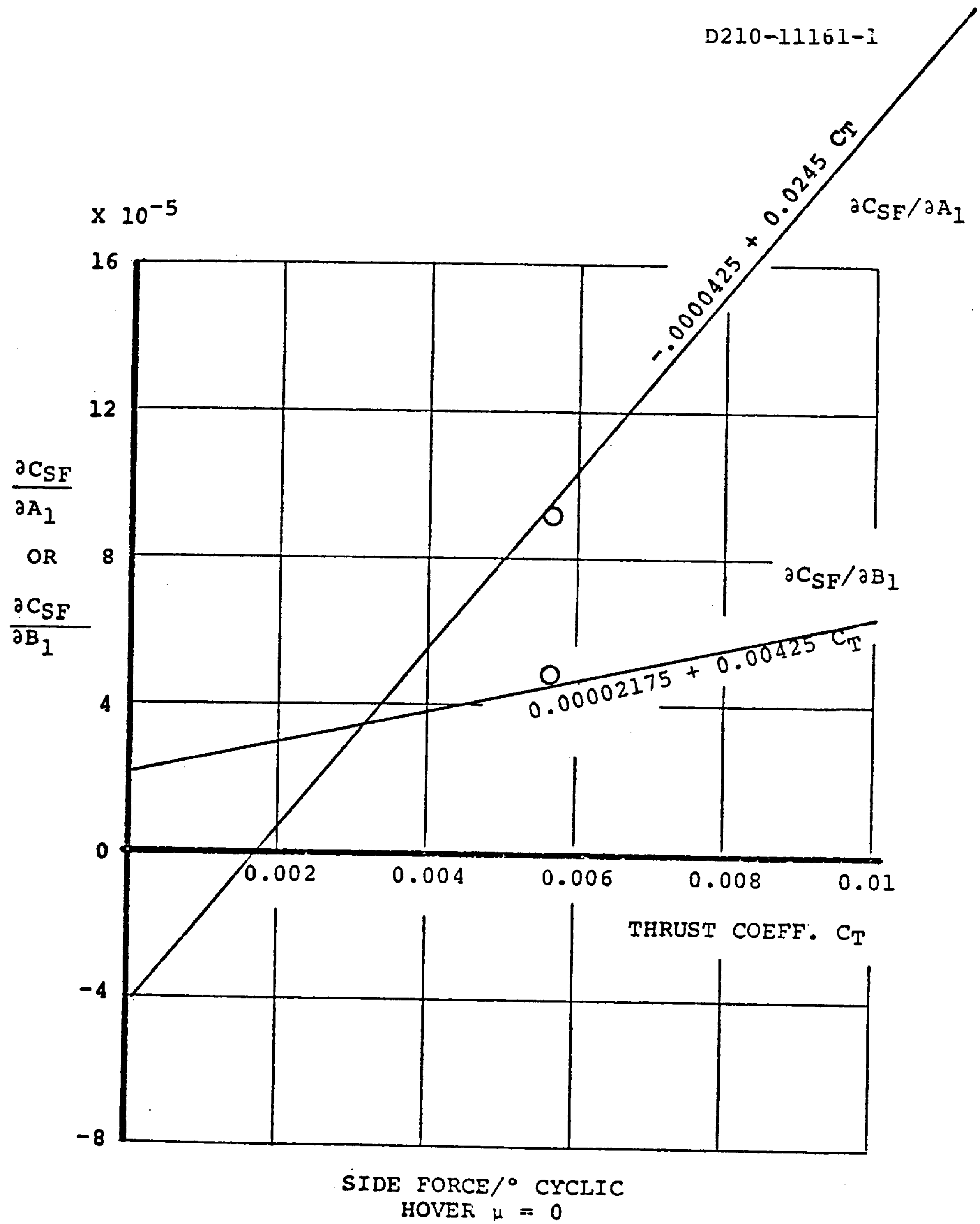

FIGURE 5.10 COMPARISON OF MATH MODEL $\partial C_{SF}/\partial A_1$ AND $\partial C_{SF}/\partial B_1$ TRENDS WITH FULL SCALE TEST DATA

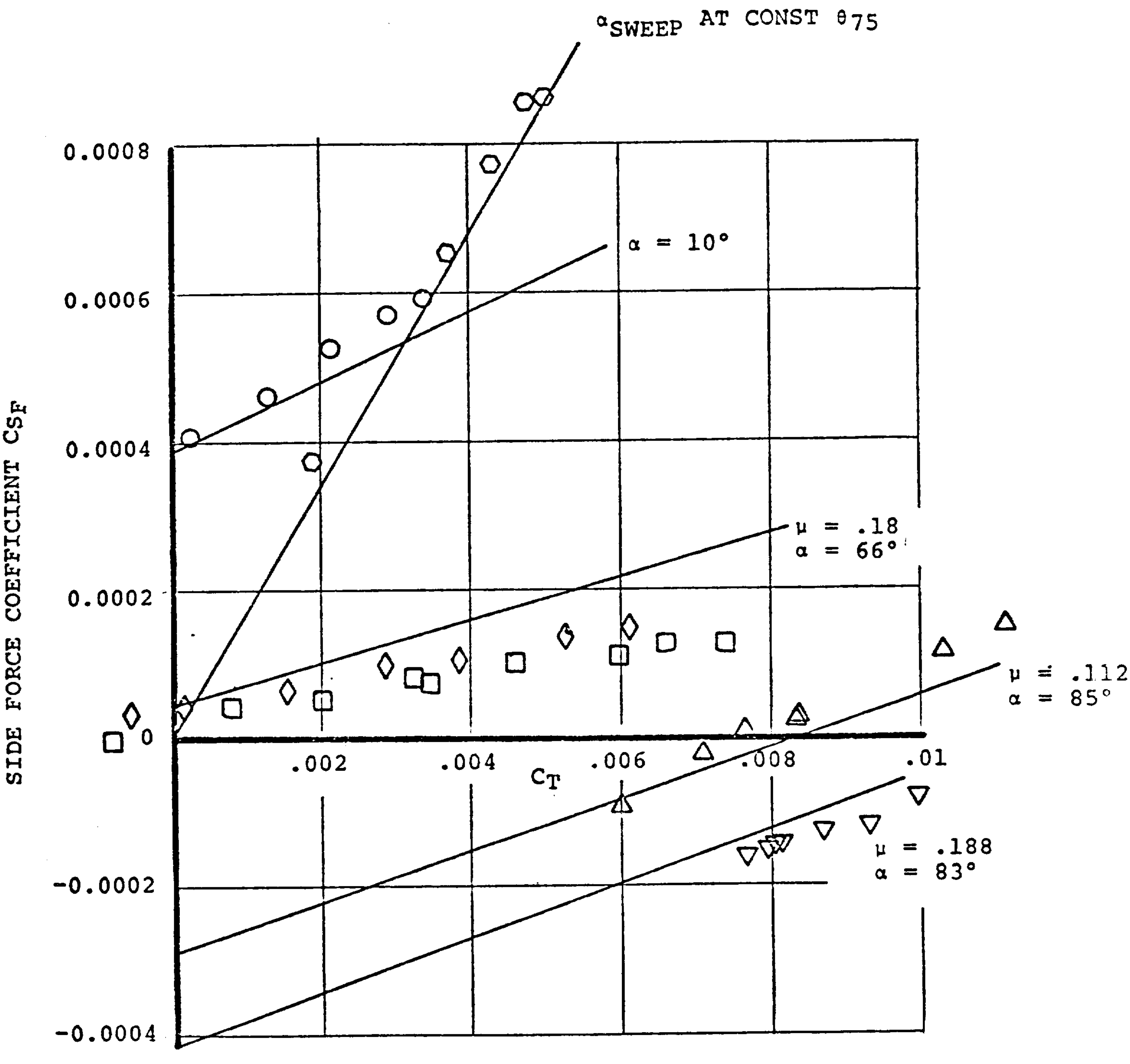

FIGURE 5.11 CORRELATION OF MATH MODEL SIDE FORCE DERIVATIVE C_{S_F} WITH FULL SCALE TEST DATA AT ZERO CYCLIC

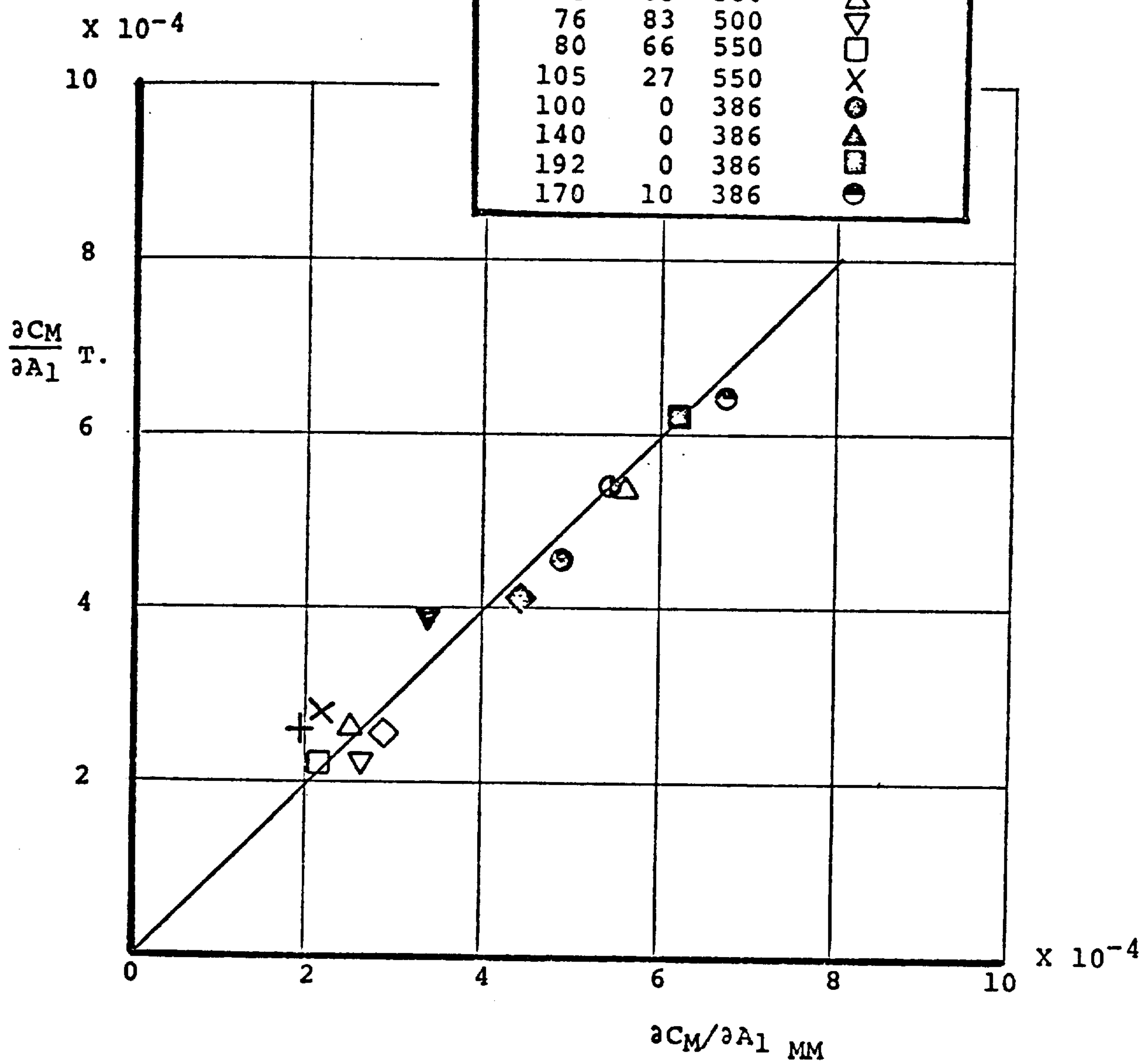

V (KT)	α	RPM	SYMBOL
45	85	500	△
76	83	500	▽
80	66	550	□
105	27	550	X
100	0	386	(shaded circle)
140	0	386	(shaded triangle)
192	0	386	(shaded square)
170	10	386	◓

FIGURE 5.12 CORRELATION OF MATH MODEL REPRESENTATION OF $\partial C_M/\partial A_1$ WITH FULL SCALE TEST DATA

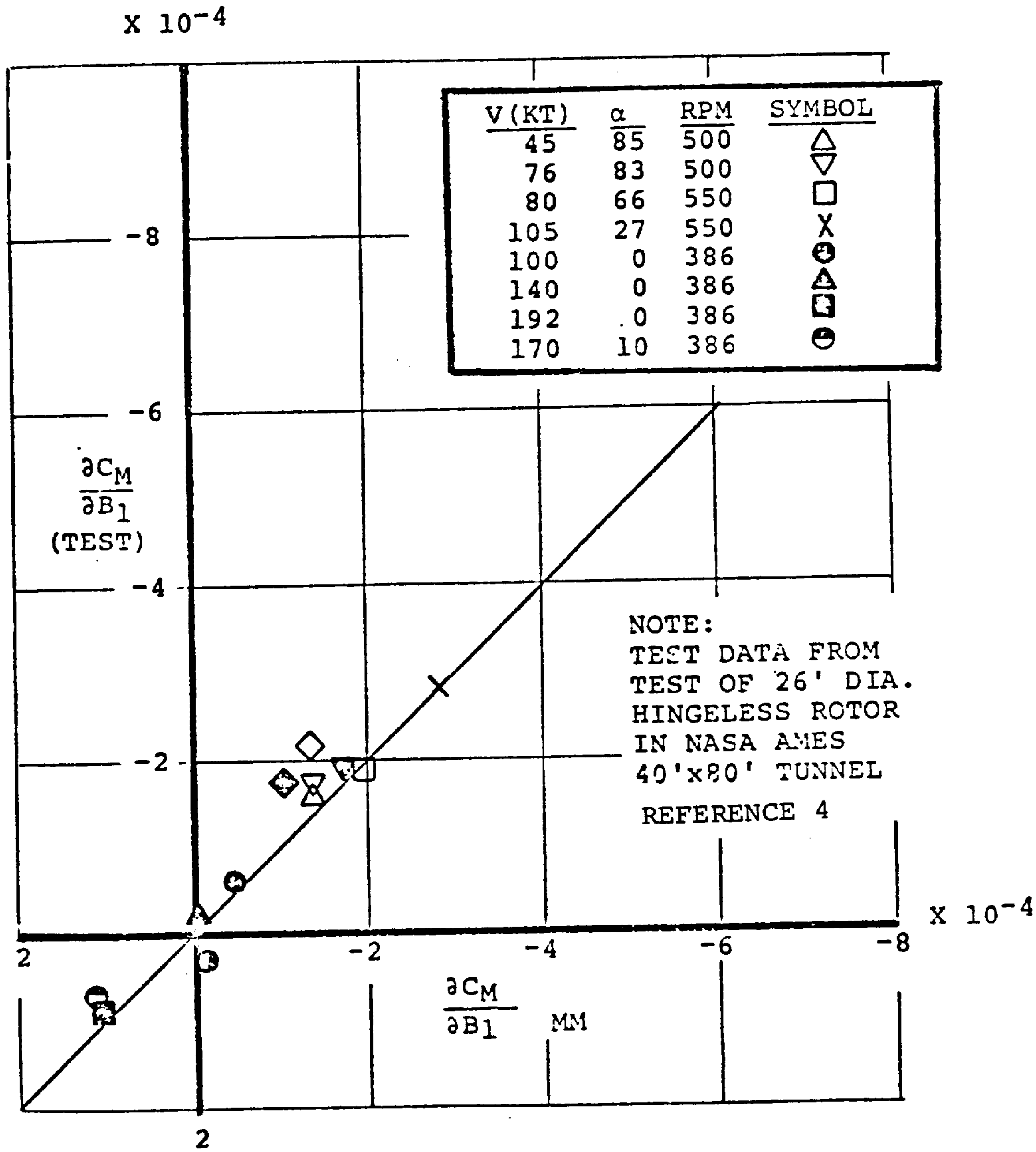

FIGURE 5.13 CORRELATION OF MATH MODEL REPRESENTATION OF $\partial C_M/\partial B_1$ WITH FULL SCALE TEST DATA

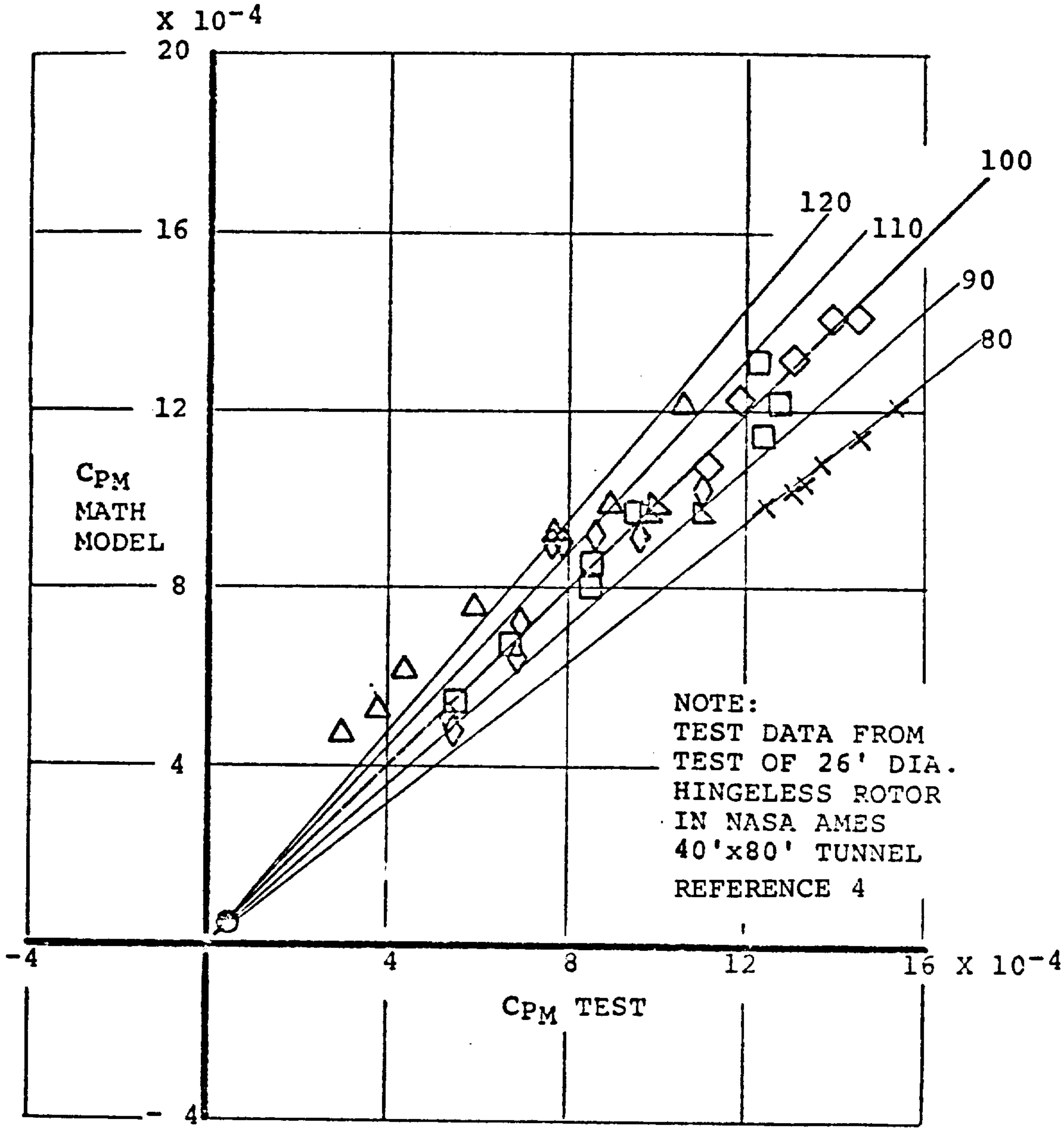

FIGURE 5.14 CORRELATION OF MATH MODEL PITCH MOMENT WITH FULL SCALE TEST DATA

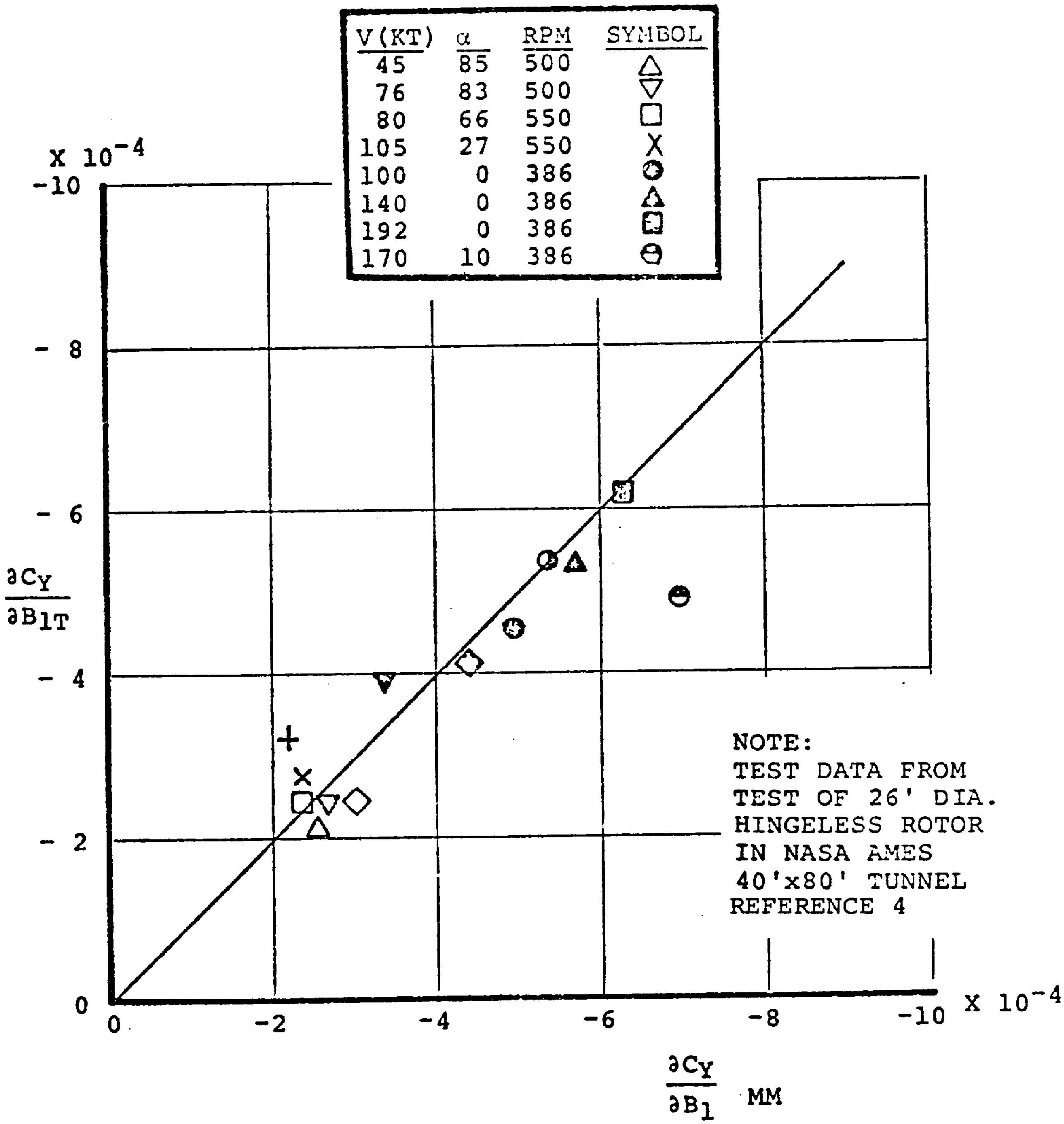

FIGURE 5.15 CORRELATION OF MATH MODEL REPRESENTATION OF $\partial C_Y/\partial B_1$ FULL SCALE TEST DATA

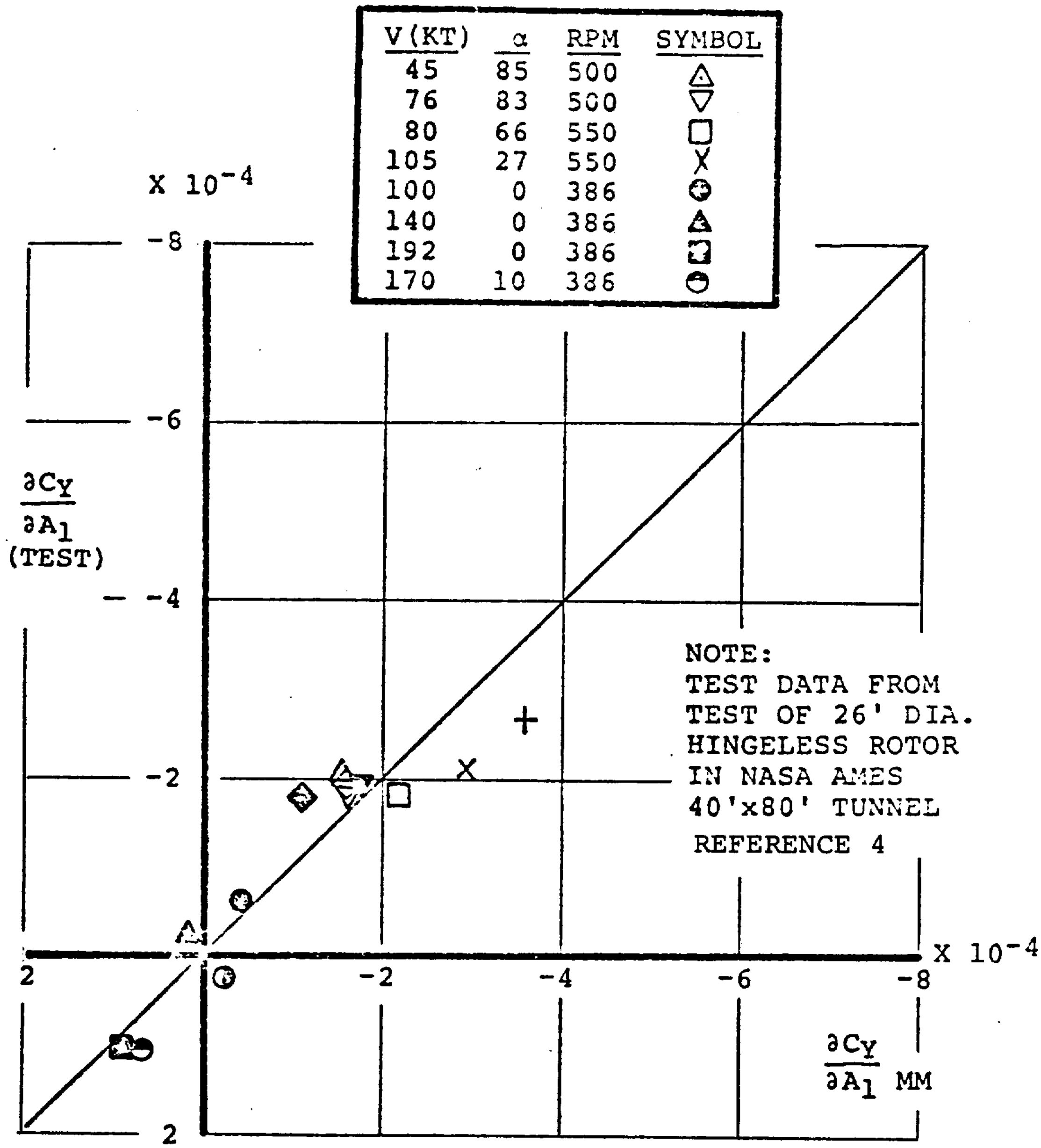

FIGURE 5.16 CORRELATION OF MATH MODEL REPRESENTATION OF $\partial C_Y/\partial A_1$ WITH FULL SCALE TEST DATA

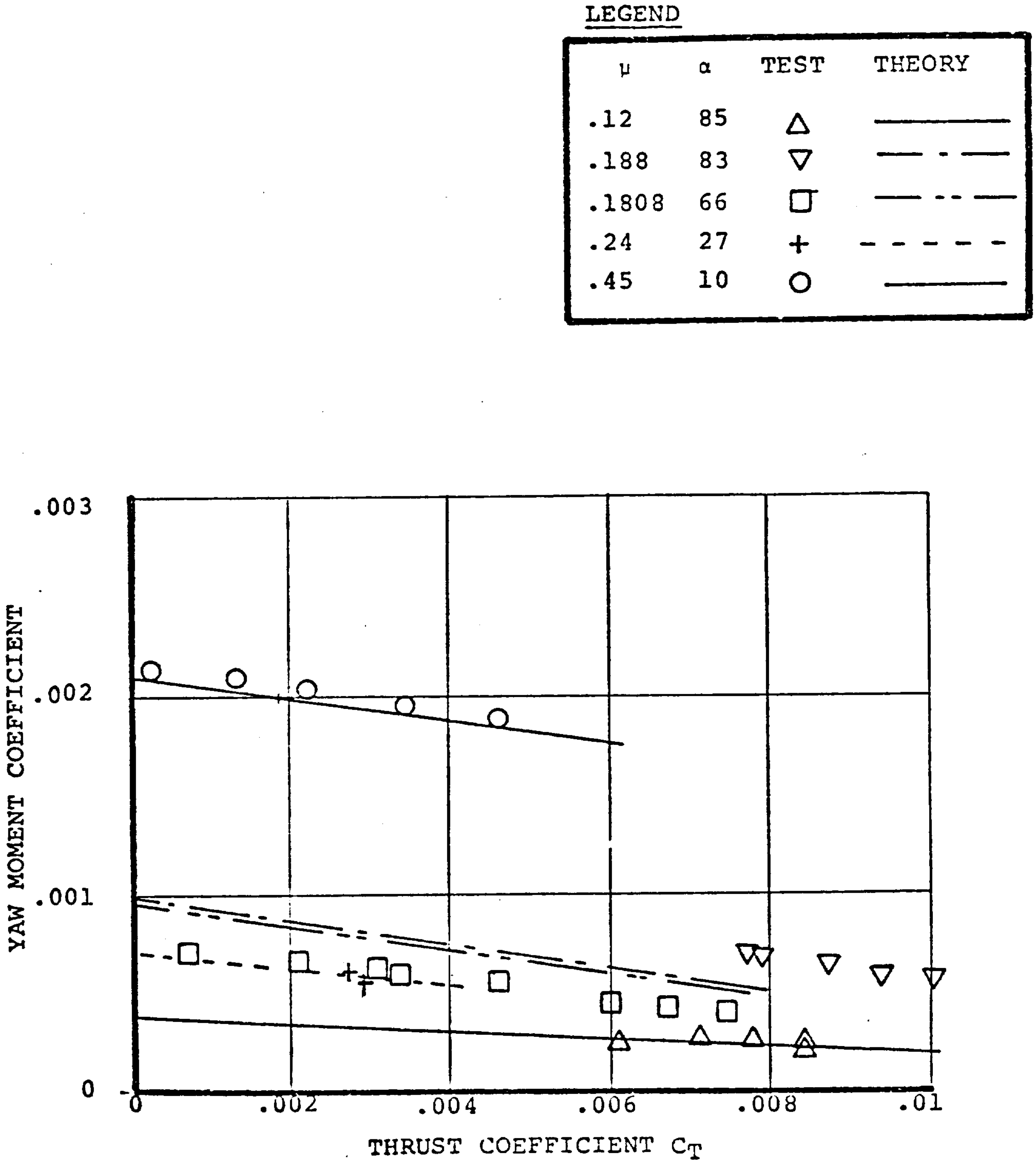

FIGURE 5.17 MATH MODEL AND TEST DATA COMPARISON OF YAW MOMENT SENSITIVITY TO THRUST COEFFICIENT

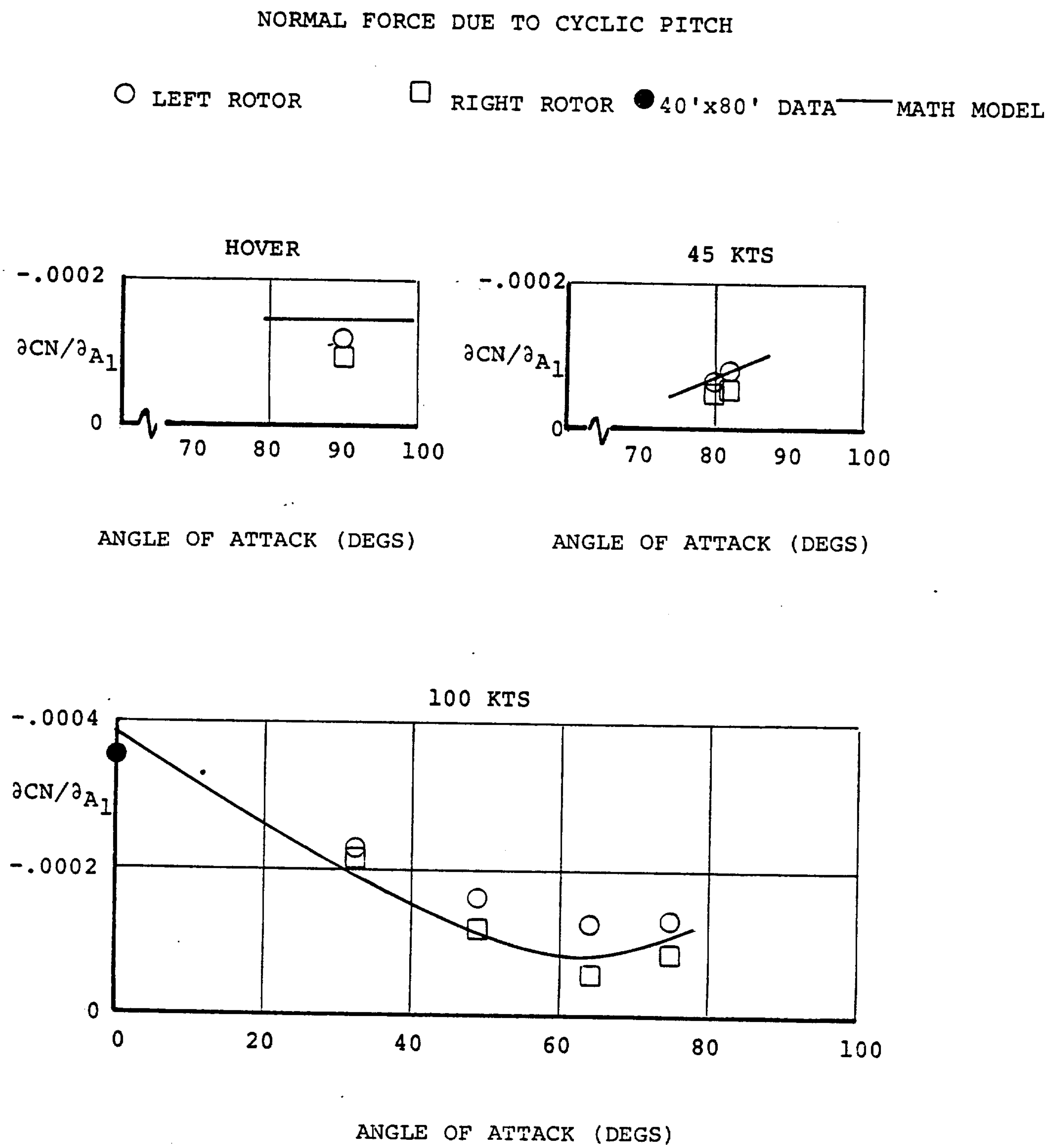

FIGURE 5.18 MATH MODEL PREDICTIONS COMPARED WITH 40' X 80' FULL SCALE AND 1/4.622 MODEL SCALE TEST DATA - $\partial C_N/\partial A_1$

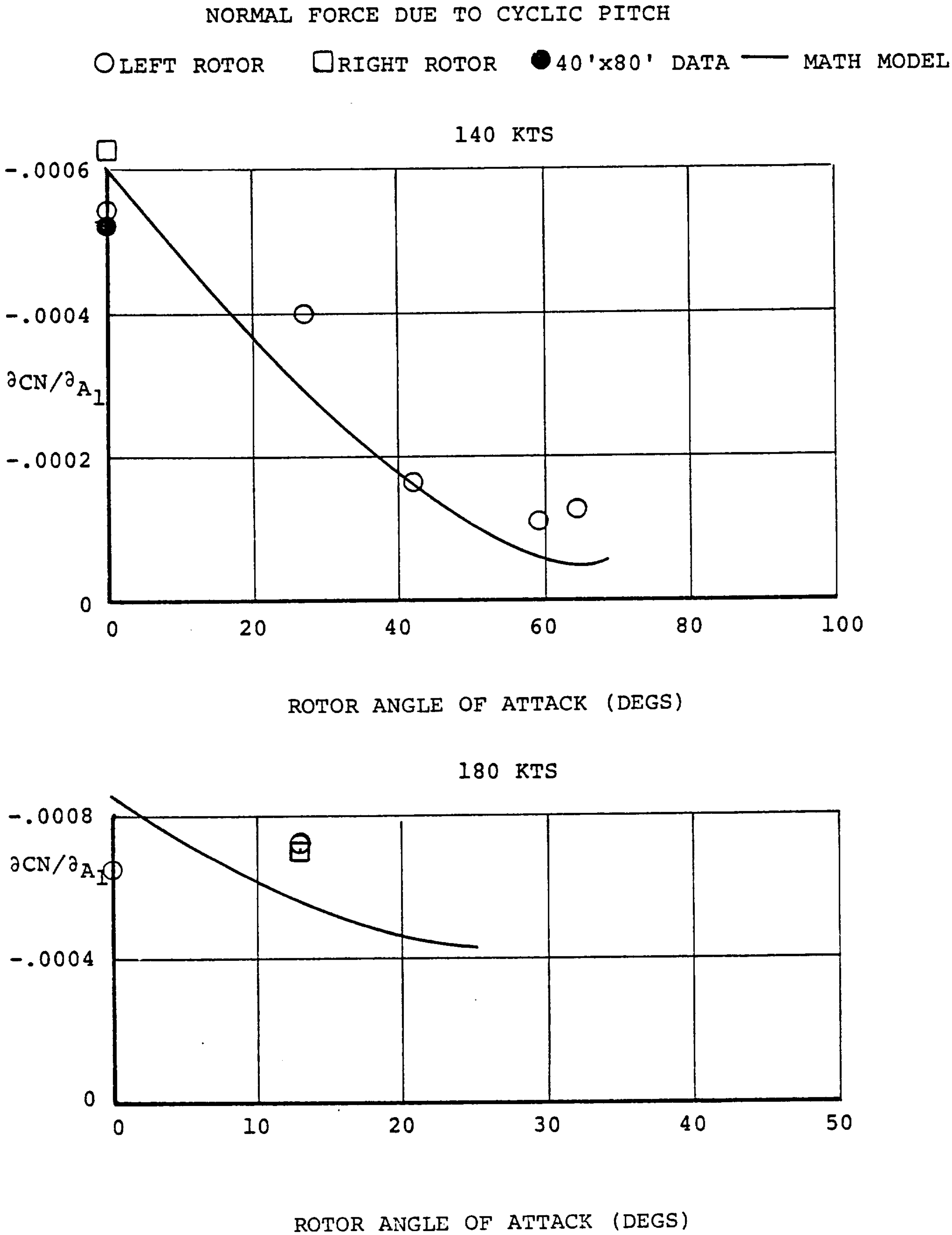

FIGURE 5.19 MATH MODEL PREDICTIONS COMPARED WITH 40' X 80' FULL SCALE AND 1/4.622 MODEL SCALE TEST DATA - $\partial C_N/\partial A_1$

NORMAL FORCE DUE TO CYCLIC PITCH

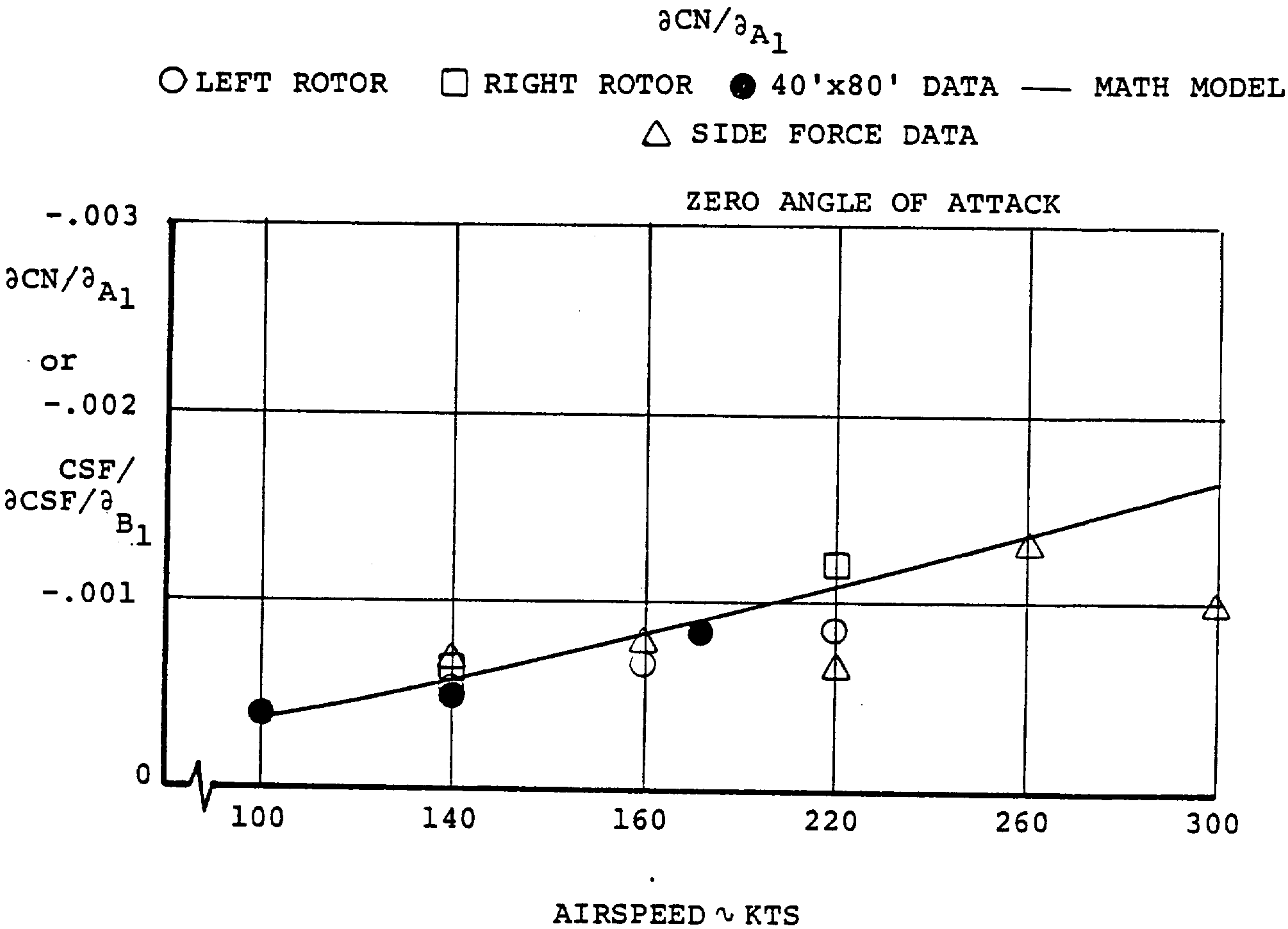

FIGURE 5.20 MATH MODEL PREDICTIONS COMPARED WITH 40' X 80' FULL SCALE AND 1/4.622 MODEL SCALE TEST DATA - $\partial C_N/\partial A_1$

NORMAL FORCE DUE TO CYCLIC PITCH $\partial CN/\partial_{B_1}$

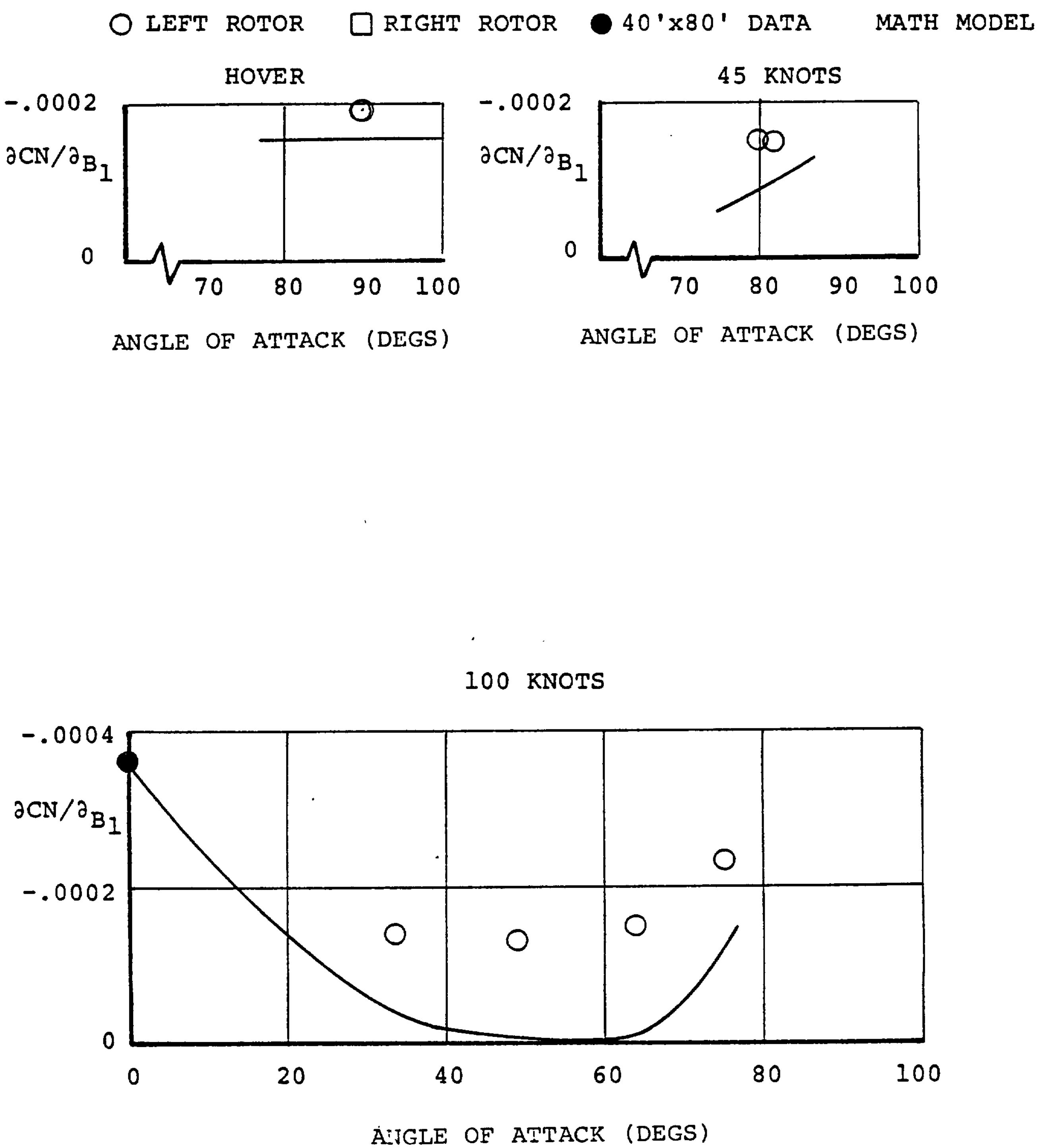

FIGURE 5.21 MATH MODEL PREDICTIONS COMPARED WITH 40' X 80' FULL SCALE AND 1/4.622 MODEL SCALE TEST DATA - $\partial C_N/\partial B_1$

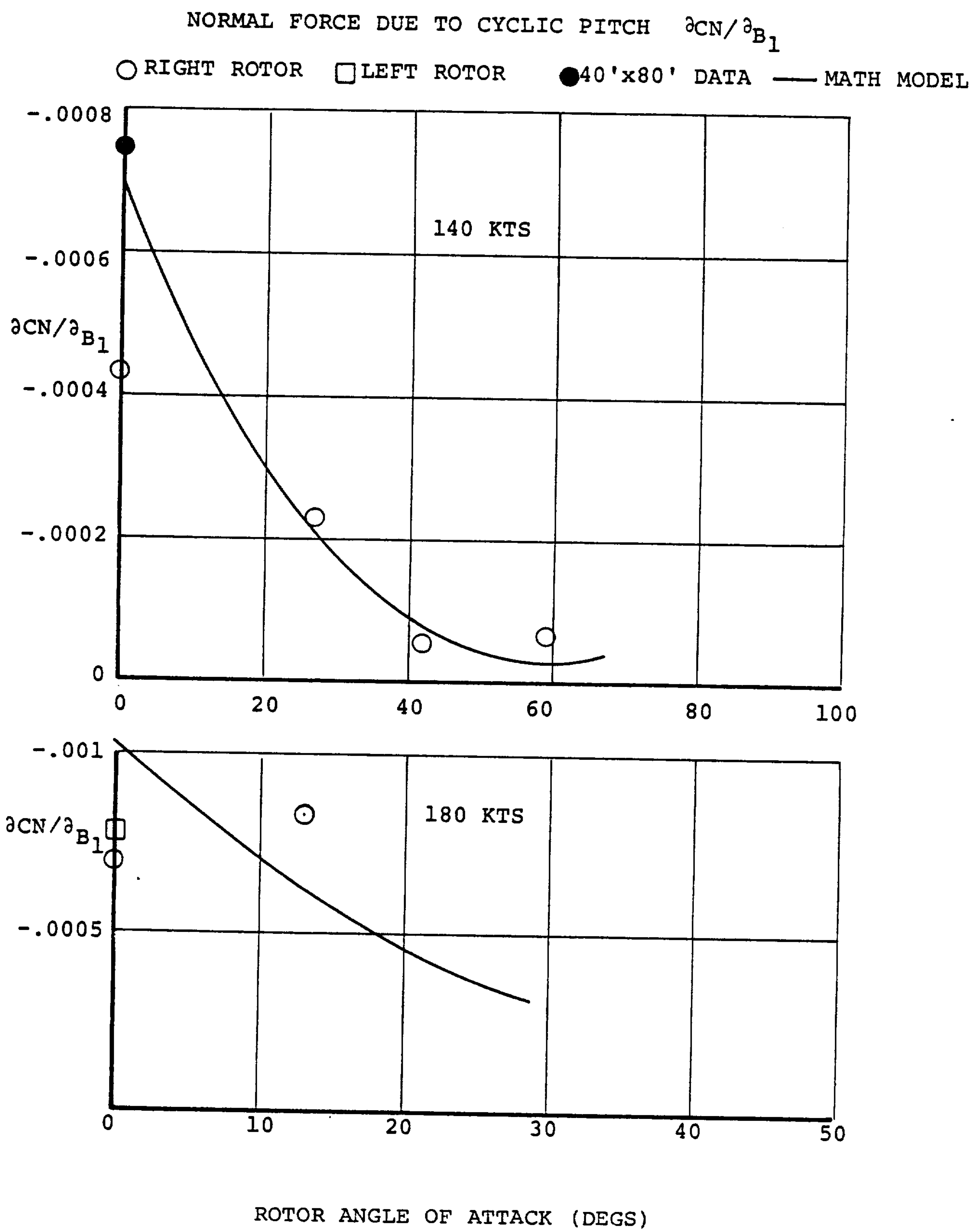

FIGURE 5.22 MATH MODEL PREDICTIONS COMPARED WITH 40' X 80' FULL SCALE AND 1/4.622 MODEL SCALE TEST DATA - $\partial C_N/\partial B_1$

NORMAL FORCE DUE TO CYCLIC PITCH $\partial CN/\partial B_1$

○ RIGHT ROTOR □ LEFT ROTOR ● 40'x80' DATA —— MATH MODEL

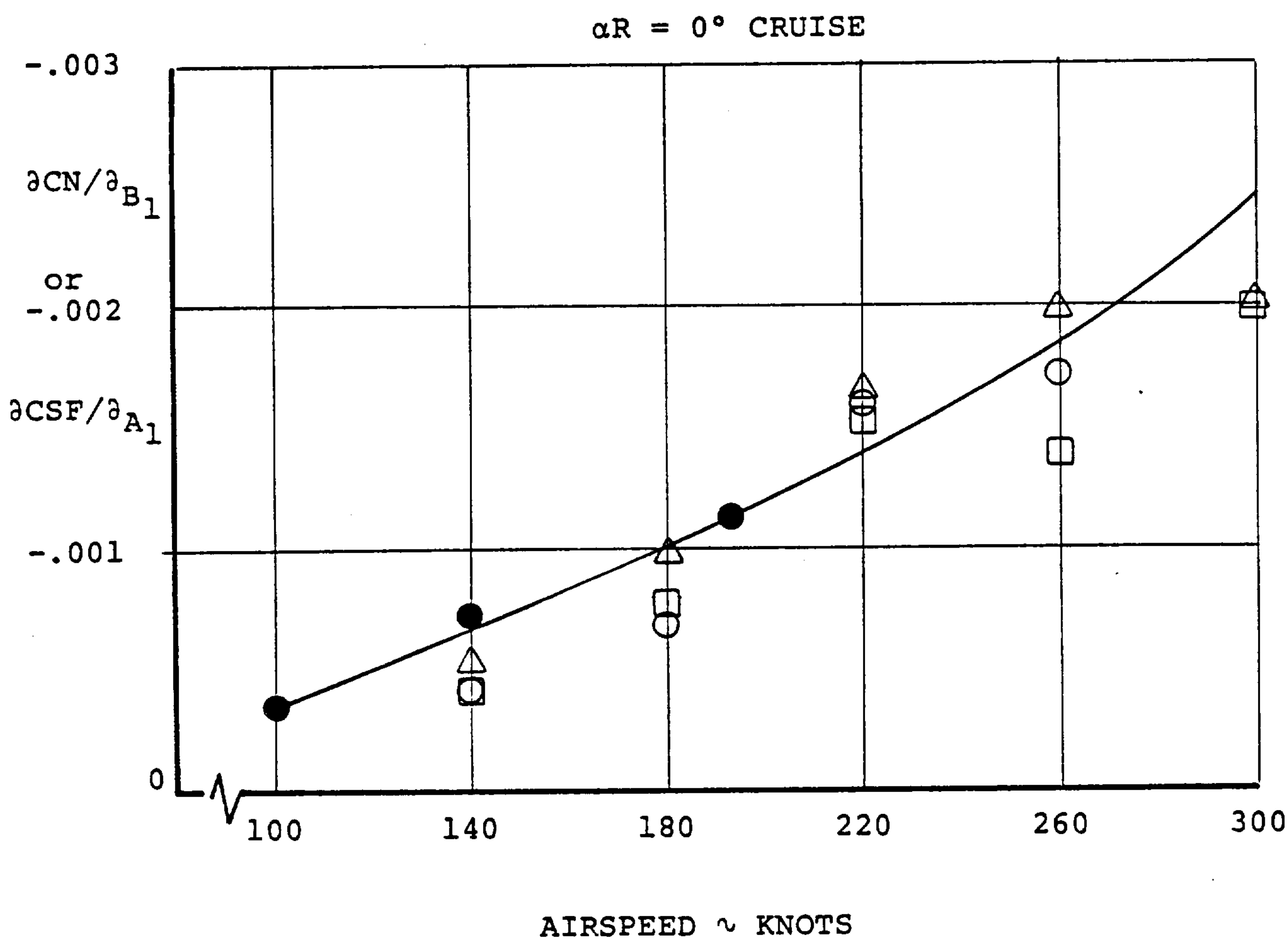

FIGURE 5.23 MATH MODEL PREDICTIONS COMPARED WITH 40' X 80' FULL SCALE AND 1/4.622 MODEL SCALE TEST DATA - $\partial C_N/\partial B_1$

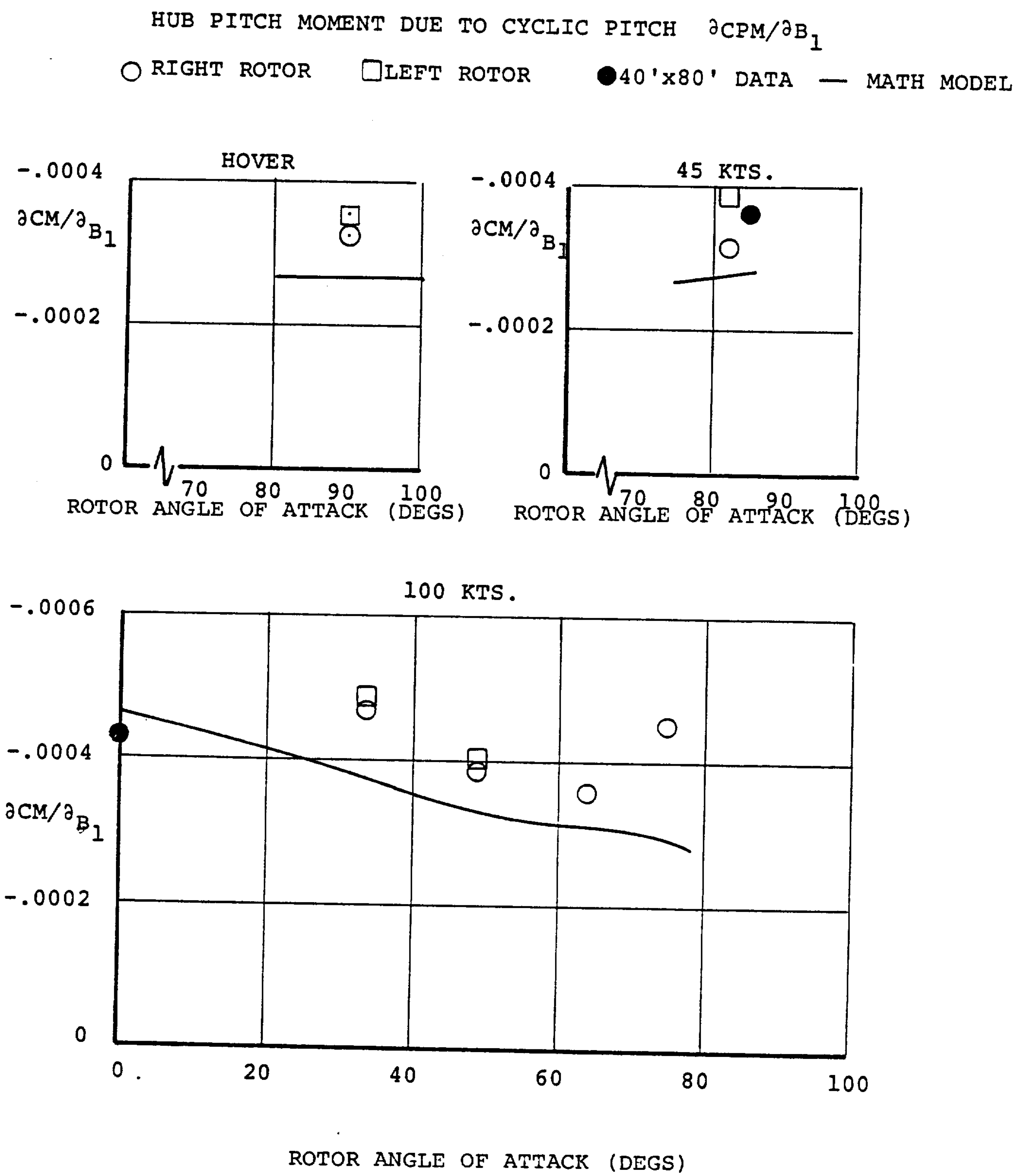

FIGURE 5.24 MATH MODEL PREDICTIONS COMPARED WITH 40' X 80' FULL SCALE AND 1/4.622 MODEL SCALE TEST DATA - $\partial C_M/\partial B_1$

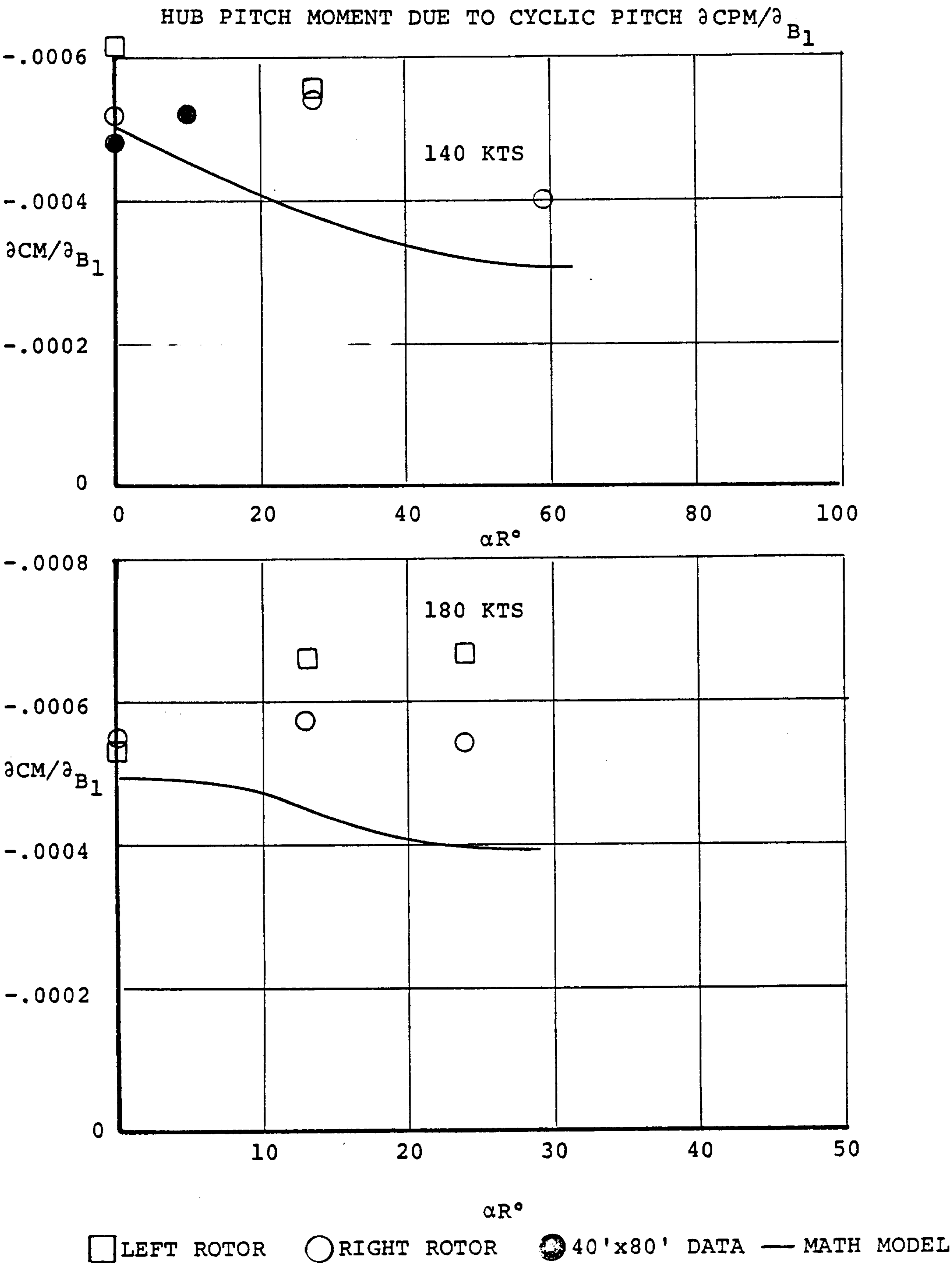

FIGURE 5.25 MATH MODEL PREDICTIONS COMPARED WITH 40' X 80' FULL SCALE AND 1/4.622 MODEL SCALE TEST DATA - $\partial C_M/\partial B_1$

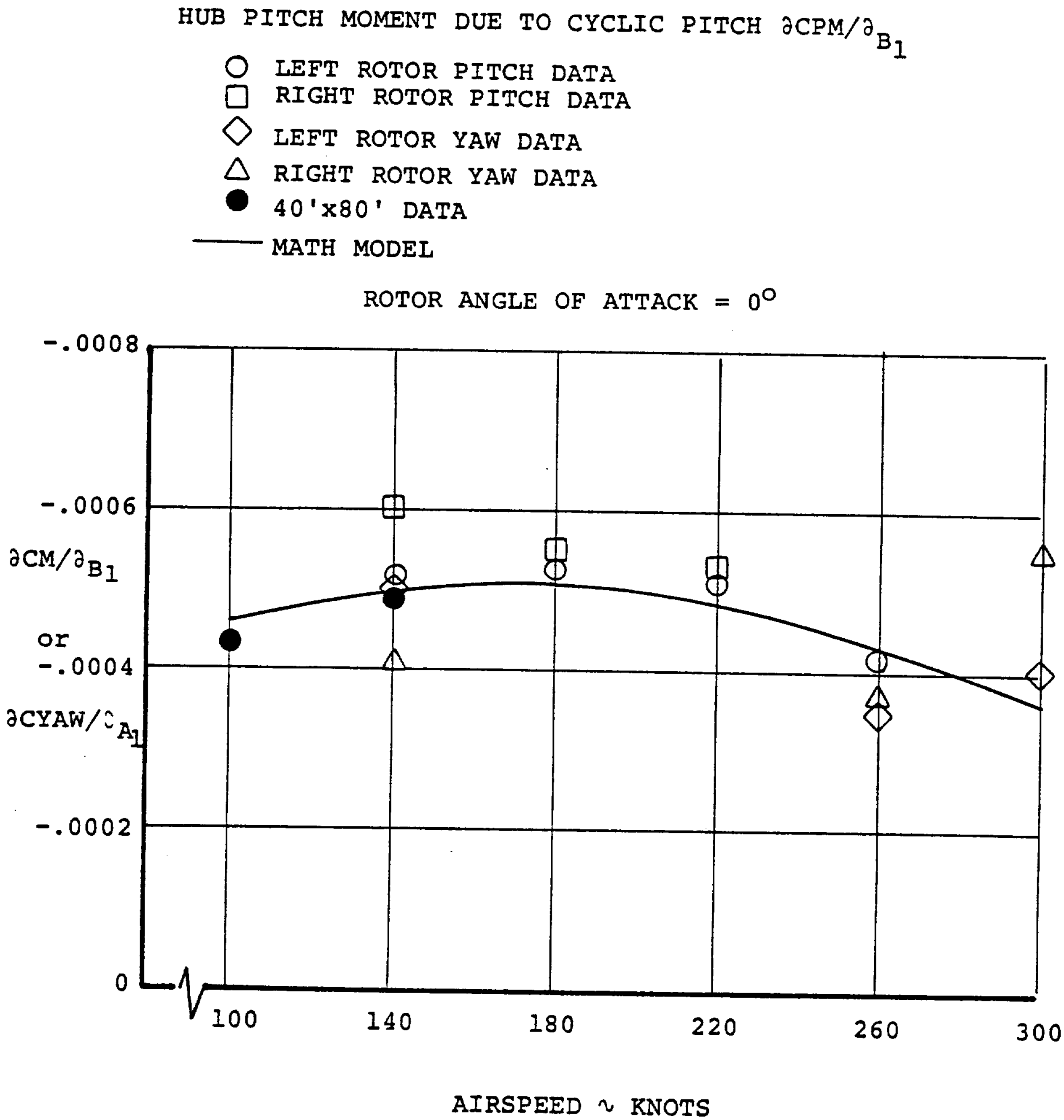

FIGURE 5.26 MATH MODEL PREDICTIONS COMPARED WITH 40' X 80' FULL SCALE AND 1/4.622 MODEL SCALE TEST DATA - $\partial C_M/\partial B_1$

CRUISE DATA

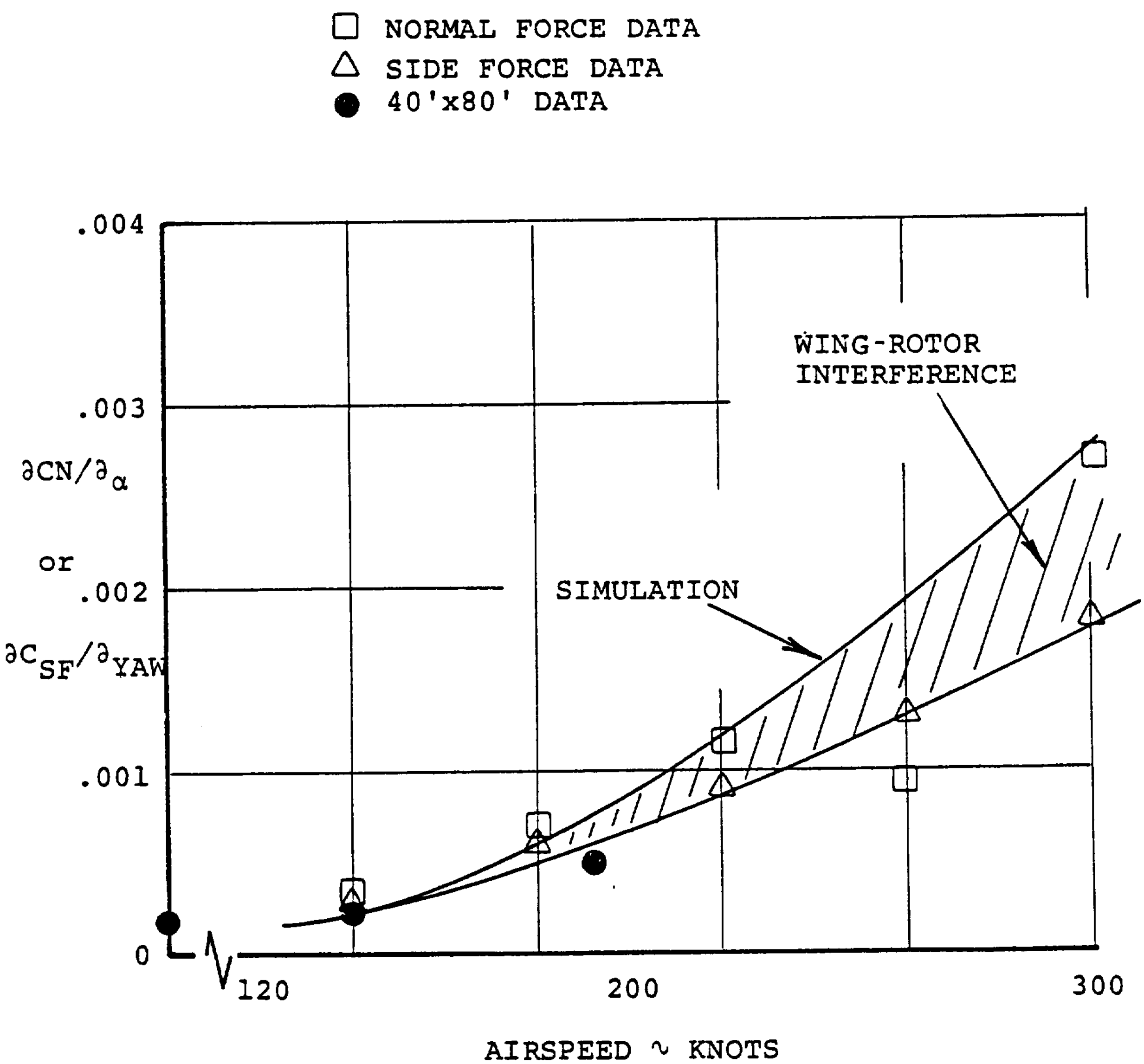

FIGURE 5.27 EFFECT OF WING-ROTOR INTERFERENCE ON ROTOR NORMAL FORCE

$$\left(\frac{T_{IGE}}{T_{OGE}}\right) = \left[\left(\frac{h}{D}\right)^2_{EFF} (.1741-.6216\mu) + \left(\frac{h}{D}\right)_{EFF} (1.4779\mu-.4143) + 1.2479 - .8806\mu\right]$$

<u>NOTE:</u> <u>If</u> $\mu > 0.283$; $\left(\frac{T_{IGE}}{T_{OGE}}\right) = 1.0$

<u>or</u>

<u>If</u> $\left(\frac{h}{D}\right)_{EFF} > 1.3$; $\left(\frac{T_{IGE}}{T_{OGE}}\right) = 1.0$

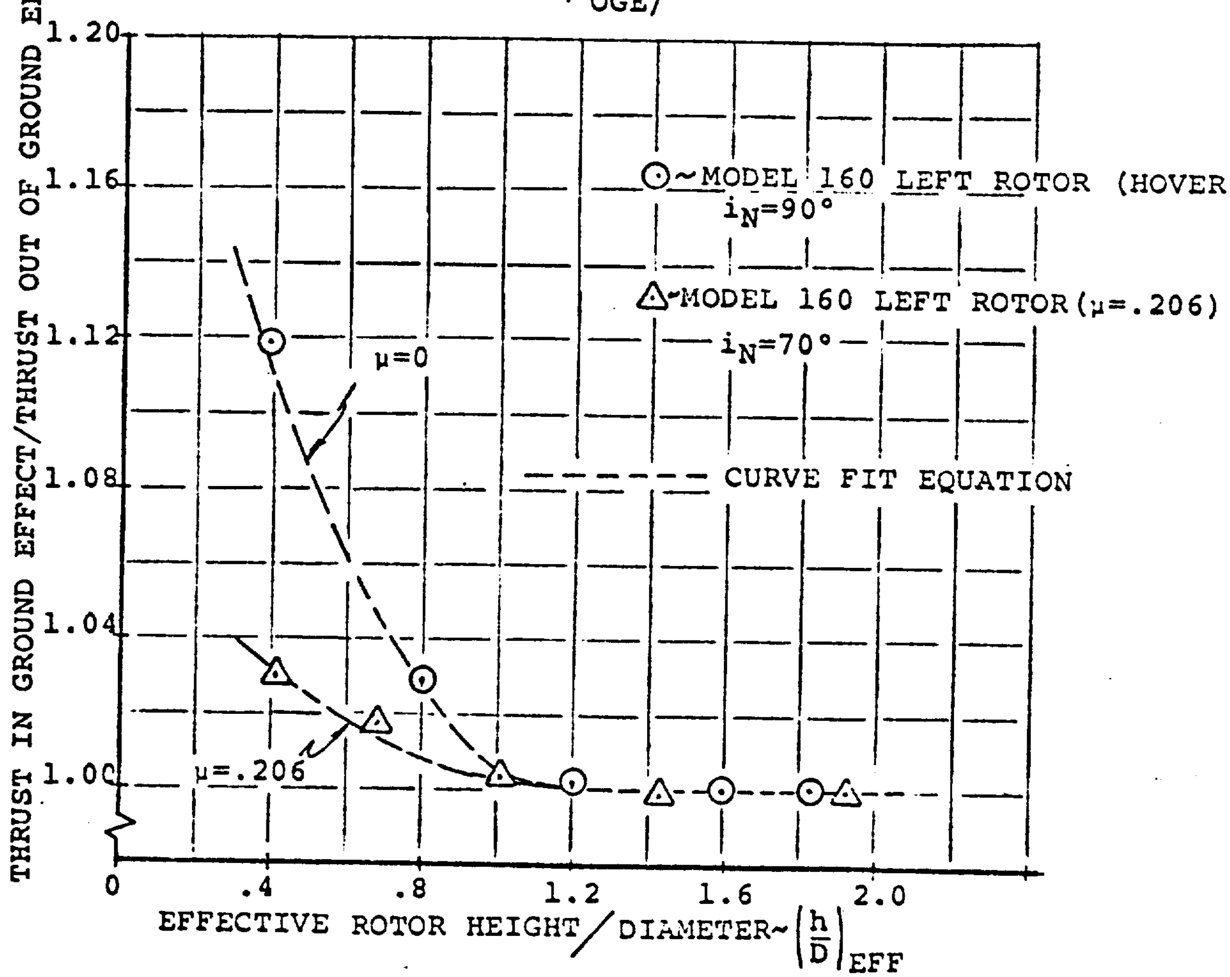

Figure 5.28. Effect of Rotor Height on Thrust Augmentation Ratio

6.0 CONTROL SYSTEM

6.0 CONTROL SYSTEM

Control of the HRXV-15 tilt rotor aircraft is accomplished by means of rotor and fixed-wing controls with the rotor controls phasing out during conversion to airplane flight. The rotor controls consist of longitudinal and lateral cyclic and differential collective. The airplane controls are differential flaperon deflection (ailerons), flaps, elevator and rudder. The airplane controls are operative during all phases of flight from hover to high speed cruise. Rotor cyclic inputs are retained beyond transition in order to reduce blade loads and provide high fatigue life. This is discussed in Section 11.0.

Cockpit controls consist of a lateral/longitudinal control stick and rudder pedals; a central throttle lever controls (via the governor) engine power and collective in hover and early transition. At the high speed end of transition and throughout cruise, movement of the throttle commands only engine power setting as in a conventional airplane. Nacelle incidence is controlled by a beep switch on the throttle lever. Flaps are selected via a flap lever operating through detents. Control stick and rudder trim is provided by hat switches on the stick. Trim rates are varied with dynamic pressure so as to maintain sensitivity at all speeds. A magnetic brake is incorporated for force zeroing. Page E-7 and E-8 of Appendix E present schematics of the overall control system layout.

6.1 Longitudinal Control

Longitudinal control in hover is by longitudinal cyclic pitch. This is phased out as the nacelles are tilted forward and becomes zero in cruise. The elevator provides pitch control in airplane flight. Elevator angle is scheduled through transition to minimize trimmed stick travel.

6.2 Lateral-Directional Control

In hover, roll control is accomplished by differential collective (thrust) and yaw control by differential longitudinal cyclic (thrust vectoring). Differential engine power accompanies differential collective in order to ensure roll control in the event of cross shaft failure and also to minimize cross shaft torque.

As transition proceeds from hover to airplane flight, the ailerons and rudder become more effective and the differential collective and differential longitudinal cyclic control gains are scheduled out with nacelle incidence. A small amount of differential collective is retained in cruise to provide favorable yaw with aileron deflection.

6.3 Thrust/Collective Control

In hover, forward motion of the throttle lever commands both increased collective pitch and increased engine power. The governor makes fine adjustments to the collective to maintain rpm. Over-travel of the pilot's throttle lever beyond the position for maximum power shuts down the governor and leaves the collective pitch connected directly with the throttle lever as in a helicopter. This feature gives a collective pitch flare landing capability in emergencies.

During transition, rotor collective pitch is scheduled with nacelle angle, thereby minimizing the amount of adjustment required from the governor. The collective authority of the throttle lever is also reduced with decreasing nacelle angle until, in cruise, movement of the throttle commands only engine power. Rotor rpm is maintained by the governor via blade pitch.

6.4 Force Feel System

The force sensitivities (force per unit displacement) of the pilot's stick and pedals are varied as a function of dynamic pressure in order to prevent excessive control sensitivities at high speeds. The force gradients were selected to provide a constant stick-force-per-g characteristic and good harmony between longitudinal and lateral controls. Control breakout forces and gradients are given in Appendix F.

6.5 Stability Augmentation Systems

Stability augmentation systems (SAS) are provided to enhance aircraft flying qualities. The systems consist of longitudinal, lateral and directional SAS. The system block diagrams are given in Appendix E.

The longitudinal (pitch) SAS incorporates a pitch rate feedback and a longitudinal stick pickoff. In addition, a pitch attitude signal is used to provide attitude stabilization without an autopilot. An autopilot is not represented in this simulation. The signals are shaped and put through an authority limit. The SAS actuators introduce control motions in series with the pilot's stick inputs. The longitudinal SAS commands longitudinal cyclic pitch to provide the required damping in hover and transition. This is not required in cruise and is phased out at 175 knots.

The lateral (roll) SAS operates in all flight modes. It consists of roll rate feedback for increased roll damping, a roll attitude feedback to give roll attitude stability, and a lateral stick pickoff. Roll attitude retention is provided when the stick is centered. In addition, a sideslip feedback is incorporated to compensate for dihedral effect. Roll SAS commands are added in series with the pilot's stick.

The directional (yaw) SAS operates throughout the flight envelope. The yaw channel consists of yaw rate feedback for increased directional damping in hover and transition, yaw attitude feedback for yaw stability, and rudder pedal pickoff for quickening. A heading-hold feature is provided when the rudder pedals are centered. A turn coordination feature enables pedal-free turns to be made down to about 50 knots. The yaw SAS command is input to the control system as inches of equivalent rudder pedal.

6.6 Thrust Management System (Governor)

The thrust and power management system for a tilt rotor aircraft must be compatible with both the helicopter and airplane configurations. Thrust control for the hover task, rpm control, gust response (especially in the cruise flight regime), and effect on aircraft flying qualities must all be considered. For a tilt rotor aircraft it is desirable from a practical viewpoint to have one type of governing for both the helicopter and fixed-wing flight regimes. Collective pitch governing offers the following advantages:

- It is more readily adapted to the hover flight regime than the fuel governor is to cruise
- It has better gust response characteristics
- It is fast acting and has high accuracy
- Thrust response to pilot control can be easily shaped with feed forward loops
- It has been demonstrated successfully in hover, transition and cruise in the CL-84 aircraft

With collective pitch governing there are two areas in the thrust management system to be considered: (1) design of the collective pitch governor; and (2) the feed forward loops for shaping pilot thrust control. The block diagram for this system is shown in Appendix E.

The governor was designed to meet the following objectives: (1) 0.3 percent steady state error in 2.5 to 3 seconds; (2) 2 percent rpm overshoot; and (3) satisfactory effect on aircraft flying qualities in the all-operational mode (i.e., all aircraft components operational and performing as designed). A single governor reference that uses the rpm signals from each rotor and averages them, satisfies the design criteria. To achieve the required accuracy and transient response goals, integral as well as proportional feedback of rpm is necessary in both the hover and cruise regimes. Governor gain is scheduled with nacelle incidence to maintain a near optimum level of governing throughout the flight envelope. Gains are varied linearly as the rotor rpm is changed from hover to cruise. The second requirement of the governor system is shaping the rotor thrust output for a pilot throttle input. Considerations in determining the proper shaping include:

(1) throttle sensitivity

(2) time constant to reach 63% of steady-state thrust

(3) allowable thrust overshoot

Variable pilot's control sensitivity is employed to give the optimum sensitivity in the hover power range yet maintain full power control within a reasonable throttle throw (8 inches). Shaping of the pilot command with collective quickening is used to improve the thrust time constant and thrust response transient shaping so that the pilot may perform the precision hover task with a minimum of difficulty. In the cruise regime, shaping of the thrust output is unnecessary and is phased out during transition.

The thrust/collective pitch control system is designed in such a manner that, during hover, when the pilot moves his control, he commands both a change in engine fuel setting and a change in collective setting. The governor then operates with a time lag to trim the collective to the value required to maintain rpm. The mechanical collective change feature is washed out as a function of nacelle incidence so that when nacelle incidence is decreased to zero, the pilot commands only engine fuel.

7.0 ENGINE MODEL

7.0 ENGINE MODEL

This section describes the representation of engine performance and dynamics. The basic engine cycle performance data consists of tabulated values of four variables: power, fuel flow, gas generator shaft rpm, and power turbine shaft rpm. These parameters are a function of Mach number and turbine inlet temperature. All data are in referred, normalized format as shown in Table 7.1. Because of the normalized, referred format, all data are valid for any ambient conditions. The effects on engine performance of operating at non-optimum power turbine speed are included in the model. The referred format also facilitates the inclusion of engine thermodynamic and mechanical limits. Limitations on engine cycle operation may be input in any combination of the following: fuel flow, torque, gas generator speed, gas generator referred rpm or output shaft speed. The flow charts which describe this routine mathematically are shown in Appendix E, and the performance data in Appendix F.

A simplified model of the Lycoming T53-L-13B engine was used in the tilt rotor mathematical model. The model basically consists of two first-order lags in series with variable time constants and gains. The output of the model is rate-limited to reflect actual engine performance. This simplified model gives satisfactory results for both large and small power transients. The block diagram for this system is shown as part of the thrust management system block diagram shown in Appendix E.

TABLE 7.1 ENGINE CYCLE DATA FORMAT

VARIABLE	SYMBOL	REFERRED NORMALIZED FORM
Thrust	F_N	$F_N/\delta F_N^*$
Power	SHP	$SHP/\delta \sqrt{\theta}\ SHP^*$
Gas Generator rpm	N_I	$N/\sqrt{\theta}\ N_I^*$
Power Turbine rpm	N_{II}	$N/\sqrt{\theta}\ N_{II}^*$
Fuel Flow	W_f	$W_f/\delta \sqrt{\theta}\ F_N^*$ $W_f/\delta \sqrt{\theta}\ SHP^*$
Turbine Inlet Temp.	T	T/θ

Where: * = Max. Power Setting, Static, Sea Level, Std. Day
θ = Ambient Temperature (^{o}R) Divided by $518.69^{o}R$
δ = Ambient Pressure (psia) Divided by 14.696 psia

8.0 AIRFRAME WEIGHT, CG AND INERTIAS

8.0 AIRFRAME WEIGHT, C.G. AND INERTIAS

In the derivation of the basic equations of motion, the aircraft was divided into three elements: the fuselage of mass m_f, the wings (m_W), and the tilting nacelles each of mass m_N. The components of these mass elements are:

o Fuselage Mass	Fuselage and contents Horizontal tail and contents Vertical tail and contents Crew and trapped liquids Cargo
o Wing Mass	Wing and contents Fuel carried in wing Fixed nacelles/engines
o Tilting Nacelle Mass	Tilting nacelle/engines including the rotor and hubs

The center of gravity of the aircraft with respect to the pivot reference line is calculated from

$$x_{CG} = \frac{m_f \ell_f + m_w \ell_w}{m} + \ell \frac{m_N}{m} [\text{Cos}(i_{NL} - \lambda) + \text{Cos}(i_{NR} - \lambda)]$$

$$z_{CG} = \frac{m_f h_f + m_w h_w}{m} - \ell \frac{m_N}{m} [\text{Sin}(i_{NL} - \lambda) + \text{Sin}(i_{NR} - \lambda)]$$

where the distances ℓ_f, ℓ_w, ℓ, and the angle λ are defined in the sketch below.

In the present simulation a weight and CG breakdown by components was not available so values of m_f, ℓ_f, m_w etc. were chosen so that the CG calculated from the above equations agreed with the centers of gravity at design gross weight 5896 Kg (13000 Lbs) as quoted in Reference 1.

The aircraft inertias were obtained from Reference 1. The variation of inertia with nacelle tilt is given by

$$I_{xx} = I_{xxo} + K_{I_1} i_N$$

$$I_{yy} = I_{yyo} + K_{I_2} i_N$$

$$I_{zz} = I_{zzo} + K_{I_3} i_N$$

$$I_{xz} = I_{xzo} + K_{I_4} i_N$$

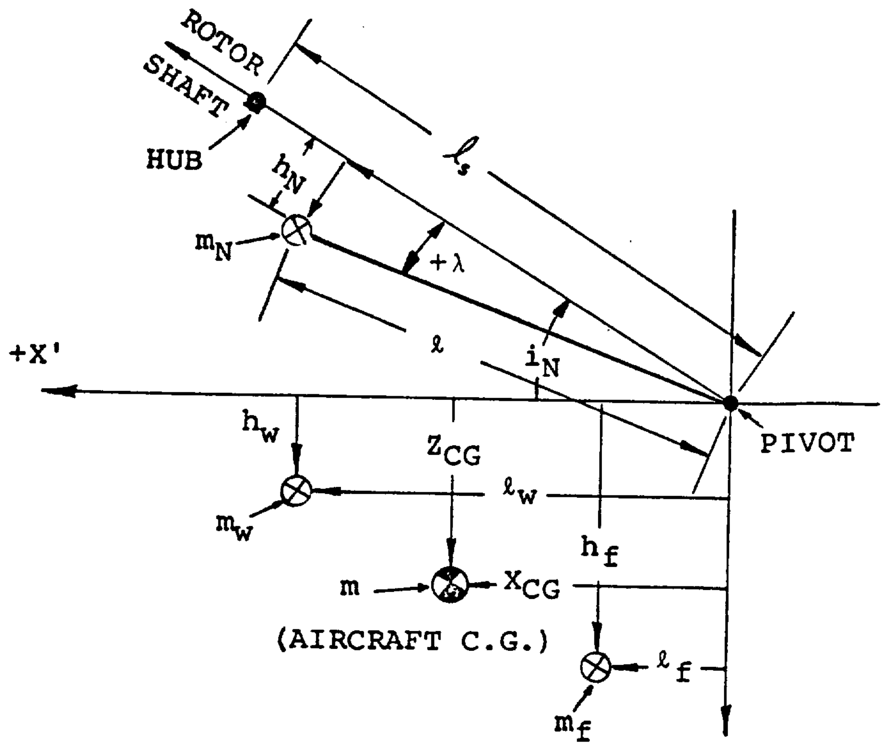

Note: Positive distances are indicated by the direction of the arrows

The quantities required to compute m_f, ℓ_f, m_w, ℓ_w, m, ℓ, m_N, λ, h_f, h_w are available from an aircraft three-view drawing and a standard mass properties buildup.

9.0 AEROELASTIC REPRESENTATION

9.0 AEROELASTIC REPRESENTATION

The stability and control characteristics of airplanes may be significantly influenced by distortions of the structure under transient loading conditions. A simplified representation of wing elastic distortion was therefore developed that could be used to study these effects.

Two aeroelastic degrees of freedom are included in the tilt rotor mathematical model. These are first mode wing vertical bending and first mode wing torsion. The assumptions made in deriving the wing bending and torsion relationships are as follows:

- No coupling between bending and torsion
- Wings are cantilevered from fuselage
- Elliptical loading for rigid untwisted wing
- Aerodynamic loads act at the quarter chord
- Wing elastic axis coincident with cross shaft
- Wing center of mass assumed to be on the elastic axis
- First torsion mode linear

The equations used to compute bending and torsion are derived in Appendix A. The wing twist at the tip is calculated from the following equation

$$K_{\theta_t}\,\theta_t = M_{NACT} - N_E I_E \Omega_E [(r \text{ Cos } i_N + p \text{ Sin } i_N) K_1 + K_2 r]$$

$$+ M^W_{AERO} - Z^W_{AERO}\, X_{WAC}$$

where K_{θ_t} is the wing torsional spring constant

θ_t is the wing twist angle in degrees

M_{NACT} is the nacelle actuator moment

N_E is the number of engines operating at the tip

I_E is the engine inertia of rotation

Ω_E is the engine speed

r	is the body axis yaw rate
p	is the body axis roll rate
K_1	is zero for non-tilting engines, unity if tilting
K_2	is zero for tilting engines, unity for non-tilting
M^W_{AERO}	is the pitching moment about the wing a.c.
$-Z^W_{AERO}$	is wing lift force
X_{WAC}	is the distance from the pivot line to the wing aerodynamic center

Assuming a linear mode shape from wing tip to root and zero twist at the root, the wing elastic twist at the wing aerodynamic center is obtained. This incremental twist is added to the rigid body twist and the resulting angle used in the wing aerodynamics equations.

The equations used to calculate wing vertical bending are:

$$\ddot{h}_1 = \omega_W^2 (F - h_1) - 2\xi_W \omega_W \dot{h}_1$$

$$F_L = -K_{w1} Z^{N'}_{AERO} - K_{w2} Z^{W'}_{AERO} - K_{w3} L^{N'}_{AERO} + K_{w4} \frac{Z_{AERO}}{m} \pm K_{w5} \dot{p}$$

$$\dot{h}_{WAC} = K_{w6} \dot{h}_1 ; \quad h_{WAC} = K_{w6} h_1$$

where

h_1	is the wing tip deflection
ω_W	is the first bending mode natural frequency
ξ_W	is the first bending mode vertical damping fraction
$Z^{N'}_{AERO}$	is the vertical nacelle aerodynamic force
$Z^{W'}_{AERO}$	is the vertical wing aerodynamic force
$L^{N'}_{AERO}$	is the aerodynamic torque at the tip
Z_{AERO}/m	is the aircraft normal acceleration

$\dot{p}$ is the roll acceleration

and K_{w1} through K_{w6} are constants

These equations determine the wing bending modal accelerations at each time frame using current values of the aerodynamic loads. Integration yields the velocity of the tip and the wing aerodynamic center. These velocities are then added to the rigid body velocities and the angle of attack are determined.

10.0 MATH MODEL CHECKOUT AND VALIDATION

10.0 MATH MODEL CHECKOUT AND VALIDATION

This section presents results of the mathematical model checkout and validation phase of the contract. Validation was made by:

(1) Comparing the HRXV-15 airplane-less-rotors component forces and moments with data from the current XV-15 Ames simulation math model.

(2) Taking stability derivatives and comparing the airframe contributions with published derivatives from the Ames simulation.

The force and moment validation was accomplished by setting up the math model at the same pitch attitudes and control settings as those quoted in the Ames data. Table 10.1 presents comparisons at 160 and 260 KTS in the airplane mode and at 40 and 80 KTS in the helicopter mode. The agreement between the two math models is generally within 10%.

Table 10.2 shows comparisons of the aircraft stability derivatives at 40 and 80 knots in helicopter flight and at 160 knots in the airplane mode. The contributions of the airframe and rotors to the total are shown separately.

The comparisons indicate that the airframe derivatives are in good agreement considering the different structures of the math models. Notable differences appear in the derivatives Y_p and, to a lesser extent, Y_r. The differences are attributed to the way in which the angles of attack at the vertical fins are computed. In the Boeing model the angle of attack and dynamic pressures at each fin are computed separately whereas in the model of Reference 1, the angle of attack seems to be computed as if the aircraft had a single fin in the plane of symmetry. This difference in treatment results in lower angles of attack at each fin (for a given roll rate) in the Boeing model and hence reduced side force.

	AIRPLANE MODE				HELICOPTER MODE			
	160 KTS		260 KTS		80 KTS		40 KTS	
	XV-15	ADV.XV-15	XV-15	ADV.XV-15	XV-15	ADV.HX-15	XV-15	ADV.HX-15
PITCH ATTITUDE, DEG.	-1.14	-1.14	.737	.739	-8.06	-8.06	-2.22	-2.22
FLAP SETTING, DEG.	40	40	0	0	40	40	40	40
ELEVATOR SETTING, DEG.	-6.8	-6.81	1.97	1.97	4.23	4.23	2.45	2.45
CG/NACELLE ANGLE, DEG.	AFT/0°		FWD/0°		AFT/90°		FWD/90°	
C_L FUSELAGE	.034	.034	.044	.0438	0	-.002	.0288	.0283
C_M FUSELAGE	-.0929	-.0924	-.0545	.0536	-.209	-.210	-.115	-.117
C_D FUSELAGE	.0126	.0124	.0123	.0122	.018	.019	.0129	.0131
TAIL DOWNWASH ANGLE, DEGREES	4.9	5.1	2.92	3.03	2.74	2.93	4.89	5.40
THRUST/ROTOR (LBS)	977	1003	989	976	6023	6052	6135	6212
X_{TAIL} (LBS)	-14.0	-5.7	-164	-148	-16.1	-16.1	-5.0	-9.0
X_{WING} (LBS)	-1886	-1906	-828	-742	-1132	-1066	-312	-212
T_{TAIL} (LBS)	673	703	939	1016	25.3	100	-38	-64
T_{WING} (LBS)	-13220	-13998	-11920	-12114	-1622.4	-1748	-536	-450
C_M WING	-17	-.169	-.0248	-.0249	-.099	-.095	-.109	-.110

TABLE 10.1 COMPARISON OF BOEING ADVANCED HRXV-15 AND NASA XV-15 TRIM DATA

		X/m		Y/m		Z/m		L/I_{xx}		M/I_{yy}		N/I_{zz}	
		XV-15	HRXV-15	XV-15	HRXV-15	XV-15	HRXV-15	XV-15	HRXV-15	XV-15	HRXV-15	XV-15	HRXV-15
δ_B	TOTAL	-1.087	-.718	---	---	-.576	.209	---	---	.373	.779	---	---
	ROTOR	-1.091	-.730	---	---	-.760	.010	---	---	.258	.658	---	---
	AIRFRAME	+.004	.012	---	---	+.184	.199	---	---	.115	.121	---	---
δ_S	TOTAL	---	---	-.041	-.161	---	---	.3043	.464	---	---	-.027	-.051
	ROTOR	---	---	-.041	-.161	---	---	.2872	.462	---	---	-.026	-.050
	AIRFRAME	---	---	0	0	---	---	.0171	.002	---	---	-.001	-.001
δ_r	TOTAL	---	---	.032	-.105	.001	.009	-.076	-.084	---	---	.151	.156
	ROTOR	---	---	.226	.086	.002	-.009	-.071	-.079	---	---	.115	.121
	AIRFRAME	---	---	-.194	-.191	-.001	0	-.005	-.005	---	---	.036	.035
p	TOTAL	---	---	-.966	-.595	-.001	.037	-1.055	-1.826	0	-.069	.091	.027
	ROTOR	---	---	-1.120	-.669	-.001	.033	-.915	-1.752	0	-.071	.119	.042
	AIRFRAME	---	---	.154	.074	0	.004	-.140	-.074	0	.002	-.028	-.015
q	TOTAL	1.420	.030	---	---	-.901	-.013	-.010	.024	-1.329	-3.259	---	---
	ROTOR	1.396	.290	---	---	.660	.795	-.010	.024	-.371	-2.222	---	---
	AIRFRAME	.024	-.260	---	---	-1.561	-.808	0	0	-.958	-1.037	---	---
r	TOTAL	.002	-.018	-.927	-.431	.044	.113	.441	.257	-.002	0	.099	-.009
	ROTOR	.002	.010	-.151	-.005	.046	.110	.431	.254	-.001	0	-.029	-.082
	AIRFRAME	0	-.028	-.776	-.426	-.002	.003	.010	.003	-.001	0	.128	.073
U	TOTAL	-.045	-.067	---	---	-.197	-.172	---	---	-.001	.015	---	---
	ROTOR	-.018	-.046	---	---	-.144	-.116	---	---	.005	.025	---	---
	AIRFRAME	-.027	-.021	---	---	-.053	-.056	---	---	-.006	-.010	---	---
V	TOTAL	---	---	.006	-.037	---	---	-.005	-.018	---	---	-.004	-.004
	ROTOR	---	---	-.005	-.040	---	---	-.004	-.019	---	---	.003	.002
	AIRFRAME	---	---	.011	.003	---	---	-.001	.001	---	---	-.007	-.006
W	TOTAL	.008	-.012	---	---	-.369	-.447	---	---	.037	.042	---	---
	ROTOR	.009	-.016	---	---	-.279	-.397	---	---	-.001	.007	---	---
	AIRFRAME	-.001	.004	---	---	-.090	-.050	---	---	.038	.035		

5896 Kg (13,000 LBS) V = 40 KT NACELLE = 90° FLAPS = 40° AFT C.G. SAS OFF

TABLE 10.2 DERIVATIVES COMPARISON - XV-15 VS HRXV-15 - 40 KTS, $i_N = 90°$

		X/m		Y/m		Z/m		L/I_{xx}		M/I_{yy}		N/I_{zz}	
		XV-15	HRXV-15	XV-15	HRXV-15	XV-15	HRXV-15	XV-15	HRXV-15	XV-15	HRXV-15	XV-15	HRXV-15
δ_B	TOTAL	-1.026	-.565	---	---	-1.268	.460	---	---	.527	.967	---	---
	ROTOR	-1.046	-.625	---	---	-1.735	.008	---	---	.254	.693	---	---
	AIRFRAME	.020	.060	---	---	.467	.452	---	---	.273	.274	---	---
δ_S	TOTAL	---	---	.006	-.239	---	---	.378	.530	---	---	-.043	-.085
	ROTOR	---	---	.006	-.239	---	---	.337	.509	---	---	-.040	-.078
	AIRFRAME	---	---	0	0	---	---	.041	.021	---	---	-.003	-.007
δ_r	TOTAL	---	---	-.372	-.330	---	---	-.136	-.070	---	---	.172	.185
	ROTOR	---	---	.168	.108	---	---	-.121	-.058	---	---	.073	.105
	AIRFRAME	---	---	-.540	-.438	---	---	-.015	-.012	---	---	.099	.080
p	TOTAL	---	---	-1.550	-.194	---	---	-1.548	-2.100	---	---	.190	.111
	ROTOR	---	---	-1.366	-.100	---	---	-1.261	-1.885	---	---	.128	.064
	AIRFRAME	---	---	-.184	-.094	---	---	-.287	-.215	---	---	.062	.047
q	TOTAL	1.317	.274	-.001	0	-2.119	-1.353	---	---	-1.744	-3.509	---	---
	ROTOR	1.376	.301	-.001	0	.116	.249	---	---	-.370	-2.377	---	---
	AIRFRAME	-.059	-.027	0	0	-2.235	-1.602	---	---	-1.374	-1.132	---	---
r	TOTAL	-.007	.008	1.059	.378	-.072	.089	.381	.339	.011	-.003	-.243	-.255
	ROTOR	0	.008	.133	-.374	0	.082	.300	.275	0	-.007	-.041	-.106
	AIRFRAME	-.007	0	.926	.752	-.072	.007	.081	.064	.011	.004	-.202	-.149
U	TOTAL	-.072	-.098	---	---	-.137	-.077	---	---	.012	.032	---	---
	ROTOR	-.020	-.048	---	---	-.079	-.033	---	---	.005	.031	---	---
	AIRFRAME	-.052	-.050	---	---	-.058	-.044	---	---	.007	.001	---	---
V	TOTAL	---	---	-.089	-.110	---	---	-.010	-.016	---	---	.004	.004
	ROTOR	---	---	-.012	-.040	---	---	-.005	-.015	---	---	.001	.002
	AIRFRAME	---	---	-.077	-.070	---	---	-.005	-.001	---	---	.003	.002
W	TOTAL	-.011	-.031	---	---	-.705	-.655	---	---	-.023	-.006	---	---
	ROTOR	-.003	-.003	---	---	-.368	-.327	---	---	.002	.023	---	---
	AIRFRAME	-.008	-.028	---	---	-.337	-.328	---	---	-.025	-.029	---	---

5896 Kg (13,000 LBS) V = 40 KT NACELLE = 90° FLAPS = 40° AFT C.G. SAS OFF

TABLE 10.3 DERIVATIVES COMPARISON - XV-15 VS HRXV-15 - 80 KTS, i_N = 90°

		X/m		Y/m		Z/m		L/I_{xx}		M/I_{yy}		N/I_{xx}	
		XV-15	HRXV-15	XV-15	HRXV-15	XV-15	HRXV-15	XV-15	HRXV-15	XV-15	HRXV-15	XV-15	HRXV-15
δ_B	TOTAL	.154	.011	---	---	1.846	1.811	---	---	1.219	1.207	---	---
	ROTOR	0	0	---	---	0	0	---	---	0	0	---	---
	AIRFRAME	.154	.011	---	---	1.846	1.811	---	---	1.219	1.207	---	---
δ_S	TOTAL	---	---	---	---	---	---	.210	.221	---	---	.087	.075
	ROTOR	---	---	---	---	---	---	.028	.046	---	---	.079	.073
	AIRFRAME	---	---	---	---	---	---	.182	.175	---	---	.008	.002
δ_r	TOTAL	---	---	-1.749	-1.727	---	---	-.061	-.060	---	---	.318	.314
	ROTOR	---	---	0	0	---	---	0	0	---	---	0	0
	AIRFRAME	---	---	-1.749	-1.727	---	---	-.061	-.060	---	---	.318	.314
p	TOTAL	---	---	-.842	-.405	---	---	-.819	-1.224	---	---	-.152	-.354
	ROTOR	---	---	-.171	.040	---	---	-.209	-.529	---	---	-.255	-.356
	AIRFRAME	---	---	-.671	-.445	---	---	-.610	-.695	---	---	.103	.002
q	TOTAL	.560	.058	---	---	-8.028	-2.266	---	---	-1.953	-4.469	---	---
	ROTOR	.980	.026	---	---	-4.553	.820	---	---	.429	-2.015	---	---
	AIRFRAME	-.420	.032	---	---	-3.475	-3.086	---	---	-2.382	-2.454	---	---
r	TOTAL	---	---	7.531	2.202	---	---	-.007	-.200	---	---	-1.303	-1.676
	ROTOR	---	---	4.559	-.604	---	---	-.278	-.359	---	---	-.742	-1.162
	AIRFRAME	---	---	2.972	2.806	---	---	.271	.159	---	---	-.561	-.514
U	TOTAL	-.060	-.027	---	---	-.257	-.170	---	---	.004	.004	---	---
	ROTOR	-.020	-.018	---	---	0	-.023	---	---	.001	.004	---	---
	AIRFRAME	-.040	-.009	---	---	-.257	-.147	---	---	.003	0	---	---
V	TOTAL	---	---	-.245	-.367	---	---	-.011	-.011	---	---	.015	.006
	ROTOR	---	---	-.046	-.169	---	---	0	-.008	---	---	-.002	-.008
	AIRFRAME	---	---	-.199	-.198	---	---	-.011	-.003	---	---	.017	-.014
W	TOTAL	.032	.109	---	---	-.865	-1.004	---	---	-.023	-.012	---	---
	ROTOR	-.011	.002	---	---	-.046	-.169	---	---	.009	.031	---	---
	AIRFRAME	.043	.107	---	---	-.819	-.835	---	---	-.032	-.043	---	---
5896 Kg (13,000 LBS) V = 40 KT NACELLE = 90° FLAPS = 40° AFT C.G. SAS OFF													

TABLE 10.4 DERIVATIVES COMPARISON - XV-15 VS HRXV-15 - 160 KTS, i_N = 0°

11.0 AIRCRAFT TRIMMED
FLIGHT CHAR. & BOUND.

11.0 AIRCRAFT TRIMMED FLIGHT CHARACTERISTICS AND BOUNDARIES

This section presents the aircraft trim attitudes and control settings both in level flight and in steady turns at constant altitude for forward and aft CG conditions at design gross weight - 5896 Kg (13,000 Lbs). Data is also presented on blade loads, as estimated using the method discussed in Appendix G. Most of the data shown was obtained at sea level standard conditions, though some results at altitude are included. All the results presented were obtained with the preliminary cyclic-on-the-stick and stick-offset schedules as determined by the parametric study described in Appendix G. It should be emphasized that the trimmed flight characteristics and boundaries presented here are preliminary only, since many of the control laws, gains, etc. are themselves preliminary and are likely to change as a result of further control system development and design studies on the Advanced Hingeless Rotor XV-15 to be completed in 1977.

In the following graphs aft CG is defined to be at sea level 301.2" (40.28% MAC) and forward CG at sea level 291.7" (25.2% MAC). The rotor blade cyclic angles quoted are the values of cyclic in the rotor wind-axes system, i.e., lateral cyclic is the value at $\psi = 0°$, and longitudinal cyclic the value at $\psi = 90°$. Wing stall is defined to occur at a wing angle of attack in the slipstream of 13°. This value is the angle of wing $C_{L_{MAX}}$ at $i_N = 90°$ and flaps set at 40°.

11.1 Steady Level Transition

The aircraft trim pitch attitudes, elevator and longitudinal stick positions, wing-in-slipstream angle of attack and A_1 and B_1 cyclic pitch required, are presented in Figures 11.1 through 11.10. The data was obtained with flaps set at 40° for both the forward and aft center of gravity positions.

The variation of trimmed fuselage pitch attitude is shown in Figure 11.1 for aft CG and Figure 11.2 for forward CG. The trimmed pitch attitudes are also the wing angles of attack on those portions of the wing not influenced by the rotor slipstream. Pitch angles are slightly lower for the forward CG condition at high nacelle angles and low airspeeds while at low to intermediate nacelle positions and higher airspeeds the trim attitudes tend to be slightly higher. For both loading conditions the variations are smooth and continuous from hover to cruise.

Figures 11.3 and 11.4 present the angles of attack of slipstream-immersed portions of the wing, if any part of the wing is, in fact, immersed.

At high nacelle angles, above approximately 40 knots airspeed, the rotor slipstream does not impinge on the wing and hence the operating wing angle of attack would be obtained from Figures 11.1 and 11.2. This point will be returned to later in connection with wing stall boundaries.

The variation of elevator deflection with airspeed at various nacelle angles is shown in Figures 11.5 and 11.6. The values shown are the total elevator deflection - scheduled elevator plus pilot-command elevator. At airspeeds below about 90 knots raising the nacelles requires more positive elevator to lower the nose to trim attitude. The close bunching of the curves near 100 knots at aft CG is due to the cruise cyclic on the stick inputs.

Longitudinal stick travel through transition is presented in Figures 11.7 and 11.8. The gradients with airspeed are stable, i.e., forward stick - increasing airspeed. At aft CG the stick gradients at $i_N = 0, 15°$ are steep below 110 knots. In this region the aircraft is approaching stall and therefore a fairly large gradient is desirable.

Figures 11.9 and 11.10 present the A_1 and B_1 values of cyclic required to trim through transition. The cyclics required above 80 knots and at nacelle angles below 60° show the increasing contribution of the cruise cyclic on the stick. The apparent sudden change in size of both A_1 and B_1 near hover arises from the fact that swashplate cyclic is input at $\psi = 30°$.

Aircraft power and thrust required from hover through cruise at fixed nacelle angles is plotted in Figures 11.11 through 11.14. The rotor torque required is presented in Figures 11.15 and 11.16. Cruise descent torque values are high because the flaps are at 40° in this plot. The torque corresponding to 100% is equivalent to 1550 horsepower at 551 RPM. Thus the MIL (30 minutes) power setting occurs at 90.6% torque and NRP occurs at 80.6% torque.

11.1.1 Blade Loads

The estimated blade alternating bending moments are presented in Figures 11.17 and 11.18. The bending moments are at 12.5% radius and were computed using one empirical blade loads equation. Comparisons of the loads calculated using the equation with measured loads obtained from tests of a full-scale rotor in the Ames 40' by 80' tunnel, indicates that the predictions are within ±20% of measured data. While more work needs to be done to improve blade loads prediction, nevertheless the computed loads are not unreasonable and can be used to assess the rotor loads and establish fatigue margins in both steady level and turning flight and maneuvers.

The blade load level of 4064 Nm (36,000 in.-lbs) is marked on the figures and is the infinite fatigue life allowable level.

The blade loads are seen to be sufficiently low throughout transition to ensure a reasonably wide conversion corridor without operating past the infinite fatibue life allowables in sustained flight

11.1.2 Transition Corridors

First estimates of the transition corridors, flaps down, at forward and aft CG are presented in Figures 11.19 and 11.20. The lower boundaries are wing stall (power on), blade loads infinite life allowables, and maximum up-elevator. In airplane flight with nacelles down the wing stalls before full up-elevator travel is reached. At aft CG, the wing stall line forms the lower boundary until at about 30° nacelle incidence the ($M-3\sigma$) 10^8 cycles blade loads line defines the limit from 80 knots to hover. At forward CG, the wing stall line defines the low speed boundary down to about 50 knots and 47° nacelle angle, after which rotor loads become limiting.

At the high speed end of transition the conversion corridor is bounded by torque limits, blade loads, flap loads and maximum elevator deflection.

The elevator and blade loads boundaries are clearly dependent on control system design and as such are functions of the cyclic and elevator schedules and gains used in the control system model. In the aft CG case the high nacelle angle cases are limited by maximum elevator deflection whereas for the forward CG case the blade loads are the limiting factor. There is room for further optimization in this area by use of a reduced elevator offset at $i_N = 90°$. At $i_N = 90°$ the envelope is limited at 96 knots by loads in the forward CG case and at 90 knots by elevator at aft CG.

Below 70° the corridor is bounded by either the blade loads limit or the transmission torque limit. Since the transmission for this vehicle is not yet designed, torque levels associated with the engine power levels have been used to provide a benchmark and to provide some insight as to the effect of transmission design criteria on the corridor width.

The loads limits are in the same general vicinity as the control and transmission limits and it seems likely that a control system can be found which will provide a corridor limited only by torque and control travel.

11.2 Transition - Sustained Turns

The data presented in Figures 11-21 to 11-83 was calculated in steady coordinated turns. Figures 11-21 to 11-27 are for a i_N of 90° at 40 knots. The control variations are normal and smooth and the maneuver capability at this condition is probably power limited, although the infinite life blade bending loads are exceeded at about 2g's with a forward CG (see Figure 11-27).

Similar data is shown in Figures 11-28 to 11-35 at $i_N = 90°$ and a velocity of 80 knots. The aft CG case is not limited up to a bank angle of 55° whereas in the forward CG case the turn is limited by fatigue blade loads at 12° bank. A better compromise between the elevator and cyclics to trim at this i_N should allow an expanded envelope at CG forward and restrict the aft CG case more until equal performance is achieved in both cases. This should also help the 1g envelope limits previously discussed. There is a small tendency to reverse the longitudinal stick travel at high Ø to hold the turn but it is less than 0.15" (0.381 cm). This reversal is probably due to the discontinuity in pitch damping from the rotors at this advance ratio. The model fidelity should be checked further in this area.

Figures 11-36 to 11-43 present the turn data for $i_N = 60°$ at 60 knots. The control positions and variations of thrust and power etc. are normal. For the aft CG case it is unlikely that rotor loads will be limiting until above Ø = 60° (2g's) whereas for the forward CG case the rotor loads become limiting at Ø = 15°.

A similar situation exists at 90 knots ($i_N = 60°$) where the aft CG case is not rotor loads limited (data Figures 11-44 to 11-47) until a bank angle of approximately 64° (2.28g's). The forward CG case is blade load limited at 31.5° bank or 1.73g's and the data is plotted in Figures 11-48 to 11-51. At 110 knots aft CG and 120 knots forward CG the data shows much the same trends, Figures 11-52 to 11-59.

Data for coordinated turns with $i_N = 30°$ are shown in Figures 11-60 to 11-83 at 110, 130 and 150 knots. At 110 knots the sustained turns are limited by fatigue blade loads to 1.86g's (aft CG) and 1.5g's (forward CG). At higher speeds rotor loads limits are higher than 2g's or a 60° banked turn.

NOTE: GW = 5896.7 Kg(13000 LB)
AFT CG
SL STD DAY
δ_F = 40°

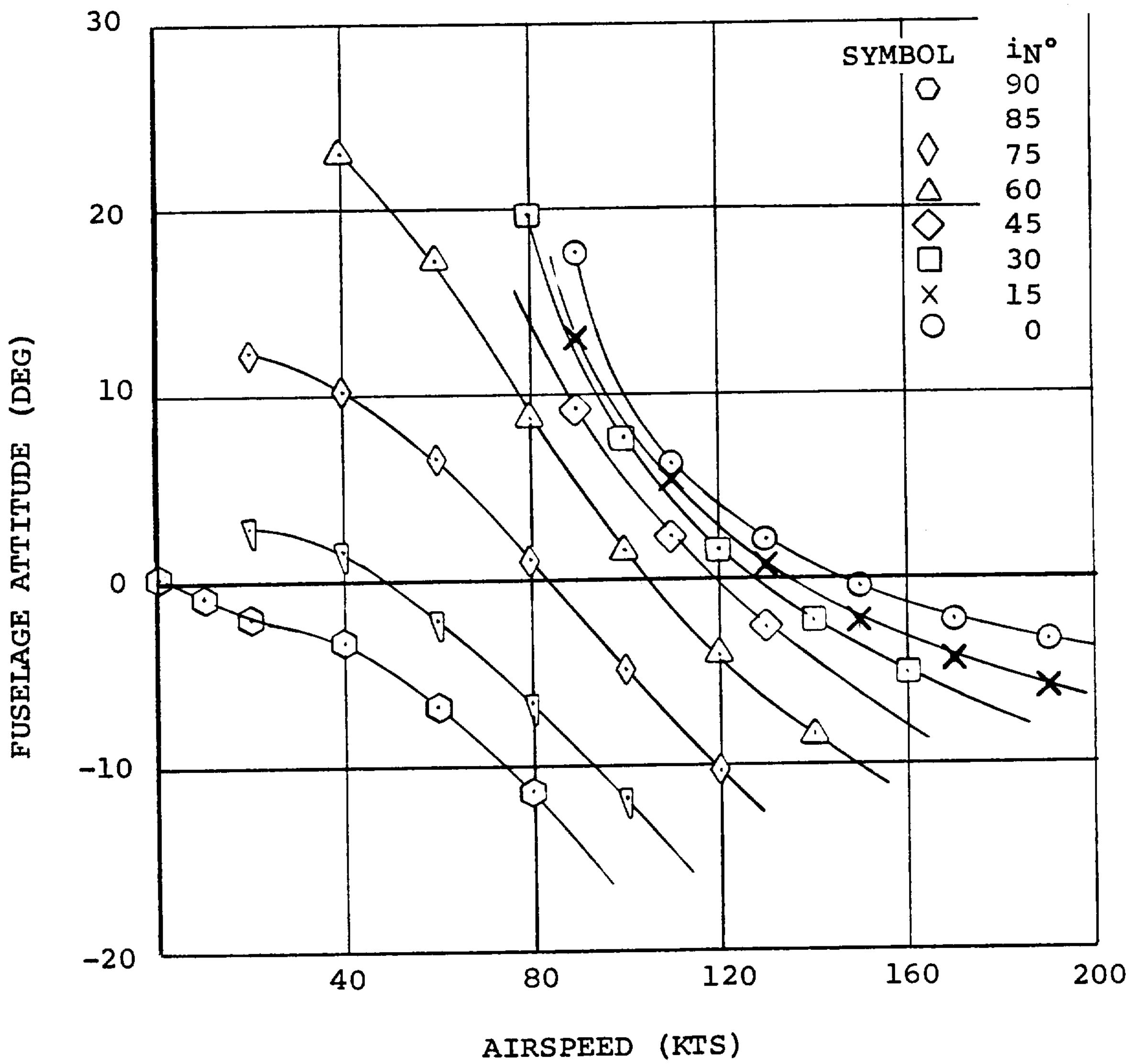

FIGURE 11.1.FUSELAGE ATTITUDE IN TRANSITION AFT CG

NOTE:
SEA LEVEL STD DAY
GW = 5896.7 Kg(13000 LB)
δ_F = 40°
FWD CG

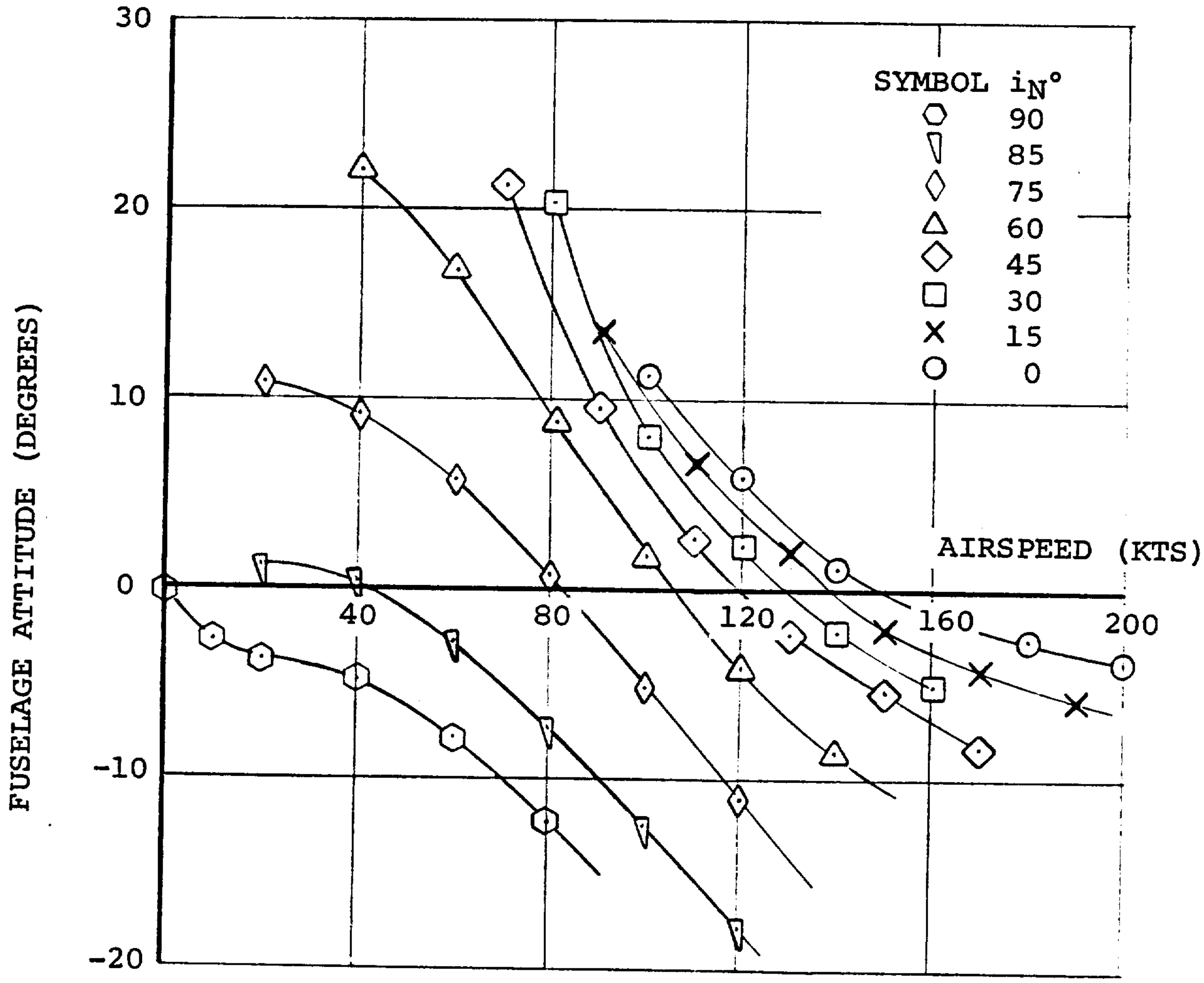

FIGURE 11.2. FUSELAGE ATTITUDE FOR TRANSITION TRIM
FWD CG, GW = 5896.7 Kg (13000 LB)

NOTE: GW = 5896.7 Kg (13000 LB)
AFT CG
SL STD DAY
δ_F = 40°

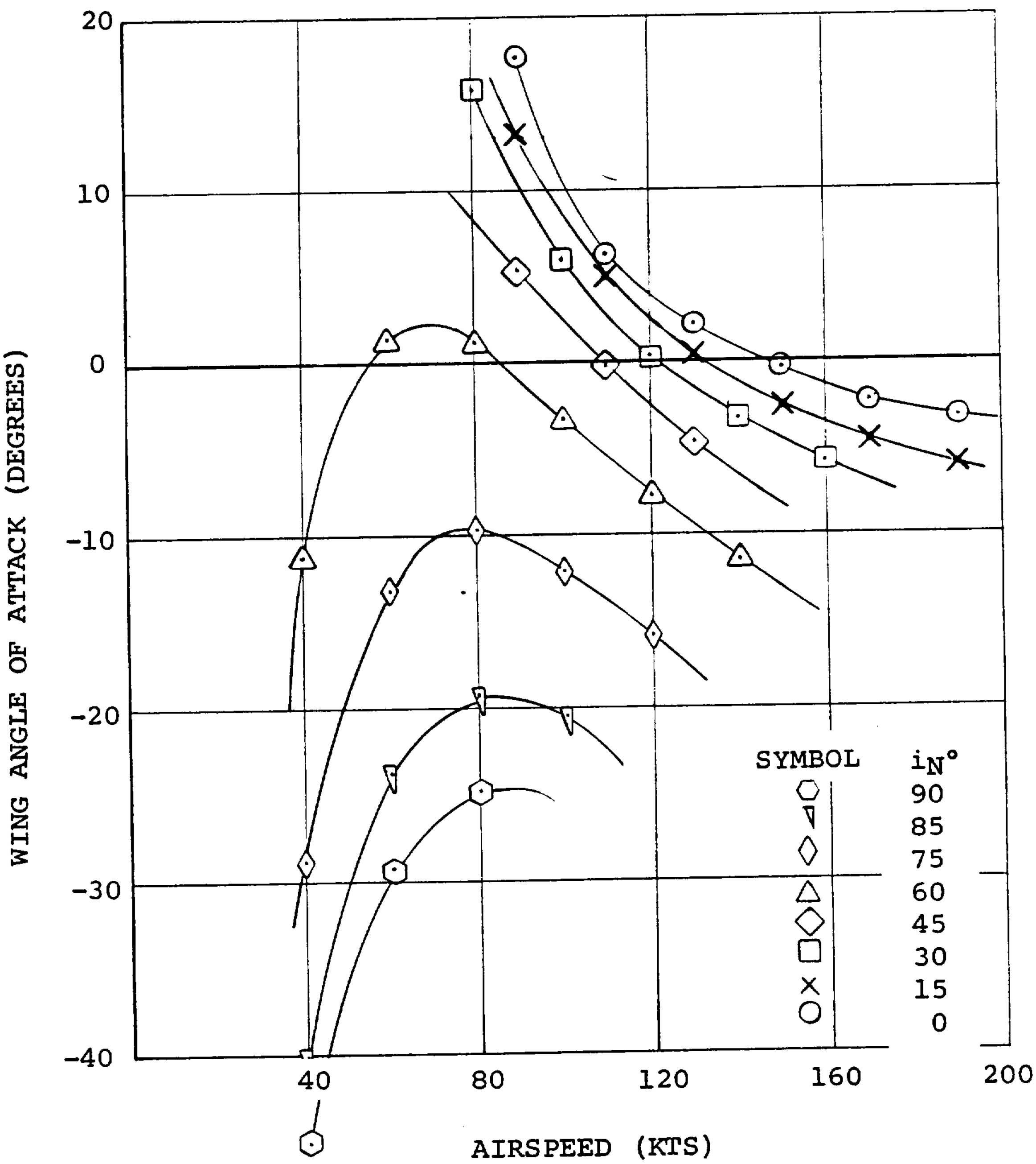

FIGURE 11.3. WING ANGLE OF ATTACK IN TRANSITION AFT CG

NOTE:
SEA LEVEL STD DAY
GW = 5896.7 Kg(13000 LB)
δ_F = 40°
FWD CG

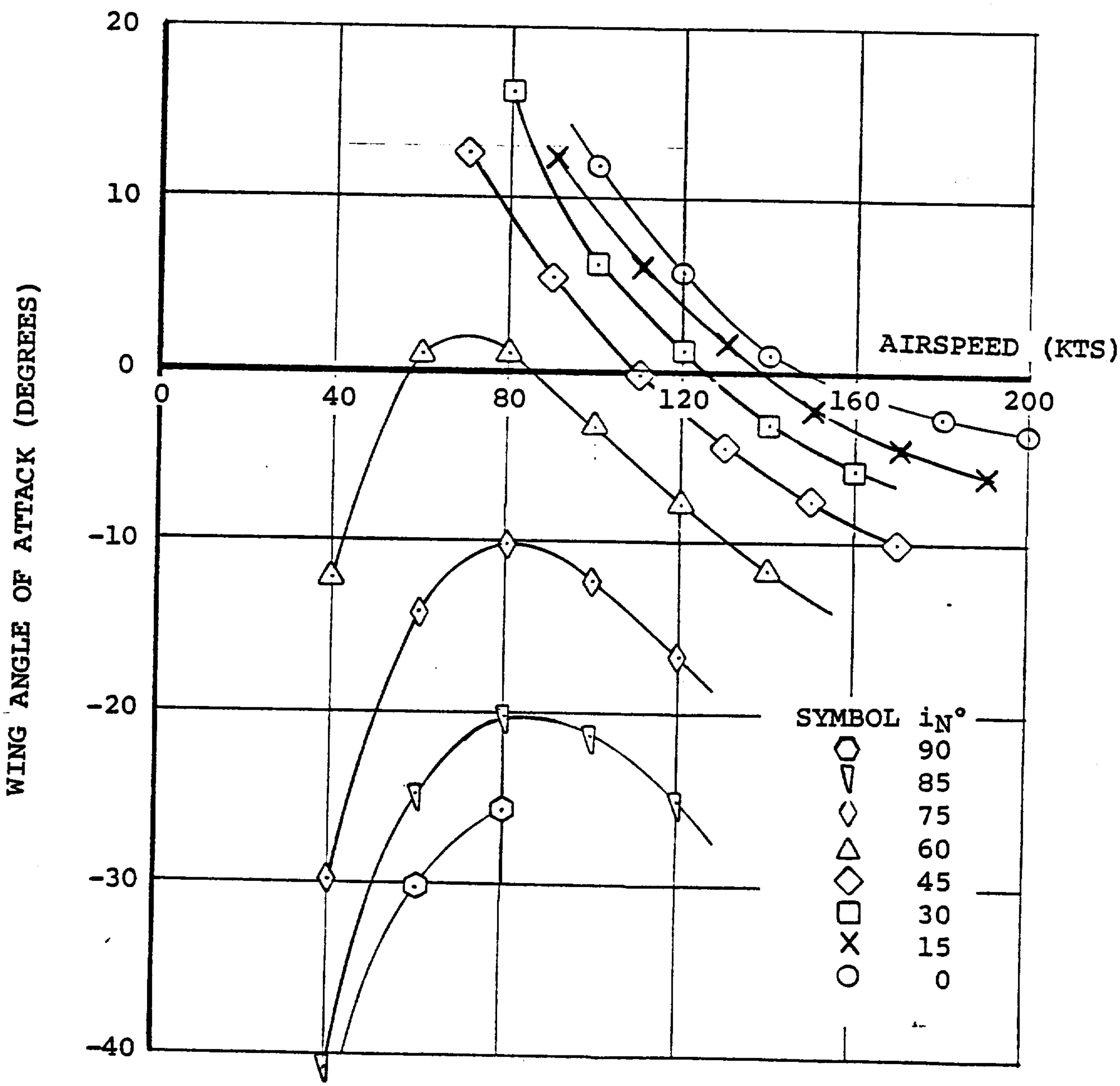

FIGURE 11.4. WING INCIDENCE IN TRANSITION FWD CG
GW = 5896.7 Kg (13000 LB) δ_F = 40°

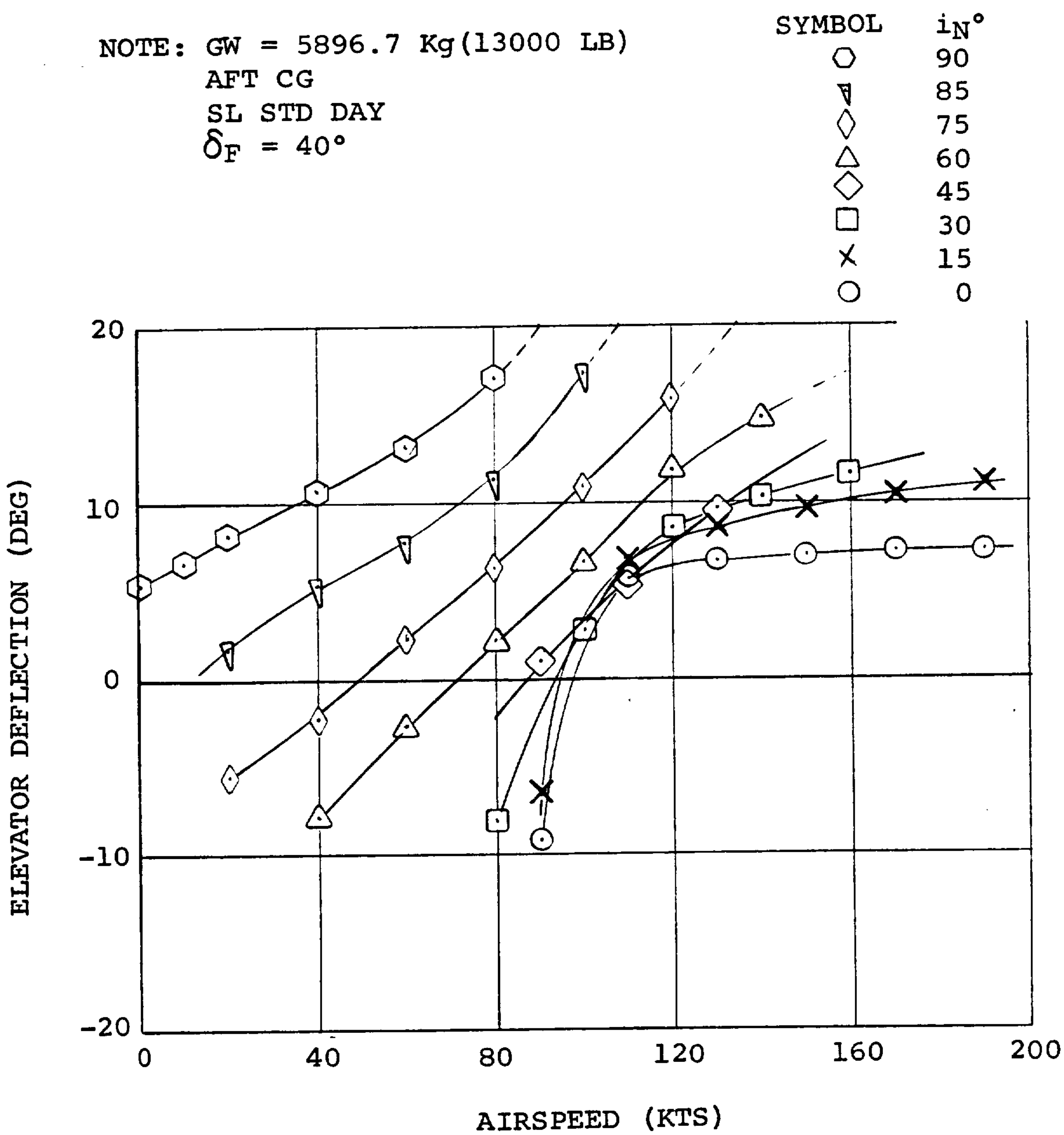

FIGURE 11.5.ELEVATOR DEFLECTION IN TRANSITION AFT CG

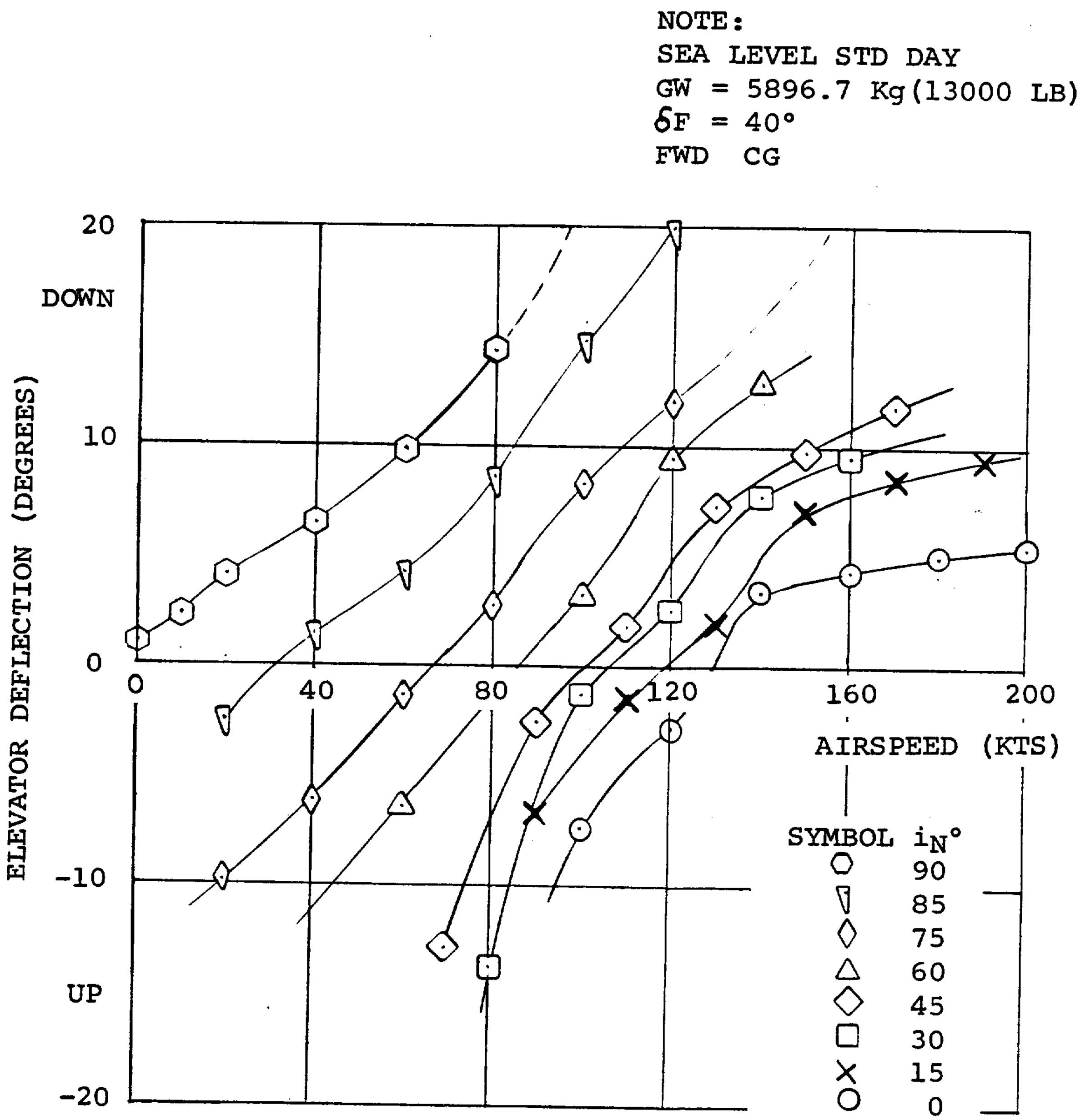

FIGURE 11.6. ELEVATOR DEFLECTION IN TRANSITION FWD CG
GW = 5896.7 Kg (13000 LB) SEA LEVEL STD DAY

NOTE: GW = 5896.7 Kg (13000 LB)
AFT CG
SL STD DAY
$\delta_F = 40°$

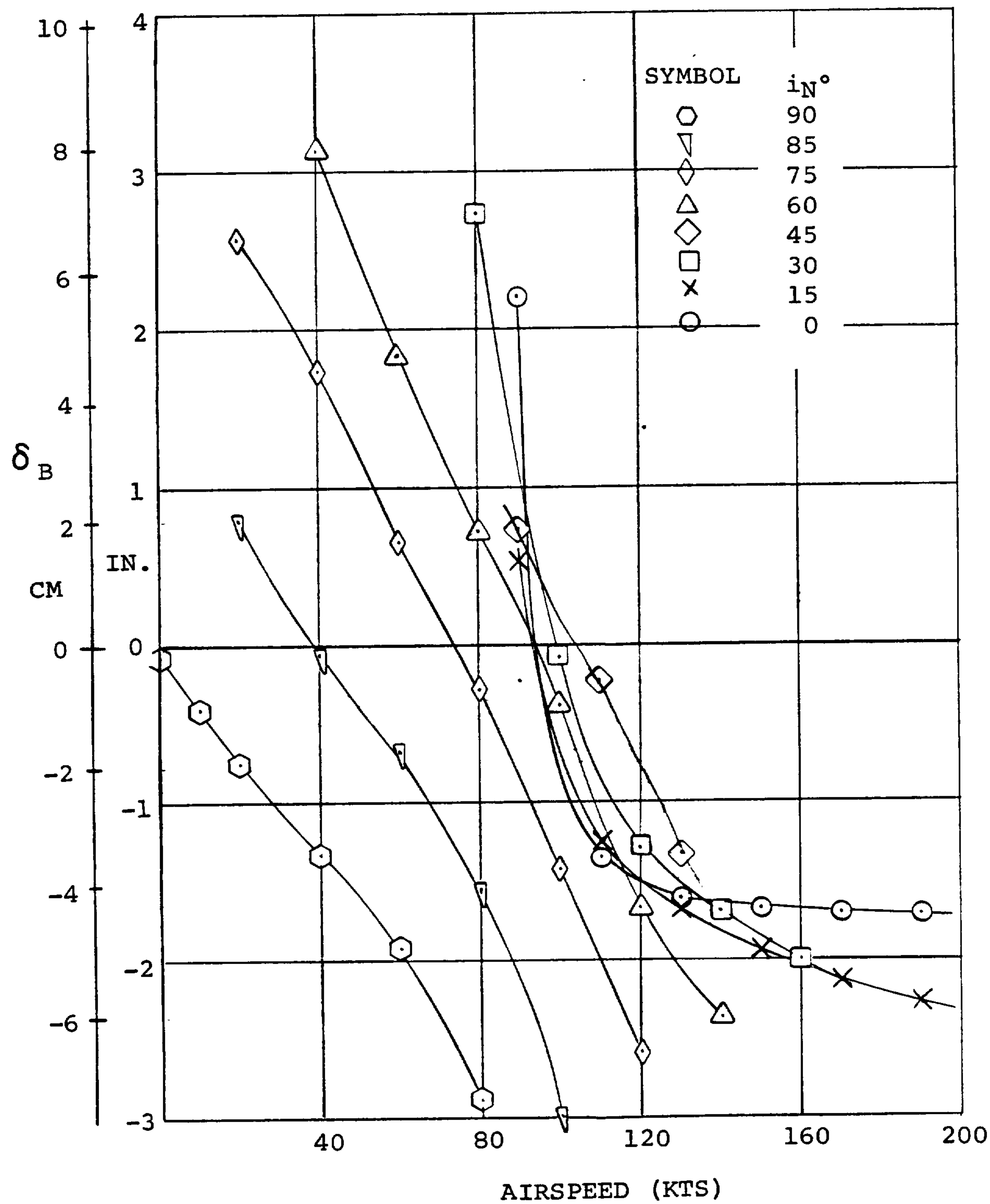

FIGURE 11.7. LONGITUDINAL STICK POSITION IN TRANSITION AFT CG

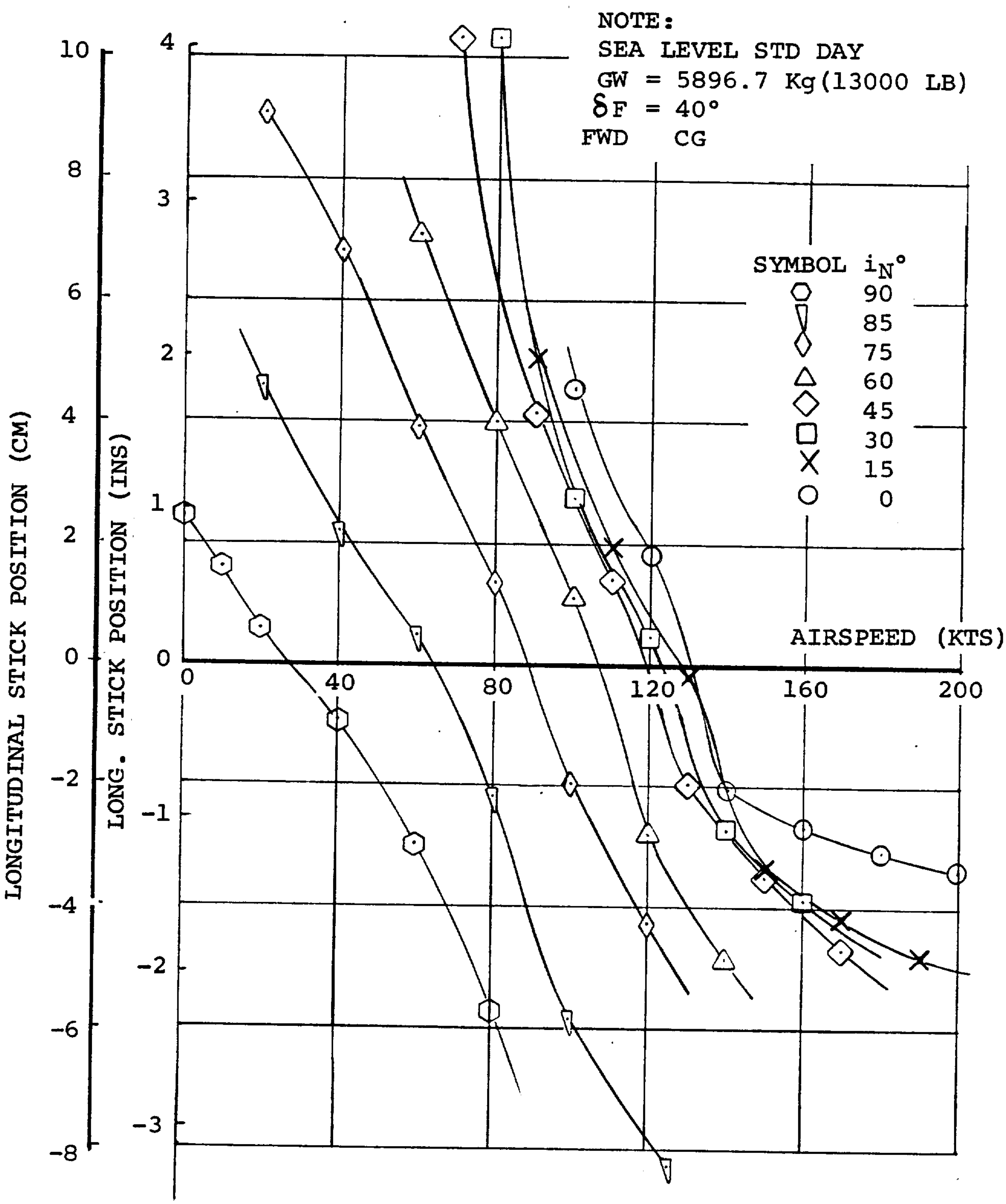

FIGURE 11.8.LONGITUDINAL STICK POSITION FOR TRIM IN TRANSITION FWD CG. GW = 5896.7 Kg (13000 LB)

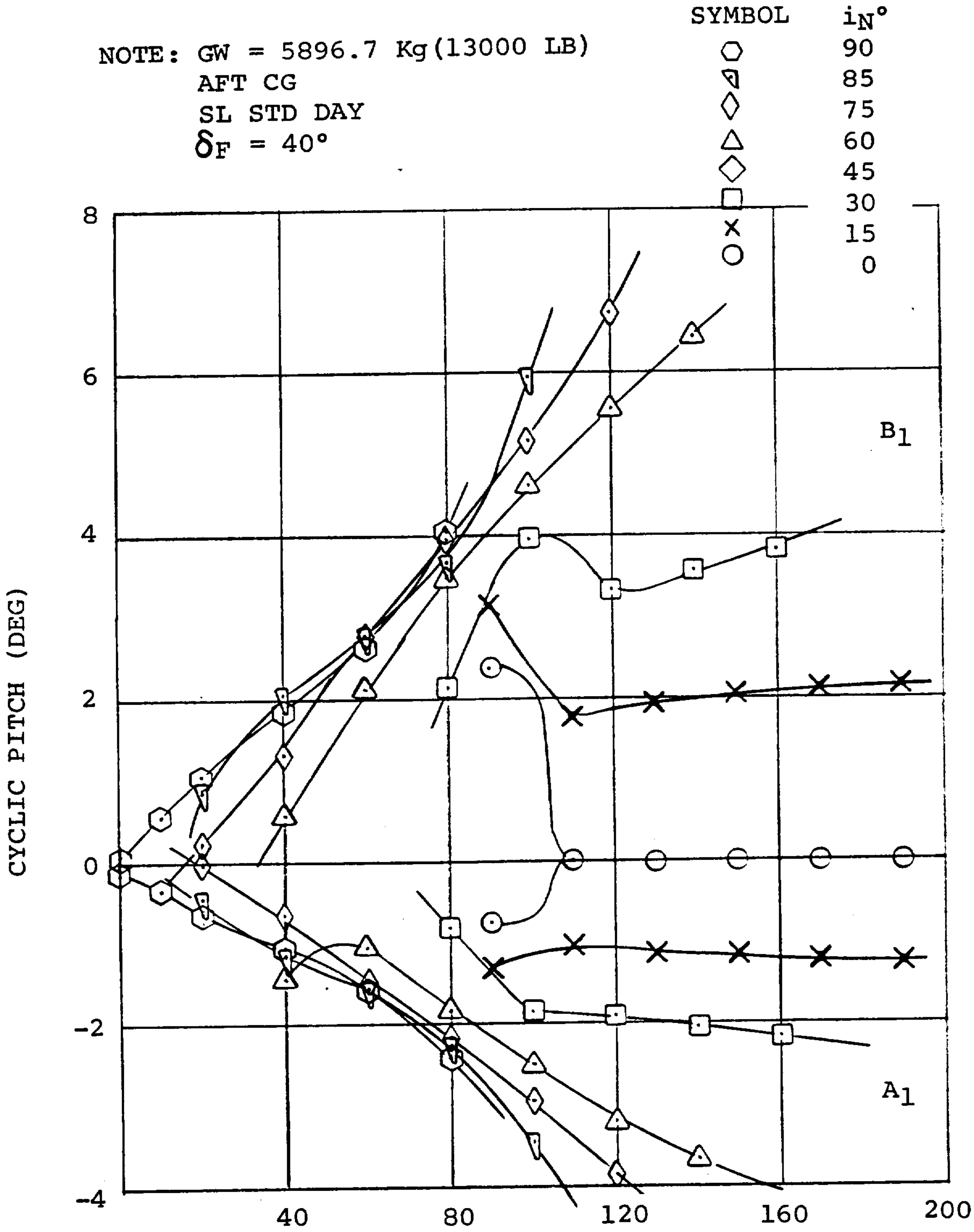

FIGURE 11.9. CYCLIC PITCH TO TRIM IN TRANSITION AFT CG

NOTE:
SEA LEVEL STD DAY
GW = 5896.7 Kg (13000 LB)
δ_F = 40°
FWD CG

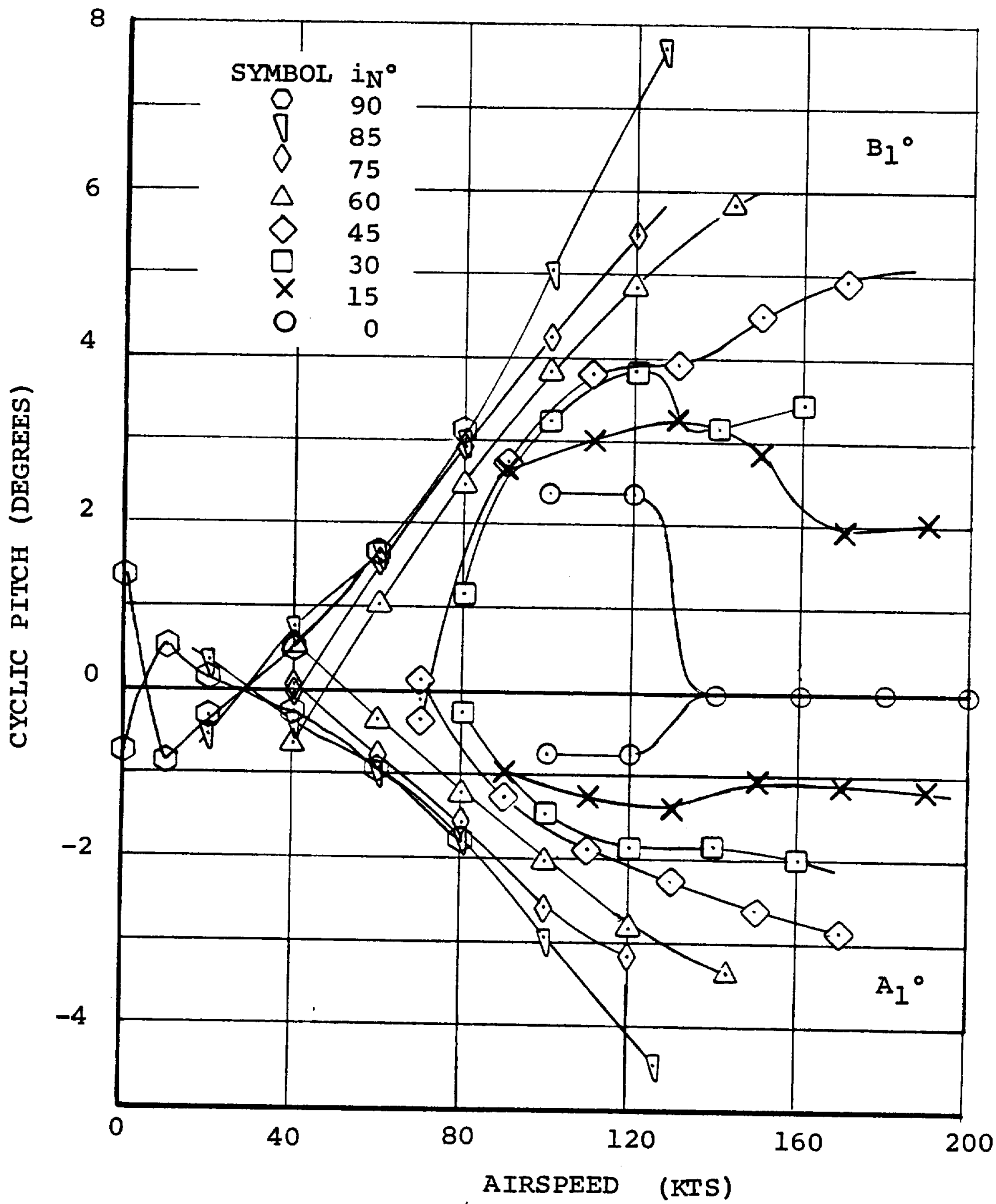

FIGURE 11.10 CYCLIC PITCH TO TRIM IN TRANSITION FWD CG
GW = 5896.7 Kg (13000 LB) SEA LEVEL STD DAY

NOTE: GW = 5896.7 Kg (13000 LB)
AFT CG
SL STD DAY
$\delta_F = 40°$

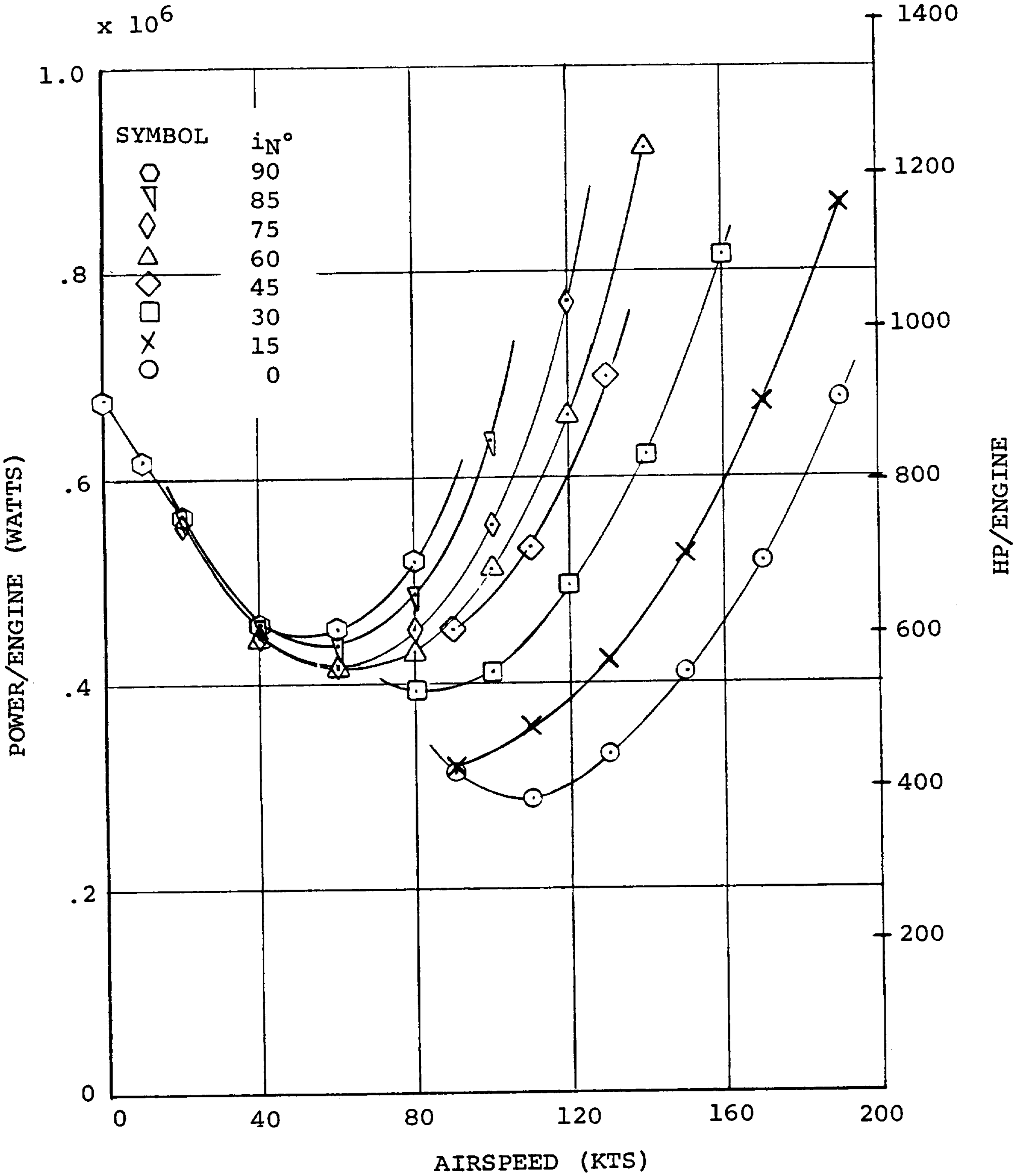

FIGURE 11.11 POWER REQUIRED IN TRANSITION AFT CG

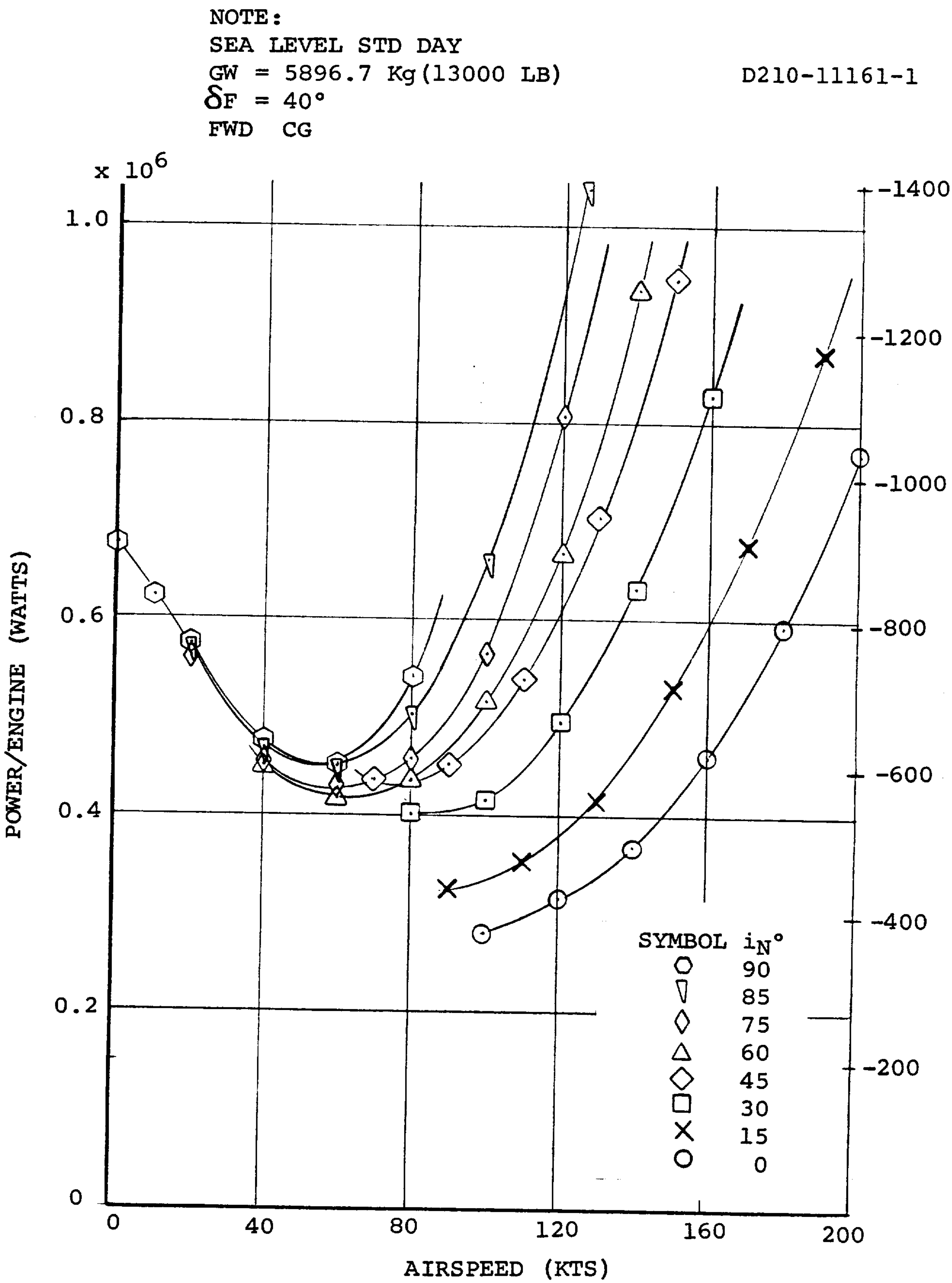

FIGURE 11.12 POWER REQUIRED IN TRANSITION FWD CG
SEA LEVEL STD DAY GW = 5896.7 Kg (13000 LB)

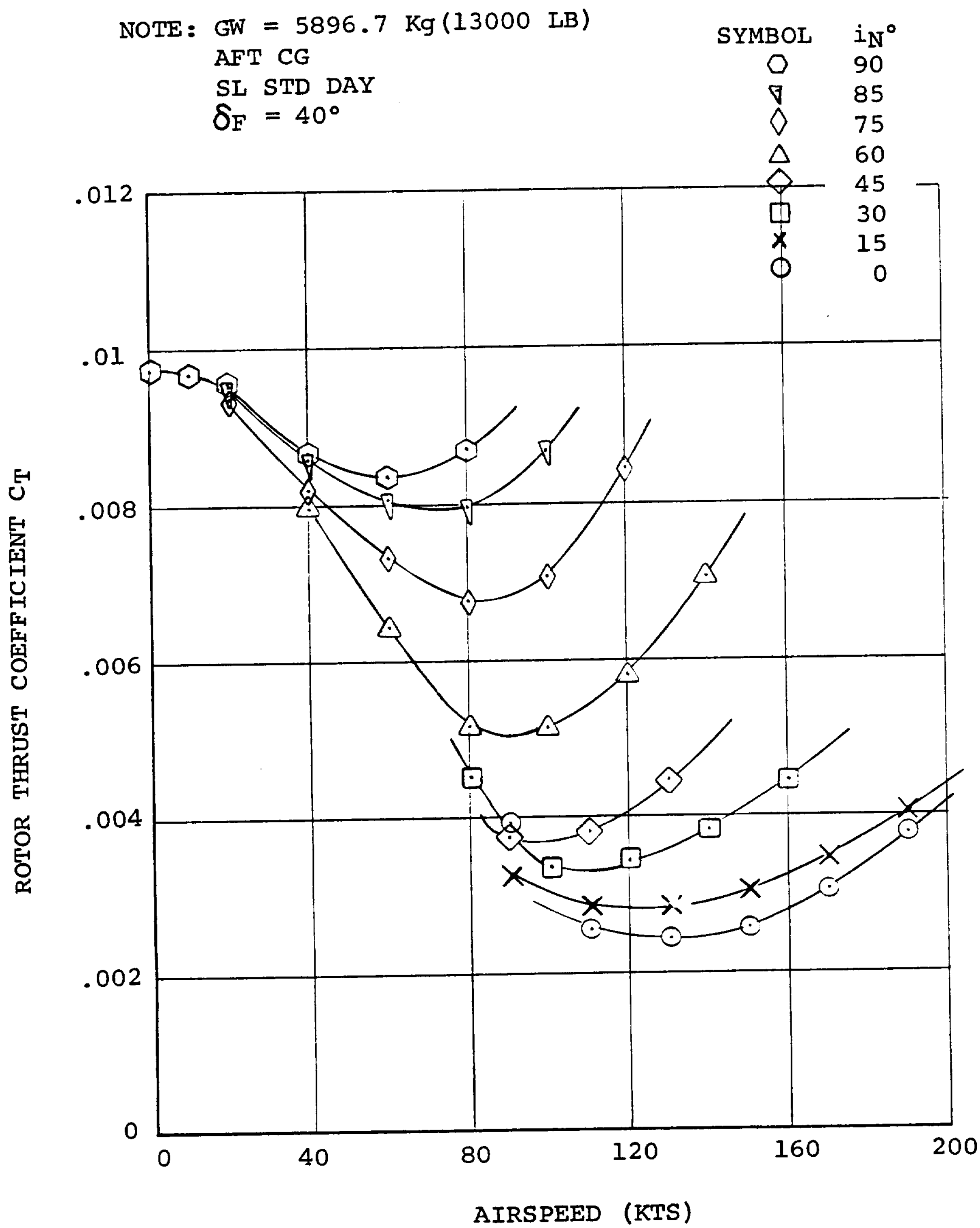

FIGURE 11.13 ROTOR THRUST COEFFICIENT IN TRANSITION AFT CG

NOTE:
SEA LEVEL STD DAY
GW = 5896.7 Kg(13000 LB)
δ_F = 40°
FWD CG

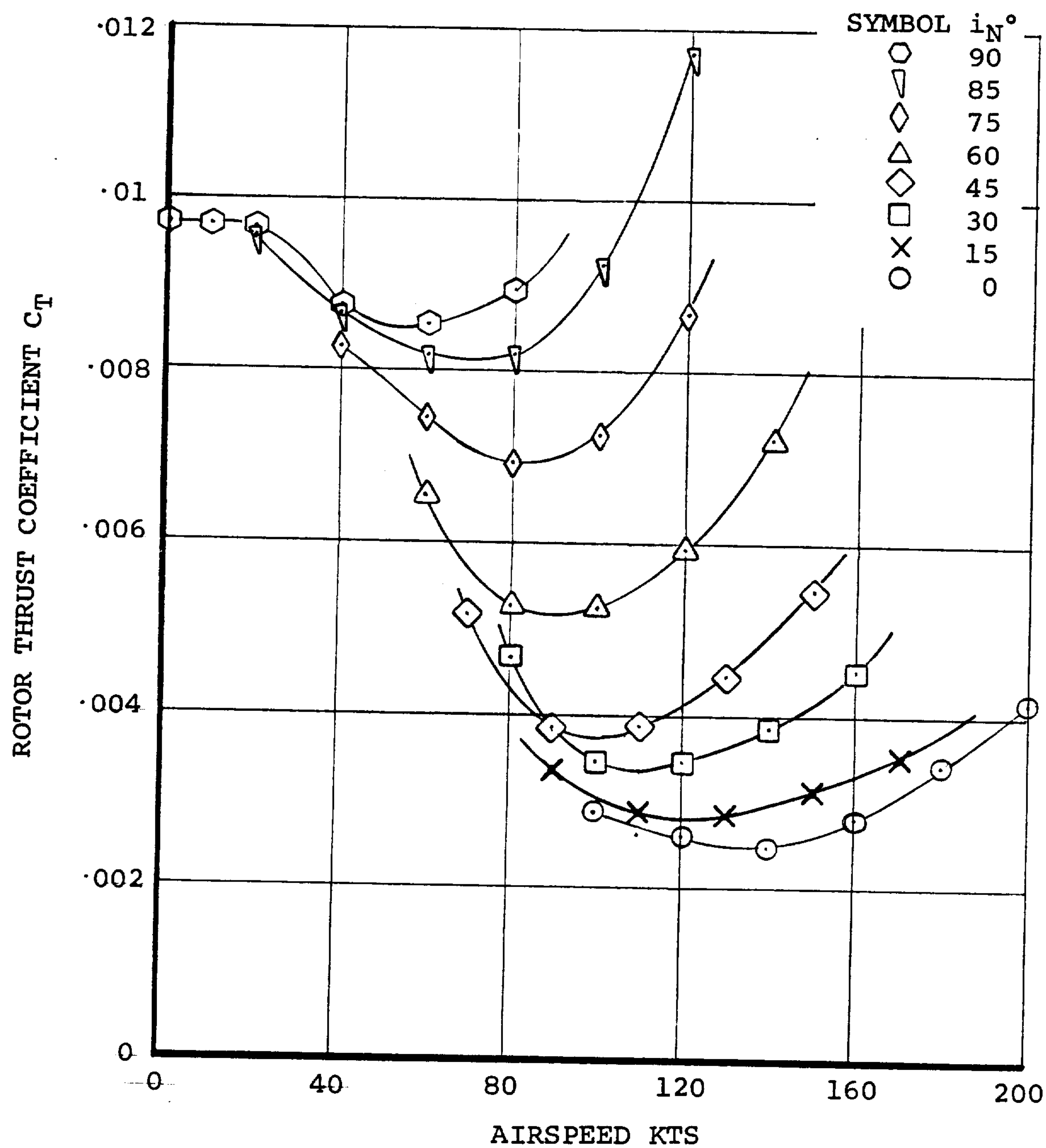

FIGURE 11.14 ROTOR THRUST COEFFICIENT IN TRANSITION
GW = 5896.7 Kg (13000 LB) FWD CG, SEA LEVEL, STD DAY

NOTE: GW = 5896.7 Kg (13000 LB)
AFT CG
SL STD DAY
δ_F = 40°

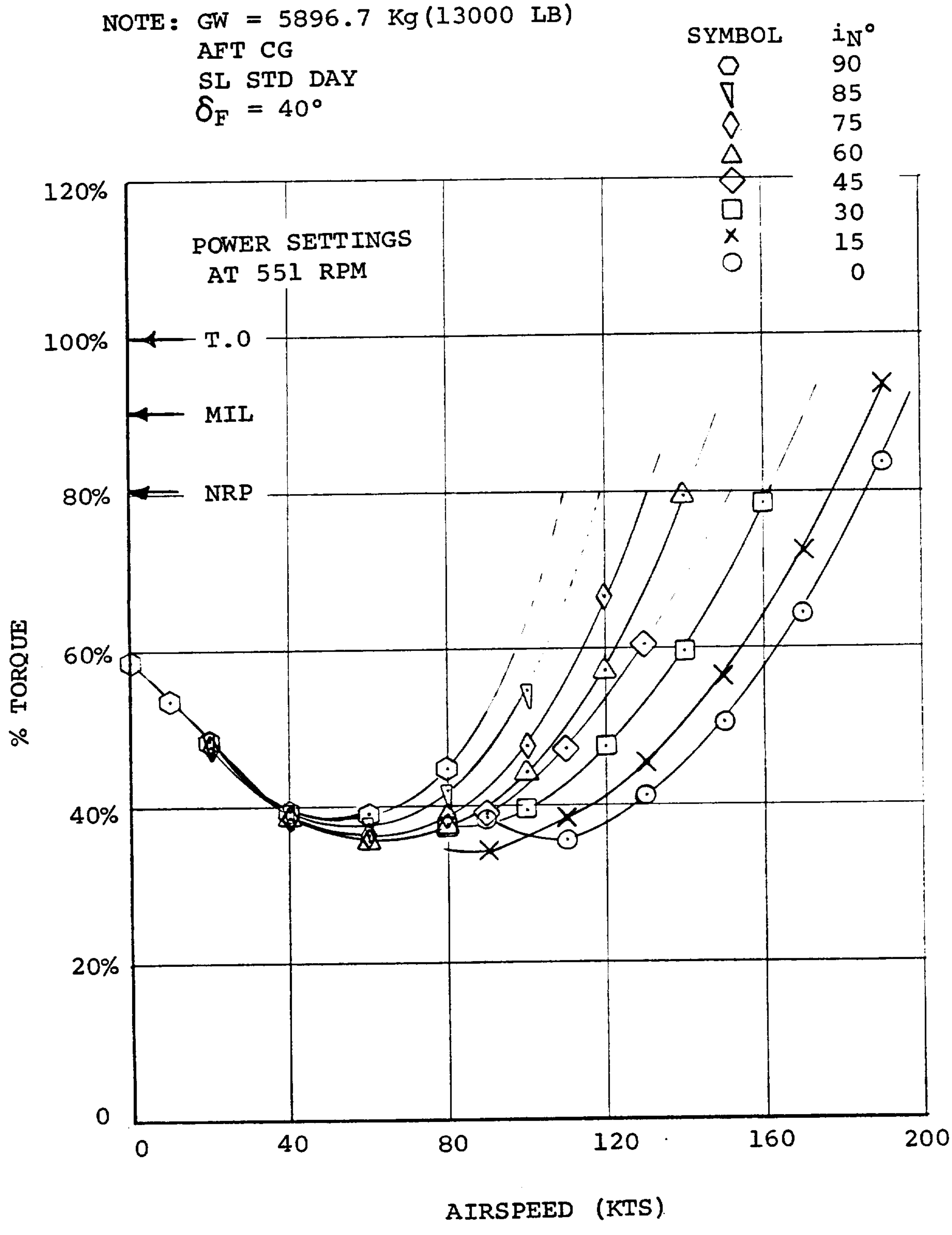

FIGURE 11.15 TORQUE VARIATION IN TRANSITION AFT CG

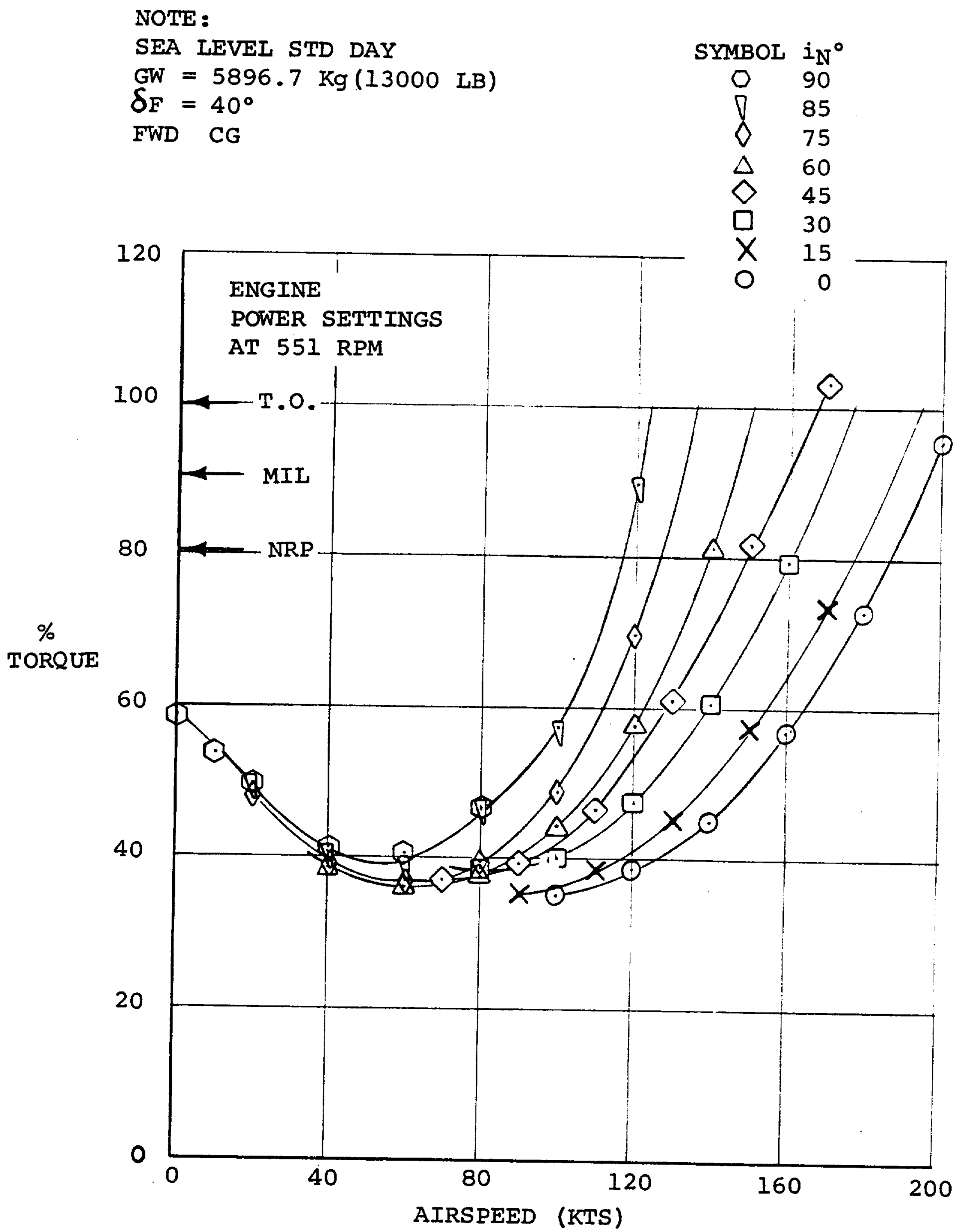

FIGURE 11.16 TORQUE VARIATION IN TRANSITION FWD CG
GW = 5896.7 Kg (13000 LB) SEA LEVEL STD DAY

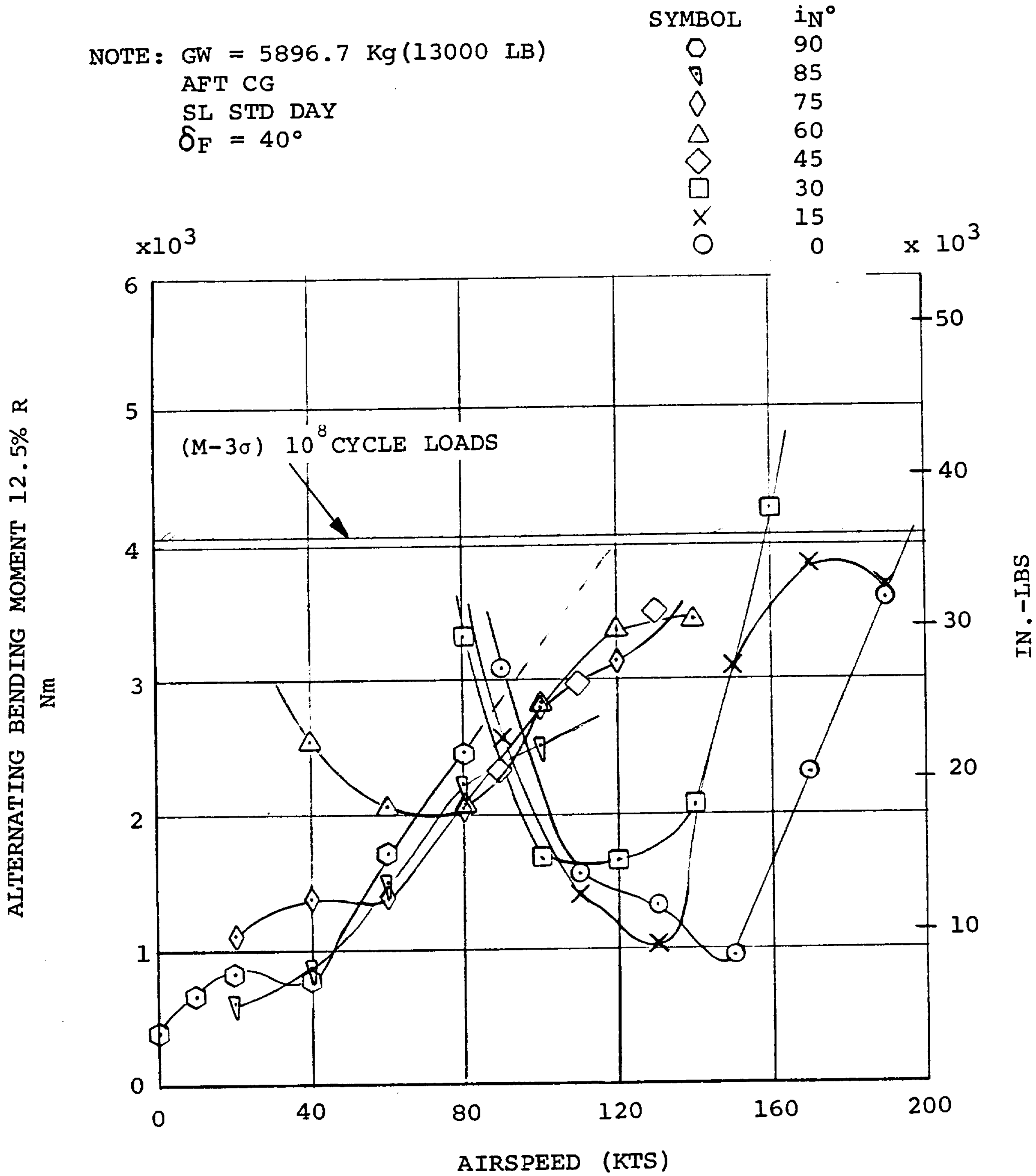

FIGURE 11.17. ESTIMATED BLADE BENDING LOADS IN TRANSITION AFT CG

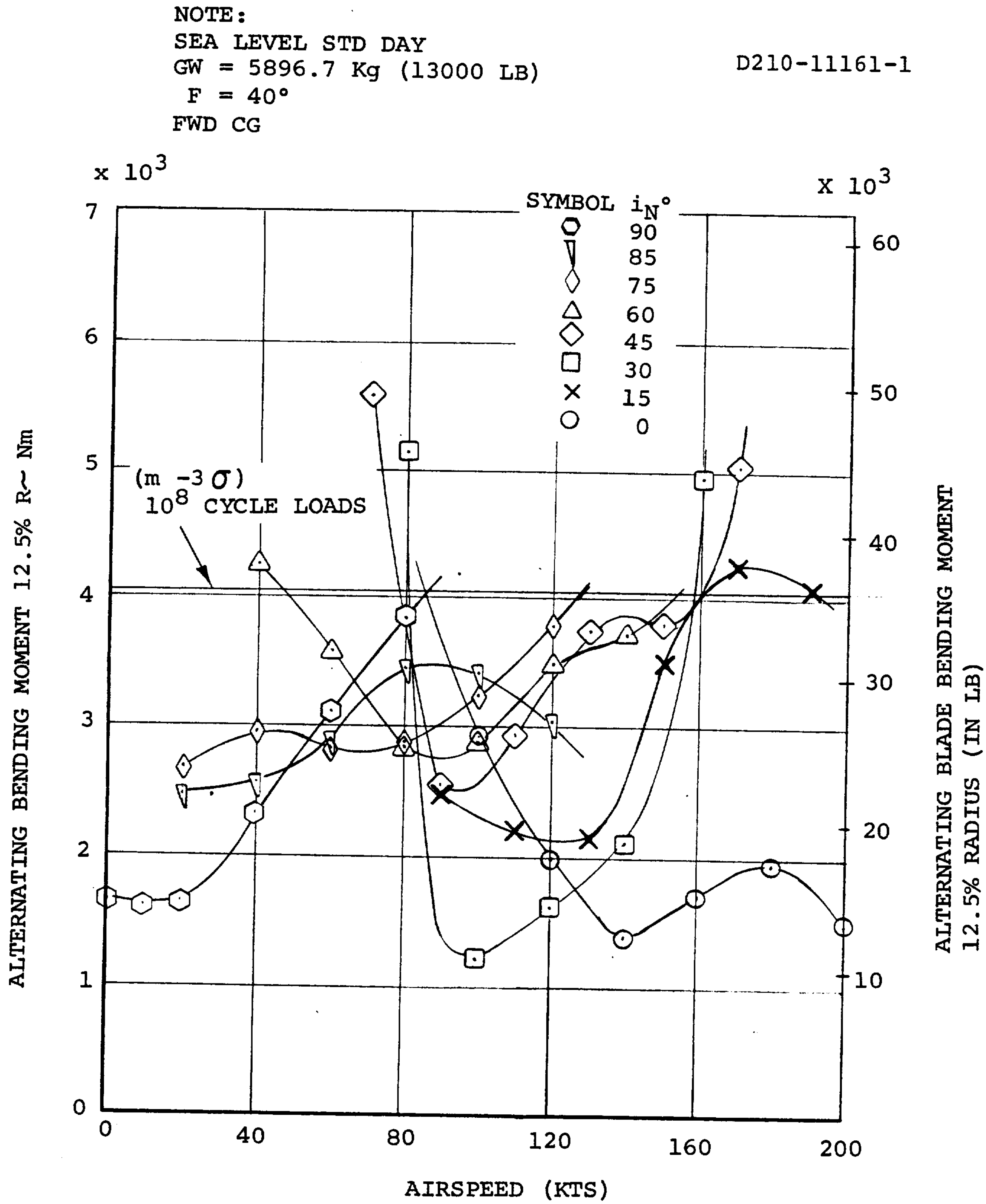

FIGURE 11.18. ESTIMATED BLADE BENDING LOADS IN TRANSITION FWD CG
GW = 5896.7 Kg (13000 LB) SEA LEVEL STD DAY

NOTE: GW = 5896.7 Kg (13000 LB)
AFT CG
SL STD DAY
$\delta_F = 40°$

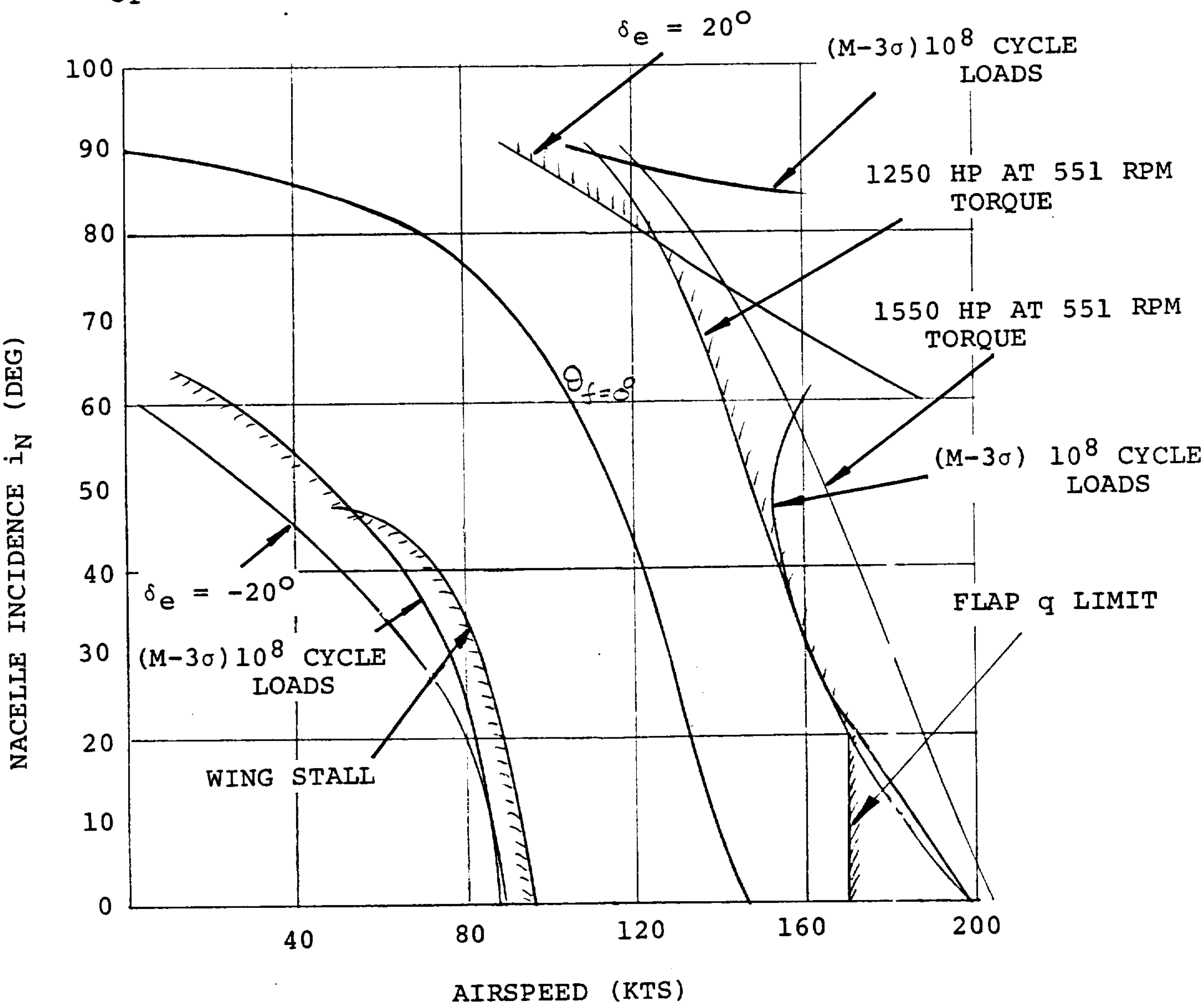

FIGURE 11.19 AFT CG - TRANSITION CORRIDOR

NOTE:
SEA LEVEL STD DAY
GW = 5896.7 Kg (13000 LB)
$\delta F = 40°$
FWD CG

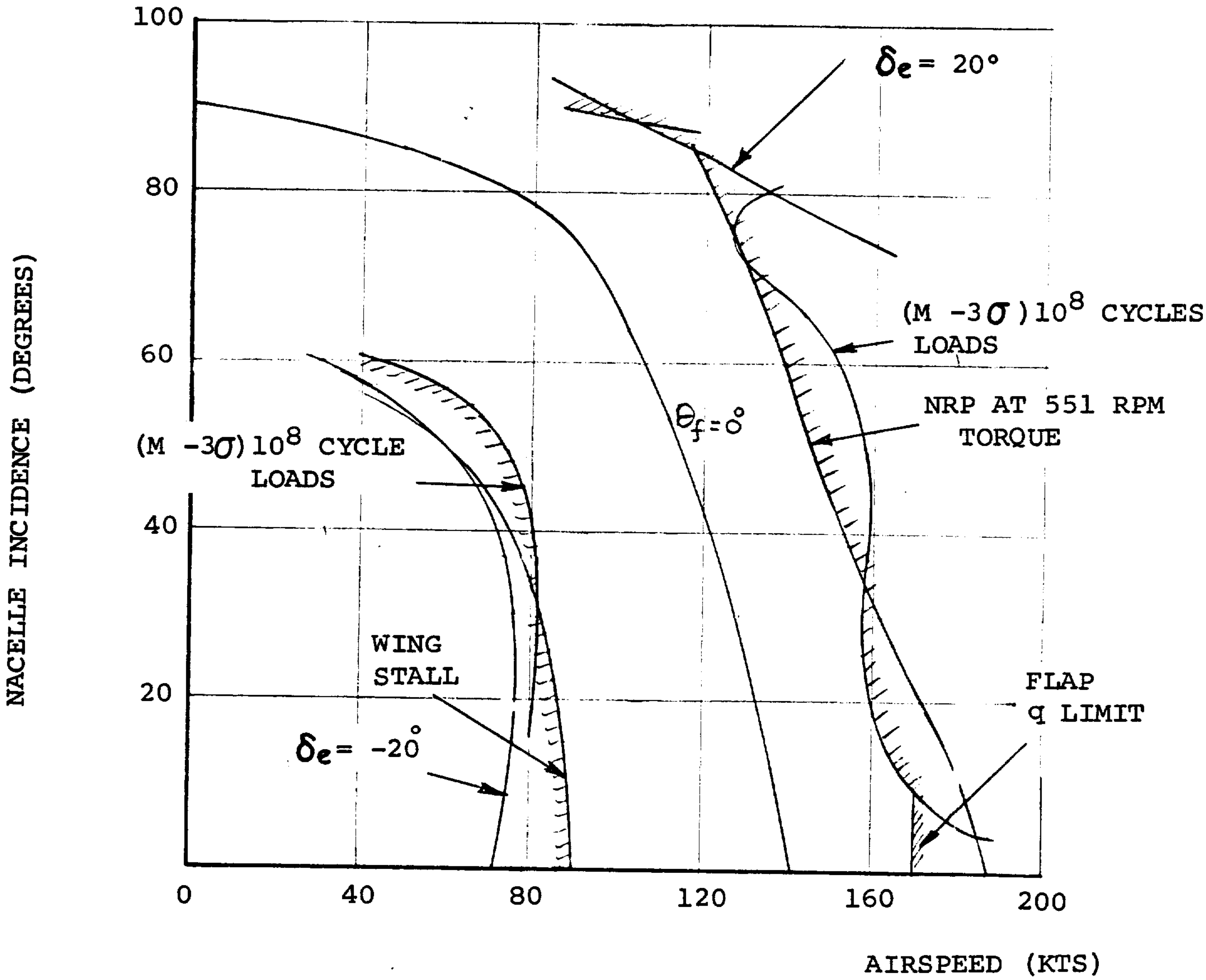

FIGURE 11.20. FWD CG TRANSITION CORRIDOR GW = 5896.7 Kg (13000 LB)
GW = 5896.7 Kg (13000 LB) SEA LEVEL STD DAY

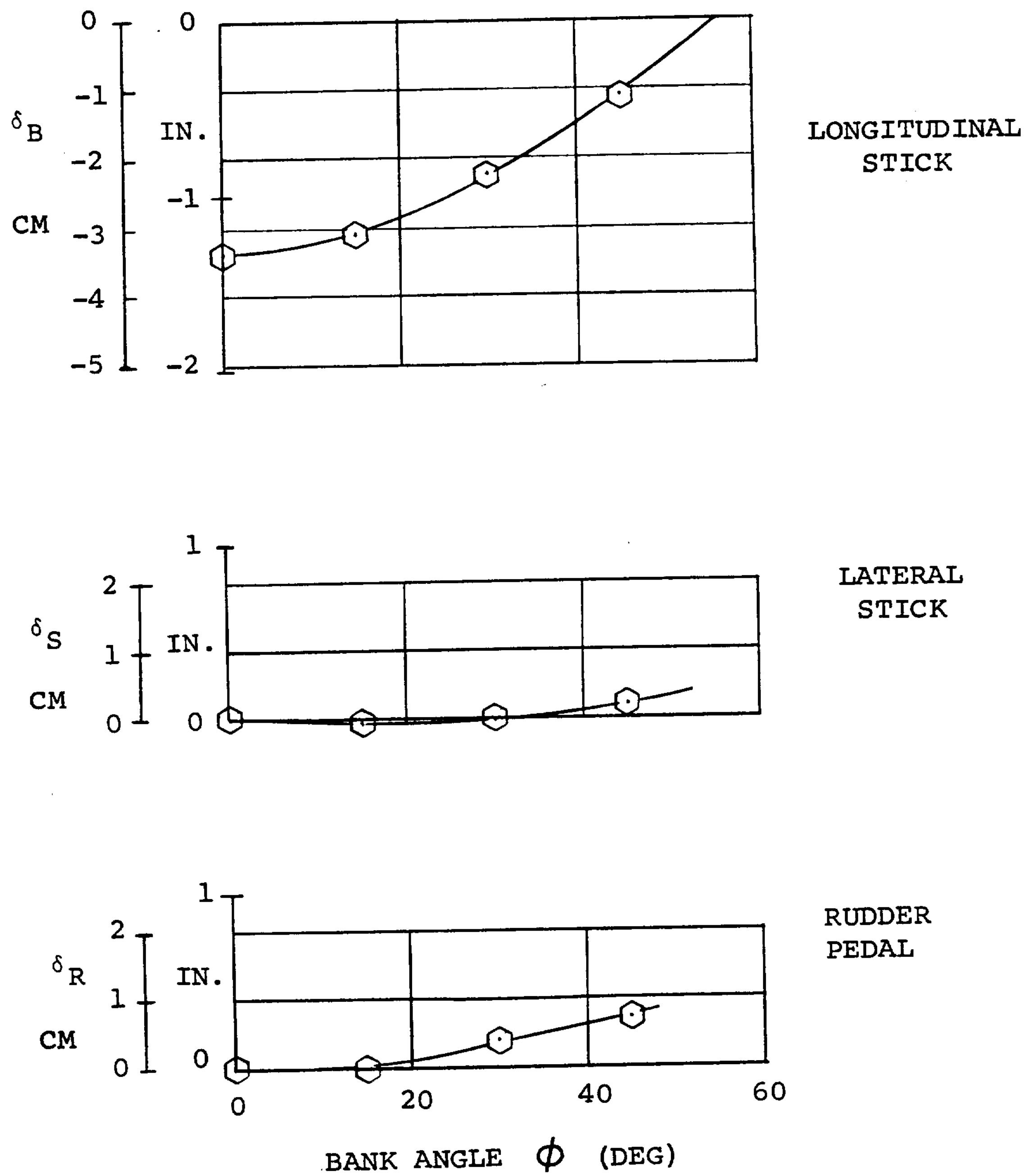

FIGURE 11.21 CONTROL POSITIONS IN COORDINATED TURNS IN TRANSITION AFT CG V = 40 KTS. $i_N = 90°$ GW = 5896.7 Kg (13000 LB) SL STD DAY $\delta_F = 40°$

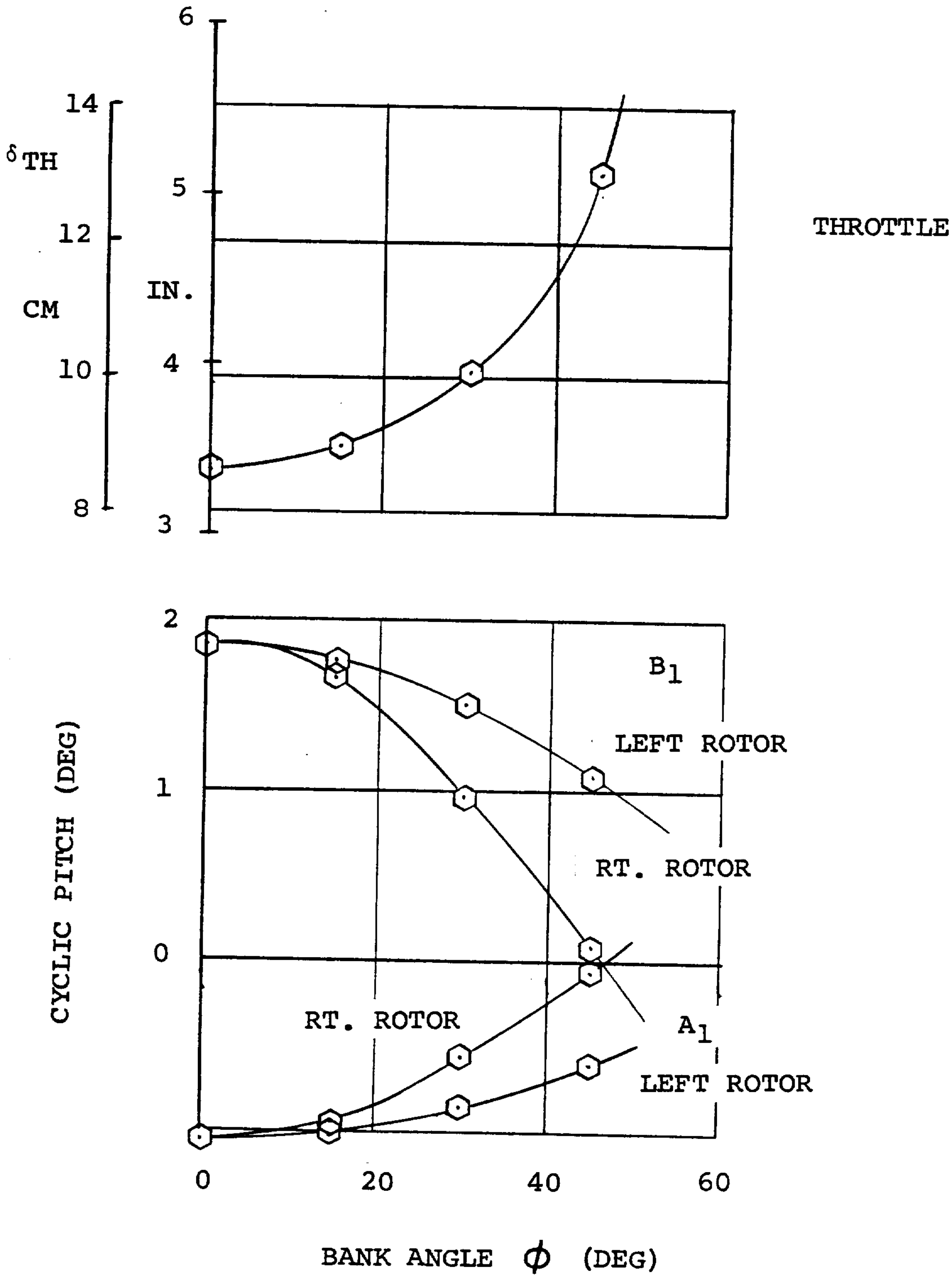

FIGURE 11.22 CONTROL DATA IN COORDINATED TURNS IN TRANSITION
AFT CG $i_N = 90°$ $V = 40$ KTS $\delta_F = 40°$
GW = 5896.7 Kg (13000 LBS) SL STD DAY

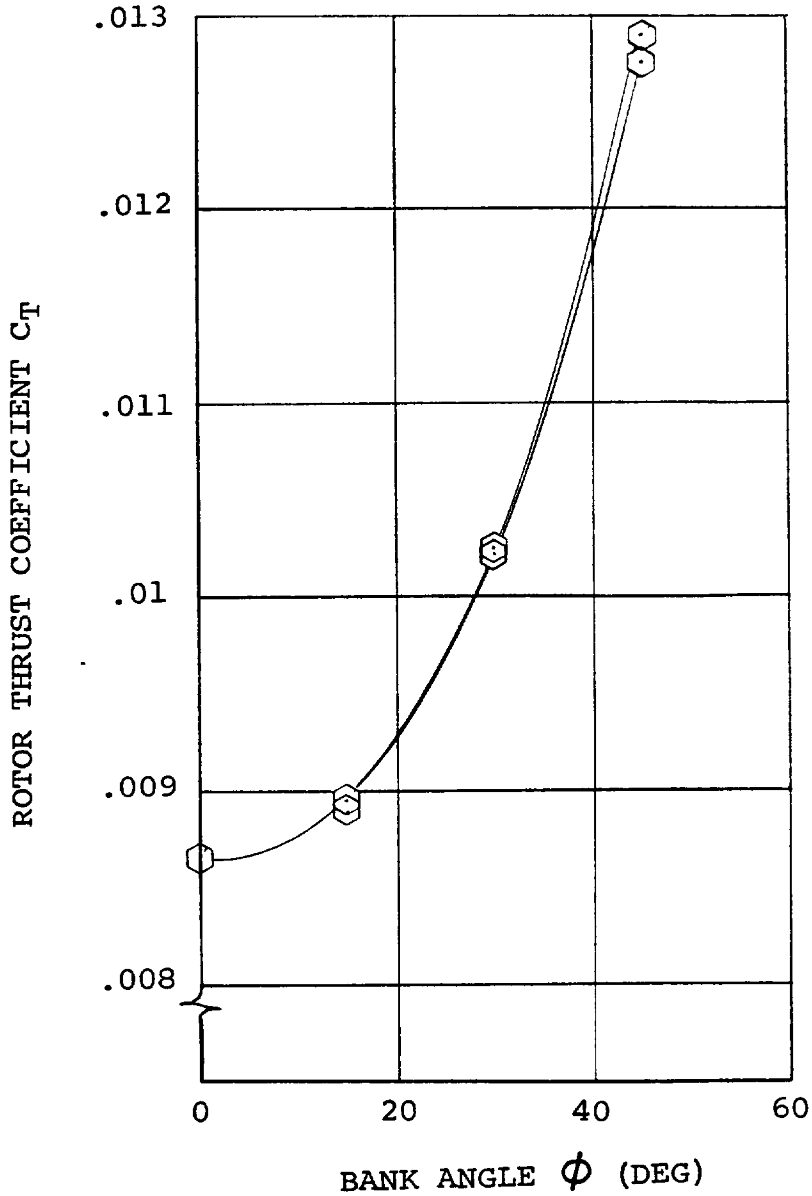

FIGURE 11.23. ROTOR THRUST IN COORDINATED TURNS IN TRANSITION
$i_N = 90°$ V = 40 KTS $\delta_F = 40°$ AFT CG
GW = 5896.7 Kg (13000 LB) SL STD DAY

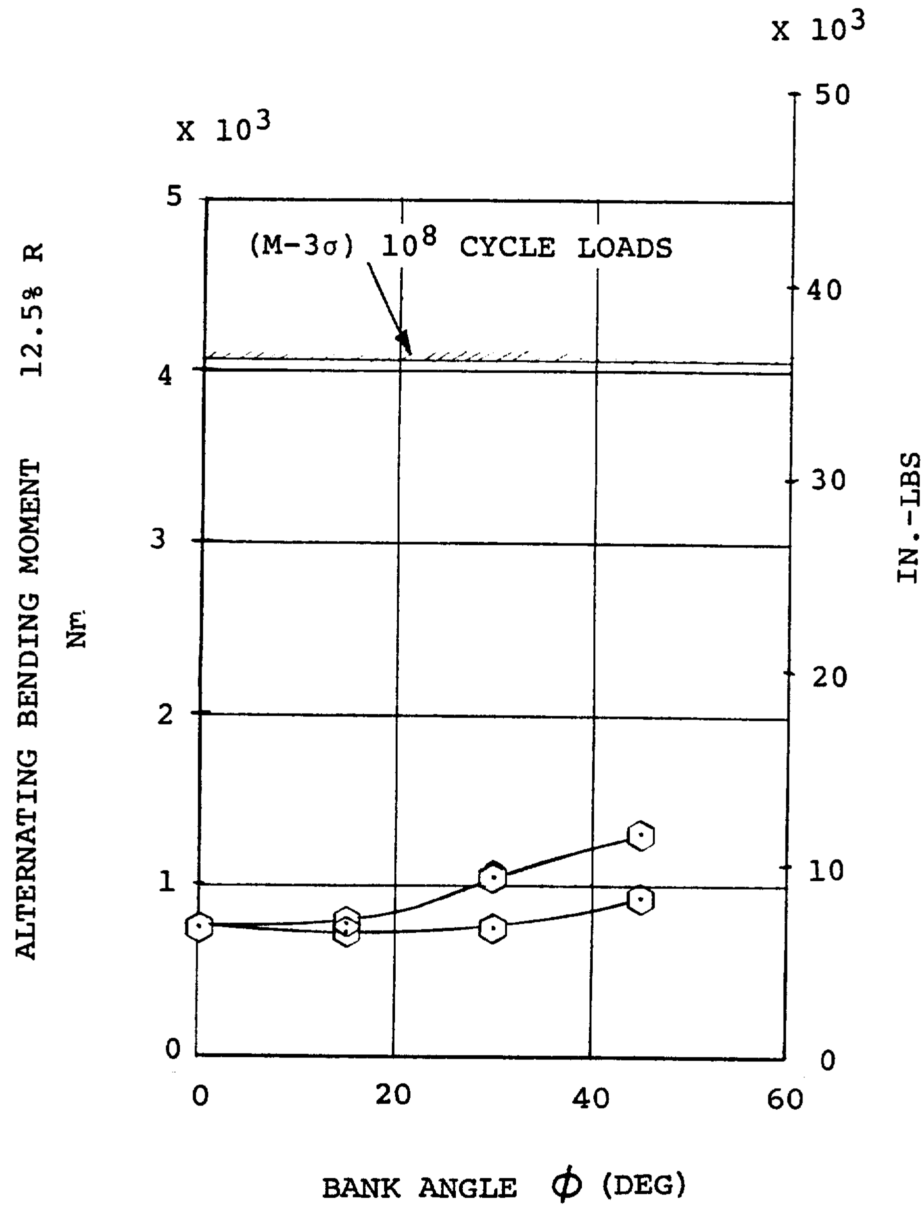

FIGURE 11.24. ESTIMATED BLADE BENDING LOADS 12.5% IN COORDINATED TURNS IN TRANSITION AFT CG $i_N = 90°$ V = 40 KTS $\delta_F = 40°$ GW = 5896.7 Kg (13000 LB) SL STD DAY

NOTE: TRANSITION COORDINATED TURNS $i_N = 90°$
40 KTS GW = 5896.7 Kg (13000 LBS)
SL STD $\delta_F = 40°$

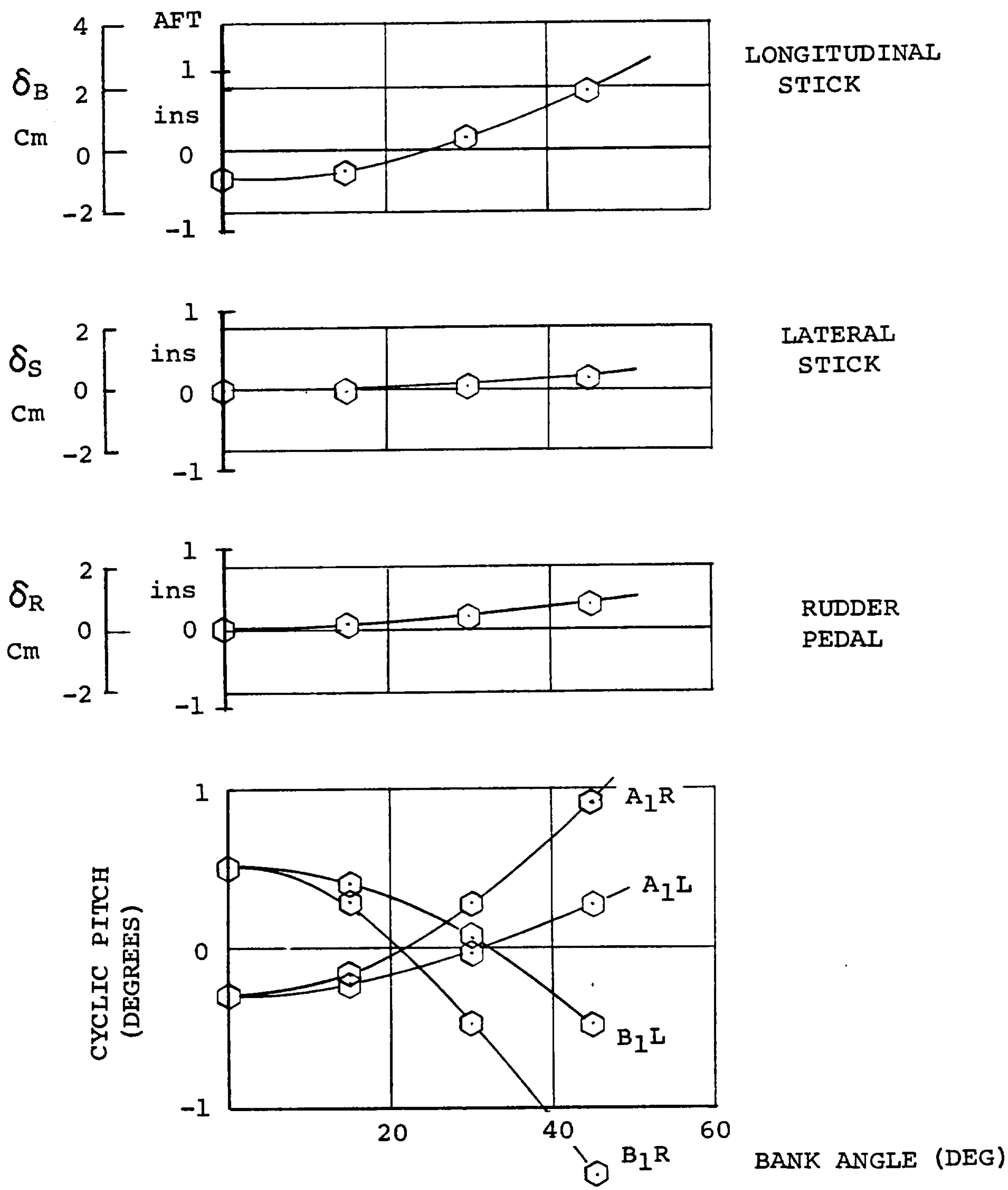

FIGURE 11.25. TRANSITION COORDINATED TURNS CONTROL DATA
$i_N = 90°$ V = 40 KTS

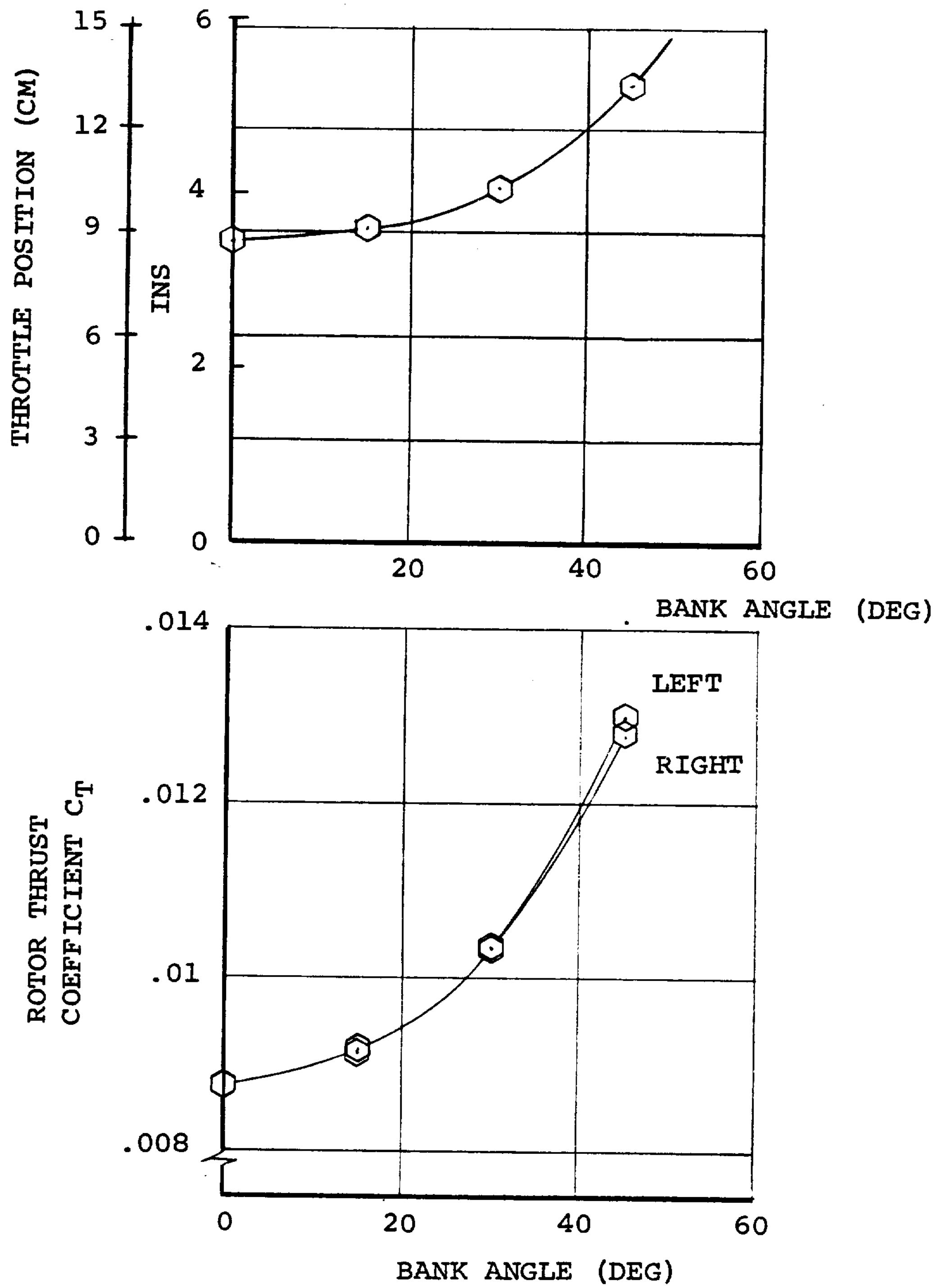

FIGURE 11.26. COORDINATED TURNS IN TRANSITION FWD CG
GW = 5896.7 Kg (13000 LBS) SL STD DAY
$\delta_F = 40°$, $i_N = 90°$ V = 40 KTS

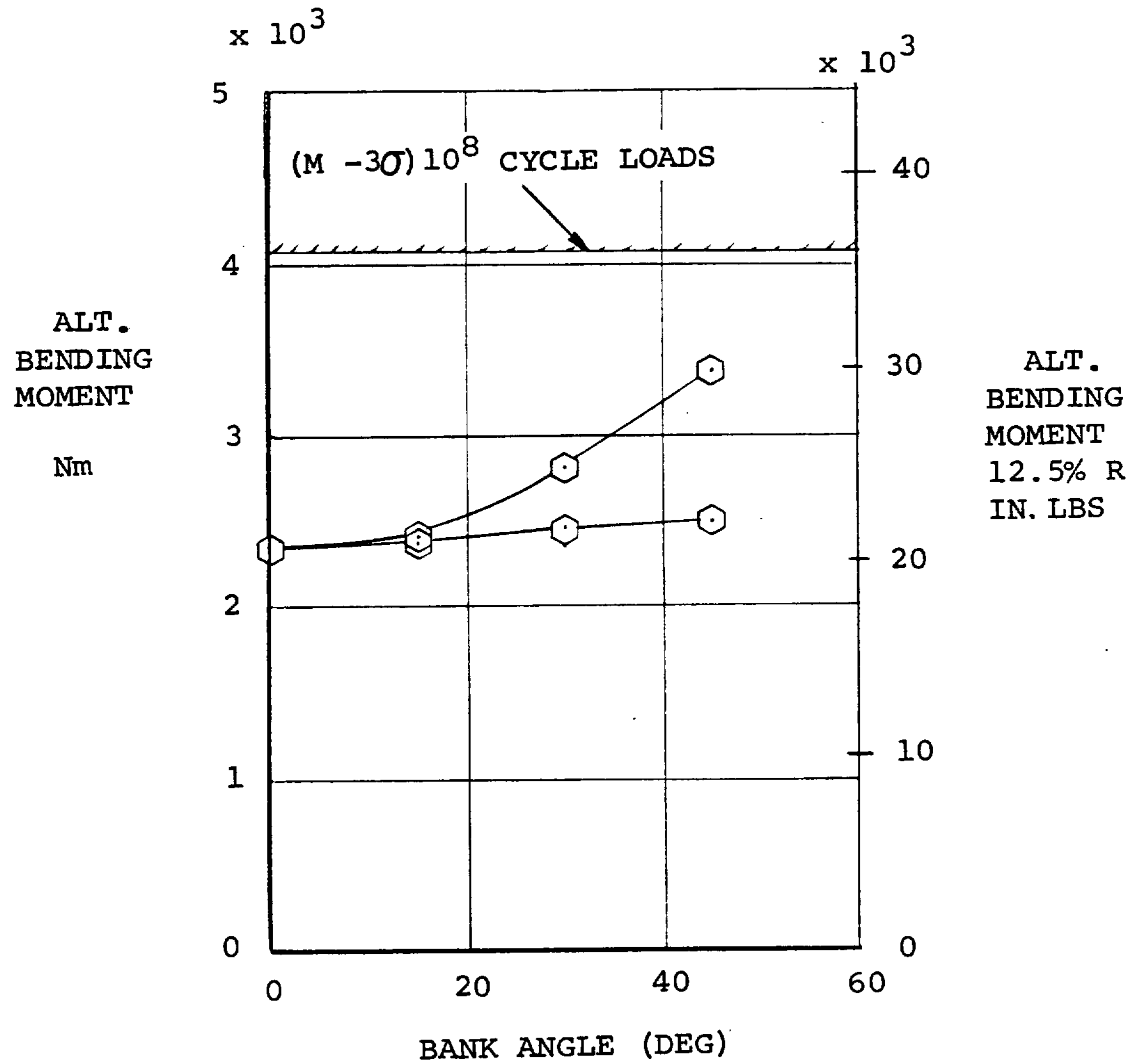

FIGURE 11.27. ESTIMATED BLADE BENDING MOMENTS IN COORDINATED TURNS - GW = 5896.7 Kg (13000 LBS) SL STD DAY $\delta_F = 40°$ $i_N = 90°$ V = 40 KTS FWD CG

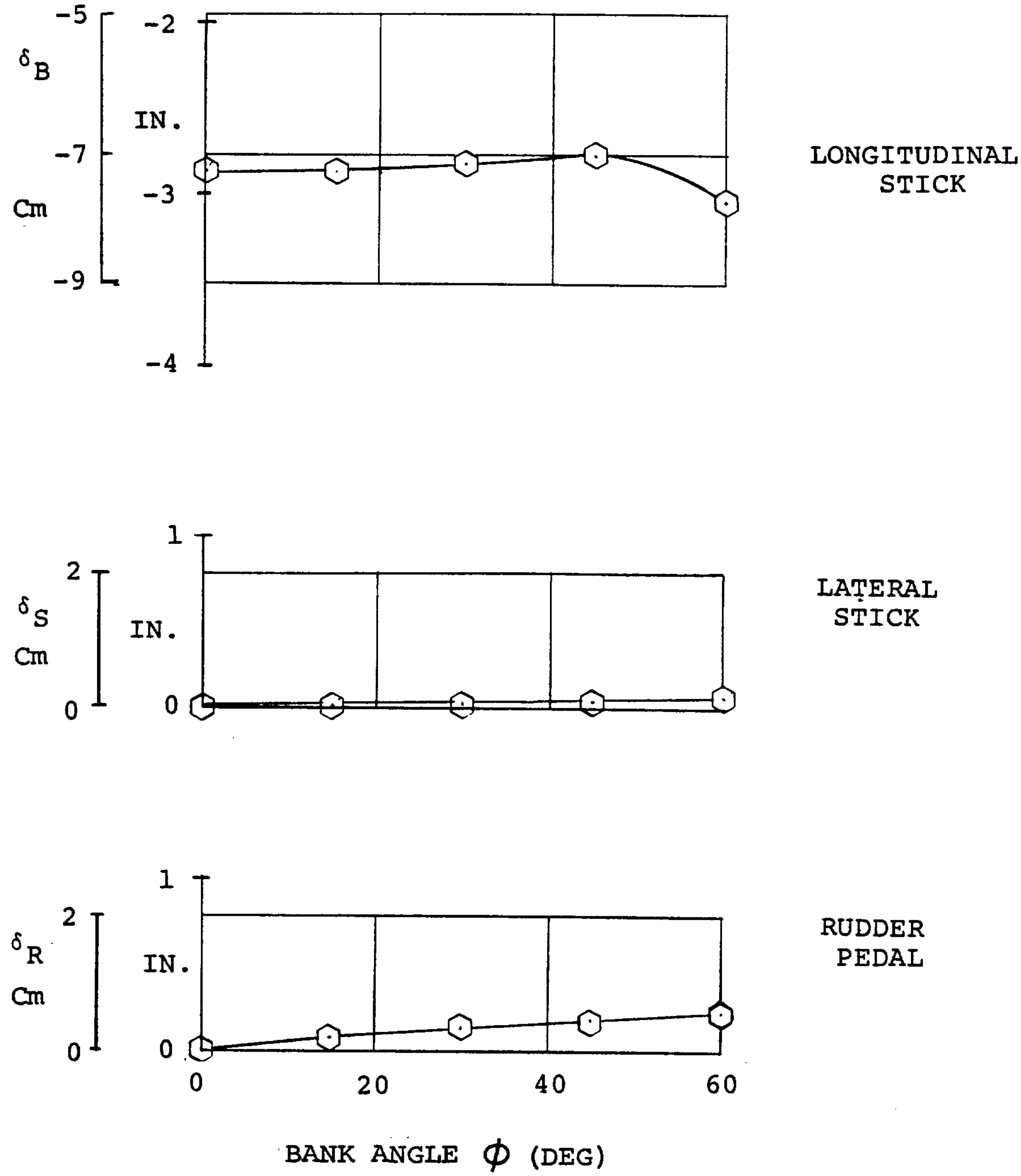

FIGURE 11.28.CONTROL POSITIONS IN COORDINATED TURNS IN TRANSITION AFT CG V = 80 KTS i_N = 90° δ_F = 40° GW = 5896.7 Kg (13000 LB) SL STD DAY

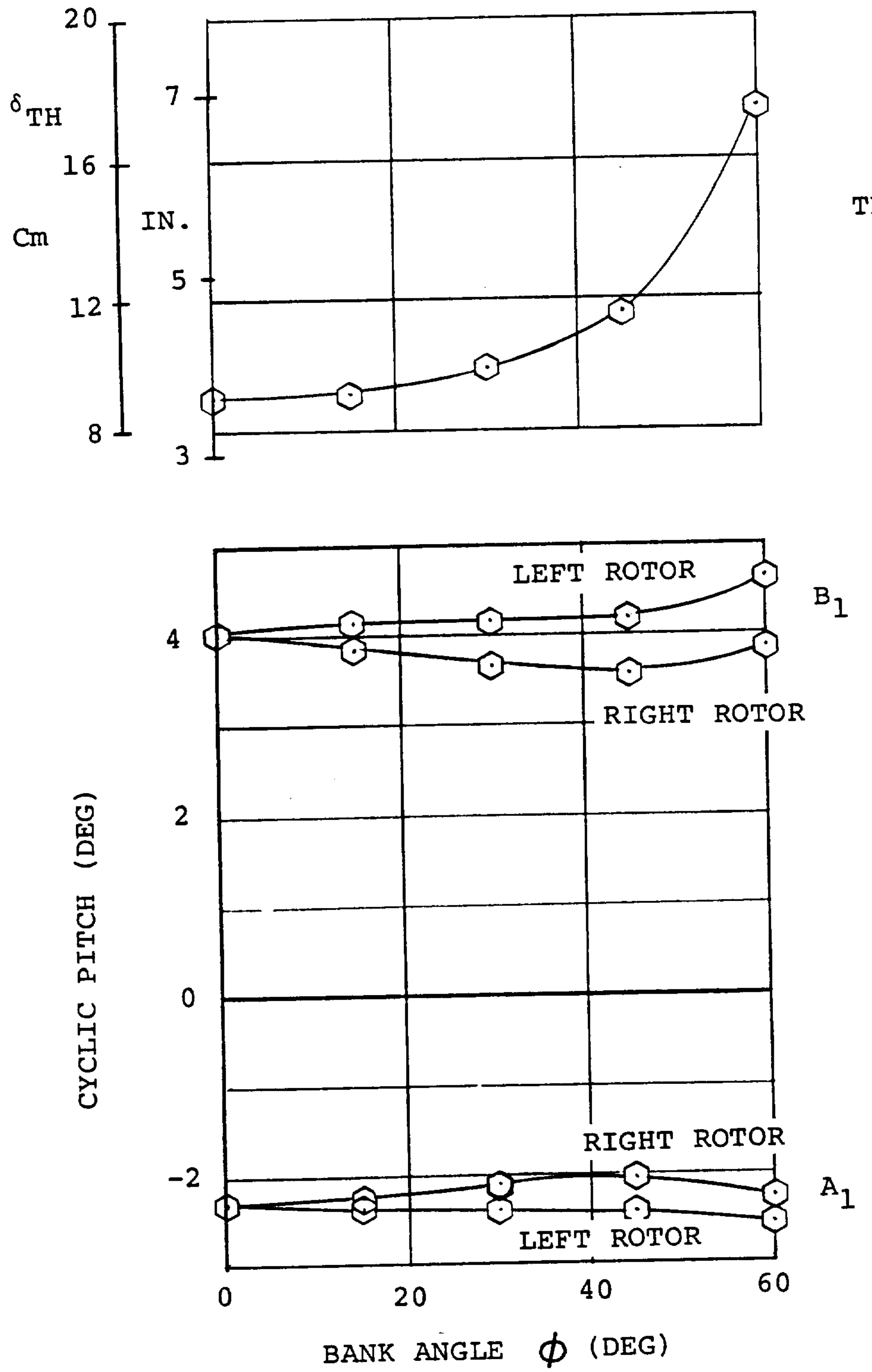

FIGURE 11.29 CONTROL DATA IN COORDINATED TURNS IN TRANSITION - $i_N = 90^\circ$ V = 80 KTS $\delta_F = 40^\circ$
AFT CG GW = 5896.7 Kg (13000 LBS) SL STD DAY

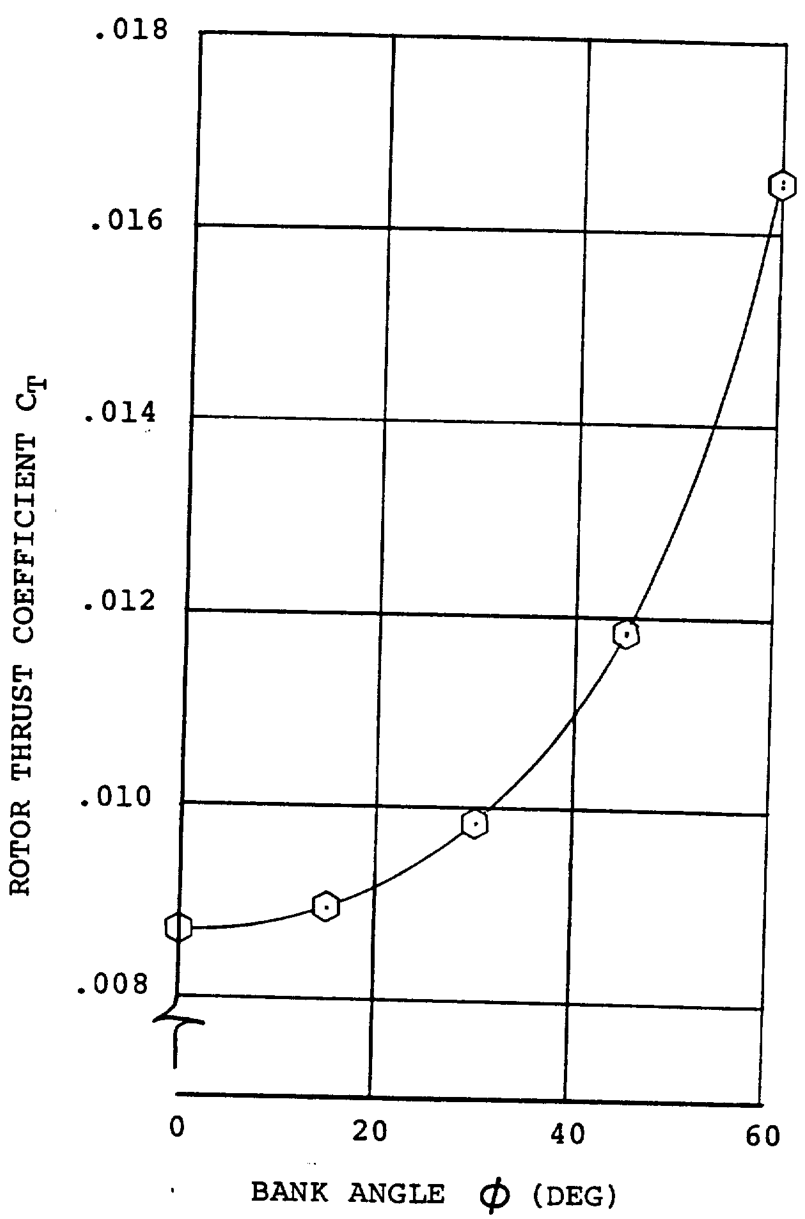

FIGURE 11.30 ROTOR THRUST IN COORDINATED TURNS IN TRANSITION - i_N = 90° V = 80 KTS δ_F = 40° AFT CG GW = 5896.7 Kg (13000 LBS) SL STD DAY

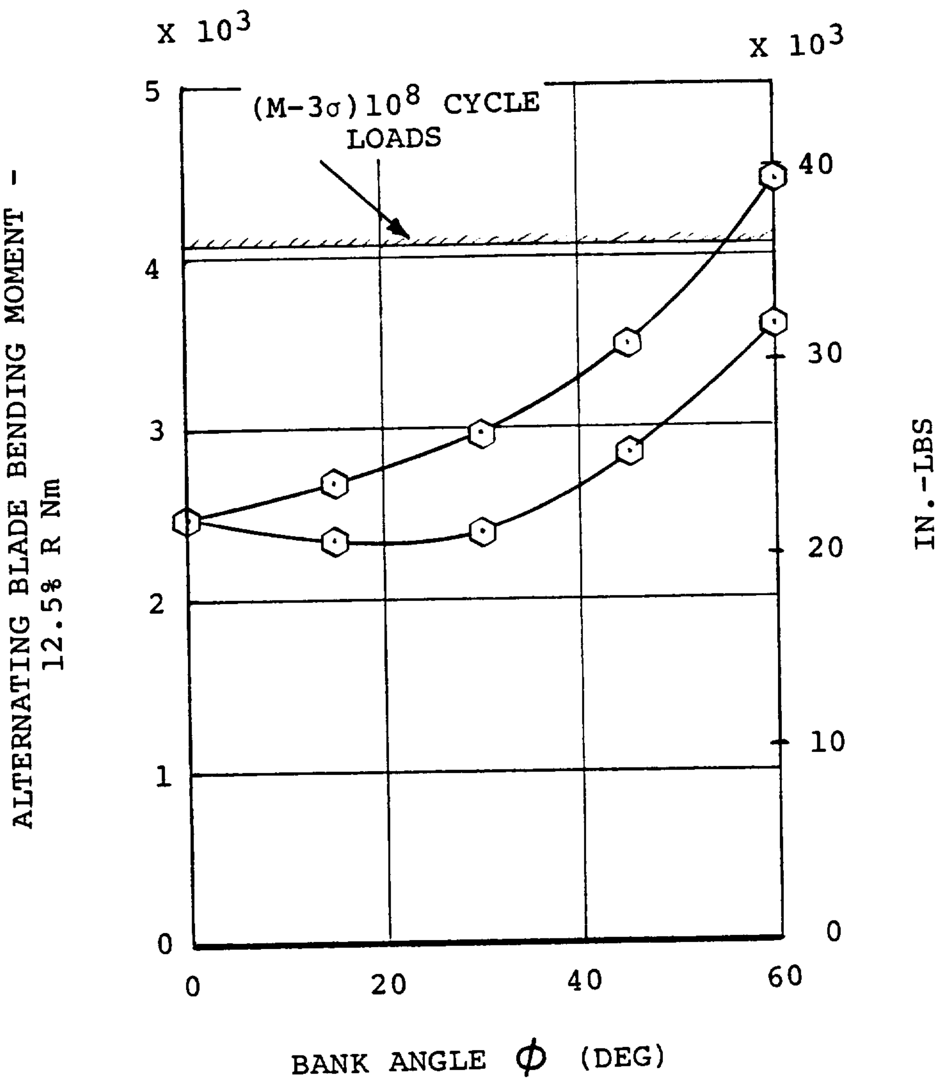

FIGURE 11.31 ESTIMATED BLADE BENDING LOADS 12.5% R IN COORDINATED TURNS IN TRANSITION - $i_N = 90^\circ$ V = 80 KTS $\delta_F = 40^\circ$ AFT CG GW = 5896.7 Kg (13000 LBS) SL STD DAY

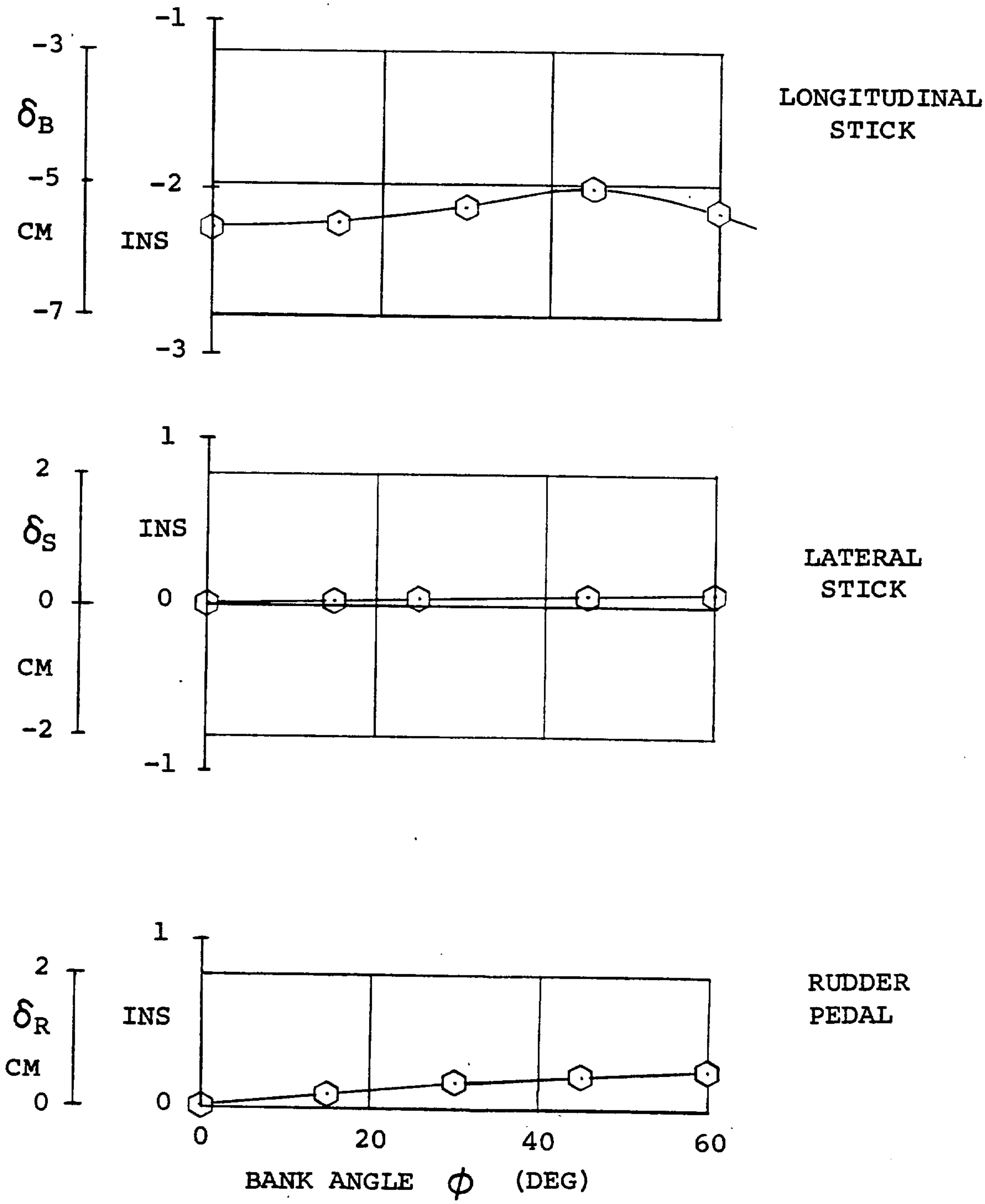

FIGURE 11.32 COORDINATED TURNS IN TRANSITION, CONTROL DATA
GW = 5896.7 Kg (13000 LB) FWD CG, SL STD DAY
i_N = 90° V = 80 KTS

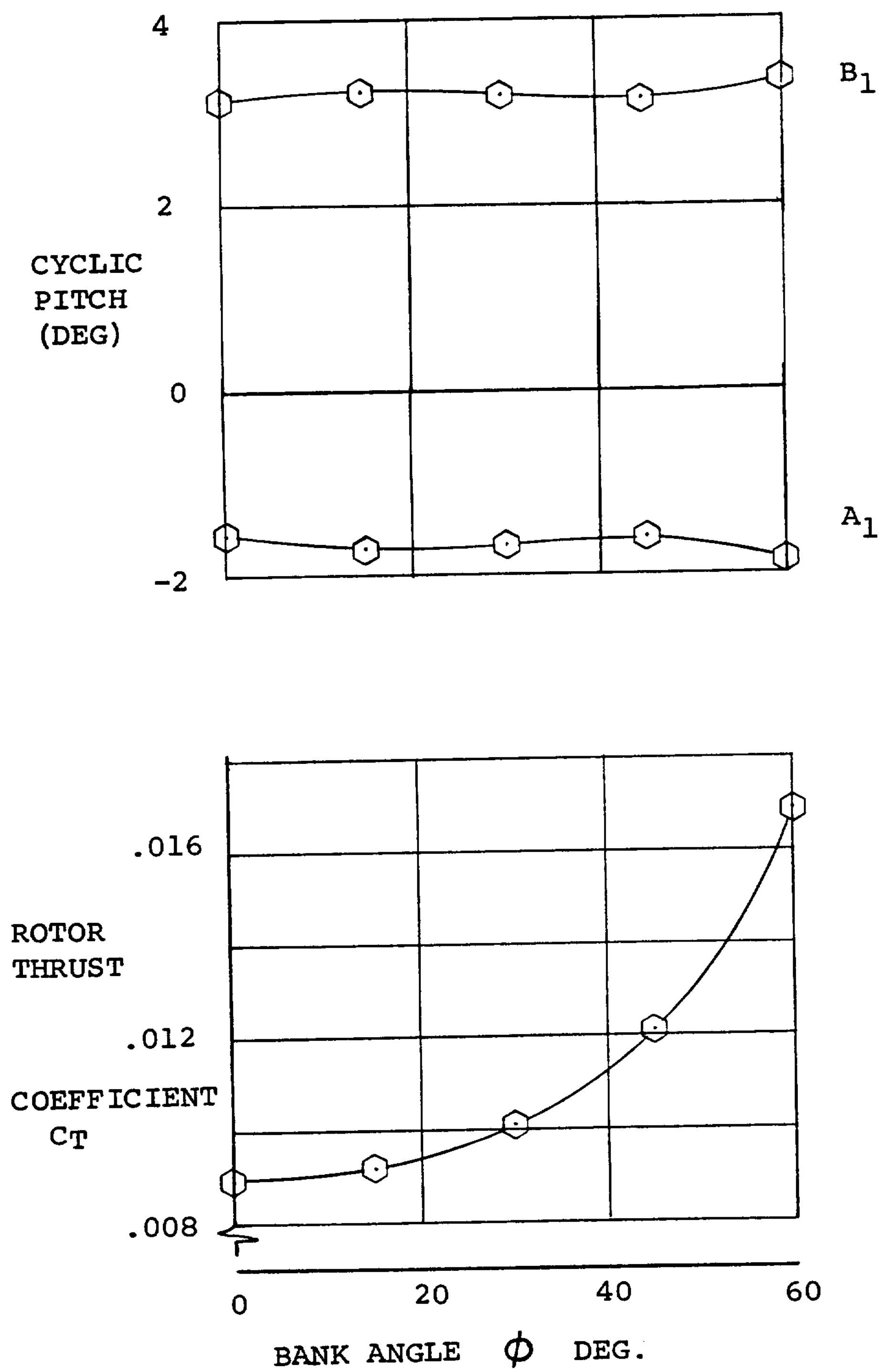

FIGURE 11.33 COORDINATED TURNS IN TRANSITION, FWD CG
GW = 5896.7 Kg (13000 LB) SL STD DAY
i_N = 90° V = 80 KTS

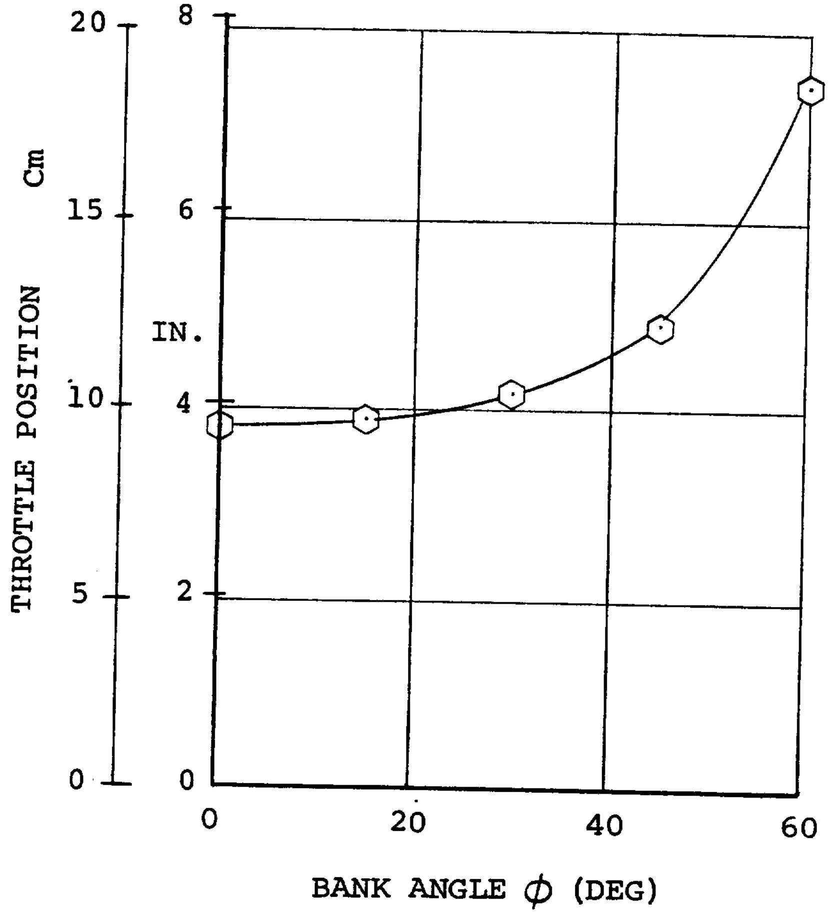

FIGURE 11.34 THROTTLE POSITION IN COORDINATED TURNS IN TRANSITION
$i_N = 90°$, $V = 80$ KTS, GW = 5896.7 Kg (13000 LB)
$\delta_F = 40°$ FWD CG

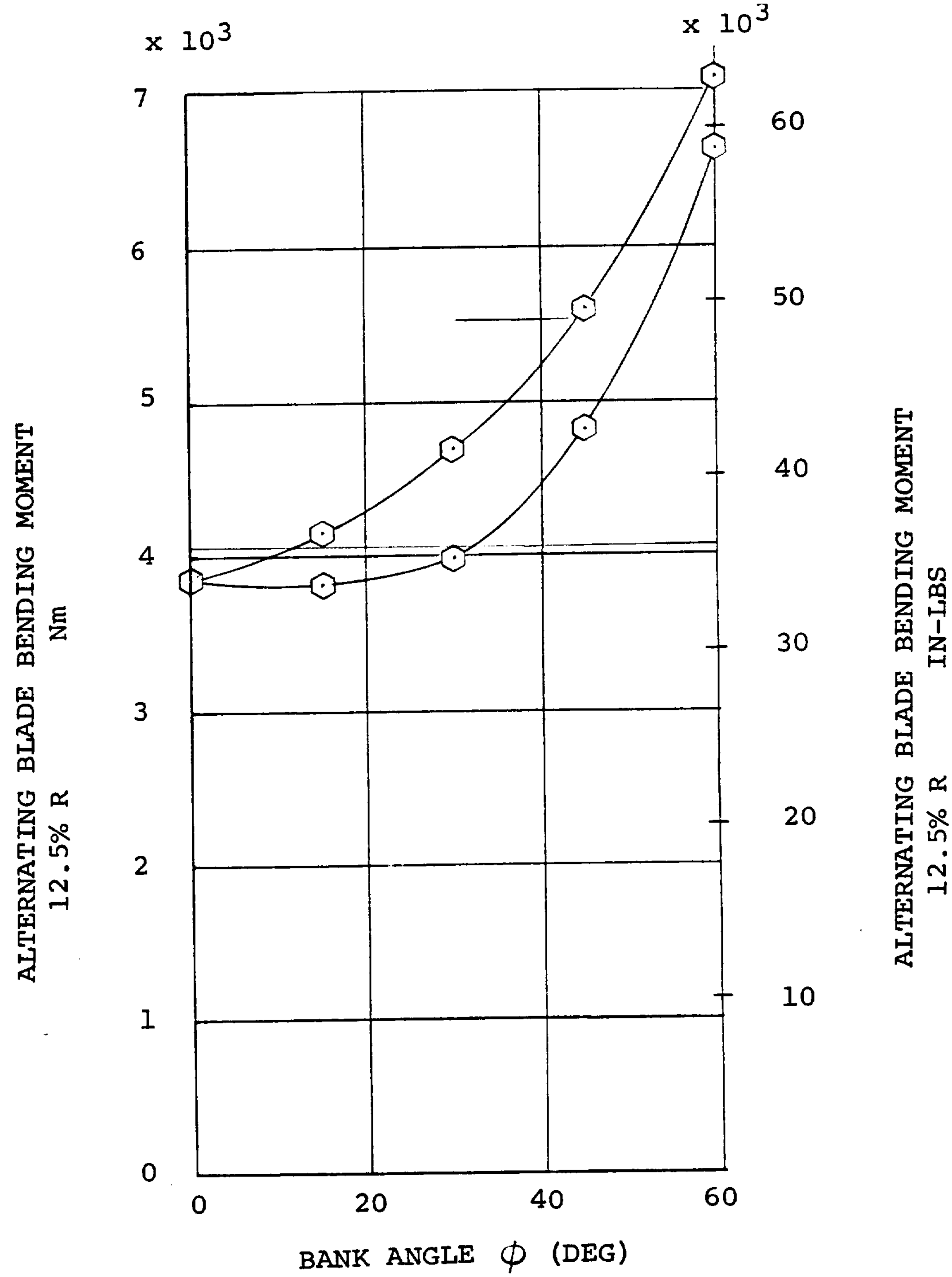

FIGURE 11.35 ESTIMATED BLADE BENDING LOADS 12.5% R IN COORDINATED TURNS GW = 5896.7 Kg (13000 LB) i_N = 90° V = 80 KTS SL STD DAY FWD CG

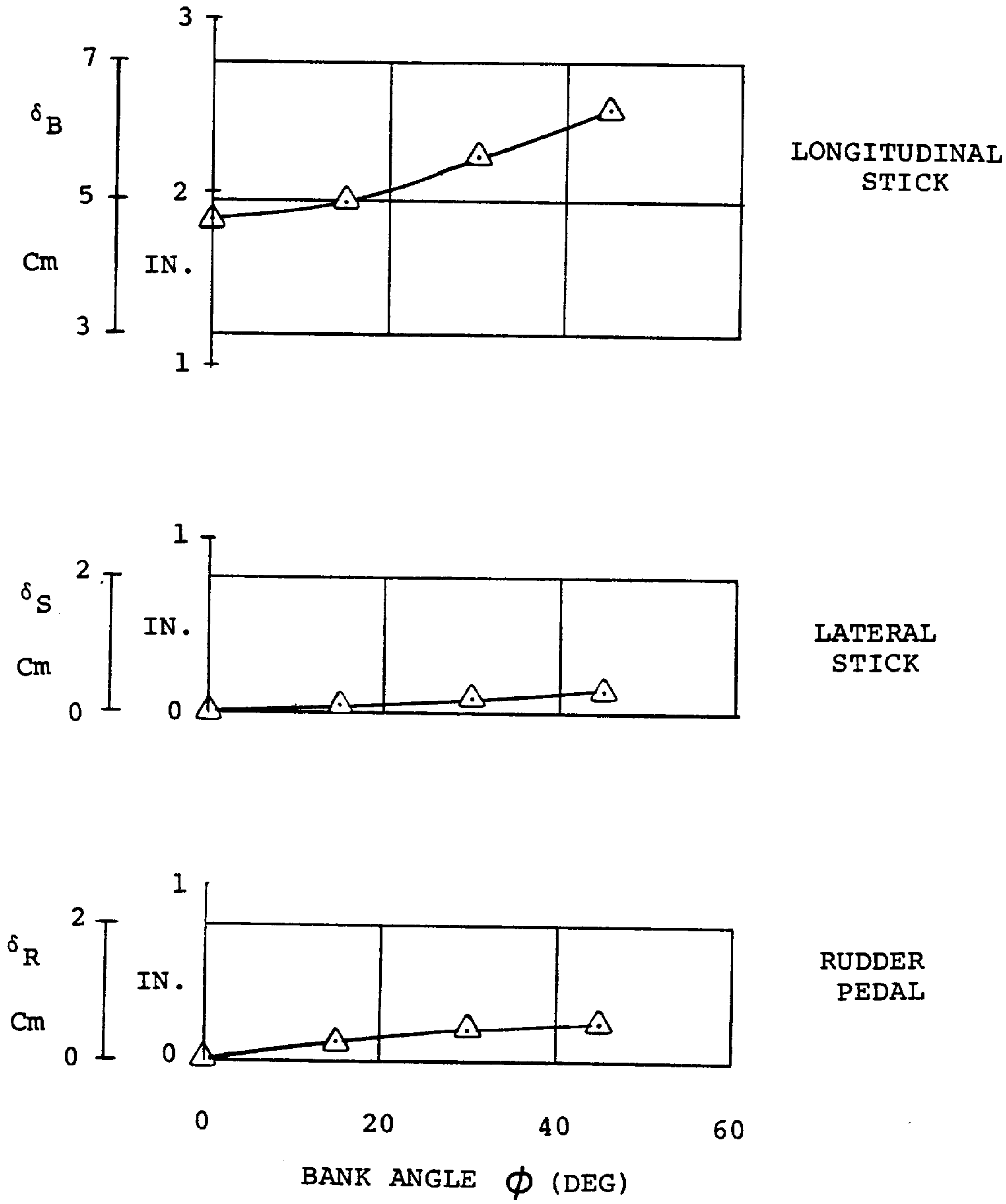

FIGURE 11.36 CONTROL POSITIONS IN COORDINATED TURNS IN TRANSITION
$i_N = 60^\circ$ V = 60 KTS $\delta_F = 40^\circ$ GW = 5896.7 Kg
(13000 LBS) SL STD DAY AFT CG

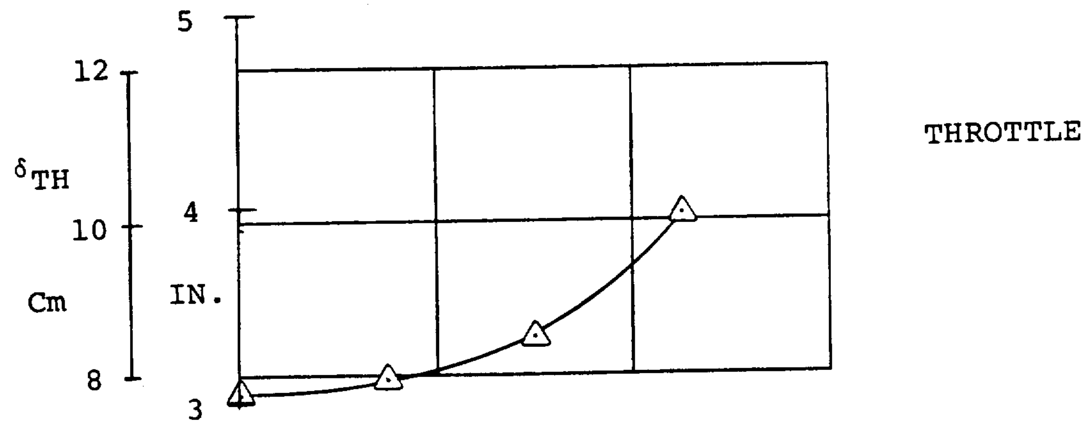

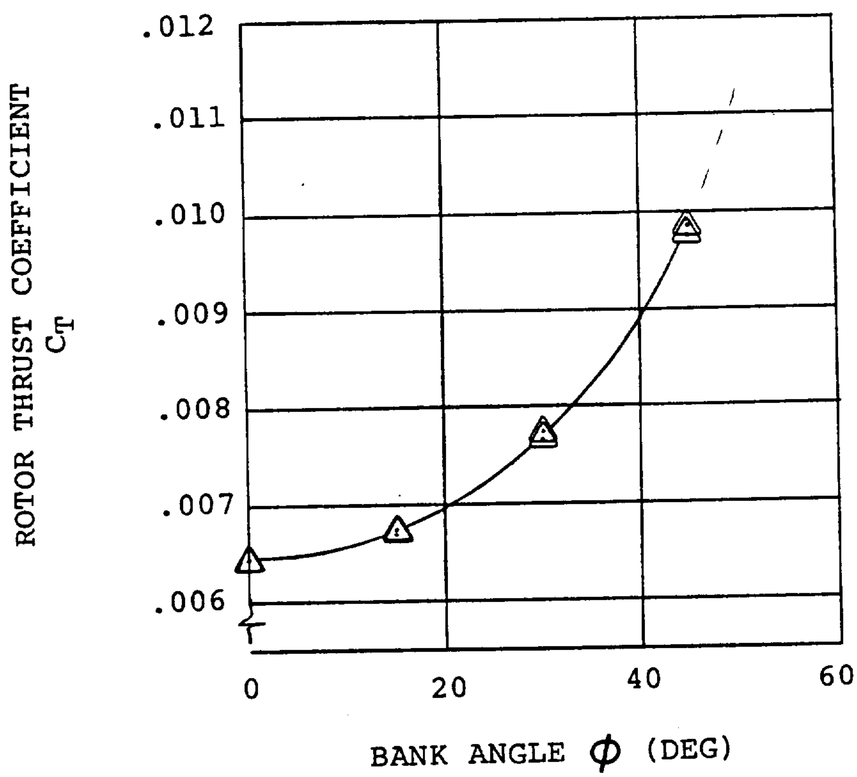

FIGURE 11·37 THROTTLE POSITION AND ROTOR THRUST IN COORDINATED TURNS IN TRANSITION - $i_N = 60°$ V = 60 KTS
$\delta_F = 40°$ AFT CG GW = 5896.7 Kg (13000 LBS)
SL STD DAY

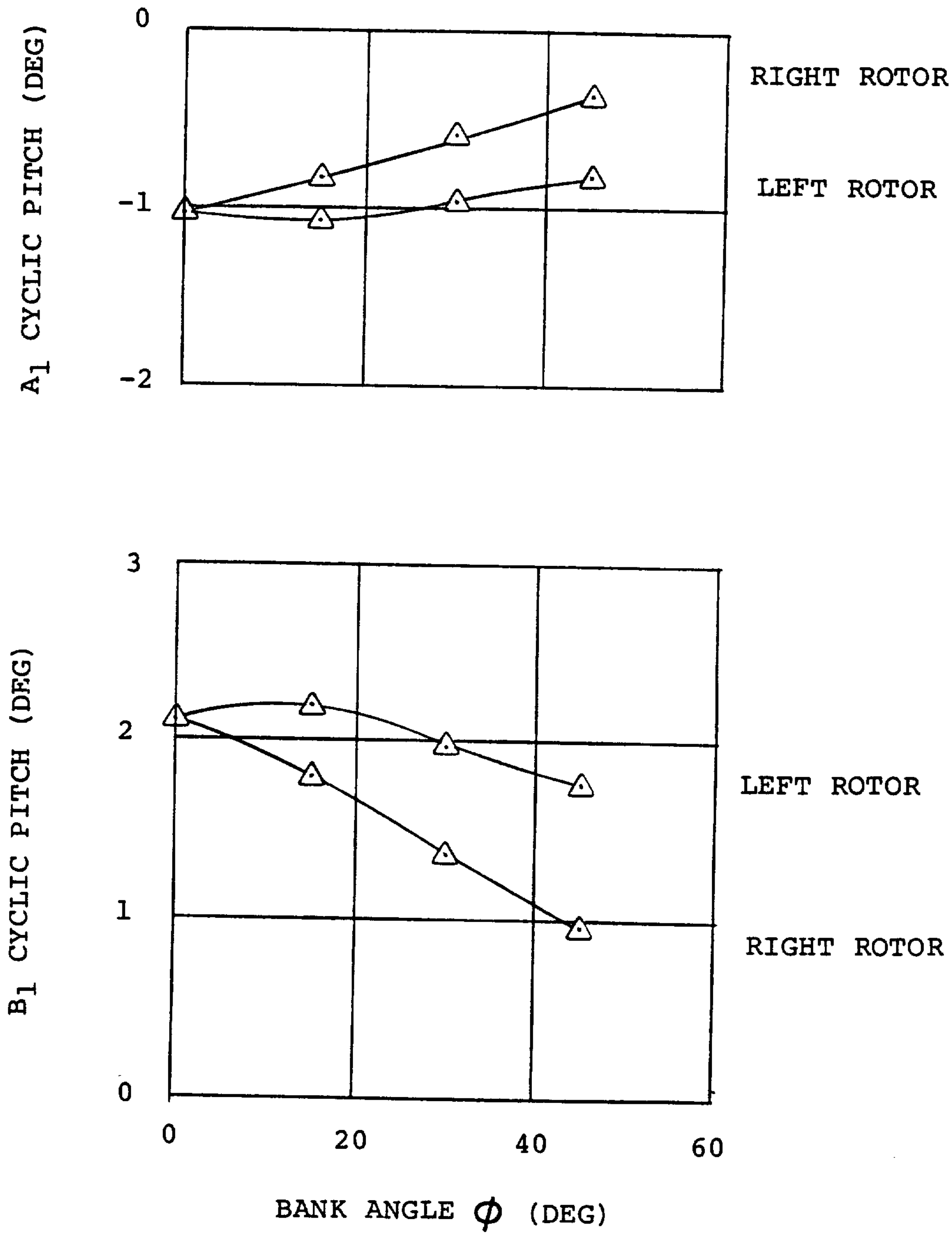

FIGURE 11.38. CYCLIC PITCH IN COORDINATED TURNS IN TRANSITION
$i_N = 60°$ V = 60 KTS $\delta_F = 40°$ AFT CG
GW = 5896.7 Kg (13000 LBS) SL STD DAY

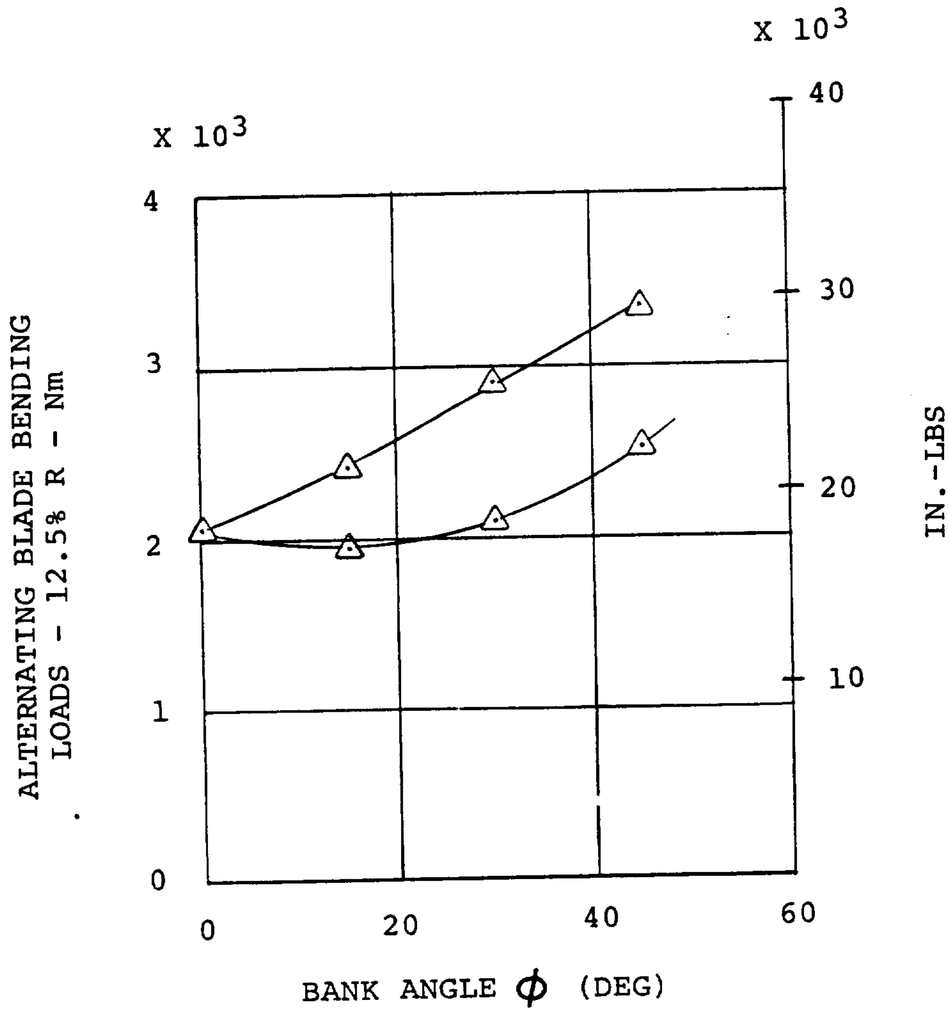

FIGURE 11.39. ESTIMATED BLADE BENDING LOADS IN COORDINATED TURNS IN TRANSITION - $i_N = 60^\circ$ V = 60 KTS $\delta_F = 40^\circ$ GW = 5896.7 Kg (13000 LBS) SL STD DAY AFT CG

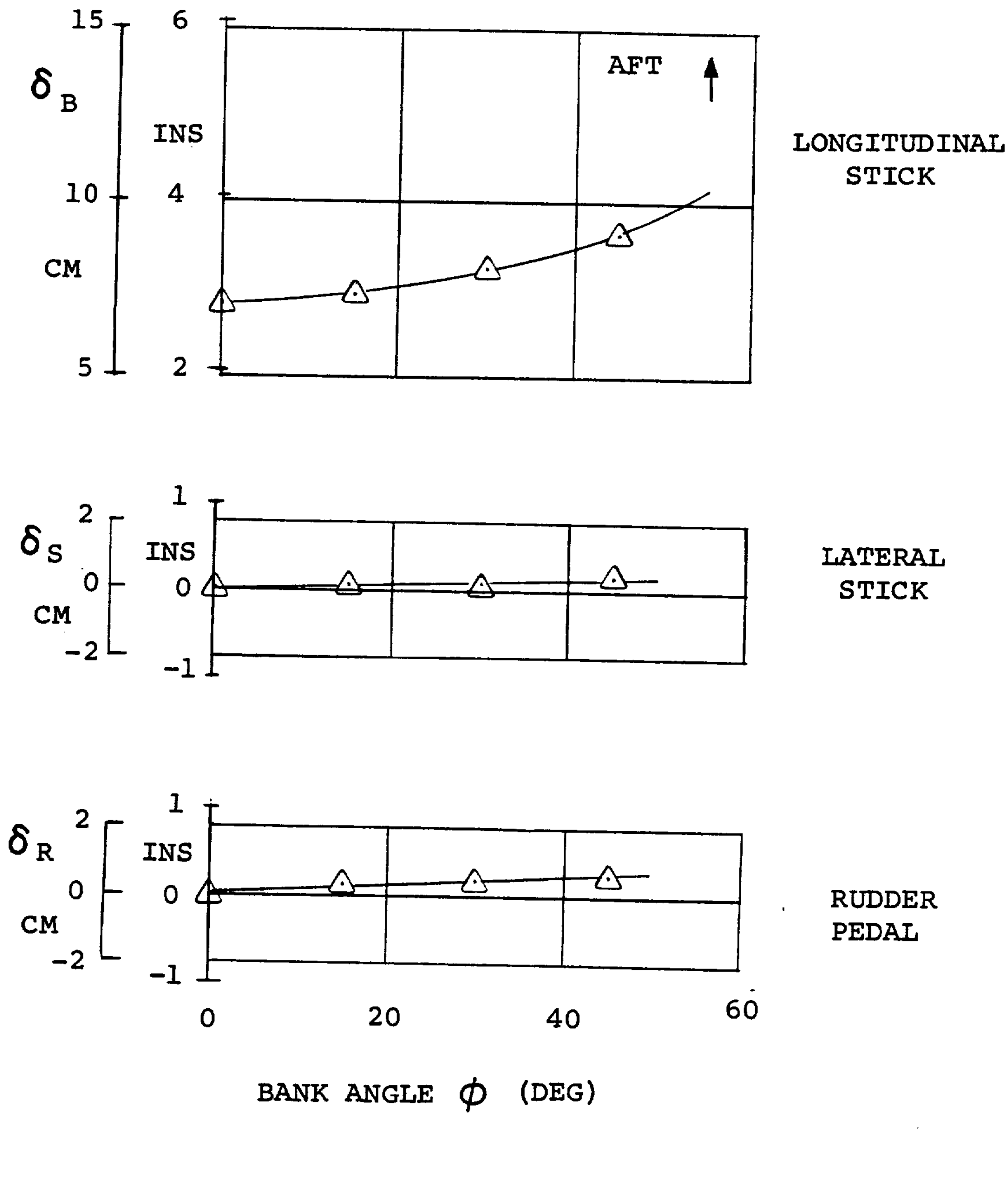

FIGURE 11.40 CONTROL POSITIONS IN COORDINATED TURNS IN TRANSITION
$i_N = 60^\circ$ V = 60 KTS GW = 5896.7 Kg (13000 LBS)
FWD CG $\delta_F = 40^\circ$

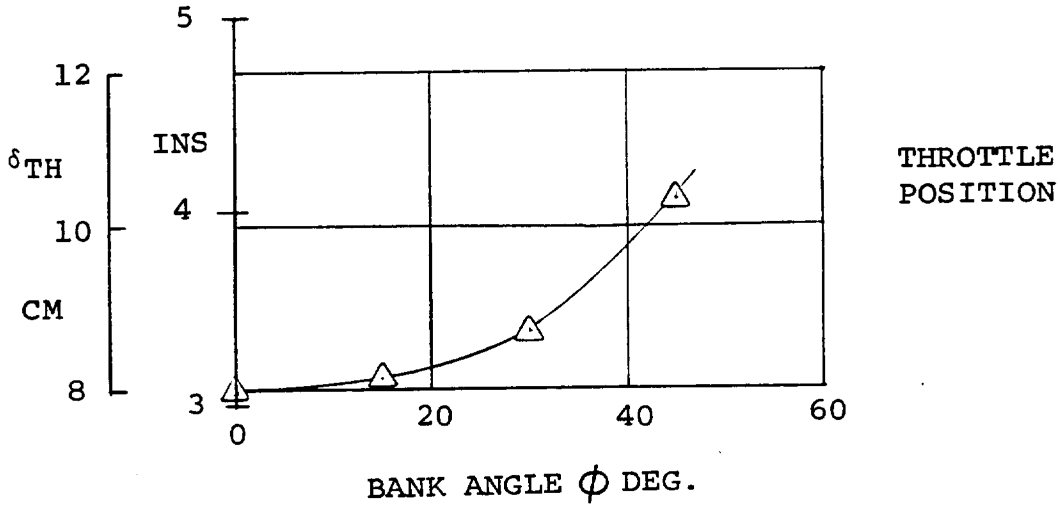

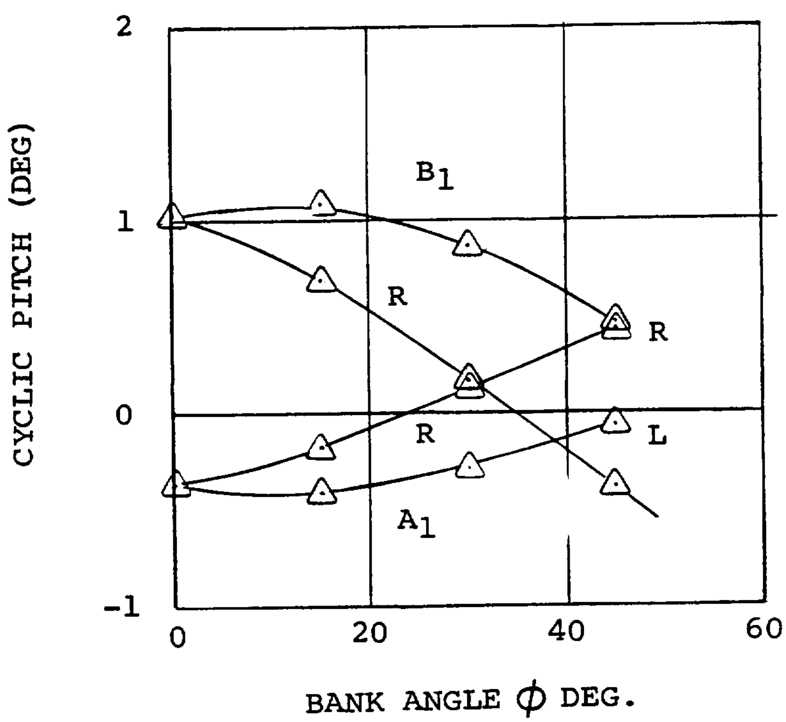

FIGURE 11.41. CONTROL POSITIONS IN COORDINATED TURNS IN TRANSITION $i_N = 60°$ V = 60 KTS
GW = 5896.7 Kg (13000 LB) FWD CG $\delta_F = 40°$

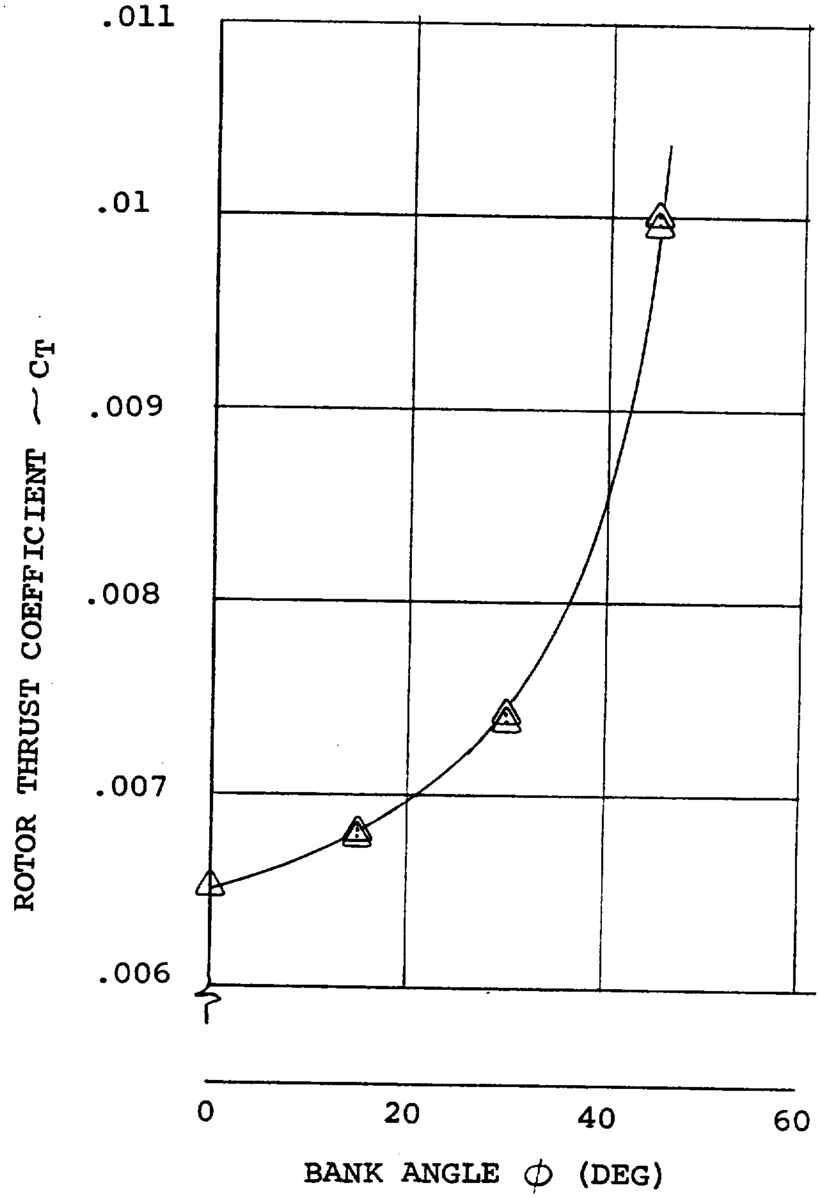

FIGURE 11.42 COORDINATED TURNS IN TRANSITION
GW = 5896.7 Kg (13000 LB) FWD CG
$\delta_F = 40°$ SL, STD DAY V = 60 KTS $i_N = 60°$

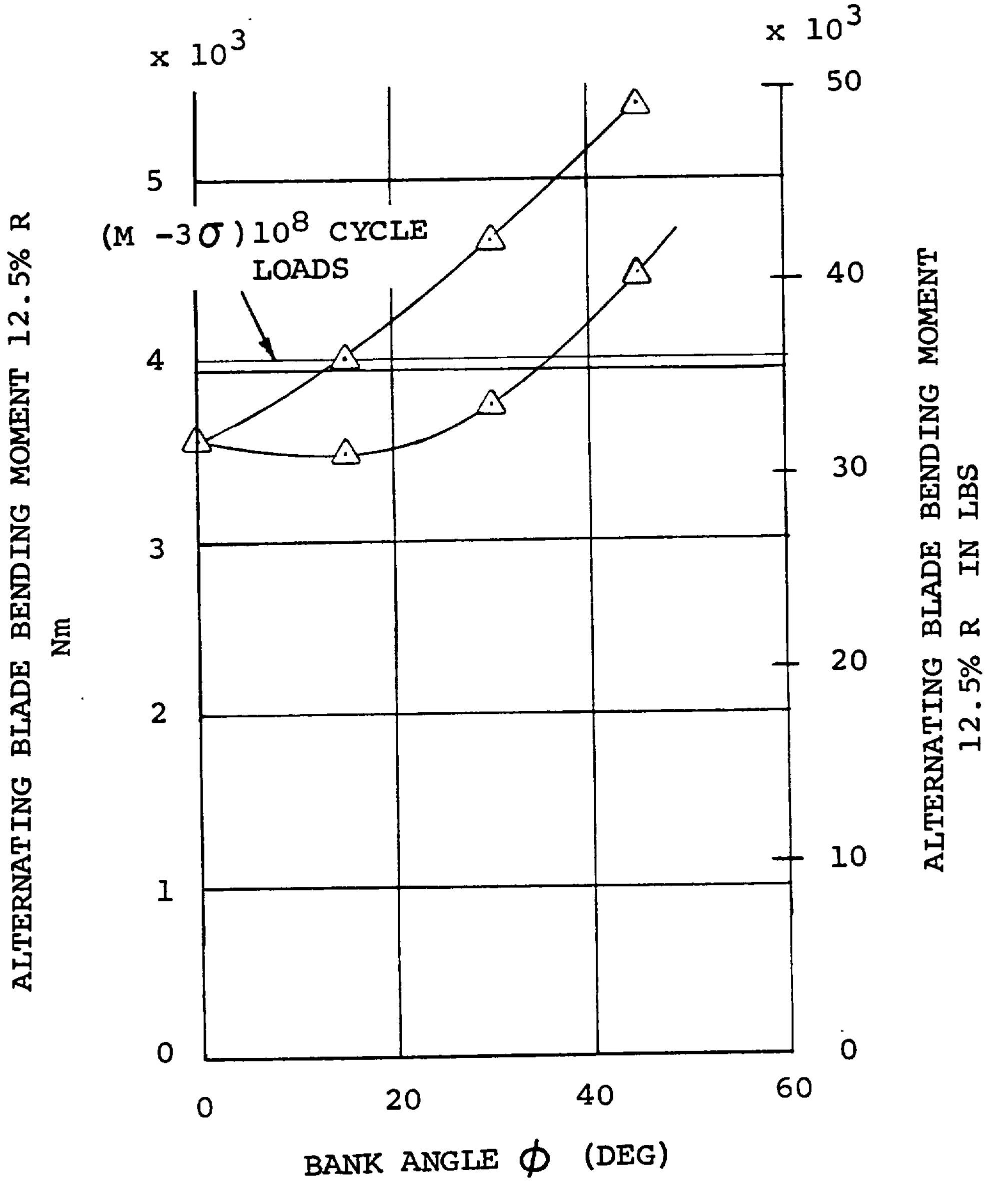

FIGURE 11.43. ALTERNATING BLADE BENDING LOADS IN COORDINATED TURNS IN TRANSITION $i_N = 60°$ V = 60KTS $\delta_F = 40°$ GW = 5896.7 Kg (13000 LB) SL STD DAY FWD CG

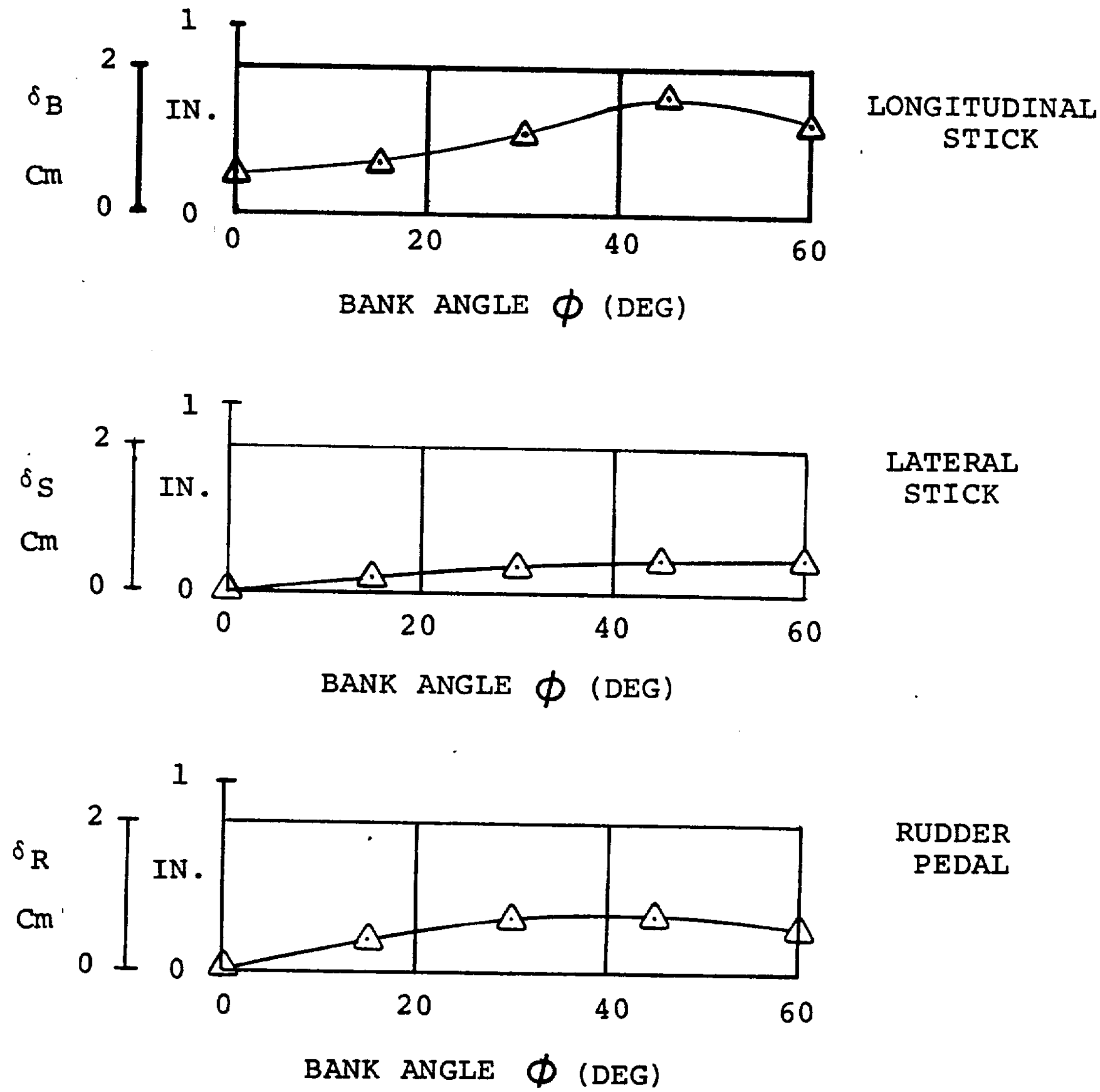

FIGURE 11.44. CONTROL POSITIONS IN COORDINATED TURNS IN TRANSITION - $i_N = 60^\circ$ V = 90 KTS AFT CG GW = 5896.7 Kg (13000 LBS) $\delta_F = 40^\circ$ SL STD DAY

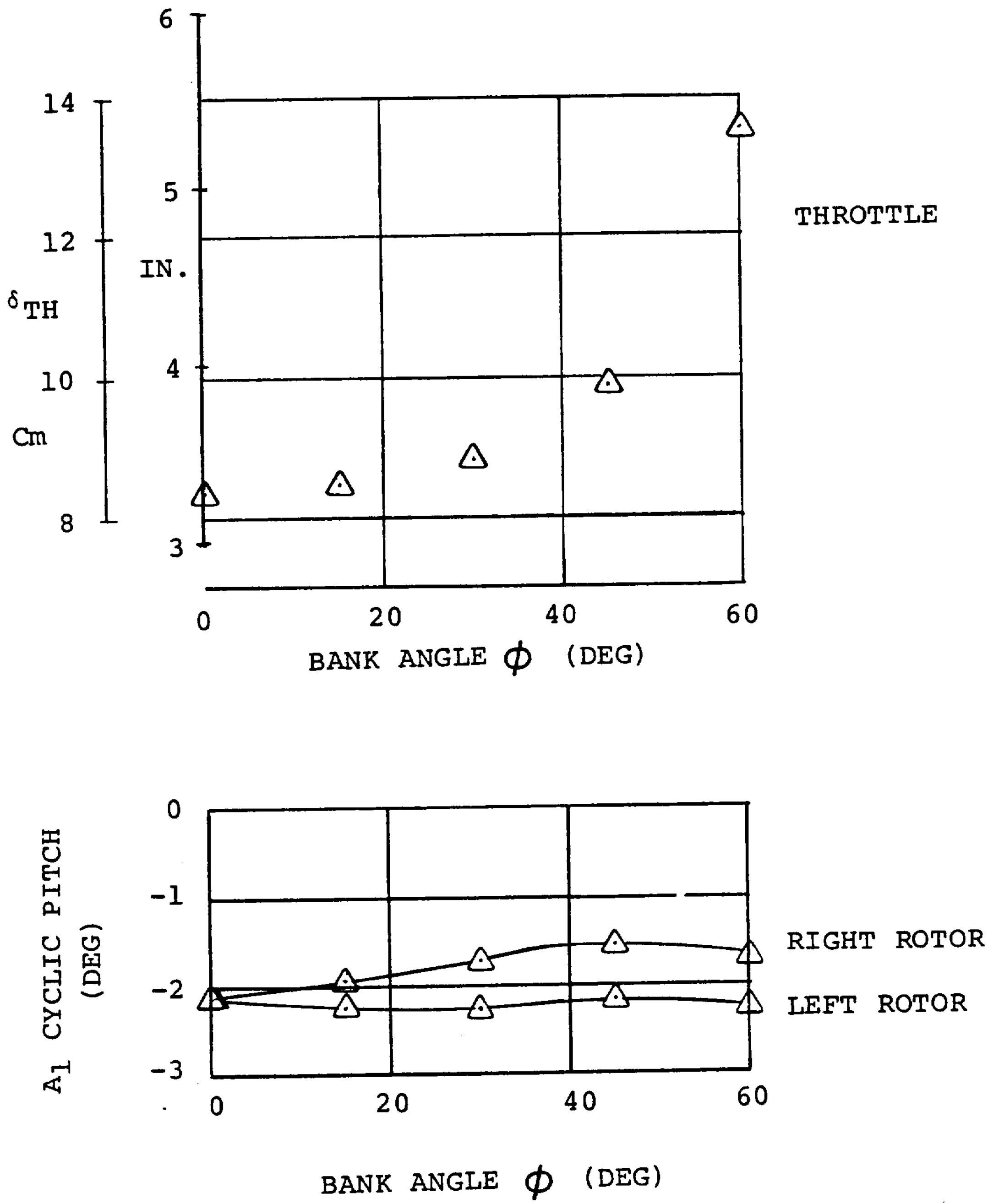

FIGURE 11.45 CONTROL DATA IN COORDINATED TURNS IN TRANSITION - $i_N = 60^\circ$ V = 90 KTS $\delta_F = 40^\circ$ AFT CG GW = 5896.7 Kg (13000 LBS) SL STD DAY

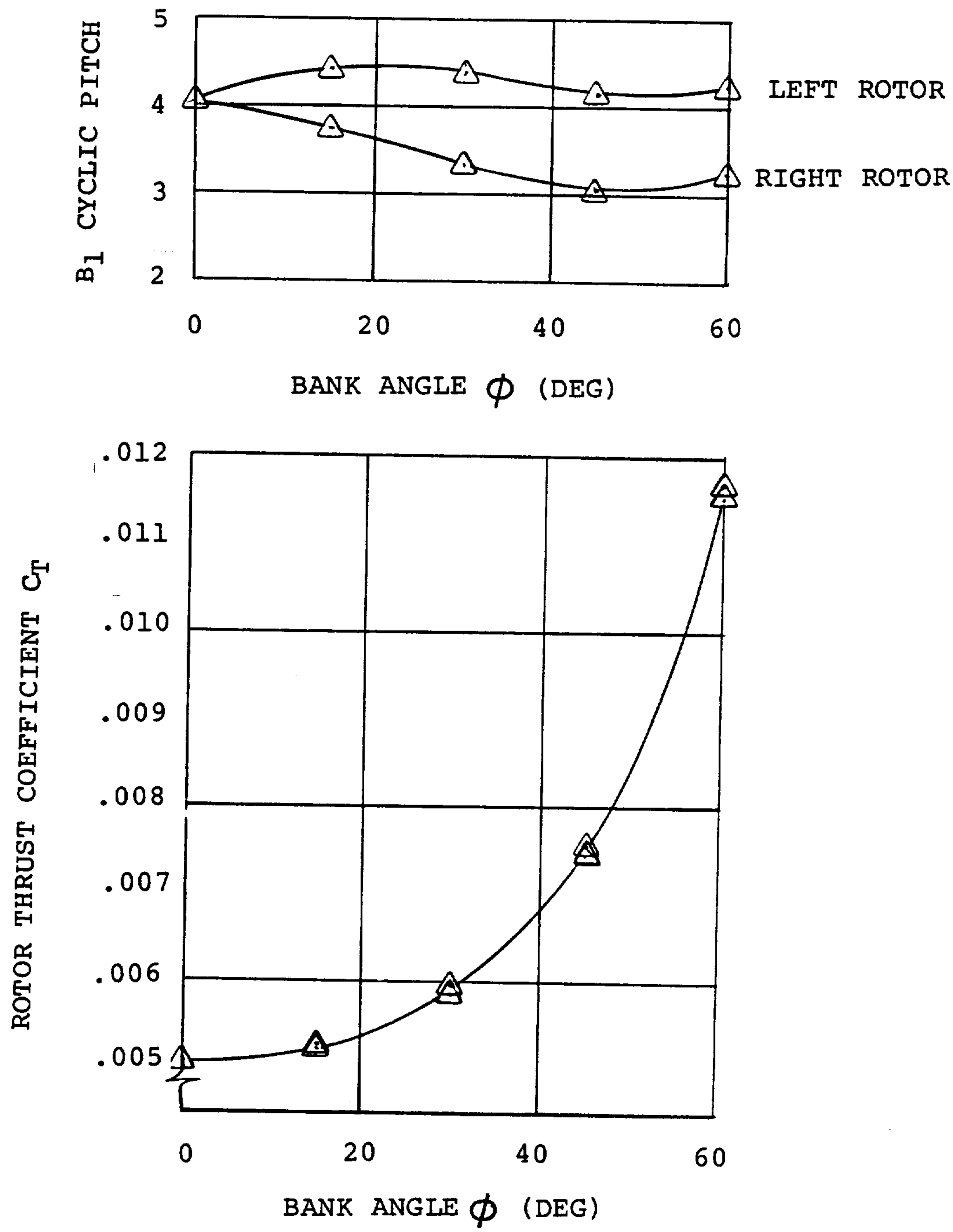

FIGURE 11.46 CYCLIC AND THRUST DATA IN COORDINATED TURNS
IN TRANSITION - $i_N = 60^\circ$ V = 90 KTS $\delta_F = 40^\circ$
AFT CG GW = 5896.7 Kg (13000 LBS) SL STD DAY

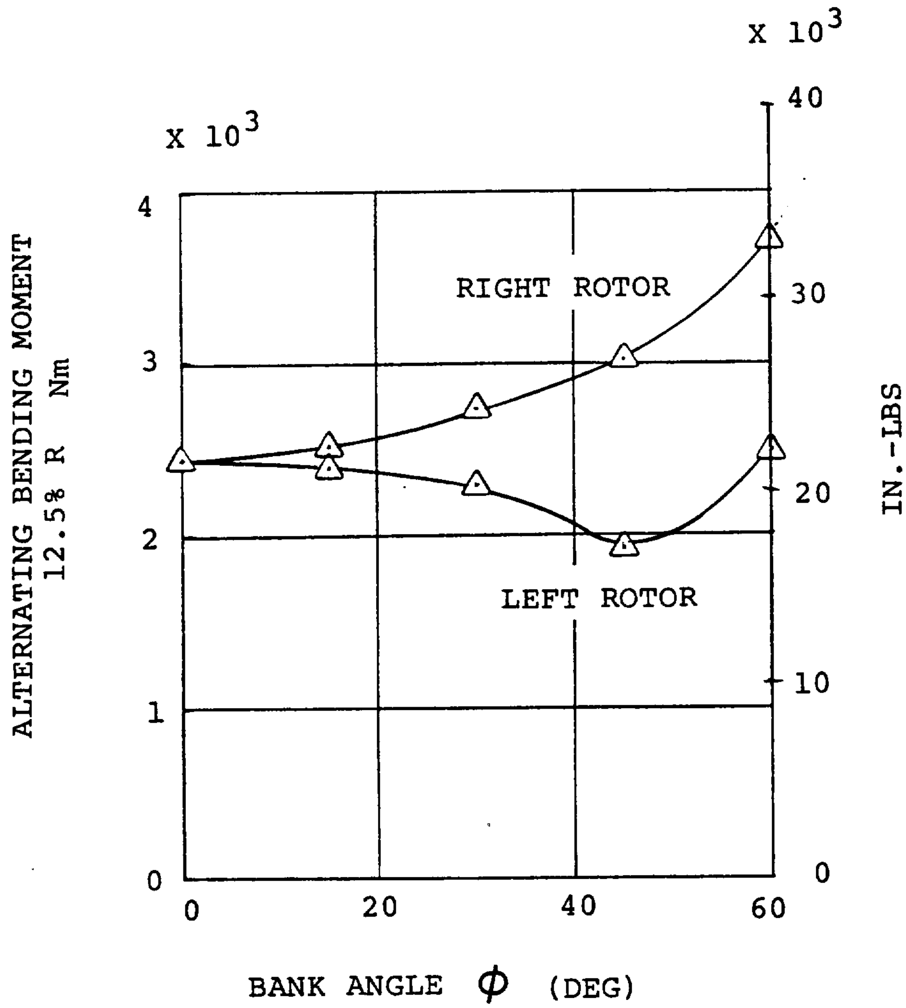

FIGURE 11.47 ESTIMATED BLADE BENDING LOADS IN COORDINATED TURNS IN TRANSITION - $i_N = 60^{\circ}$ V = 90 KTS
$\delta_F = 40^{\circ}$ AFT CG GW = 5896.7 Kg (13000 LBS)
SL STD DAY

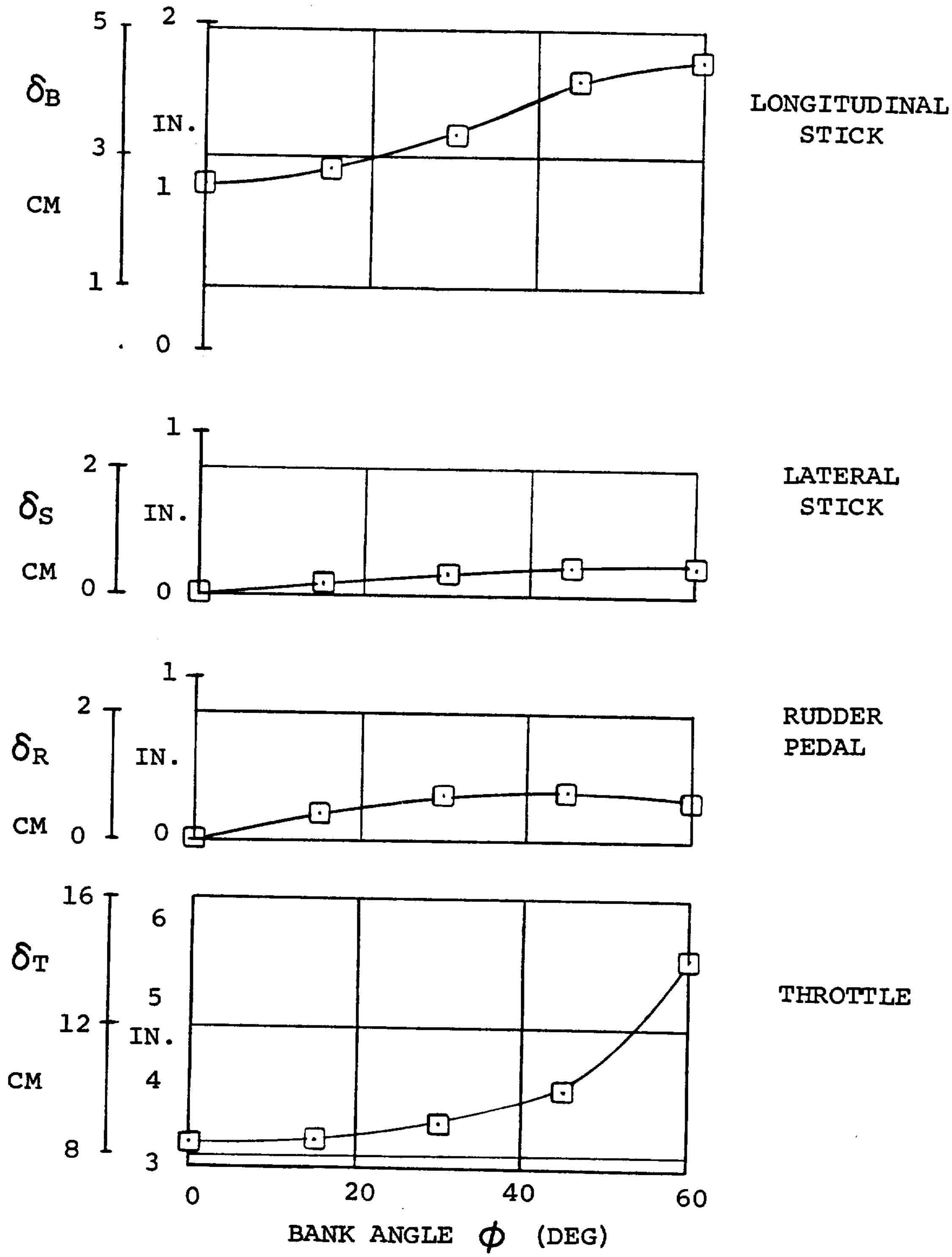

FIGURE 11.48 CONTROL POSITION IN TRANSITION COORDINATED TURNS $i_N = 60°$ V = 90 $\delta_F = 40°$ FWD CG GW = 5896.7 Kg (13000 LB) SL STD DAY

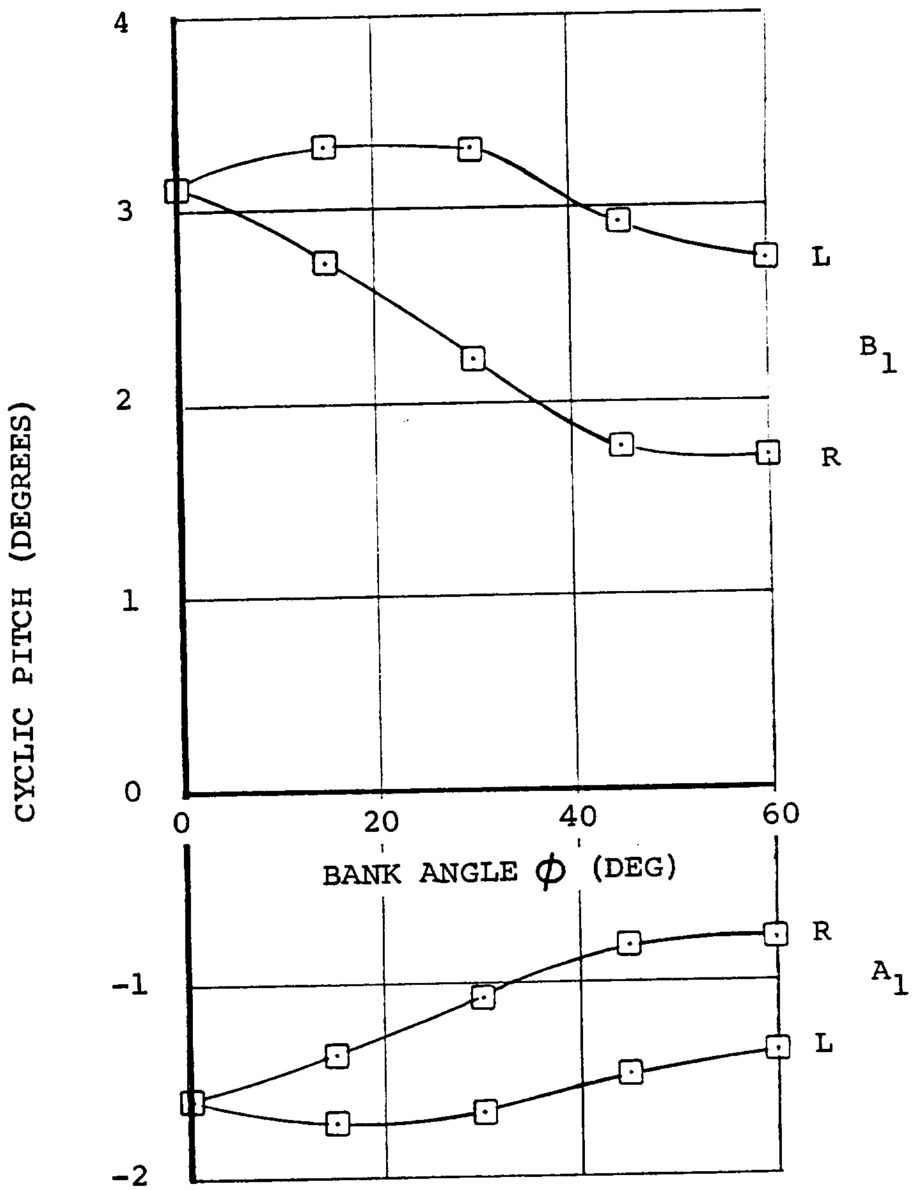

FIGURE 11.49 CYCLIC PITCH IN COORDINATED TRANSITION TURNS
$i_N = 60°$ V = 90 KTS $\delta_F = 40°$ FWD CG
GW = 5896.7 Kg (13000 LB) SL STD DAY

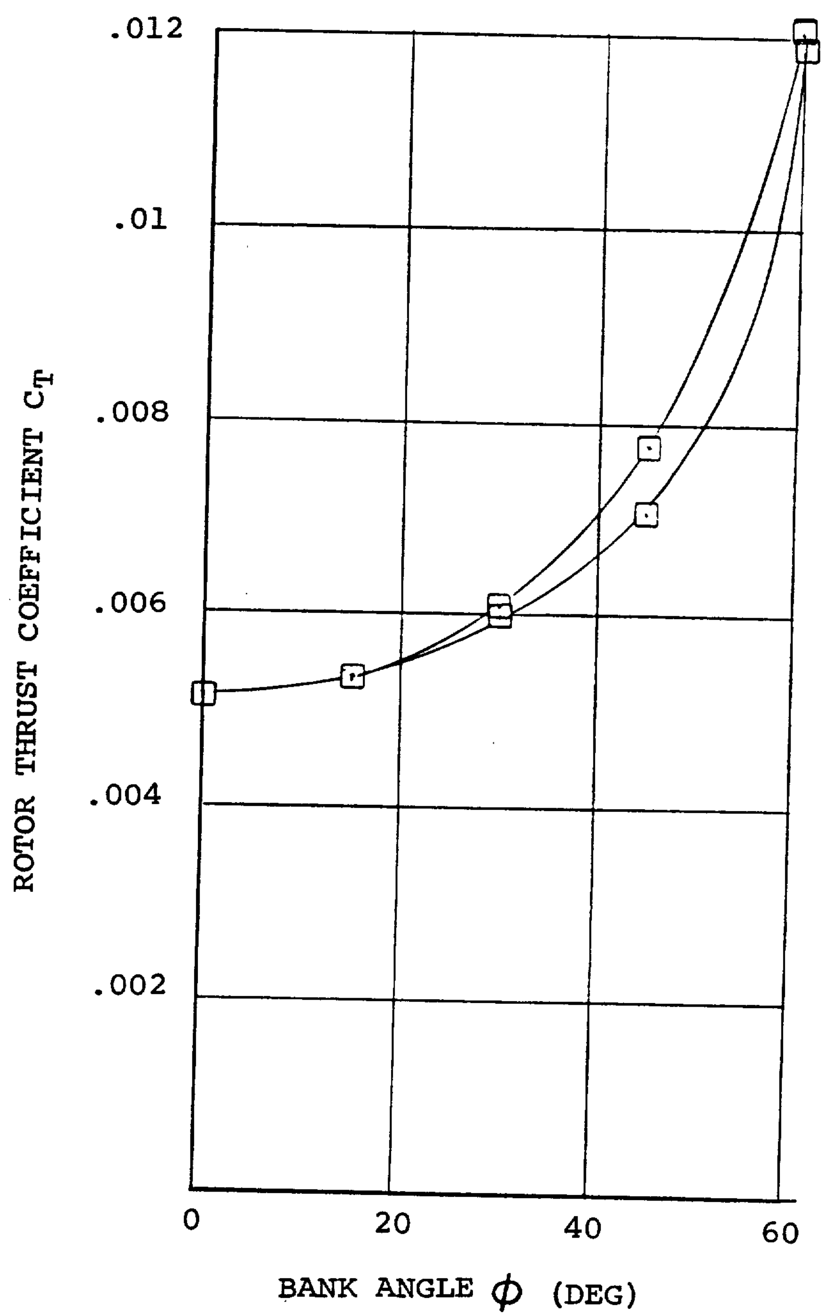

FIGURE 11.50 ROTOR THRUST COEFFICIENT IN TRANSITION COORDINATED TURNS $i_N = 60°$ V = 90 KTS $\delta_F = 40°$ GW = 5896.7 Kg (13000 LB) FWD CG SL STD DAY

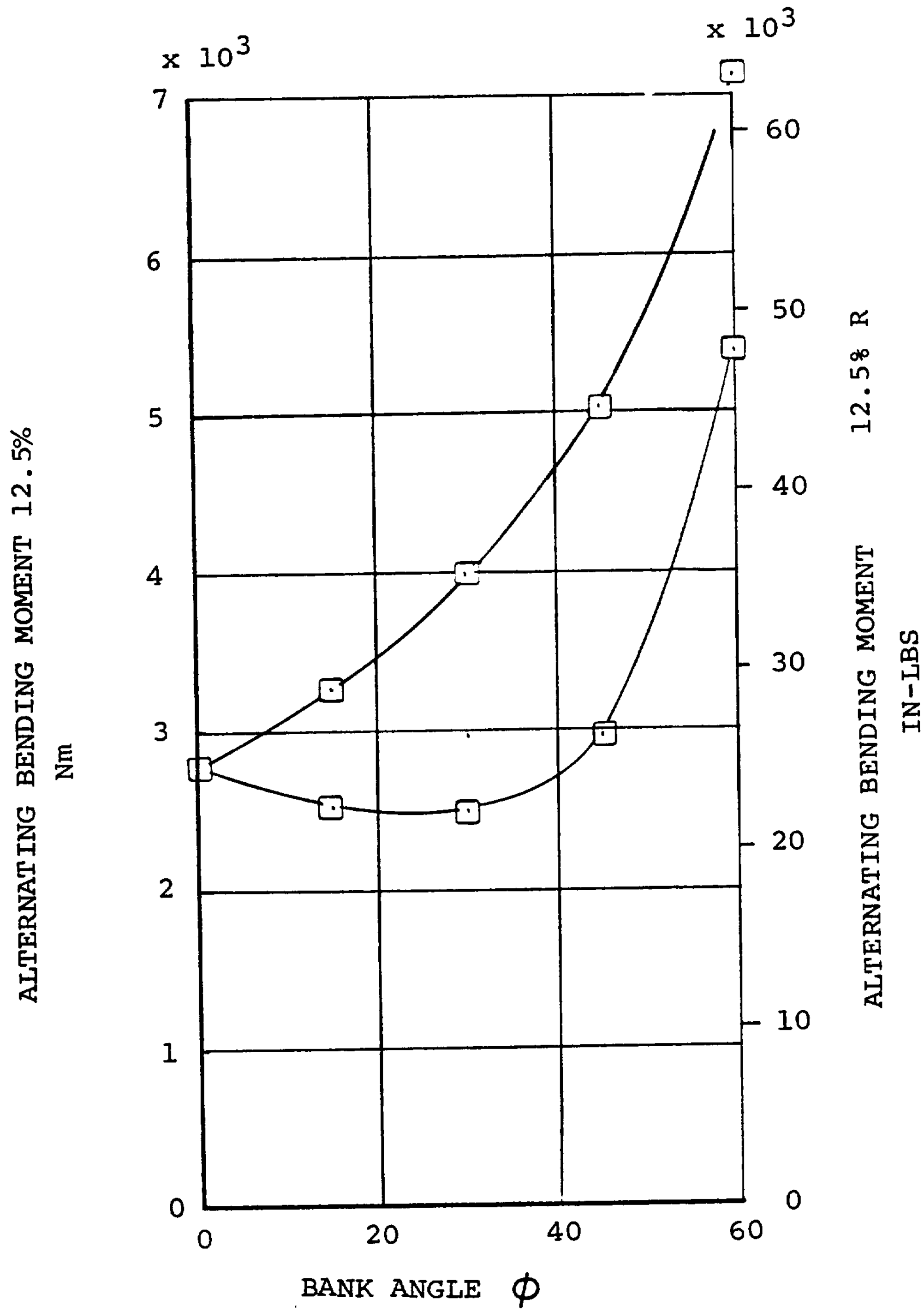

FIGURE 11.51 ESTIMATED BLADE BENDING LOADS IN COORDINATED TURNS IN TRANSITION $i_N = 60°$ V = 90 KTS $\delta_F = 40°$ GW = 5896.7 Kg (13000 LB) FWD CG SL STD DAY

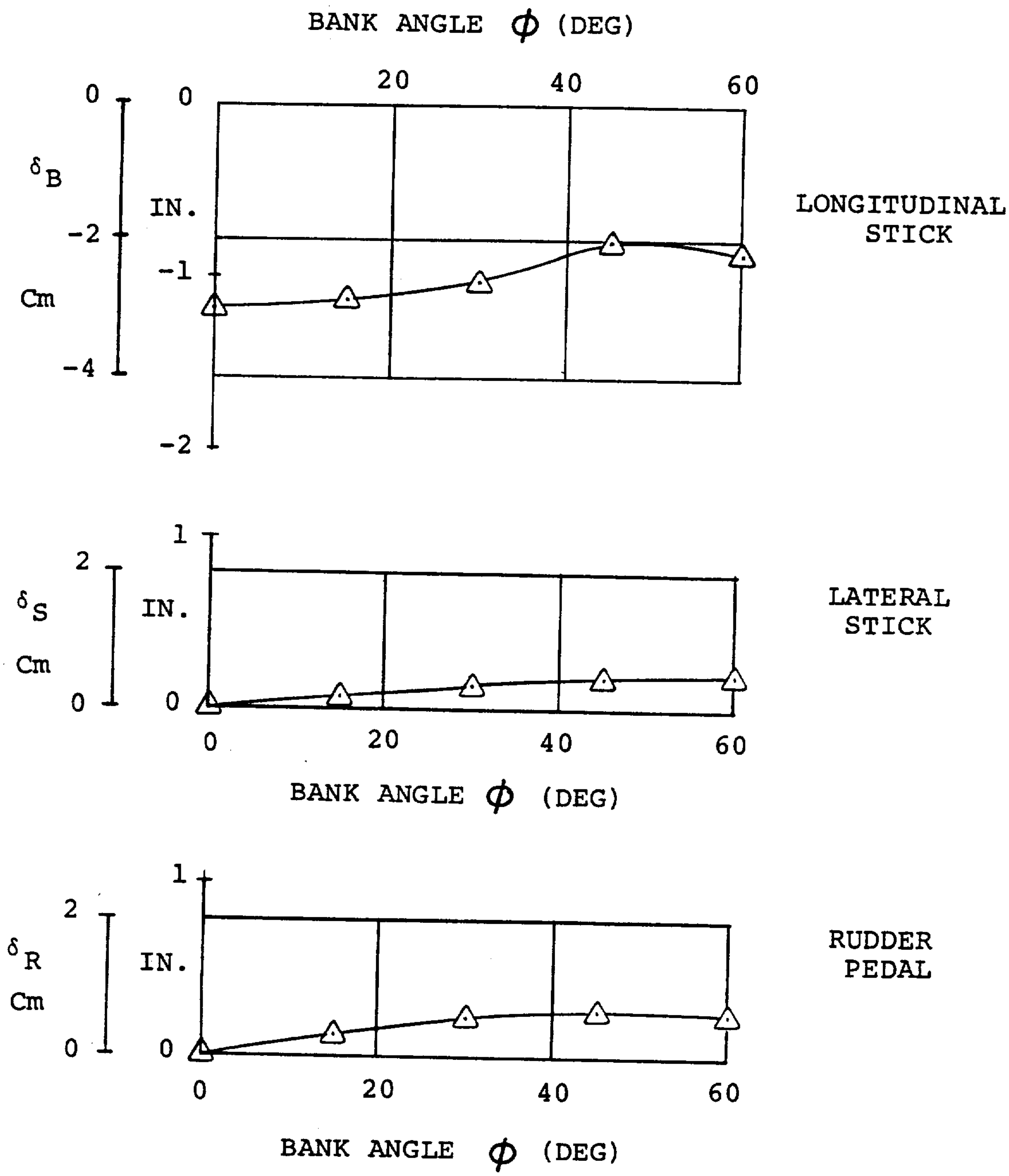

FIGURE 11.52 CONTROL POSITIONS IN COORDINATED TURNS IN TRANSITION - $i_N = 60^o$ V = 110 KTS $\delta_F = 40^o$ GW = 5896.7 Kg (13000 LBS) SL STD DAY AFT CG

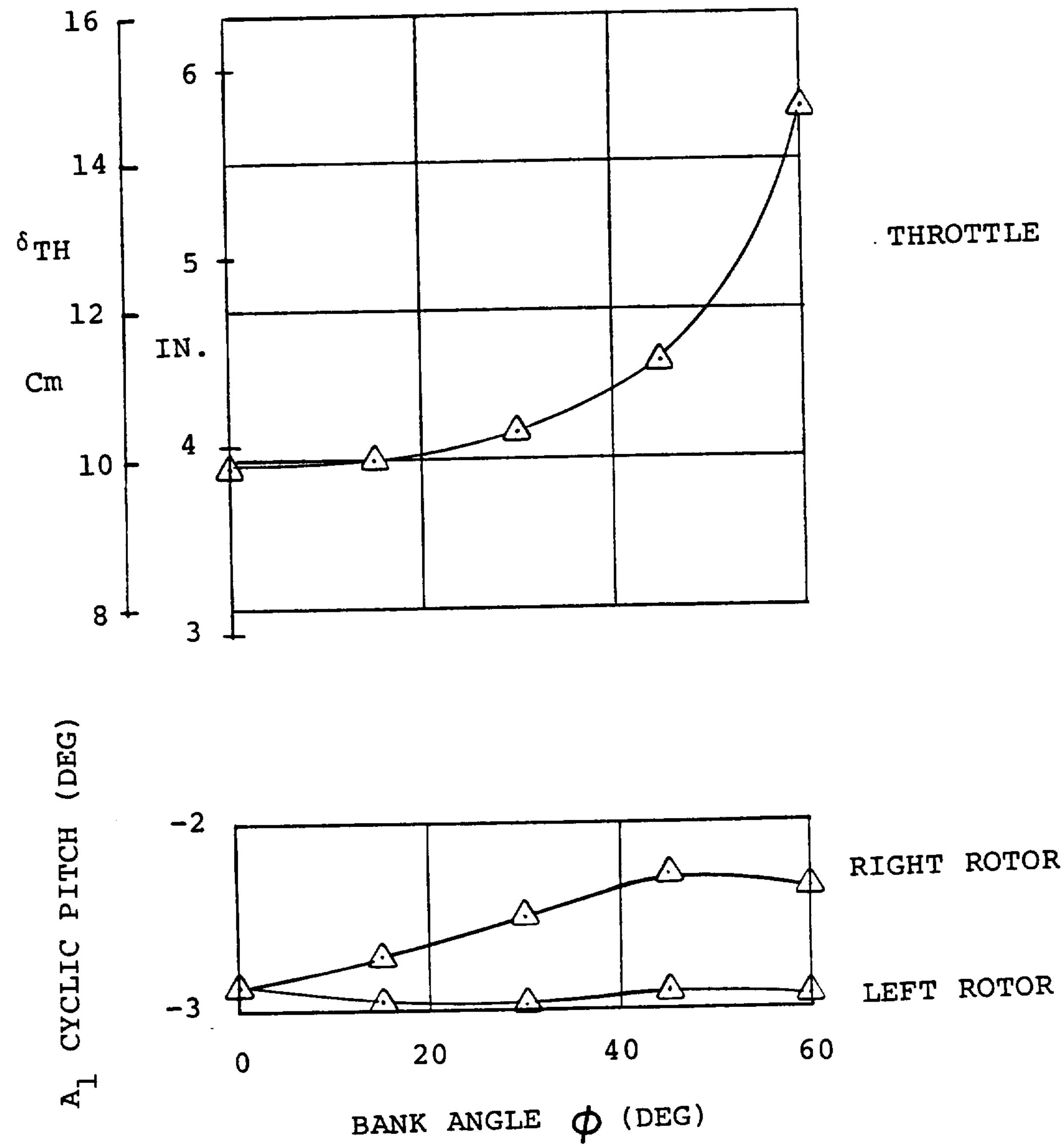

FIGURE 11.53 CONTROL DATA IN COORDINATED TURNS IN TRANSITION - $i_N = 60°$ V = 110 KTS
$\delta_F = 40°$ AFT CG GW = 5896.7 Kg (13000 LBS) SL STD DAY

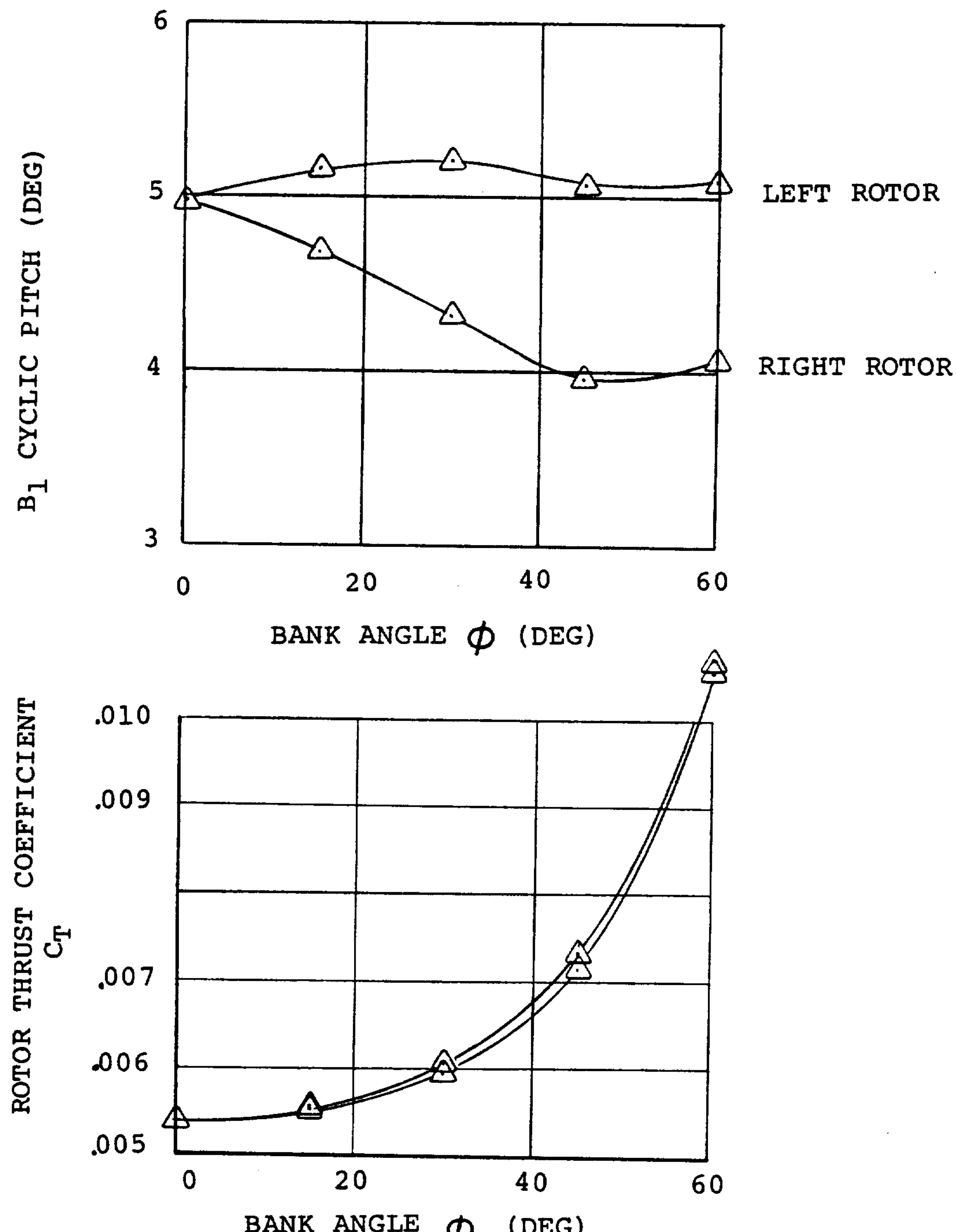

FIGURE 11.54 CYCLIC AND THRUST DATA IN COORDINATED TURNS IN TRANSITION - i_N = 60° V - 110 KTS δ_F = 40° AFT CG GW = 5896.7 Kg (13000 LBS) SL STD DAY

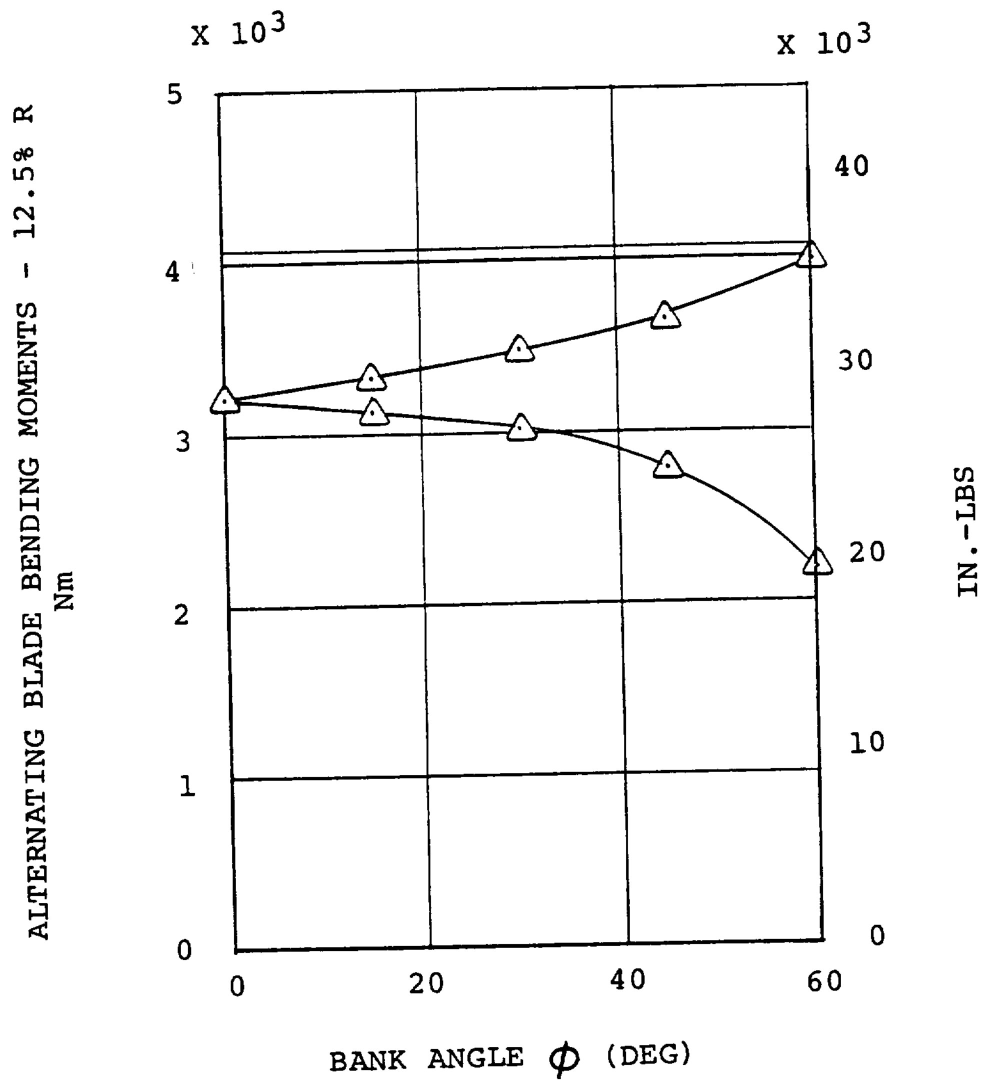

FIGURE 11.55 ESTIMATED BLADE BENDING LOADS IN COORDINATED TURNS IN TRANSITION - $i_N = 60°$ V = 110 KTS $\delta_F = 40°$ AFT CG GW = 5896.7 Kg (13000 LBS) SL STD DAY

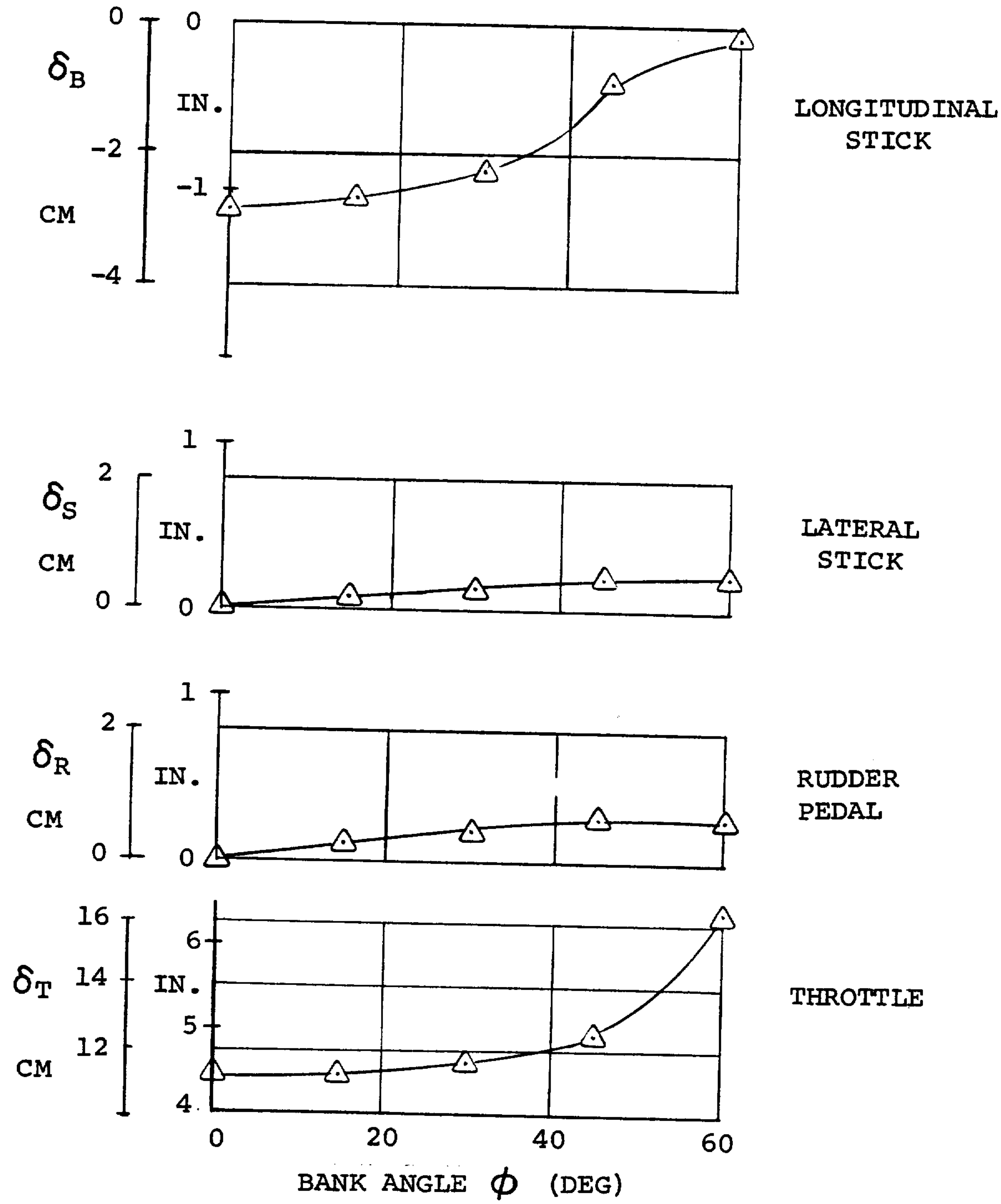

FIGURE 11.56 CONTROL POSITIONS IN TRANSITION COORDINATED TURNS $i_N = 60°$ V = 120 KTS $\delta_F = 40°$ FWD CG GW = 5896.7 Kg (13000 LB) SL STD DAY

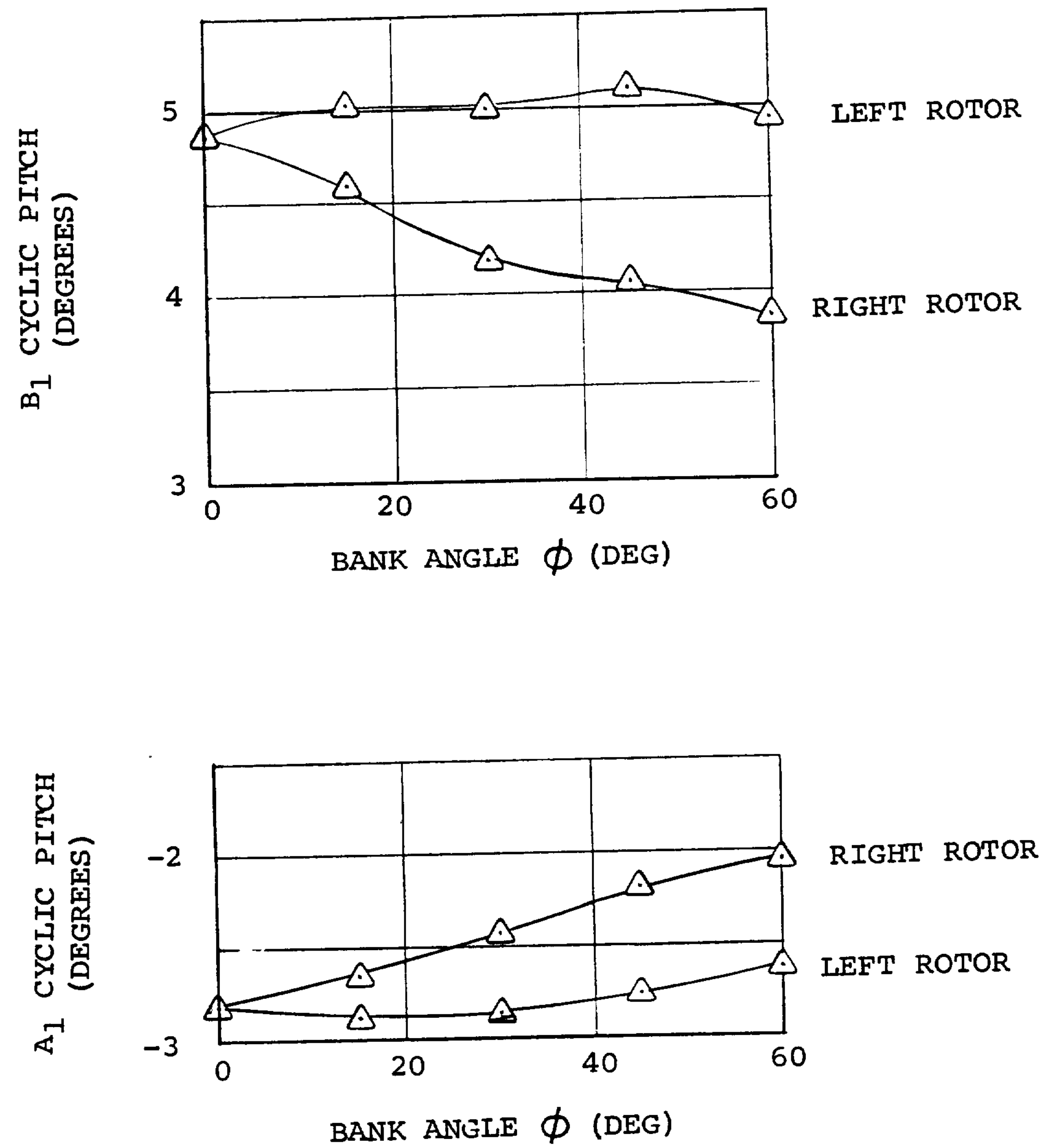

FIGURE 11.57 CYCLIC PITCH IN COORDINATED TURNS IN TRANSITION
$i_N = 60°$ V = 120 KTS $\delta_F = 40°$ FWD CG SL STD DAY
GW = 5896.7 Kg (13000 LB)

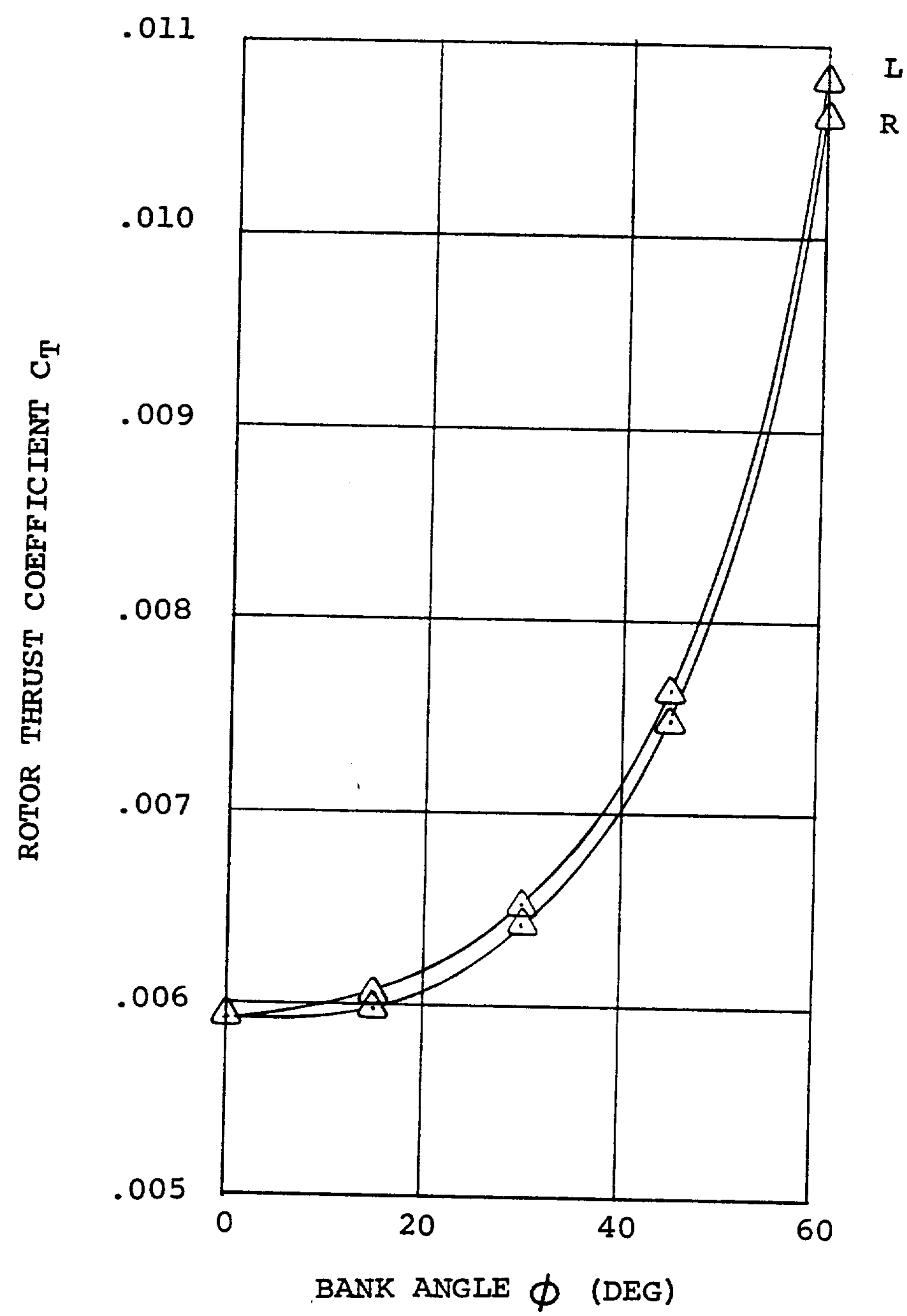

FIGURE 11.58 ROTOR THRUST COEFFICIENT IN COORDINATED TURNS IN TRANSITION $i_N = 60°$ V = 120 KTS $\delta_F = 40°$ FWD CG GW = 5896.7 Kg (13000 LB) SL STD DAY

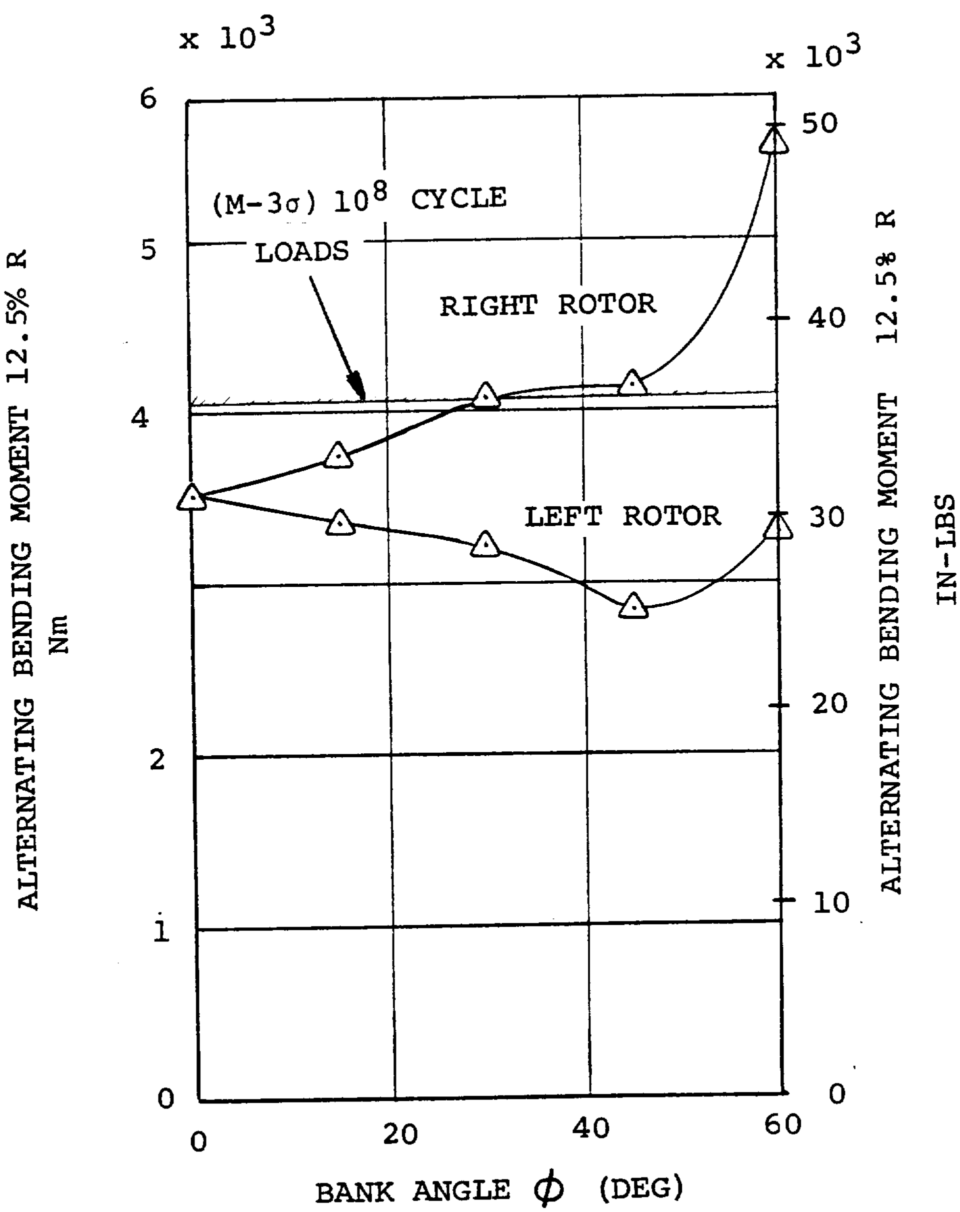

FIGURE 11.59 ESTIMATED BLADE LOADS IN COORDINATED TURNS IN TRANSITION $i_N = 60°$ V=120KTS $\delta_F = 40°$ FWD CG GW = 5896.7 Kg (13000 LB) SL STD DAY

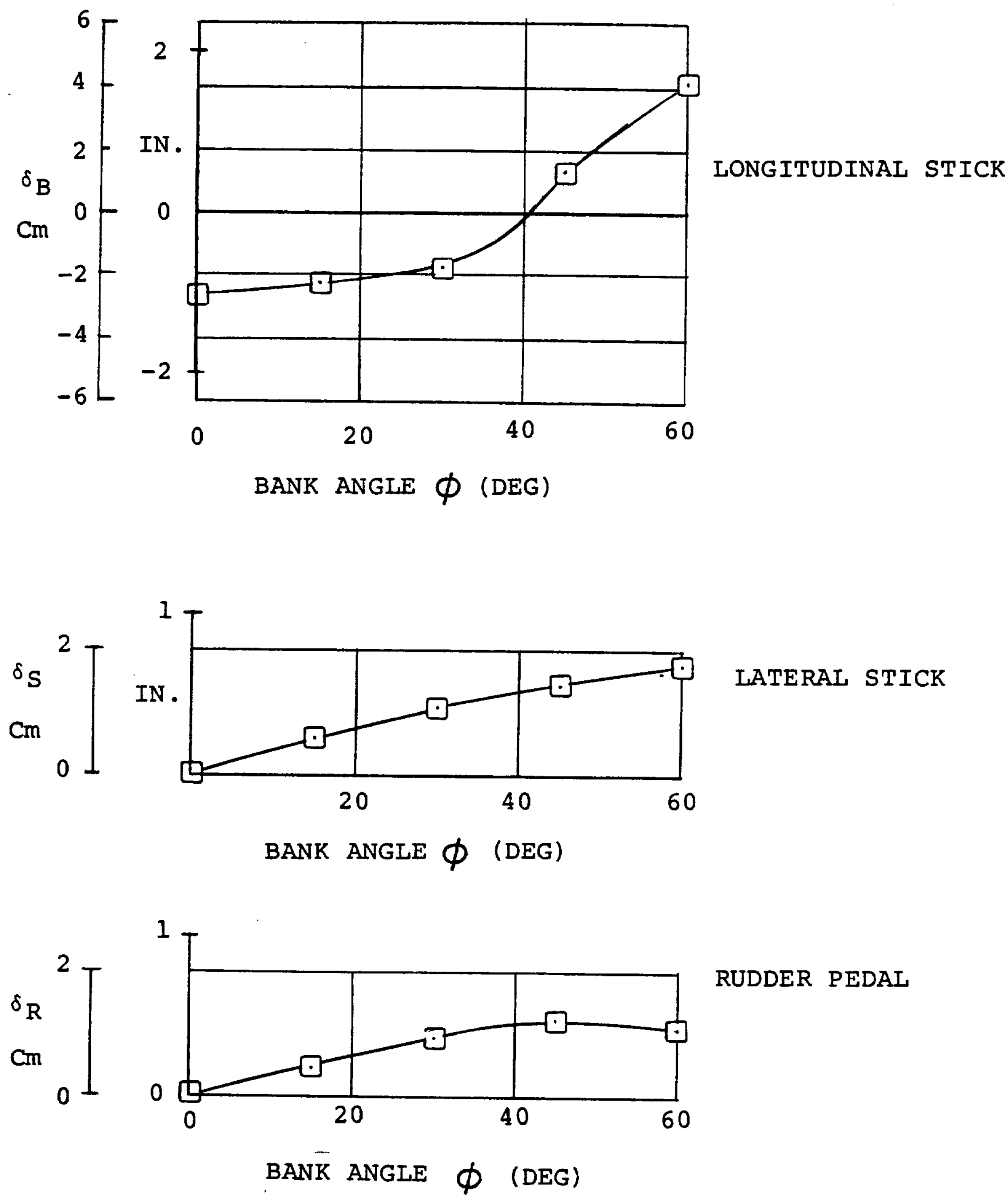

FIGURE 11.60 CONTROL POSITIONS IN COORDINATED TURNS IN TRANSITION - $i_N = 30^\circ$ V = 110 KTS $\delta_F = 40^\circ$ AFT CG

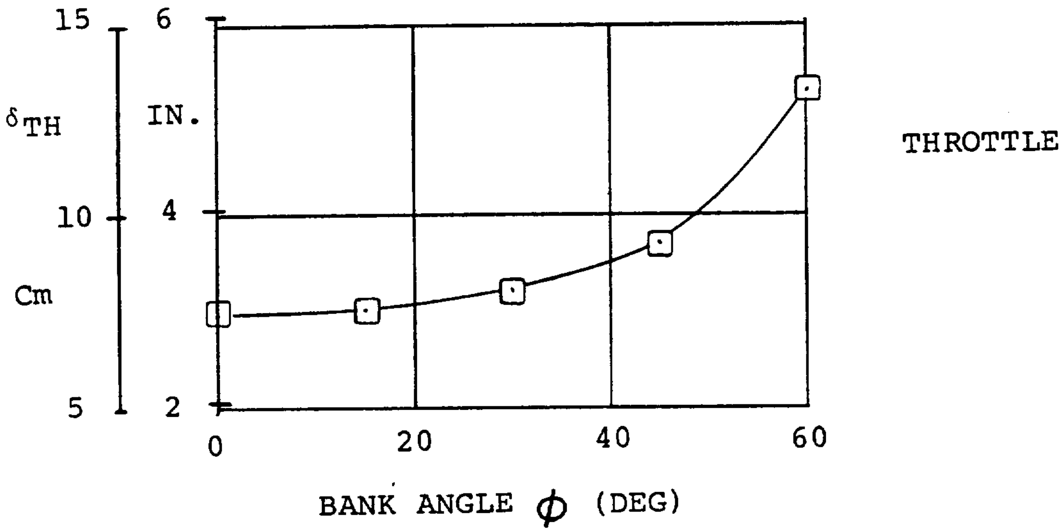

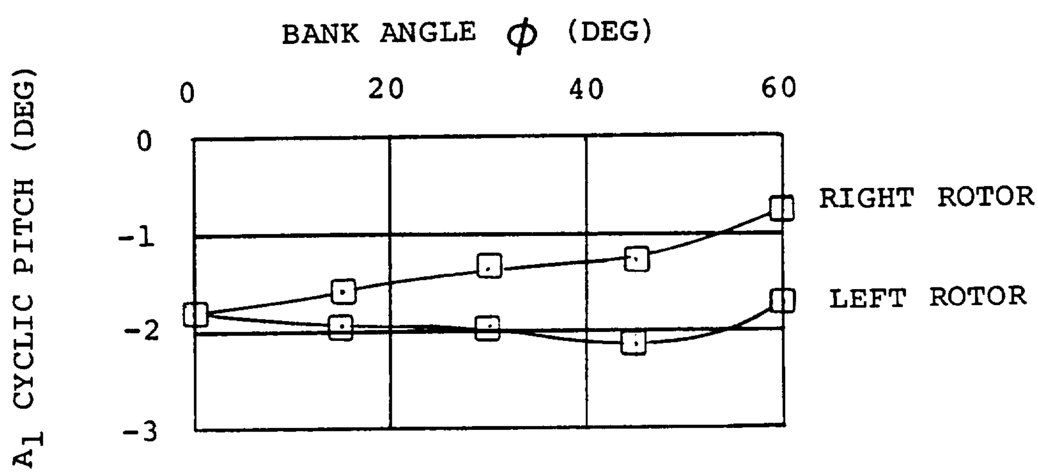

FIGURE 11.61 CONTROL DATA IN COORDINATED TURNS IN TRANSITION
AFT CG $i_N = 30°$ V = 110 KTS $\delta_F = 40°$
GW = 5896.7 Kg (13000 LBS) SL STD DAY

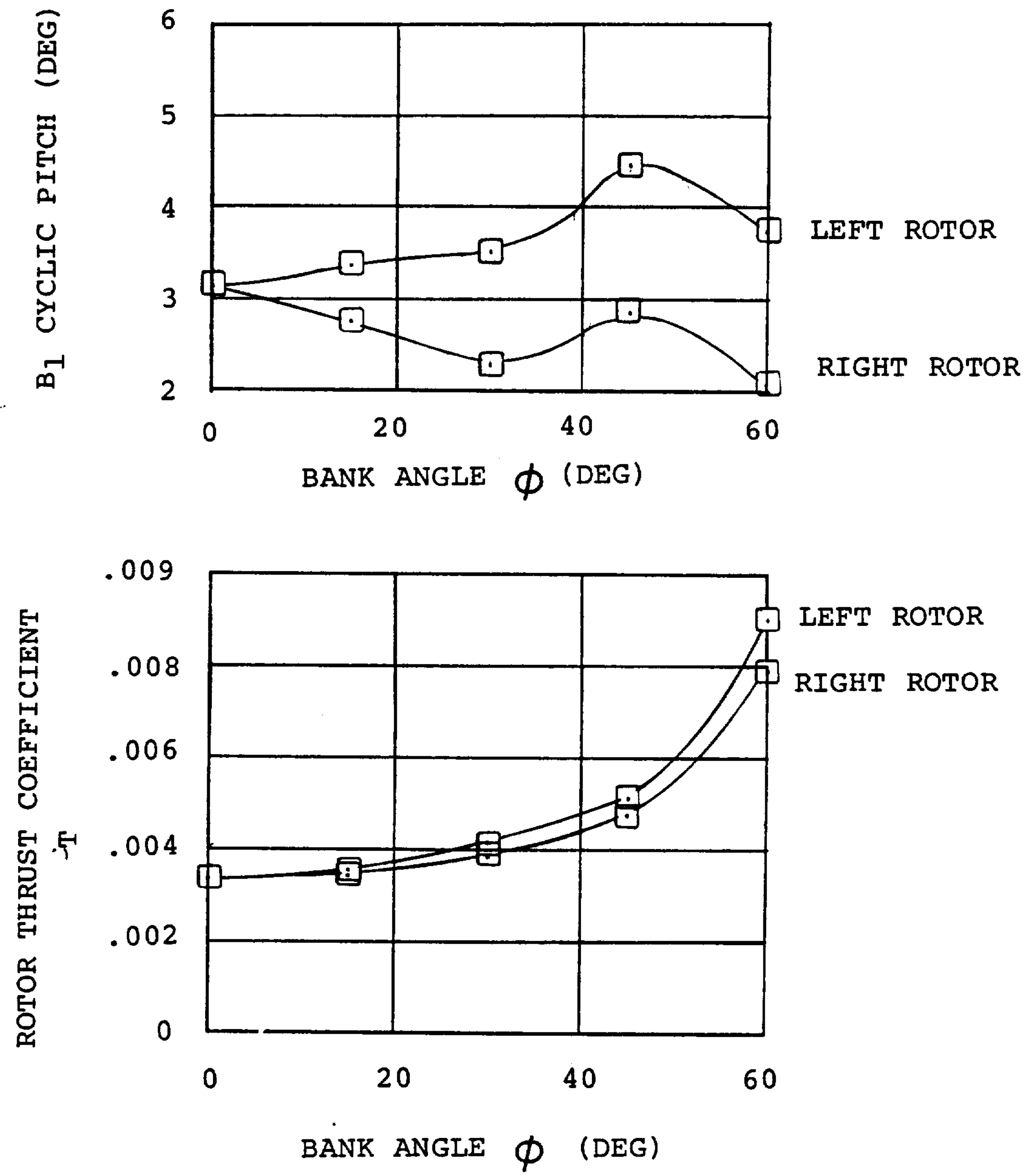

FIGURE 11.62 CYCLIC AND THRUST DATA IN COORDINATED TURNS IN TRANSITION - $i_N = 30°$ V = 110 KTS $\delta_F = 40°$ AFT CG GW = 5896.7 Kg (13000 LBS) SL STD DAY

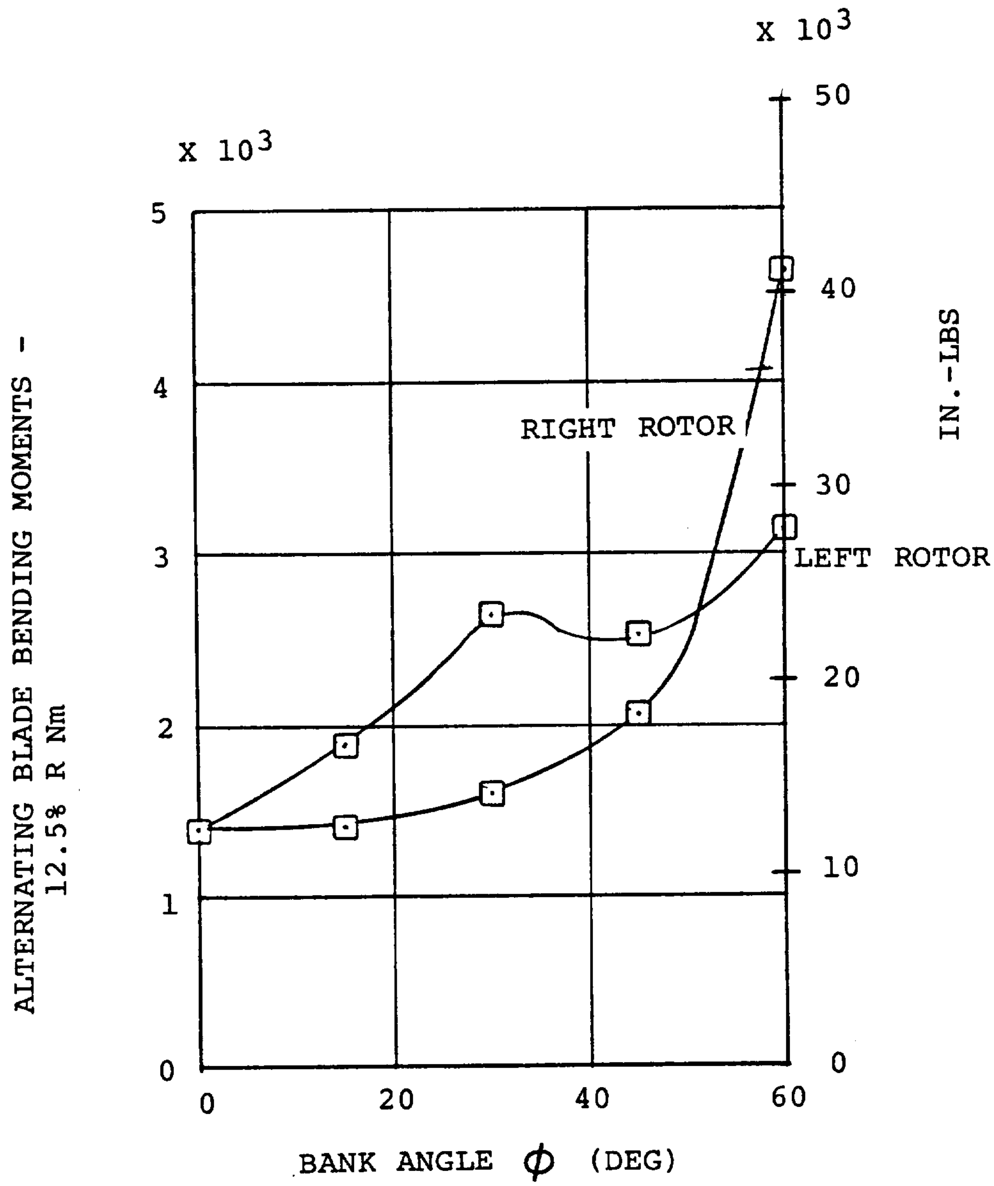

FIGURE 11.63 ESTIMATED BLADE BENDING LOADS 12.5% R
$\delta_F = 40^o$ AFT CG GW = 5896.7 Kg (13000 LBS)
SL STD DAY V = 110 KTS $i_N = 30°$

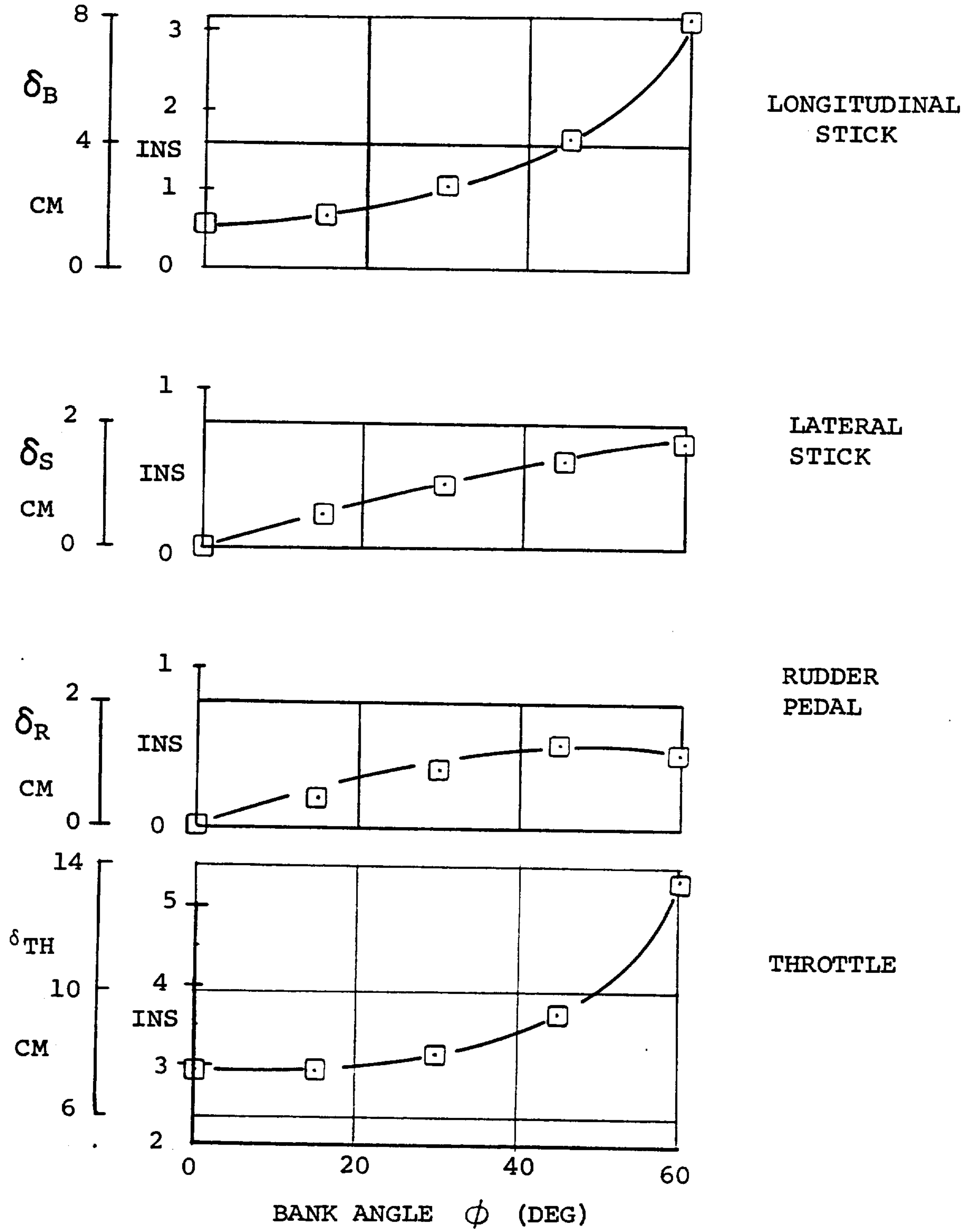

FIGURE 11.64 CONTROL POSITIONS IN COORDINATED TURNS
$i_N = 30°$ V = 110 KTS GW = 5896.7 Kg (13000 LB)
FWD CG $\delta_F = 40°$ SL STD DAY

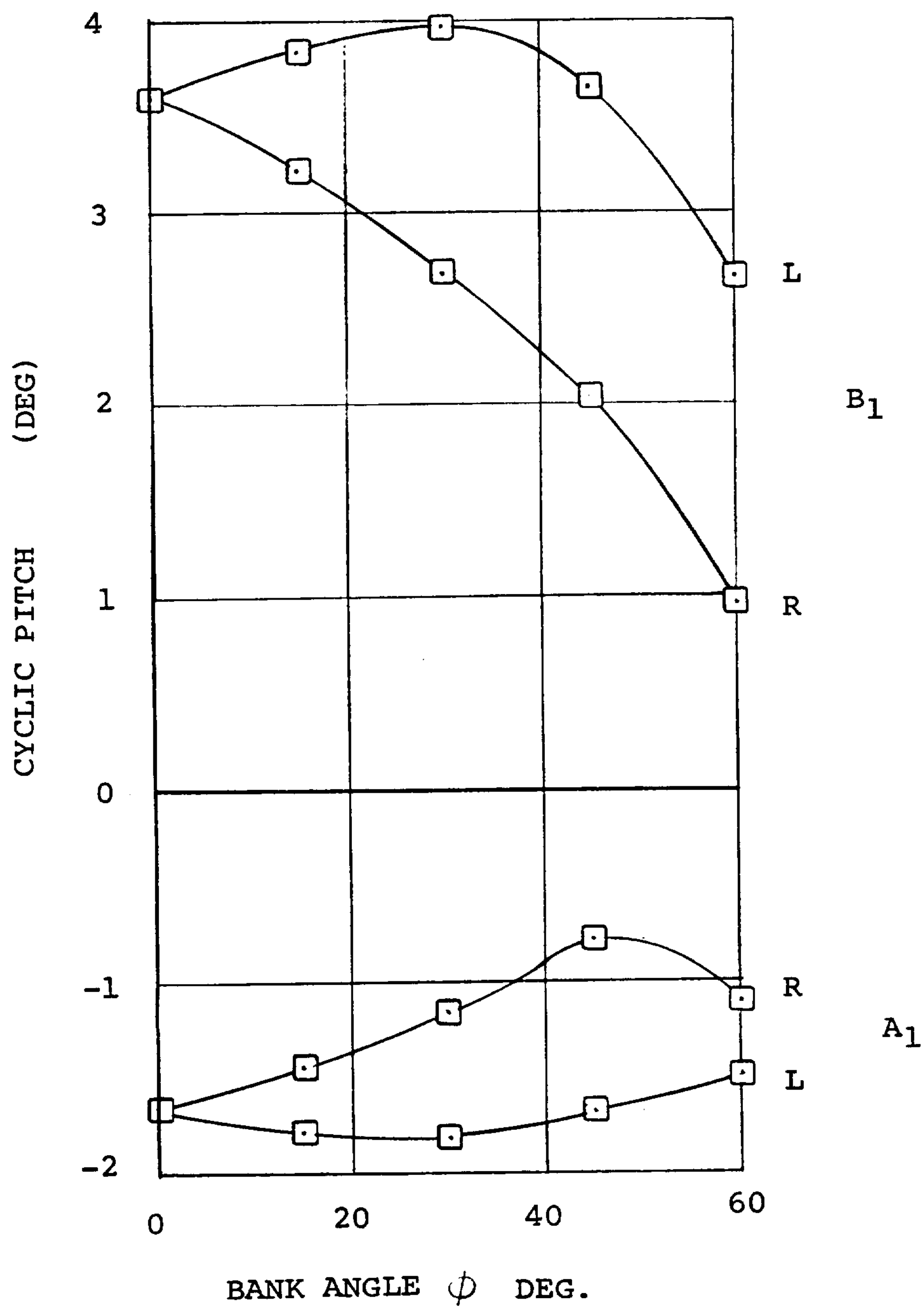

FIGURE 11.65 COORDINATED TURNS IN TRANSITION - CYCLIC PITCH
FWD CG $i_N = 30°$ v = 110 KTS SL STD DAY
$\delta_F = 40°$ GW = 5896.7 Kg (13000 LB)

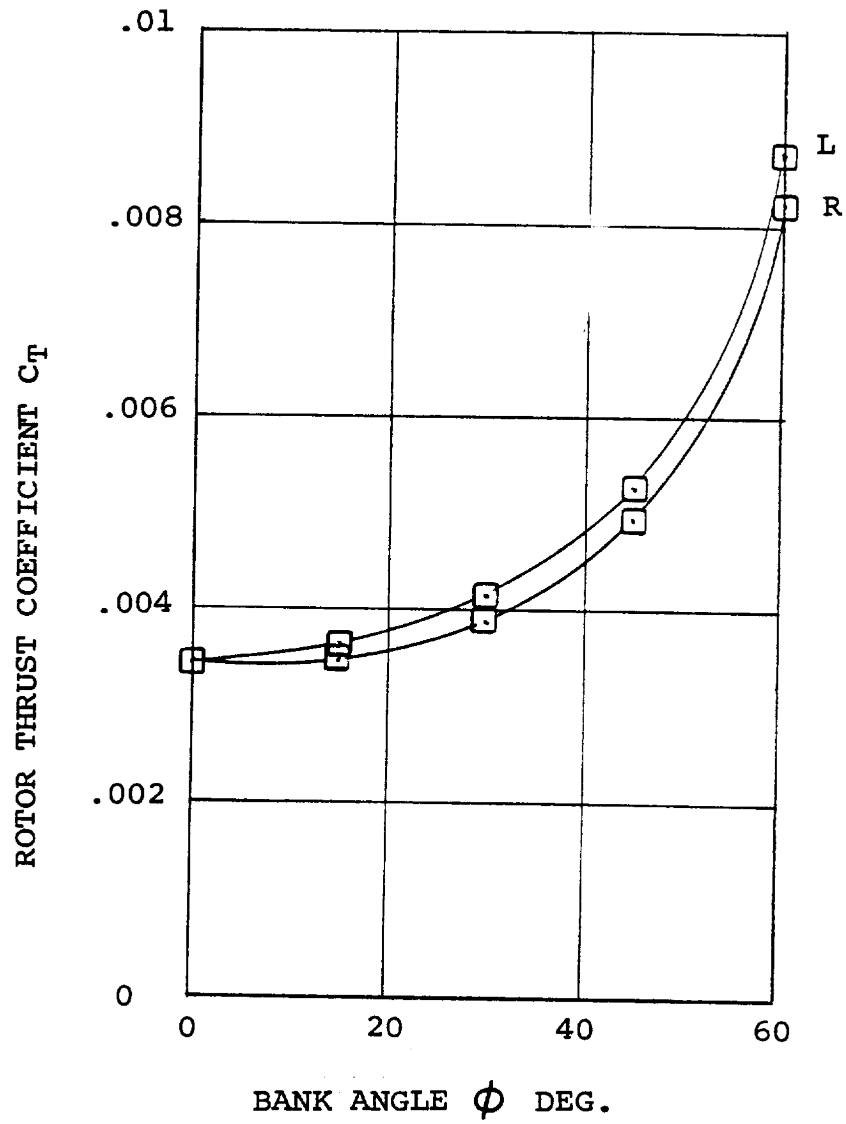

FIGURE 11.66 ROTOR THRUST IN COORDINATED TURNS SL STD DAY
$i_N = 30°$ V = 110 KTS $\delta_F = 40°$ FWD CG
GW = 5896.7 Kg (13000 LB)

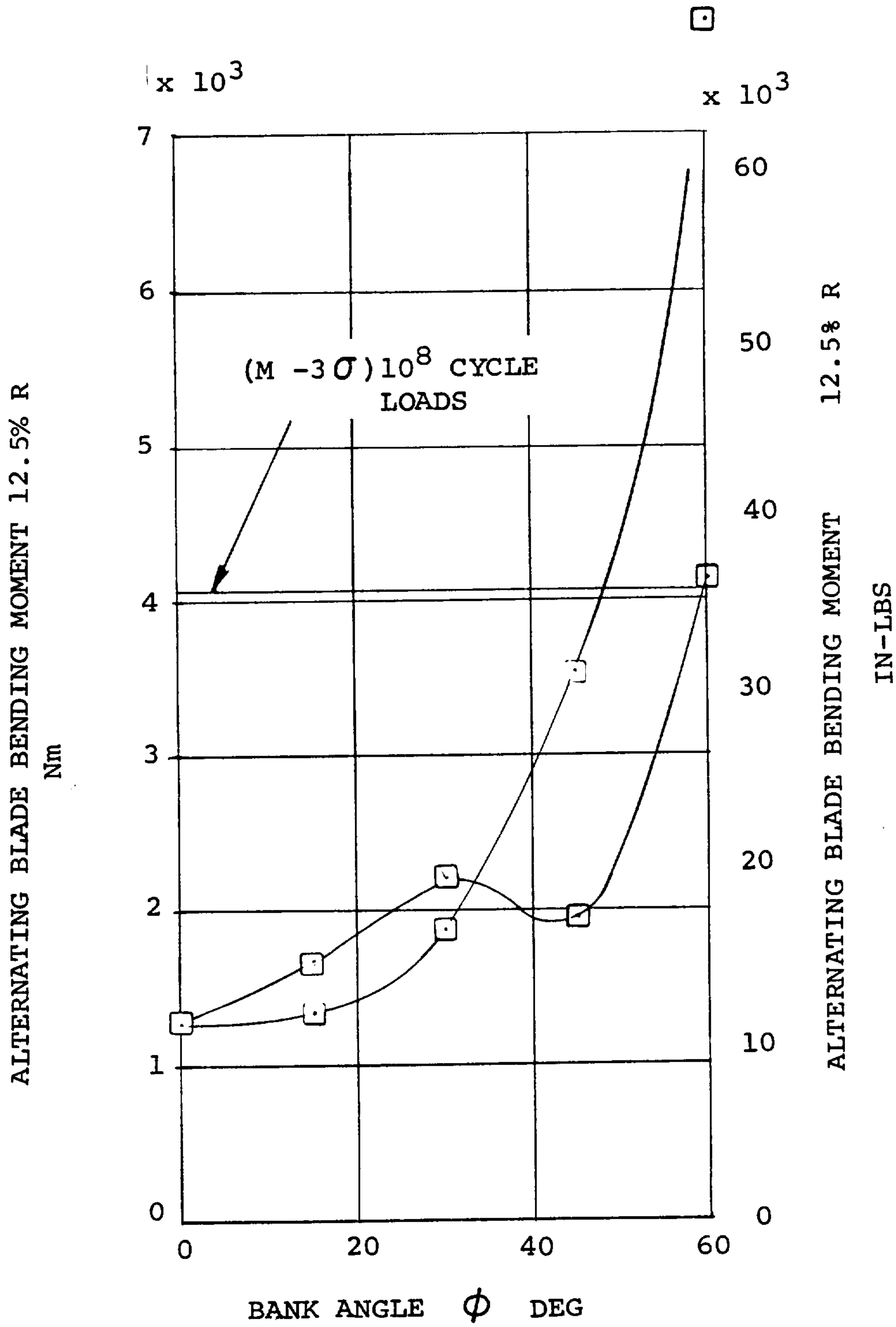

FIGURE 11.67 ESTIMATED BLADE LOADS IN COORDINATED TURNS
$i_N = 30^\circ$ V = 110 KTS FWD CG $\delta_F = 40^\circ$
GW = 5896.7 Kg (13000 LBS) SL STD DAY

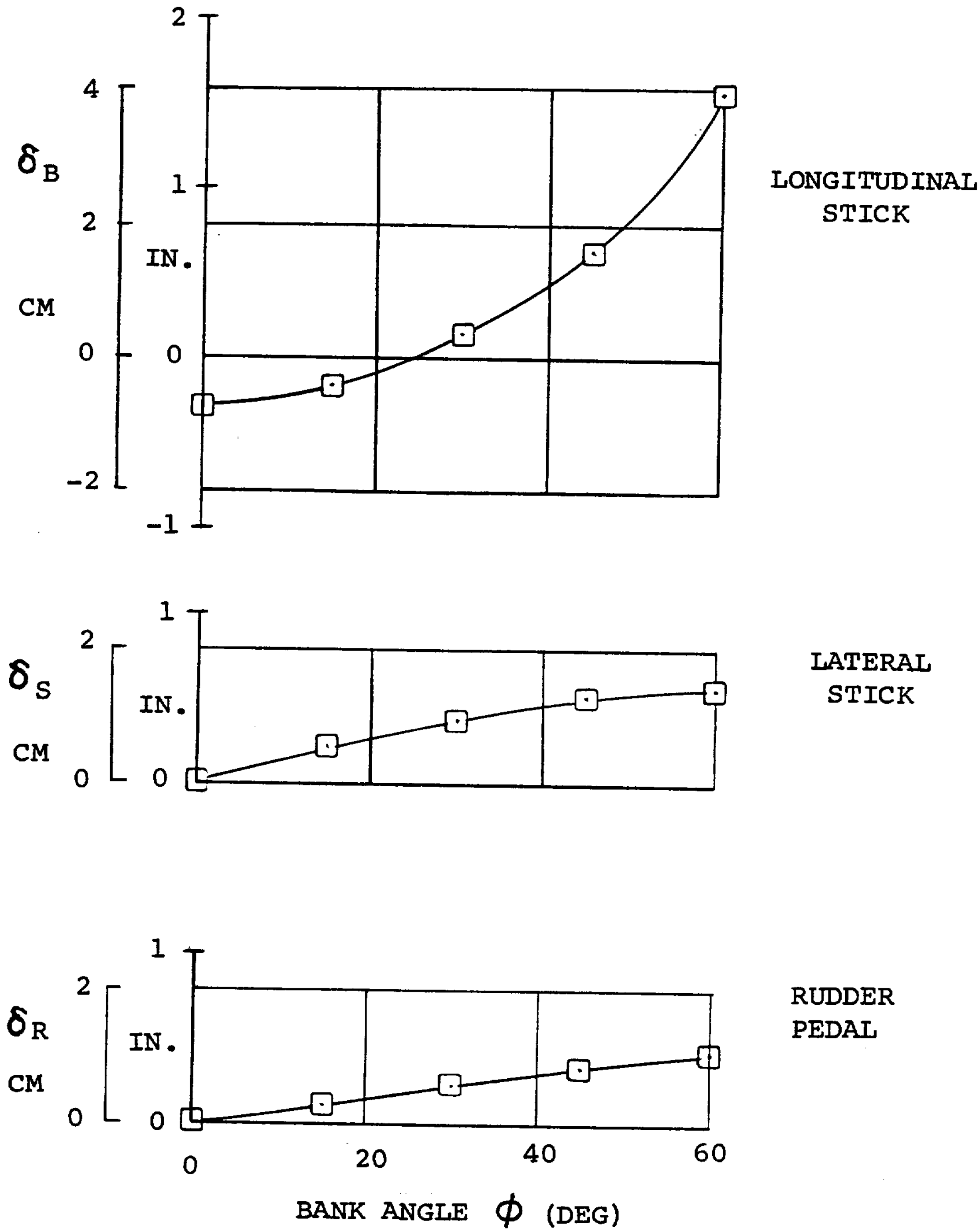

FIGURE 11.68 CONTROL POSITIONS IN COORDINATED TURNS IN TRANSITION $i_N = 30°$ V = 130 KTS $\delta_F = 40°$ FWD CG GW = 5896.7 Kg (13000 LB) SL STD DAY

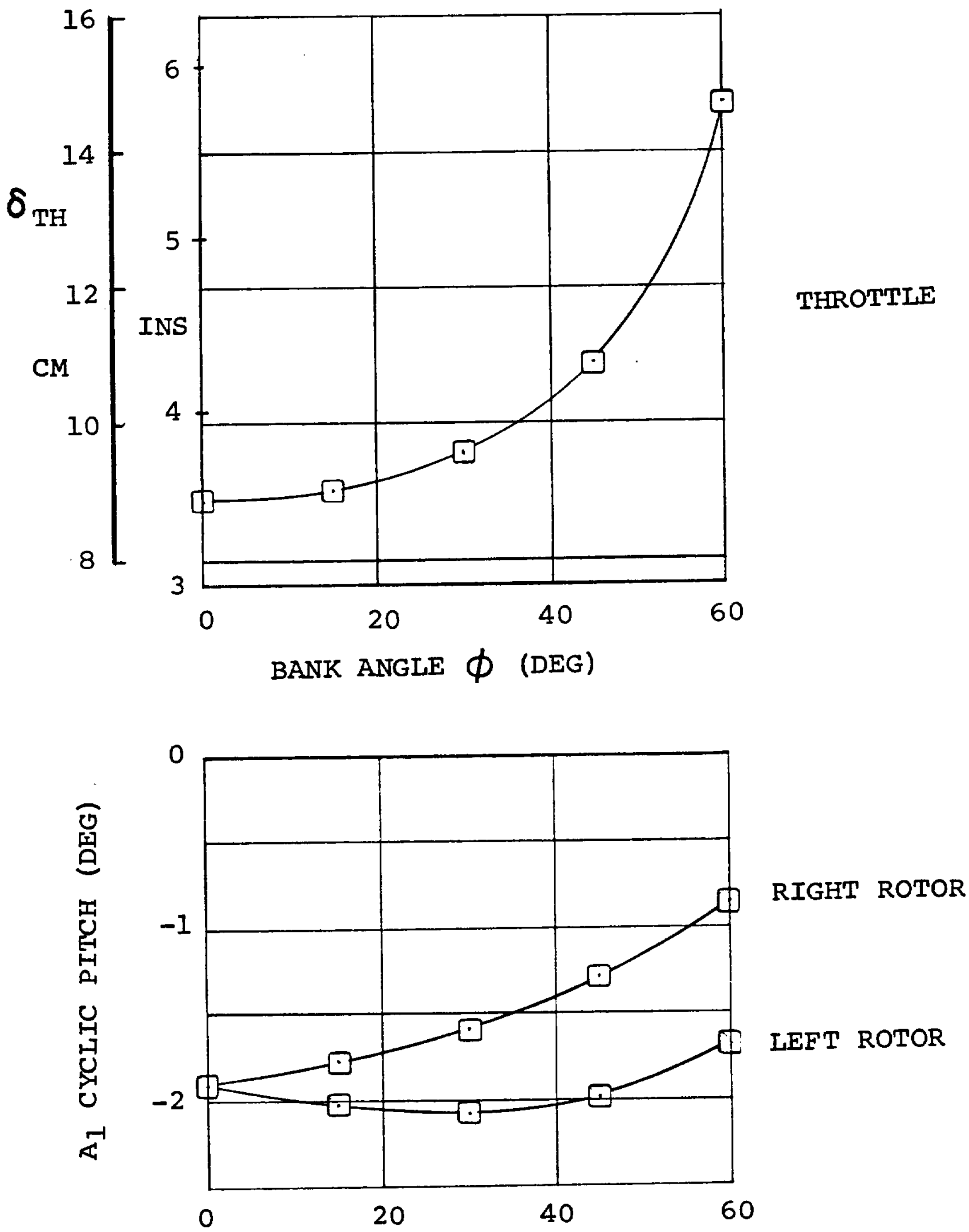

FIGURE 11.69 CONTROL POSITIONS IN COORDINATED TURNS IN TRANSITION $i_N = 30°$ V = 130 KTS $\delta_F = 40°$ FWD CG GW = 5896.7 Kg (13000 LB) SL STD DAY

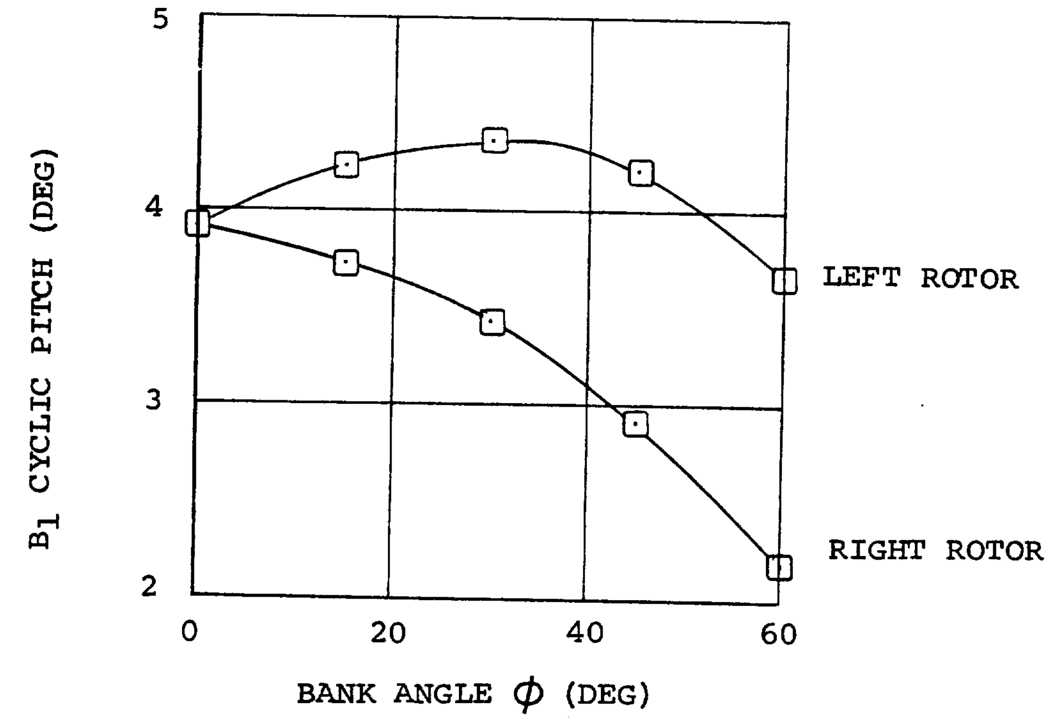

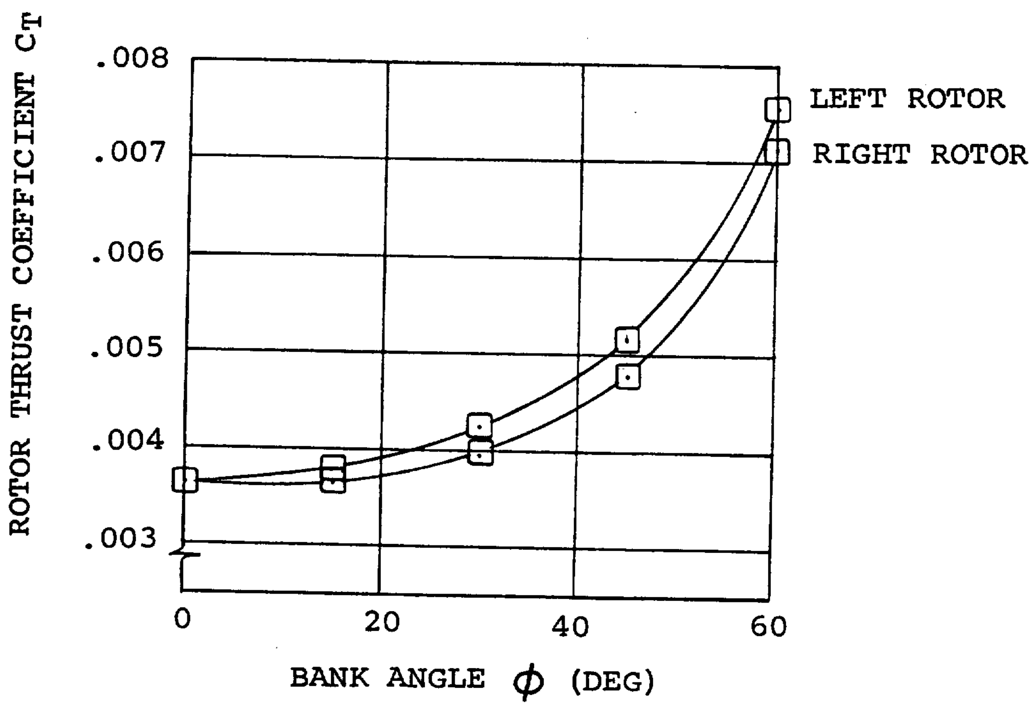

FIGURE 11.70. TRIM DATA IN COORDINATED TURNS IN TRANSITION
$i_N = 30°$ V = 130 KTS $\delta_F = 40°$ FWD CG
GW = 5896.7 Kg (13000 LB) SL STD DAY

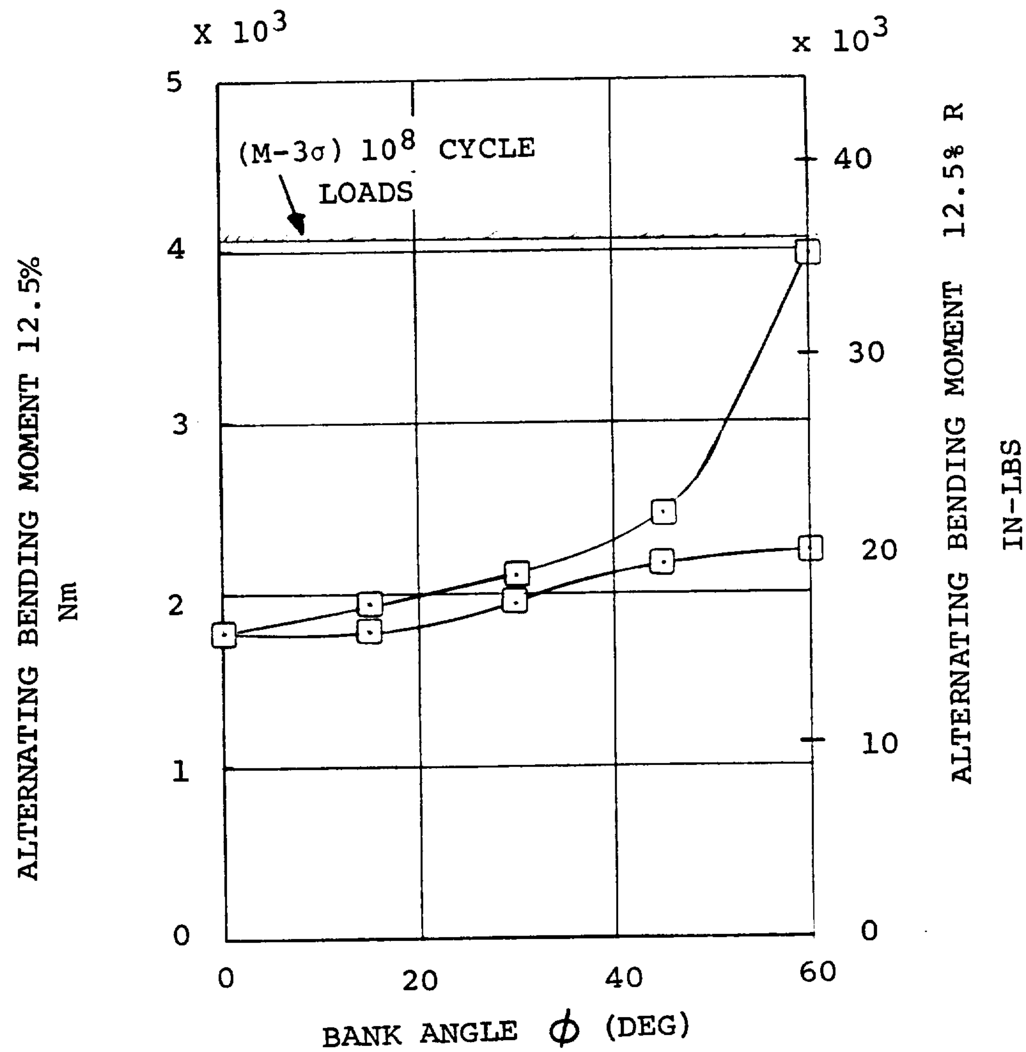

FIGURE 11.71. ESTIMATED BLADE BENDING LOADS AT 12.5% R IN COORDINATED TURNS IN TRANSITION $i_N = 30^\circ$ V = 130 KTS $\delta_F = 40^\circ$ FWD CG SL STD DAY GW = 5896.7 Kg (13000 LB)

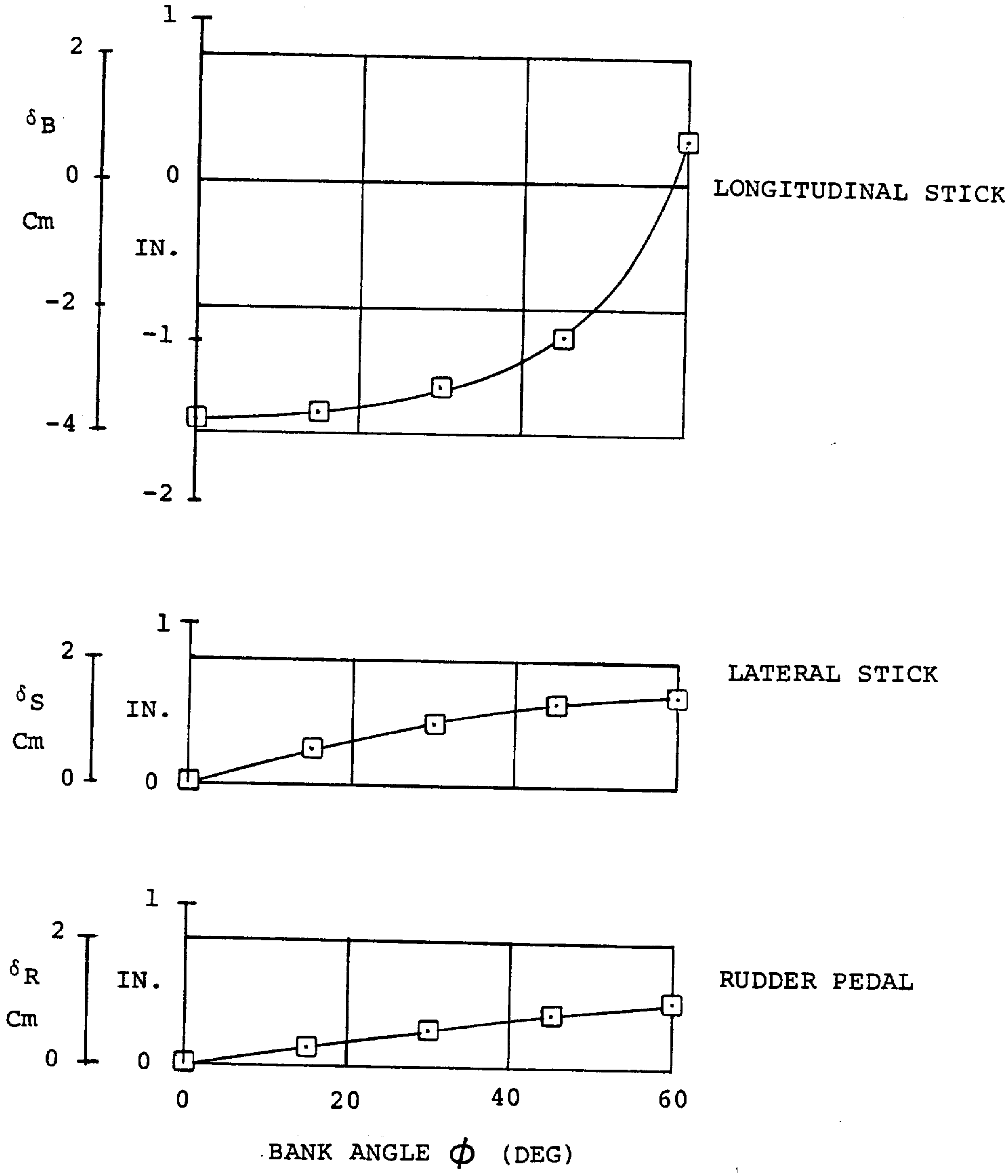

FIGURE 11. 72. CONTROL POSITIONS IN COORDINATED TURNS IN TRANSITION
$i_N = 30^\circ$ V = 130 KTS $\delta_F = 40^\circ$ AFT CG
GW = 5896.7 Kg (13000 LBS) SL STD DAY

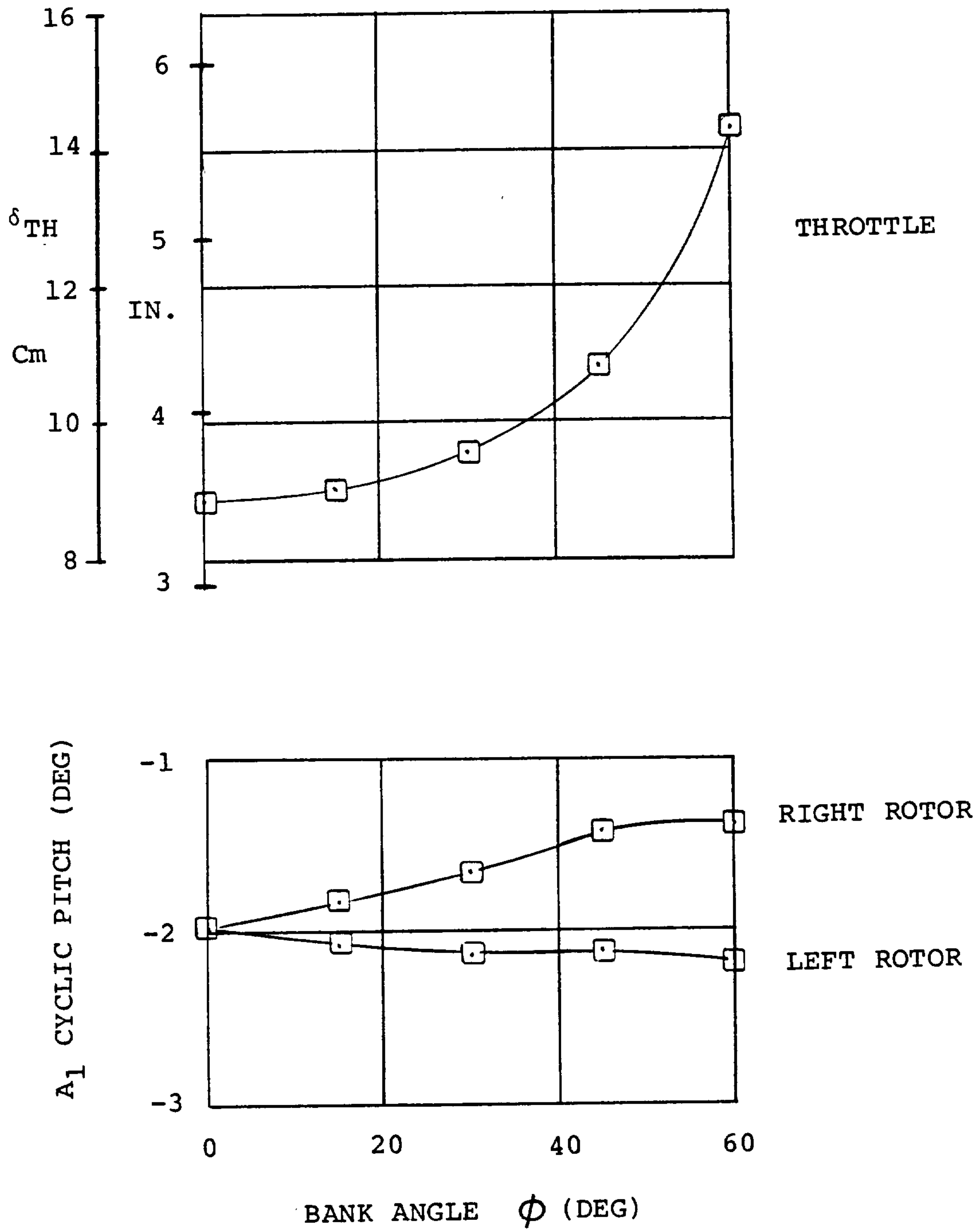

FIGURE 11.73 CONTROL DATA IN COORDINATED TURNS IN TRANSITION
$i_N = 30^\circ$ V = 130 KTS AFT CG $\delta_F = 40^\circ$
GW = 5896.7 Kg (13000 LBS) SL STD DAY

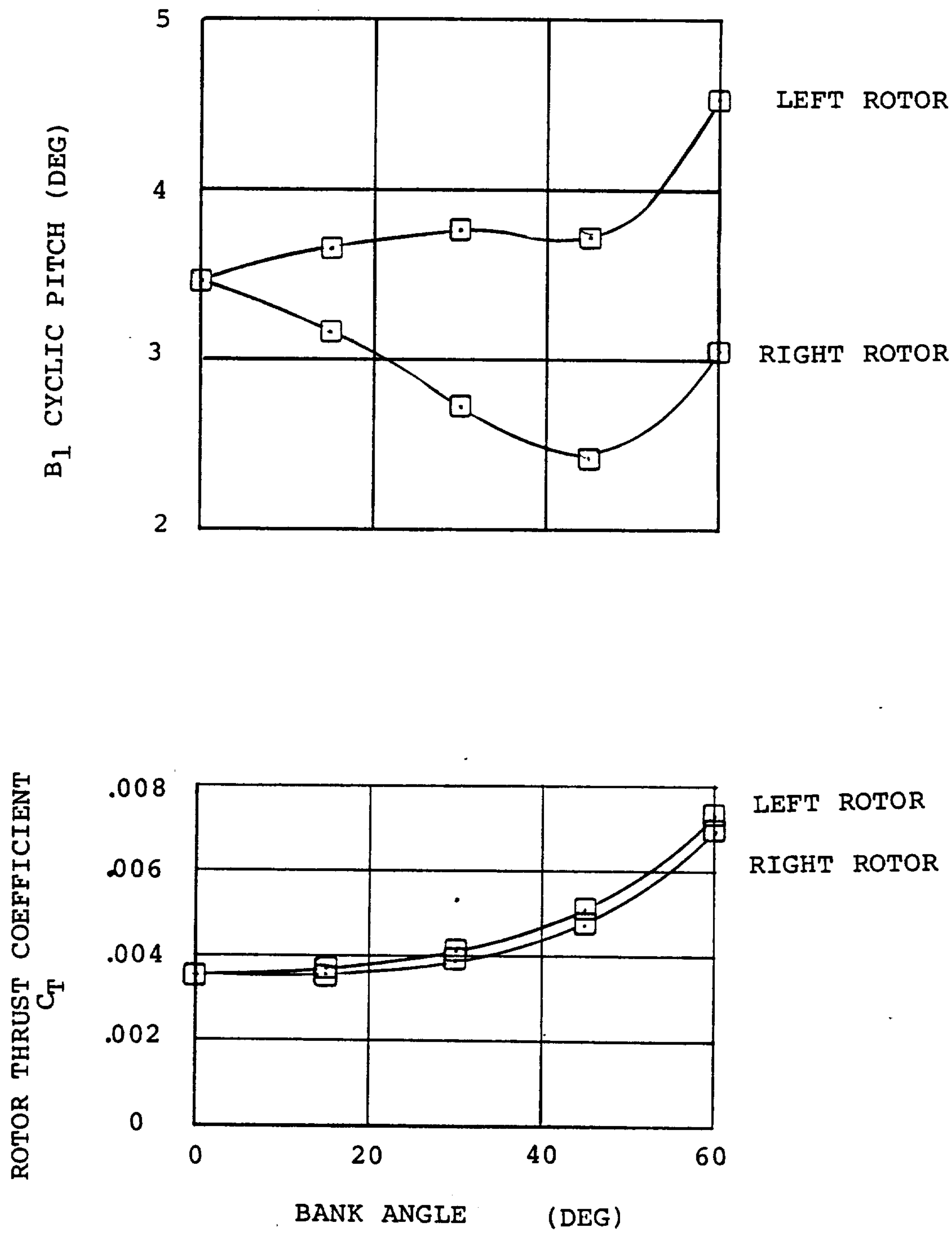

FIGURE 11.74 CYCLIC AND THRUST DATA IN COORDINATED TURNS IN TRANSITION - $i_N = 30^o$ V = 130 KTS $\delta_F = 40^o$ AFT CG GW = 5896.7 Kg (13000 LBS) SL STD DAY

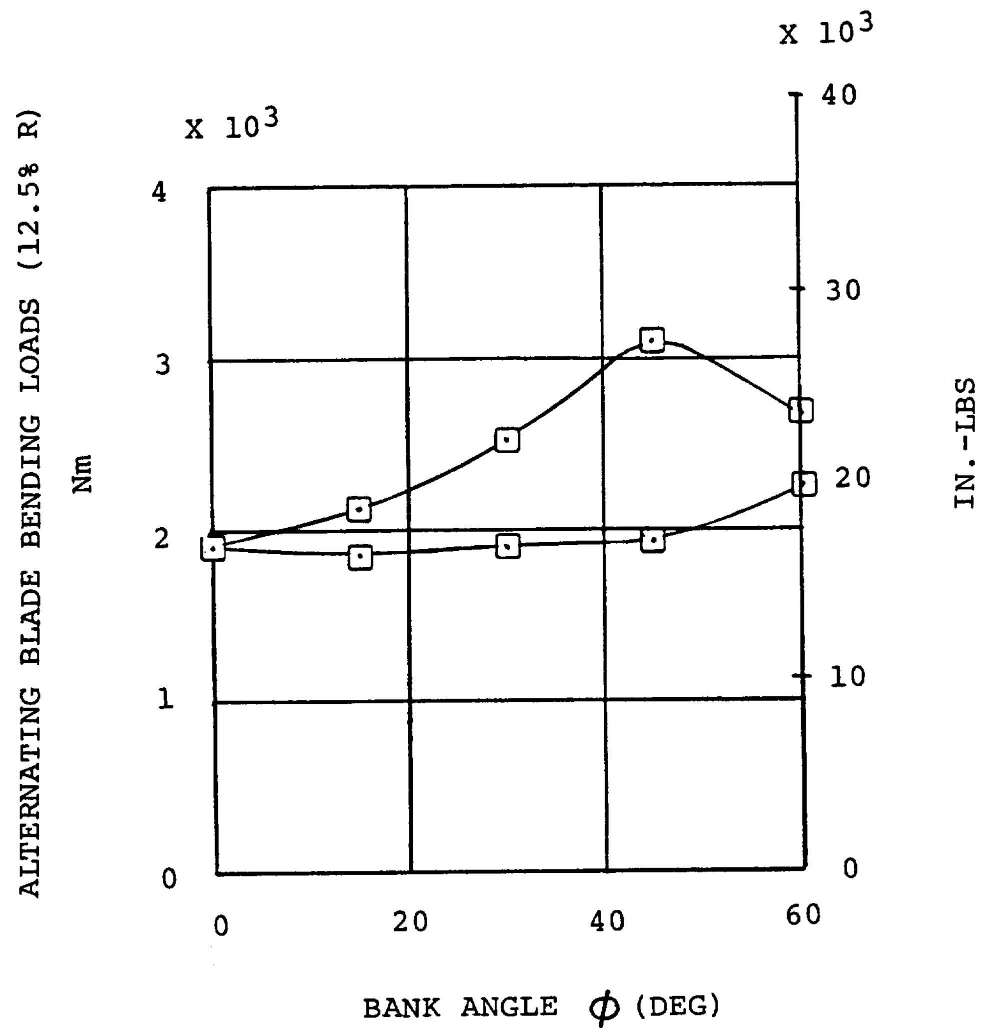

FIGURE 11.75 ESTIMATED BLADE BENDING LOADS IN COORDINATED TURNS IN TRANSITION - $i_N = 30^\circ$ V = 130 KTS $\delta_F = 40^\circ$ AFT CG GW = 5896.7 Kg (13000 LBS) SL STD DAY

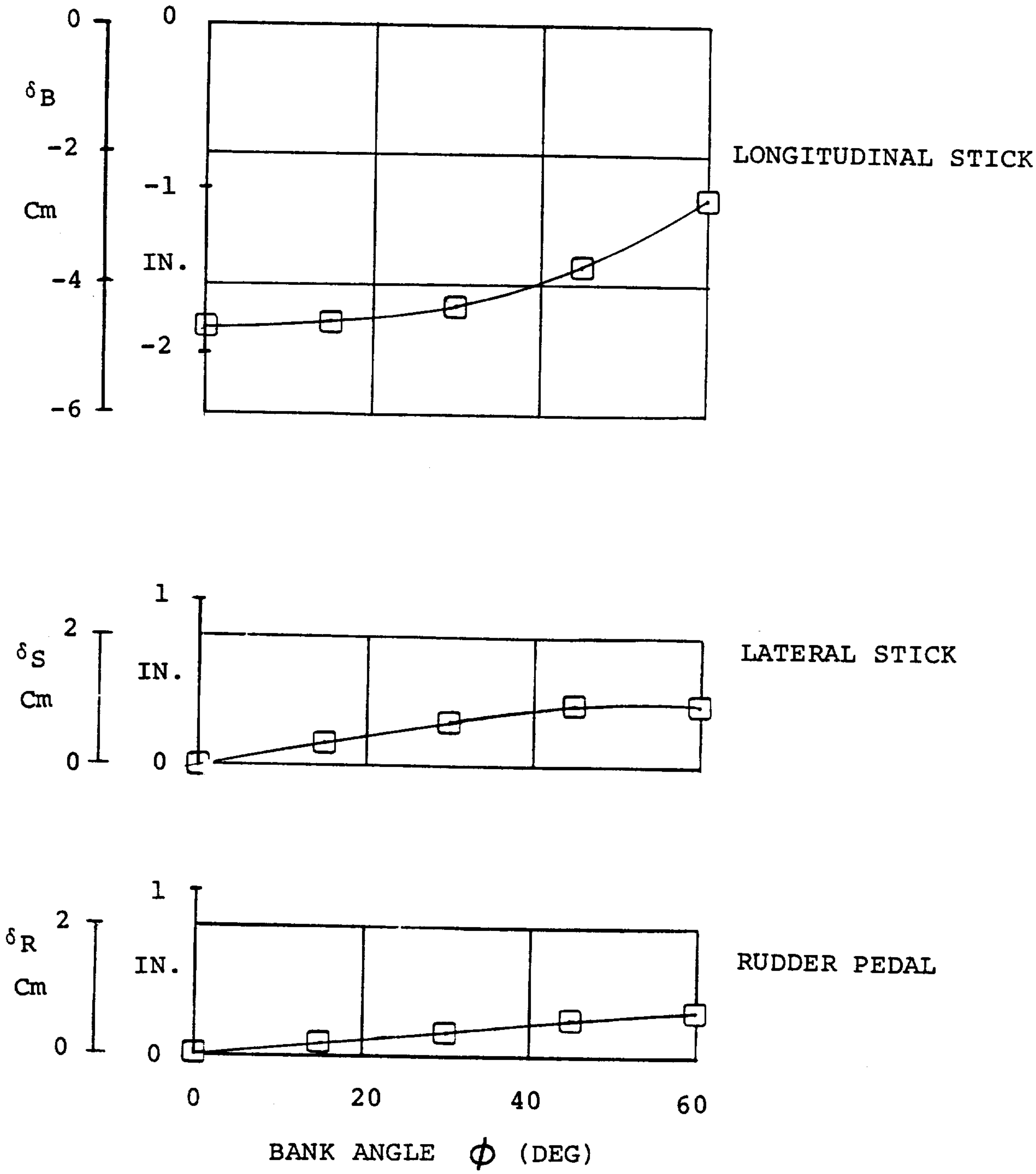

FIGURE 11.76 CONTROL POSITIONS IN COORDINATED TURNS IN TRANSITION - i_N = 30° V - 150 KTS δ_F = 40° GW = 5896.7 Kg (13000 LBS) AFT CG SL STD DAY

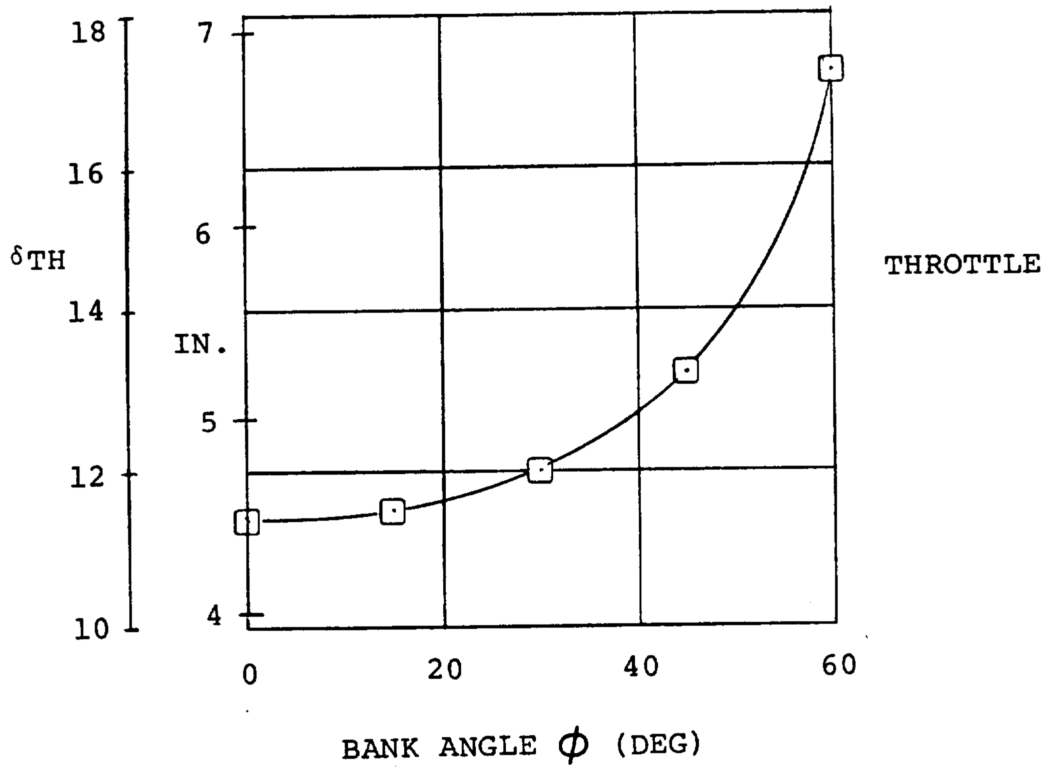

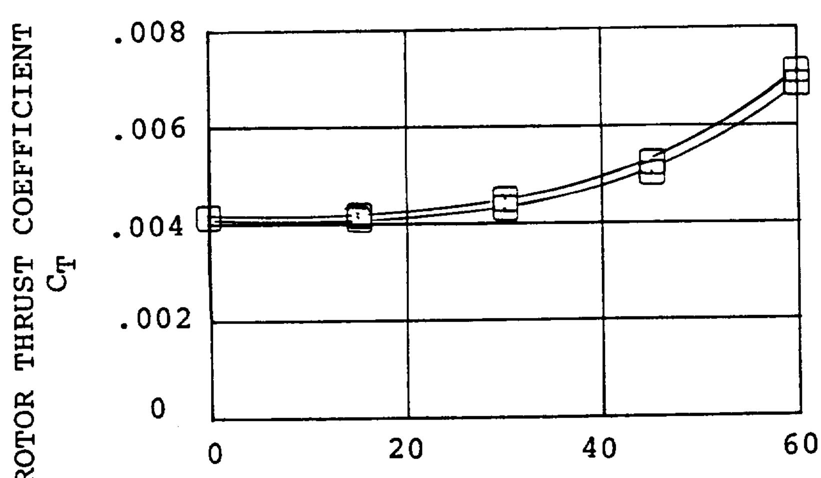

FIGURE 11.77 THROTTLE POSITION AND THRUST DATA IN COORDINATED TURNS IN TRANSITION - i_N = 30° V = 150 KTS δ_F = 40° AFT CG GW = 5896.7 Kg (13000 LBS) SL STD DAY

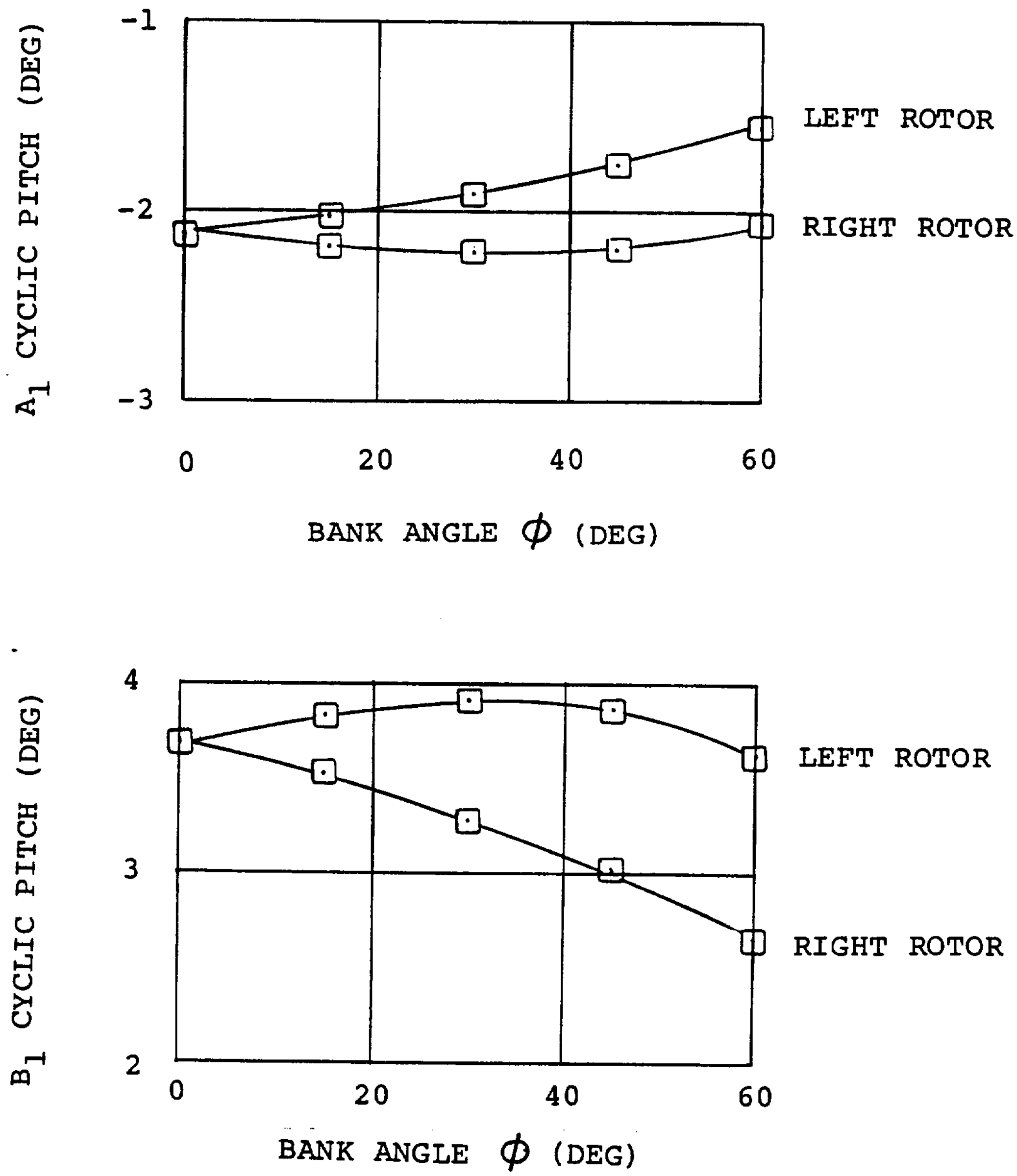

FIGURE 11.78 CYCLIC PITCH IN COORDINATED TURNS IN TRANSITION - $i_N = 30^\circ$ V = 150 KTS
$\delta_F = 40^\circ$ GW = 5896.7 Kg (13000 LBS)
AFT CG SL STD DAY

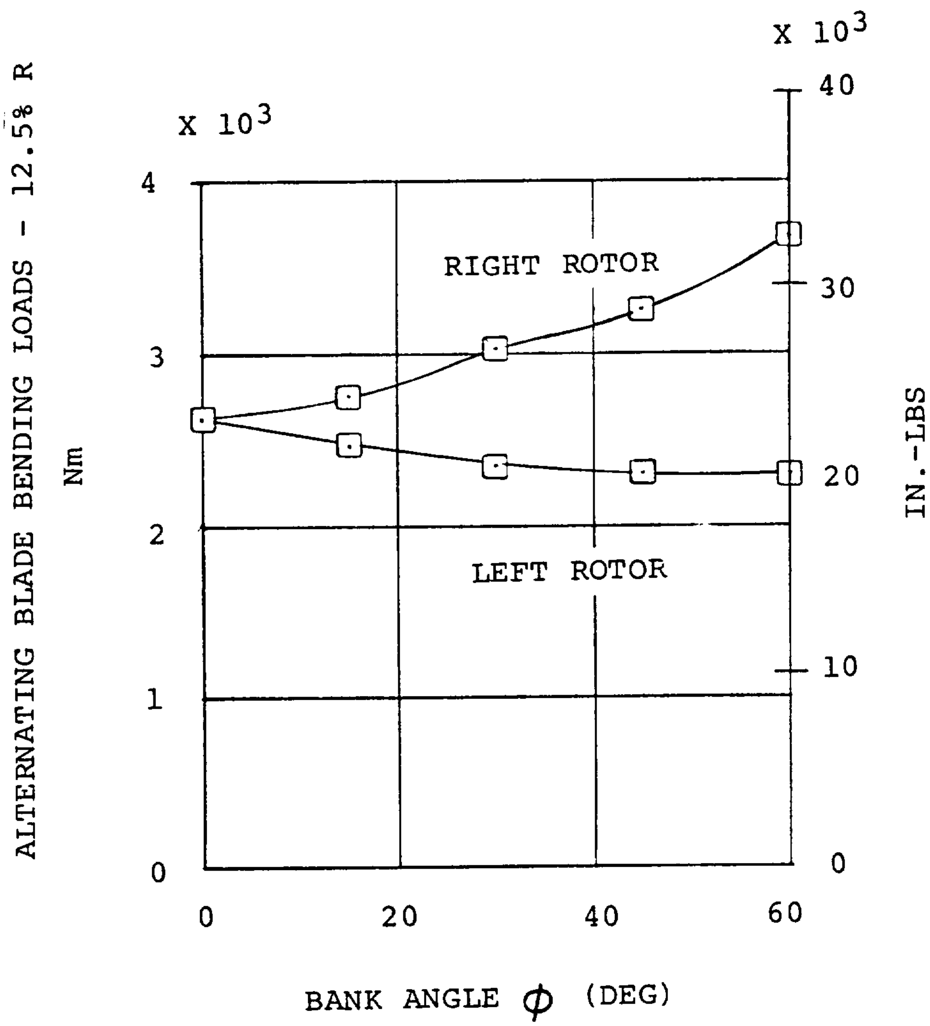

FIGURE 11.79 ESTIMATED BLADE BENDING LOADS IN COORDINATED TURNS IN TRANSITION - $i_N = 30^\circ$ V = 150 KTS $\delta_F = 40^\circ$ AFT CG GW - 5896.7 Kg (13000 LBS) SL STD DAY

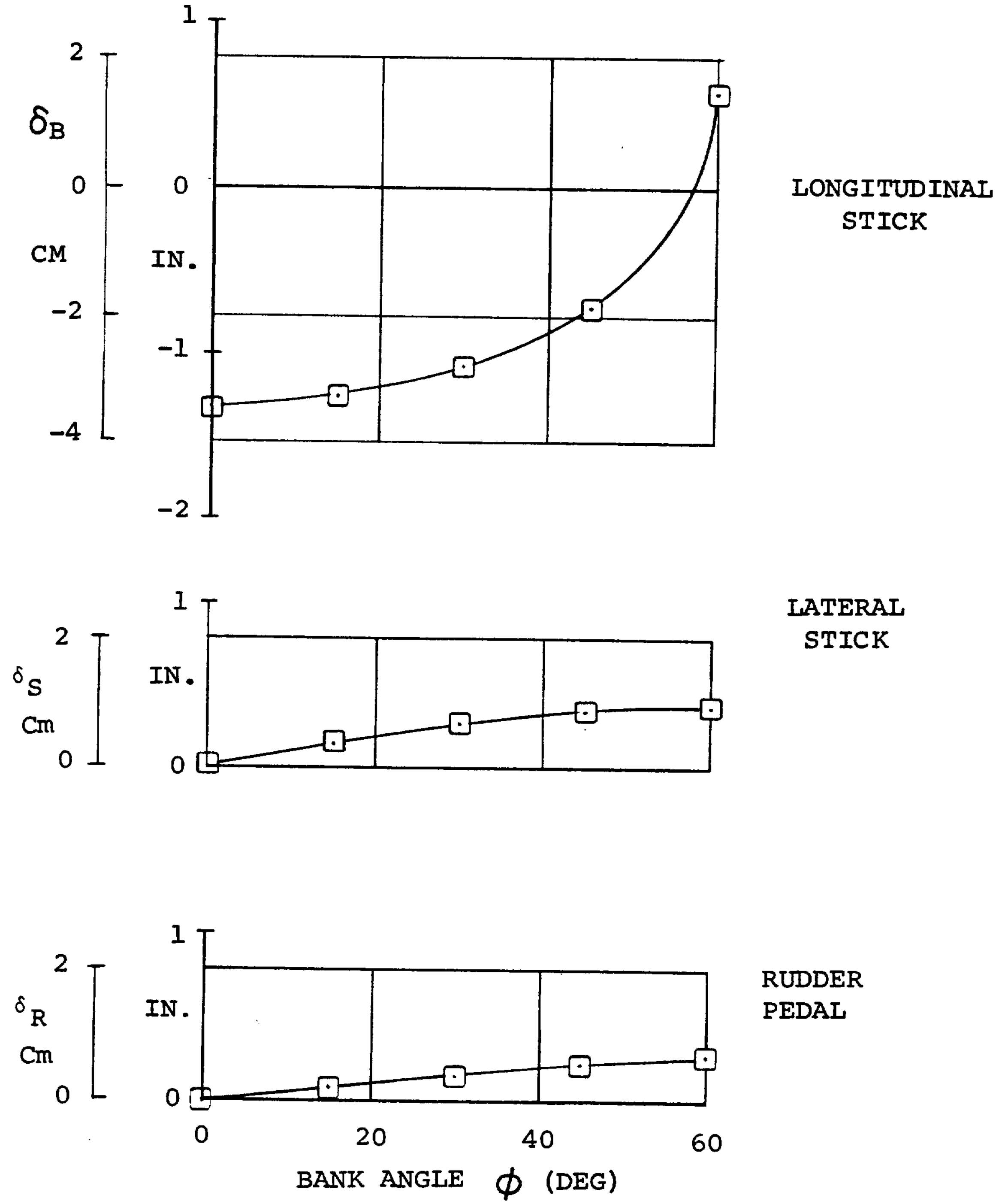

FIGURE 11.80 CONTROL POSITIONS IN COORDINATED TURNS IN TRANSITION $i_N = 30°$ V = 150 KTS FWD CG GW = 5896.7 Kg (13000 LB) SL STD DAY

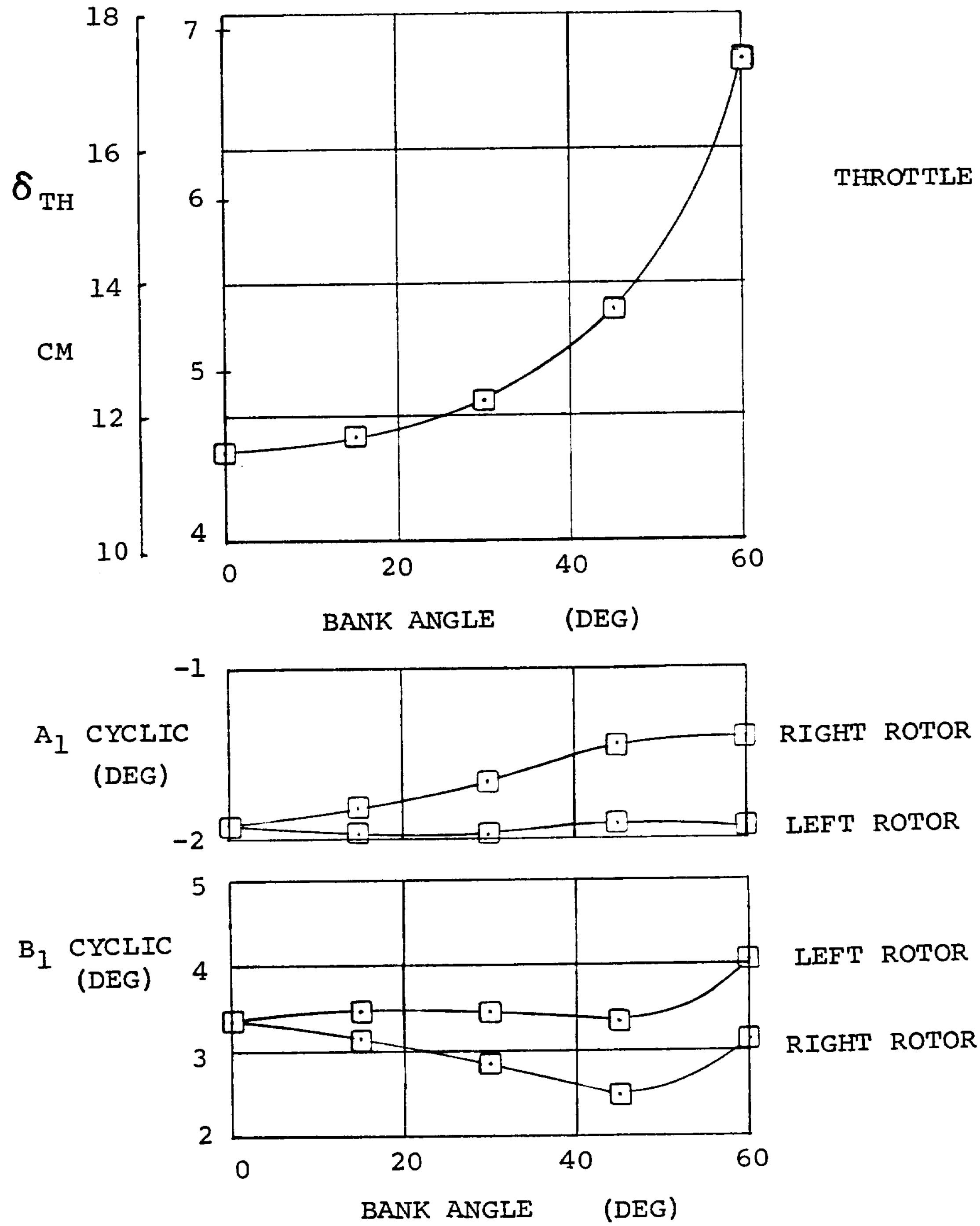

FIGURE 11.81 CONTROL DATA IN COORDINATED TURNS IN TRANSITION
$i_N = 30°$ V = 150 KTS $\delta_F = 40°$ SL STD DAY FWD CG
GW = 5896.7 Kg (13000 LB)

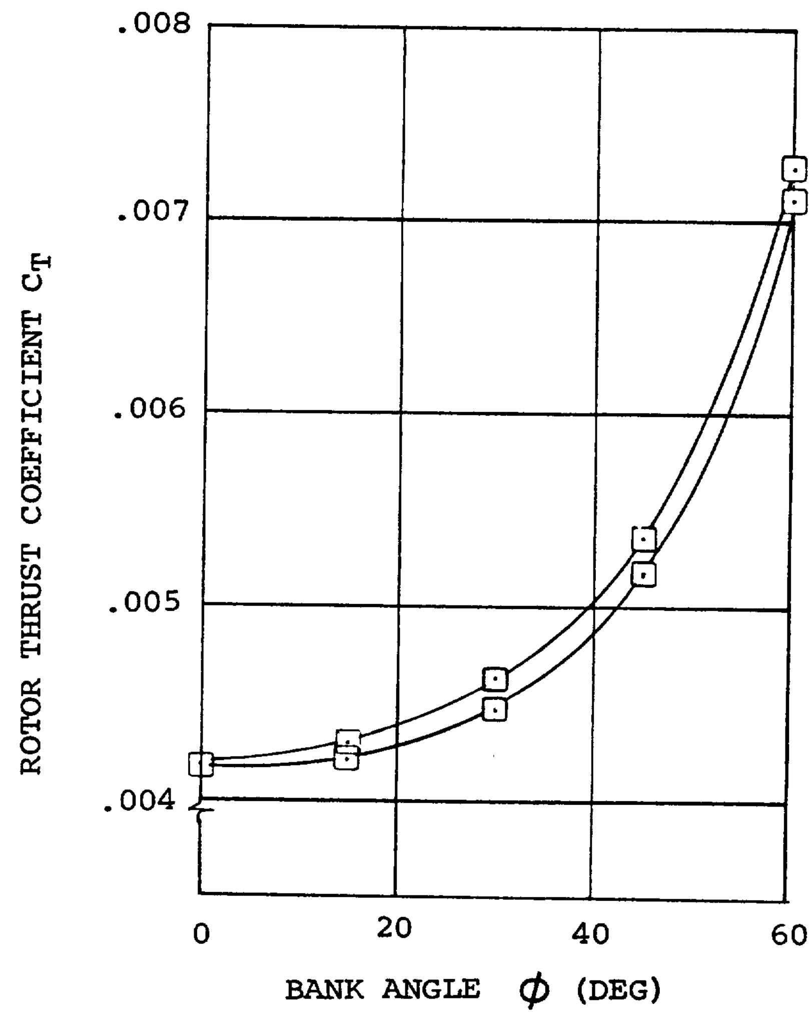

FIGURE 11.82 ROTOR THRUST COEFFICIENT IN COORDINATED TURNS IN TRANSITION $i_N = 30°$ V = 150 FWD CG SL STD DAY GW = 5896.7 Kg (13000 LB)

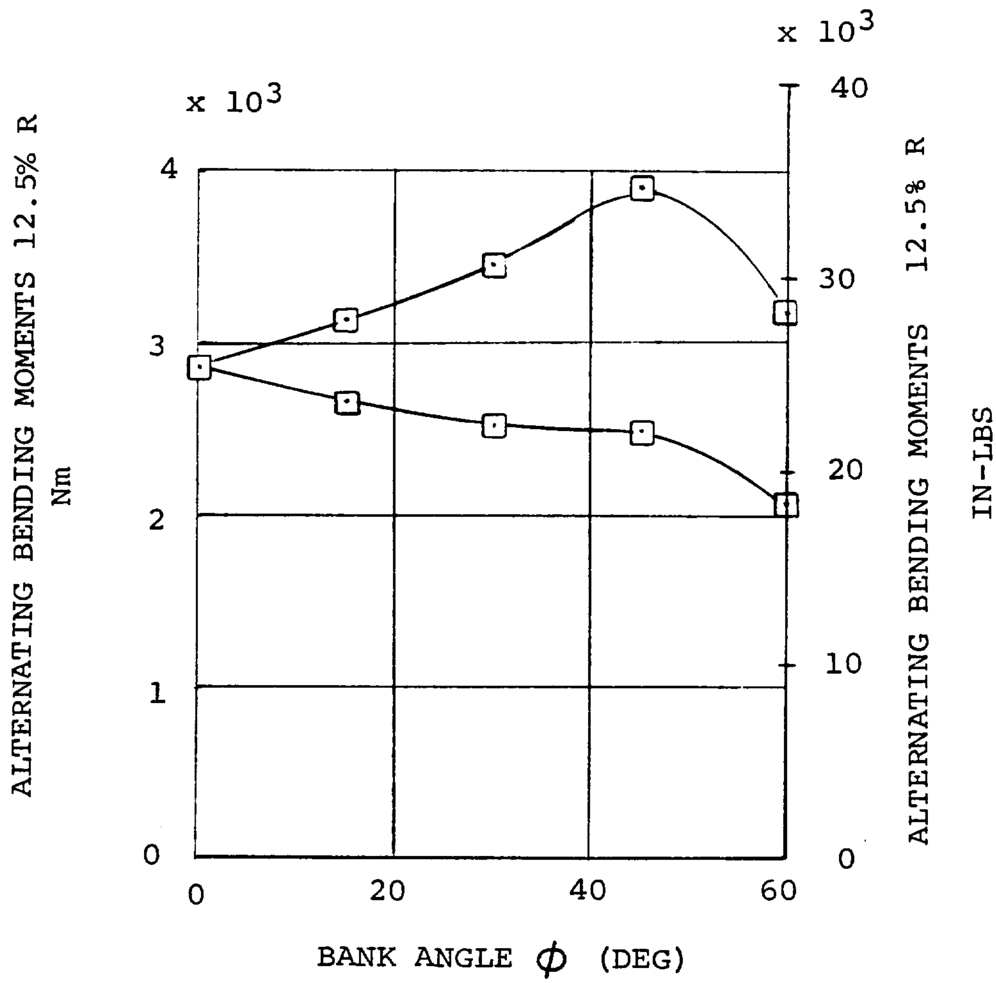

FIGURE 11.83 ESTIMATED BLADE LOADS IN COORDINATED TURNS IN TRANSITION $i_N = 30°$ V = 150 KTS $\delta_F = 40°$ FWD CG GW = 5896.7 Kg (13000 LB) SL STD DAY

11.3 Trimmed Cruise Flight

The aircraft steady flight characteristics with $i_N = 0°$ are shown in Figures 11-84 to 11-90 at sea level for forward and aft CG locations and 0, 20 and 40° of flap.

In cruise flight the fuselage attitude is approximately equal to the wing angle of attack. Power on stall occurs at $\alpha = 13°$ and lies between 93 Kts and 110 Kts depending on flap setting. The stick position data, Figure 11-85, show that as stall is approached the stick gradient become steep. For $\delta_F = 40°$ the stick gradients become small, but are still stable (i.e., stick forward with increased speed). No adverse pilot reaction was received to this low gradient. The small discontinuity in the stick travel at 205 Kts (aft CG) is due to the cyclic pitch input from the longitudinal stick. This cyclic pitch input is rate limited. The elevator deflection to trim is shown in Figure 11-86 and reflects the same characteristics as the stick position data.

The transmission torque levels in cruise at 386 RPM are shown for 0, 20 and 40° of flap in Figure 11-87. The torque level of 100% is equivalent to 1550 HP at 551 RPM and corresponds to a transmission designed to take the full takeoff power available. This of course means that the normal rated power torque level at 551 RPM is at 80.6% and this level reflects a transmission designed for 1250 HP. At this level the aircraft will fly at 197 Kts with 40° of flap which exceeds the flap placard speed. At $\delta_F = 0$ the same torque level would limit the sea level cruise speed to 240 Kts. At 100% torque the aircraft can fly up to 264 Kts at sea level.

Figure 11-88 shows the cruise cyclic pitch inputs used to control the alternating blade loads. The alternating loads at $i_N = 0$ for $\delta_F = 20$ and 40° are shown in Figure 11-89 and indicate load levels less than endurance limit loads from stall up to the flaps down q limit. Apart from the flap limit the loads do not limit the $\delta_F = 40°$ case until a speed of 200 Kts. Figure 11-90 shows the alternating loads as a function of airspeed for both forward and aft CG positions for the $\delta_F = 0$ case. The loads are not a problem in 1g flight.

Figures 11-91, 11-92 and 11-93 show similar data at 1524m (5000 Ft) and 3047m (10,000 Ft) altitude.

The trimmed flight characteristics are much the same as before except that the torque becomes limiting at higher speeds. Rotor loads are not a problem anywhere in the flight envelope shown.

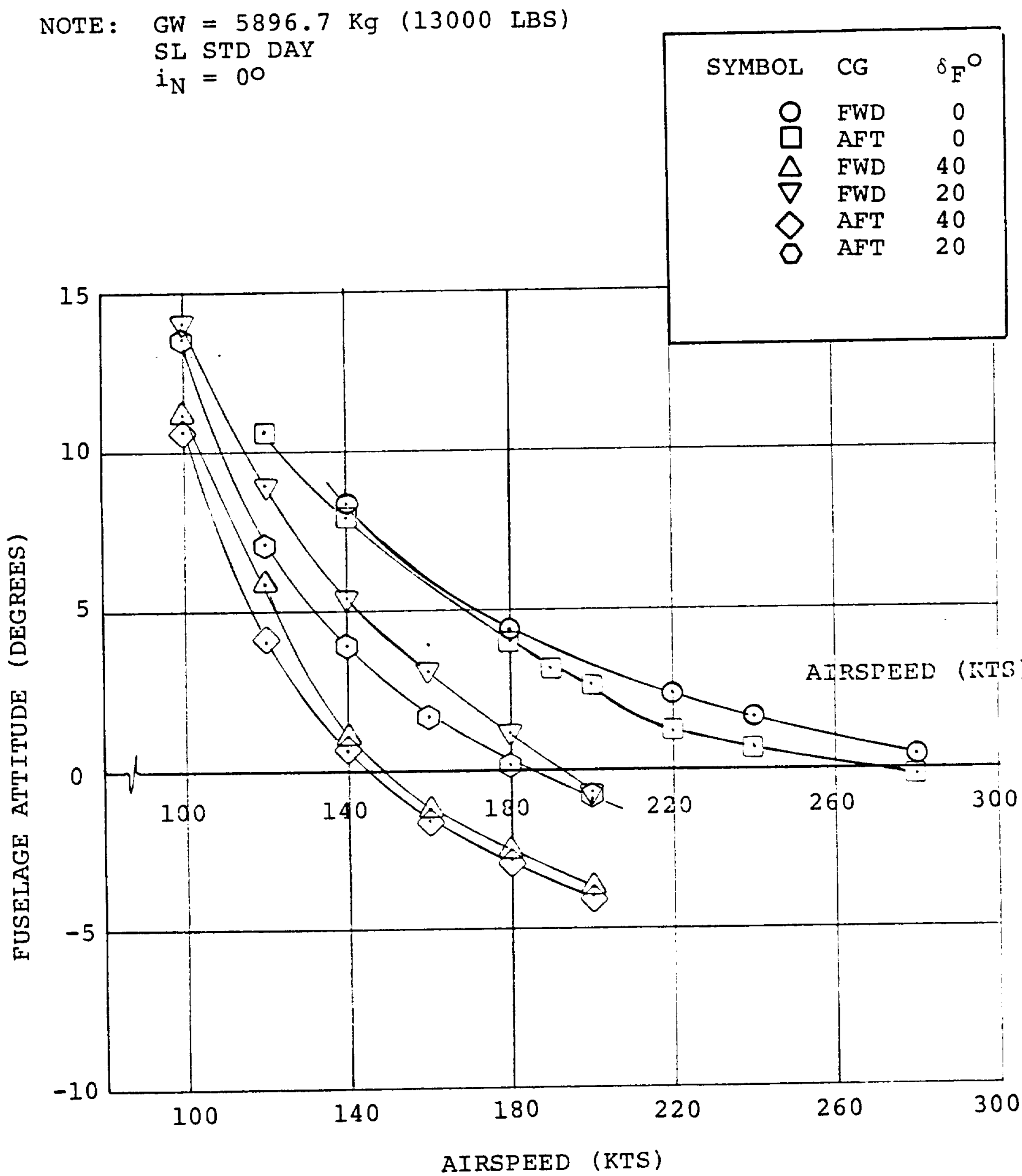

FIGURE 11.84. FUSELAGE ATTITUDE IN CRUISE FLIGHT

NOTE: GW = 5896.7 Kg (13000 LBS)
SL STD DAY
$i_N = 0^\circ$

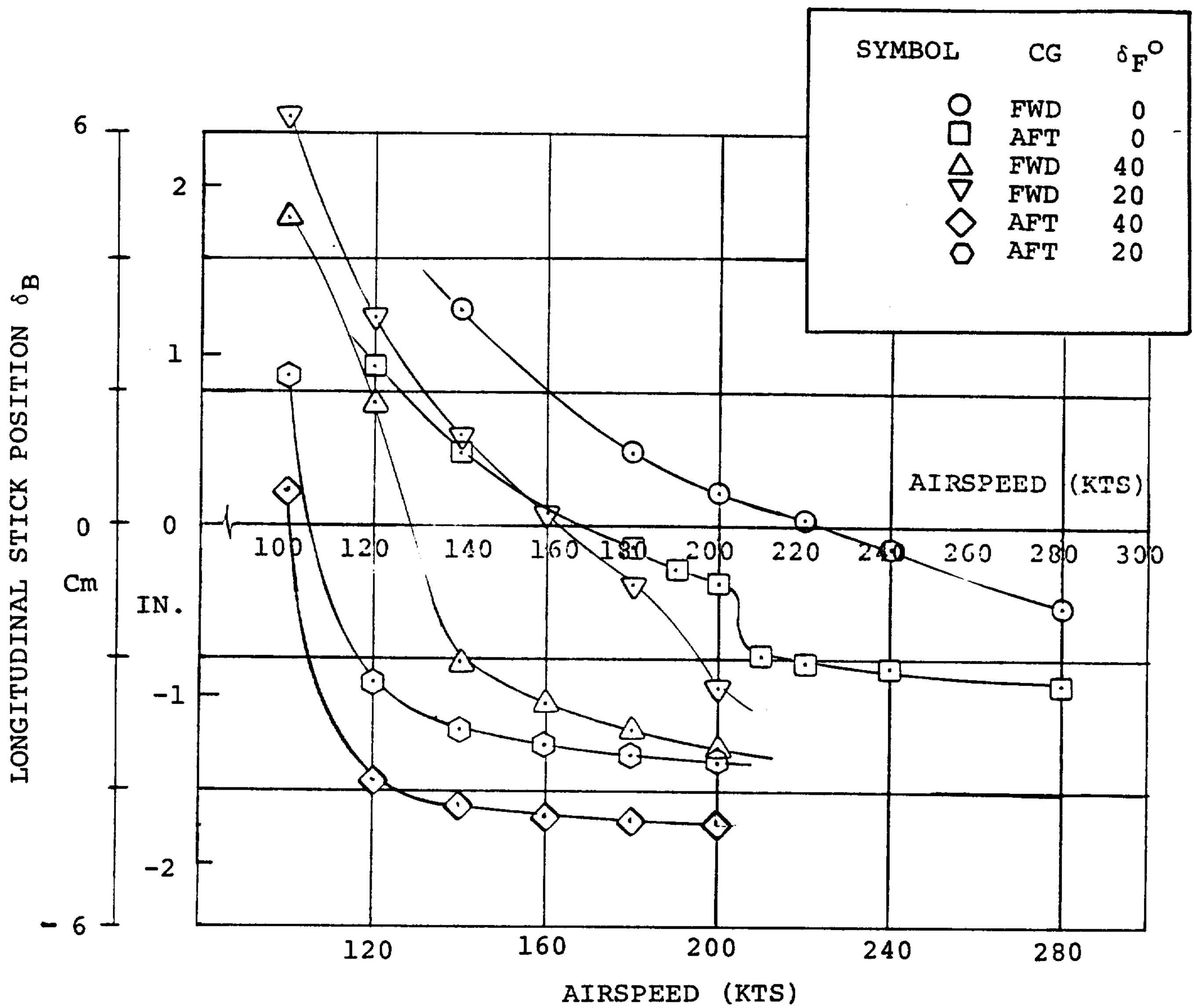

FIGURE 11.85. LONGITUDINAL STICK POSITION IN CRUISE FLIGHT

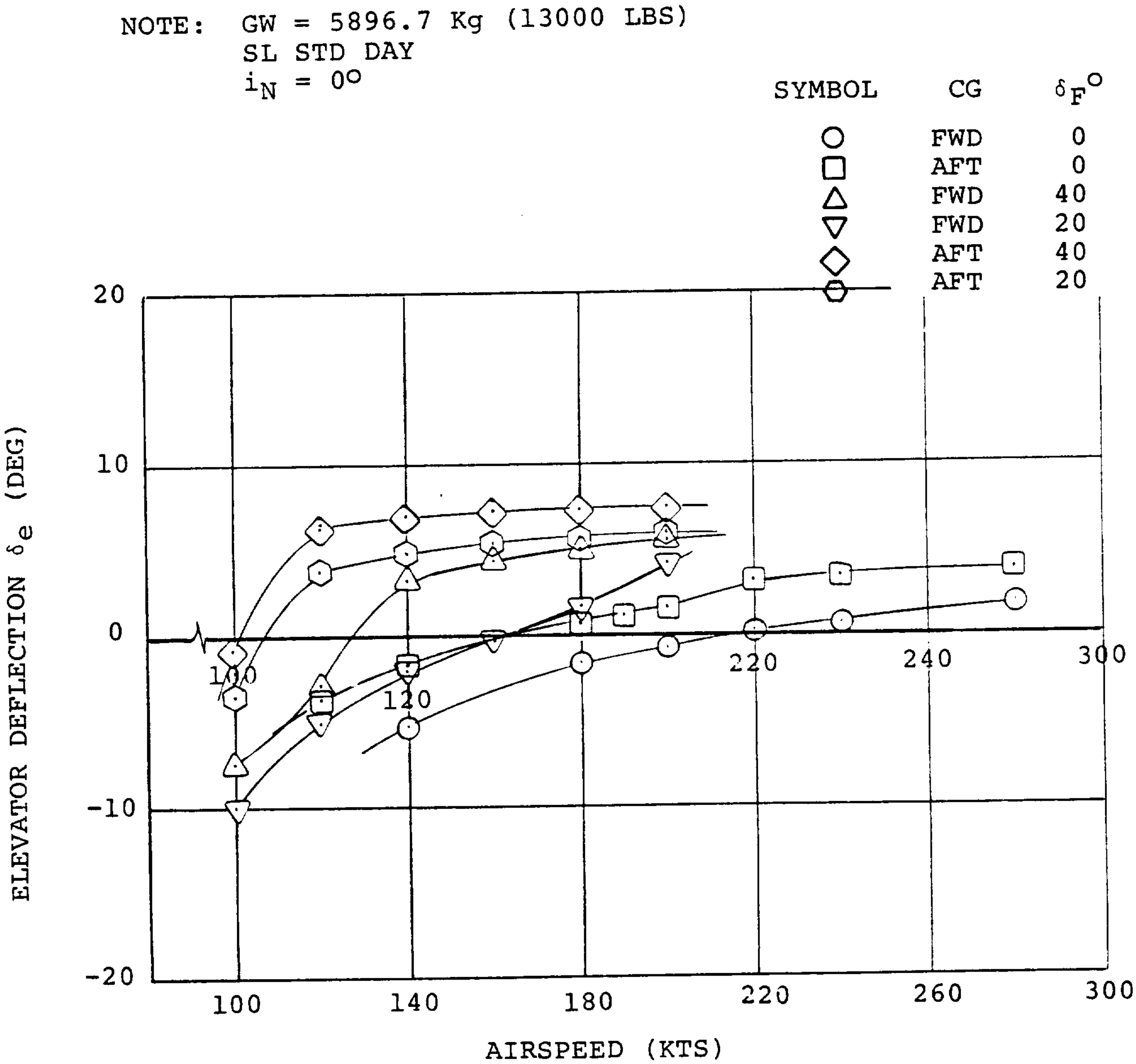

FIGURE 11.86. ELEVATOR DEFLECTION IN CRUISE FLIGHT

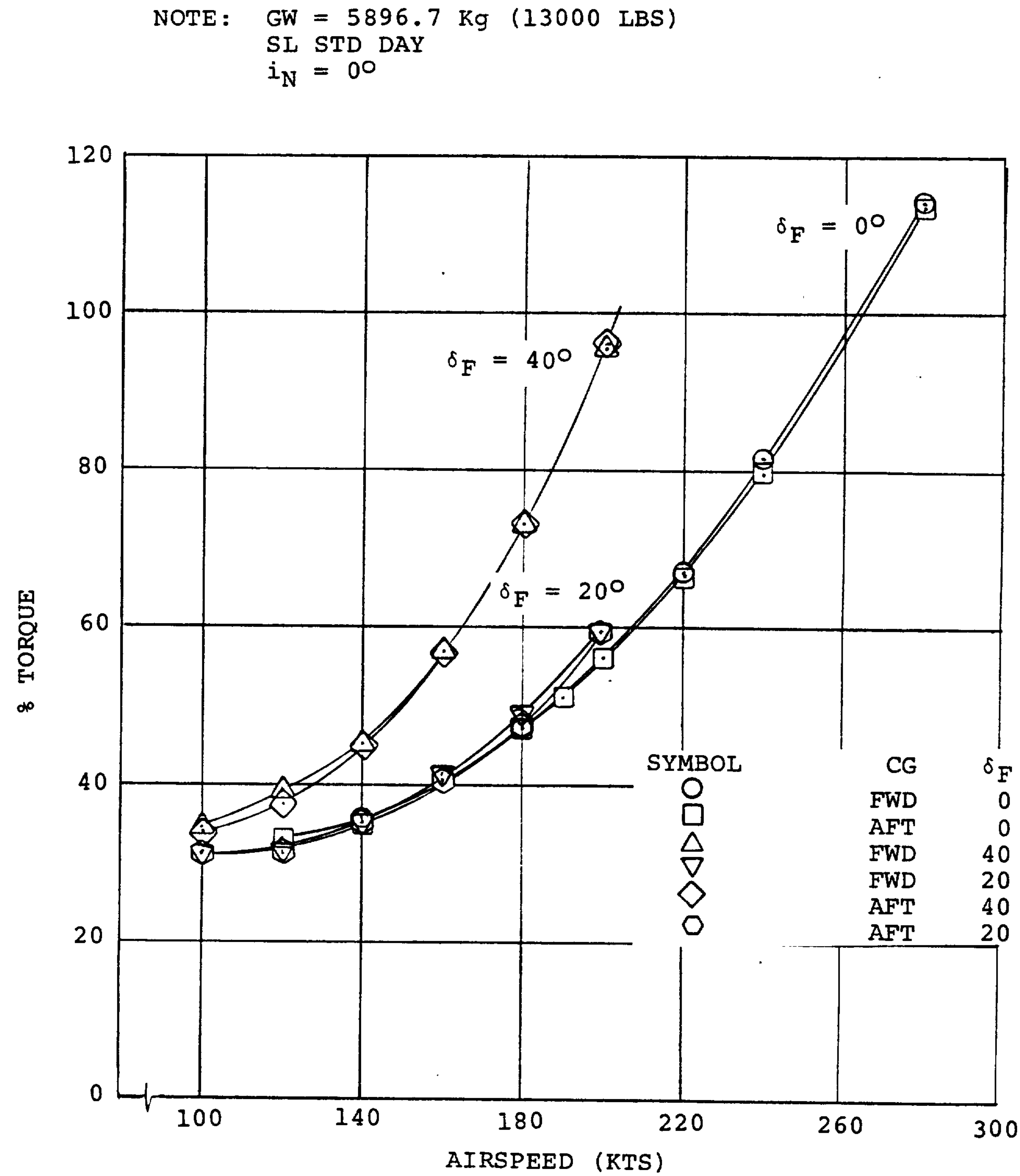

FIGURE 11.87. TORQUE LEVELS IN CRUISE FLIGHT

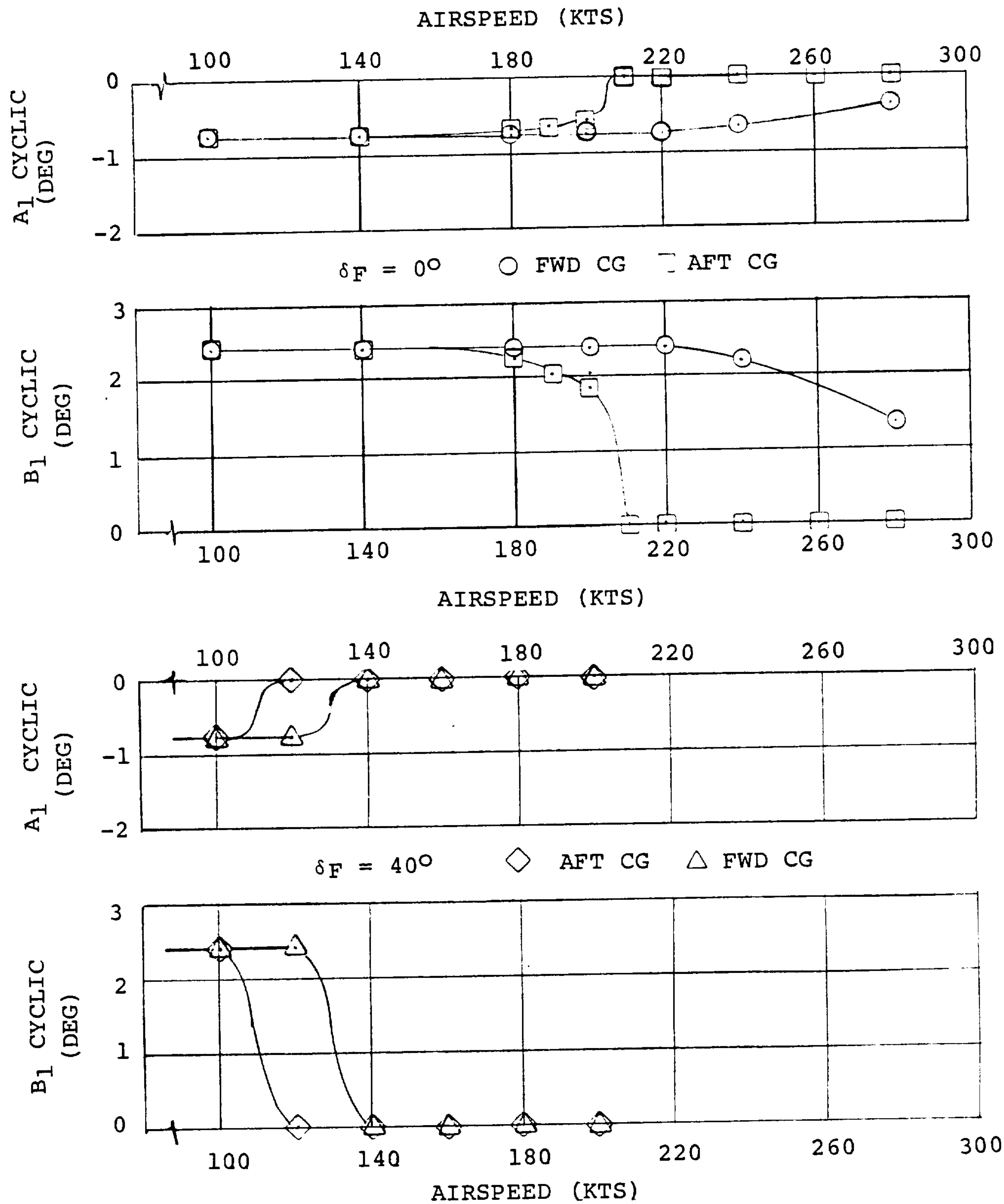

FIGURE 11.88. CYCLIC PITCH IN CRUISE FLIGHT - $i_N = 0^{\circ}$
GW = 5896.7 Kg (13000 LBS) SL STD DAY

NOTE: GW = 5896.7 Kg (13000 LBS)
SL STD DAY
$i_N = 0^\circ$

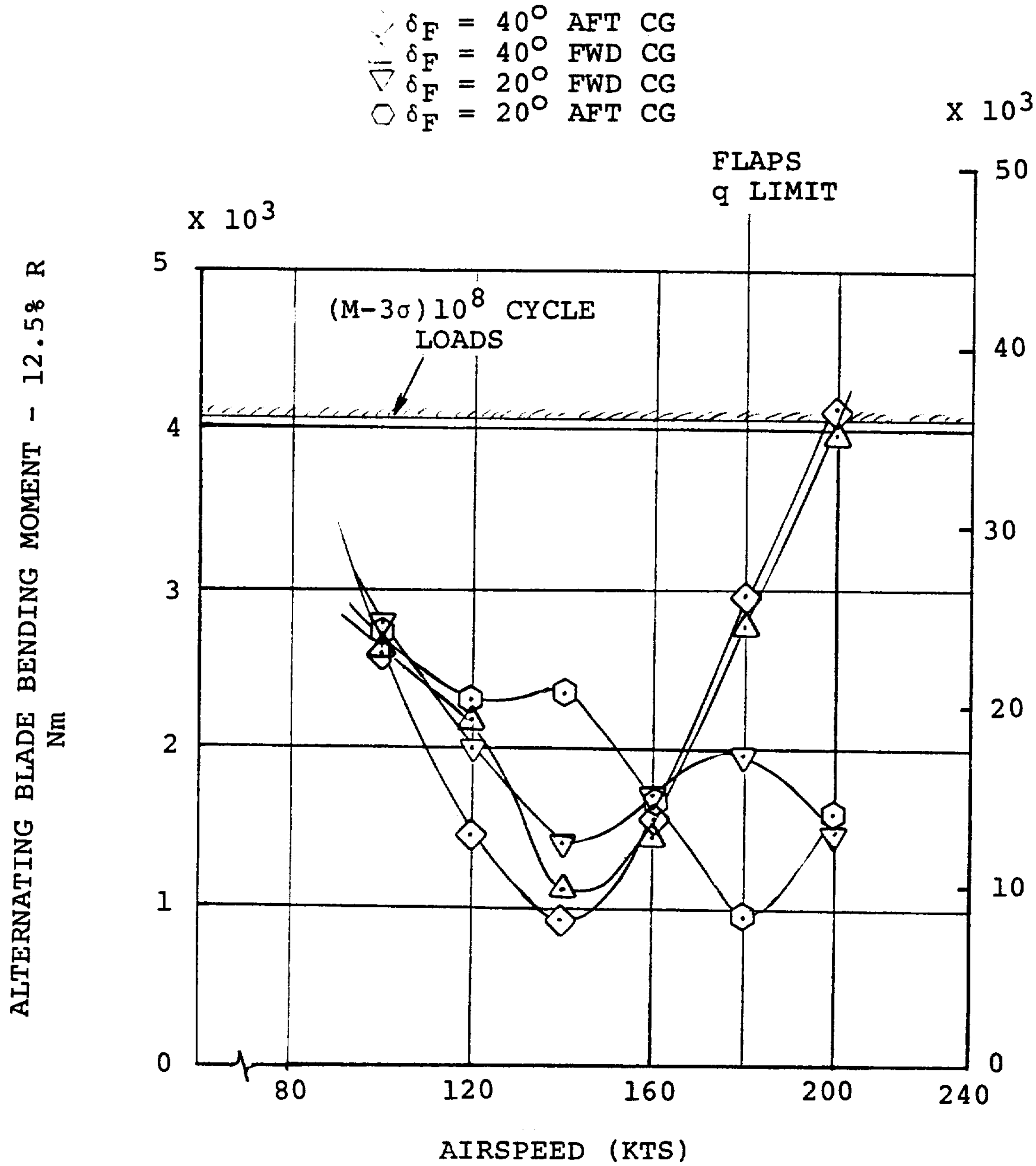

FIGURE 11.89. ESTIMATED BLADE BENDING LOADS 12.5% R IN CRUISE FLIGHT - FLAPS DOWN

NOTE: GW = 5896.7 (Kg) - 13000 LBS
SL STD DAY
$i_N = 0°$

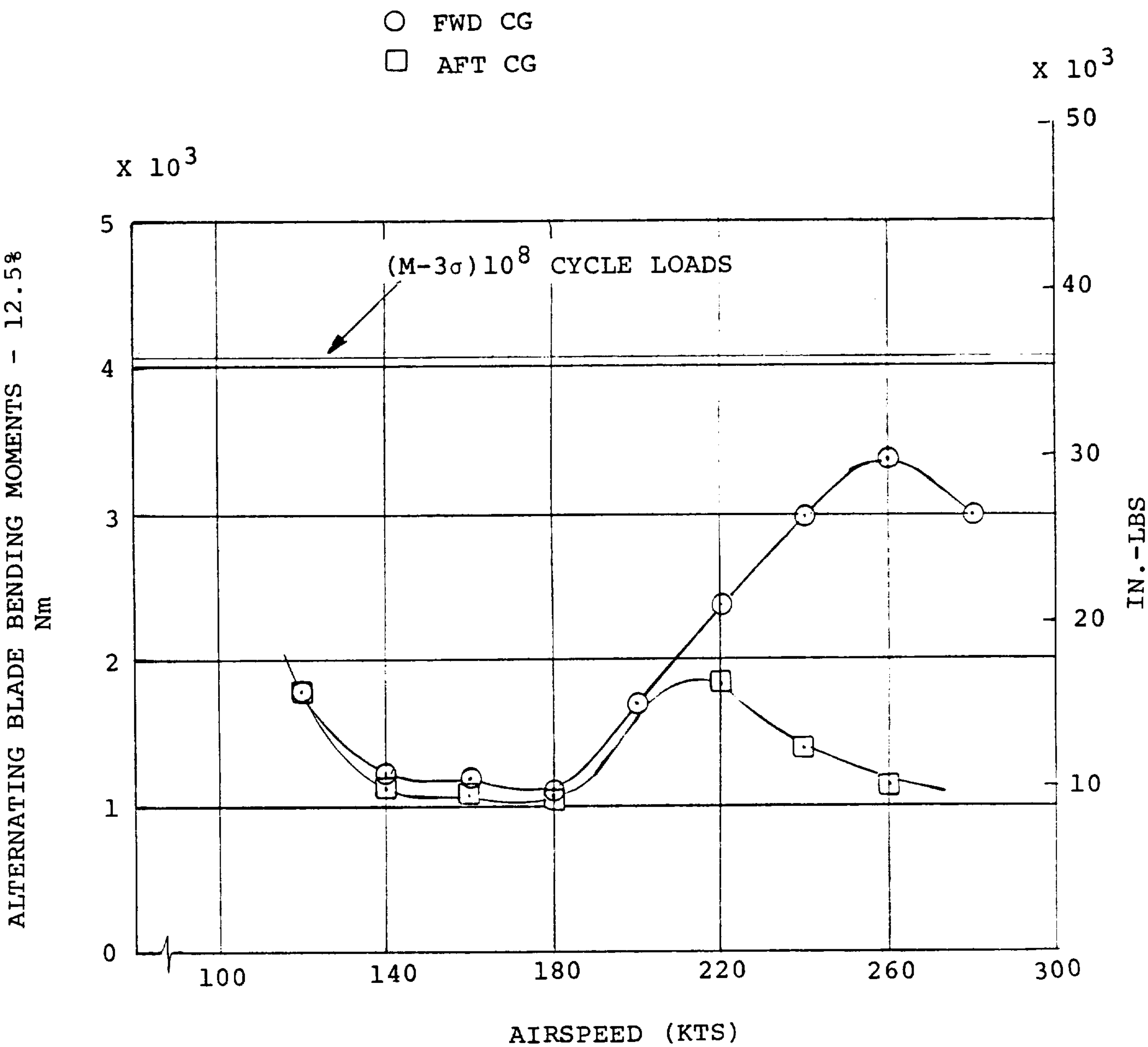

FIGURE 11.90. ESTIMATED BLADE BENDING LOADS IN STEADY CRUISE FLIGHT - FLAPS UP

ALT (m)	SYMBOL	ALT (FT)	CG
1524	[illegible]	5000	AFT
1524	[illegible]	5000	FWD
3045	×	10000	AFT
3045	◊	10000	FWD

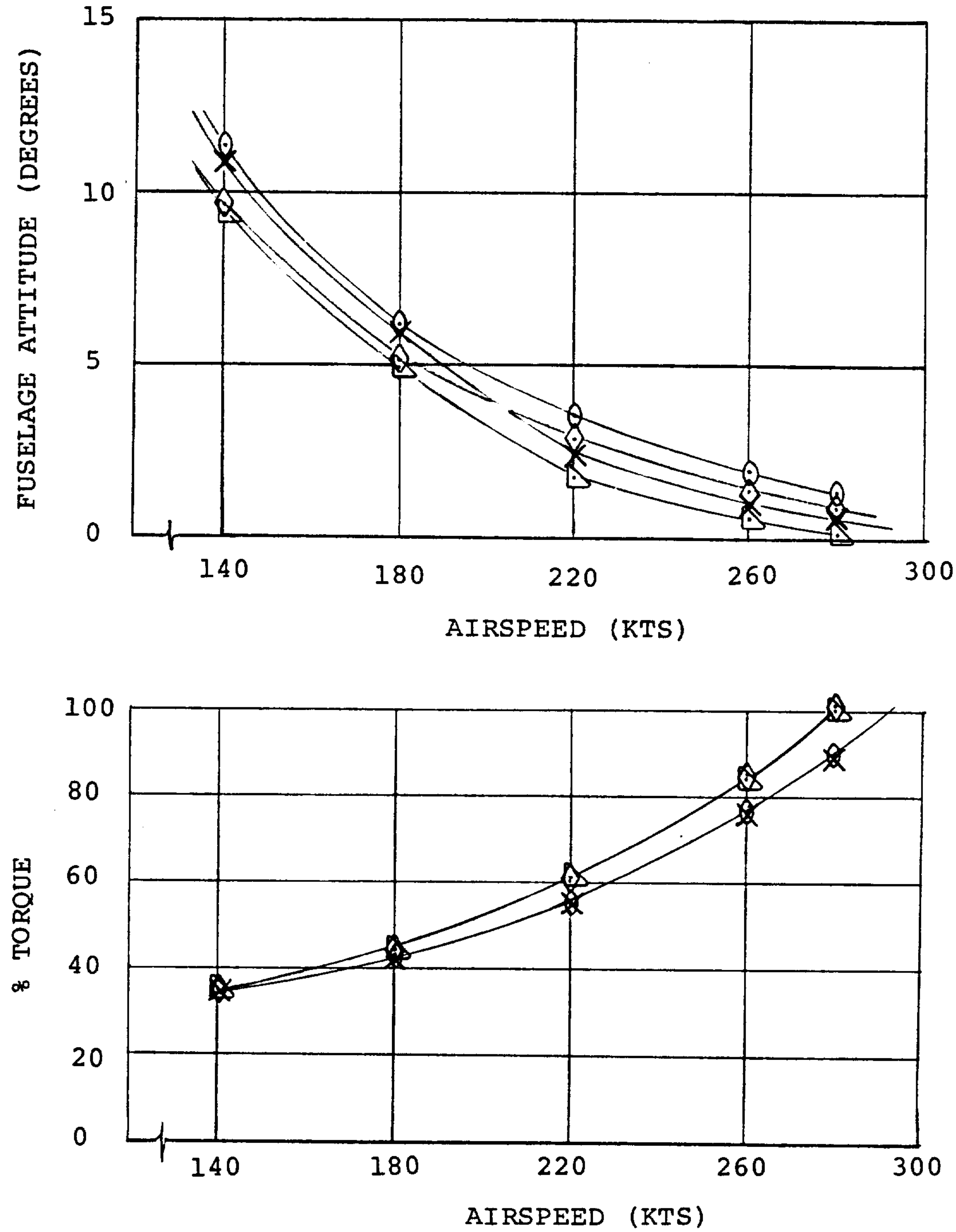

FIGURE 11.91. TRIM DATA IN CRUISE $i_N = 0^o$ AT ALTITUDE
GW = 5896.7 Kg (13000 LBS) $\delta_F = 0^o$
386 RPM STANDARD DAY

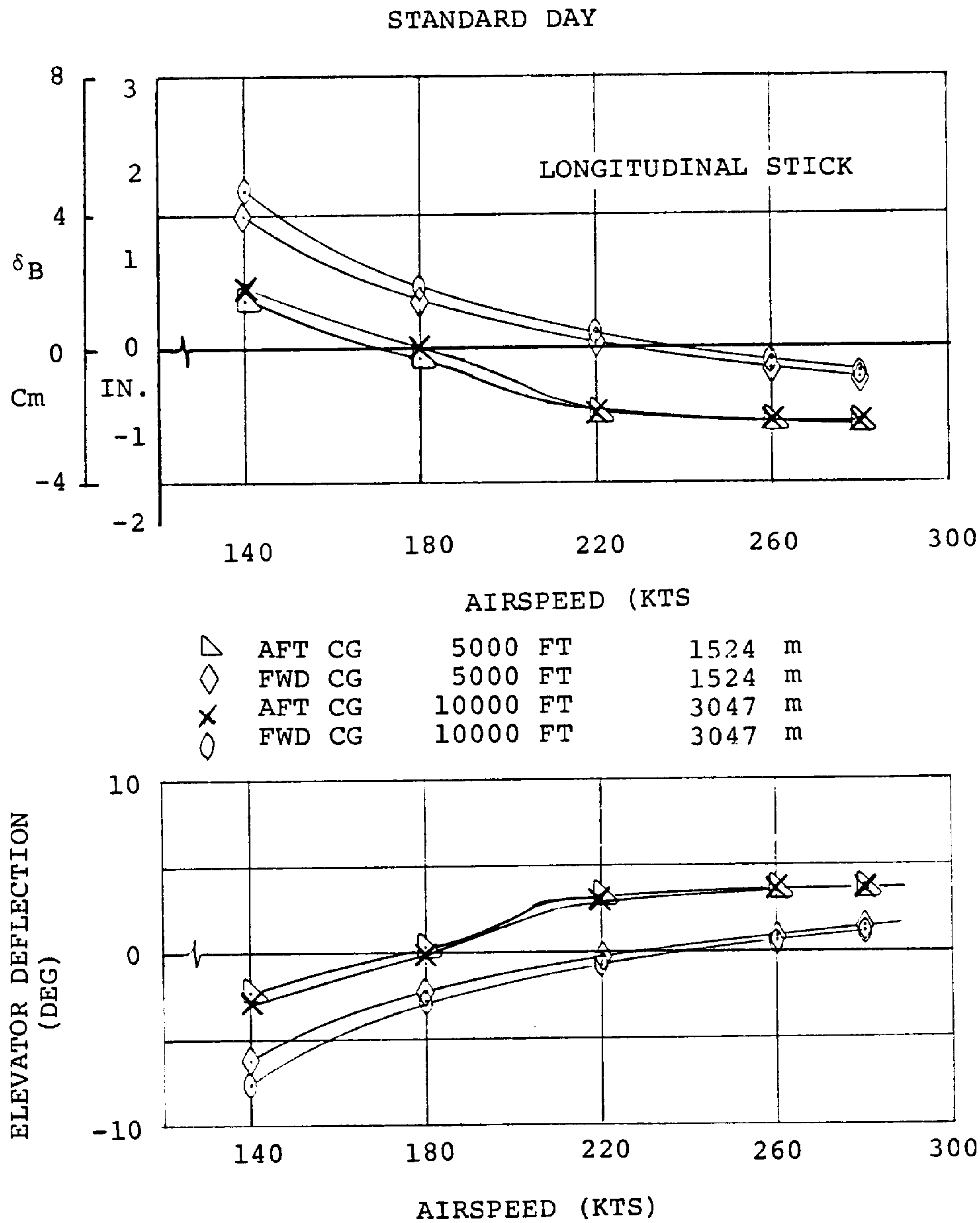

FIGURE 11.92. TRIM DATA IN CRUISE AT ALTITUDE
GW = 5896.7 Kg (13000 LBS) 386 RPM
$\delta_F = 0^\circ$ $i_N = 0^\circ$

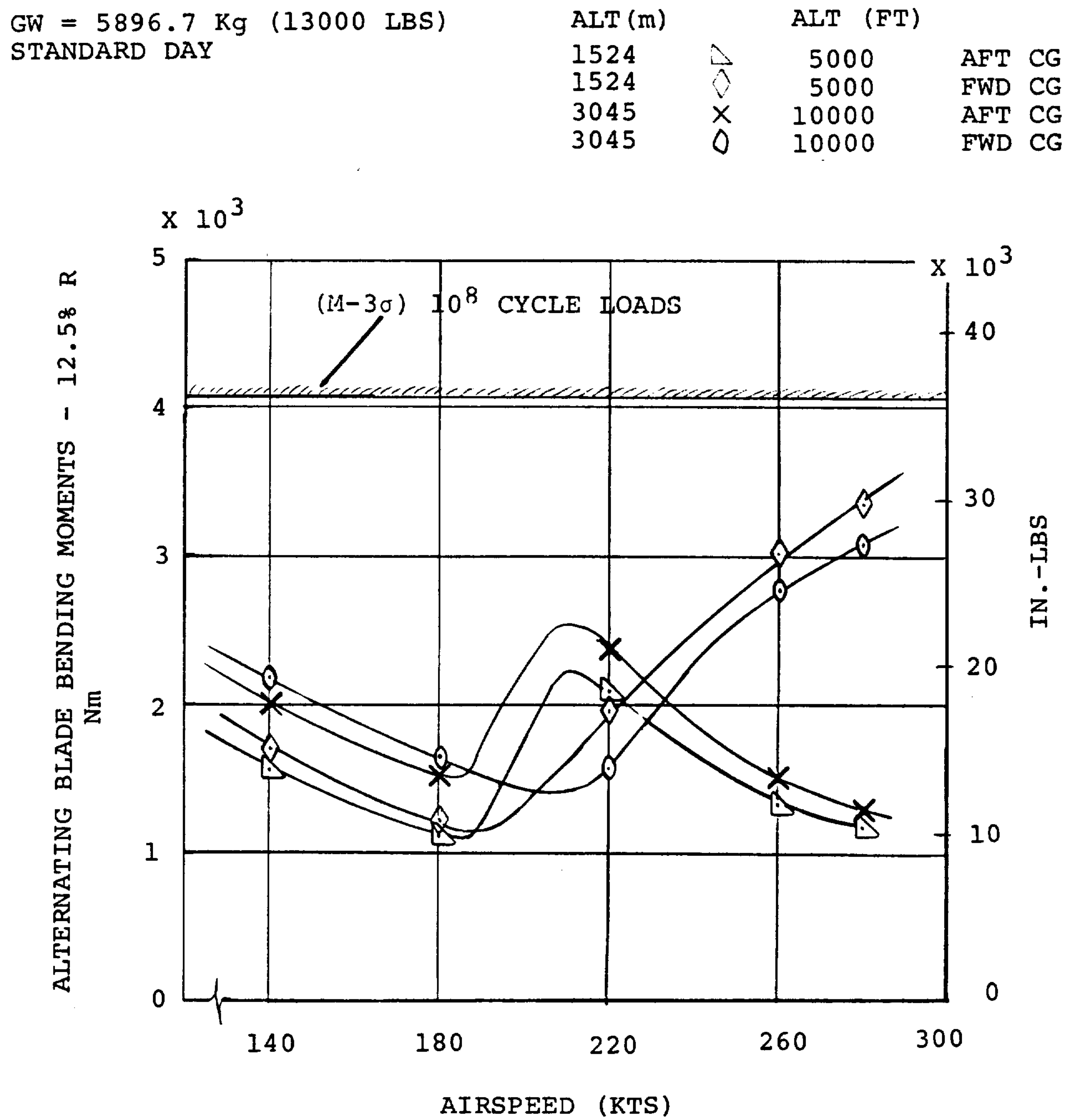

FIGURE 11-93. ESTIMATED BLADE BENDING LOADS IN CRUISE AT 5000 AND 10000 FEET $\delta_F = 0^{\circ}$ $i_N = 0^{\circ}$ 386 RPM

11.4 Coordinated Turns in Cruise

The control positions for trimmed coordinated turns in cruise at GW = 5896.7 Kg (13,000 lbs) at sea level are shown in Figures 11-94 to 11-97 and display normal fixed wing airplane control inputs. The maneuver envelope is limited by transmission torque limits, stall and blade fatigue loads as shown in Figure 11-98. The loads boundary shown in Figure 11-98 is the fatigue endurance limit of the fiberglass spar. Up to 180 knots the airplane's turn capability is limited by wing stall. After 180 knots the limiting factors are transmission torque then blade endurance limit loads and wing stall. The blade endurance limit line lies very close to the wing stall limit. The transmission torque limit is likely to be the limiting factor in excess of 163 knots. The "torque 1" limit corresponds to a transmission designed for 1250 HP rotor in hover. Uprating the transmission limit to 1550 HP (engine T.O. power setting) at 551 RPM increases the available speed by approximately 20 knots.

11.5 Sidewards Flight

The airplane characteristics in sidewards flight with $i_N = 90°$ are shown in Figures 11-99 and 11-100. The control data show that a sidewards velocity of 49 knots can be achieved before running out of rudder pedal travel. The alternating blade bending loads in sidewards flight are shown in Figure 11-100. Alternating loads exceed 4064 Nm (36,000 lbs) at 29.5 knots sidewards. The airplane is controllable up to higher speeds but blade fatigue damage would result.

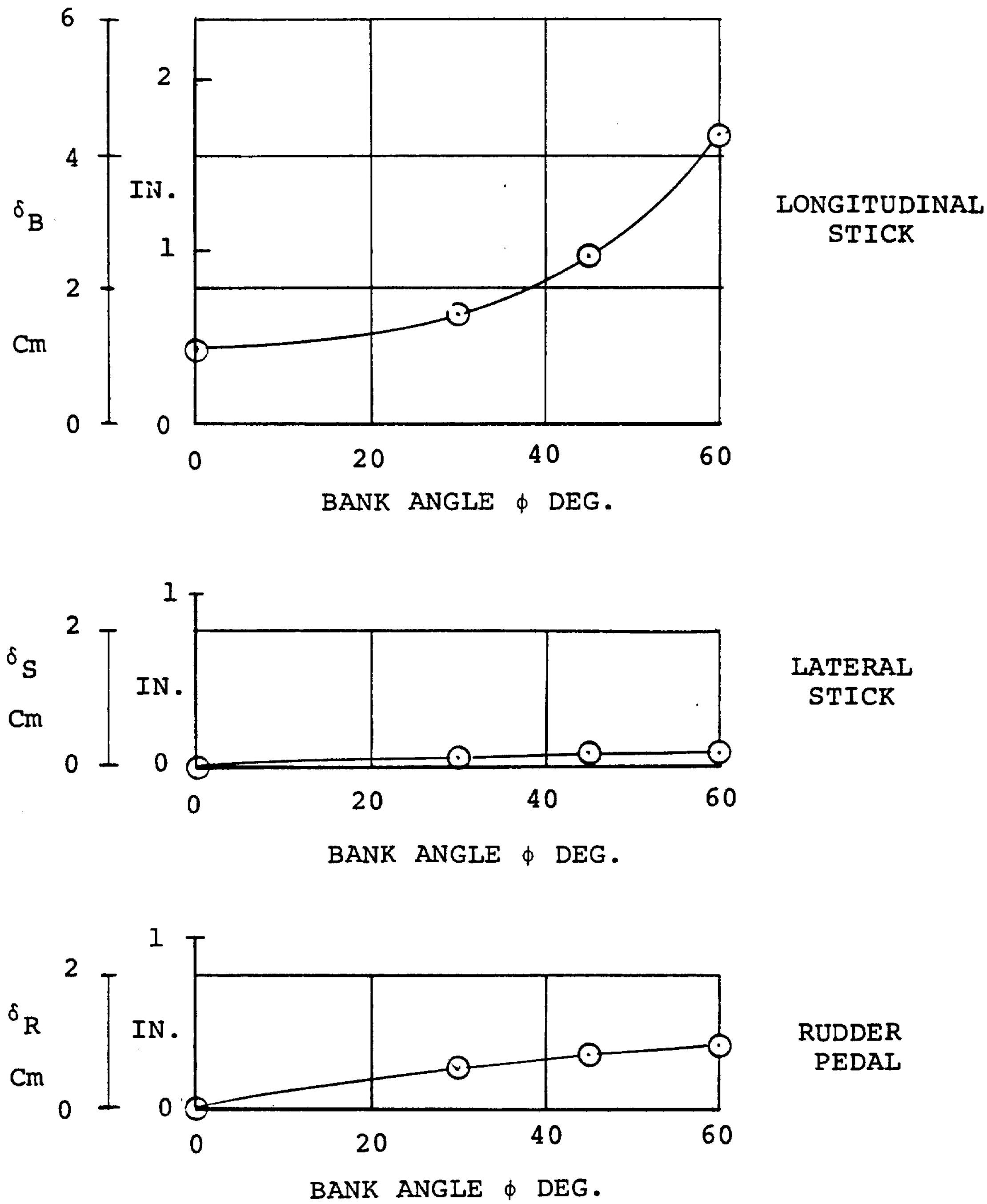

FIGURE 11.94. CONTROL POSITIONS IN COORDINATED TURNS IN CRUISE FLIGHT - $i_N = 0^\circ$ $\delta_F = 0^\circ$ AFT CG GW = 5896.7 Kg (13000 LBS) SL STD DAY 140 KTS

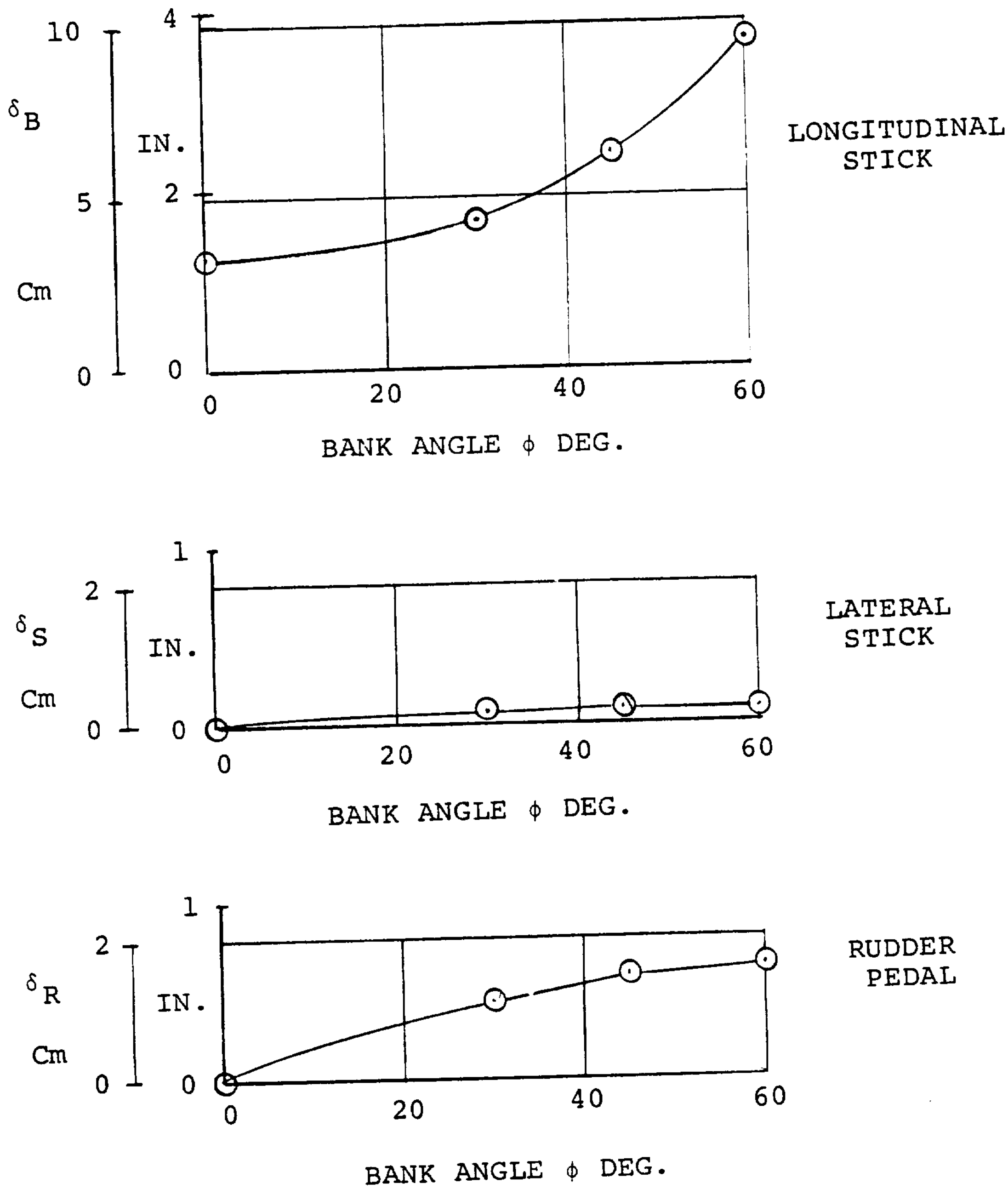

FIGURE 11.95. CONTROL POSITIONS IN COORDINATED TURNS IN CRUISE - $i_N = 0^\circ$ $\delta_F = 0^\circ$ FWD CG
GW = 5896.7 Kg (13000 LBS) SL STD DAY
140 KTS

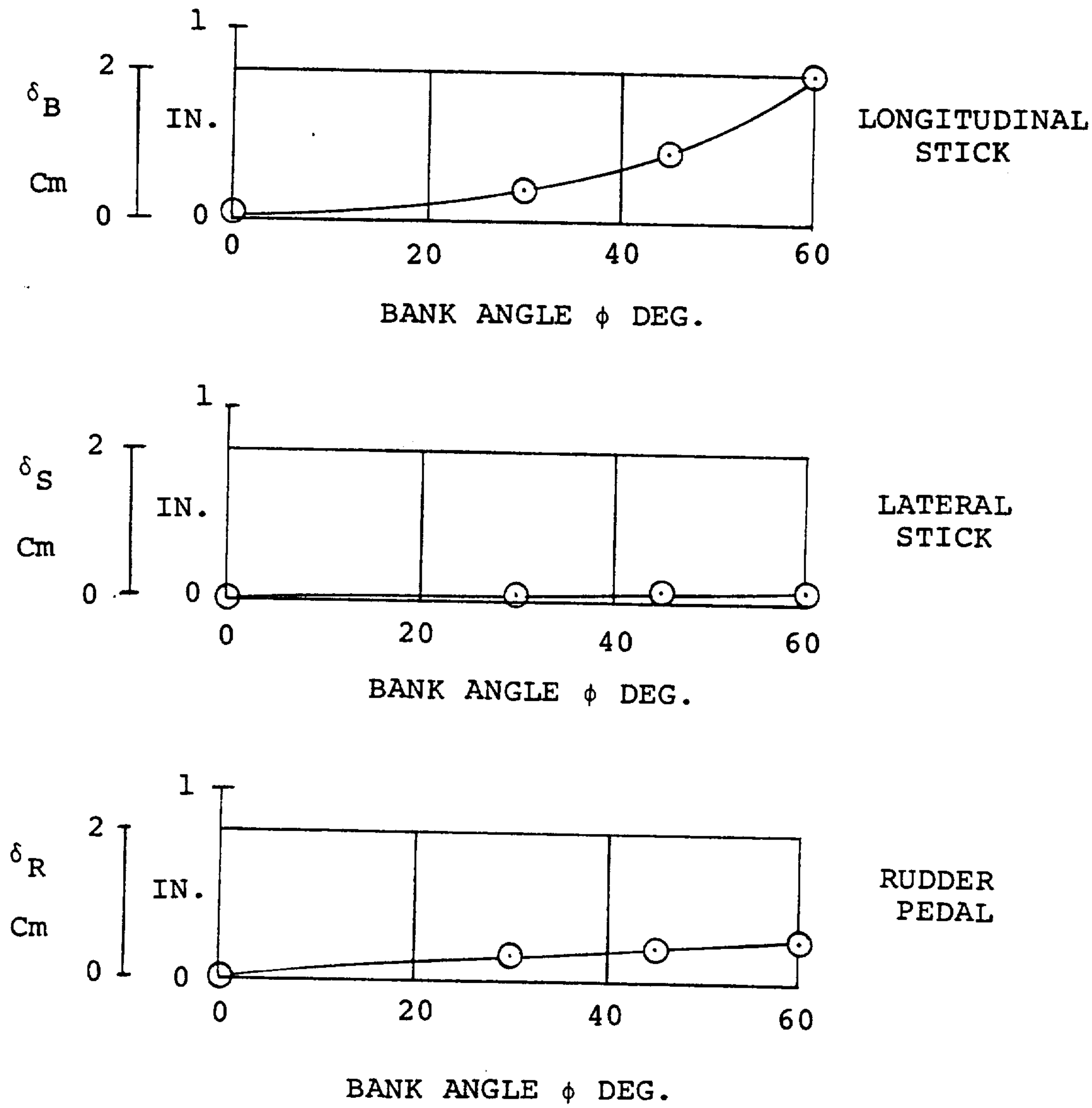

FIGURE 11.96. CONTROL POSITIONS IN COORDINATED TURNS IN CRUISE FLIGHT - $i_N = 0^\circ$ $\delta_F = 0^\circ$ FWD CG
GW = 5896.7 Kg (13000 LBS) SL STD DAY
220 KTS

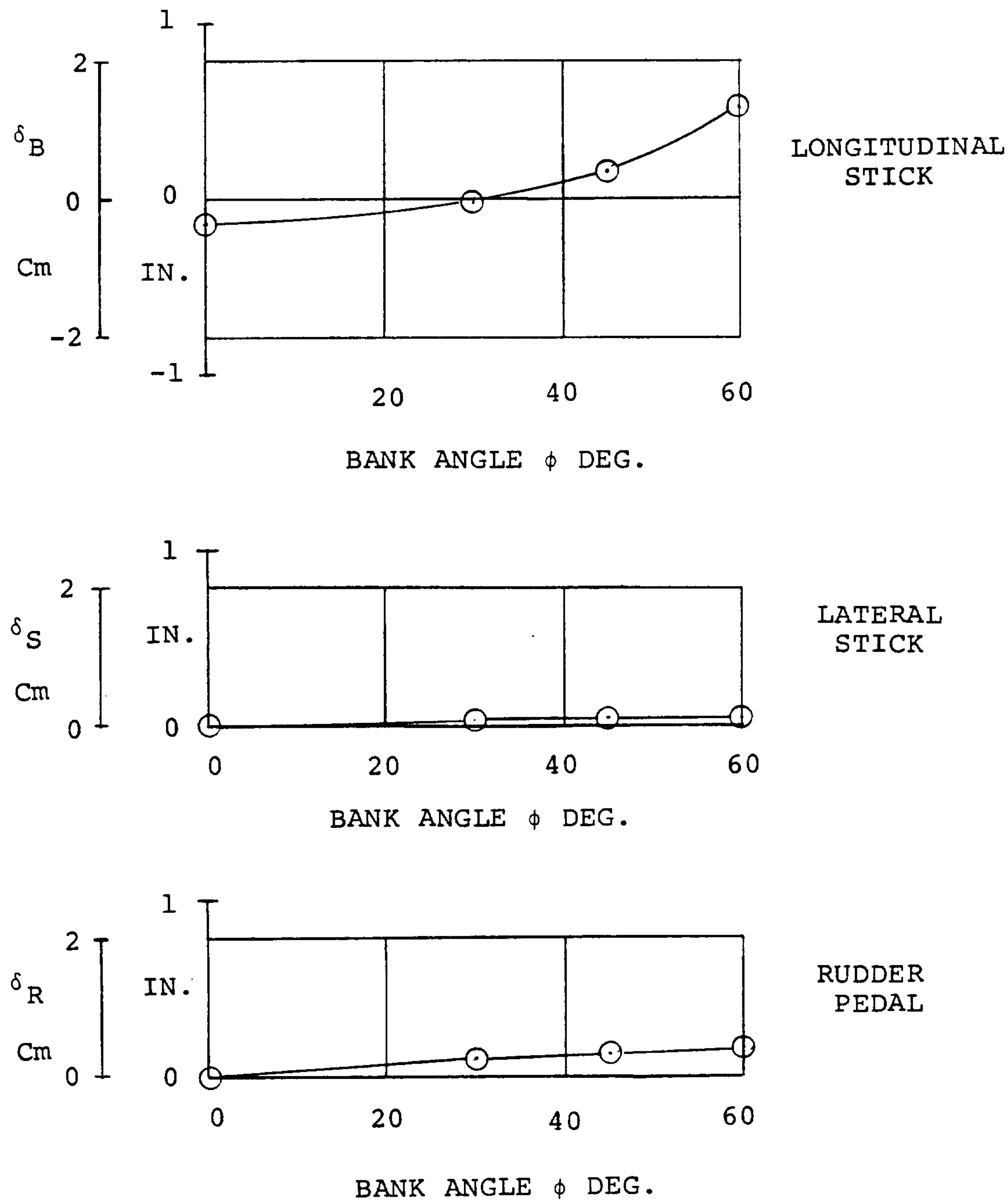

FIGURE 11.97. CONTROL POSITIONS IN COORDINATED TURNS IN CRUISE FLIGHT - $i_N = 0^\circ$ $\delta_F = 0^\circ$
FWD CG GW = 5896.7 Kg (13000 LBS)
SL STD DAY 240 KTS

*NOTES: 1. TORQUE 1 EQUIVALENT TO 1250 HP AT 551 RPM
2. TORQUE 2 EQUIVALENT TO 1550 HP AT 551 RPM
3. LOADS = $(M-3\sigma)10^8$ CYCLE LOADS IN GLASS SPAR (FWD CG)

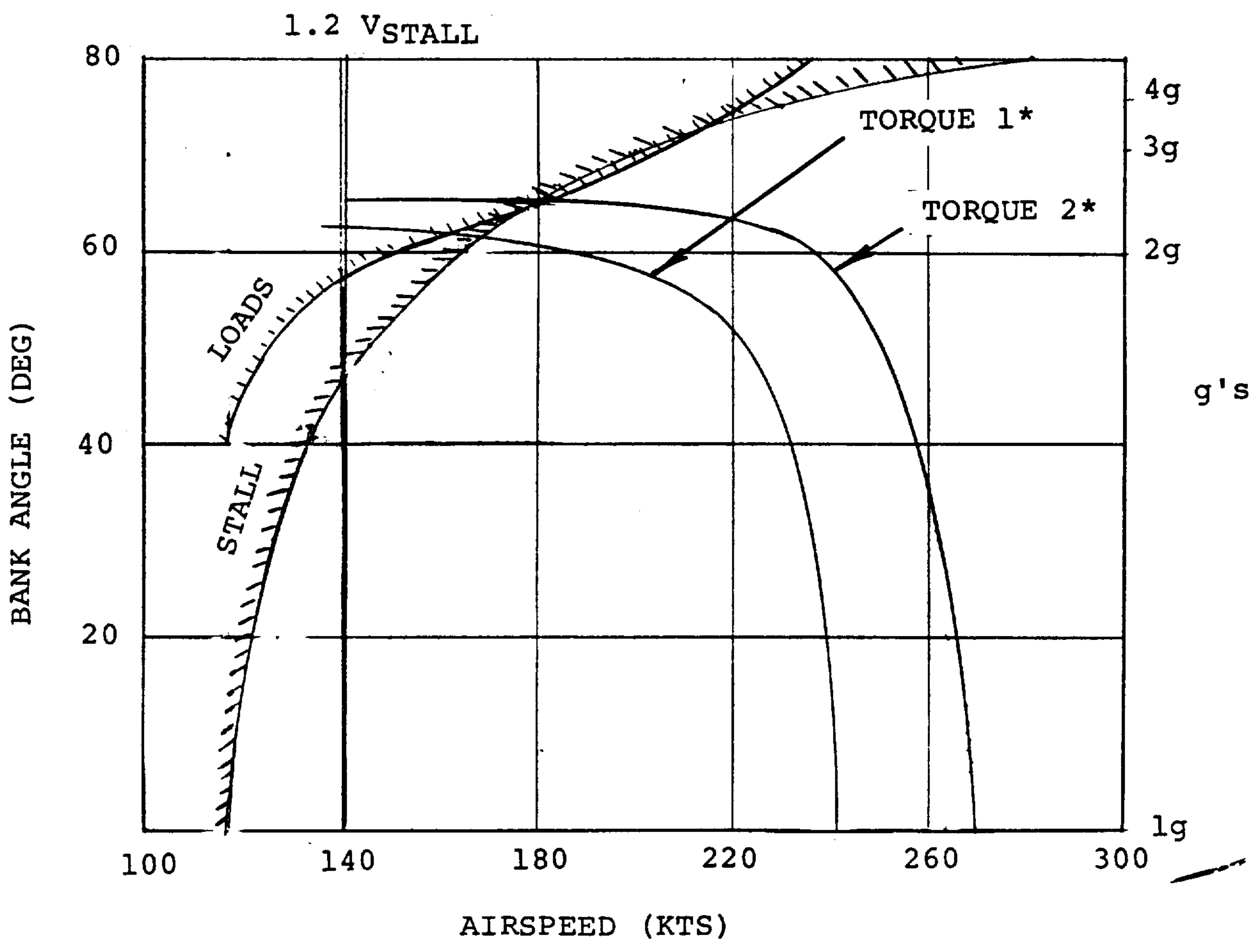

FIGURE 11.98. FLIGHT ENVELOPE LIMITS IN SUSTAINED TURNS
$\delta_F = 0^\circ$ SL STD DAY $i_N = 0^\circ$ 386 RPM
GW = 5896.7 Kg (13000 LBS)

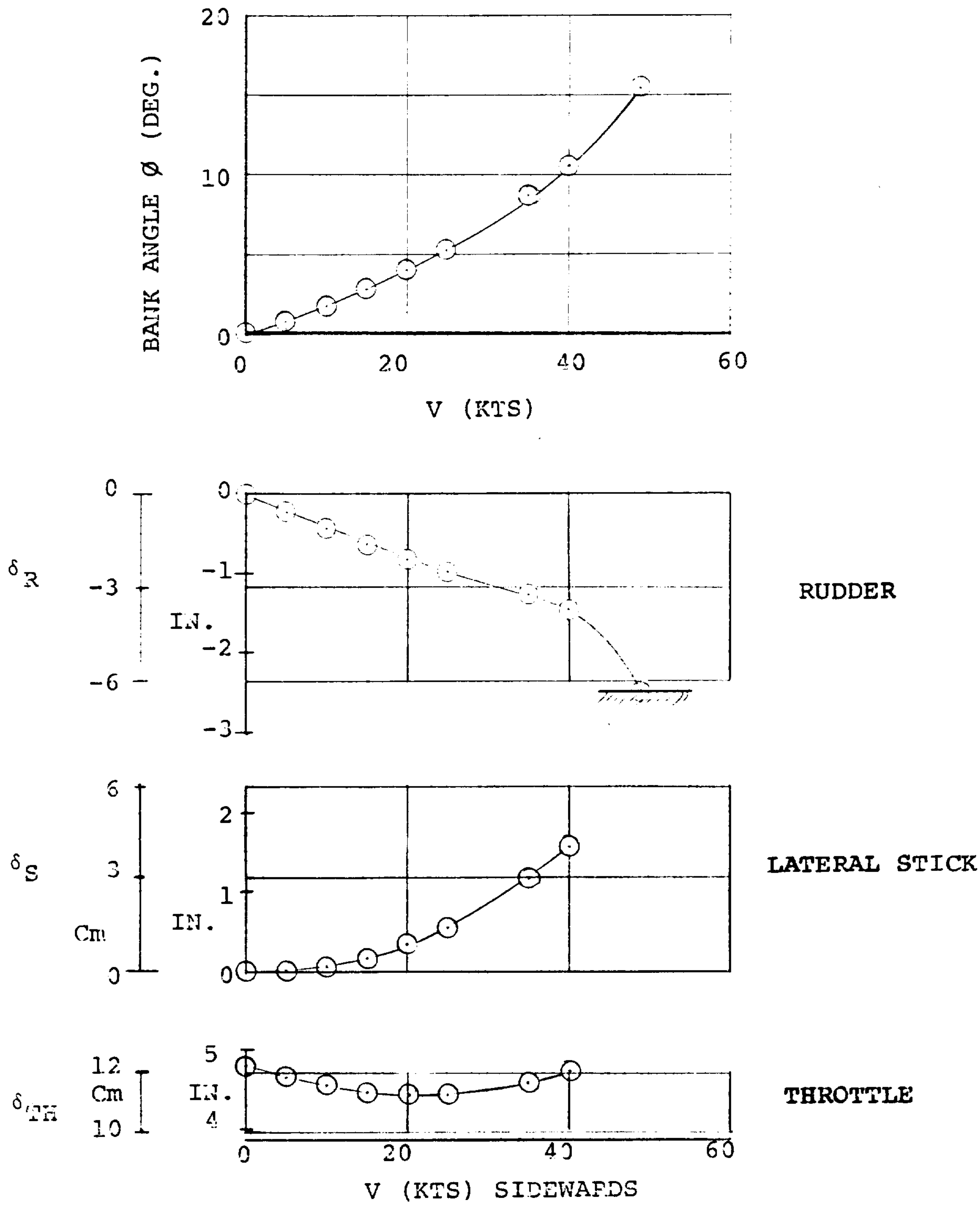

FIGURE 11.99. CONTROL DATA IN SIDEWARDS FLIGHT - GW = 5896.7 Kg (13,000 LBS) - AFT CG - $i_N = 90°$

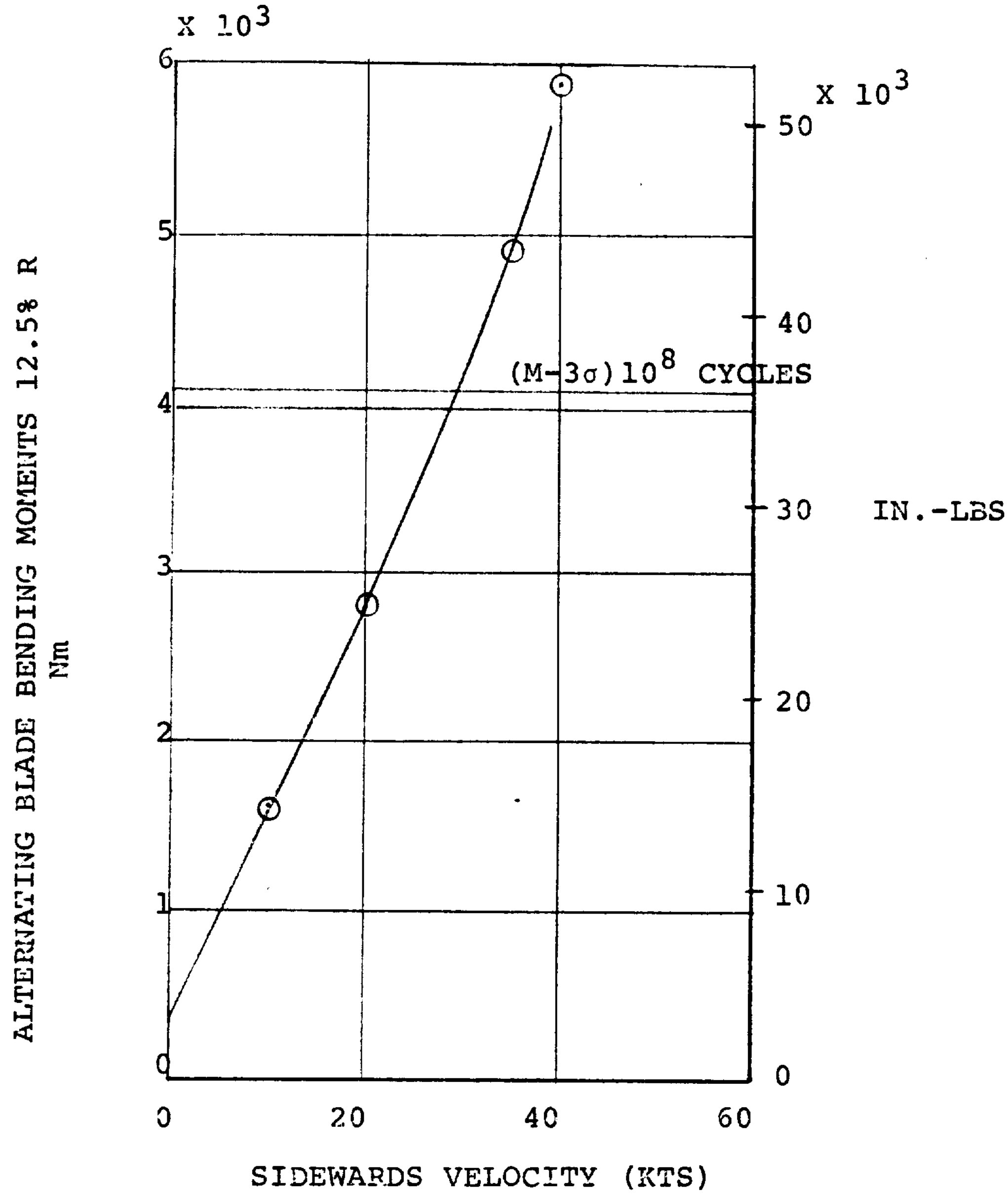

FIGURE 11.100. ESTIMATED BLADE BENDING LOADS IN SIDEWARDS FLIGHT $i_N = 90°$ GW = 5896.7 Kg (13,000 LBS) AFT CG

12.0 STABILITY AND CONTROL

12.0 STABILITY AND CONTROL

Preliminary stability and control characteristics of the Hingeless Rotor XV-15 Aircraft were evaluated over the range of airspeed from hover to high speed cruise. The evaluation was performed using the mathematical model to obtain dynamic responses to pulses and to provide stability derivatives. The stability derivatives were used in a small perturbation, coupled lateral/directional analysis to yield the stability roots. The evaluation was conducted at sea level, at aft CG and at 13000 pounds gross weight with the rotor rpm governor operating. All results presented are for SAS-off. Laboratory and piloted evaluation indicates that the SAS provides adequate augmentation.

It should be noted that the results presented here do not reflect rotor loads control systems (cyclic-on-the-stick). The effect of these systems on stability and control will be investigated during an upcoming design study.

12.1 Control Power

Pitch, roll and yaw control power of the Hingeless Rotor XV-15 at selected nacelle angles and airspeeds through transition and cruise, is presented in Figures 12.1 through 12.3. The amount of control power available per inch of control displacement at a given nacelle angle depends on the rotor cyclic and aerodynamic control surface gains. For the HRXV-15 the elevator, rudder and aileron gains (degrees/inch) were kept the same as the current XV-15. The cyclic gains were chosen by selecting values in hover that produced good hover control without compromising blade fatigue life. These values were then reduced by the sine of the nacelle angle as conversion progressed. No further optimization of control gains was attempted at this time until further work is completed on the cyclic-on-the-stick loads control system.

As can be seen from the figures, pitch control power about all three axes in hover, transition and cruise is high and well above the minimums specified in MIL-F-83300. The hover pitch control power of 0.66 rads/sec^2/inch is comparable to present-day helicopters. Roll control power at nacelle angles above 30 degrees is in excess of requirements at all airspeeds. At 30° nacelle angle and below 160 knots, roll control power is near specification minimums due to a combination of non-optimum gains and the low nacelle angles. It is planned to improve the control power in roll at these configurations by reworking the gain schedules. Yaw control power is above minimums throughout the envelope except at 60° nacelle angle and 70 knots. This condition is, however, close to the stall boundary for the aircraft.

As determined from the simulator evaluation, pilot opinion of the control power for the unaugmented aircraft is favorable.

12.2 Control Feel and Stick Force/g

The control force-feel gradients and breakouts utilized in the HRXV-15 piloted simulation were the same as those used in the NASA/Army XV-15. During the simulation the pilot stated that the stick forces felt high during low speed flight. In high speed flight the stick force per g was noted as being low. The force gradients were changed accordingly to yield a virtually constant 15 lbs/g at mid CG position. Figures 12.4 and 12.5 present the revised force gradients and breakouts and Figure 12.6 shows the stick force/g variation with airspeed in the airplane mode. Also shown are the stick force/g for the current XV-15 force-feel schedules.

12.3 Dynamic Stability

Dynamic stability of the HRXV-15 was investigated in hover, transition and cruise flight. The simulator mathematical model was used to generate time histories of aircraft response to control applications. The model was also used to provide stability derivatives which were then used to obtain the roots of the characteristic equations from a longitudinal lateral-directional coupled analysis.

12.3.1 Longitudinal

The responses of the HRXV-15 to longitudinal stick pulse inputs were obtained SAS-off, governor-on, at aft CG, 13,000 pounds gross weight. The selected responses covering the flight range from hover to cruise are presented in Figures 12.7 through 12.14.

The short period mode, as shown by the pitch attitude responses, is well-damped throughout the flight envelope. In hover, the initial response (Figure 12.7) is well damped and is followed by a phugoid oscillation of period 15 seconds. This long period oscillation is slowly divergent with a time to double amplitude of 57 seconds and damping ratio -.03. The hover pitch response, SAS-off, is annoying but manageable by the pilot.

Figure 12.8 shows the pitch response for 90° nacelle angle and 60 knots, a typical mid-transition configuration. The short period is nearly dead beat, ensuring precise pilot command of pitch attitude. The ensuing phugoid is divergent oscillatory of 16 seconds period and time to double is 16 seconds. If the nacelles are lowered to 60° at 60 knots (Figure 12.9) the short period remains highly damped and the phugoid becomes lightly damped (ζ = .19) with period 23 seconds and time-to-half-amplitude 13 seconds.

Figures 12.10 through 12.12 show the effect of reducing nacelle angle at constant (100 knots) airspeed. Short period response is very highly damped and response reduces as nacelles are lowered because of the cyclic gain reduction with nacelle angle. The phugoid is positively damped throughout, with $t_{1/2}$ varying from 10 seconds at i_N = 60° to 21 seconds at i_N = 0°.

The longitudinal response in cruise mode with flaps up and nacelles fully down is shown in Figures 12.13 and 12.14 representing the low and high speed conditions. Initial pitch response is highly damped and the phugoid period varies from 38 seconds at 140 knots to 46 seconds at 240 knots. Times to half amplitude are 66 seconds and 46 seconds respectively.

Longitudinal response characteristics are summarized in Figures 12.15 through 12.17, which present the frequencies, damping, and periodic times of the short period and phugoid, as determined from analysis of the characteristic roots.

In general, the longitudinal characteristics of the unaugmented HRXV-15 are estimated to be acceptable throughout the flight range. At airspeeds below 80 knots and nacelle angles above 75° the phugoid is mildly divergent. Pilot experience in the simulator showed that this condition is readily controllable.

12.3.2 Lateral-Directional

Lateral-directional responses of the unaugmented aircraft to lateral stick and rudder pulses are presented in Figures 12.18 through 12.24.

In the helicopter configuration (i_N = 90°) at 60 knots, Figure 12.18 shows the response to a right stick pulse of 0.5" for 1 second. The initial roll damping is high and the resulting roll/yaw coupled oscillation is slightly negatively damped (-.08) and period 9 seconds. The roll/yaw coupling arises from the rotor aerodynamic contributions. This response meets Level 2 requirements of MIL-F-83300. Application of a 0.5 inch rudder pulse shows that the requirement to change yaw angle by 6 degrees in 1 second is met, and that the aircraft rolls right for right pedal, thus satisfying the dihedral requirement.

Figure 12.19 presents the aircraft response to stick and rudder with 60° nacelle angle and 60 knots. The dutch roll response meets Level 2 requirements ($\zeta\omega_N$ = -.032 ω_D = .489).

Figures 12.20, 12.21 and 12.22 show the responses with nacelle angle of 60°, 30° and 0° at 100 knots. The dutch roll response rapidly improves, meeting Level 1 requirements at 60° and exceeding them at 30° and 0° nacelle settings. The spiral mode is stable throughout. At all conditions proverse yaw response to lateral stick is attained. There is, however, a small amount of negative dihedral in response to rudder pulses, i.e., the aircraft initially rolls left during a right pedal input.

Cruise lateral-directional responses are shown in Figure 12.23 at 140 knots and in Figure 12.24 at 240 knots with flaps up. The roll mode is well damped with positive spiral stability evident at each speed. The dutch roll response is also well damped and meets the requirements of Level 1.

The lateral-directional characteristics are summarized in Figures 12.25 through 12.27 in the form of characteristic frequencies, damping, etc. Figure 12.27 compares the unaugmented aircraft response in dutch roll with the various levels of MIL-F-83300.

SYMBOL	i_N°	δ_N°
⬡	90	40
◇	75	40
△	60	40
□	30	40
×	0	40
○	0	40
	0	0

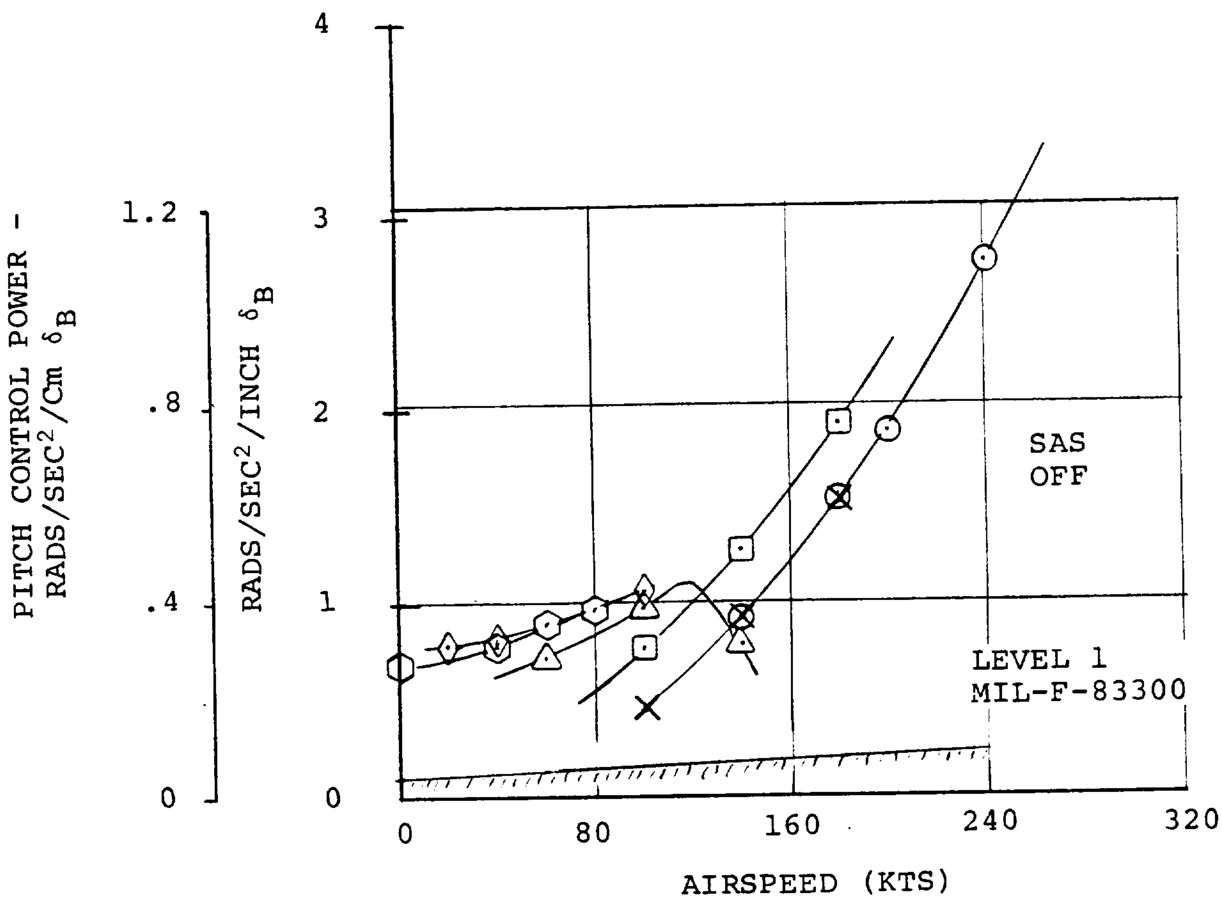

FIGURE 12.1. PITCH CONTROL POWER - AFT CG

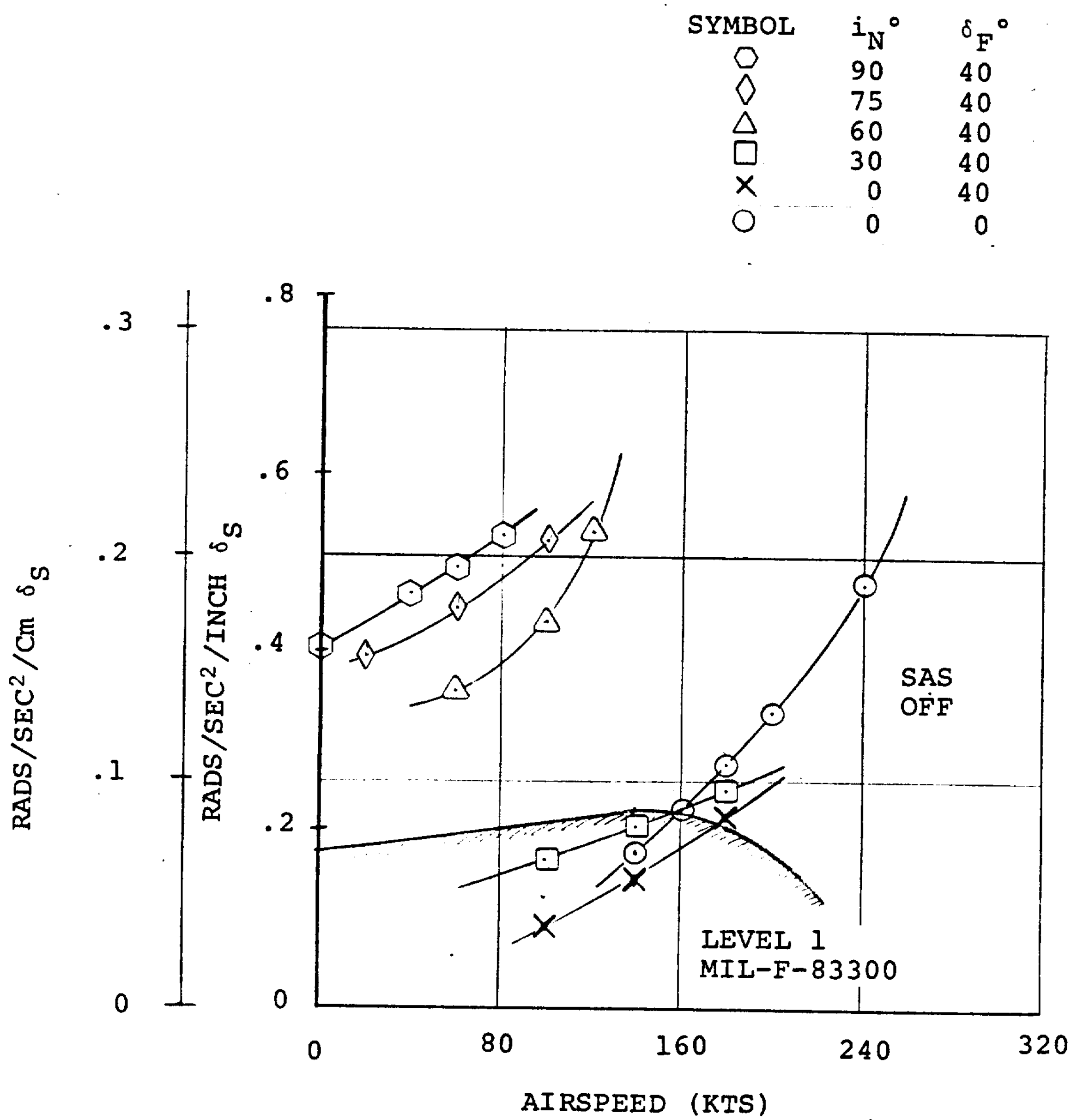

FIGURE 12.2. ROLL CONTROL POWER - AFT CG

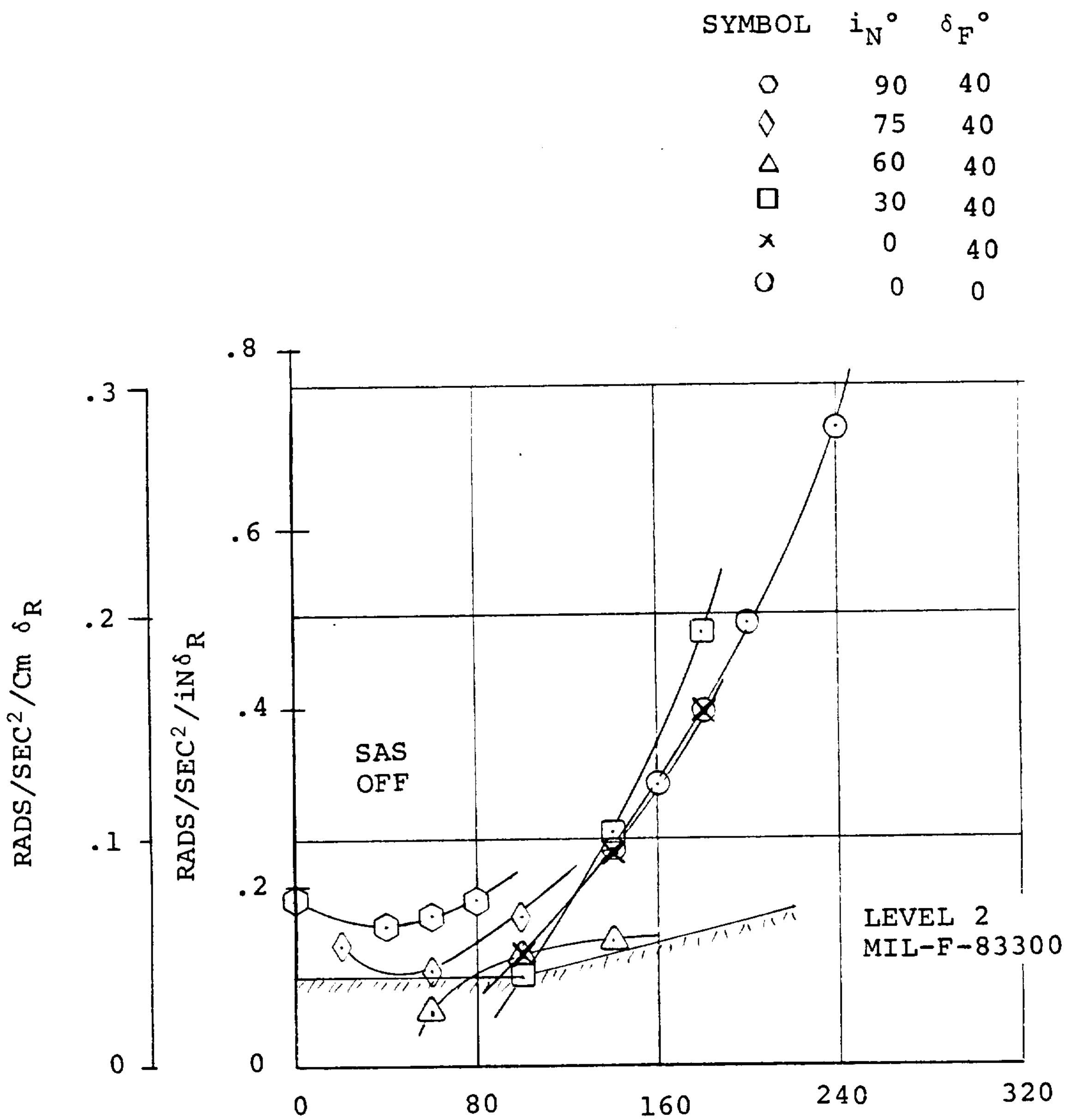

FIGURE 12.3. YAW CONTROL POWER - AFT CG

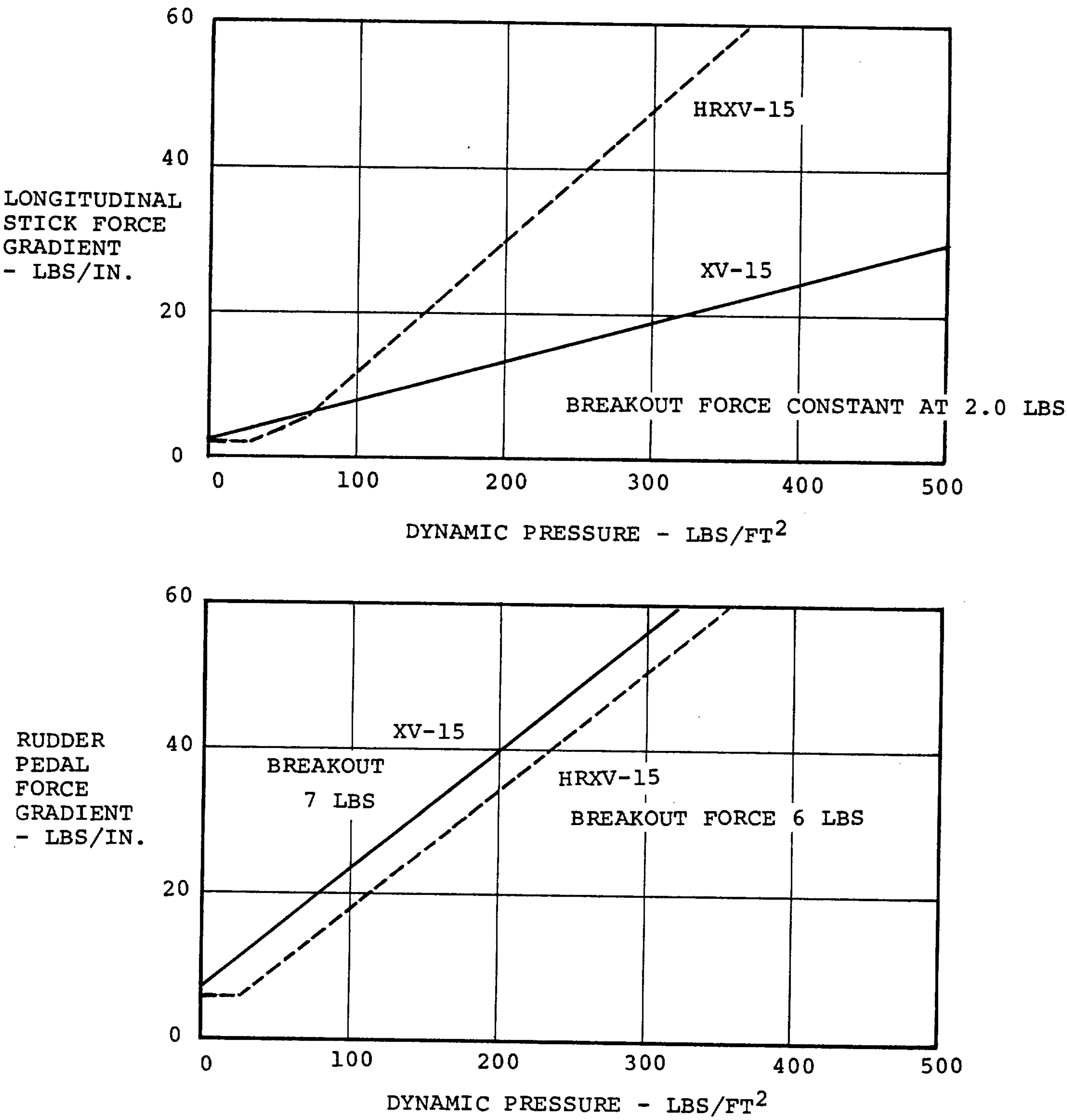

FIGURE 12.4. REVISED LONGITUDINAL AND PEDAL FORCE GRADIENTS

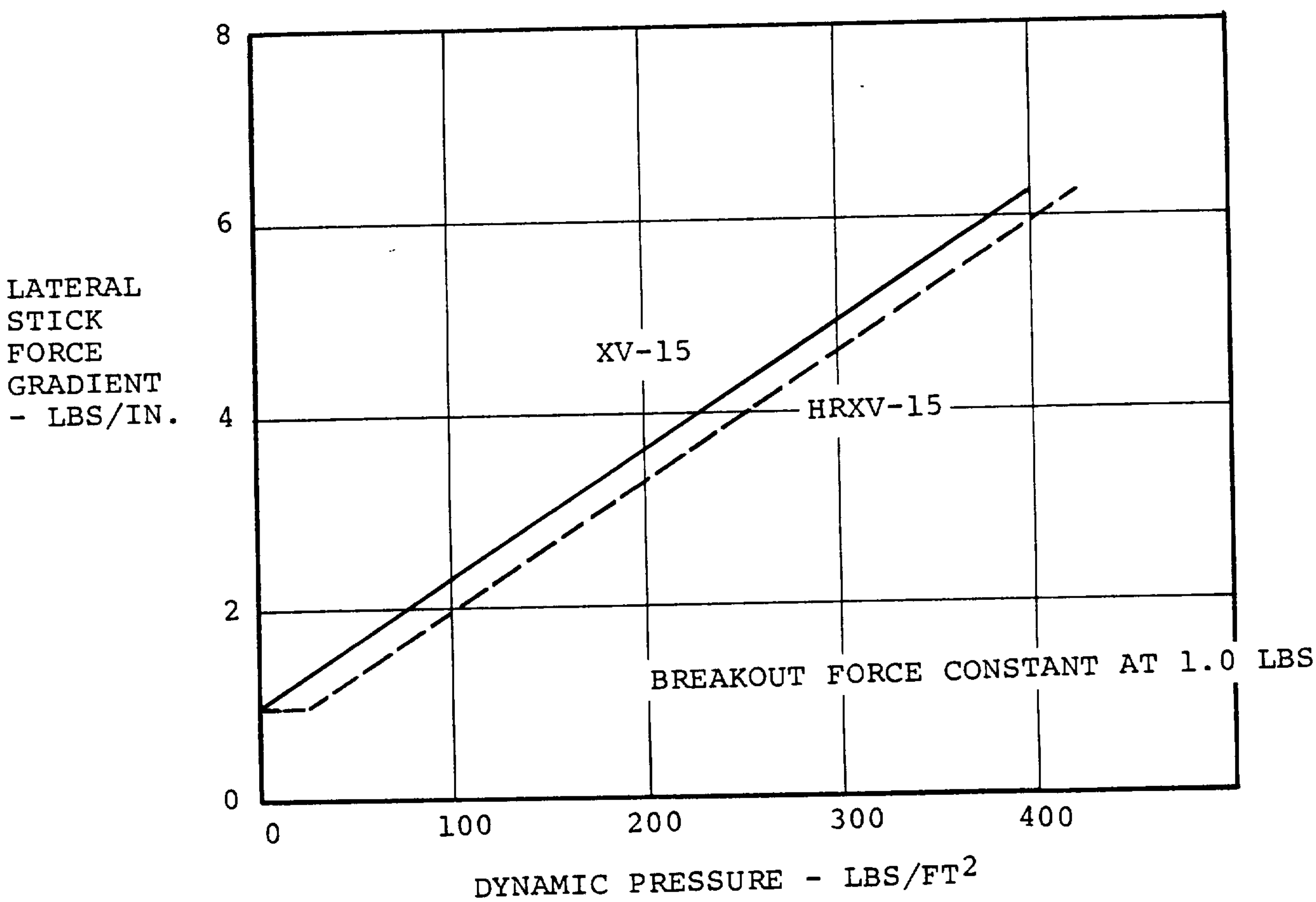

FIGURE 12.5. REVISED LATERAL STICK GRADIENT

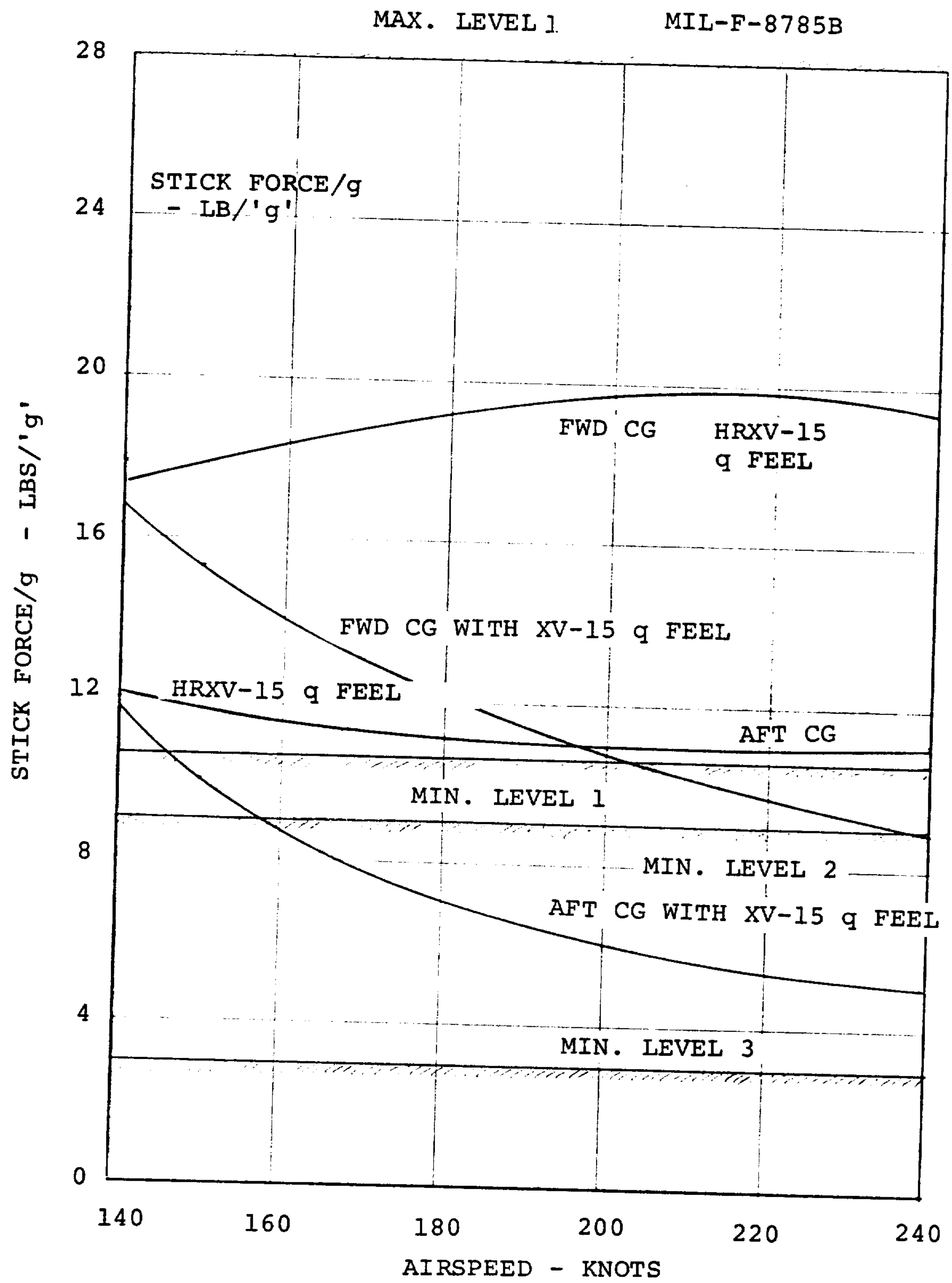

FIGURE 12.6. STICK FORCE/g VARIATION WITH AIRSPEED IN AIRPLANE MODE

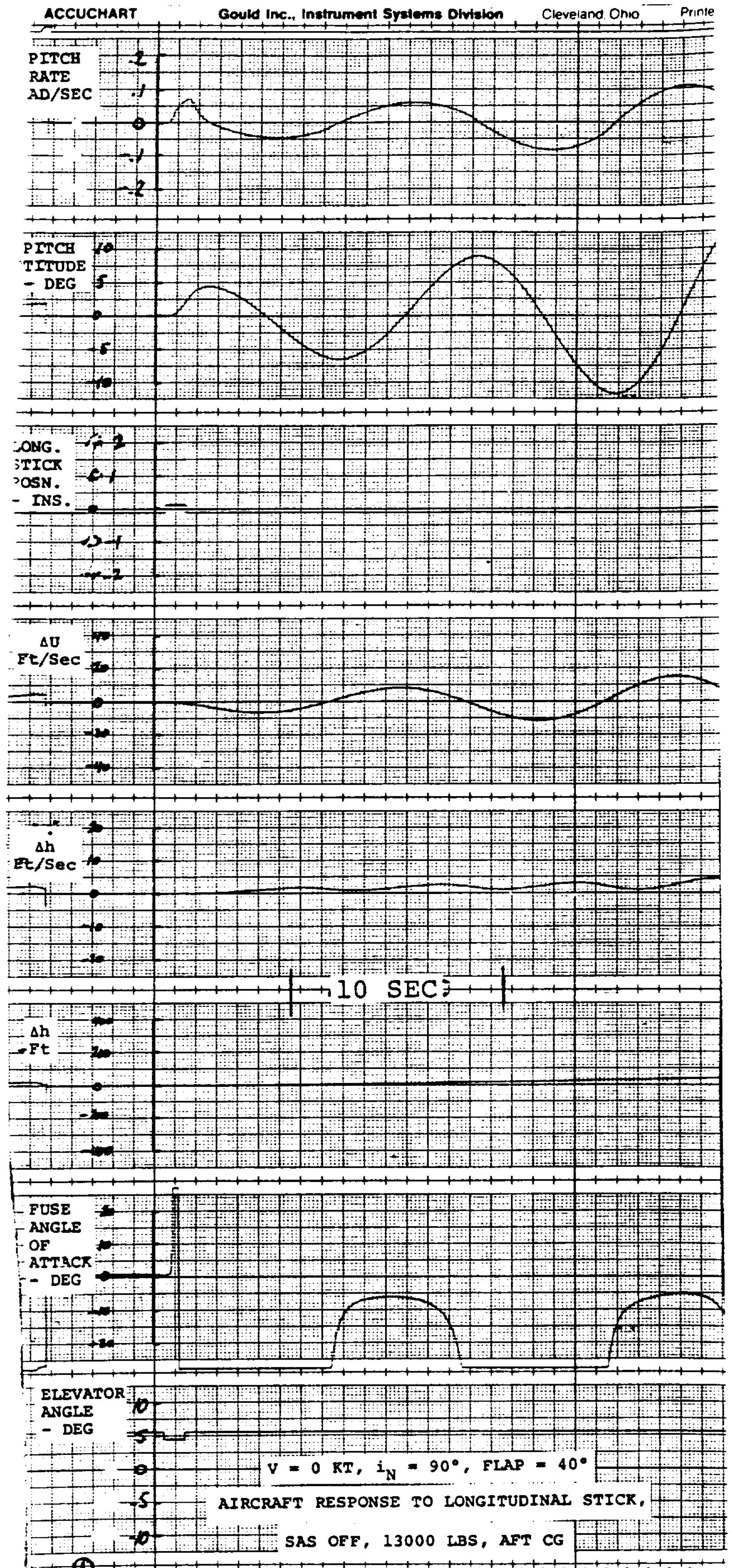
ACCUCHART
Gould Inc., Instrument Systems Division
Cleveland, Ohio
PITCH RATE AD/SEC
PITCH TITUDE - DEG
LONG. STICK POSN. - INS.
ΔU Ft/Sec
Δh Ft/Sec
10 SEC
Δh Ft
FUSE ANGLE OF ATTACK - DEG
ELEVATOR ANGLE - DEG
V = 0 KT, i_N = 90°, FLAP = 40°
AIRCRAFT RESPONSE TO LONGITUDINAL STICK,
SAS OFF, 13000 LBS, AFT CG

FIGURE 12.7

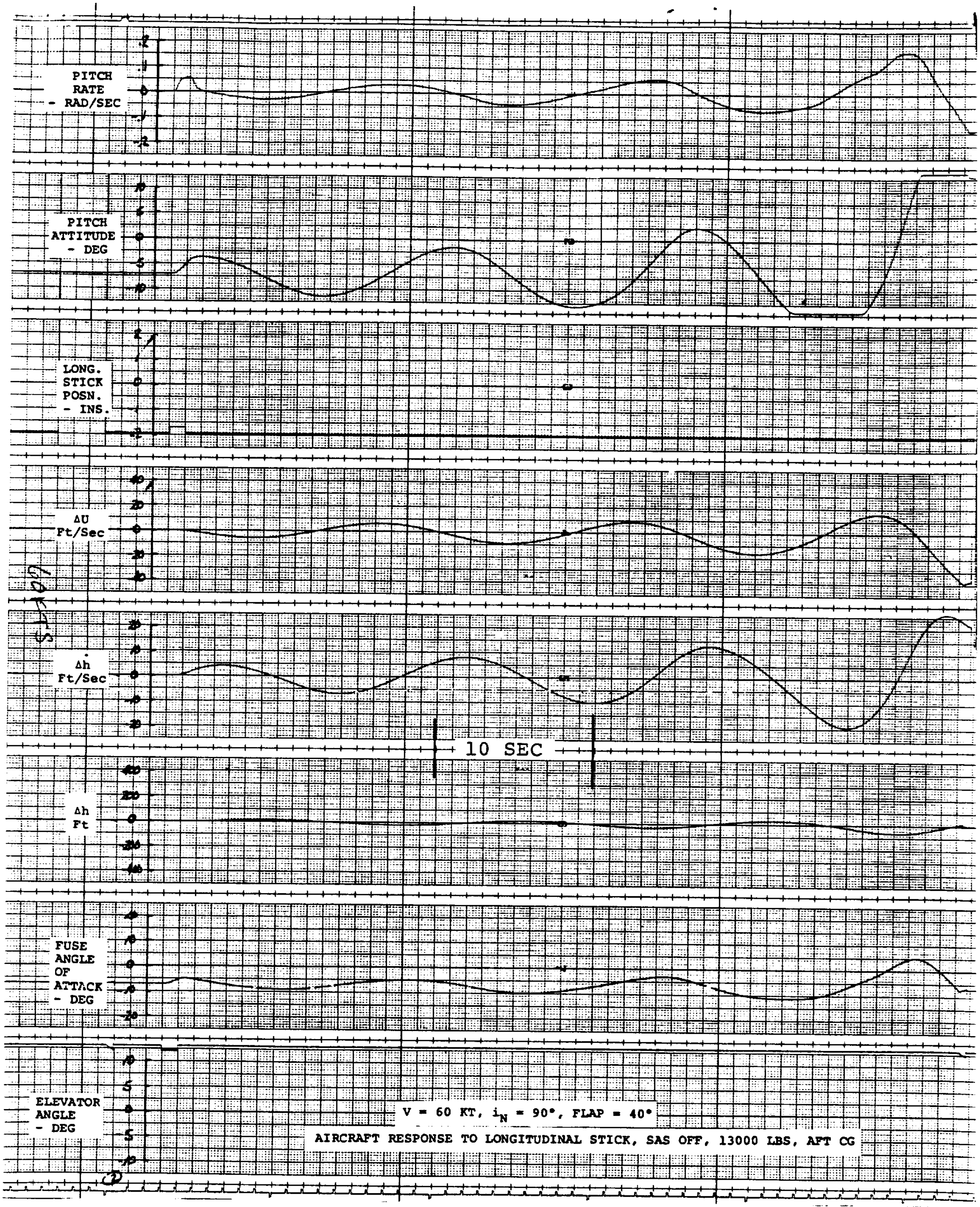
PITCH
RATE
- RAD/SEC
PITCH
ATTITUDE
- DEG
LONG.
STICK
POSN.
- INS.
ΔU
Ft/Sec
Δḣ
Ft/Sec
10 SEC
Δh
Ft
FUSE
ANGLE
OF
ATTACK
- DEG
ELEVATOR
ANGLE
- DEG
V = 60 KT, i_N = 90°, FLAP = 40°
AIRCRAFT RESPONSE TO LONGITUDINAL STICK, SAS OFF, 13000 LBS, AFT CG

FIGURE 12.8

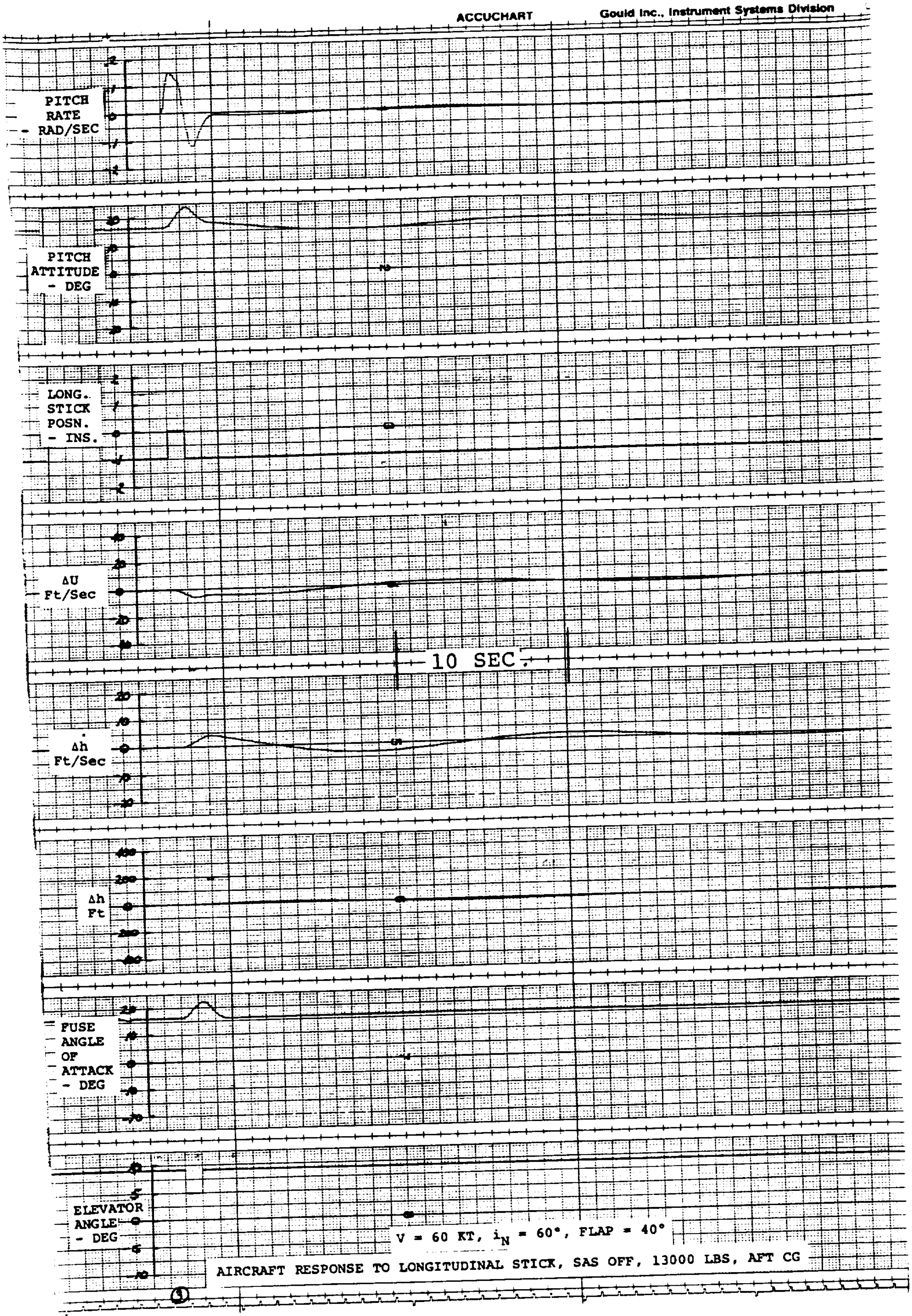
ACCUCHART
Gould Inc., Instrument Systems Division
PITCH RATE RAD/SEC
PITCH ATTITUDE - DEG
LONG. STICK POSN. - INS.
ΔU Ft/Sec
10 SEC
Δḣ Ft/Sec
Δh Ft
FUSE ANGLE OF ATTACK - DEG
ELEVATOR ANGLE - DEG
V = 60 KT, i_N = 60°, FLAP = 40°
AIRCRAFT RESPONSE TO LONGITUDINAL STICK, SAS OFF, 13000 LBS, AFT CG

FIGURE 12.9

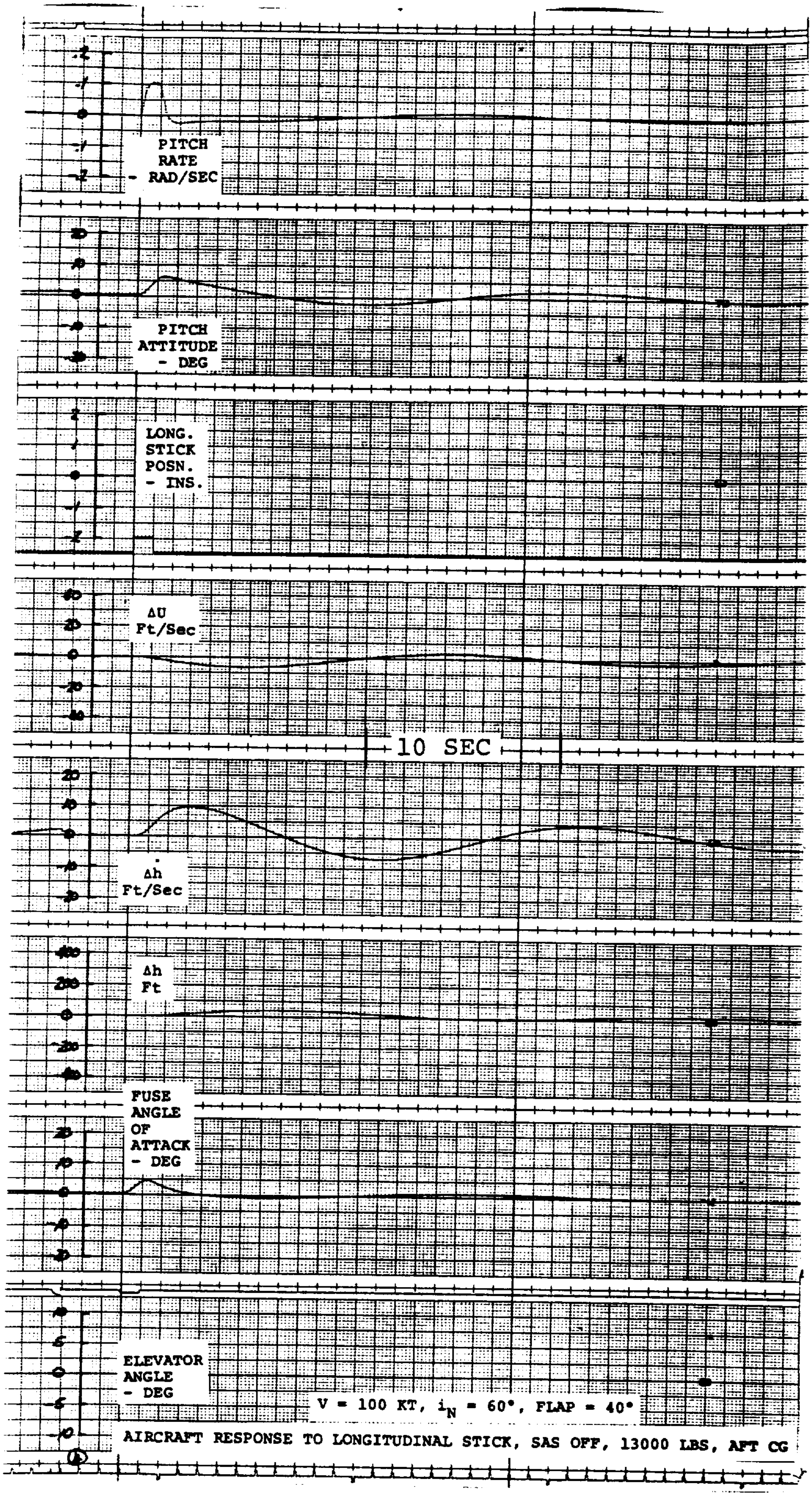
PITCH RATE - RAD/SEC
PITCH ATTITUDE - DEG
LONG. STICK POSN. - INS.
ΔU Ft/Sec
10 SEC
Δḣ Ft/Sec
Δh Ft
FUSE ANGLE OF ATTACK - DEG
ELEVATOR ANGLE - DEG
V = 100 KT, i_N = 60°, FLAP = 40°
AIRCRAFT RESPONSE TO LONGITUDINAL STICK, SAS OFF, 13000 LBS, AFT CG

FIGURE 12.10

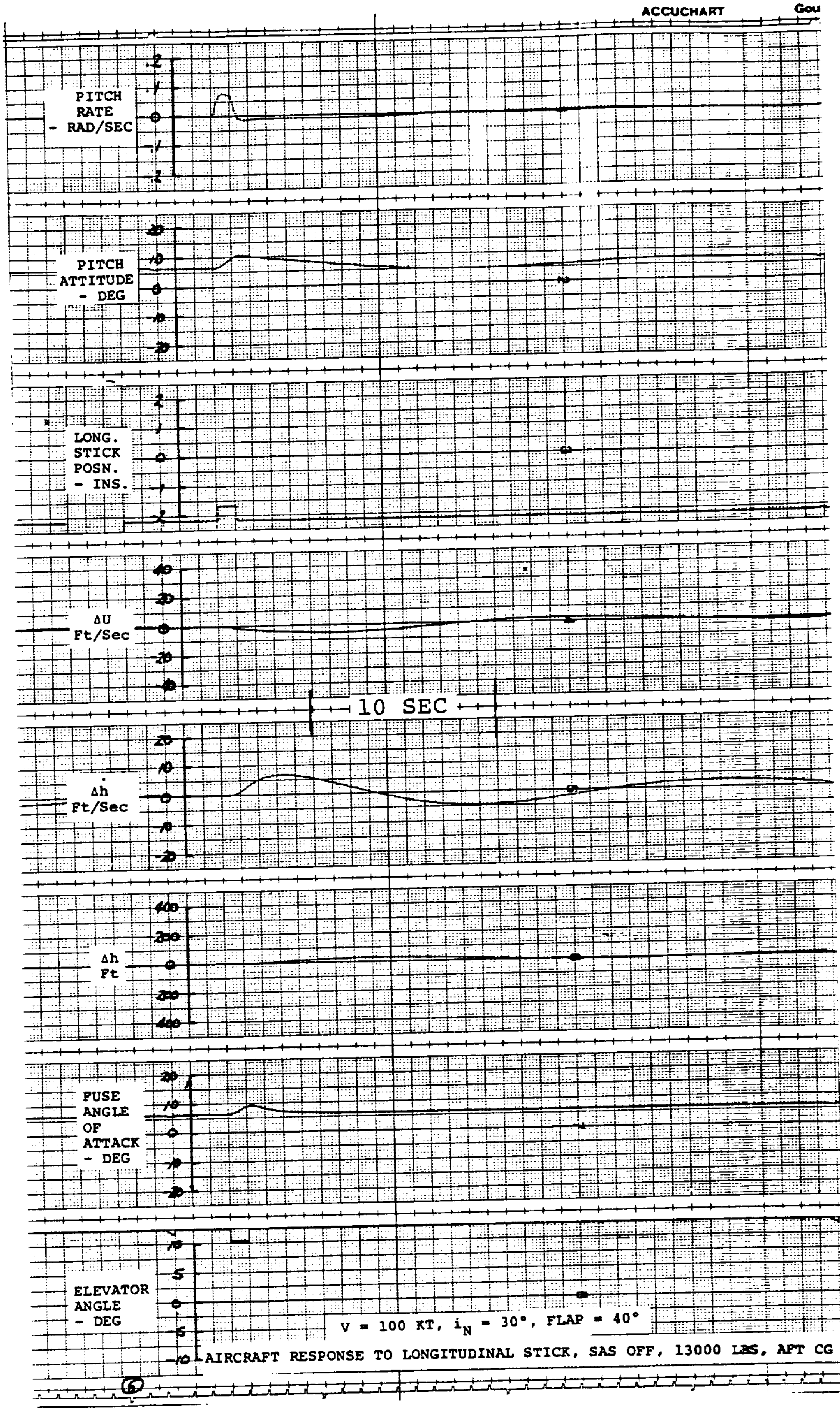
ACCUCHART
PITCH RATE - RAD/SEC
PITCH ATTITUDE - DEG
LONG. STICK POSN. - INS.
ΔU Ft/Sec
10 SEC
Δḣ Ft/Sec
Δh Ft
FUSE ANGLE OF ATTACK - DEG
ELEVATOR ANGLE - DEG
V = 100 KT, i_N = 30°, FLAP = 40°
AIRCRAFT RESPONSE TO LONGITUDINAL STICK, SAS OFF, 13000 LBS, AFT CG

FIGURE 12.11

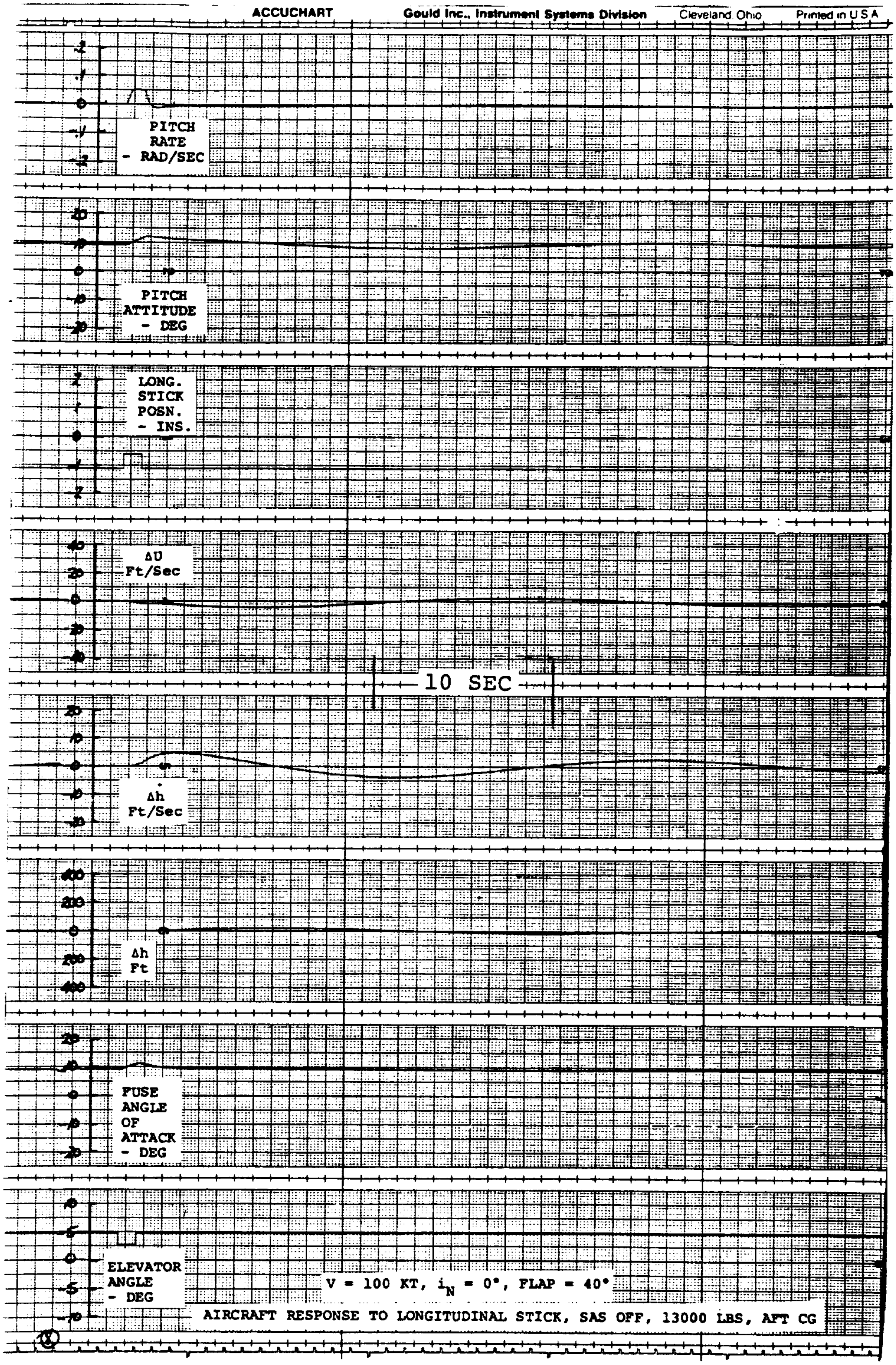
ACCUCHART
Gould Inc., Instrument Systems Division
Cleveland Ohio
Printed in U S A
PITCH
RATE
- RAD/SEC
PITCH
ATTITUDE
- DEG
LONG.
STICK
POSN.
- INS.
ΔU
Ft/Sec
10 SEC
Δḣ
Ft/Sec
Δh
Ft
FUSE
ANGLE
OF
ATTACK
- DEG
ELEVATOR
ANGLE
- DEG
V = 100 KT, i_N = 0°, FLAP = 40°
AIRCRAFT RESPONSE TO LONGITUDINAL STICK, SAS OFF, 13000 LBS, AFT CG

FIGURE 12.12

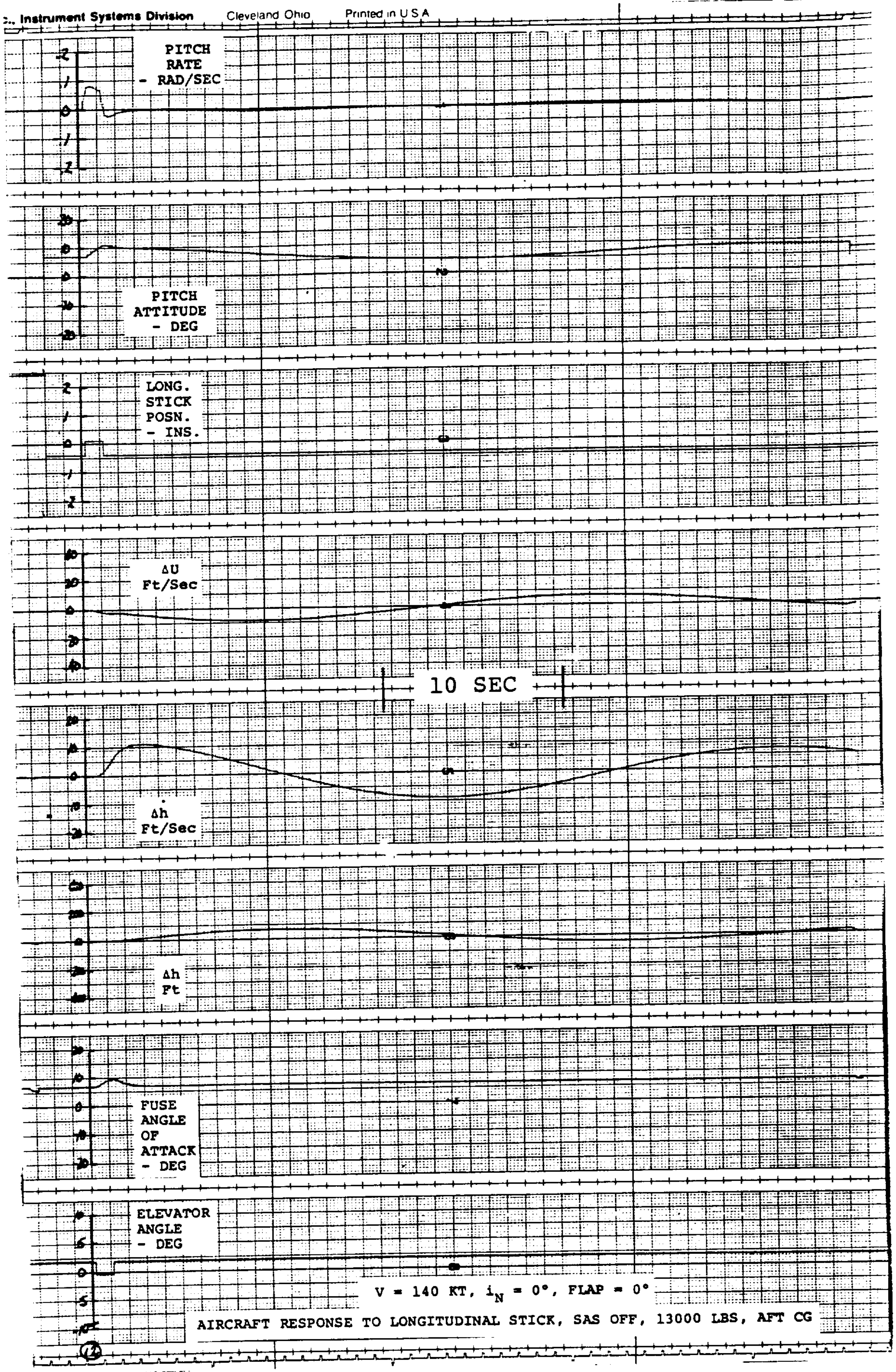
Instrument Systems Division
Cleveland Ohio
Printed in U S A
PITCH RATE - RAD/SEC
PITCH ATTITUDE - DEG
LONG. STICK POSN. - INS.
ΔU Ft/Sec
10 SEC
Δḣ Ft/Sec
Δh Ft
FUSE ANGLE OF ATTACK - DEG
ELEVATOR ANGLE - DEG
V = 140 KT, i_N = 0°, FLAP = 0°
AIRCRAFT RESPONSE TO LONGITUDINAL STICK, SAS OFF, 13000 LBS, AFT CG

FIGURE 12.13

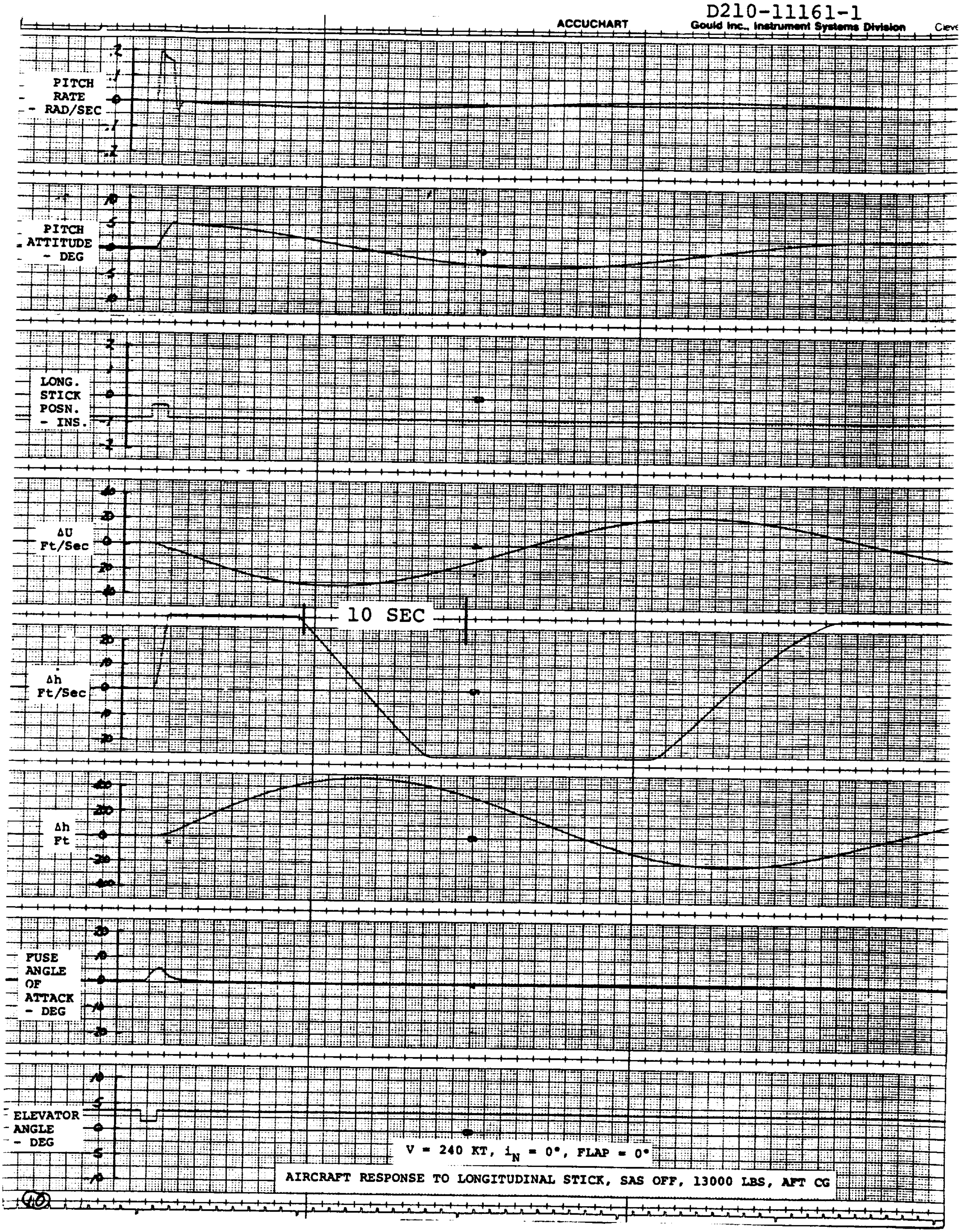
ACCUCHART
Gould Inc., Instrument Systems Division
PITCH RATE - RAD/SEC
PITCH ATTITUDE - DEG
LONG. STICK POSN. - INS.
ΔU Ft/Sec
10 SEC
Δḣ Ft/Sec
Δh Ft
FUSE ANGLE OF ATTACK - DEG
ELEVATOR ANGLE - DEG
V = 240 KT, i_N = 0°, FLAP = 0°
AIRCRAFT RESPONSE TO LONGITUDINAL STICK, SAS OFF, 13000 LBS, AFT CG

FIGURE 12.14

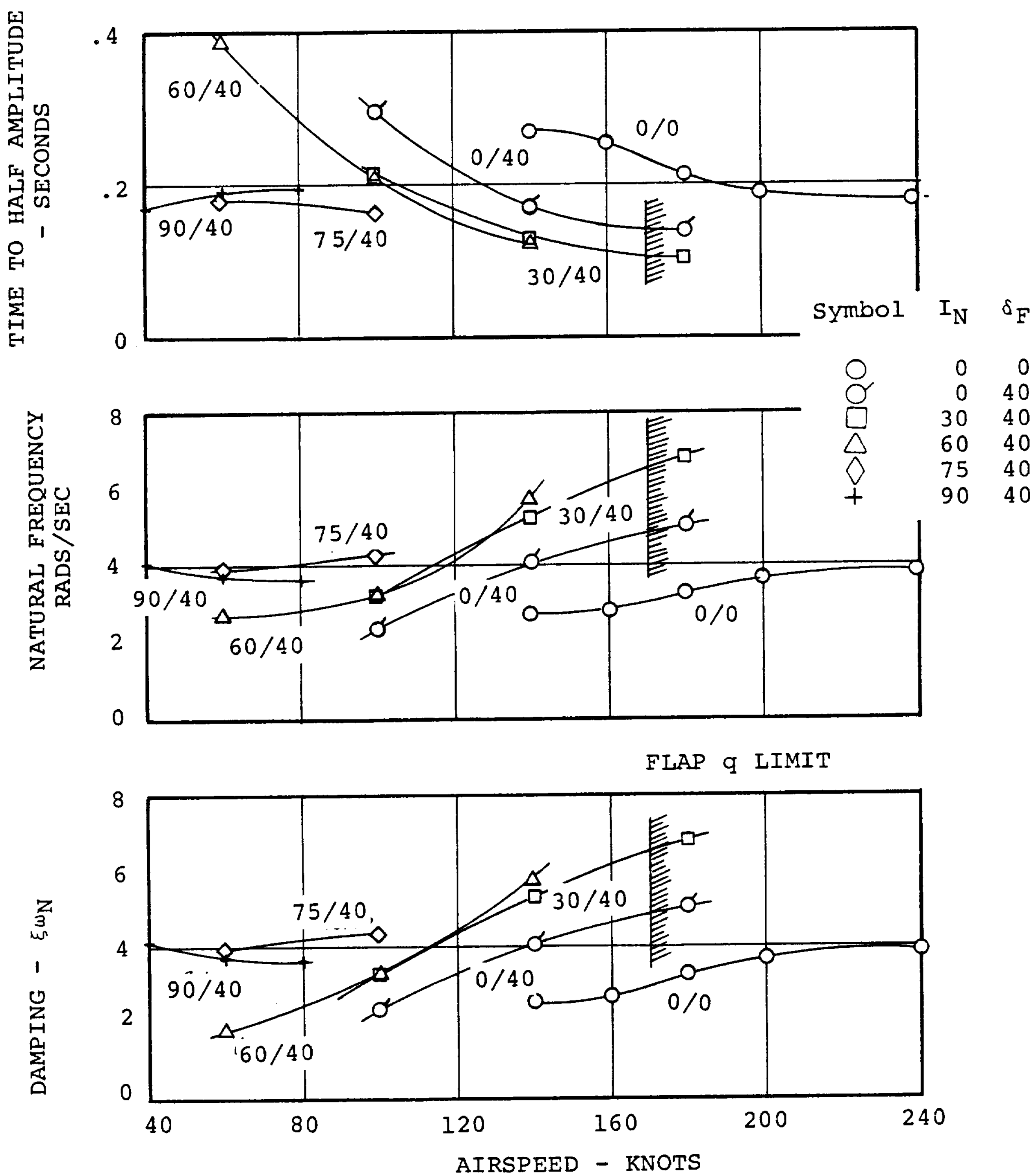

FIGURE 12.15. SHORT PERIOD CHARACTERISTICS, 13,000 LBS, AFT CG, GOVERNOR ON, SEA LEVEL

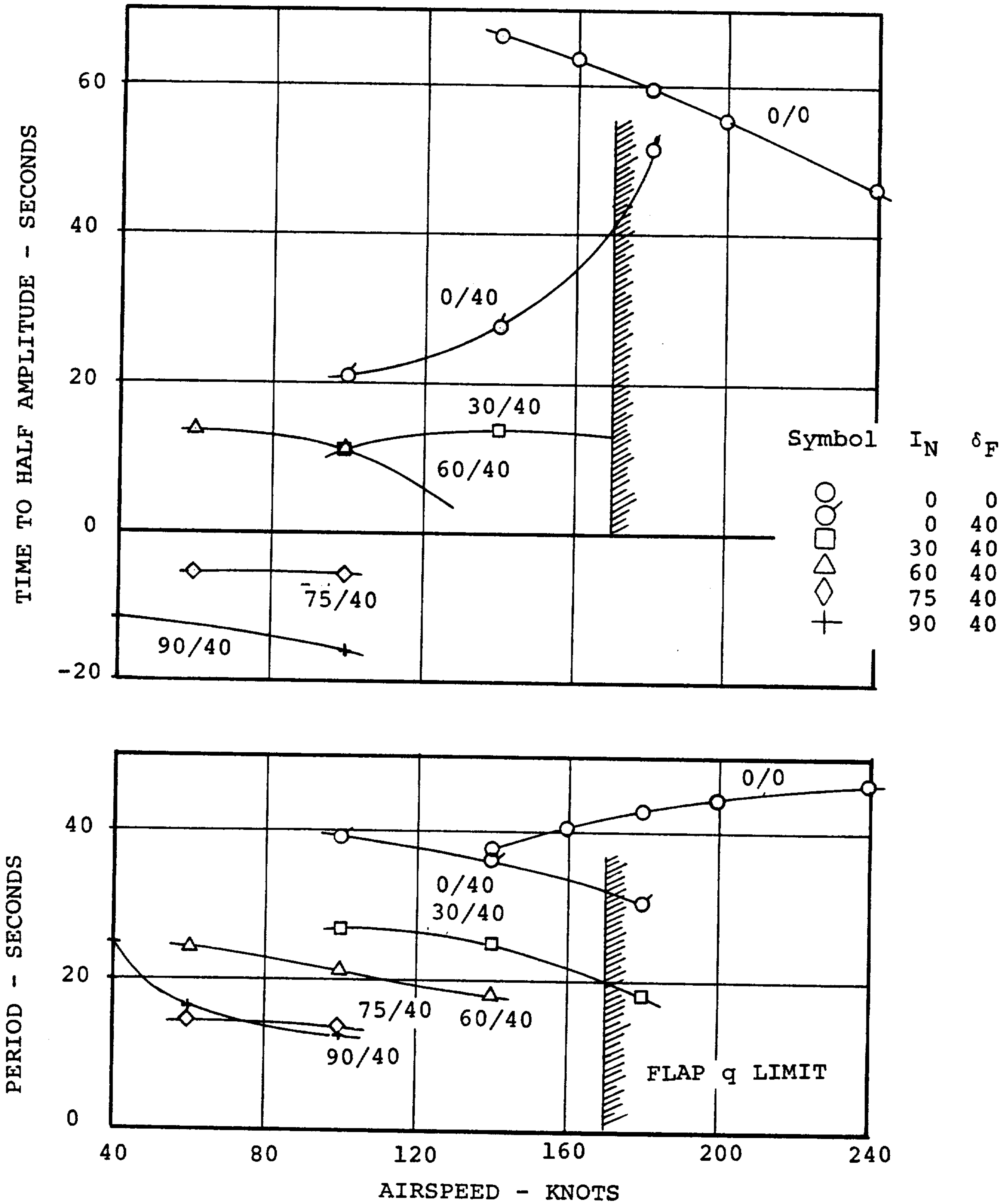

FIGURE 12.16. PHUGOID CHARACTERISTICS, 13,000 LBS, AFT CG, SAS-OFF, GOVERNOR ON

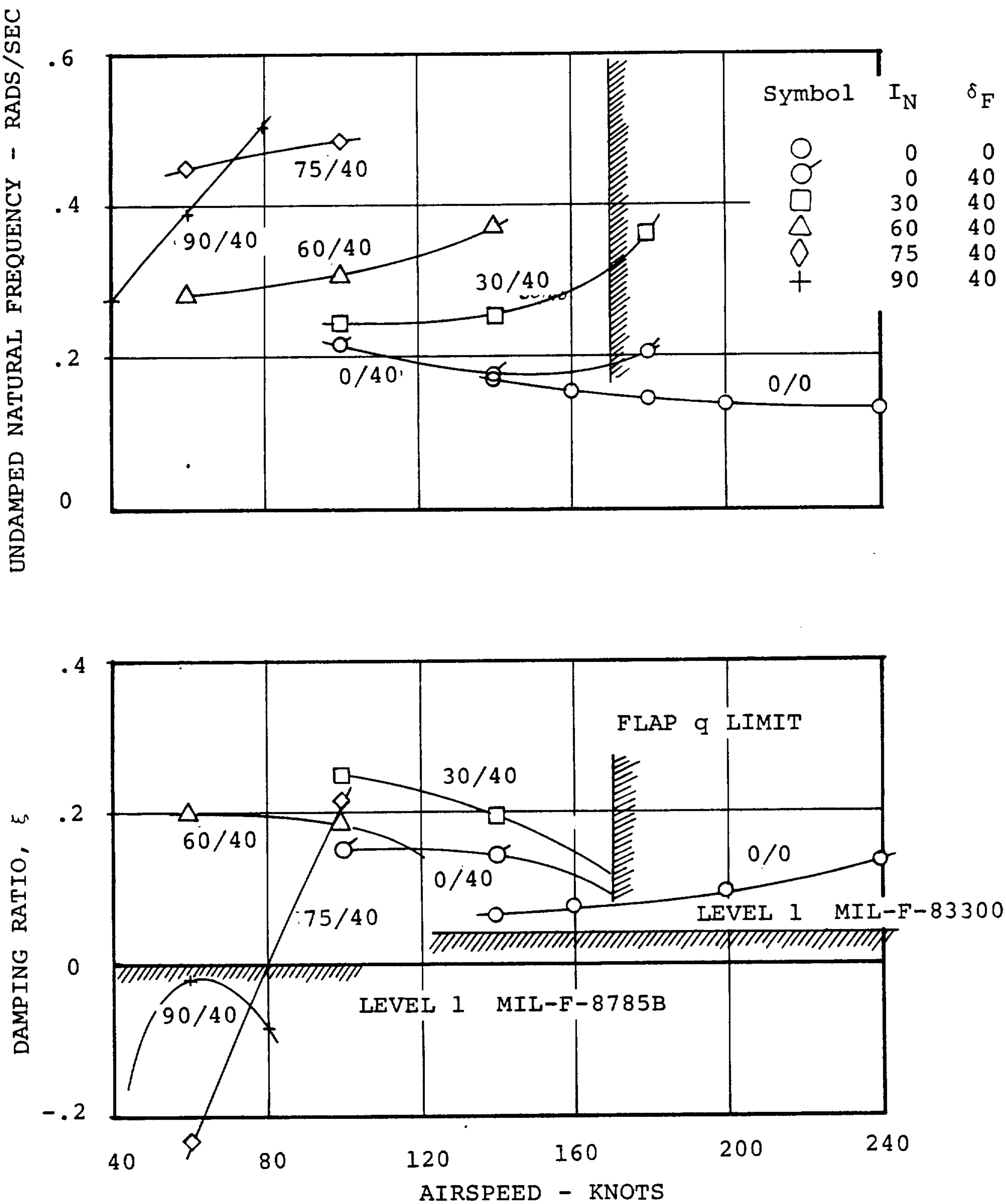

FIGURE 12.17. PHUGOID CHARACTERISTICS, 13,000 LBS, AFT CG, SAS-OFF, GOVERNOR ON

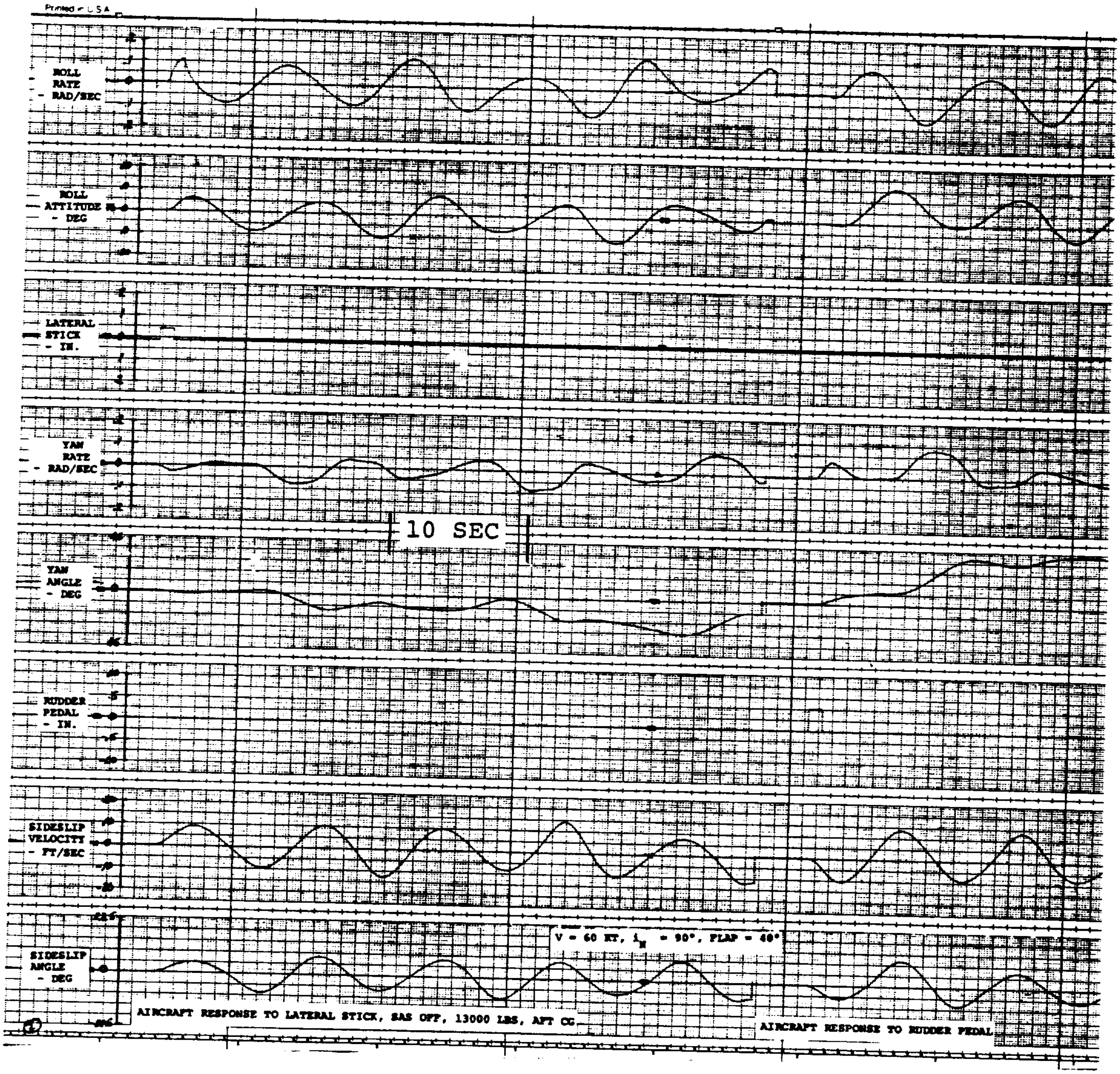
ROLL RATE - RAD/SEC
ROLL ATTITUDE - DEG
LATERAL STICK - IN.
YAW RATE - RAD/SEC
10 SEC
YAW ANGLE - DEG
RUDDER PEDAL - IN.
SIDESLIP VELOCITY - FT/SEC
SIDESLIP ANGLE - DEG
V = 60 KT, i_N = 90°, FLAP = 40°
AIRCRAFT RESPONSE TO LATERAL STICK, SAS OFF, 13000 LBS, AFT CG.
AIRCRAFT RESPONSE TO RUDDER PEDAL

FIGURE 12.18

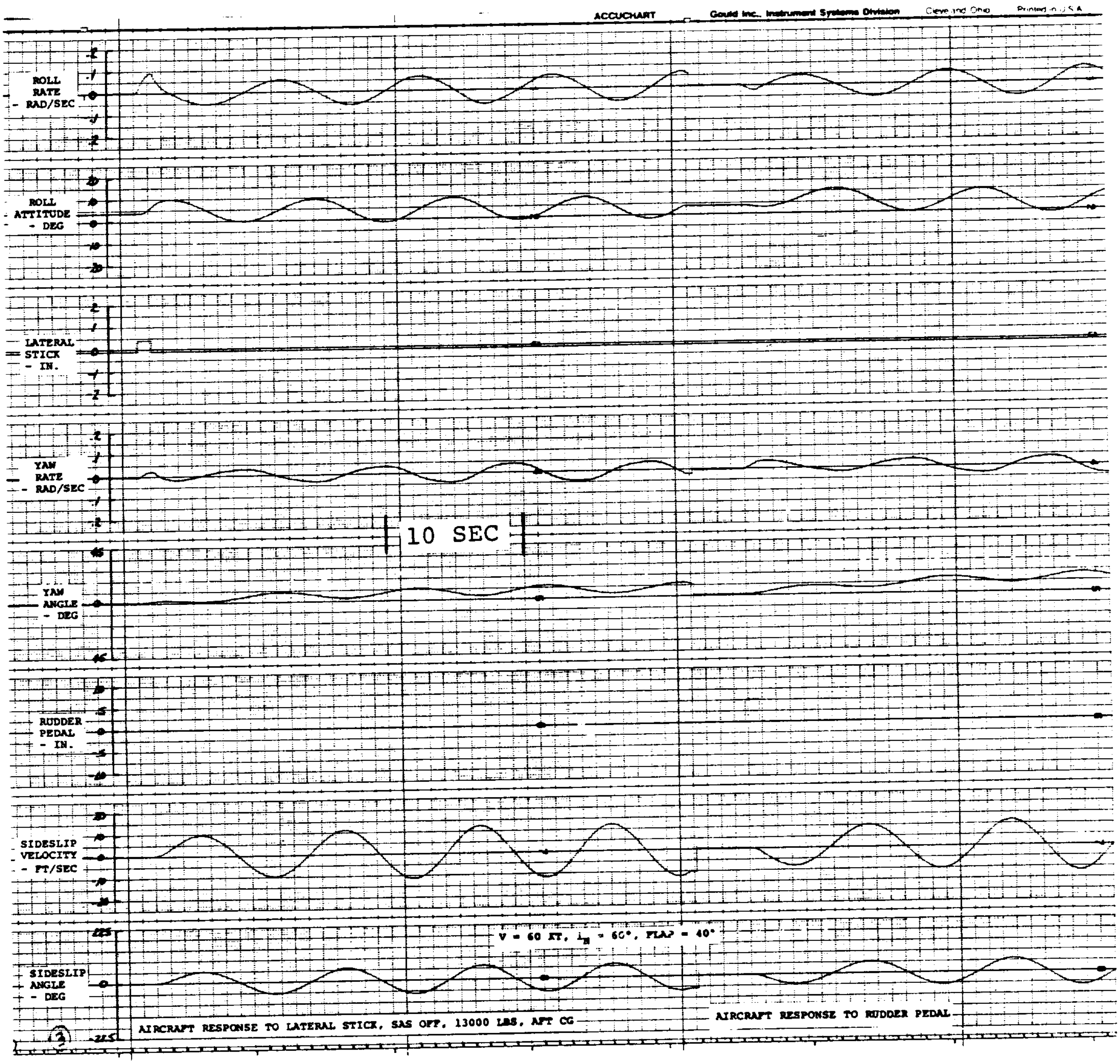
ACCUCHART
Gould Inc., Instrument Systems Division
ROLL RATE - RAD/SEC
ROLL ATTITUDE - DEG
LATERAL STICK - IN.
YAW RATE - RAD/SEC
10 SEC
YAW ANGLE - DEG
RUDDER PEDAL - IN.
SIDESLIP VELOCITY - FT/SEC
V = 60 KT, i_N = 60°, FLAP = 40°
SIDESLIP ANGLE - DEG
AIRCRAFT RESPONSE TO LATERAL STICK, SAS OFF, 13000 LBS, AFT CG
AIRCRAFT RESPONSE TO RUDDER PEDAL

FIGURE 12.19

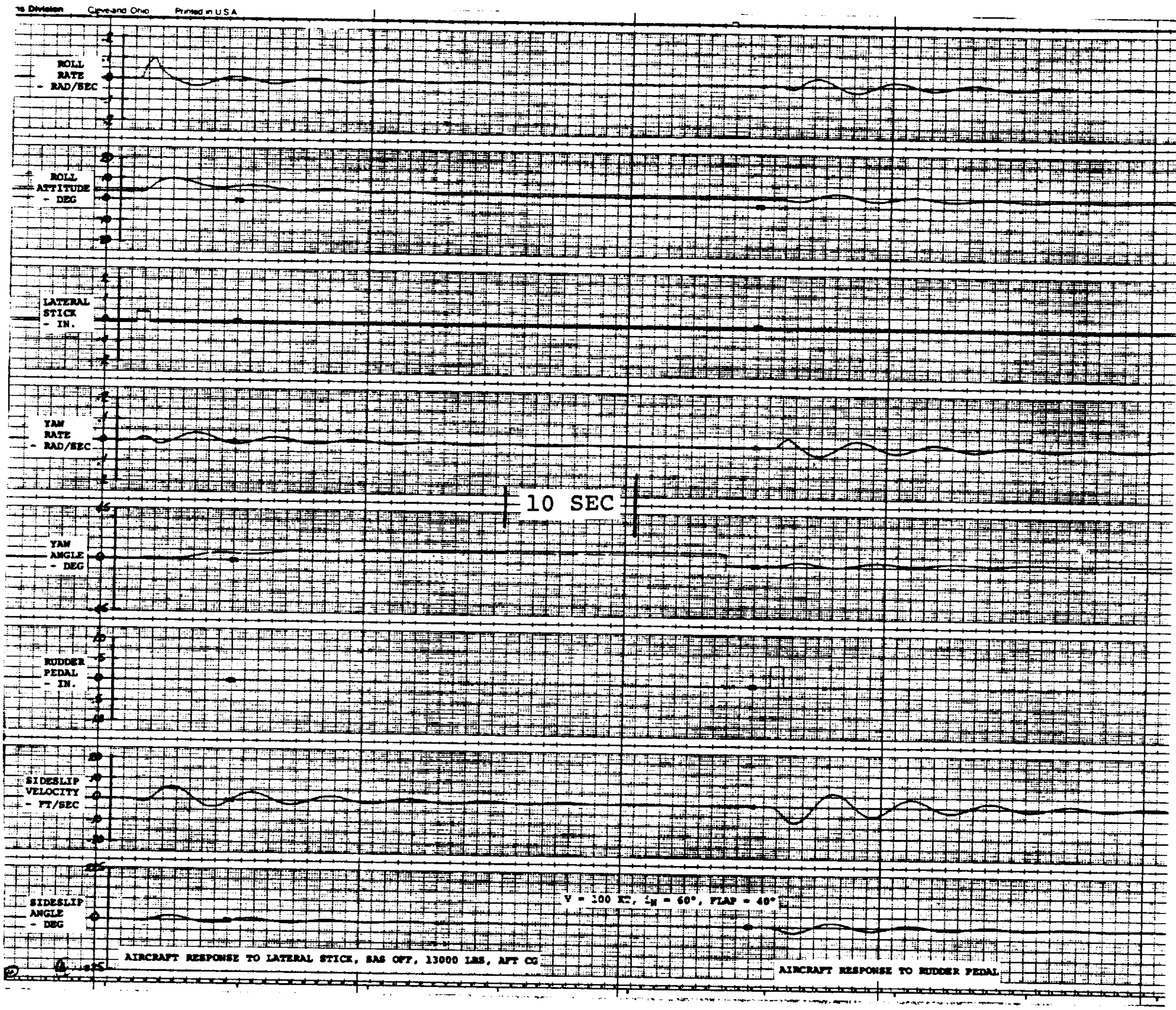

ROLL RATE - RAD/SEC
ROLL ATTITUDE - DEG
LATERAL STICK - IN.
YAW RATE - RAD/SEC
10 SEC
YAW ANGLE - DEG
RUDDER PEDAL - IN.
SIDESLIP VELOCITY - FT/SEC
SIDESLIP ANGLE - DEG
V = 100 KT, i_W = 60°, FLAP = 40°
AIRCRAFT RESPONSE TO LATERAL STICK, SAS OFF, 13000 LBS, AFT CG
AIRCRAFT RESPONSE TO RUDDER PEDAL

FIGURE 12.20

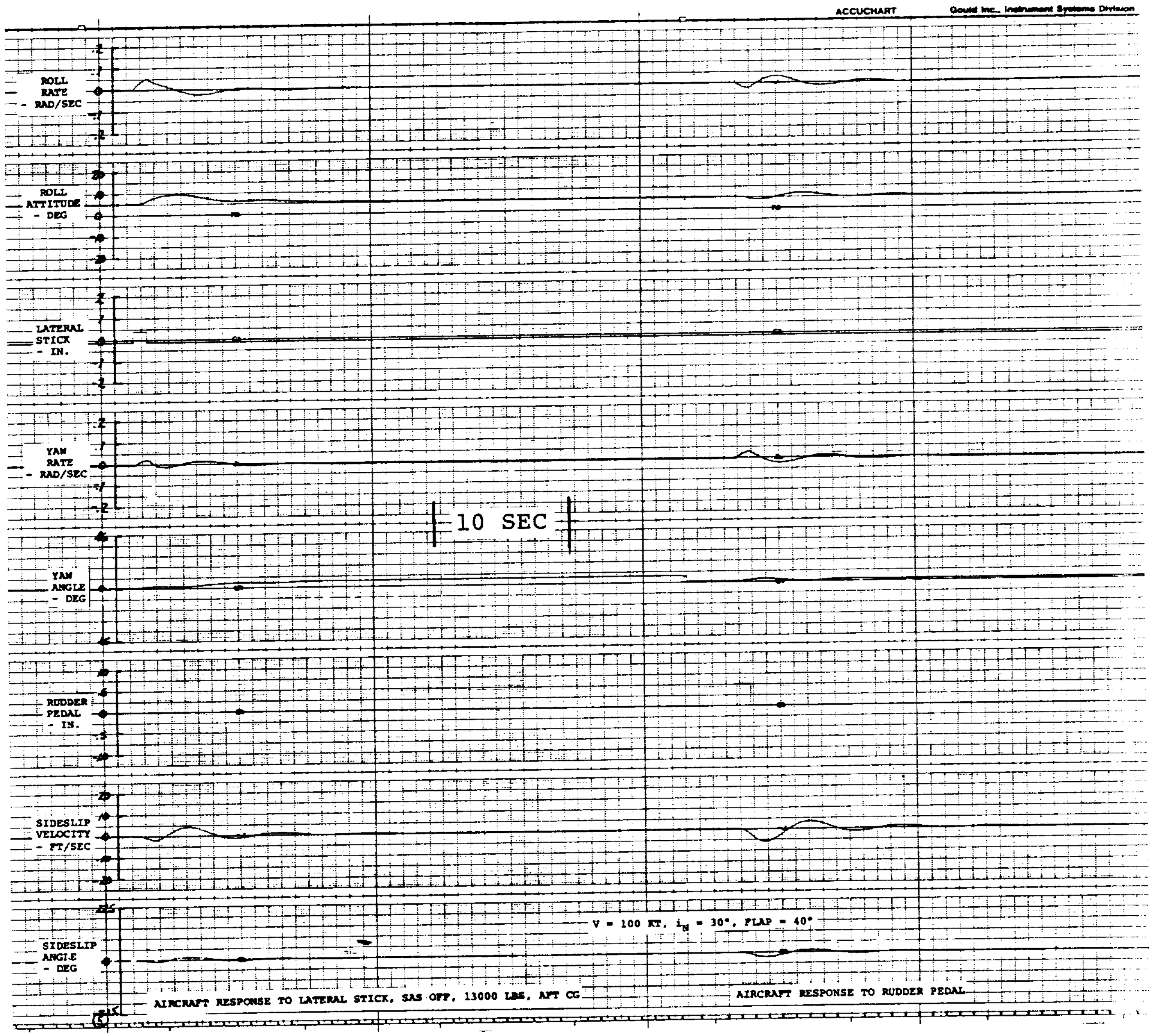

ACCUCHART
Gould Inc., Instrument Systems Division
ROLL RATE - RAD/SEC
ROLL ATTITUDE - DEG
LATERAL STICK - IN.
YAW RATE - RAD/SEC
10 SEC
YAW ANGLE - DEG
RUDDER PEDAL - IN.
SIDESLIP VELOCITY - FT/SEC
SIDESLIP ANGLE - DEG
V = 100 KT, i_N = 30°, FLAP = 40°
AIRCRAFT RESPONSE TO LATERAL STICK, SAS OFF, 13000 LBS, AFT CG
AIRCRAFT RESPONSE TO RUDDER PEDAL

FIGURE 12.21

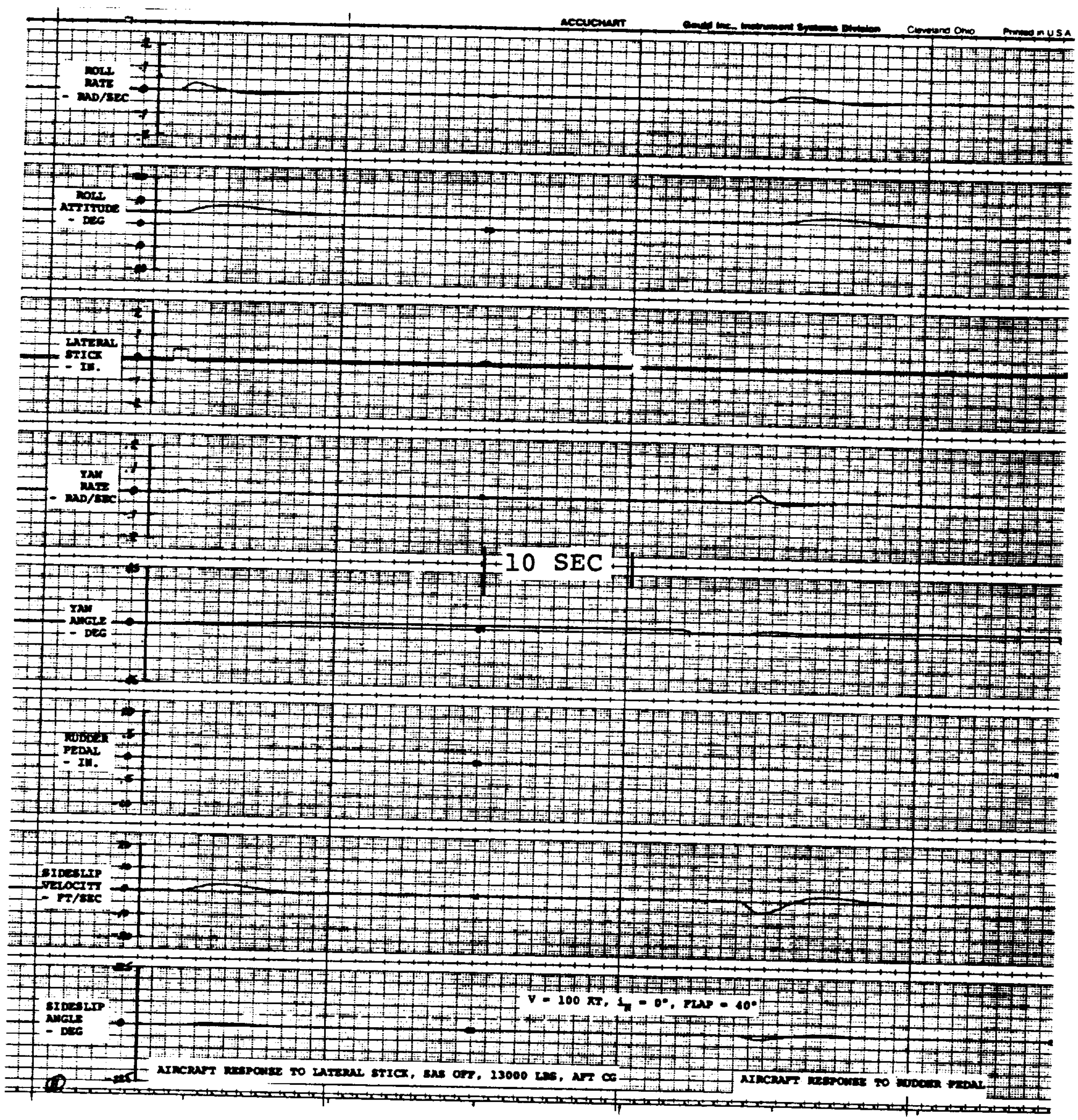
ACCUCHART
Gould Inc., Instrument Systems Division
Cleveland Ohio
Printed in U.S.A.
ROLL RATE - RAD/SEC
ROLL ATTITUDE - DEG
LATERAL STICK - IN.
YAW RATE - RAD/SEC
10 SEC
YAW ANGLE - DEG
RUDDER PEDAL - IN.
SIDESLIP VELOCITY - FT/SEC
SIDESLIP ANGLE - DEG
V = 100 KT, i_H = 0°, FLAP = 40°
AIRCRAFT RESPONSE TO LATERAL STICK, SAS OFF, 13000 LBS, AFT CG
AIRCRAFT RESPONSE TO RUDDER PEDAL

FIGURE 12.22

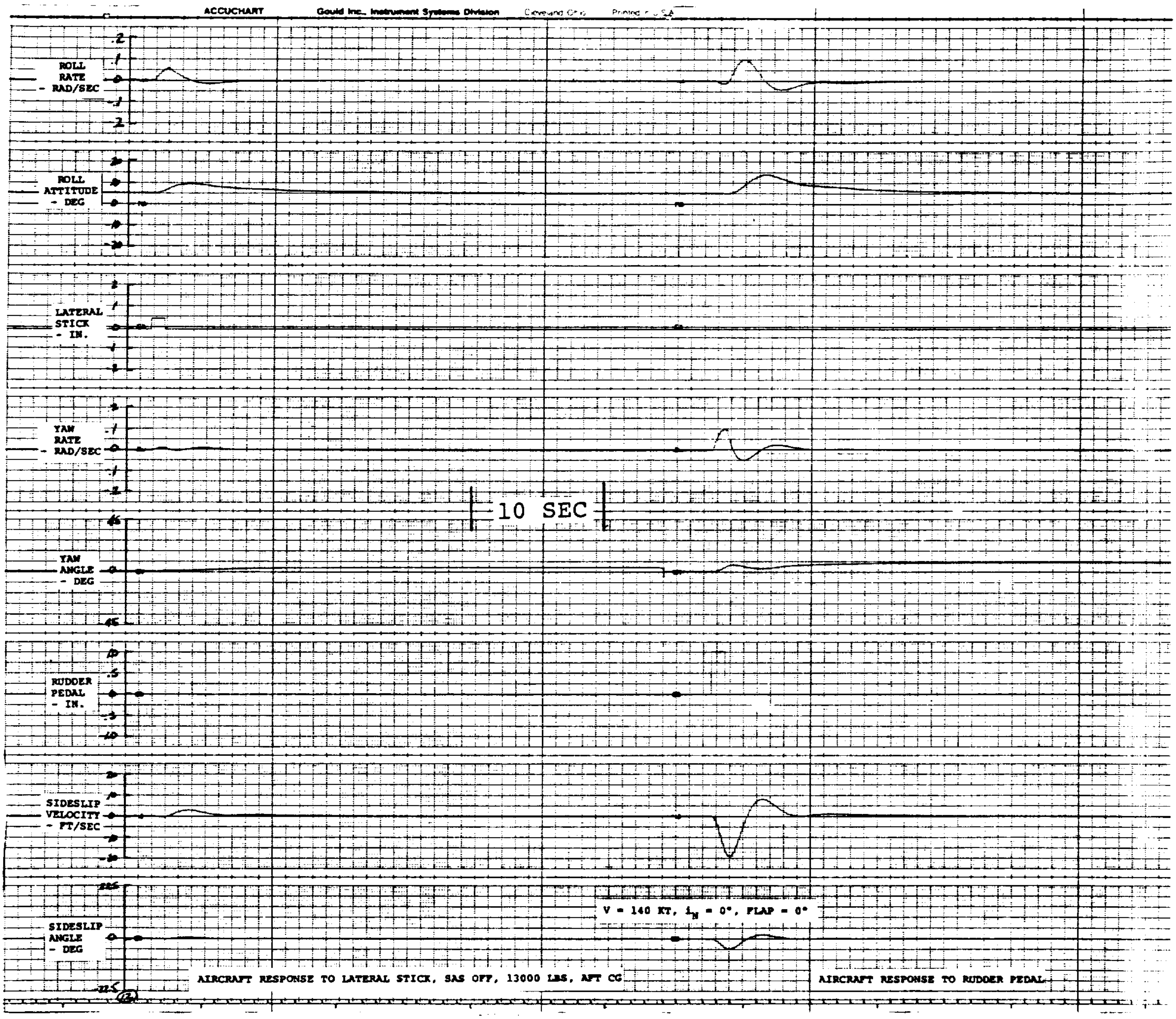

ACCUCHART
Gould Inc., Instrument Systems Division
ROLL RATE - RAD/SEC
ROLL ATTITUDE - DEG
LATERAL STICK - IN.
YAW RATE - RAD/SEC
10 SEC
YAW ANGLE - DEG
RUDDER PEDAL - IN.
SIDESLIP VELOCITY - FT/SEC
SIDESLIP ANGLE - DEG
V = 140 KT, i_N = 0°, FLAP = 0°
AIRCRAFT RESPONSE TO LATERAL STICK, SAS OFF, 13000 LBS, AFT CG
AIRCRAFT RESPONSE TO RUDDER PEDAL

FIGURE 12.23

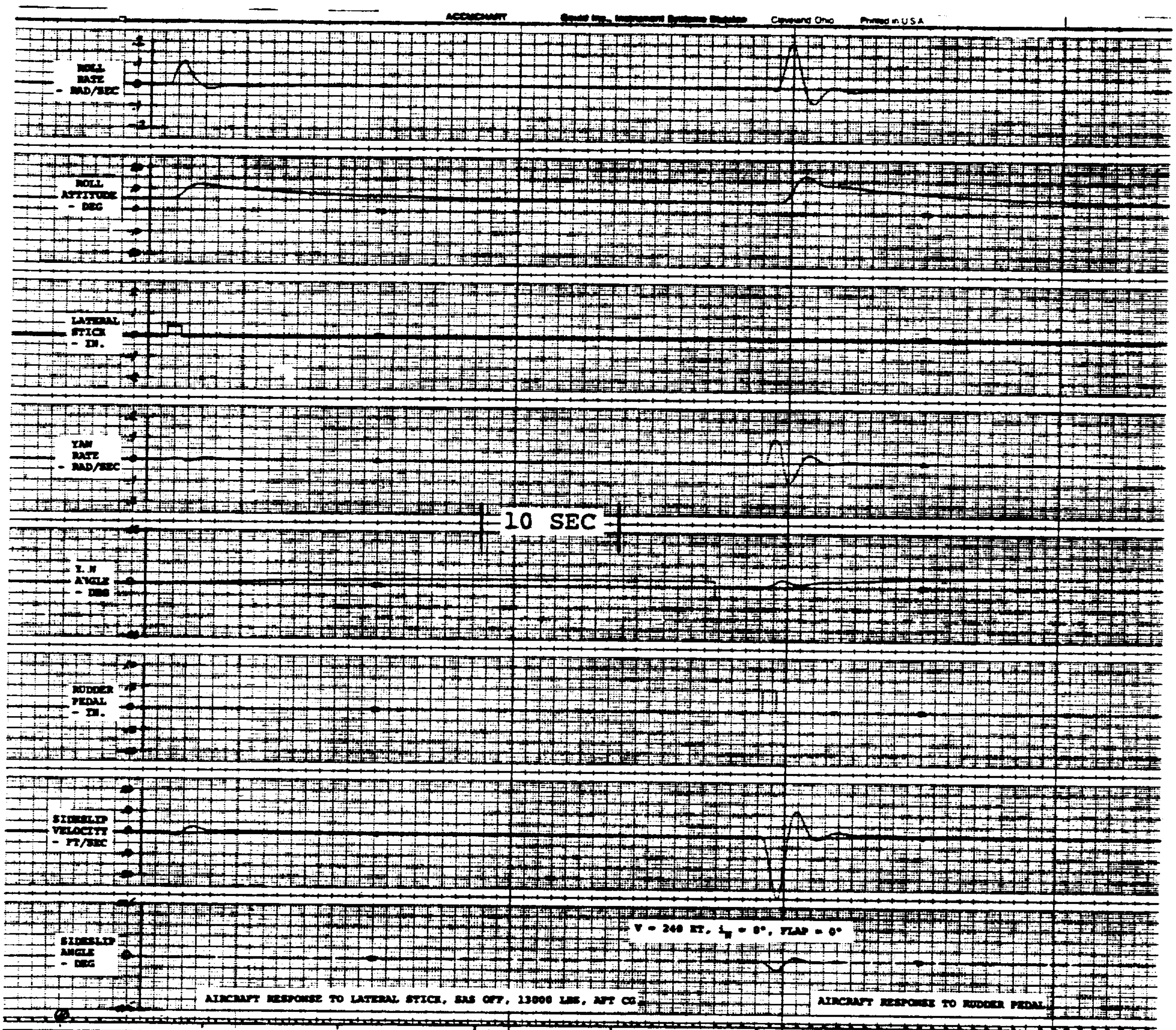
ROLL RATE - RAD/SEC
ROLL ATTITUDE - DEG
LATERAL STICK - IN.
YAW RATE - RAD/SEC
10 SEC
YAW ANGLE - DEG
RUDDER PEDAL - IN.
SIDESLIP VELOCITY - FT/SEC
SIDESLIP ANGLE - DEG
V = 240 KT, i_H = 0°, FLAP = 0°
AIRCRAFT RESPONSE TO LATERAL STICK, SAS OFF, 13000 LBS, AFT CG
AIRCRAFT RESPONSE TO RUDDER PEDAL

FIGURE 12.24

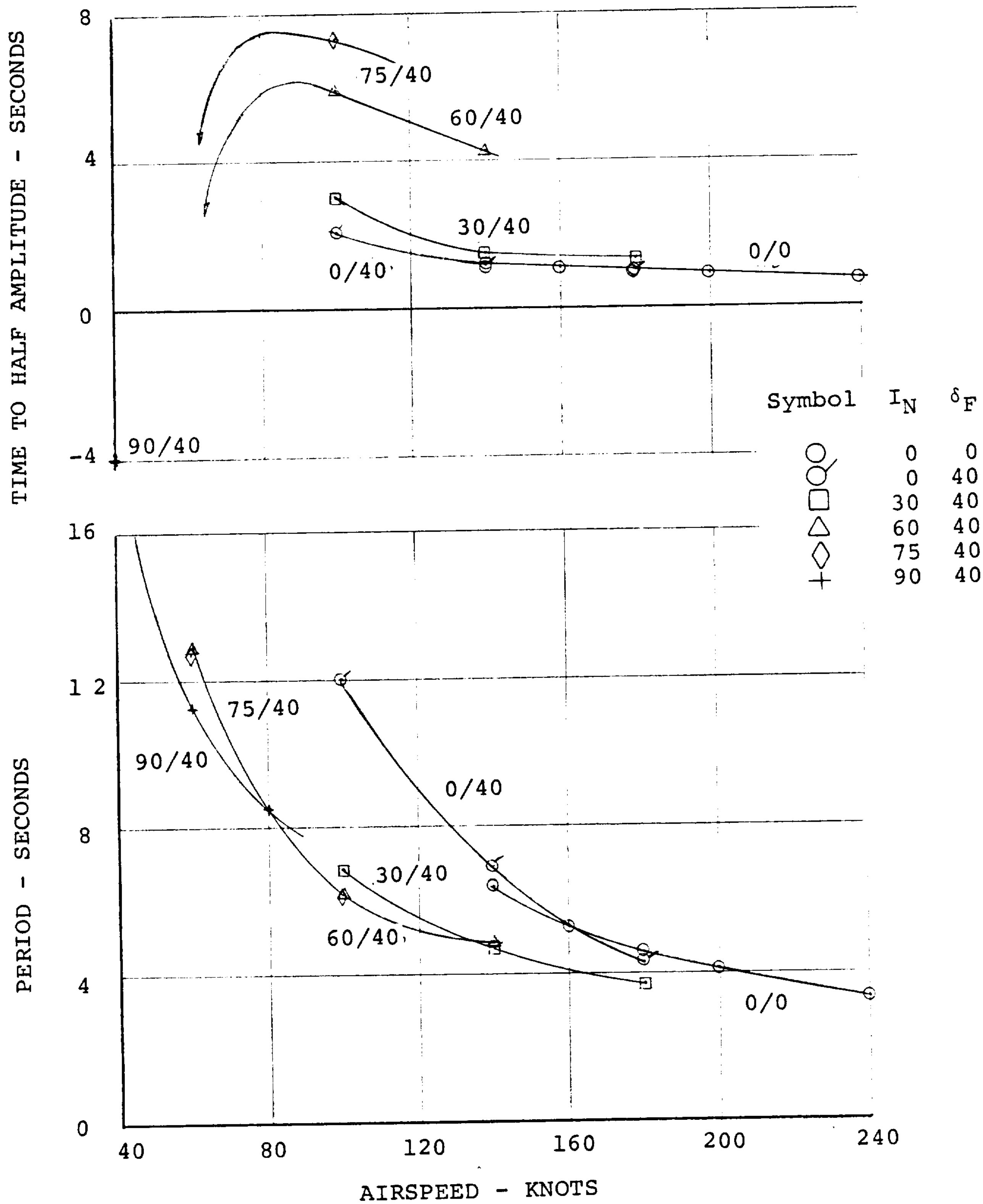

FIGURE 12.25. DUTCH ROLL, CHARACTERISTICS, SAS-OFF, AFT CG, SEA LEVEL STANDARD

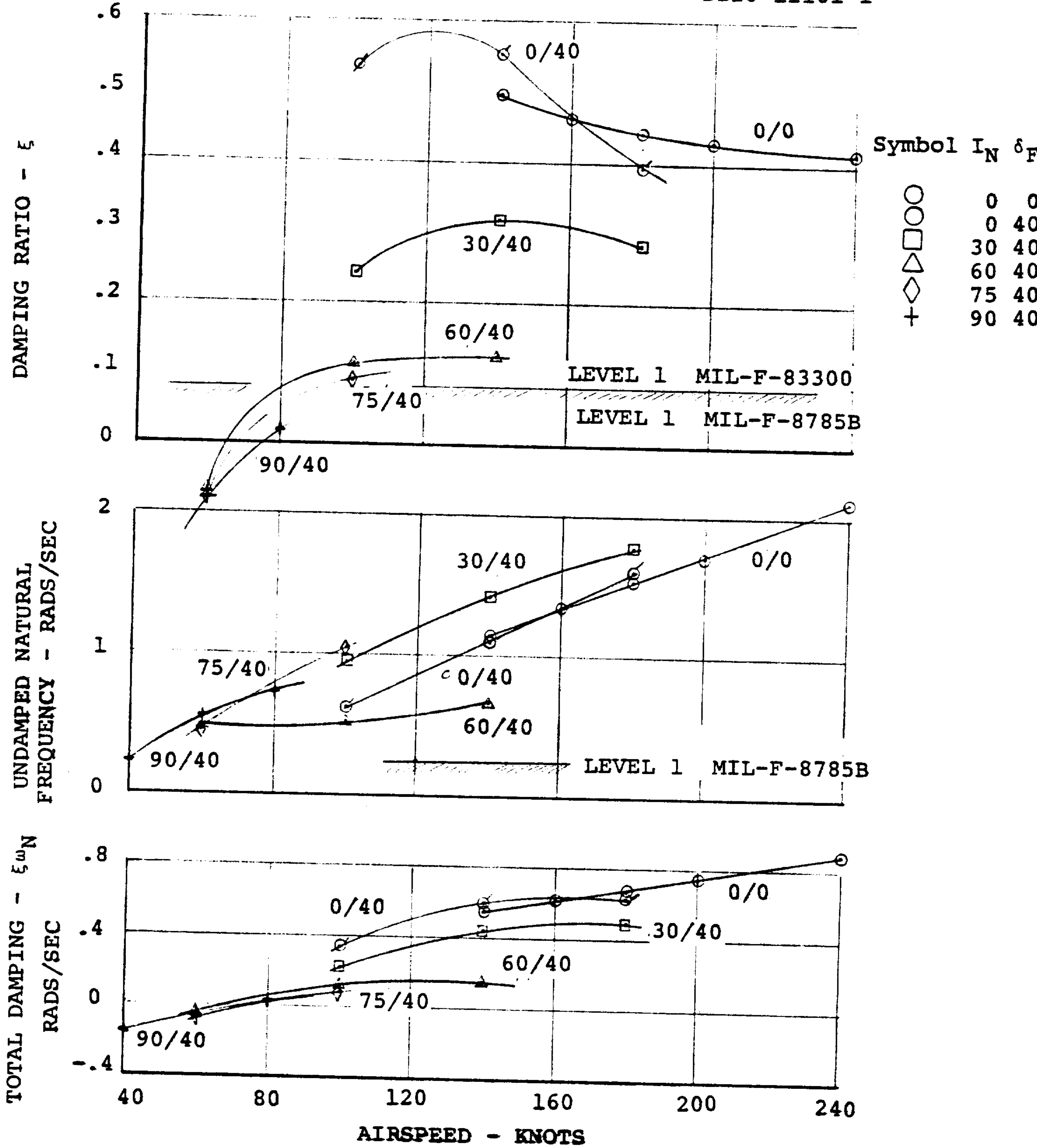

FIGURE 12.26. DUTCH ROLL CHARACTERISTICS, SAS-OFF, AFT CG, GOVERNOR ON, SEA LEVEL

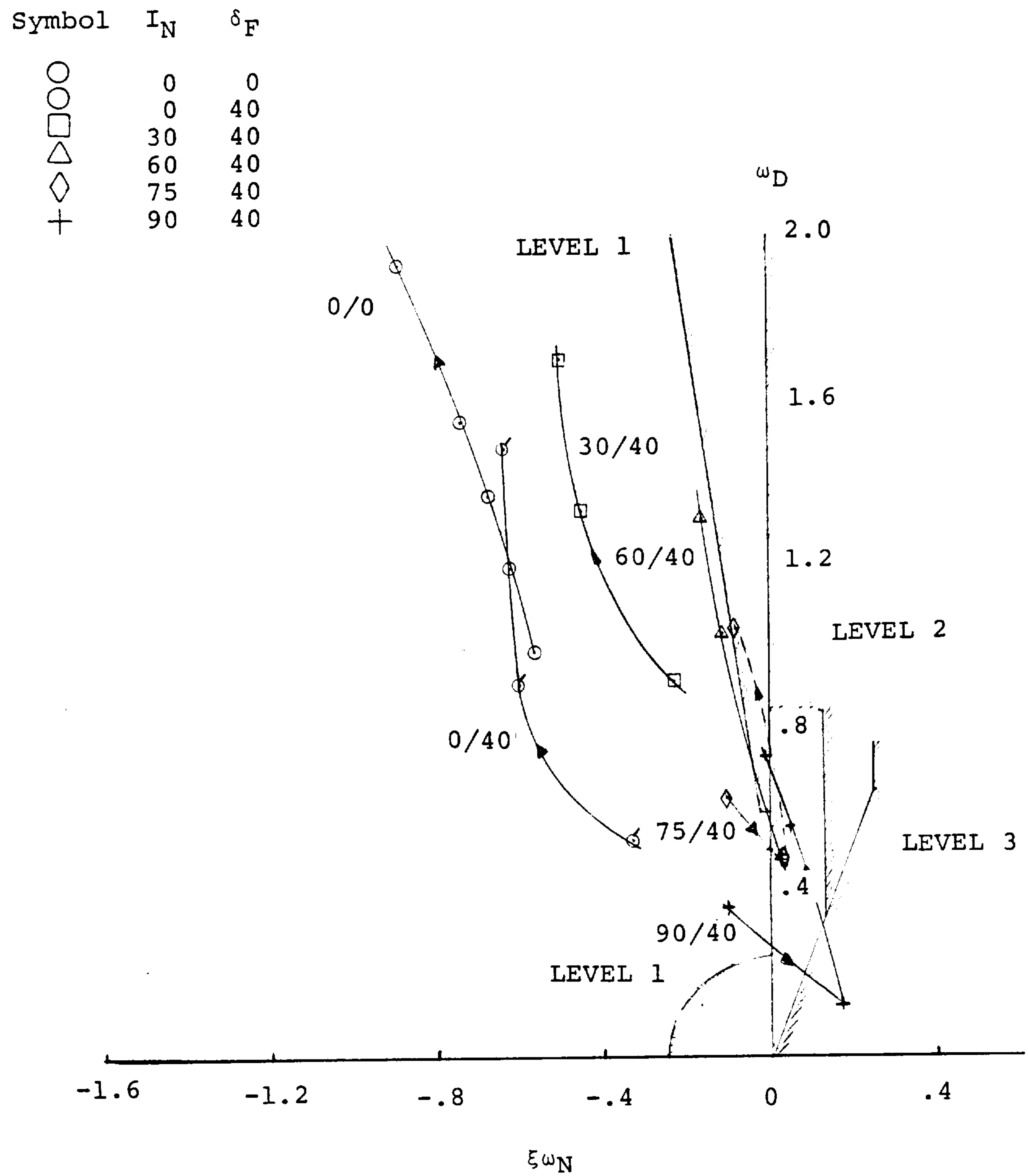

FIGURE 12.27. SUMMARY - DUTCH ROLL CHARACTERISTICS VS REQUIREMENTS OF MIL-F-83300, SAS-OFF

13.0 PILOTED SIMULATION

13.0 PILOTED SIMULATION

This section presents the results of the real-time piloted simulation conducted to evaluate the handling qualities of the Advanced Hingeless Rotor XV-15 Aircraft. The mathematical model of the airframe that was used to drive the simulator is as described in the body of this report except that the cyclic schedules used to control rotor loads were not available for incorporation in time for the simulation.

The effect of cyclic on the stick on the aircraft flying qualities and handling will require careful evaluation during subsequent studies.

The mathematical model of the rotor forces and moments was that detailed in Section 5.0. As pointed out in that section, rotor performance at lower power settings and in autorotation is obtained essentially by mathematical extrapolation, since the rotor has not yet been tested in these ranges of operation. Therefore, aircraft performance and pilot comments on low power descents and autorotation should be weighed accordingly. Approximately 15 hours was spent in actual piloted evaluation with about 40 hours tie-in time used to debug the system and make changes in response to pilot comments.

13.1 Simulator Description

The Boeing Vertol simulation facility consists of a 6 degree-of-freedom, small-motion pilot cabin driven by signals from a Xerox Σ9 digital computing system. The pilot's cabin is equipped with an adaptable instrument panel, a variable flight control force-feel system, and an out-of-the-window visual display. The visual display is generated by a black-and-white television camera moving over a terrain model. The image is viewed by the pilot through a large collimating lens providing a field of view measuring 38 degrees vertically by 53 degrees azimuthally with 0 degrees depression angle.

The limited-motion, 6 degrees-of-freedom pilot's cabin has the following performance:

Motion System Performance

Payload (including pilot)	770 Lbs

Travel Limits (stop-to-stop total):

Vertical Longitudinal Lateral	12.7 cm (5 in.)

Pitch	13 deg.
Roll	19 deg.
Yaw	19 deg.
Pitch Tilt	26 deg.

Rate Limits with Zero Acceleration:

Vertical	±0.66m/s (±26 in./sec.)
Longitudinal	±1.04m/s (±41 in./sec.)
Lateral	±0.66m/s (±26 in./sec.)
Pitch	±69 deg./sec.
Roll	±97 deg./sec.
Yaw	±155 deg./sec.

Acceleration Limits for Zero Rates (incremental values):

Vertical	19.63m/s^2 (±64.4 ft./sec.^{2})
Longitudinal	10.79m/s^2 (±35.4 ft./sec.^{2})
Lateral	8.81m/s^2 (±28.9 ft./sec.^{2})
Pitch	±248 deg./sec.^{2}
Roll	±414 deg./sec.^{2}
Yaw	±745 deg./sec.^{2}

13.2 Configuration of Pilot's Cabin

The cabin of the simulator was configured to represent approximately the layout of the NASA-Army XV-15 aircraft instrument panel and controls. Because the simulator was also being used to evaluate current Company helicopter designs, some compromises had to be made in instrument placement so as to minimize configuration changes when switching back and forth between aircraft models.

13.2.1 Instruments and Controls

Instruments and primary controls were positioned in the single-seat cabin such that the pilot flew as if from the right seat. Figure 13-1 shows the instrument panel layout used throughout the simulation and Table 13.1 details the instruments and ranges. The pilot's force-feel system was programmed to deliver breakout forces and gradients according to the current XV-15 force-feel system shown in Figure 13.2.

The control stick in the simulator was mechanically limited to ±4.8" longitudinally and laterally, and the pedals to ±2.5". A beep force-trim hat switch was mounted on the stick enabling the pilot to zero out stick forces and to make small trim adjustments to the aircraft. Initially a constant beep trim rate of 1/2 degree per second was used. Later in the program beep rate was washed out as a function of dynamic pressure according to the equation

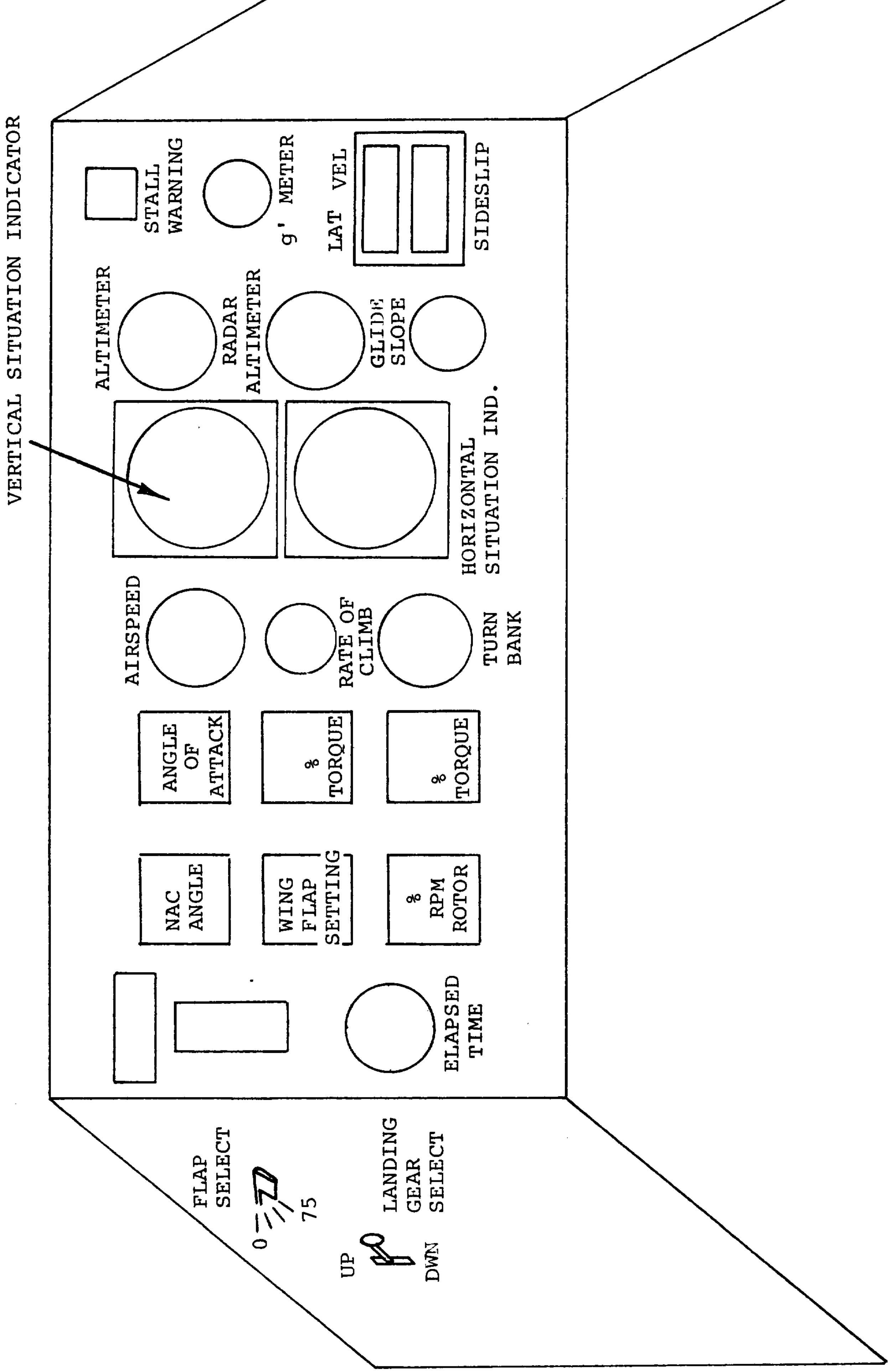

FIGURE 13.1. INSTRUMENT PANEL LAYOUT

CAB INSTRUMENTATION

Instrument	Range
Vertical Situation Indicator	±90° Pitch and Roll
Horizontal Situation Indicator	±120° Heading
Airspeed	0 → 520 KIAS
Pressure Altimeter	0 → 10,000 Ft
Radar Altimeter	0 → 1,000 Ft
Rate of Climb	± 6,000 Ft/Min
Turn and Bank	± Needle Widths
	±1-1/2 Ball Widths
'g' Meter	-1, +3 'g'
Nacelle Angle	0 → 120°
Clock	
Sideward Velocity	±40 Knots
Angle of Attack	±20°
Wing Flap Position	0 → 100°
Rotor Speed	0 → 125%
Engine Torque Meters (2)	0 → 125%

PRIMARY FLIGHT CONTROLS

Stick (±4.8" Longitudinal and Lateral)
Pedals (±2.5")
Power Lever (0 → 8" Normal; 0 → 10" Emergency)
Nacelle Position Thumb Switch on Power Lever

MISCELLANEOUS EQUIPMENT AND FEATURES

Back Drives to Trim Stick and Pedals while in Initial Condition (I.C.)
Landing Gear Up - Down Switch with Indicator Light
Flap Select Lever 0°, 20°, 40°, 75°
Detent Switches on Spring Cartridges (Pedals & Lateral Stick)
Magnetic Brake on Pedals, Longitudinal and Lateral Controls
Longitudinal and Lateral Beep Force Trim on Stick
Power Lever Null Meter
Toe Brakes
Specified Force Feel System

TABLE 13.1. HRXV-15 PILOT STATION FEATURE SUMMARY

$$\text{beep trim rate} = 0.5 - .00131\ q_F \text{ inches/second}$$

A magnetic brake, operated by a button on the stick, was used to zero stick and pedal forces simultaneously. This was used mostly in hover and low speeds since at higher speeds an objectionable stick 'jump' was experienced by the pilot. Detents on the lateral stick and pedals were set to ± 0.05 inches.

The HRXV-15 uses a single throttle lever, side-arm controller style, to command the power of both engines and to provide collective pitch lead in hover and transition with rotor speed controlled by the governor. Rotor rpm is scheduled with nacelle angle. A proportional thumb switch,loaded-to-center, with detent, breakout and gradient was mounted on the hand grip and controlled nacelle tilt angle. Figure 13.3 shows the power lever mounted beside the left arm rest of the pilot's seat. The power lever has a normal travel of 8-inches encompassing the range of engine powers from flight idle to maximum. For single or dual engine features, direct pilot control of rotor collective pitch is obtained by moving the lever through a detent set at the 8-inch travel point. Once through the detent, the rotor governor is switched off and an additional 2-inches of travel is available with the power lever acting as a collective lever.

A flap lever and a landing gear up-down select lever were mounted on the left sidewall of the simulator cabin. The flap lever commanded flap settings of 0, 20, 40 and 75 degrees only. Flap extend/retract rate was fixed at 5 degrees per second. A 4 second cycle time on the landing gear switch was used.

A stall warning light was mounted on the right side of the instrument panel but failed to function during the test period. Approach to stall was monitored by the pilot using the angle of attack indicator.

13.3 Piloted Evaluation

During the simulator evaluation period much time was spent in correcting errors in the visual display and in trouble-shooting computer/simulator interface problems. Some of these problems were solved, but many persisted throughout the period. Nevertheless, about 15 hours of productive pilot flying was logged, sufficient to provide a basis for a preliminary evaluation of the Hingeless Rotor XV-15.

The problems that persisted during the evaluation were associated with the motion base and the visual display. The visual display was the subject of frequent comments by the pilot concerning poor resolution, field of view and brightness.

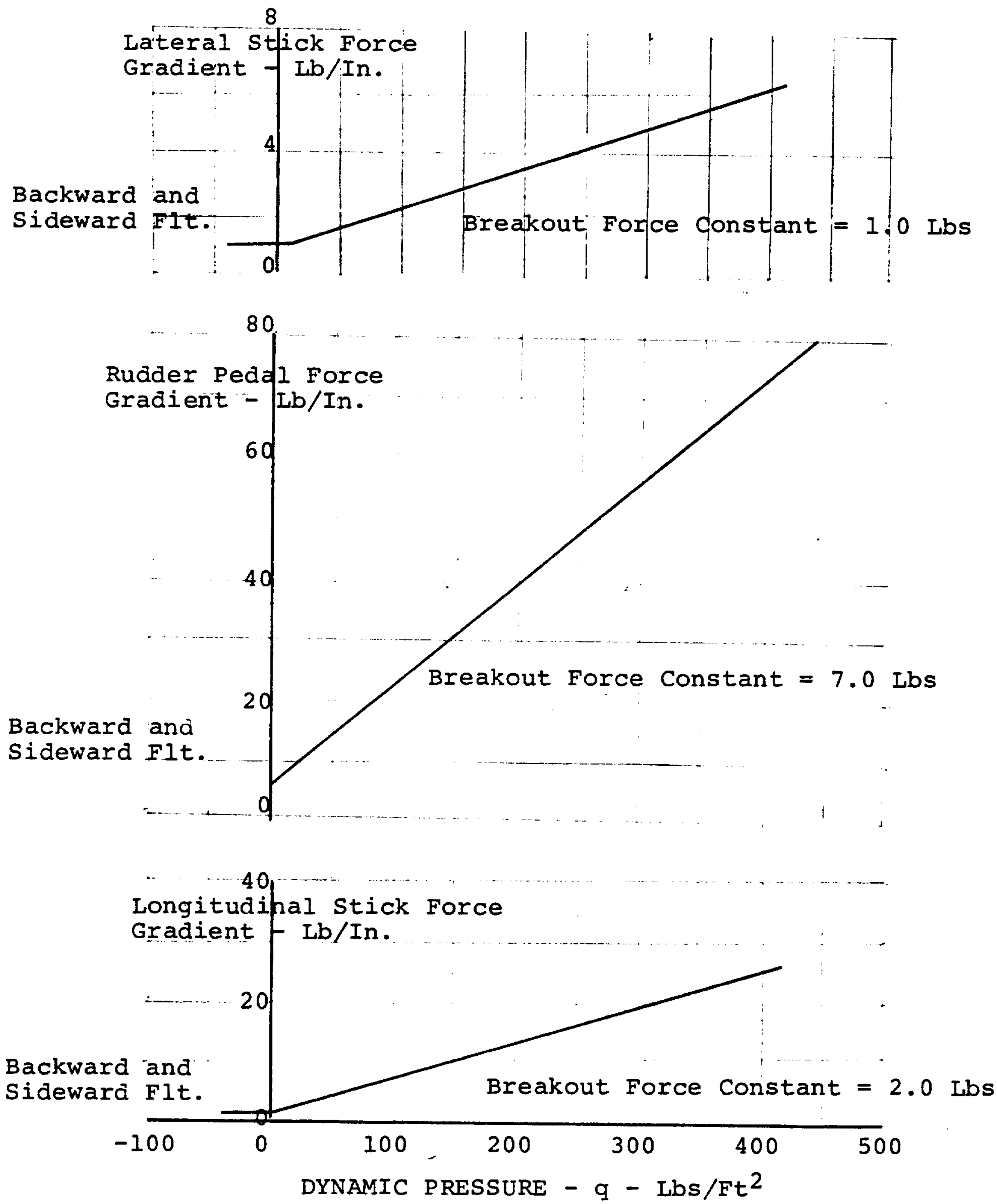

FIGURE 13.2. CONTROL FORCE GRADIENTS AND BREAKOUT FORCES

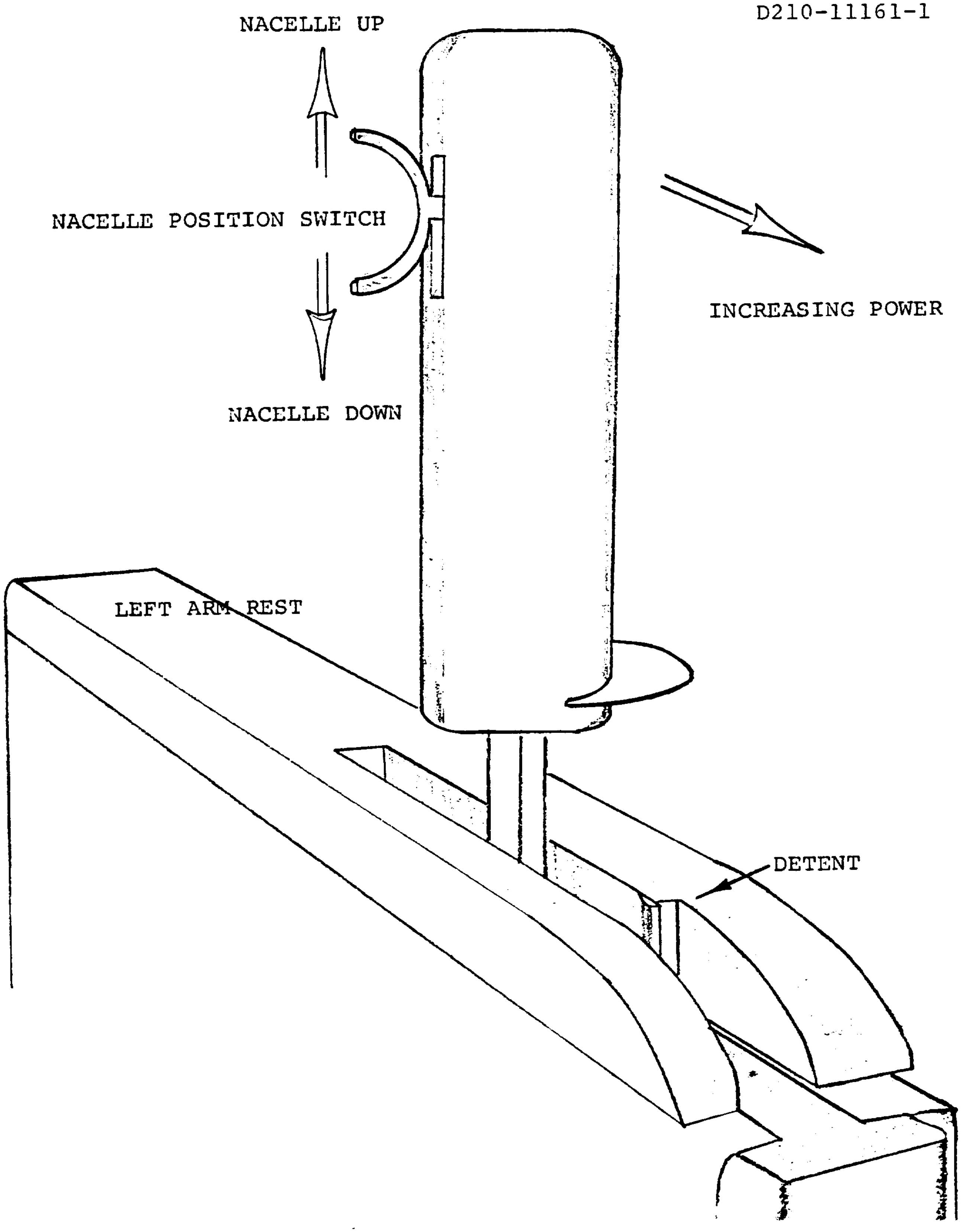

FIGURE 13.3. POWER LEVER/COLLECTIVE CONTROL FOR HRXV-15 SIMULATION

Some degree of improvement in brightness-of-scene was achieved by repositioning the terrain illumination and by altering the television camera brightness/contrast contacts. Image resolution was found to be especially poor when flying in the hover mode near the ground and this contributed to increased pilot workload in precision hover and low speed maneuvers close to the ground. The limitations on field of view, especially the down and side views, resulted in a degradation in the quality of visual cues available during turns and in sidewards flight.

The motion base realism was criticized by the pilot throughout the evaluation period. He complained of abrupt washout and recentering motions especially at low airspeed. At higher airspeeds, noise on the pitch and roll acceleration channels produced an annoying small amplitude, rapid pitching/rolling sensation. Attempts were made to filter out the noise with limited success.

Prior to the forthcoming evaluation by a NASA pilot it is hoped to be able to adjust the simulator motion base to the pilot's satisfaction.

13.3.1 Pilot's Report and Engineering Comments

Presented below is the pilot's preliminary evaluation of the aircraft, followed by Engineering comments, which are keyed to pilot remarks by the numbers in the righthand margin.

Pilot's Report

During the period October 2 through October 29, 1976, approximately 15 "flight" hours, in 6 sessions, were spent in qualitative evaluation of the XV-15 simulation. Detailed comments are presented below. It should be noted that evaluation results of dynamic maneuvers would probably be tempered in real world by stress/structural limitations which were not presented or displayed to the pilot.

The pilot did not use standard pilot ratings, since there was no baseline of simulation fidelity to measure against. Ideally, for a program of this type where the simulated aircraft is a "paper" aircraft, prior to the evaluation the pilot should fly a simulated aircraft in which he has actual flight experience to establish a simulation baseline. It is recommended for the forthcoming NASA pilot evaluation, a CH-47 simulation be available for his assessment. 1

Prior to the NASA evaluation, some work needs to be done on the Boeing Vertol simulator to optimize visual and motion cues and improve cockpit displays and functions. Specific shortcomings are:

- Visual Display - Poor resolution and brightness, inadequate field of view. The Cab Fresnel lens apparently degrades picture quality, since the monitor picture is more distinct than the cockpit display. A second window would improve field of view; the present field inhibits maneuvering, particularly in pitch up maneuvers at low altitude when visual reference is lost and pilot must revert to cockpit instruments to maintain adequate control. The ultimate objective should be a 2-3 window color picture, since strong visual cueing is mandatory with a limited or "nudge" motion base. 2

- Motion Base - Primary complaints were acceleration washout and recentering time constants appeared too short. Response to pulse control inputs was too abrupt and unreal. Lateral or roll cues for low speed side force conditions appeared to be exaggerated and tended to be disorienting. Spuriour jolts and jostles unrelated to aircraft happenings occurred, evidently due to "noise". These were disconcerting and annoying, but not disorienting. If the above recommended CH-47 simulation is mechanized for the NASA pilot, the motion settings can be optimized by a Boeing Vertol pilot during this simulation checkout phase. 3

- Cockpit Display - Power lever/nacelle beep switch configuration should be changed to approximate the Bell/NASA simulator configuration. Present nacelle switch is thumb operated up and down. It is felt that a fore-aft switch operation would be more acceptable human factors-wise. 4

  Much difficulty was experienced trying to establish and maintain vertical speed velocity trim conditions due to apparently oversensitive vertical speed indications. The instrument displays simulated instantaneous vertical speed, and some attempt was made to filter the signal. However, the optimum balance between good sensitivity and excessive lag was not achieved. 5

  Lateral velocity and sideslip angle indicators should be relocated closer to the primary scan area and have better illumination. 6

  If the NASA evaluation math model should include stress parameters, some form of cockpit indication related to stress limits, like the C.G.I., should be installed. Also, a stall warning light should be provided. 7

Flying Qualities Evaluation (Pilot's Comments)

Introduction

Approximately 15 simulation hours were flown to evaluate flying qualities of the Hingeless Rotor XV-15 Tilt Rotor Aircraft throughout its normal flight spectrum. Cooper-Harper pilot ratings were not used because the pilot did not have an opportunity to fly a simulated actual aircraft to establish a simulator fidelity baseline.

Test Conditions

The initial flight period was devoted to pilot familiarization of the aircraft and simulator. The subsequent evaluation included hover and low speed maneuvering and forward flight to 80 KIAS in the helicopter mode (90° nacelle angle), forward flight characteristics at various intermediate nacelle angles; conversions at normal and max nacelle rates; power on and off wing stalls clean and with landing gear and flaps extended; single engine failures at cruise in the airplane mode and from hover, IGE and OGE, in the helicopter mode; helicopter mode autorotations; optimum airspeed approaches at 90° and 75° nacelle angles. Most conditions were evaluated SAS on and off and at most forward and aft center of gravity locations. Helicopter approaches to hover in 15 knot crosswind, helicopter and airplane cruise in turbulence were performed.

Test Results

Helicopter Mode (Hover and Low Speed Maneuvering). Configuration - 90° nacelle angle, 40° flap angle, landing gear down.

Response to pitch, roll and yaw pulses, SAS on, was good with
dead beat return to trim in pitch and roll attitude and yaw
rate. Initial pitch response appeared to have approximately 8
.25 second lag, noticeable but not objectionable. SAS off,
pitch appeared statically stable, dynamically unstable; roll
and yaw statically stable. Precision maneuvering laterally,
longitudinally and vertically was difficult, requiring excessive
pilot workload. However, considering that response character-
istics were comparable to contemporary helicopters, this was
attributed to weak visual and motion cues.

Acceleration from hover to 80 KIAS was sluggish, requiring an initial uncomfortable (up to 15°) nose down attitude with a trim attitude of 10° nose down required at 80 knots. Decelerations also appeared sluggish but were affected by pilot inhibition to steep flare attitudes, since with the limited visual field of view, flares much in excess of 10° nose up lost visual ground reference.

Low speed turns, 40 to 80 Kts, were acceptable, with reasonably good coordination (1/4 ball or less).

Transitions (0° - 90° - 0° Nacelle Angles)

Normal rate transitions were accomplished SAS on and off with no problem except maintaining zero R/C in pitch. Again, it 9
felt that stronger cues would have greatly diminished pilot workload. Maximum rate transitions (90° in 7 seconds), SAS on and off, were controllable with considerable pilot effort. With so many parameters to monitor and control (flight path, torque, nacelle and flap angles, angle of attack) this maneuver is not recommended for normal operations and should be reserved for emergency situations with adequate altitude.

STOL Mode (45° to 75° Nacelle Angles)

Level flight and turns were acceptable. During 75° approach at 80 kts, power was reduced to establish a 1,000 ft/min descent rate and control was lost thru rotor rpm decay caused by an exceedance of the governor limits. This was corrected by
a governor change. 10

Airplane Mode - SAS On

Good attitude stability and maneuver response. Some difficulty was experienced in maintaining zero vertical speed in trimmed level flight. This may have been poor simulation display, but regardless, an altitude hold capability in pitch would be a desirable feature. Roll attitude hold about any bank angle, comparable to YUH-61A and CH-147, is possibly a questionable characteristic for a fixed wing airplane. This provides neutral spiral stability, where possibly positive stability would be more desirable. Yaw steps produced pure sideslip with zero bank angle; roll
attitude hold results in no apparent dihedral effect. 11

This is not necessarily undesirable but is abnormal for an airplane. Turns to 45°, pedal fixed, were well coordinated and rolling pullouts ±45° bank angle with 3g were performed with no problem.

Airplane Mode - SAS Off

Response to pitch, roll and yaw pulses was satisfactory with slow return toward initial trim. Turn coordination, pedals fixed, was somewhat degraded (less than 1/4 ball slip) and more pilot effort in pitch was required to maintain zero R/C than SAS on.

Stalls

Power on and off, clean and gear and flaps down were docile and easily recoverable. Stalls were evidenced by angle of attack and sink rate indications, with some nose drop tendency but no roll off. Recovery was effected by releasing back pressure and allowing airspeed to increase by diving and/or power application. No stalls were performed from steep banked turns.

Turbulence

No problems experienced SAS-on, other than an increase in pilot workload to maintain zero R/C. SAS-off pilot workload increased to degree where IFR capability would be marginal if mission tasks over and above flight path
control were greater than moderate. 12

Single Engine Failures

Helicopter mode - IGE. Single engine power cuts from a 20
foot hover were performed. Remaining engine increased to maxi- 13
mum torque and aircraft settled to the ground, with reasonable ground contact. Prior to attempting failures from an O.G.E. hover, minimum single engine level flight speed was determined to be 20 KIAS. O.G.E. engine cuts were initialed from 800 feet, pilot reaction delayed one second, and aircraft pitched over to achieve 20 Kts, with a height loss of 100 feet (repeatable). This indicates a height velocity diagram of 20 - 200 with the nose at 20 Kts would probably be conservative.

Airplane Mode

No noticeable effect other than a light longitudinal deceleration.

Dual Engine Failures

Helicopter Mode

Initialed from 70 Kts by retarding power lever to minimum at a moderate rate. The first attempt resulted in an unrecoverable pitch down. Subsequent attempts were con-
trollable but resulted in an indicated 5,000 feet/minute 14
autorotative rate of descent. No attempt was made to flare to a landing. This power off condition requires considerable investigation to determine if it is possible to land either in the helicopter, STOL or airplane configuration. It should be noted that in the airplane mode, without pilot control of rotor pitch (feathering), windmill braking effect of these large rotors would result in

excessive rates of descent. The alternative to a satisfactory power off landing capability is crew ejection.

Airplane Mode

Throttle cuts from level flight cruise resulted in no aircraft response other than a rapid longitudinal deceleration.

General

Controls

Pitch, roll and yaw controls are conventional and common to both helicopters and fixed wing aircraft. The power lever motion is fore and aft like an airplane throttle and compromises standard helicopter thrust control orientation, with the exception of the forward cockpit side arm thrust control in the Bell AH-1G Cobra. No problems were encountered using this control in the helicopter mode. Although sensitivity per unit displacement is greater than a conventional thrust lever, the side arm location allows wrist action control of minor power changes permitting precise pilot control of the vertical axis.

Vernier beep trim is provided on the stick for pitch and roll force and attitude trim adjustments, while a mag brake button on the stick allows instantaneous force retrimming in pitch, roll and yaw. It was found that if pitch and roll trim rates were optimized for good force and attitude trimming in hover, the rates were too fast for vernier attitude trimming in airplane forward flight, and vice versa. If some compromise rate cannot be established, it is possible the trim rate may have to be variable with q. 15

Nacelle Angle Control is provided by a power lever mounted, thumb operated, variable rate switch. The motion axis is up and down, functionally related to nacelle movement. It is felt that this switch orientation should be related to resultant aircraft response, which is acceleration-deceleration, and should therefore be actuated fore and aft. This is the orientation in the NASA Bell XV-15 simulator, which would be more familiar to a NASA evaluation pilot. 16

Conclusions and Recommendations

1. Except for the helicopter autorotative and airplane power-off landing problems noted above, overall flying qualities, SAS on and off, are considered acceptable throughout the flight envelope.

2. Some real world limitations may be imposed by stress/ structural considerations not mechanized in this simulation.

3. It is recommended that for any follow-on evaluation of this aircraft simulation, the pilot should be provided a simulated known aircraft to establish a baseline of simulation fidelity.

4. Improvement of cockpit controls and instrument panel displays is highly desirable.

5. Optimization of simulator visual and motion cues is mandatory.

Engineering Comments

A CH-47 simulation will be made available for NASA pilot baseline familiarization. 1

The visual display system will be reviewed and attempts made 2
to improve resolution and brightness. It is unlikely, however, that much can be done to extend the field of view since this is governed by the existing television camera arrangement and cockpit display system. Work is in process to build an improved simulation visual system that will provide forward, sidewards and downwards vision. Unfortunately this work will not be completed until mid 1977.

It is planned to try to adjust the motion base, using a Boeing 3
Vertol pilot, prior to evaluation by the Ames pilot.

The existing up-down nacelle switch will be repositioned on 4
the throttle lever to operate in the fore-and-aft directions. This will involve some reworking of the present throttle lever hardware.

This will be corrected for the upcoming NASA pilot's evalu- 5
ation.

Space considerations on the simulator instrument panel may not 6
permit this, but it will be investigated.

A monitor will be installed to provide the pilot with an indi- 7
cation of blade loads. In addition, an aural warning is being considered. A stall warning light was provided during the simulation, however, it did not function. This will be corrected.

The 1/4 second lag in pitch was subsequently traced to the 8
visual system and has been corrected.

The difficulty experienced by the pilot in maintaining zero 9
rate of climb was due, in part, to the oversensitive rate-of-climb meter as mentioned in Number 5.

The cause of the governor failure was traced to the rotor power 10
versus collective relationship. This is discussed in Section 12.0.

The roll attitude hold feature in cruise flight will be modi- 11
fied such that it is inoperative except during feet-and-hands off level flight.

Turbulence level was set at 5 fps RMS about all axes. 12

The engine dynamic model used in the simulation is that of a 13
single engine. Dual engine performance is simulated by doubling of the single engine model output during each time frame. Engine failures were, therefore, simulated by multiplying the output by a factor which decayed from 2.0 to 1.0 in 3 seconds.

As stated in the introduction to this section, the rotor math 14
model is not yet validated for low power descents or autorotation.

Beep trim rate was reduced as a function of dynamic pressure 15
during the final stages of pilot evaluation and appeared to be acceptable.

The nacelle angle control will be repositioned. 16

14.0 CONCLUSIONS AND RECOMMENDATIONS

14.0 CONCLUSIONS AND RECOMMENDATIONS

A simulator mathematical model of the NASA/Army XV-15 tilt rotor aircraft equipped with a Boeing hingeless rotor system was developed and used to perform preliminary studies of the aircraft's performance, handling qualities, and stability. The following conclusions are drawn:

1. The aircraft has good overall flying qualities, SAS On and SAS Off, throughout the flight envelope. With no stability augmentation, the aircraft is easily controlled with some increase in pilot work load at low airspeeds.

2. Control power and damping are adequate in hover and low-speed transition. At higher transition speeds and in cruise flight, control provides good attitude and maneuver response.

3. A wide speed-maneuver corridor free from structural limitations has been provided throughout transition and cruise regimes. This is the result of careful control parameter scheduling and the use of cyclic-on-the-stick in transition and cruise. Closed-loop load alleviation systems are not required and will not be used.

Recommendations for Future Work

1. Update of Simulation Model

   The mathematical model should be updated to reflect the results of design studies projected under an extension to Contract NAS2-9015 (Hingeless Rotor XV-15 Design Integration Feasibility Study and checks of the critical flight areas repeated as required. In addition, it is recommended that the rotor representation should be upgraded to fully reflect data obtained in wind tunnel tests under Contract NAS2-9015 (Wind Tunnel Test of 1/4.622 Scale Model, NASA-CR 151936-151939).

2. Autorotation

Additional wind tunnel tests and analysis should be performed to determine the performance of the rotor at low power settings and in autorotation. The existing rotor math model does not cover these regions of rotor operation adequately and new data are required to extend the range of validity of the model. While the pilot's comments concerning autorotative landing capability are, no doubt, due in large part to inadequate modelling of this region, nevertheless, this phase of flight operation requires further investigation.

3. Control System Failure Simulation and Evaluations

Specialized modifications to the systems simulation should be made to allow representation of failure modes (e.g., hydraulic pressure loss, hardovers and recovery, etc.).

4. Further Development of Load Alleviation

Development of the cyclic-on-the-stick load reduction feature should be continued and evaluated with the pilot in the loop. This is required as part of the general updating noted in (1).

15.0 REFERENCES

15.0 REFERENCES

1. Harendra, P. B., et al; "Mathematical Model for Real-Time Flight Simulation of the Bell Model 301 Tilt Rotor Research Aircraft"; Bell Helicopter Company Report No. 301-099-001, Revision F.

2. Anon; "V/STOL Tilt Rotor Research Aircraft - Volume 1 and 2", Bell Helicopter Company Report No. 301-199-001.

3. Etkin, Bernard; "Dynamics of Flight", John Wiley and Sons, Inc., 1959.

4. Magee, J. P., and Alexander, H. R.: "Wind Tunnel Tests of a Full-Scale Hingeless Prop/Rotor Designed for the Boeing Model 222 Tilt Rotor Aircraft", NASA CR 114644, September 1973.

5. Heyson, Harry, H., and Katzoff, S.; "Induced Velocities Near a Lifting Rotor with Non-Uniform Disk Loading", NACA Report 1319, December 7, 1956.

6. Smith, M. C.; "University of Maryland Wind Tunnel Test 489, Force, Moment and Downwash Measurements on a Rigid Rotor and Semispan Wing", Boeing Document D8-10062-1, The Boeing Vertol Company.

7. Study of V/STOL Tilt Rotor Research Program, Volume 8, Boeing Document D222-10050-8, March 1973.

APPENDIX A

APPENDIX A - TREATMENT OF WING FLEXIBILITY

As described in Section 10 the large separation which exists between the natural frequencies of vibration of the wing structure and the aircraft rigid body motions, enables the elastic deformations of the wing structure to be calculated on a quasi-static basis.

In the simple treatment presented below, the bending and torsion modes are considered to be uncoupled. The wing is treated as a cantilever with a built-in root end. The wing is free to twist about the elastic axis which is assumed to coincide with the nacelle pivot line. The center of mass of each chordwise strip is also taken to lie on the pivot line. The unloaded wing has neither geometric nor aerodynamic twist.

WING TWIST

Spanwise twisting of the wing takes place under the action of the nacelle aerodynamic and inertial moments, the wing lift distribution, and the spanwise distribution of aerodynamic pitching moment. The nacelle aerodynamic moments consist of rotor hub loads, transferred to the pivot, together with the aerodynamic loads on the nacelle itself. Nacelle inertial moments include the gyroscopic effects of the rotor drive system.

With reference to Figure A.1, M_N is the moment supplied or absorbed by the nacelle tilt actuator. If K_θ is the wing stiffness as seen by the wing tip, then

$$M_N = K_\theta \, \theta_T \tag{A-1}$$

The total moment about the elastic axis due to wing aerodynamics, nacelle loads and engine gyroscopic torque is

$$T = \int_0^{b/2} m \, dy + M_N + M_{gyro} \tag{A-2}$$

The aerodynamic moment about the elastic axis at any station y is given by

$$M = M_{c/4} + \ell x \tag{A-3}$$

where ℓ is the section lift and x is the distance from the quarter chord to the elastic axis. In terms of the section aerodynamic coefficients,

$$m(y) = \frac{1}{2}\rho V^2 c^2 \; C_{m_{c/4}} + \frac{1}{2}\rho V^2 c^2 C_\ell \frac{x}{c} \tag{A-4}$$

The section lift coefficient, C_ℓ, is given by

$$c_\ell = k \frac{dC_\ell}{d\alpha} (\alpha - \alpha_o) \sqrt{1 - \left(\frac{2y}{b}\right)^2}$$

$$= k\ a_o\ (\alpha_R - \varepsilon_p - \alpha_o + \theta_t(y)) \sqrt{1 - \left(\frac{2y}{b}\right)^2} \qquad \text{(A-5)}$$

where α_R is the wing root section angle of attack

ε_p is the rotor induced downwash, assumed constant spanwise

α_o is the section zero-lift angle

θ_t is the structural twist at station y

The factor $k \sqrt{1 - \left(\frac{2y}{b}\right)^2}$ is introduced so that, for the untwisted wing, the lift distribution is elliptical. The value of k is obtained from the rigid wing elliptical loading as

$$k = \frac{4}{\pi} \frac{C_{L_\alpha}}{a_o} \qquad \text{(A-6)}$$

Thus the equation for C_ℓ becomes, with $\alpha_{RIGID} = \alpha_R - \varepsilon_p - \alpha_o$,

$$C_\ell = \frac{4}{\pi} C_{L_\alpha} \left[\alpha_{RIGID} \sqrt{1 - \left(\frac{2y}{b}\right)^2} + \theta_t \sqrt{1 - \left(\frac{2y}{b}\right)^2}\right] \qquad \text{(A-7)}$$

In equation (A-4) we can write, for low angles of attack,

$$C_{m_{c/4}} = C_{m_o} + \frac{dC_{m_{c/4}}}{dC_\ell} C_\ell \qquad \text{(A-8)}$$

and therefore

$$m(y) = \frac{1}{2} \rho V^2 c^2 \left\{ C_{m_o} + \left(\frac{dC_{m_{c/4}}}{dC_\ell} + \frac{x}{c}\right) C_\ell \right\} \qquad \text{(A-9)}$$

The equation for the total wing twisting moment, equation (A-2), can now be written as,

$$T = M_{actuator} + M_{GYRO} + \frac{1}{4} \rho V^2 c^2 C_{m_o} b + \frac{1}{2} \rho V^2 c^2$$

$$\left(\frac{dC_{m_{c/4}}}{dC_\ell} + \frac{x}{c}\right) \int_0^{b/2} C_\ell dy \qquad \text{(A-10)}$$

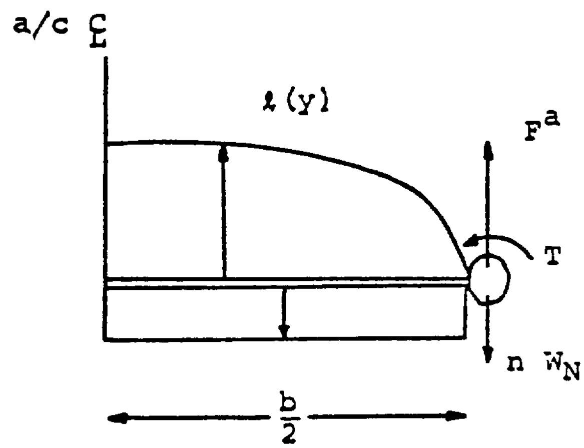

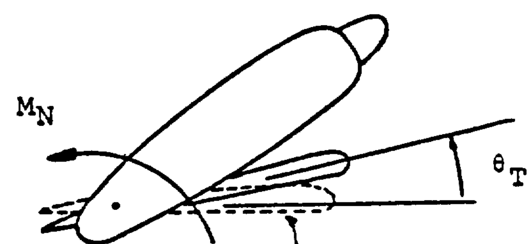

Figure A.1. Wing Geometry for Derivation of Flexibility

Using equation (A-7), assuming a linear structural twist from root to tip and performing the indicated integrations, the equation for total wing twisting moment becomes

$$T = K_\theta \theta_T = M_{actuator} + M_{gyro} + \frac{1}{4}\rho V^2 bc^2 C_{m_o} + \frac{1}{2}\rho V^2 c^2 \left(\frac{dC_{m_{c/4}}}{dC_\ell} + \frac{x}{c}\right)$$
$$\times \frac{C_{L_\alpha} b}{6\pi}\left(3\pi\alpha_{RIGID} + 4\theta_T\right) \qquad \text{(A-11)}$$

The equation for the actuator moment is given in the equations of motion, Section 5.0.

Rearranging, and writing $q = q_s\ (1-C_{T_s}) = \frac{1}{2}\ \rho V^2$

$$\theta_T = \frac{M_N + M_{gyro} + \frac{1}{2}q_s(1-C_{T_s})c_w^2\left[6\pi\alpha_{rigid}\left(\frac{dC_m}{dC_L} + \frac{x}{c}\right) + b_w C_{m_o}\right]}{K_\theta - \frac{2}{3\pi}\ q_s b_w c_w^2\ C_{L_\alpha}\ (1-C_{T_s})\left(\frac{dC_m}{dC_L} + \frac{x}{c}\right)} \qquad \text{(A-12)}$$

where C_{M_o}, the zero-lift wing section pitching moment coefficient, is a function of flap deflection:

$$C_{m_o} = C_1 + C_2\delta_f + C_3\delta_f^2 \qquad \text{(A-13)}$$

Knowing the tip value of twist, the twist at any other spanwise station is obtained by assuming a linear variation of twist from zero at the root to the tip value.

WING VERTICAL BENDING

The spanwise bending moment at any spanwise station y, on the wing is the sum of the bending moments due to wing aerodynamic lift, wing weight, nacelle lift, nacelle weight and net torque on the nacelle. The expressions for each contribution to the bending moments are derived below.

- Bending moment due to wing loading.

  Assuming an elliptical distribution of lift the bending moment is given by

$$M^a\ (y_1) = \int_{y_1}^{b/2} \ell(y)\ (y-y_1)dy \qquad \text{(A-14)}$$

$$= \frac{\ell_o b^2}{4} \int_{y_1}^{b/2} \sqrt{1-\left(\frac{2y}{b}\right)^2}\left(\frac{2y}{b} - \frac{2y_1}{b}\right)d\left(\frac{2y}{b}\right)$$

where ℓ_o is the lift per unit length at the wing root. Introducing the spanwise variable $\theta=\cos^{-1}\left|\frac{2y}{b}\right|$ making the required substitutions and integrating, the bending moment at any point y is:

$$M(y) = \frac{\ell_o b^2}{4}\left[\frac{1}{2}(\sin\theta-\theta\cos\theta)-\frac{1}{6}\sin^3\theta\right] \quad \text{(A-15)}$$

- <u>Bending due to nacelle net vertical load</u>.

  The net vertical force on nacelle is

  $$F=F^a - nW_N$$

  where F^a is the aerodynamic force and nW_N is the inertial load on the nacelle. The bending moment due to nacelle force is

  $$M^N(y) = \frac{Fb}{2}(1-\cos\theta) \quad \text{(A-16)}$$

- <u>Bending due to wing weight</u>.

  Assuming a uniform distribution of wing weight

  $$M^W(y_1) = -n\int_{y_1}^{b/2} w(y)\,(y-y_1)dy$$

  and $w(y) = 2W/b$ where W is the weight of one wing panel

  $$\therefore\ M^W(y_1) = \frac{2nW}{b}\int_{y_1}^{b/2}(y-y_1)dy \quad \text{(A-17)}$$

  i.e. $$M^W(y) = -\frac{nWb}{2}\left(1-\cos\theta-\frac{1}{2}\sin^2\theta\right)$$

- <u>Bending due to nacelle torque (rolling moment)</u>

  $$T(y) = \text{constant} = T \quad \text{(A-18)}$$

Total bending moment at station y is therefore

$$M(y) = M^a(y) + M^N(y) + M^W(y) + T \quad \text{(A-19)}$$

Assuming a linear variation of EI from root to tip given by

$$EI(y) = EI_o\left[1-a\left|\frac{2y}{b}\right|\right] = EI_o\,(1-a\cos\theta), \quad \text{(A-20)}$$

the curvature of the wing due to bending is

$$\frac{M(y)}{EI(y)} = \frac{d^2z}{dy^2} = \frac{\ell_o b^2}{8EI_o}\left[\frac{(\sin\theta-\theta\cos\theta)-1/3\sin^3\theta)}{1-a\cos\theta}\right] + \frac{F^a b}{2EI_o}\left[\frac{1-\cos\theta}{1-a\cos\theta}\right]$$

$$-\frac{nW_N b}{2EI_o}\left[\frac{1-\cos\theta}{1-a\cos\theta}\right] - \frac{nW_w b}{2EI_o}\left[\frac{1-\cos\theta-\frac{1}{2}\sin^2\theta}{1-a\cos\theta}\right]$$

$$+\frac{T}{EI_o}\left[\frac{1}{(1-a\cos\theta)}\right] \qquad \text{(A-21)}$$

Double integration of this equation yields the following expression for the bending deflection of the wing at any point y on the span:-

$$z(y) = \frac{Lb^3}{8\pi EI_o}\phi_1 + \frac{b^3F^a}{8EI_o}\phi_2 - \frac{nW_N b^3}{8EI_o}\phi_3$$

$$-\frac{nW_w b^3}{8EI_o}\phi_4 + \frac{Tb^3}{4EI_o}\phi_5 \qquad \text{(A-22)}$$

where $\phi_1 = \frac{b^2}{4}\int_o^y\left\{\int_o^y \frac{(\sin\theta-\theta\cos\theta)-\frac{1}{3}\sin^3\theta}{1-a\cos\theta}dy\right\}dy$

$$\phi_2 = \phi_3 = \frac{b^2}{4}\int_o^y\left\{\int_o^y \frac{1-\cos\theta}{1-a\cos\theta}dy\right\}dy$$

$$\phi_4 = \frac{b^2}{4}\int_o^y\left\{\int_o^y \frac{1-\cos\theta-\frac{1}{2}\sin^2\theta}{1-a\cos\theta}dy\right\}dy$$

$$\phi_5 = \frac{b^2}{4}\int_o^y\left\{\int_o^y \frac{dy}{1-a\cos\theta}\right\}dy$$

and where the wing lift (2 wing panels) $L = \frac{\pi}{4}\ell_o b$. The function ϕ_1 through ϕ_5 were obtained numerically and are presented in Figure A.2.

Since $L = -2\,Z^W_{AERO}$

$F^a = -\,Z^N_{AERO}$

$T = -\,L^N_{AERO}$

$$nW_w = \frac{1}{2} m_w \frac{Z_{AERO}}{m} = \frac{1}{2} m_w \bar{a}_{WAC}$$

$$nW_N = m_N \bar{a}_T$$

where m_w is the mass of two wing panels

m is the total aircraft mass

$\bar{a}_{WAC}$ is the acceleration of the wing aerodynamic center

$\bar{a}_T$ is the acceleration of the wing tip

and since the values of ϕ_1 through ϕ_5 are constant for any given station y on the wing we can write the final equation for wing bending in the form

$$h_1 = K_{W_1} Z^N_{AERO} + K_{W_2} Z^W_{AERO} - K_{W_3} L^N_{AERO} - K_{W_4} \bar{a}_T - K_{W_5} \bar{a}_{WAC}$$

where $h_1 = -z$

$$K_{W_1} = \frac{b^3 \phi_2}{8EI_o}$$

$$K_{W_2} = \frac{b^3 \phi_1}{4\pi EI_o}$$

$$K_{W_3} = \frac{b^3 \phi_5}{4EI_o}$$

$$K_{W_4} = \frac{m_N b^3 \phi_2}{8EI_o}$$

$$K_{W_5} = \frac{m_W b^3 \phi_4}{8EI_o}$$

This is the form given in the computer representation. The bending deflection at the aerodynamic center and at the wing tip are obtained using the values of $\phi_1 \rightarrow \phi_5$ appropriate to these stations.

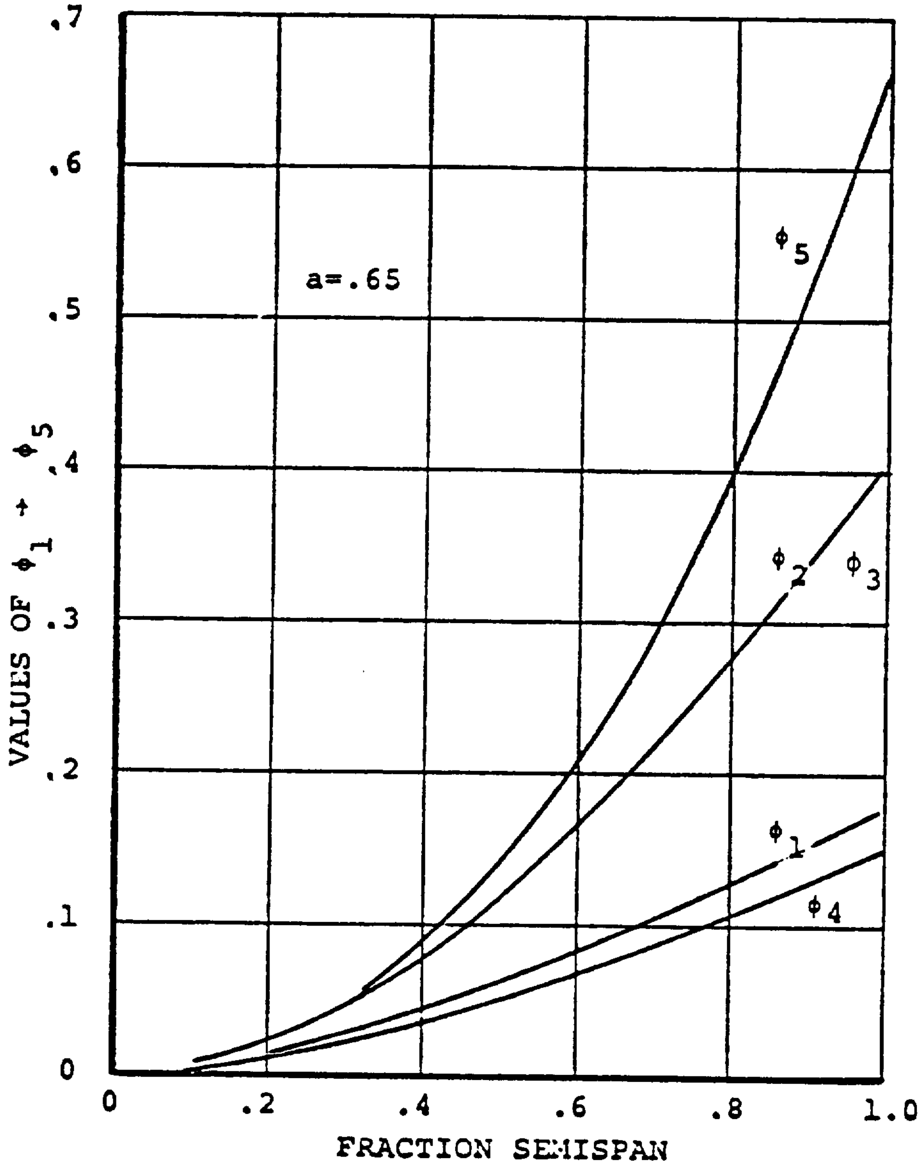

Figure A.2. Wing Bending Functions

APPENDIX B

APPENDIX B - DERIVATION OF LANDING GEAR EQUATIONS

Presented below are the equations for landing gear forces and moments arising from ground contact. The derivation accounts for brake and friction forces together with a simplified representation of the oleo dynamics. Nose wheel steering is not included.

With reference to Figure B-1 the distance from the center of gravity to the bottom of the right main wheel following a positive pitch rotation is

$$h_\theta = X \sin\theta - Z\cos\theta - r \qquad \text{(B-1)}$$

where X and Z are the coordinates of the hub of the wheel relative to the C.G. and r is the tire radius. If the aircraft is now rolled right, through the angle ϕ, the bottom of the right gear moves through a distance.

$$h_\phi = \left[Y \sin\phi + (Z+r)\ (\cos\phi - 1)\right] \cos\theta \qquad \text{(B-2)}$$

The height of the bottom of the wheel above the ground is therefore

$$h = H_{CG} + h_\theta - h_\phi \qquad \text{(B-3)}$$

and the oleo deflection during ground contact is given by

$$h_T = \frac{H_{CG} + h_\theta - h_\phi}{\cos\phi\ \cos\theta} \qquad \text{(B-4)}$$

By differentiation of equation B-4 and making small angle assumptions regarding the aircraft pitch and roll angles during touchdown, the rate of change of oleo strut deflection is obtained as

$$\dot{h}_T = \frac{\dot{H}_{CG}}{\cos\phi\ \cos\theta} + XQ - YP \qquad \text{(B-5)}$$

Assuming that the oleo response is that of a second order system, the equation of motion for the landing gear is

$$F_G = K_{ST}\ h_T + D_{ST}\ \dot{h}_T \qquad \text{(B-6)}$$

where K_{ST} and D_{ST} are the equivalent spring rates and damping for the oleo, and F_G is the force on the landing gear strut.

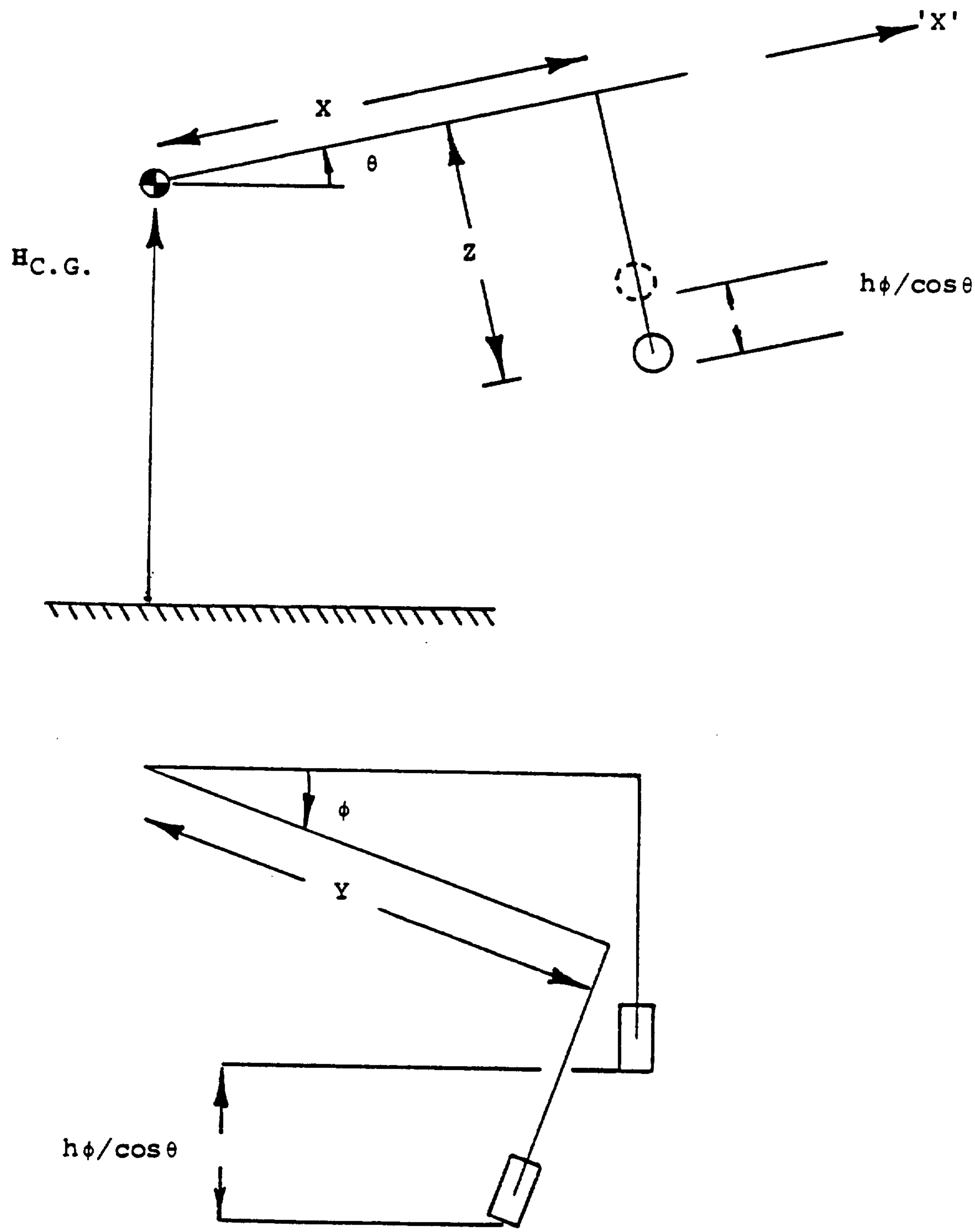

VIEW IN DIRECTION OF 'X'

FIGURE B.1 GEOMETRY OF LANDING GEAR

Tire Friction and Side Force

The friction force acting on each tire during ground contact is resolved into a force F_μ along the line of intersection of the plane of the wheel and the ground plane, positive forward, and a side force F_μ at right angles to F_μ lying in the ground plane and positive to starboard. The friction force F_s is assumed to be proportional to oleo force and the amount of braking exerted by the pilot. The side force is proportional to the oleo force.

The components of tire friction are:

$$F_\mu = (\mu_0 + \mu_1 B_G) F_{GZ} \frac{u}{|u|} \tag{B-7}$$

$$F_s = \mu_s F_{GZ} \frac{v}{|v|} \tag{B-8}$$

where μ_O, μ_1 and μ_s are the coefficients for rolling friction, brake friction and sliding friction. B_G is expressed as a percentage of full brake pedal deflection. The signs of the forward and sidewards velocity are introduced to properly orient the tire forces.

The force and moment contributions of each landing gear to the aircraft total forces and moments are, assuming small angles;

$$\Delta X_n = F_{\mu_n} - F_{GZ_n} \theta \tag{B-9}$$

$$\Delta Y_n = F_{s_n} + F_{GZ_n} \phi \tag{B-10}$$

$$\Delta Z_n = F_{\mu_n} \theta - F_{s_n} \phi + F_{GZ_n} \tag{B-11}$$

$$\Delta M_n = -\Delta Z_n X_n + \Delta X_n (Z_n + r_n + h_{T_n}) \tag{B-12}$$

$$\Delta L_n = \Delta Z_n Y_n - \Delta Y_n (Z_n + r_n + h_T) \tag{B-13}$$

$$\Delta N_n = -\Delta X_n Y_n + X_n \Delta Y_n \tag{B-14}$$

where n=1, 2 and 3 denote the left main gear, right main gear and nose gear, respectively.

The total contribution of the landing gear forces to the forces and moments at the center of gravity of the aircraft are:

$$\Delta X_{LG} = \sum_{n=1}^{3} \Delta X_n$$

$$\Delta Y_{LG} = \sum_{n=1}^{3} \Delta Y_n$$

$$\Delta Z_{LG} = \sum_{n=1}^{3} \Delta Z_n$$

$$\Delta L_{LG} = \sum_{n=1}^{3} \Delta L_n$$

$$\Delta M_{LG} \quad \sum_{n=1}^{3} \Delta M_n$$

$$\Delta N_{LG} \quad \sum_{n=1}^{3} \Delta N_n$$

APPENDIX C

APPENDIX C - VELOCITY AND ACCELERATION TRANSFORMATIONS AND CENTER OF GRAVITY/INERTIA EQUATIONS

C.1 Velocity Transformations

The calculation of aerodynamic forces on wings, fuselage, nacelles, and tail surfaces requires that the angle of attack and relative wind velocity at these surfaces be known. These velocities are obtained most conveniently in terms of the velocity of the pivot reference point.

With reference to Figure C.1, the velocity of a general point in the aircraft relative to the airplane center of gravity is

$$\underline{V} = \frac{\delta \underline{r}}{\delta t} + \underline{\Omega} \times \underline{r} \qquad \text{(C-1)}$$

where $\underline{r}$ is the radius vector from the c.g. to the point and $\underline{\Omega}$ is the angular velocity of the aircraft. Thus, expanding equation C-1, the velocity of the pivot relative to the c.g. is

$$\begin{aligned} u_p' &= \dot{X}_p + QZ_p - Y_pR \\ v_p' &= \dot{Y}_p - PZ_p - X_pR \\ w_p' &= \dot{Z}_p + PY_p - QX_p \end{aligned} \qquad \text{(C-2)}$$

where X_p, Y_p and Z_p are the distances of the pivot from the c.g., measured positively forward, to the right and downwards, respectively. If we measure all distances from the pivot location then $X_p = -X_{CG}$, $Y_p = -Y_{CG} = 0$, $Z_p = -Z_{CG}$ and the velocity of the pivot relative to inertial space can be written,

$$\begin{aligned} u_p &= U + u_p' = U - \dot{X}_{CG} - QZ_{CG} \\ v_p &= V + v_p' = V + PZ_{CG} - X_{CG}R \\ w_p &= W + w_p' = W + QX_{CG} - \dot{Z}_{CG} \end{aligned} \qquad \text{(C-3)}$$

where U, V, and W are the components of the velocity of the airplane center of gravity.

The velocity of a point in the aircraft relative to the pivot is

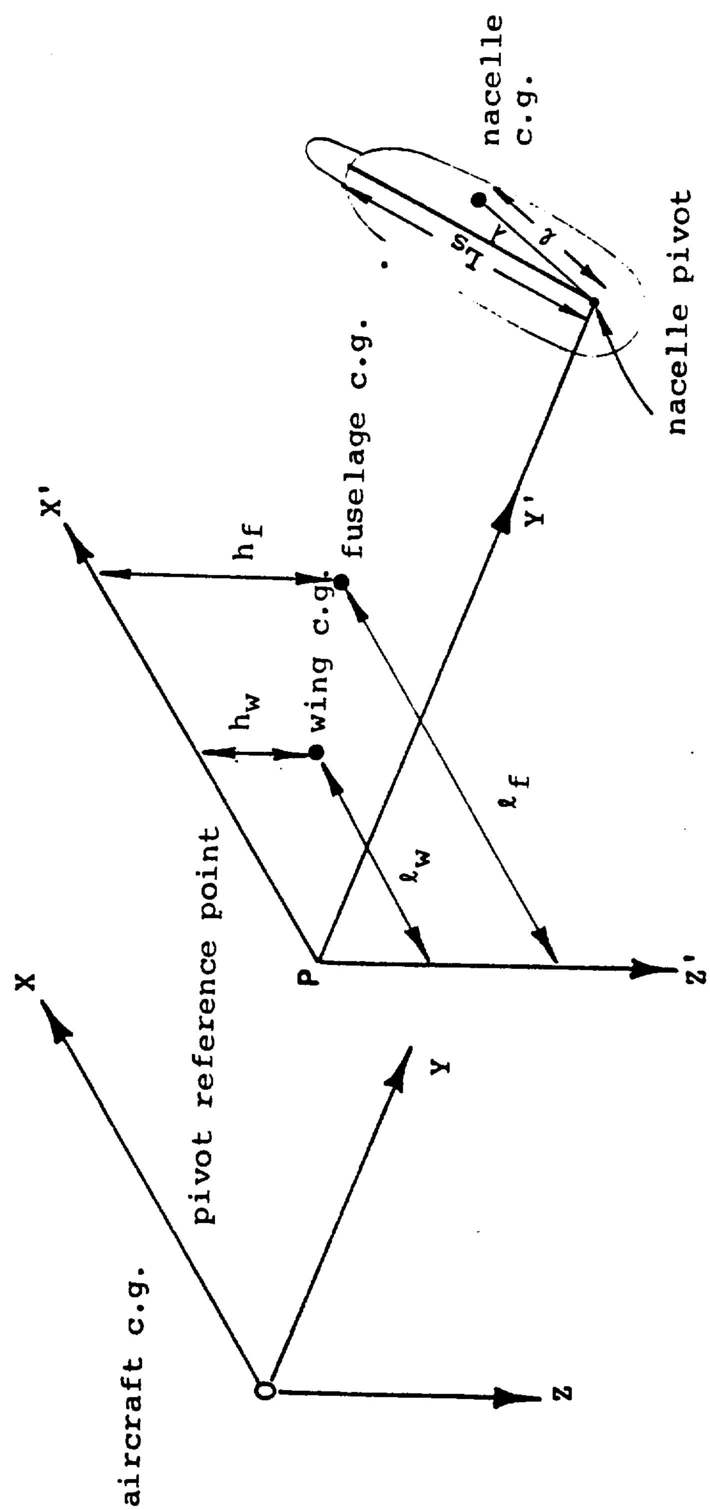

O and P are coplanar

FIGURE C.1 REFERENCE AXES SYSTEMS

$$u = \dot{X} + QZ - YR$$
$$v = \dot{Y} + RX - PZ \qquad \text{(C-4)}$$
$$w = \dot{Z} + PY - QX$$

where X, Y, and Z are measured from the pivot to the point. By adding equations (C-3) and (C-4) the velocities of the following components are obtained relative to inertial space. The indicated distances are measured relative to the pivot.

Velocity of Horizontal Tail Aerodynamic Center

$$u_{HT} = u_P + Z_{HT}Q$$
$$v_{HT} = v_P + X_{HT}R - Z_{HT}P \qquad \text{(C-5)}$$
$$w_{HT} = w_P - X_{HT}Q$$

Velocity of Vertical Tail Aerodynamic Center

$$u_{VT} = u_P + Z_{VT}Q$$
$$v_{VT} = u_P + X_{VT}R - Z_{VT}P \qquad \text{(C-6)}$$
$$w_{VT} = w_P + X_{VT}Q$$

Velocity of Left Wing Aerodynamic Center - Body Axes

$$u'_{LW} = u_P + Q\ (Z_{WAC} + h_{1_{LWAC}}) + Y_{WAC}R$$
$$v'_{LW} = u_P + X_{WAC}R - P(Z_{WAC} + h_{1_{LWAC}}) \qquad \text{(C-7)}$$
$$w'_{LW} = w_P - Y_{WAC}P - X_{WAC}Q + \dot{h}_{1_{LWAC}}$$

where $h_{1_{LWAC}}$ is the elastic deflection of the left wing aerodynamic center. The equations for the right wing are obtained by substituting

$$Y_{RWAC} = -Y_{LWAC}$$

and $h_{1_{RWAC}} = h_{1_{LWAC}}$

Velocity of Left Wing Aerodynamic Center-Chord Axes

In order to compute wing angle-of-attack the velocity components are required relative to the wing chord line. If the wing chord makes an angle i_w with the body centerline then

$$u_{LW} = u'_{LW} \cos i_w - w'_{LW} \sin i_w$$

$$v_{LW} = v'_{LW} \qquad (C-8)$$

$$w_{LW} = w'_{LW} \cos i_w + w'_{LW} \sin i_w$$

The equations for the right wing are obtained by changing the subscript.

Velocity of Left Rotor Hub - Body Axes

$$u'_{RL'} = u_P + RY_N - L_s (\dot{i}_{NL} + Q) \sin i_{NL} + Qh_{1_L}$$

$$v'_{RL} = v_P + L_s (R \cos i_{NL} + P \sin i_{NL}) - Ph_{1_L} \qquad (C-9)$$

$$w'_{RL} = w_P - PY_N - L_s (\dot{i}_{NL} + Q) \cos i_{NL} + \dot{h}_{1_L}$$

where L_s is the distance from the rotor pivot point to the rotor hub and h_{1_L} is the deflection of the wing tip. The equations for the right hub are obtained by changing subscripts and substituting $Y_N = -Y_N$.

Velocity of Left Rotor Hub - Shaft Axes

Since the rotor aerodynamic forces and moments are functions of the shaft angle of attack and sideslip, the velocity components are required relative to shaft axes.

$$u_{RL} = u'_{RL} \cos i_{NL} - w'_{RL} \sin i_{NL}$$

$$v_{RL} = v'_{RL} \qquad (C-10)$$

$$w_{RL} = w'_{RL} \sin i_{NL} + w'_{RL} \cos i_{NL}$$

The corresponding equations for the right hub are obtained by changing the subscript.

C.2 Center of Gravity and Inertia Equations

Equations are required that express the overall aircraft center of gravity position and inertias in terms of the centers of gravity and inertias of the individual mass components. In order to do this a fixed reference point is chosen in the aircraft defined by the intersection of the line joining the nacelle pivots and the vertical plane of symmetry of the aircraft, see Figure C.1. A set of axes $P_{x'y'z'}$ is taken at this pivot reference point, parallel to the axes OXYZ at the aircraft center of gravity. If the location of the aircraft center of gravity with respect to the pivot reference axes is $(X'_{CG}, Y'_{CG}, Z'_{CG})$ and if (ℓ_f, h_f) and (ℓ_w, h_w) are the x and z coordinates of the fuselage and wing masses measured from the pivot, then the following relationships are obtained between the centers of mass of the components and the aircraft center of gravity.

Fuselage CG Relative to Aircraft CG

$$X_f = \ell_f - X'_{CG}$$

$$X_f = h_f - Z_{CG} \qquad \text{(C-11)}$$

Wing CG Relative to Aircraft CG

$$X_w = \ell_w - X'_{CG}$$

$$Z_w = h_w - Z'_{CG} \qquad \text{(C-12)}$$

Nacelle CG Relative to Aircraft CG

$$X_{NR} = \ell \cos (i_{NR} - \lambda) - X'_{CG}$$

$$X_{NL} = \ell \cos (i_{NL} - \lambda) - X'_{CG} \qquad \text{(C-13)}$$

$$Z_{NR} = \ell \sin (i_{NR} - \lambda) - Z'_{CG}$$

$$Z_{NL} = \ell \sin (i_{NL} - \lambda) - Z'_{CG}$$

where ℓ is the distance from the nacelle pivot point to the nacelle c.g., and λ is the angular depression of the nacelle center of mass below the nacelle pivot, when the nacelle is in the down position, see Figure C.1.

Aircraft Center of Gravity Position

By taking moments about the pivot, the aircraft center of gravity is given by

$$x'_{CG} = \frac{m_f \ell_f + m_w \ell_w}{m} + \ell \left(\frac{m_N}{m}\right) \left[\cos(i_{NL}-\lambda) + \cos(i_{NR}-\lambda)\right]$$

$$z'_{CG} = \frac{m_f h_f + m_w h_w}{m} - \ell \left(\frac{m_N}{m}\right) \left[\sin(i_{NL}-\lambda) + \sin(i_{NR}-\lambda)\right] \qquad \text{(C-14)}$$

The equations of motion (Section 3) require the first and second time derivatives of the center of gravity position. They are as follows:

Center of Gravity Velocity Relative to Pivot Point

$$\dot{x}'_{CG} = -\ell \left(\frac{m_N}{m}\right) \left[\dot{i}_{NR}\sin(i_{NR}-\lambda) + \dot{i}_{NL}\sin(i_{NL}-\lambda)\right]$$

$$\dot{z}'_{CG} = -\ell \left(\frac{m_N}{m}\right) \left[\dot{i}_{NR}\cos(i_{NR}-\lambda) + \dot{i}_{NL}\cos(i_{NL}-\lambda)\right] \qquad \text{(C-15)}$$

Center of Gravity Acceleration Relative to Pivot Point

$$\ddot{x}'_{CG} = -\ell \left(\frac{m_N}{m}\right) \left[\ddot{i}_{NR}\sin(i_{NR}-\lambda) + \ddot{i}_{NL}\sin(i_{NL}-\lambda) + \dot{i}_{NL}^2 \cos(i_{NL}-\lambda) + \dot{i}_{NR}^2 \cos(i_{NR}-\lambda)\right] \qquad \text{(C-16)}$$

$$\ddot{z}'_{CG} = -\ell \left(\frac{m_N}{m}\right) \left[\ddot{i}_{NR}\cos(i_{NR}-\lambda) + \ddot{i}_{NL}\cos(i_{NL}-\lambda) - \dot{i}_{NL}^2\sin(i_{NL}-\lambda) - \dot{i}_{NR}^2\sin(i_{NR}-\lambda)\right]$$

Pilot Station Velocities - Body Axes

The velocities at the pilot's station are required in order to drive the visual display. From Equations (C-3) and (C-4) the components of velocity of the pilot's station in body axes are:

$$: \quad u_{PA} = u_P + QZ_{PA} - RY_{PA}$$

$$v_{PA} = v_P + R\ell_{PA} - PZ_{PA}$$

$$w_{PA} = w_P + PY_{PA} - Q\ell_{PA}$$

C-3 Pilot Station Acceleration - Body Axes

The pilot station acceleration is also required to drive the visual display. These accelerations are derived here.

The velocity at the pilot's station is

$$\underline{V}_{PA} = \underline{V}_{CG} + \underline{\Omega} \times \underline{r}_{PA} + \frac{\delta \underline{r}_{PA}}{\delta t}$$

where $\underline{r}_{PA}$ is the vector from the aircraft CG to the pilot's station and $\frac{\delta \underline{r}_{PA}}{\delta t}$ is the rate of change of the pilot's station with respect to the aircraft CG.

The pilot's station acceleration is

$$\underline{a}_{PA} = \frac{d\underline{V}_{PA}}{dt} = \frac{d\underline{V}_{CG}}{dt} + \frac{d}{dt}(\underline{\Omega} \times \underline{r}_{PA}) + \frac{d}{dt}\left(\frac{\delta \underline{r}_{PA}}{\delta t}\right)$$

$$= \underline{a}_{CG} + \frac{\delta}{\delta t}(\underline{\Omega} \times \underline{r}_{PA}) + \underline{\Omega} \times (\underline{\Omega} \times \underline{r}_{PA}) + \frac{\delta^2 \underline{r}_{PA}}{\delta t^2} + \underline{\Omega} \times \frac{\delta \underline{r}_{PA}}{\delta t}$$

$$= \underline{a}_{CG} + \frac{\delta \underline{\Omega}}{\delta t} \times \underline{r}_{PA} + 2\underline{\Omega} \times \frac{\delta \underline{r}_{PA}}{\delta t} + \underline{\Omega}\,(\underline{r}_{PA} \cdot \underline{\Omega}) - \Omega^2 \underline{r}_{PA} + \frac{\delta^2 \underline{r}_{PA}}{\delta t^2}$$

with $\underline{\Omega} = P\hat{\underline{i}} + Q\hat{\underline{j}} + R\hat{\underline{k}}$

$$\frac{\delta \Omega}{\delta t} = \dot{P}\hat{\underline{i}} + \dot{Q}\hat{\underline{j}} + \dot{R}\hat{\underline{k}}$$

$$\underline{r}_{PA} = (X_{PA} - X_{CG})\,\hat{\underline{i}} + (Y_{PA} - Y_{CG})\,\hat{\underline{j}} + (Z_{PA} - Z_{CG})\,\hat{\underline{k}}$$

$$\frac{\delta \underline{r}_{PA}}{\delta t} = (\dot{X}_{PA} - \dot{X}_{CG})\,\hat{\underline{i}} + (\dot{Y}_{PA} - \dot{Y}_{CG})\,\hat{\underline{j}} + (\dot{Z}_{PA} - \dot{Z}_{CG})\,\hat{\underline{k}}$$

and noting that Y_{CG} and the time derivatives of X_{PA}, Y_{PA}, Z_{PA} are always zero, the above equation yields the pilot's station accelerations as:

$$a_{x_{PA}} = \frac{X_{AERO}}{m} + (\dot{Q} + PR)(Z_{PA} - Z_{CG}) + (Q^2 + R^2)(X_{CG} - \ell_{PA})$$

$$+ Y_{PA}(PQ - \dot{R}) - 2Q\dot{Z}_{CG} - \ddot{X}_{CG}$$

$$a_{y_{PA}} = \frac{Y_{AERO}}{m} + (\dot{P} - QR)(Z_{CG} - Z_{PA}) + (\dot{R} + PQ)(\ell_{PA} - X_{CG})$$

$$- Y_{PA}(R^2 + P^2) + 2(P\dot{Z}_{CG} - R\dot{X}_{CG})$$

$$a_{z_{PA}} = \frac{Z_{AERO}}{m} + (\dot{Q} - PR)(X_{CG} - \ell_{PA}) + (P^2 + Q^2)(Z_{CG} - Z_{PA})$$

$$+ Y_{PA}(\dot{P} + QR) + 2Q\dot{X}_{CG} - \ddot{Z}_{CG}$$

where $a_{x_{CG}} = \dfrac{Z_{AERO}}{m}$ etc.

and $X_{PA} = \ell_{PA}$, the distance from the pivot to the pilot's station

C.4 Aircraft Inertias

The aircraft roll inertia about the aircraft center of gravity is, from the parallel axis theorem,

$$I_{xx} = I_{xx}^{f} + I_{xx}^{W} + I_{xx}^{NL} + I_{xx}^{NR} + m_f Z_f^2 + m_W Z_W^2 + 2m_N Y_N^2 + m_N Z_{NL}^2 + m_N Z_{NR}^2 \qquad \text{(C-17)}$$

where I_{xx}^{f}, etc., are the inertias of the various components about their individual centers of gravity.

In the case of the nacelles the inertias I_{xx}^{NL}, I_{xx}^{NR} are dependent on the nacelle tilt angle, i_N. These inertias are related to the inertias of the nacelle with respect to a set of nacelle-fixed axes O"xyz placed as shown in Figure 3.1. The relationships are

$$
\begin{aligned}
I_{xx}^{N} &= I_{xx_o}^{N} + (I_{zz_o}^{N} - I_{xx_o}^{N}) \sin^2 i_N - I_{xz_o} \sin 2i_N \\
I_{yy}^{N} &= I_{yy_o}^{N} \\
I_{zz}^{N} &= I_{zz_o}^{N} + (I_{xx_o}^{N} - I_{zz_o}^{N}) \sin^2 i_N + I_{xz_o} \sin 2i_N \\
I_{xz}^{N} &= I_{xz_o}^{N} \cos 2i_N + \frac{1}{2} (I_{xx_o} - I_{zz_o}) \sin 2i_N
\end{aligned}
\qquad \text{(C-18)}
$$

Using equations (C-18) together with (C-13), (C-11), and (C-12), in equation (C-17), the roll inertia becomes

$$
\begin{aligned}
I_{xx} = {} & I_{xx}^{f} + I_{xx}^{w} + 2I_{xx_o}^{N} + (I_{zz_o}^{N} - I_{xx_o}^{N}) (\sin^2 i_{NL} + \sin^2 i_{NR}) \\
& - I_{xz_o}^{N} (\sin 2i_{NL} + \sin 2i_{NR}) + 2\, m_N Y_N^2 + m_f h_f Z_f \\
& + m_w h_w z_w - m_f Z_f Z'_{CG} - m_w Z_w Z'_{CG} \\
& - m_N Z_{NL} Z'_{CG} - m_N Z_{NR} Z'_{CG} \\
& - \ell m_N \left[Z_{NR} \sin (i_{NR} - \lambda) + Z_{NL} \sin (i_{NL} - \lambda) \right] \\
= {} & I_{xx}^{f} + I_{xx}^{w} + 2I_{xx_o}^{N} + (I_{zz_o}^{N} - I_{xx_o}^{N}) (\sin^2 i_{NL} + \sin^2 i_{NR}) \\
& - I_{xz_o}^{N} (\sin 2i_{NL} + \sin 2i_{NR}) + 2\, m_N Y_N^2 + m_f h_f Z_f \\
& + m_w h_w Z_w - \ell m_N \left[Z_{NR} \sin (i_{NR} - \lambda) + Z_{NL} \sin (i_{NL} - \lambda) \right]
\end{aligned}
$$

since the terms containing Z'_{CG} sum to zero.

Similarly

$$I_{xz} = I_{xz}^{f} + I_{xz}^{w} + I_{xz}^{N} \left(\cos 2i_{NL} + \cos 2i_{NR}\right)$$

$$+ \frac{1}{2} \left(I_{xx_o}^{N} - I_{zz_o}^{N}\right) \left(\sin 2i_{NL} + \sin 2i_{NR}\right) + m_f \ell_f Z_f$$

$$+ m_w Z_w \ell_w + \ell m_N \left[Z_{NR} \cos\left(i_{NR} - \lambda\right) + Z_{NL} \cos\left(i_{NL} - \lambda\right)\right]$$

$$(I_{zz} - I_{yy}) = I_{zz}^{f} - I_{yy}^{f} + I_{zz}^{w} - I_{yy}^{w} + 2\left(I_{zz_o}^{N} - I_{yy_o}^{N}\right)$$

$$+ \left(I_{xx_o}^{N} - I_{zz_o}^{N}\right)\left(\sin^2 i_{NL} + \sin^2 i_{NR}\right) + I_{xz_o}^{N}\left(\sin 2i_{NL}\right.$$

$$\left. + \sin Zi_{NR}\right) - \left(m_f h_f Z_f + m_w h_w Z_w\right) + m_N \ell \left[Z_{NL} \sin\left(i_{NL} - \lambda\right)\right.$$

$$\left. + Z_{NR} \sin\left(i_{NR} - \lambda\right)\right] + 2m_N Y_N^2$$

Similar expressions are obtained for I_{yy} and I_{zz} and these are presented in Appendix E.

APPENDIX D

APPENDIX D - CALCULATION OF SLIPSTREAM-IMMERSED WING AREAS

The wing areas washed by the rotor slipstreams are required in the calculation of wing lift and drag. These immersed areas depend on rotor shaft inclination, wing angle of attack and sideslip, and rotor thrust. The equations presented in Appendix E for the immersed areas Si_L and Si_R were obtained as follows.

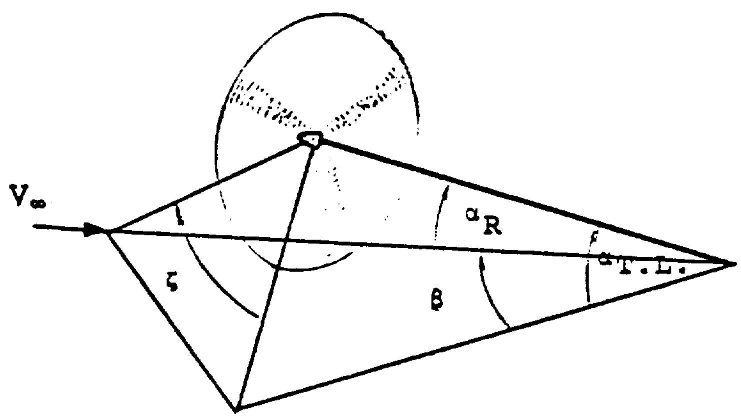

The above sketch shows a rotor under conditions of combined angle of attack ($\alpha_{T.L.}$) and sideslip (β). The resultant angle of attack of the shaft is given by

$$\alpha_R = \cos^{-1}(\cos \alpha_{T.L.} \cos \beta) \tag{D-1}$$

If the rotor shaft is inclined to the fuselage centerline at angle i_N and the fuselage is at angle of attack α_f then

$$\alpha_{T.L.} = \alpha_f + i_N \tag{D-2}$$

The rotor "sideslip" angle, ζ, is defined by

$$\zeta = \mathrm{Tan}^{-1} \frac{\mathrm{Tan}\ \beta}{\mathrm{Sin}\ \alpha_{T.L.}} \tag{D-3}$$

and is the angle shown in the sketch.

Figure D.1 presents four views of the geometry of rotor slipstream/wing planform interaction.

Figure D.1[a] is a view of the plane taken through the rotor shaft parallel to the aircraft vertical plane of symmetry. The line PT is the wing chord, the distances PC and h_p are the horizontal and vertical coordinates of the pivot measured from the wing leading edge, and ℓ is the spinner-to-pivot shaft length.

Figure D.1[b] is a view taken normal to the rotor disc plane. In this view, the traces of the slipstream on planes taken through the wing leading and trailing edges parallel to the disc plane appear as circles. This assumes that the slipstream is a sheared circular cylinder.

Figure D.1[c] is a section taken in the plane containing the rotor shaft and the freestream velocity vector V_∞. The angle ε is the deflection of the slipstream relative to the freestream direction. Planes are taken through the wing leading and trailing edges parallel to the rotor disc. These intersect the rotor shaftline at the points O and T, and intersect the slipstream centerline at the points O' and O". These points enable the slipstream traces shown in (b) to be constructed.

Figure D.1[d] is a view taken perpendicular to the wing surface showing the areas washed by the slipstream. For convenience, this view combines the immersed areas of both left and right wings. In general, the imprint of the slipstream on the wing will be bounded in the chordwise direction by curves lines; however, the approximation is made that these lines are straight.

The immersed area of the right wing panel is (assuming that the tip is immersed),

$$S_{i_R} = \frac{1}{2}(PM + TN)c$$

$$= \frac{1}{2}(PR + RM + TS + SN)c \qquad (D-4)$$

From Figure D.1[b] $\quad PR = OO' \sin \zeta \qquad$ (D-5)

From Figure D.1[c] $\quad OO' = (\ell - OD) \tan (\alpha_R - \varepsilon) \qquad$ (D-6)

From Figure D.1[a] $\quad OD = PC \cos (i_N - i_W) - h_p \sin (i_N - i_W) \qquad$ (D-7)

From Figure D.1[b] $\quad RM = R'M' = \sqrt{\frac{D_S^2}{4} - O'R'^2} \qquad$ (D-8)

From Figure D.1[b] $\quad O'R' = OO' \cos \zeta + OP \qquad$ (D-9)

From Figure D.1[a] $\quad OP = PC \sin (i_N - i_W) + h_p \cos (i_N - i_W) \qquad$ (D-10)

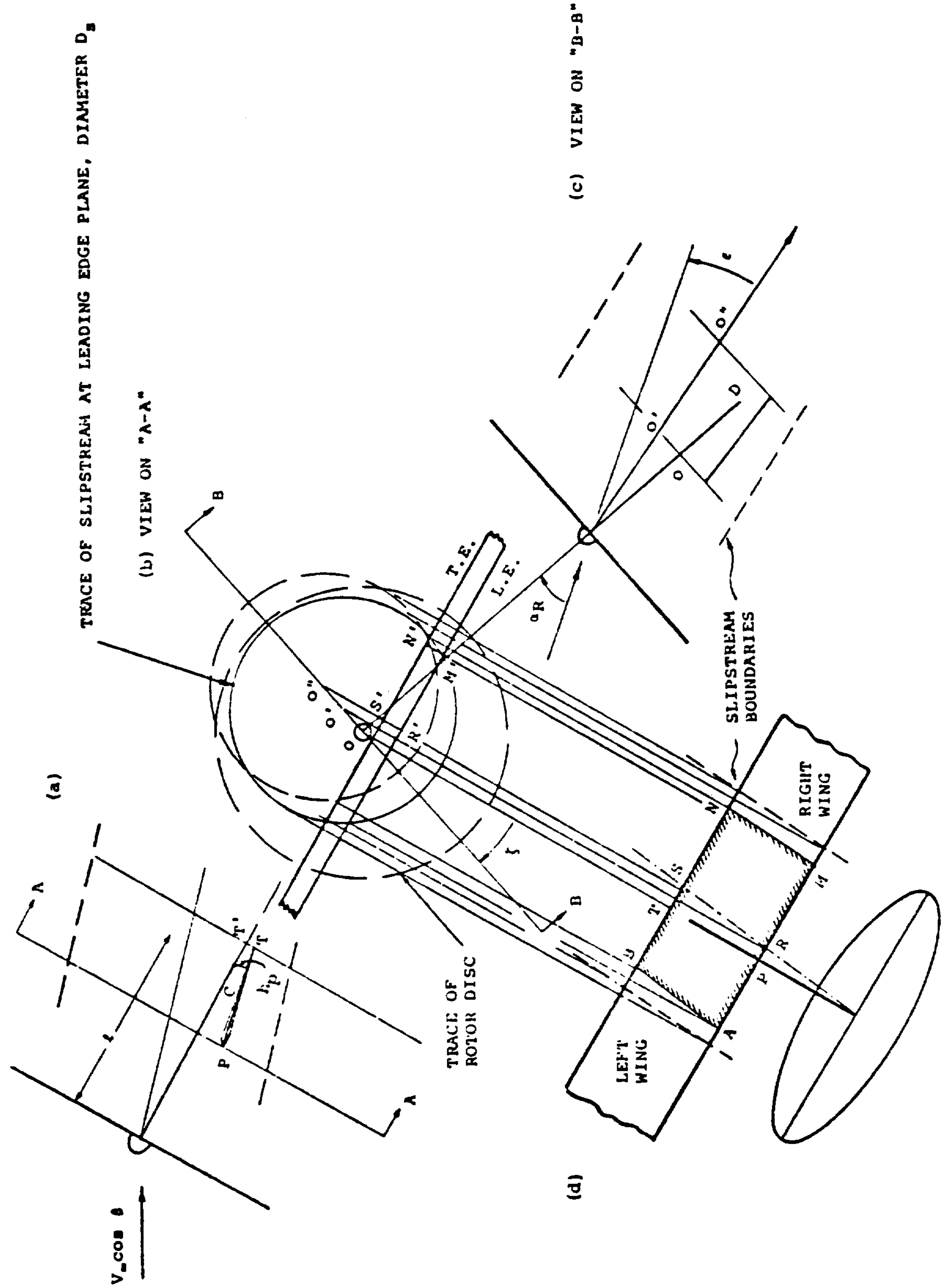

Figure D.1. Geometry of Rotor Slipstream/Wing Planform Interaction

These equations define the leading edge intersection PM. If RM is zero or negative, the slipstream does not intersect the leading edge and the wing is considered to be unaffected by the slipstream.

For the trailing edge intersection, TN:

$$TS = OO'' \sin \zeta \tag{D-11}$$

$$OO'' = (\ell + c \cos (i_N - i_W) - OD) \operatorname{Tan} (\alpha_R - \varepsilon) \tag{D-12}$$

$$SN = S'N' = \frac{D_s^2}{4} - O''S'^2 \tag{D-13}$$

$$O''S' = OO'' \cos \zeta + TT' \tag{D-14}$$

$$TT' = OP - c \sin (i_N - i_W) \tag{D-15}$$

If we write

$$\xi_1 = PR,\ \xi_2 = RM,\ \xi_3 = TS, \text{ and } \xi_4 = SN$$

then, using the above equations,

$$\xi_1 = [\ell - PC \cos (i_N - i_W) + h_p \sin (i_N - i_W)] \operatorname{Tan}(\alpha_R - \varepsilon) \sin \xi \tag{D-16}$$

and

$$\xi_2 = \sqrt{\frac{D_s^2}{4} - \{[\ell - PC \cos (i_N - i_W) + h_p \sin (i_N - i_W)] \operatorname{Tan}(\alpha_R - \varepsilon) \cos \zeta + PC \sin (i_N - i_W) + h_p \cos (i_N - i_W)\}} \tag{D-17}$$

The corresponding equations for ξ_3 and ξ_4 are obtained by replacing PC in (D-16) and (D-17) and (PC-c)

Thus the immersed area of the right wing panel is given by

$$S_{i_R} = \frac{1}{2} c \ (\xi_1 + \xi_2 + \xi_3 + \xi_4) \tag{D-18}$$

From the symmetry of Figure D.1[d], SN=BS and RM=AR. The total immersed area of both wing panels is

$$S_{i_T} = \frac{1}{2} c \ (AM + BN) = \frac{1}{2} c \ (2\xi_2 + 2\xi_4) = c(\xi_2 + \xi_4) \tag{D-19}$$

and therefore the immersed area of the left wing is obtained from

$$S_{i_L} = S_{i_T} - S_{i_R} \tag{D-20}$$

The above equations correspond to those presented in Appendix E for calculating immersed wing area.

APPENDIX E

Appendix E

The equations and control diagrams that form the mathematical model of the hingeless rotor XV-15 tilt rotor aircraft are presented in the following pages. Input data for the model is provided in Appendix F. The simulation block diagram is shown on page E-6. Each element of the diagram is numbered. The reference table on page E-2 lists the block diagram element number, the function of the element, and the starting number of the pages containing the equations for the element.

APPENDIX E - TABLE OF CONTENTS

TABLE OF CONTENTS
(Cont'd)

TABLE OF CONTENTS

(Cont'd)

INDEX TO BLOCK DIAGRAM EQUATIONS

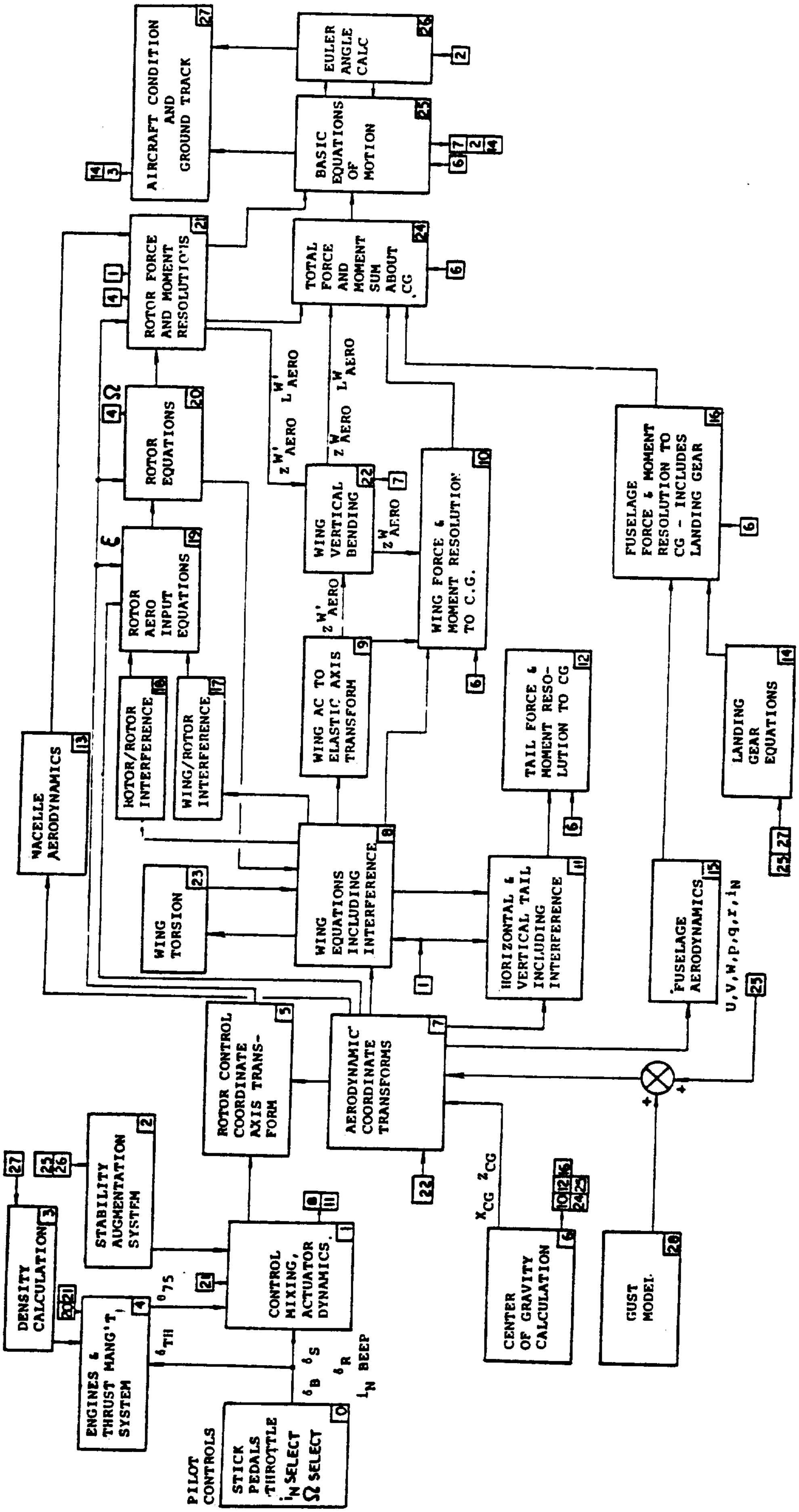
PILOT CONTROLS
STICK
PEDALS
THROTTLE
i_N SELECT
Ω SELECT
ENGINES & THRUST MANG'T SYSTEM
DENSITY CALCULATION
STABILITY AUGMENTATION SYSTEM
CONTROL MIXING, ACTUATOR DYNAMICS
ROTOR CONTROL COORDINATE AXIS TRANSFORM
AERODYNAMIC COORDINATE TRANSFORMS
CENTER OF GRAVITY CALCULATION
GUST MODEL
NACELLE AERODYNAMICS
ROTOR/ROTOR INTERFERENCE
WING/ROTOR INTERFERENCE
ROTOR AERO INPUT EQUATIONS
ROTOR EQUATIONS
ROTOR FORCE AND MOMENT RESOLUTIONS
WING TORSION
WING EQUATIONS INCLUDING INTERFERENCE
WING AC TO ELASTIC AXIS TRANSFORM
WING VERTICAL BENDING
WING FORCE & MOMENT RESOLUTION TO C.G.
HORIZONTAL & VERTICAL TAIL INCLUDING INTERFERENCE
TAIL FORCE & MOMENT RESOLUTION TO CG
FUSELAGE AERODYNAMICS
LANDING GEAR EQUATIONS
FUSELAGE FORCE & MOMENT RESOLUTION TO CG - INCLUDES LANDING GEAR
TOTAL FORCE AND MOMENT SUM ABOUT CG
BASIC EQUATIONS OF MOTION
EULER ANGLE CALC
AIRCRAFT CONDITION AND GROUND TRACK
U,V,W,P,q,r,i_N
X_{CG} Z_{CG}

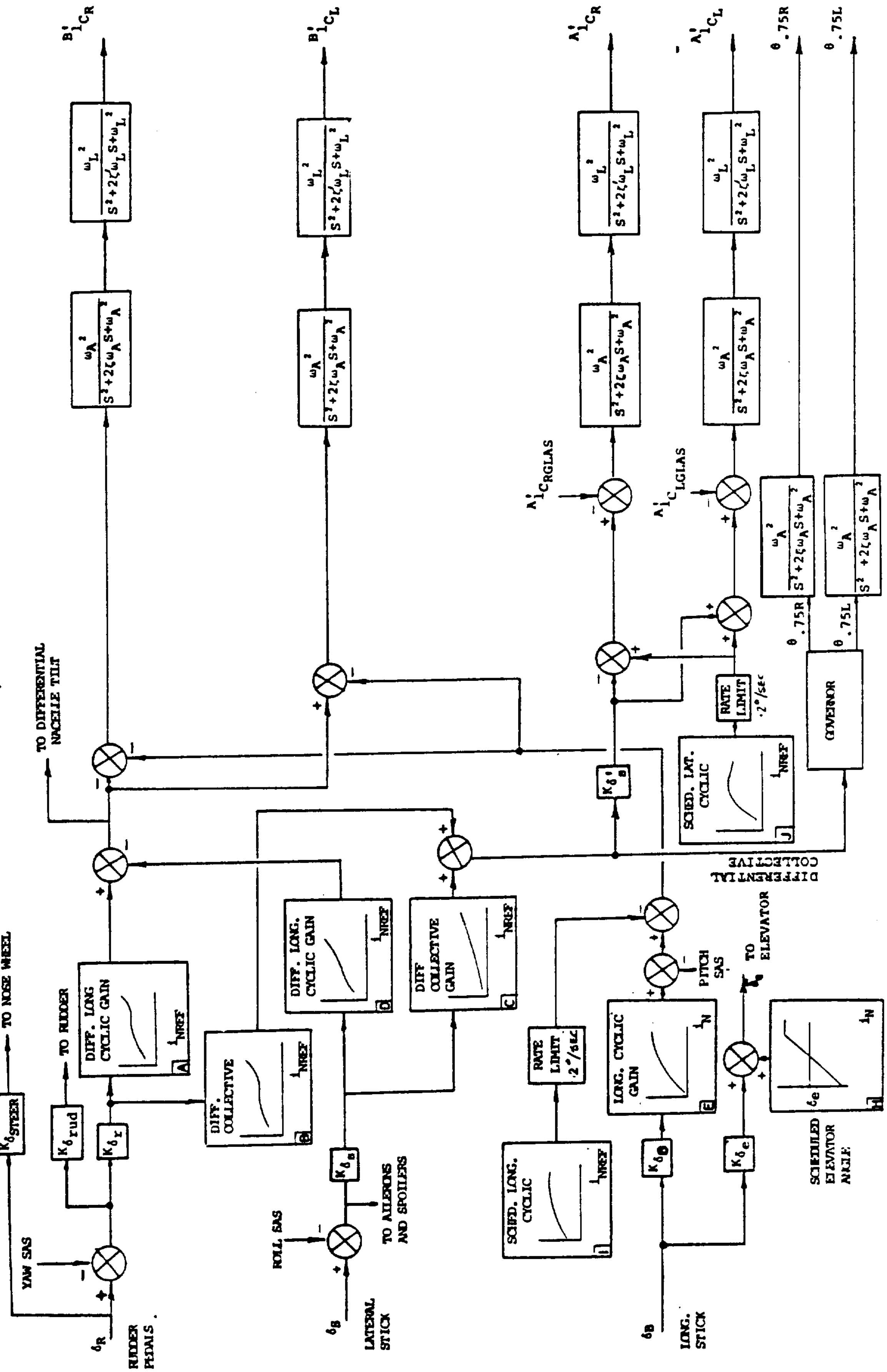

PRELIMINARY CONTROL SYSTEM BLOCK DIAGRAM

NACELLE, FLAPS, AND AILERON CONTROLS

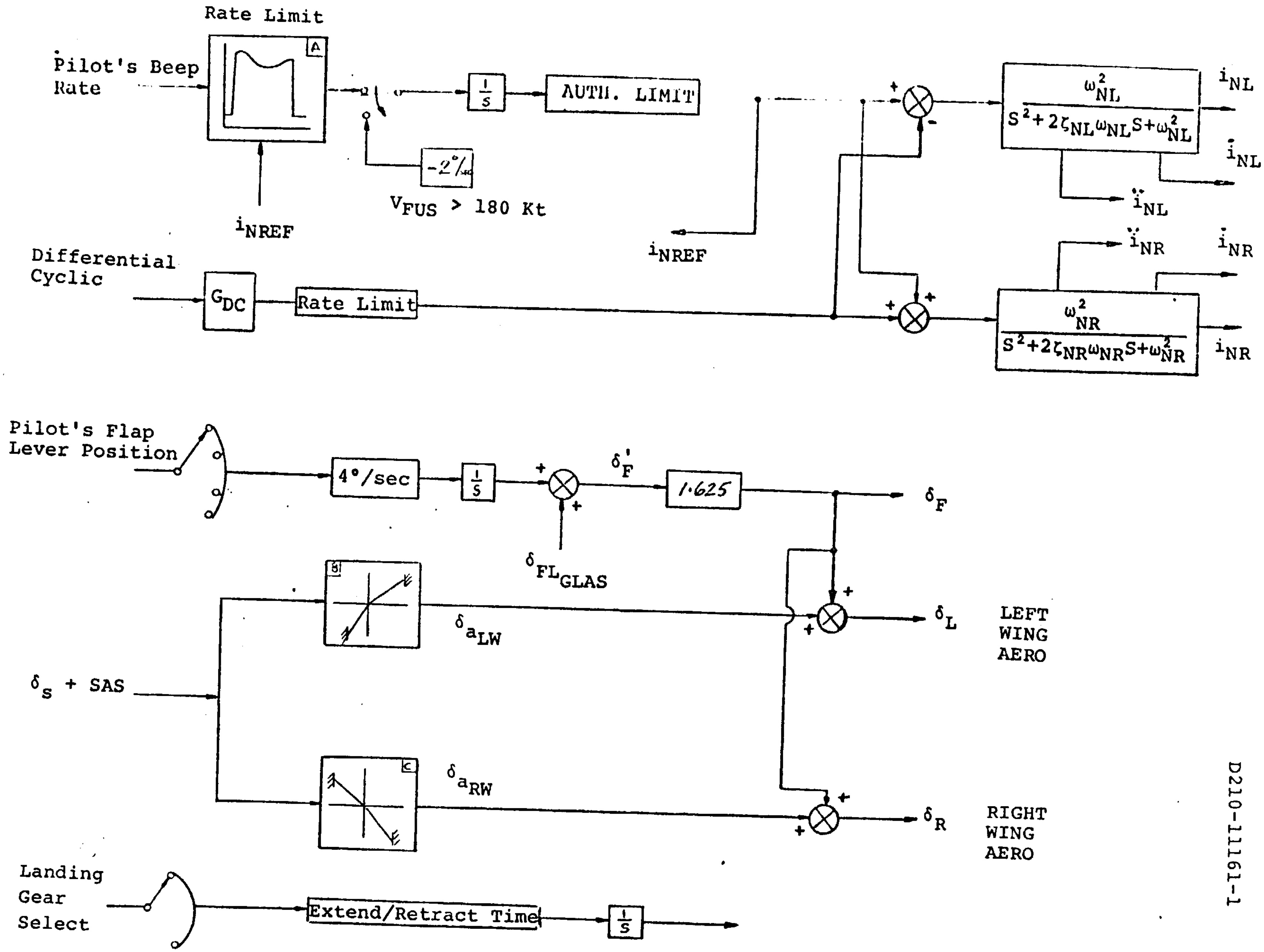

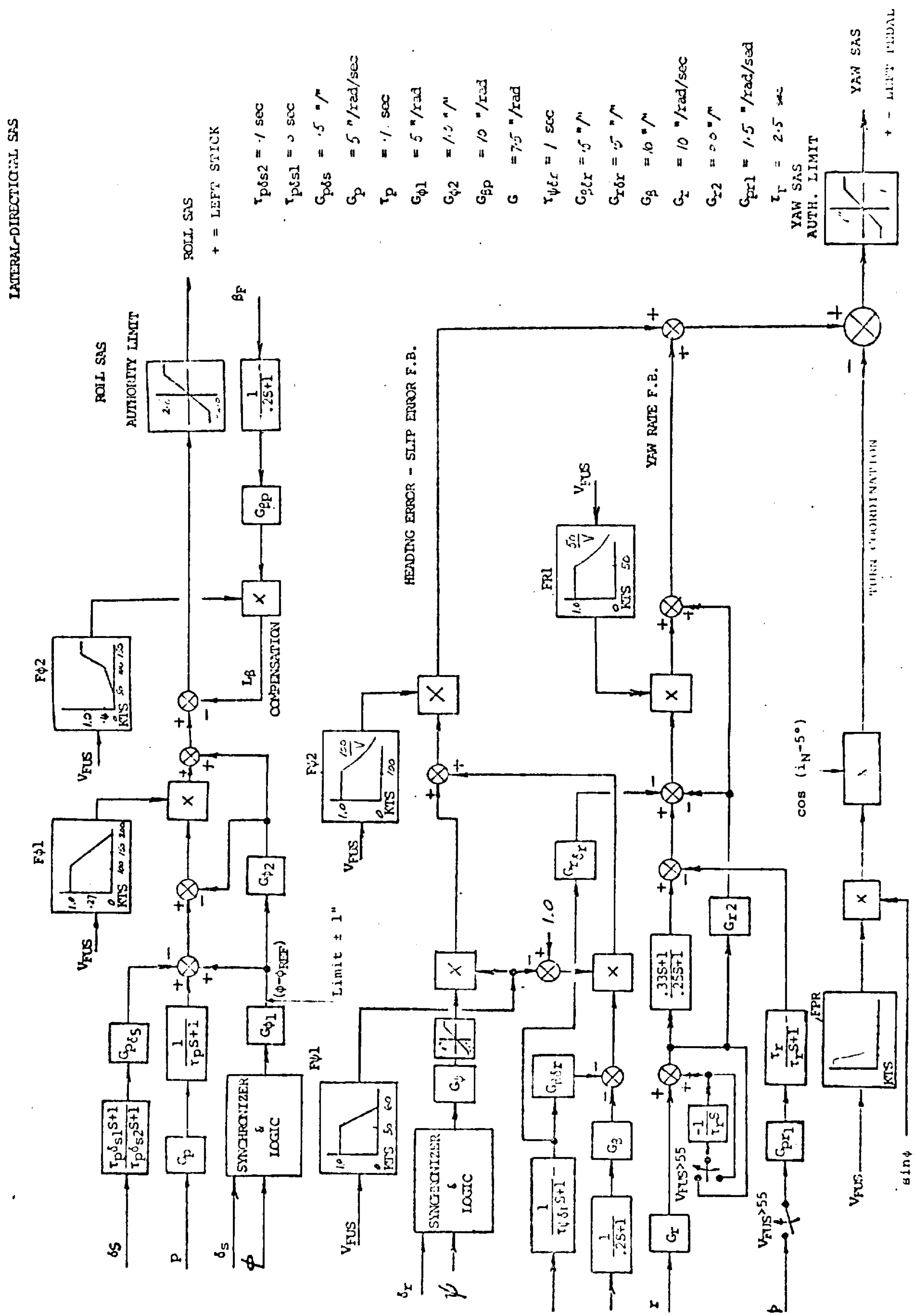

LATERAL-DIRECTIONAL SAS
ROLL SAS
+ = LEFT STICK
ROLL SAS AUTHORITY LIMIT
COMPENSATION
HEADING ERROR - SLIP ERROR F.B.
YAW RATE F.B.
TURN COORDINATION
YAW SAS AUTH. LIMIT
YAW SAS
+ - LEFT PEDAL
SYNCHRONIZER & LOGIC
Limit ± 1"
cos (iN-5°)
VFUS>55
KTS

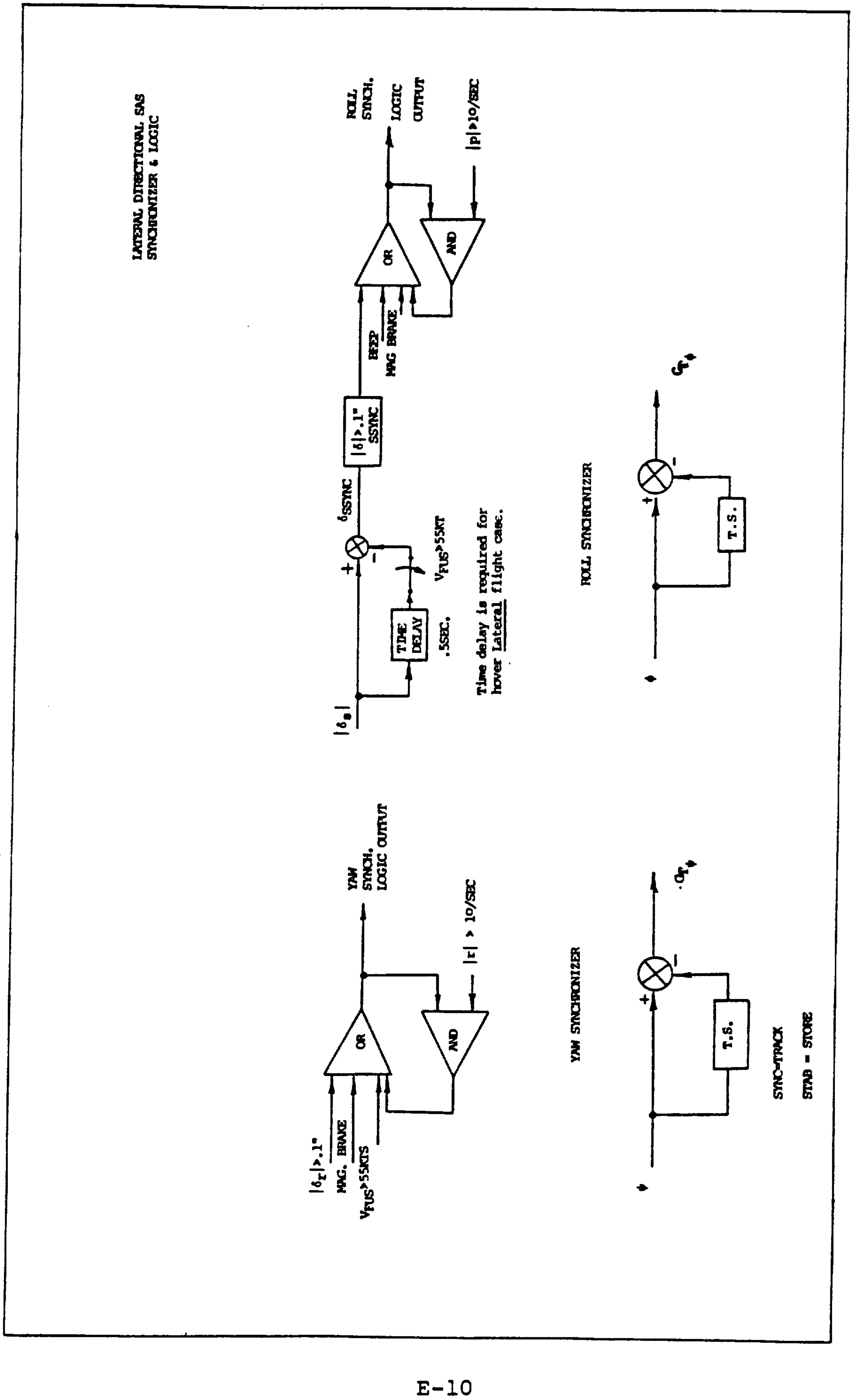
LATERAL DIRECTIONAL SAS
SYNCHRONIZER & LOGIC
SHEET
ROLL
SYNCH.
LOGIC
OUTPUT
|p|>1°/SEC
OR
AND
BEEP
MAG BRAKE
|δ|>.1"
SSYNC
δSSYNC
+
-
TIME
DELAY
.5SEC.
VFUS>55KT
|δa|
Time delay is required for
hover Lateral flight case.
ROLL SYNCHRONIZER
T.S.
YAW
SYNCH.
LOGIC OUTPUT
|r| > 1°/SEC
|δr|>.1"
MAG. BRAKE
VFUS>55KTS
YAW SYNCHRONIZER
SYNC=TRACK
STAB = STORE

LONGITUDINAL SAS

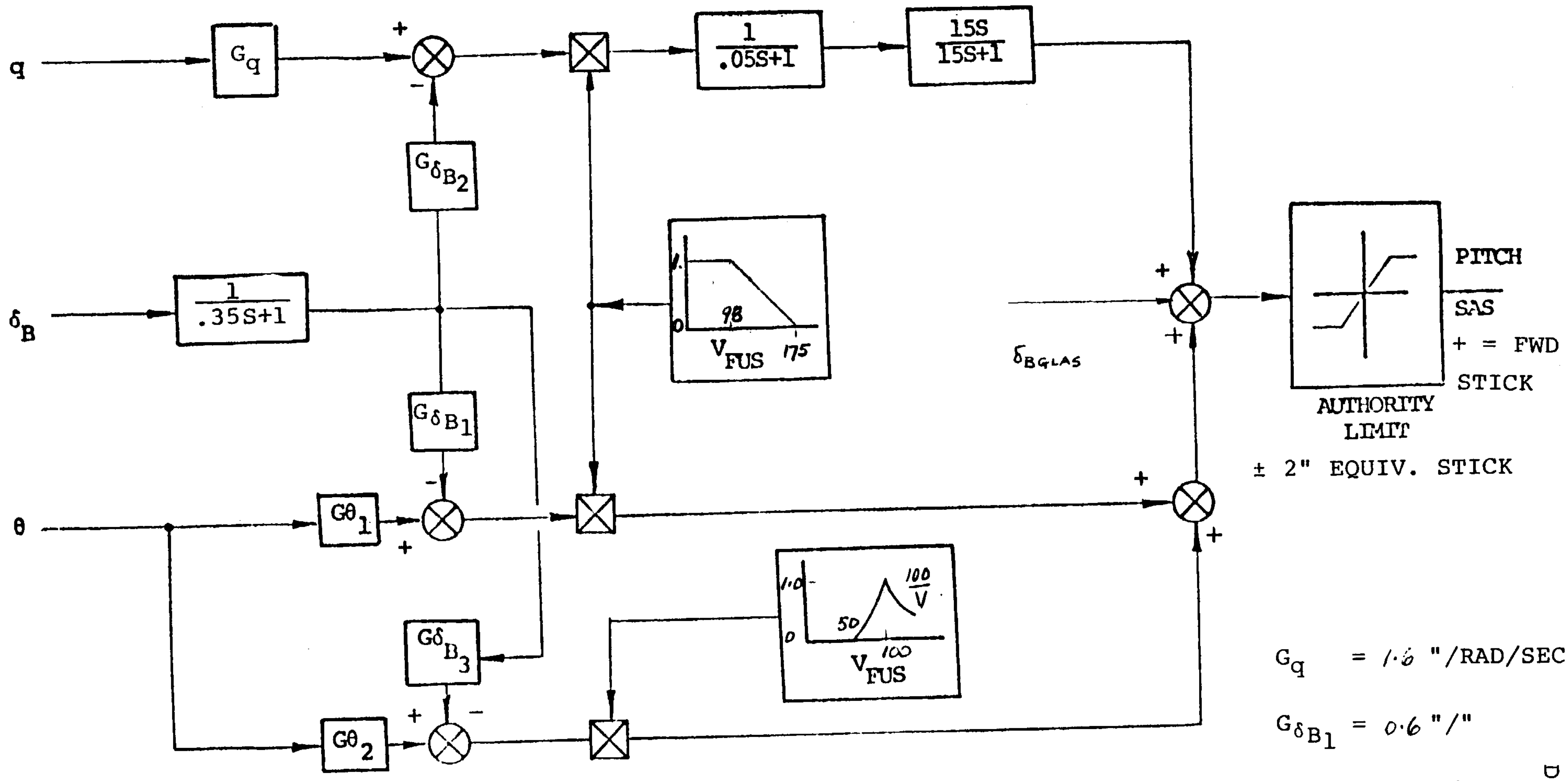

G_q = 1.6 "/RAD/SEC

$G_{\delta B_1}$ = 0.6 "/"

$G_{\delta B_2}$ = 0.0 "/"

$G\theta_1$ = 8.0 "/RAD

$G_{\delta B_3}$ = 0.17 "/"

$G\theta_2$ = [illegible] "/RAD

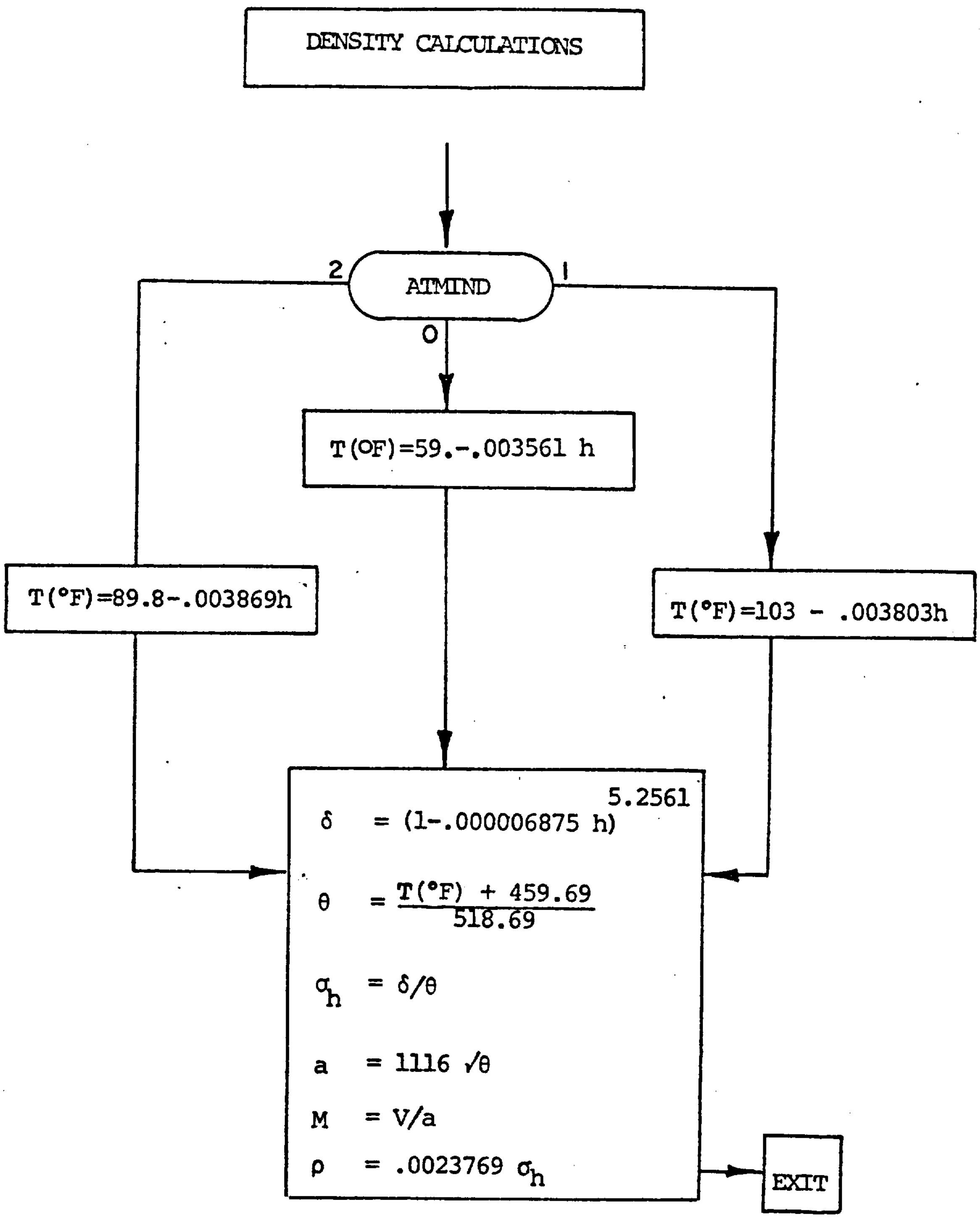

INPUT: h

ATMIND 0 STD ATMOS

1 HOT ATMOS

2 TROPICAL ATMOS

OUTPUT: δ, θ, σ_h, a, M, ρ

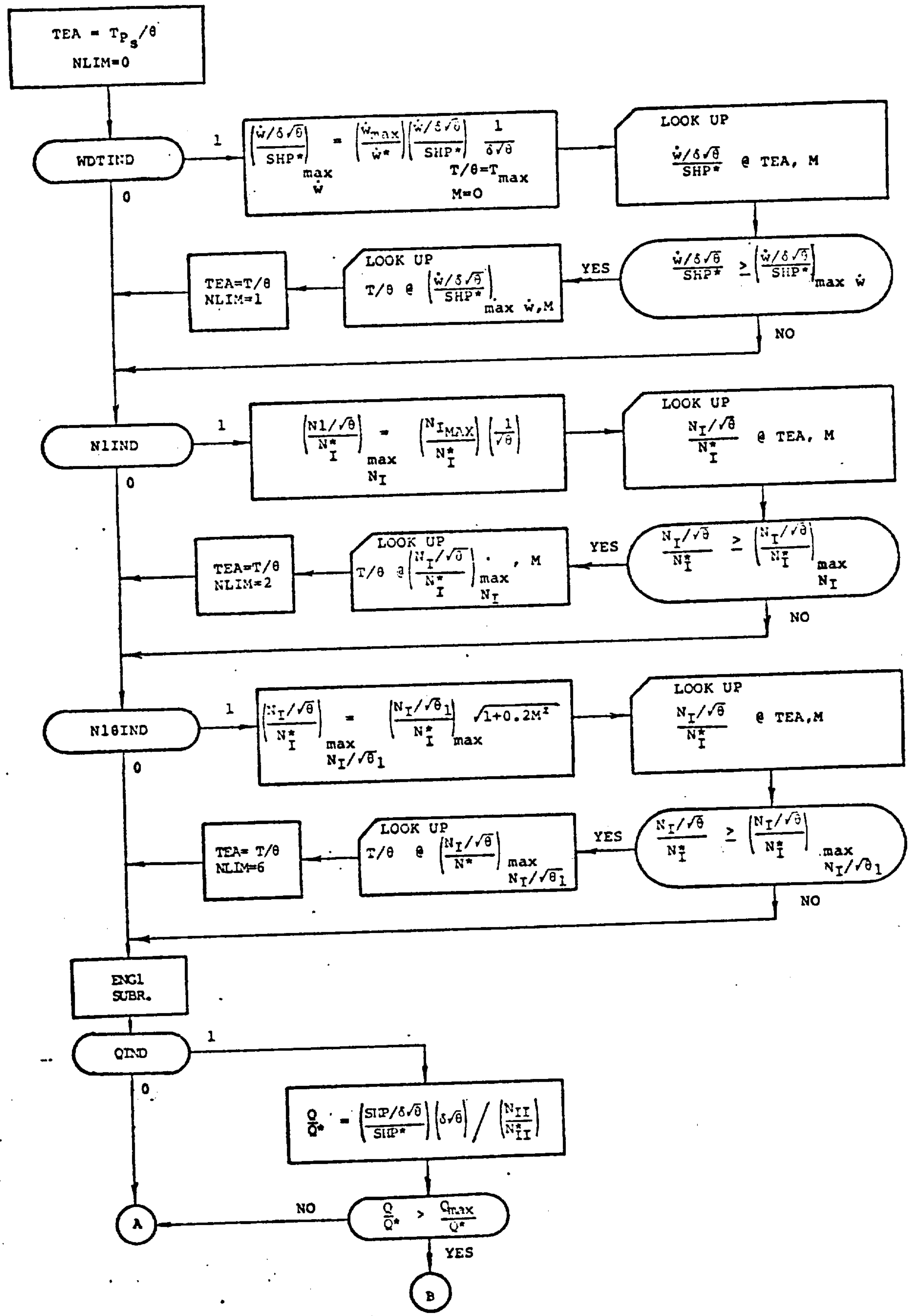

ENGINE ROUTINE POWER AVAILABLE

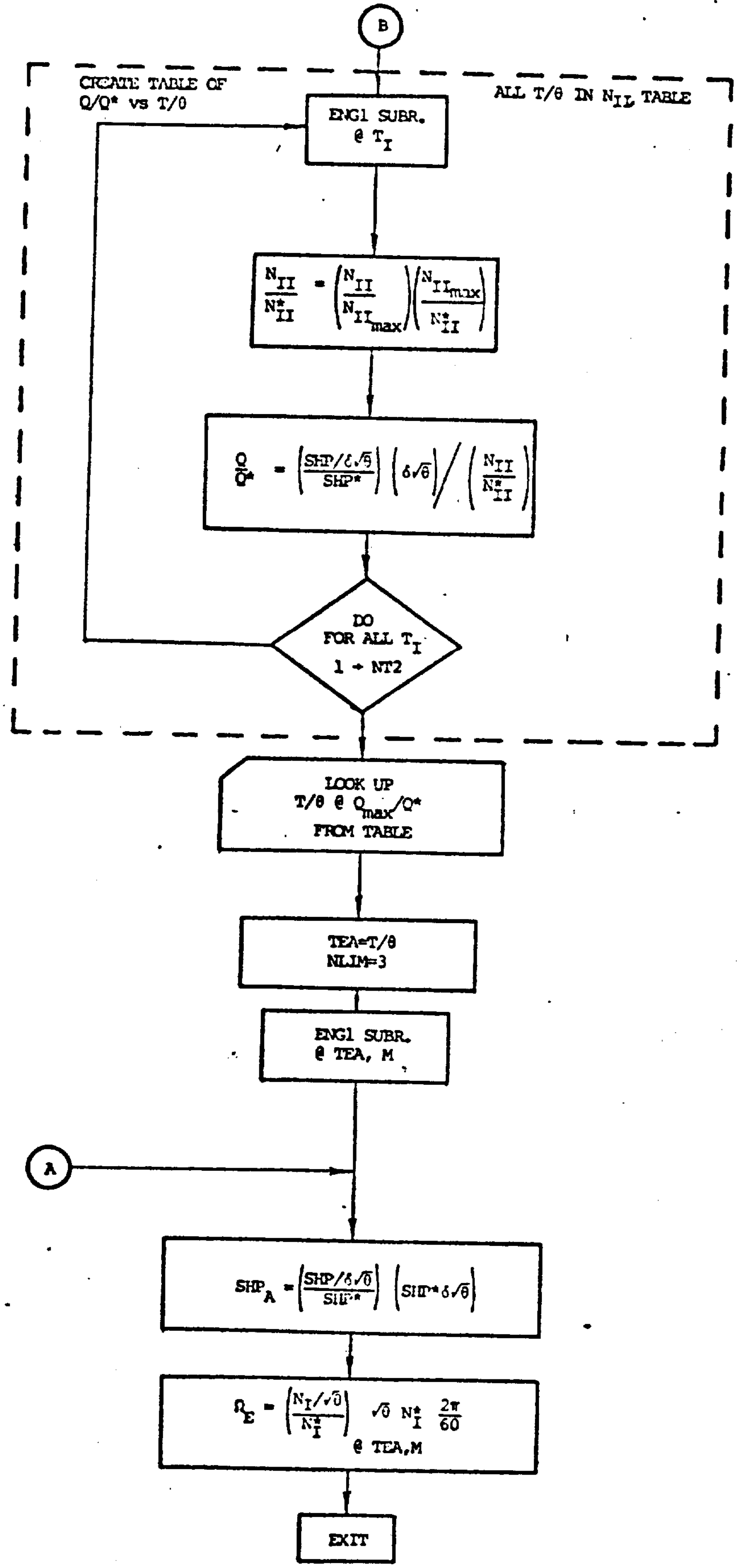

ENGINE ROUTINE POWER AVAILABLE

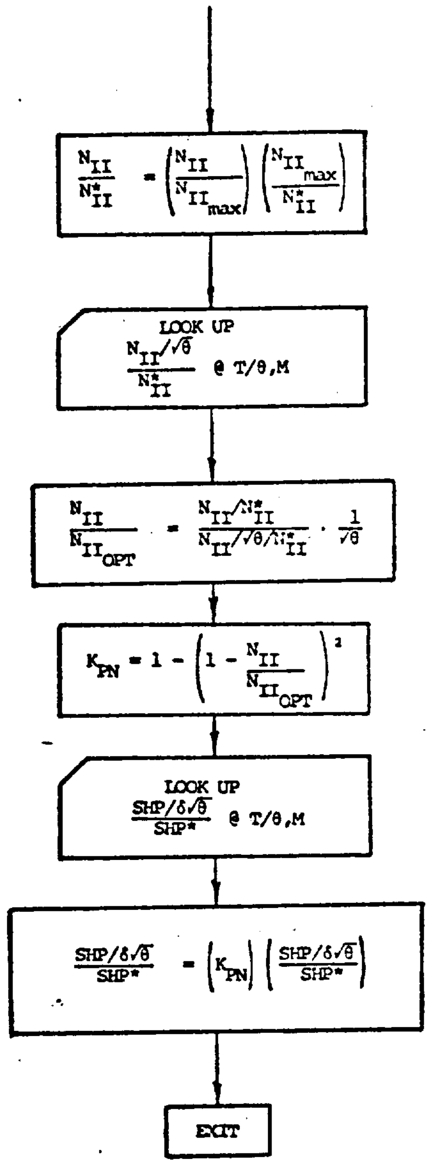

FLOW CHART FOR SUBROUTINE ENG 1 OF ENGINE ROUTINE

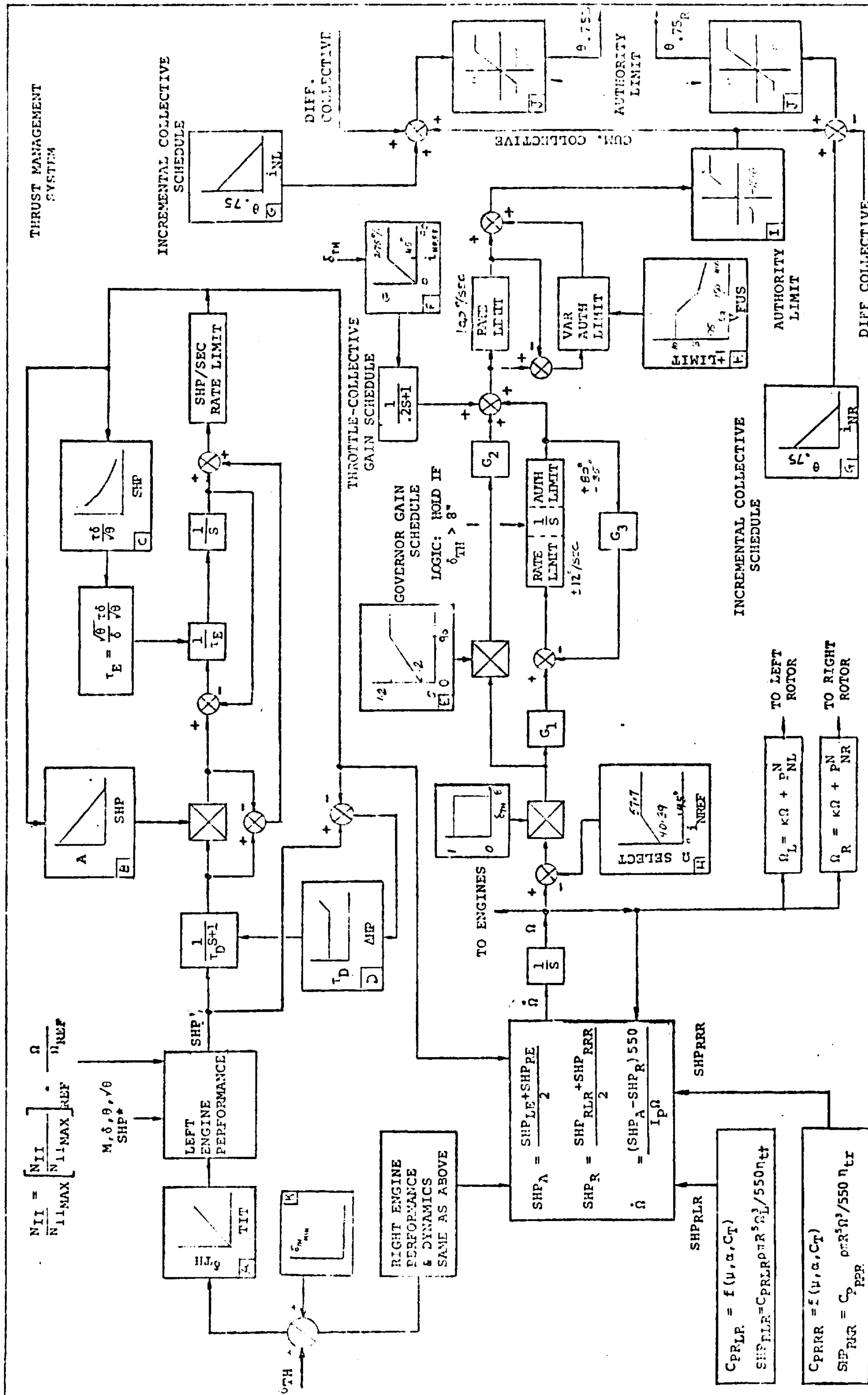
THRUST MANAGEMENT SYSTEM
INCREMENTAL COLLECTIVE SCHEDULE
DIFF. COLLECTIVE
AUTHORITY LIMIT
CUM. COLLECTIVE
SHEET
SHP/SEC RATE LIMIT
THROTTLE-COLLECTIVE GAIN SCHEDULE
RATE LIMIT
VAR AUTH LIMIT
AUTHORITY LIMIT
DIFF COLLECTIVE
GOVERNOR GAIN SCHEDULE
LOGIC: HOLD IF
RATE LIMIT
AUTH LIMIT
INCREMENTAL COLLECTIVE SCHEDULE
TO LEFT ROTOR
TO RIGHT ROTOR
SELECT
TO ENGINES
LEFT ENGINE PERFORMANCE
RIGHT ENGINE PERFORMANCE & DYNAMICS SAME AS ABOVE

ROTOR CONTROL COORDINATE AXIS TRANSFORM

LEFT

$$A1''_{CL} = A1'_{CL} \cos \phi_P + B1'_{CL} \sin \phi_P$$

$$B1''_{CL} = -A1'_{CL} \sin \phi_P + B1'_{CL} \cos \phi_P$$

$$A1_{CL} = A1''_{CL} \cos \xi_{HL} - B1''_{CL} \kappa \sin \xi_{HL}$$

$$B1_{CL} = A1''_{CL} \kappa \sin \xi_{HL} + B1''_{CL} \cos \xi_{HL}$$

NOTE: ϕ_P is the control phase angle. ϕ_P is positive for the control axis moved opposite to rotor rotation.

RIGHT

$$A1''_{CR} = A1'_{CR} \cos \phi_P + B1'_{CR} \sin \phi_P$$

$$B1''_{CR} = -A1'_{CR} \sin \phi_P + B1'_{CR} \cos \phi_P$$

$$A1_{CR} = A1''_{CR} \cos \xi_{HR} + B1''_{CR} \kappa \sin \xi_{HR}$$

$$B1_{CR} = -A1''_{CR} \kappa \sin \xi_{HR} + B1''_{CR} \cos \xi_{HR}$$

CENTER OF GRAVITY CALCULATION

C.G. LOCATION RELATIVE TO PIVOT

$$X_{CG} = \frac{m_f \ell_f + m_w \ell_w}{m} + \ell \left(\frac{m_N}{m}\right)\left[\cos\,(i_{NL}-\lambda) + \cos\,(i_{NR}-\lambda)\right]$$

$$Z_{CG} = \frac{m_f h_f + m_w h_w}{m} - \ell \left(\frac{m_N}{m}\right)\left[\sin\,(i_{NL}-\lambda) + \sin\,(i_{NR}-\lambda)\right]$$

C.G. VELOCITY RELATIVE TO PIVOT

$$\dot{X}_{CG} = -\ell \left(\frac{m_N}{m}\right)\left[\dot{i}_{NL}\,\sin\,(i_{NL}-\lambda) + \dot{i}_{NR}\,\sin\,(i_{NR}-\lambda)\right]$$

$$\dot{Z}_{CG} = -\ell \left(\frac{m_N}{m}\right)\left[\dot{i}_{NL}\,\cos\,(i_{NL}-\lambda) + \dot{i}_{NR}\,\cos\,(i_{NR}-\lambda)\right]$$

C.G. ACCELERATION RELATIVE TO PIVOT

$$\ddot{X}_{CG} = -\ell \left(\frac{m_N}{m}\right)\Big[\ddot{i}_{NL}\,\sin\,(i_{NL}-\lambda) + \dot{i}_{NL}^2\,\cos\,(i_{NL}-\lambda)$$

$$+ \ddot{i}_{NR}\,\sin\,(i_{NR}-\lambda) + \dot{i}_{NR}^2\,\cos\,(i_{NR}-\lambda)\Big]$$

$$\ddot{Z}_{CG} = -\ell \left(\frac{m_N}{m}\right)\Big[\ddot{i}_{NL}\,\cos\,(i_{NL}-\lambda) - \dot{i}_{NL}^2\,\sin\,(i_{NL}-\lambda)$$

$$+ \ddot{i}_{NR}\,\cos\,(i_{NR}-\lambda) - \dot{i}_{NR}^2\,\sin\,(i_{NR}-\lambda)\Big]$$

FUSELAGE PIVOT VELOCITY

$$U_P = U - Z_{CG}q - \dot{X}_{CG}$$

$$V_P = V + Z_{CG}p - X_{CG}r$$

$$W_P = W + X_{CG}q - \dot{Z}_{CG}$$

VELOCITIES OF AIRCRAFT COMPONENTS

LEFT WING A.C. VELOCITY - BODY AXES

$$U'_{LW} = U_P + Z_{WAC}q + Y_{WAC}r + q\ h_{1_{LWAC}}$$

$$V'_{LW} = V_P + X_{WAC}r - Z_{WAC}p - p\ h_{1_{LWAC}}$$

$$W'_{LW} = W_P - Y_{WAC}p - X_{WAC}q + \dot{h}_{1_{LWAC}}$$

ROTOR WING A.C. VELOCITY - BODY AXES

$$U'_{RW} = U_P + Z_{WAC}q - Y_{WAC}r + q\ h_{1_{RWAC}}$$

$$V'_{RW} = V_P + X_{WAC}r - Z_{WAC}p - p\ h_{1_{RWAC}}$$

$$W'_{RW} = W_P + Y_{WAC}p - X_{WAC}q + \dot{h}_{1_{RWAC}}$$

LEFT ROTOR HUB VELOCITY - BODY AXES

$$U'_{RL} = U_P + r\ Y_N - L_S \sin i_{NL}\ (\dot{i}_{NL} + q) + q\ h_{1_L}$$

$$V'_{RL} = V_P + L_S\ (r \cos i_{NL} + p \sin i_{NL}) - p\ h_{1_L}$$

$$W'_{RL} = W_P - p\ Y_N - L_S(\dot{i}_{NL} + q) \cos i_{NL} + \dot{h}_{1_L}$$

RIGHT ROTOR HUB VELOCITY - BODY AXES

$$U'_{RR} = U_P - r\ Y_N - L_S \sin i_{NR}\ (\dot{i}_{NR} + q) + q\ h_{1_R}$$

$$V'_{RR} = V_P + L_S\ (r \cos i_{NR} + p \sin i_{NR}) - p\ h_{1_R}$$

$$W'_{RR} = W_P + p\ Y_N - L_S\ (\dot{i}_{NR} + q) \cos i_{NR} + \dot{h}_{1_R}$$

LEFT ROTOR HUB VELOCITY - SHAFT AXES

$$U_{RL} = U'_{RL} \cos i_{NL} - W'_{RL} \sin i_{NL}$$

$$V_{RL} = V'_{RL}$$

$$W_{RL} = U'_{RL} \sin i_{NL} + W'_{RL} \cos i_{NL}$$

RIGHT ROTOR HUB VELOCITY - SHAFT AXES

$$U_{RR} = U'_{RR} \cos i_{NR} - W'_{RR} \sin i_{NR}$$

$$V_{RR} = V'_{RR}$$

$$W_{RR} = U'_{RR} \sin i_{NR} + W'_{RR} \cos i_{NR}$$

LEFT WING A.C. VELOCITY - CHORD AXES

$$U_{LW} = U'_{LW} \cos i_W - W'_{LW} \sin i_W$$

$$V_{LW} = V'_{LW}$$

$$W_{LW} = U'_{LW} \sin i_W + W'_{LW} \cos i_W$$

RIGHT WING A.C. VELOCITY - CHORD AXES

$$U_{RW} = U'_{RW} \cos i_W - W'_{RW} \sin i_W$$

$$V_{RW} = V'_{RW}$$

$$W_{RW} = U'_{RW} \sin i_W + W'_{RW} \cos i_W$$

HORIZONTAL STABILIZER A.C. VELOCITY - BODY AXES

$$U_{HT} = U_P + Z_{HT}q$$

$$V_{HT} = V_P + X_{HT}r - Z_{HT}p$$

$$W_{HT} = W_P - X_{HT}q$$

VERTICAL FIN A.C. VELOCITY - BODY AXES

RIGHT FIN

$$U_{VT_R} = U_P + Z_{VT}q - Y_{VT}r$$

$$V_{VT_R} = V_P + X_{VT}r - Z_{VT}p$$

$$W_{VT_R} = W_P - X_{VT}q + Y_{VT}p$$

LEFT FIN

$$U_{VT_L} = U_P + Z_{VT}q + Y_{VT}r$$

$$V_{VT_L} = V_P + Y_{VT}r - Z_{VT}p$$

$$W_{VT_L} = W_P - X_{VT}q - Y_{VT}p$$

WING AERODYNAMICS

CALCULATE ROTOR INTERFERENCE TERMS:

$$\tau_{RR} = \alpha_{RR}$$

$$R_{RR} = T_R$$

$$V_{*_R} = \frac{V_{RR}}{\sqrt{\frac{|R_{RR}|+10}{2\rho A}}} \quad ; \quad v_{i_R} = v_{*_R}\sqrt{\frac{|R_{RR}|+10}{2\rho A}}$$

$$v_{*_R}^4 + 2 V_{*_R} v_{*_R}^3 \cos \tau_{RR} + v_{*_R}^2 V_{*_R}^2 = 1 \text{ (Solve for } v_{*_R})$$

$$\varepsilon_{P_{RR}} = K_S \operatorname{Tan}^{-1}\left[\frac{\sqrt{W_{RR}^2 + V_{RR}^2}}{2v_{i_R} + U_{RR}}\right] \text{ limit } 90°$$

$$C_{TS_{RR}} = \frac{\cos(\tau_{RR} - \alpha_{RR})}{\cos(\tau_{RR} - \alpha_{RR}) + \frac{V_{*_R}^2}{4}}$$

$$\tau_{LR} = \alpha_{LR}$$

$$R_{LR} = T_L$$

$$V_{*_L} = \frac{V_{LR}}{\sqrt{\frac{|R_{LR}|+10}{2\rho A}}} \quad ; \quad v_{i_L} = v_{*_L}\sqrt{\frac{|R_{LR}|+10}{2\rho A}}$$

$$v_{*_L}^4 + 2 V_{*_L} v_{*_L}^3 \cos \tau_{LR} + v_{*_L}^2 V_{*_L}^2 = 1 \text{ (Solve for } v_{*_L})$$

$$\varepsilon_{P_{LR}} = K_S \operatorname{Tan}^{-1}\left[\frac{\sqrt{W_{LR}^2 + V_{LR}^2}}{2V_{i_L} + U_{L_R}}\right] \text{ limit } 90°$$

$$C_{TS_{LR}} = \frac{\cos(\tau_{LR} - \alpha_{LR})}{\cos(\tau_{LR} - \alpha_{LR}) + \frac{V_{*_L}^2}{4}}$$

$$\xi_{HR} = \mathrm{Tan}^{-1}\ [V_{RR}/(W_{RR} + \varepsilon_{WRR}\ U_{RR})]$$ Used in rotor transformations

$$\xi_{HL} = \mathrm{Tan}^{-1}\ [V_{RL}/(W_{RL} + \varepsilon_{WRL}\ U_{RL})]$$

$$\bar{\xi} = (\xi_{HR} + \xi_{HL})/2 \qquad \bar{\varepsilon}_P = (\varepsilon_{PRR} + \varepsilon_{PLR})/2$$

$$\bar{\alpha}_R = (\alpha_{RR} + \alpha_{LR})/2 \qquad \bar{i}_N = (i_{NL} + i_{NR})/2$$

$$D_S = D\left[\frac{W_{RR}^2 + (U_{RR} + v_{i_R})^2}{W_{RR}^2 + (U_{RR} + 2v_{i_R})^2}\right]^{0.25}$$

$$\xi_{R1} = [L_S - PC\ \mathrm{Cos}\ (\bar{i}_N - i_W) + h_P\ \mathrm{Sin}\ (\bar{i}_N - i_W)]\ \mathrm{Tan}\ \bar{\varepsilon}_P\ \mathrm{Sin}\ \bar{\xi}$$

$$\xi_{R2} = \sqrt{\frac{D_S^2}{4} - \left[\xi_{R1}\ \mathrm{Cot}\ \bar{\xi} + PC\ \mathrm{Sin}\ (\bar{i}_N - i_W) + h_P\ \mathrm{Cos}\ (\bar{i}_N - i_W)\right]^2}$$

If $\xi_{R2} \leq 0$ or imaginary, set $\xi_{R2} = 0$ and $\xi_{R1} = 0$

If $|\bar{\varepsilon}_P| > 89°$ set $= 89°$ and $\xi_{R2} = \frac{D_S}{2}$

Form ξ_{R3}, ξ_{R4} by setting $PC = PC - c_W$

If $\xi_{R4} \leq 0$ or imaginary, set $\xi_{R4} = 0$ and $\xi_{R3} = 0$

$R_S = D_S/2$

$$c_W' = c_W - PC + \frac{R_S\ \mathrm{Cos}\ \bar{\varepsilon}_P - (L_S\ \mathrm{Sin}\ \bar{\varepsilon}_P + h_P\ \mathrm{Cos}\ \bar{i}_N - i_W - \bar{\varepsilon}_P)}{\mathrm{Sin}\ (\bar{i}_N - i_W - \bar{\varepsilon}_P)}$$

If $c_W' \geq c$ set $c_W' = c$

If $c_W' < o$ set $c_W' = 0$

$$S_{i_{RW}} = c'_w/2 \quad [\xi_{R1} + \xi_{R2} + \xi_{R3} + \xi_{R4}] = S_{i_R}$$

$$(S_i/S)_{RW} = 2 \ (S_{i_R}/S_w)$$

$$S_{i_T} = c'_w \ [\xi_{R2} + \xi_{R4}]$$

$$S_{i_{LW}} = S_{i_T} - S_{i_R} = S_{i_L}$$

$$(S_i/S)_{LW} = 2 \ (S_{i_L}/S_w)$$

$$(AR_i)_{LW} = (S_{i_L}/c_w^2)$$

$$(AR_i)_{RW} = (S_{i_R}/c_w^2)$$

$$AR_w = S_w/c_w^2 \qquad \text{(FROM PREPROCESSOR)}$$

$$(C_{L\alpha i}/C_{L\alpha})_{LW} = \frac{\pi}{\pi + C_{L\alpha w} \ [1/(AR_i)_{LW} - 1/AR_w]}$$

$$(C_{L\alpha i}/C_{L\alpha})_{RW} = \frac{\pi}{\pi + C_{L\alpha w} \ [1/(AR_i)_{RW} - 1/AR_w]}$$

$$K'_{AL} = \frac{V_L^* + (C_{L\alpha i}/C_{L\alpha})_{LW} \ v_L^*}{V_L^* + v_L^*}$$

$$K'_{AR} = \frac{V_R^* + (C_{L\alpha i}/C_{L\alpha})_{RW} \ v_R^*}{V_R^* + v_R^*}$$

$$q_{S_{LW}} = 0.5\,\rho \left[[W_{LW} - 2v_{i_L} \text{ Sin } (i_{N_L} - i_W)]^2 + [U_{LW} + 2v_{i_L} \text{ Cos } (i_{N_L} - i_W)]^2 \right]$$

$$q_{S_{RW}} = 0.5\,\rho \left[[W_{RW} - 2v_{i_R} \text{ Sin } (i_{N_R} - i_W)]^2 + [U_{RW} + 2v_{i_R} \text{ Cos } (i_{N_R} - i_W)]^2 \right]$$

$$\bar{q}_S = (q_{S_{RW}} + q_{S_{LW}})/2$$

$$q_F = \rho\,(U^2 + V^2 + W^2)/2$$

$$\frac{q}{q_{SRW}} = \frac{q_F}{q_{SRW}} \quad ; \quad \frac{q}{q_{SLW}} = \frac{q_F}{q_{SLW}}$$

$$\frac{q}{q_S} = \left[\frac{q}{q_{SRW}} + \frac{q}{q_{SLW}}\right]/2$$

Wing height for ground effect:

$$h_{W_{C/4}} = -Z_{DOWN} + (X_{WAC} - X_{CG}) \text{ Sin } \theta + (Z_{CG} - Z_{WAC}) \text{ Cos } \theta$$

WING ANGLE OF ATTACK AND SIDESLIP

$$\alpha_{LWO} = \sin^{-1}\left[\frac{W_{LW}}{\sqrt{U_{LW}^2 + W_{LW}^2}}\right] + \theta_{tLWAC}$$

$$\alpha_{RWO} = \sin^{-1}\left[\frac{W_{RW}}{\sqrt{U_{RW}^2 + W_{RW}^2}}\right] + \theta_{tRWAC}$$

$$\beta_{LWO} = \sin^{-1}\left[\frac{V_{LW}}{\sqrt{U_{LW}^2 + V_{LW}^2 + W_{LW}^2}}\right]$$

$$\beta_{RWO} = \sin^{-1}\left[\frac{V_{RW}}{\sqrt{U_{RW}^2 + V_{RW}^2 + W_{RW}^2}}\right]$$

$$\bar{\alpha}_W = (\alpha_{LWO} + \alpha_{RWO})/2$$

$$\alpha'_{LWO} = \alpha_{LWO} - i_W - \theta_{tLWAC}$$

$$\alpha'_{RWO} = \alpha_{RWO} - i_W - \theta_{tRWAC}$$

$$\alpha_{LWSSO} = \tan^{-1}\left[\frac{W_{LW} - 2v_{iL}\,\mathrm{Sin}\,(i_{NL} - i_W)}{U_{LW} + 2v_{iL}\,\mathrm{Cos}\,(i_{NL} - i_W)}\right] + \theta_{tLWAC}$$

$$\alpha_{RWSSO} = \tan^{-1}\left[\frac{W_{RW} - 2v_{iR}\sin(i_{NR} - i_W)}{U_{RW} + 2v_{iR}\cos(i_{NR} - i_W)}\right] + \theta_{tRWAC}$$

CALCULATION OF INCREMENTAL LIFT, DRAG AND MOMENT COEFFICIENTS

CALCULATE:*

$$C_{LLW_O} = C_L \text{ @ } \alpha = \alpha_{LW_{SS_O}},\ \delta = \delta_{LW} + \delta_f$$

$$C_{DLW_O} = C_D \text{ @ } \alpha = \alpha_{LW_{SS_O}},\ \delta = \delta_{LW} + \delta_f$$

$$C_{LRW_O} = C_L \text{ @ } \alpha = \alpha_{RW_{SS_O}},\ \delta = \delta_{RW} + \delta_f$$

$$C_{DRW_O} = C_D \text{ @ } \alpha = \alpha_{RW_{SS_O}},\ \delta = \delta_{RW} + \delta_f$$

$$C^*_{LLW_O} = C_L \text{ @ } \alpha = \alpha_{LW_O},\ \delta = \delta_{LW} + \delta_f$$

$$C^*_{DLW_O} = C_D \text{ @ } \alpha = \alpha_{LW_O},\ \delta = \delta_{LW} + \delta_f$$

$$C^*_{LRW_O} = C_L \text{ @ } \alpha = \alpha_{RW_O},\ \delta = \delta_{RW} + \delta_f$$

$$C^*_{DRW_O} = C_D \text{ @ } \alpha = \alpha_{RW_O},\ \delta = \delta_{RW} + \delta_f$$

$$C_{L_O} = C_L \text{ @ } \alpha = \alpha_F + i_W,\ \delta = \delta_f$$

USING THE FOLLOWING EQUATIONS:

$$\Delta C_{L_\delta} = a_7\delta \qquad (0^\circ \le \delta \le \delta_2)$$

$$= a_8 + a_9\delta + a_{10}\delta^2 \qquad (\delta_2 < \delta \le \delta_3)$$

$$= a_{11} + a_{12}\delta + a_{13}\delta^2 \qquad (\delta > \delta_3)$$

$$\Delta C_{DO_\delta} = a_{29}|\delta| + a_{30}\delta^2 \qquad (0 \le \delta \le \delta_5)$$

$$= a_{31} + a_{32}\delta \qquad (\delta > \delta_5)$$

*DO for i_N = 90° and 0°; interpolate linearly for i_N

$$\alpha_{NL}^{+} = a_0 + a_1\delta \qquad (0° \leq \delta \leq \delta_1)$$

$$= a_2 \qquad (\delta > \delta_1)$$

$$\alpha_{NL}^{-} = a_3 + a_4\delta \qquad (0° \leq \delta \leq \delta_1)$$

$$= a_5 \qquad (\delta > \delta_1)$$

If $\alpha_{NL}^{-} \leq \alpha \leq \alpha_{NL}^{+}$ calculate:

$$C_L = a_6 + C'_{L\alpha_W}\alpha + \Delta C_{L_\delta}$$

$$C_{LW_1} = C_L$$

$$C_{LW_2} = C_{LW_1} - \Delta C_{L_\delta}$$

$$C_D = C_{DO_W} + a_{26}\, C_{LW_2}^2 + a_{27}\, C_{LW_1}^2 + a_{28}\,(C_{LW_1} - C_{LW_2})^2 + \Delta C_{DO_\delta}$$

If $\alpha^{+}_{NL} < \alpha \leq \alpha^{+}_{NL} + a_{18}$ calculate:

$$C'_{L_{NL}} = a_6 + C'_{L\alpha_W} \alpha^{+}_{NL} + \Delta C_{L\delta}$$

$$\alpha_{DUM} = \alpha - \alpha^{+}_{NL} + a_0$$

$$\Delta C_{L_{NL}} = a_{20} + a_{21} \alpha_{DUM} + a_{22} \alpha^{2}_{DUM}$$

$$C_L = C'_{L_{NL}} + \Delta C_{L_{NL}}$$

$$C_{LW_1} = a_6 + C'_{L_{\alpha W}} \alpha + \Delta C_{L\delta}$$

$$C_{LW_2} = a_6 + C_{L\alpha_W} \alpha$$

$$C_D = C_{DO_W} + a_{26} C^{2}_{LW_2} + a_{27} C^{2}_{LW_1} + a_{28} (C_{LW_1} - C_{LW_2})^2$$

$$+ \Delta C_{DO_\delta} + \Delta C_{D_{SP}}$$

If $\alpha^{+}_{NL} + a_{18} < \alpha \leq 90°$ calculate:

$$C_L = (a_6 + C'_{L\alpha_W} \alpha^{+}_{NL} + \Delta C_{L_\delta})(90° - \alpha)/(90° - \alpha^{+}_{NL} - a_{18})$$

$$\alpha_2 = \alpha^{+}_{NL} + a_{18}$$

$$C_{LW_1} = a_6 + C'_{L\alpha_W} \alpha_2 + \Delta C_{L_\delta}$$

$$C_{LW_2} = a_6 + C'_{L\alpha_W} \alpha_2$$

$$C_{D_1} = C_{DO_W} + a_{26}\, C_{LW_2}^2 + a_{27}\, C_{LW_1}^2 + a_{28}\, (C_{LW_1} - C_{LW_2})^2$$
$$+ \Delta C_{DO_\delta}$$

$$C_D = C_{D_1} + (1.2 - C_{D_1})\ (\alpha - \alpha_2)/(90° - \alpha_2)$$

If $\bar{\alpha}_{NL} - a_{19} \leq \alpha < \alpha_{\overline{NL}}$ calculate:

$$C'_{L_{NL}} = a_6 + C'_{L_{\alpha_w}}\ \alpha_{\overline{NL}} + \Delta C_{L_\delta}$$

$$\alpha_{DUM} = \alpha - \alpha_{\overline{NL}} + a_3$$

$$\Delta C_{L_{NL}} = a_{23} + a_{24}\, \alpha_{DUM} + a_{25}\, \alpha_{DUM}^2$$

$$C_L = C'_{L_{NL}} + \Delta C_{L_{NL}}$$

$$C_{LW_1} = a_6 + C'_{L_{\alpha_W}}\ \alpha + \Delta C_{L_\delta}$$

$$C_{LW_2} = a_6 + C'_{L_{\alpha_w}}\ \alpha$$

$$C_D = C_{D_{W_o}} + a_{26}\, C_{L_{W_2}}^2 + a_{27}\, C_{L_{W_1}}^2 + a_{28}\, (C_{L_{W_1}} - C_{L_{W_2}})^2$$
$$+ \Delta C_{D_{O_\delta}}$$

If $-90° \leq \alpha \leq \alpha_{\overline{NL}} - a_{19}$ calculate:

$$\alpha_1 = \alpha_{\overline{NL}} - a_{19}$$

$$C'_{L_{NL}} = a_6 + C'_{L_{\alpha_w}}\ \alpha_{\overline{NL}} + \Delta C_{L_\delta}$$

$$\alpha_{DUM} = \alpha - \overline{\alpha_{NL}} + a_3$$

$$\Delta C_{L_{NL}} = a_{23} + a_{24}\ \alpha_{DUM} + a_{25}\ \alpha_{DUM}^2$$

$$C_L = C'_{L_{NL}} + \Delta C_{L_{NL}} \qquad (\alpha \geq \alpha_1)$$

$$= C'_{L_{NL}}\ (90° + \alpha)/(90° + \alpha_1) \qquad (\alpha < \alpha_1)$$

$$C_{L_{W_1}} = a_6 + C'_{L_{\alpha_W}}\ \alpha_1 + \Delta C_{L_\delta}$$

$$C_{L_{W_2}} = a_6 + C'_{L_{\alpha_W}}\ \alpha_1$$

$$C_{D_1} = C_{D_{W_o}} + a_{26}\ C_{L_{W_2}}^2 + a_{27}\ C_{L_{W_1}}^2 + a_{28}\ (C_{L_{W_1}} - C_{L_{W_2}})^2$$

$$+ \Delta C_{D_{o_\delta}}$$

$$C_D = C_{D_1} - (1.2 - C_{D_1})(\alpha - a_3 + a_{19})/(90° + a_3 - a_{19})$$

Stall warning logic:

$$\alpha^+_{stall} = 14 + \delta\ (.000122\ i_N - .058) \qquad 0 \leq \delta \leq 122°$$

$$= 9.42 + .0150\ i_N \qquad \delta > 122°$$

$$\alpha^+_{stall} = -21$$

Actuate warning if

either $\alpha^+_{stall} < \alpha_{RWSSO} < \alpha^-_{stall}$

or $\alpha^+_{stall} < \alpha_{RWO} < \alpha^-_{stall}$

CALCULATE:

$$C_{M_{LW}} = C_M \text{ @ } \alpha = \alpha_{LW_{SS_O}},\ \delta = \delta_f + \delta_{a_{LW}}$$

$$C_{M_{RW}} = C_M \text{ @ } \alpha = \alpha_{RW_{SS_O}},\ \delta = \delta_f + \delta_{a_{RW}}$$

$$C^{*'}_{M_{LW_O}} = C_M \text{ @ } \alpha = \alpha_{LW_O},\ \delta = \delta_f + \delta_{a_{LW}}$$

$$C^{*'}_{M_{RW_O}} = C_M \text{ @ } \alpha = \alpha_{RW_O},\ \delta = \delta_f + \delta_{a_{RW}}$$

AS FOLLOWS:

If $\alpha_1 \leq \alpha \leq \alpha_2$

Calculate $C'_M = b_2 + b_3\,\alpha$

$$\Delta C_{M_\delta} = b_4 + b_5\,\delta + b_6\,\delta^2 + b_7\,i_N$$

$$C_M = C'_M + \Delta C_{M_\delta}$$

If $\alpha > \alpha_2$

$$C'_M = b_2 + b_3\,\alpha_2 + \Delta C_{M_\delta}$$

$$C_M = C'_M\,(90 - \alpha)/(90 - \alpha_2)$$

If $\alpha < \alpha_1$

$$C'_M = b_2 + b_3\,\alpha_1 + \Delta C_{M_\delta}$$

$$C_M = C'_M\,(90 + \alpha)/(90 + \alpha_1)$$

CALCULATE:

$$C'''_{L_{LW}} = C_{L_{LWO}};\quad C'''_{D_{LW}} = C_{D_{LW}};\quad C''_{M_{LW}} = C_{M_{LW}}$$

$$C'''_{L_{RW}} = C_{L_{RWO}};\quad C'''_{D_{RW}} = C_{D_{RW}};\quad C''_{M_{RW}} = C_{M_{RW}}$$

$$C''_{L_{LWMAX}} = C_{L_{MAX}} + \Delta C_{L_{\delta}} + \Delta C_{L_{SP}}$$

$$C''_{L_{RWMAX}} = C_{L_{MAX}} + \Delta C_{L_{\delta}} + \Delta C_{L_{SP}}$$

$$C^{*'}_{L_{RW}} = C^{*}_{L_{RWO}};\quad C^{*'}_{D_{RW}} = C^{*'}_{D_{RWO}};\quad C^{*}_{M_{RW}} = C^{*'}_{M_{RWO}}$$

$$C^{*'}_{L_{LW}} = C^{*}_{L_{LWO}};\quad C^{*'}_{D_{LW}} = C^{*'}_{D_{LWO}};\quad C^{*}_{M_{LW}} = C^{*'}_{M_{LWO}}$$

$$C^{*}_{L_{LWMAX}} = C''_{L_{LWMAX}};\quad PGFW = \frac{2 + \sqrt{AR_W^2 + 4}}{2 + \sqrt{AR_W^2\,(1 - M^2) + 4}}$$

$$C^{*}_{L_{RWMAX}} = C''_{L_{RWMAX}}$$

$$\overline{C}_L = C_{L_0}\,(ag/a)w \times PGFW;\quad (ag/a)_W = f_1\,(h_{WC/4})$$

$$C''^{IGE}_{L_{LW}} = C'''_{L_{LW}}\,(ag/a)w \times PGFW;\quad C''^{IGE}_{L_{RW}} = C'''_{L_{RW}}\,(ag/a)w \times PGFW$$

$$C^{*IGE}_{L_{LW}} = C^{*'}_{L_{LW}}\,(ag/a)w \times PGFW;\quad C^{*IGE}_{L_{RW}} = C^{*'}_{L_{RW}}\,(ag/a)w \times PGFW$$

$$\Delta C''^{IGE}_{DLW} = K_{99}\ (C''^{IGE}_{LLW} - C'''_{LLW})^2/\pi AR_w;\ \ \Delta C''^{IGE}_{DRW} = K_{99}(C''^{IGE}_{LRW} - C'''_{LRW})^2/\pi AR_w;$$

$$\Delta C^{*IGE}_{DLW} = K_{99}\ (C^{*IGE}_{LLW} - C^{*\prime}_{LLW})^2/\pi AR_w;\ \ \Delta C^{*IGE}_{DRW} = K_{99}(C^{*IGE}_{LRW} - C^{*\prime}_{LRW})^2/\pi AR_w$$

IF: $C''^{IGE}_{LLW} \geq C''_{LLW\ MAX}$; SET $\Delta C''^{IGE}_{DLW} = 0.0$ & $C''^{IGE}_{LLW} = C''_{LLW\ MAX}$

IF: $C''^{IGE}_{LRW} \geq C''_{LRW\ MAX}$; SET $\Delta C''^{IGE}_{DRW} = 0.0$ & $C''^{IGE}_{LRW} = C''_{LRW\ MAX}$

IF: $C^{*IGE}_{LLW} \geq C^{*}_{LLW\ MAX}$; SET $\Delta C^{*IGE}_{DLW} = 0.0$ & $C^{*IGE}_{LLW} = C^{*}_{LLW\ MAX}$

IF: $C^{*IGE}_{LRW} \geq C^{*}_{LRW\ MAX}$; SET $\Delta C^{*IGE}_{DRW} = 0.0$ & $C^{*IGE}_{LRW} = C^{*}_{LRW\ MAX}$

IF: $(ag/a) > 1.0$; SET $K_{99} = -1.0$

$(ag/a) \leq 1.0$; SET $K_{99} = +1.0$

<u>CALCULATE</u>

$$C''_{LLW} = C''^{IGE}_{LLW}$$

$$C''_{DLW} = C'''_{DLW} + \Delta C''^{IGE}_{DLW}$$

$$C''_{LRW} = C''^{IGE}_{LRW}$$

$$C''_{DRW} = C'''_{DRW} + \Delta C''^{IGE}_{DRW}$$

$$C^{*}_{LLW} = C^{*IGE}_{LLW}$$

$$C^{*}_{DLW} = C^{*\prime}_{DLW} + \Delta C^{*IGE}_{DLW}$$

$$C^{*}_{LRW} = C^{*IGE}_{LRW}$$

$$C^{*}_{DRW} = C^{*\prime}_{DRW} + \Delta C^{*IGE}_{DRW}$$

$$x_L = \alpha_{LWO} - \alpha_{LWSSO}$$

$$x_R = \alpha_{RWO} - \alpha_{RWSSO}$$

$$C_{LSLW} = K'_{A_L} \left[\left(\frac{S_i}{S}\right)_{LW} (C''_{LLW} \cos x_L - C''_{DLW} \sin x_L) + C^*_{LLW} \; q/q_{SLW} \left[1 - \left(\frac{S_i}{S}\right)_{LW}\right]\right]$$

$$C_{LSRW} = K'_{A_R} \left[\left(\frac{S_i}{S}\right)_{RW} (C''_{LRW} \cos x_R - C''_{DRW} \sin x_R) + C^*_{LRW} \; q/q_{SRW} \left[1 - \left(\frac{S_i}{S}\right)_{RW}\right]\right]$$

$$C_{DSLW} = K'_{A_L} \left[\left(\frac{S_i}{S}\right)_{LW} (C''_{LLW} \sin x_L + C''_{DLW} \cos x_L) + C^*_{DLW} \; q/q_{SLW} \left[1 - \left(\frac{S_i}{S}\right)_{LW}\right]\right]$$

$$C_{DSRW} = K'_{A_R} \left[\left(\frac{S_i}{S}\right)_{RW} (C''_{LRW} \sin x_R + C''_{DRW} \cos x_R) + C^*_{DRW} \; q/q_{SRW} \left[1 - \left(\frac{S_i}{S}\right)_{RW}\right]\right]$$

$$C_{MSLW} = K'_{A_L} \left[\left(\frac{S_i}{S}\right)_{LW} (C''_{MLW} + C^*_{MLW} \; q/q_{SLW} \left[1 - \left(\frac{S_i}{S}\right)_{LW}\right]\right]$$

$$C_{MSRW} = K'_{A_R} \left[\left(\frac{S_i}{S}\right)_{RW} (C''_{MRW} + C^*_{MRW} \; q/q_{SRW} \left[1 - \left(\frac{S_i}{S}\right)_{RW}\right]\right]$$

FORCE AND MOMENT TRANSFORMATIONS FROM WING A. C. TO ELASTIC AXIS

PITCHING MOMENT

$$q'_{SRW} = q_{SRW} \cos \beta_F \quad ; \quad q'_{SLW} = q_{SLW} \cos \beta_F$$

$$M^{RW}_{AERO} = C_{MSRW}\, q'_{SRW}\, \frac{S_W}{2}\, c_w - X_{WAC}\, Z^{RW}_{AERO}$$

$$+ Z_{WAC}\, X^{RW}_{AERO}$$

$$M^{LW}_{AERO} = C_{MSLW}\, q'_{SLW}\, \frac{S_W}{2}\, c_w - X_{WAC}\, Z^{LW}_{AERO}$$

$$+ Z_{WAC}\, X^{LW}_{AERO}$$

VERTICAL FORCES

$$Z^{RW'}_{AERO} \quad [-C_{LSRW} \cos \alpha'_{RWO} - C_{DSRW} \sin \alpha'_{RWO}]\, q_{SRW}\, \frac{SW}{2}$$

$$Z^{LW'}_{AERO} = [-C_{LSLW} \cos \alpha'_{LWO} - C_{D_{SLW}} \sin \alpha'_{RWO}]\, q_{SLW}\, \frac{SW}{2}$$

NOTE: $Z^{RW'}_{AERO}$ and $Z^{LW'}_{AERO}$ ARE USED IN VERTICAL BENDING EQUATIONS.

WING FORCE AND MOMENT RESOLUTION - BODY AXES AT C.G.

$$X^{LW}_{AERO} = [-C_{DSLW} \cos \alpha'_{LWO} + C_{LSLW} \sin \alpha'_{LWO}]\ q'_{SLW} \frac{SW}{2}$$

$$X^{RW}_{AERO} = [-C_{DSRW} \cos \alpha'_{RWO} + C_{LSRW} \sin \alpha'_{RWO}]\ q'_{SRW} \frac{SW}{2}$$

$$Y^{LW}_{AERO} = -C_{DSLW}\ q_{SLW} \sin \beta_F \cos \bar{i}_N \frac{SW}{2}$$

$$Y^{RW}_{AERO} = -C_{DSRW}\ q_{SRW} \sin \beta_F \cos \bar{i}_N \frac{SW}{2}$$

$$Z^{LW}_{AERO} = Z^{LW'}_{AERO}$$

$$Z^{RW}_{AERO} = Z^{RW'}_{AERO}$$

$$\mathcal{L}^{W}_{AERO} = (K_{20} + K_{21} \bar{C}_L)\ q_F\ S_W\ b_W \sin \beta_F + K_{\mathcal{L}} (Z^{RW}_{AERO} - Z^{LW}_{AERO}) \bar{Y}_{AC}$$

$$M^{W}_{AERO} = M^{LW}_{AERO} + M^{RW}_{AERO} + X_{CG} (Z^{LW}_{AERO} + Z^{RW}_{AERO})$$

$$- Z_{CG} (X^{LW}_{AERO} + X^{RW}_{AERO})$$

$$N^{W}_{AERO} = (X^{LW}_{AERO} - X^{RW}_{AERO}) \bar{Y}_{AC} + q_F\ S_W\ b_W (K_{22} + K_{23} \bar{C}^2_L) \sin \beta_F$$

HORIZONTAL TAIL AERODYNAMICS

TAIL ALTITUDE FOR GROUND EFFECT

$$h_{Tc/4} = -Z_{DOWN} + (X_{HT} - X_{CG}) \sin\theta + (Z_{CG} - Z_{HT}) \cos\theta$$

$$\ell_{AC} = X_{WAC} - X_{HT}$$

$$GEF = [b_W^2 + 4\,(h_{Tc/4} - h_{Wc/4})^2]/[b_W^2 + 4\,(h_{Tc/4} + h_{Tc/4})^2]$$

ROTOR-ON-TAIL INTERFERENCE

$$\bar{v}_i = (v_{iL} + v_{iR})/2$$

$$v_{iHT} = \left(\frac{v_{iHT}}{\bar{v}_i}\right) K_{H\beta}\, \bar{v}_i \frac{1}{(\tau S + 1)}$$

WHERE $\tau = (L_S \cos \bar{i}_N - X_{HT})/U_P$

$$\frac{v_{iHT}}{\bar{v}_i} = f_2\,(\alpha_F, \bar{i}_N, V_F)$$

AND $K_{H\beta} = f_3\,(|\beta_F|, \bar{i}_N)$

$$U'_{HT} = U_{HT} + v_{iHT} \cos \bar{i}_N$$

$$W'_{HT} = W_{HT} - v_{iHT} \sin \bar{i}_N$$

$$q_{HT} = \frac{1}{2}\rho\,[U'^2_{HT} + V^2_{HT} + W'^2_{HT}]$$

DOWNWASH ANGLE

$$\varepsilon = [\varepsilon_o + \frac{d\varepsilon}{d\alpha}(\bar{\alpha}_W - \ell_{AC}\ \dot{W}/U^2)]\ (1\text{-}GEF)/\sqrt{1-M^2}$$

WHERE $\varepsilon_o = f_4\,(\bar{i}_N, \delta) = 2.55 - .0303\,\bar{i}_N + 4.56\times10^{-4} i_N^2 + .0673\delta - 3.609\times10^{-4}\delta^2$

$$\frac{d\varepsilon}{d\alpha} = f_5(\bar{i}_N, \delta) = 0.317 + .00078\bar{i}_N + 1.008\times10^{-3}|\delta| - 5.567\times10^{-6}\delta^2$$

FOR $\alpha_W > 16°$, $\varepsilon = \varepsilon_{@16}\,(1-(\alpha-16)/12)$

$\alpha_W < -16°$, $\varepsilon = \varepsilon_{@-16}(1+(\alpha+16)/12)$

$|\alpha_W| > 28°$ $\varepsilon = o$

HORIZONTAL TAIL LIFT AND DRAG

$$*\alpha_{HT} = i_{HT} + \mathrm{Tan}^{-1}\ (W'_{HT}/U'_{HT}) - \epsilon \quad U>0$$

$$= i_{HT} + \mathrm{Tan}^{-1}\ (W'_{HT}/U'_{HT}) \quad U<0$$

$$\hat{\alpha}_{HT_+} = (\alpha_{HT_{STALL}} - 2°) + \tau_{HT}\ \delta_e$$

$$\hat{\alpha}_{HT-} = -(\alpha_{HT_{STALL}} - 2°) + \tau_{HT}\ \delta_e$$

$$C_{L\alpha} = C_{L\alpha_{HT}}\ (ag/a)_{HT}\ \text{X PGFHT}$$

WHERE $(ag/a)_{HT} = f_6(h_{TC/4})$, $\text{PGFHT} = \dfrac{2 + \sqrt{AR^2_{HT} + 4}}{2 + \sqrt{AR^2_{HT}(1-M^2)+4}}$

IF: $\hat{\alpha}_{HT_-} \leq \alpha_{e_{HT}} \leq \hat{\alpha}_{HT_+}$

$$C_{L_{HT}} = C_{L\alpha}\ \alpha e_{HT} + C_{LH\beta}\ |\beta_F| \quad ; \quad \alpha_{e_{HT}} = \alpha_{HT} + \tau_{HT}\ \delta_e$$

$$C_{D_{HT}} = C_{DO_{HT}} + C^2_{L_{HT}}/\pi AR_{HT}E_{HT}$$

IF: $\hat{\alpha}_{HT_+} < \alpha_{e_{HT}} \leq 90°$

$$C_{L_{HT}} = C_{L\alpha}\ \hat{\alpha}_{HT_+}\ (90° - \alpha_{e_{HT}})\ /(90° - \hat{\alpha}_{HT_+})$$

$$C_{L_{HT_{STALL}}} = C_{L\alpha}\ \hat{\alpha}_{HT_+}$$

$$C_{D_{HT_{STALL}}} = C_{DO_{HT}} + C^2_{L_{HT_{STALL}}}/\pi AR_{HT}E_{HT}$$

$$C_{D_{HT}} = C_{D_{HT_{STALL}}} + \frac{(\alpha e_{HT} - \hat{\alpha}_{HT_+})(1.1 - C_{D_{HT_{STALL}}})}{90° - \hat{\alpha}_{HT_+}}$$

*This form to be used for resolution of forces and moments only. If $|\alpha_{HT}| > 180°$, $\alpha_{HT} = -(\text{sign}\ \alpha_{HT})\ 360° + \alpha_{HT}$ and use this value to obtain forces and moments.

HORIZONTAL TAIL LIFT AND DRAG (CONTINUED)

IF: $90° < \alpha_{e_{HT}} \leq (180° - .5\ \hat{\alpha}_{HT-})$

$$C_{L_{HT}} = .5\ C_{L\alpha}\ \hat{\alpha}_{HT\_}\ (\alpha_{e_{HT}} - 90°)/(90° - .5\ \alpha_{HT\_})$$

$$C_{L_{HT_{STALL}}} = .5\ C_{L\alpha}\ \hat{\alpha}_{HT\_}$$

$$C_{D_{HT_{STALL}}} = C^2_{L_{HT_{STALL}}}/\pi AR_{HT} E_{HT} + C_{D_{O_{HT}}}$$

$$C_{D_{HT}} = C_{D_{HT_{STALL}}} + \frac{\left(\alpha_{e_{HT}} + .5\ \hat{\alpha}_{HT\_} - 180°\right)\left(1.1 - C_{D_{HT_{STALL}}}\right)}{(.5\ \hat{\alpha}_{HT\_} - 90°)}$$

IF: $(180° - .5\ \hat{\alpha}_{HT-}) \leq \alpha_{e_{HT}} \leq 180°$

$$C_{L_{HT}} = C_{L\alpha}\ (\alpha_{e_{HT}} - 180°)$$

$$C_{D_{HT}} = C_{DO_{HT}} + C^2_{L_{HT}}/\pi AR_{HT} E_{HT}$$

IF: $-90 \leq \alpha_{e_{HT}} < \hat{\alpha}_{HT\_}$

$$C_{L_{HT}} = C_{L\alpha}\ \hat{\alpha}_{HT-}\ (-90° - \alpha_{e_{HT}})/(-90° - \hat{\alpha}_{HT\_})$$

$$C_{L_{HT_{STALL}}} = C_{L\alpha}\ \hat{\alpha}_{HT\_}$$

$$C_{DHT_{STALL}} = C_{DOHT} + C^2_{LHT_{STALL}}/\pi AR_{HT} E_{HT}$$

$$C_{D_{HT}} = C_{D_{HT_{STALL}}} + \frac{\left(\alpha_{e_{HT}} - \hat{\alpha}_{HT\_}\right)\left(1.1 - C_{D_{HT_{STALL}}}\right)}{(-90° - \hat{\alpha}_{HT\_})}$$

HORIZONTAL TAIL LIFT AND DRAG (CONTINUED)

IF: $(-180° + .5\hat{\alpha}_{HT_+}) < \alpha e_{HT} < -90°$

$$C_{L_{HT}} = .5\ C_{L\alpha}\ \hat{\alpha}_{HT_+}\ (\alpha e_{HT} + 90°)/(-90° + .5\ \hat{\alpha}_{HT_+})$$

$$C_{L_{HT_{STALL}}} = .5\ C_{L\alpha}\ \hat{\alpha}_{HT_+}$$

$$C_{D_{HT_{STALL}}} = C_{DO_{HT}} + C^2_{L_{HT_{STALL}}} / \pi AR_{HT} E_{HT}$$

$$C_{D_{HT}} = C_{D_{HT\ STALL}} - \frac{(\alpha e_{HT} + 180° - .5\ \hat{\alpha}_{HT_+})(1.1 - C_{D_{HT_{STALL}}})}{(.5\ \hat{\alpha}_{HT_+} - 90°)}$$

IF: $-180° \leq \alpha e_{HT} < (-180° + .5\ \hat{\alpha}_{HT_+})$

$$C_{L_{HT}} = C_{L\alpha}\ (\alpha e_{HT} + 180°)$$

$$C_{D_{HT}} = C_{DO_{HT}} + C^2_{L_{HT}} / \pi AR_{HT} E_{HT}$$

VERTICAL TAIL AERODYNAMICS

ROTOR ON TAIL INTERFERENCE

$$v_{i_{VT}} = \frac{v_{i_{HT}}}{\bar{v}_i} \quad \bar{v}_i \frac{1}{(\tau S+1)}$$

$$\left.\begin{aligned} U_{i_{VTL}} &= v_{i_{VT}} \cos \bar{i}_N \\ W_{i_{VTL}} &= -v_{i_{VT}} \sin \bar{i}_N \end{aligned}\right\} = 0 \quad \begin{aligned} &\text{for } 5° < \beta_F < 28° \\ &\text{and for } |\beta_F| \geq 60° \end{aligned}$$

$$\left.\begin{aligned} U_{i_{VTR}} &= v_{i_{VT}} \cos \bar{i}_N \\ W_{i_{VTR}} &= -v_{i_{VT}} \sin \bar{i}_N \end{aligned}\right\} = 0 \quad \begin{aligned} &\text{for } -28° < \beta_F < -5° \\ &\text{and for } |\beta_F| \geq 60° \end{aligned}$$

$$U'_{VTL} = U_{VTL} + U_{i_{VTL}}$$

$$U'_{VTR} = U_{VTR} + U_{i_{VTR}}$$

$$V'_{VTL} = V_{VTL}$$

$$V'_{VTR} = V_{VTR}$$

$$W'_{VTL} = W_{VTL} + W_{i_{VTL}}$$

$$W'_{VTR} = W_{VTR} + W_{i_{VTR}}$$

$$\bar{q}_{VTR} = 1/2\ \rho\ (U'^2_{VTR} + V'^2_{VTR} + W'^2_{VTR})$$

$$\bar{q}_{VTL} = 1/2\ \rho\ (U'^2_{VTL} + V'^2_{VTL} + W'^2_{VTL})$$

$$\sigma = \frac{d\sigma}{d\beta} \beta_F$$

FIN SIDESLIP ANGLES

$$\beta_{VTR} = \mathrm{Tan}^{-1}\left[V'_{VTR} / \sqrt{U'^2_{VTR} + W'^2_{VTR}} \right]$$

$$\beta_{VTL} = \mathrm{Tan}^{-1}\left[V'_{VTL} / \sqrt{U'^2_{VTL} + W'^2_{VTL}} \right]$$

FIN ANGLES OF ATTACK

$$\alpha_{VTR} = -\beta_{VTR} + \sigma$$

$$\alpha_{VTL} = -\beta_{VTL} + \sigma$$

These values to be used in resolution of fin forces and moments.

FIN LIFT AND DRAG

For $\alpha_{VT} = \alpha_{VTR}$ and α_{VTL} obtain $C_{D_{VTR}}$, $C_{D_{VTL}}$, $C_{Y_{VTR}}$, $C_{Y_{VTL}}$ as follows

$$\tau'_{VT} = \tau_{VT}/\kappa_\beta \qquad \kappa_\beta = f_8 \quad (|\beta_F|, V_F)$$

IF: $|\alpha_{VT}| > 180°; \alpha_{VT} = \alpha_{VT} - (\text{sign } \alpha_{VT})(360°)$

NOTE: This value of α_{VT} only used in calculation of force and moment coefficients.

$$\alpha_{e_{VT}} = (\alpha_{VT} + \tau'_{VT}\ \delta_{RUD})$$

$$\hat{\alpha}_{VT_+} = (\alpha_{VT_{STALL}} - 2°) + \tau'_{VT}\ \delta_{RUD}$$

$$\hat{\alpha}_{VT_-} = (\alpha_{VT_{STALL}} - 2°) + \tau'_{VT}\ \delta_{RUD}$$

$$C_{Y\alpha} = C_{Y\alpha_{VT}} \times PGVT, \quad PGVT = \frac{2 + \sqrt{AR^2_{VT} + 4}}{2 + \sqrt{AR^2_{VT}(1-M^2) + 4}}$$

VERTICAL TAIL LIFT AND DRAG

IF: $\hat{\alpha}_{VT_-} \leq \alpha_{e_{VT}} < \hat{\alpha}_{VT_+}$

$$C_{Y_{VT}} = C_{Y_\alpha}\ \alpha_{e_{VT}}$$

$$C_{D_{VT}} = C_{DO_{VT}} + C^2_{Y_{VT}} / \pi AR_{VT} E_{VT}$$

VERTICAL TAIL LIFT AND DRAG (CONTINUED)

IF: $\hat{\alpha}_{VT+} < \alpha_{e_{VT}} \leq 90°$

$$C_{Y_{VT}} = C_{Y\alpha}\ \hat{\alpha}_{VT_+}\ (90° - \alpha_{e_{VT}})/(90° - \hat{\alpha}_{VT_+})$$

$$C_{Y_{VT_{STALL}}} = C_{Y\alpha}\ \hat{\alpha}_{VT_+}$$

$$C_{D_{VT_{STALL}}} = C_{DO_{VT}} + C^2_{Y_{VT_{STALL}}}/\pi AR_{VT}E_{VT}$$

$$C_{D_{VT}} = C_{D_{VT_{STALL}}} + \frac{(\alpha_{e_{VT}} - \hat{\alpha}_{VT_+})(1.1 - C_{D_{VT_{STALL}}})}{(90° - \hat{\alpha}_{VT_+})}$$

IF: $90° < \alpha_{e_{VT}} \leq (180° - .5\ \hat{\alpha}_{VT\_})$

$$C_{Y_{VT}} = .5\ C_{Y\alpha}\ \hat{\alpha}_{VT\_}\ (\alpha_{e_{VT}} - 90°)/(90° - .5\ \hat{\alpha}_{VT\_})$$

$$C_{Y_{VT_{STALL}}} = .5\ C_{Y\alpha}\ \hat{\alpha}_{VT\_}$$

$$C_{Y_{VT_{STALL}}} = C_{DO_{VT}} + C^2_{Y_{VT_{STALL}}}/\pi AR_{VT}E_{VT}$$

$$C_{D_{VT}} = C_{D_{VT_{STALL}}} + \frac{(\alpha_{e_{VT}} + .5\ \hat{\alpha}_{VT\_} - 180°)(1.1 - C_{D_{VT_{STALL}}})}{(.5\ \hat{\alpha}_{VT\_} - 90°)}$$

IF: $(180° - .5\ \hat{\alpha}_{VT\_}) \leq \alpha_{e_{VT}} < 180°$

$$C_{Y_{VT}} = C_{Y\alpha}\ (\alpha_{e_{VT}} - 180°)$$

$$C_{D_{VT}} = C_{DO_{VT}} + C^2_{Y_{VT}}/\pi AR_{VT}E_{VT}$$

VERTICAL TAIL LIFT AND DRAG (CONTINUED)

IF: $-90° \leq \alpha_{e_{VT}} < \hat{\alpha}_{VT-}$

$$C_{Y_{VT}} = C_{Y\alpha}\ \hat{\alpha}_{VT_-}\ (-90° - \alpha_{e_{VT}})/(-90° - \hat{\alpha}_{VT_-})$$

$$C_{Y_{VT_{STALL}}} = C_{Y\alpha}\ \hat{\alpha}_{VT_-}$$

$$C_{D_{VT_{STALL}}} = C_{DO_{VT}} + C^2_{Y_{VT_{STALL}}}/\pi AR_{VT}E_{VT}$$

$$C_{D_{VT}} = C_{D_{VT_{STALL}}} + \frac{(\alpha_{e_{VT}} - \hat{\alpha}_{VT-})(1.1 - C_{D_{VT_{STALL}}})}{(-90° - \hat{\alpha}_{VT_-})}$$

IF: $(-180° + .5\ \hat{\alpha}_{VT_+}) < \alpha_{e_{VT}} < -90°$

$$C_{Y_{VT}} = .5\ C_{Y\alpha}\ \hat{\alpha}_{VT_+}\ (\alpha_{e_{VT}} + 90°)/(-90° + .5\ \hat{\alpha}_{VT_+})$$

$$C_{Y_{VT_{STALL}}} = .5\ C_{Y\alpha}\ \hat{\alpha}_{VT_+}$$

$$C_{D_{VT_{STALL}}} = C_{DO_{VT}} + C^2_{Y_{VT_{STALL}}}/\pi AR_{VT}E_{VT}$$

$$C_{D_{VT}} = C_{D_{VT_{STALL}}} - \frac{(\alpha_{e_{VT}} + 180° - .5\ \hat{\alpha}_{VT_+})(1.1 - C_{D_{VT_{STALL}}})}{(.5\ \hat{\alpha}_{VT_+} - 90°)}$$

IF: $-180° \leq \alpha_{e_{VT}} < (-180° + .5\ \hat{\alpha}_{VT_+})$

$$C_{Y_{VT}} = C_{Y\alpha}\ (\alpha_{e_{VT}} + 180°)$$

$$C_{D_{VT}} = C_{DO_{VT}} + C^2_{Y_{VT}}/\pi AR_{VT}E_{VT}$$

TAIL FORCE AND MOMENT RESOLUTION TO C.G.

HORIZONTAL TAIL

$$\eta_{HT} = \eta_{VT} = f_9\ (V_F,\ \alpha_F,\ \bar{i}_N);\quad \eta'_{HT} = \eta'_{VT} = 1-(1-\eta_{HT})\ \cos\ \beta_F$$

$$X^{HT}_{AERO} = \left[-C_{DHT}\ \cos\ (\alpha_{HT} - i_{HT})\ \cos\ (\beta_{VT} - \sigma) + C_{LHT}\ \sin\ (\alpha_{HT} - i_{HT})\right]\ \bar{q}_{HT}\ S_{HT}\ \eta'_{HT}$$

$$Y^{HT}_{AERO} = -C_{DHT}\ \sin\ (\beta_{VT} - \sigma)\ \bar{q}_{HT}\ S_{HT}\ \eta'_{HT}$$

$$Z^{HT}_{AERO} = \left[-C_{LHT}\ \cos\ (\alpha_{HT} - i_{HT}) - C_{DHT}\ \cos\ (\beta_{VT} - \sigma)\ \sin\ (\alpha_{HT} - i_{HT})\right]\ \bar{q}_{HT}\ S_{HT}\ \eta'_{HT}$$

$$\mathcal{L}^{HT}_{AERO} = -Y^{HT}_{AERO}\ (Z_{HT} - Z_{CG})$$

$$M^{HT}_{AERO} = Z^{HT}_{AERO}\ (X_{CG} - X_{HT}) + X^{HT}_{AERO}\ (Z_{HT} - Z_{CG})$$

$$N^{HT}_{AERO} = -Y^{HT}_{AERO}\ (X_{CG} - X_{HT})$$

VERTICAL TAIL - RIGHT FIN

$$X^{VTR}_{AERO} = \left[-C_{DVTR}\ \cos\ (\beta_{VTR} - \sigma)\ \cos\ (\alpha_{HT} - i_{HT}) - C_{YVTR}\ \sin\ (\beta_{VTR} - \sigma)\ \cos\ (\alpha_{HT} - i_{HT})\right]\ \bar{q}_{VTR}\ S_{VT}\ \eta'_{VT}\ \kappa_\beta$$

$$Y^{VTR}_{AERO} = \left[C_{YVTR}\ \cos\ (\beta_{VTR} - \sigma) - C_{DVTR}\ \sin\ (\beta_{VTR} - \sigma)\right]\ \bar{q}_{VTR}\ S_{VT}\ \eta'_{VT}\ \kappa_\beta$$

$$Z^{VTR}_{AERO} = \left[-C_{DVTR}\ \cos\ (\beta_{VTR} - \sigma)\ \sin\ (\alpha_{HT} - i_{HT}) - C_{YVTR}\ \sin\ (\beta_{VTR} - \sigma)\ \sin\ (\alpha_{HT} - i_{HT})\right]\ \bar{q}_{VTR}\ S_{VT}\ \eta'_{VT}\ \kappa_\beta$$

VERTICAL TAIL - RIGHT FIN (CONTINUED)

Repeat, with subscripts changed, for left fin.

$$\mathcal{L}^{VT}_{AERO} = -(Z_{VT} - Z_{CG})\ (Y^{VTR}_{AERO} + Y^{VTL}_{AERO}) + (Z^{VTR}_{AERO} - Z^{VTL}_{AERO})\ Y_{VT}$$

$$M^{VT}_{AERO} = (Z^{VTL}_{AERO} + Z^{VTL}_{AERO})\ (X_{CG} - X_{VT}) + (X^{VTR}_{AERO} + X^{VTL}_{AERO})\ (Z_{VT} - Z_{CG})$$

$$N^{VT}_{AERO} = -(Y^{VTL}_{AERO} + Y^{VTR}_{AERO})\ (X_{CG} - X_{VT}) + (X^{VTR}_{AERO} - X^{VTL}_{AERO})\ Y_{VT}$$

TOTAL TAIL CONTRIBUTION

$$X^{T}_{AERO} = X^{VTR}_{AERO} + X^{HT}_{AERO} + X^{VTL}_{AERO}$$

$$Z^{T}_{AERO} = Z^{VTR}_{AERO} + Z^{HT}_{AERO} + Z^{VTL}_{AERO}$$

$$M^{T}_{AERO} = M^{VT}_{AERO} + M^{HT}_{AERO}$$

$$Y^{T}_{AERO} = Y^{VTR}_{AERO} + Y^{HT}_{AERO} + Y^{VTL}_{AERO}$$

$$\mathcal{L}^{T}_{AERO} = \mathcal{L}^{VT}_{AERO} + \mathcal{L}^{HT}_{AERO}$$

$$N^{T}_{AERO} = N^{VT}_{AERO} + N^{HT}_{AERO}$$

NACELLE AERODYNAMICS

NACELLE ANGLE OF ATTACK AND SIDESLIP

$$\alpha_{RN} = \mathrm{Tan}^{-1}\left[W_{RR}/U_{RR}\right] \quad , \quad q_{RN} = 1/2\ \rho\ V_{RR}^2$$

$$\alpha_{LN} = \mathrm{Tan}^{-1}\left[W_{RL}/U_{RL}\right] \quad , \quad q_{LN} = 1/2\ \rho\ V_{LR}^2$$

$$\beta_{RN} = \mathrm{Tan}^{-1}\left[V_{RR}/\ \sqrt{U_{RR}^2 + W_{RR}^2}\right]$$

$$\beta_{LN} = \mathrm{Tan}^{-1}\left[V_{RL}/\ \sqrt{U_{RL}^2 + W_{RL}^2}\right]$$

NACELLE WIND AXIS FORCE & MOMENT COEFFICIENTS

$$C_{DRN} = C_{DON} + K_{30}|\alpha_{RN}| + K_{31}|\alpha_{RN}^2|$$

$$C_{DLN} = C_{DON} + K_{30}|\alpha_{LN}| + K_{31}|\alpha_{LN}^2|$$

NOTE: CHECK RANGE OF αRN & αLN TO DETERMINE VALUES FOR CONSTANTS.

$$C_{LRN} = K_{32}\ \mathrm{Sin}\ \alpha_{RN}\ \cos\ \alpha_{RN}$$

$$C_{LLN} = K_{32}\ \mathrm{Sin}\ \alpha_{LN}\ \cos\ \alpha_{LN}$$

$$C_{MRN} = C_{MON} + K_{34}\ \mathrm{Sin}\ \alpha_{RN}\ \cos\ \alpha_{RN} + K_{35}\ (\sin\ \alpha_{RN}\ \cos\ \alpha_{RN})|\sin\ \alpha_{RN}\ \cos\ \alpha_{RN}|$$

$$C_{MLN} = C_{MON} + K_{34}\ \sin\ \alpha_{LN}\ \cos\ \alpha_{LN} + K_{35}\ (\sin\ \alpha_{LN}\ \cos\ \alpha_{LN})|\sin\ \alpha_{LN}\ \cos\ \alpha_{LN}|$$

SPECIAL CONDITIONS

1. IF: $V_{RR}^2 \leq 1\,(FT/SEC)^2$; RIGHT NACELLE AERO $\equiv$ 0.0 & HOLD VALUE OF α_{RN} & β_{RN}

2. IF: $V_{LR}^2 \leq 1\,(FT/SEC)^2$; LEFT NACELLE AERO $\equiv$ 0.0 & HOLD VALUE OF α_{LN} & β_{LN}

$$C_{YRN} = K_{36} \text{ Sin } \beta_{RN} \text{ Cos } \beta_{RN} + K_{37}(\text{Sin } \beta_{RN} \text{ Cos } \beta_{RN})|\text{Sin } \beta_{RN} \text{ Cos } \beta_{RN}|$$

$$C_{YLN} = K'_{36} \text{ Sin } \beta_{LN} \text{ Cos } \beta_{LN} + K'_{37}(\text{Sin } \beta_{LN} \text{ Cos } \beta_{LN})|\text{Sin } \beta_{LN} \text{ Cos } \beta_{LN}|$$

$$C_{NRN} = C_{NORN} + K_{38}\text{Sin } \beta_{RN}\text{Cos } \beta_{RN} + K_{39}(\text{Sin } \beta_{RN}\text{Cos}\beta_{RN})|\text{Sin}\beta_{RN} \text{ Cos } \beta_{RN}|$$

$$C_{NLN} = C_{NOLN} + K_{40}\text{Sin } \beta_{LN}\text{Cos } \beta_{LN} + K_{41}(\text{Sin } \beta_{LN}\text{Cos}\beta_{LN})|\text{Sin}\beta_{LN} \text{ Cos } \beta_{LN}|$$

$$C_{\mathcal{L}RN} = C_{\mathcal{L}LN} = 0.0$$

<u>NACELLE FORCES & MOMENTS - NACELLE AXES</u>

$$\Delta X'_{RN} = q_{RN}S_W[-C_{DRN}\cos\alpha_{RN} + C_{LRN}\sin\alpha_{RN} - C_{YRN}\sin\beta_{RN}\cos\alpha_{RN}]1/2$$

$$\Delta Y'_{RN} = q_{RN}S_W[C_{YRN} \cos\beta_{RN} - C_{DRN}\sin\beta_{RN}]1/2$$

RIGHT

$$\Delta Z'_{RN} = q_{RN}S_W[-C_{LRN}\cos\alpha_{RN} - C_{DRN}\cos\beta_{RN} \sin\alpha_{RN} - C_{YRN}\sin\beta_{RN}\sin\alpha_{RN}]1/2$$

$$\Delta \mathcal{L}'_{RN} = q_{RN}S_W b_W[-\frac{c_W}{b_W} C_{MRN} \sin\beta_{RN} \cos\alpha_{RN} - C_{NRN} \sin\alpha_{RN}]1/2$$

$$\Delta M'_{RN} = q_{RN}S_W c_W [C_{MRN} \cos \beta_{RN}]1/2$$

$$\Delta N'_{RN} = q_{RN}S_W b_W [C_{NRN} \cos \alpha_{RN} - \frac{c_W}{b_W} C_{MRN} \sin \beta_{RN} \cos\alpha_{RN}]1/2$$

$$\Delta X'_{LN} = q_{LN}S_W [-C_{DLN} \cos \alpha_{LN} + C_{LLN} \sin \alpha_{LN} - C_{YLN} \sin \beta_{LN} \cos\alpha_{LN}]1/2$$

$$\Delta Y'_{LN} = q_{LN}S_W [C_{YLN} \cos \beta_{LN} - C_{DLN} \sin \beta_{LN}]1/2$$

$$\Delta Z'_{LN} = q_{LN}S_W[-C_{LLN}\cos\alpha_{LN}-C_{DLN}\cos\beta_{LN}\sin\alpha_{LN}-C_{YLN}\sin\beta_{LN}\sin\alpha_{LN}]1/2$$

LEFT

$$\Delta \mathcal{L}'_{LN} = q_{LN}S_W b_W[-\frac{c_W}{b_W} C_{MLN} \sin \beta_{LN} \cos \alpha_{LN} - C_{NLN} \sin \alpha_{LN}]1/2$$

$$\Delta M'_{LN} = q_{LN}S_W c_W[C_{MLN}\cos \beta_{LN}]1/2$$

$$\Delta N'_{LN} = q_{LN}S_W b_W [C_{NLN} \cos \alpha_{LN} - \frac{c_W}{b_W} C_{MLN} \sin \beta_{LN} \cos\alpha_{LN}]1/2$$

LANDING GEAR EQUATIONS

PERFORM THE FOLLOWING CALCULATIONS FOR EACH WHEEL OF THE LANDING GEAR WHERE - $n = 1$ LEFT MAIN GEAR
$n = 2$ RIGHT MAIN GEAR
$n = 3$ NOSE GEAR

LANDING GEAR - A/C LOCATION

$$X_n = - X_{CG} + X_{Gn}$$

$$Y_n = Y_{Gn}$$

$$Z_n = - Z_{CG} + Z_{Gn}$$

STRUT DEFLECTION

$$h_{G\theta n} = X_n \sin\theta - Z_n \cos\theta - r_n$$

$$h_{G\phi n} = \left[Y_n \sin\phi + (Z_n + r_n)(\cos\phi - 1)\right] \cos\theta$$

$$h_{Tn} = (-Z_{DOWN} + h_{G\theta n} - h_{G\phi n})/(\cos\phi \cos\theta)$$

RATE OF STRUT DEFLECTION

$$\dot{h}_{Tn} = -\dot{Z}_{DOWN} / (\cos\phi \cos\theta) + X_n q - Y_n p$$

VERTICAL FORCE

$$F_{GZn} = K_{STn} h_{Tn} + D_{STn} \dot{h}_{Tn}$$

NOTE: COMPUTE F_{GZn} ONLY IF $h_{Tn} < 0$;

IF $h_{Tn} > 0$; $F_{GZn} = 0.0$ &

REMAINING CALCULATIONS MAY BE SET

TO ZERO.

LONGITUDINAL FORCE:

$$F_{\mu n} = (\mu_0 + \mu_1 B_{Gn}) F_{GZn} \quad \text{Sign } U$$

NOTE: B_{Gn} is percent brake pedal deflection.

SIDE FORCE:

$$F_{Sn} = \mu_S F_{GZn} \quad \text{Sign } V$$

FORCE AND MOMENT CONTRIBUTION OF EACH WHEEL

$$\Delta X_n = F_{\mu n} - F_{GZn} \theta \quad (n = 1,2);$$

$$\Delta X_3 = F_{\mu 3} \cos \delta_{STEER} - F_{S3} \sin \delta_{STEER} - F_{GZ3} \theta$$

$$\Delta Y_n = F_{Sn} + F_{GZn} \phi \quad (n = 1,2);$$

$$\Delta Y_3 = F_{S3} \cos \delta_{STEER} + F_{\mu 3} \sin \delta_{STEER} + F_{GZ3} \phi$$

$$\Delta Z_n = F_{\mu n} \theta - F_{Sn} \phi + F_{GZn}$$

$$\Delta M_n = - \Delta Z_n X_n + \Delta X_n (Z_n + r_n + h_{Tn})$$

$$\Delta \mathcal{L}_n = \Delta Z_n Y_n - \Delta Y_n (Z_n + r_n + h_{Tn})$$

$$\Delta N_n = - \Delta X_n Y_n + X_n \Delta Y_n$$

$$\Delta X_{LG} = \sum_{1}^{3} \Delta X_n$$

$$\Delta Y_{LG} = \sum_{1}^{3} \Delta Y_n$$

$$\Delta Z_{LG} = \sum_{1}^{3} \Delta Z_n$$

$$\Delta \mathcal{L}_{LG} = \sum_{1}^{3} \Delta \mathcal{L}_n$$

$$\Delta M_{LG} = \sum_{1}^{3} \Delta M_n$$

$$\Delta N_{LG} = \sum_{1}^{3} \Delta N_n$$

FUSELAGE AERODYNAMICS

FUSELAGE INPUT EQUATIONS

$$\alpha_F = \mathrm{Tan}^{-1}\ (W/U) \qquad \beta_F = \mathrm{Tan}^{-1}\left[V/\sqrt{U^2 + W^2} \right]$$

$$\alpha_F' = \sin\ \alpha_F\ \cos\ \alpha_F \qquad \beta_F' = \mathrm{Sin}\ \beta_F\ \cos\ \beta_F$$

$$V_F = \sqrt{U^2 + V^2 + W^2}$$

$$q_F = 1/2\rho\ V_F^2$$

$$V_{FUS} = V_F\ \sqrt{\sigma_h}$$

FUSELAGE WIND AXIS COEFFICIENTS

$$C_{DF} = (C_{DOF} + K_1|\alpha_F| + K_2\alpha_F^2)\ \cos^2\ \beta_F + K_O\ C_{DOF}|1-\cos\ (.18\beta_F)| + \Delta C_{D_{LG}}\ (1 - \ell^{-t/t_G})$$

$$C_{LF} = (K_{42} + K_3\ \alpha_F')\ \cos^2\beta_F - K_4\ \sin^3\ |\beta_F|$$

$$C_{YF} = K_7\ \beta_F' + K_8\ \beta_F'\ |\beta_F'|$$

$$C_{\mathcal{L}F} = K_{13}\ \beta_F'$$

$$C_{MF} = [-.11 + .36\ \sin\ (6.6 + 3.3\ \alpha_F^O)]\ \cos^2\beta_F + K_5\ |\beta_F'| + \Delta C_{M_{LG}}\ (1 - \ell^{-t/t_G})$$

$$C_{NF} = C_{NOF} + K_9\ \beta_F' + K_{10}\ \beta_F'|\beta_F'|$$

NOTE: IF GEAR IS UP; ΔC_{DLG} & $\Delta C_{MLG} \equiv 0.0$

SPECIAL CONDITIONS

1. If $V_F^2 \leq 1$ (ft/sec)^2 FUSELAGE AERO = 0.0 & HOLD VALUE OF α_F & β_F

FUSELAGE FORCES AND MOMENT ABOUT A/C C.G.

$$X^{F'}_{AERO} = [-C_{DF} \cos\alpha_F \cos\beta_F + C_{LF} \sin\alpha_F - C_{YF} \sin\beta_F \cos\alpha_F]\, q_F S_W$$

$$Y^{F'}_{AERO} = [C_{YF} \cos\beta_F - C_{DF} \sin\beta_F]\, q_F S_W$$

$$Z^{F'}_{AERO} = [-C_{LF} \cos\alpha_F - C_{DF} \cos\beta_F \sin\alpha_F$$

$$-C_{YF} \sin\beta_F \sin\alpha_F]\, q_F S_W$$

$$\mathcal{L}^{F'}_{AERO} = [-(c_w/b_w) C_{MF} \sin\beta_F \cos\alpha_F - C_{NF} \sin\alpha_F]\, q_F S_W b_W + {}^{*}\mathcal{L}_{GEF}$$

$$+ Y^{F'}_{AERO} [Z_{CG} - Z_{FAC}] + C_{\mathcal{L}_F} \cos\alpha_F \cos\beta_F\, q_F S_W b_W$$

$$M^{F'}_{AERO} = [C_{MF} \cos\beta_F]\, q_F S_W c_W + Z^{F'}_{AERO} [X_{CG} - X_{FAC}]$$

$$-X^{F'}_{AERO} [Z_{CG} - Z_{FAC}] + C_{\mathcal{L}_F} \sin\beta_F\, q_F S_W b_W$$

$$N^{F'}_{AERO} = [C_{NF} \cos\alpha_F - (c_w/b_w) C_{MF} \sin\beta_F \sin\alpha_F]\, q_F S_W b_W$$

$$-Y^{F'}_{AERO} [X_{CG} - X_{FAC}] + C_{\mathcal{L}_F} \sin\alpha_F \cos\beta_F\, q_F S_W b_W$$

$$X^{F}_{AERO} = X^{F'}_{AERO} + \Delta X_{LG}$$

$$Y^{F}_{AERO} = Y^{F'}_{AERO} + \Delta Y_{LG}$$

$$Z^{F}_{AERO} = Z^{F'}_{AERO} + \Delta Z_{LG}$$

$$\mathcal{L}^{F}_{AERO} = \mathcal{L}^{F'}_{AERO} + \Delta\mathcal{L}_{LG}$$

$$M^{F}_{AERO} = M^{F'}_{AERO} + \Delta M_{LG}$$

$$N^{F}_{AERO} = N^{F'}_{AERO} + \Delta N_{LG}$$

$${}^{*}\mathcal{L}_{GEF} = [-8270 + 26186\,(h/D) - 23369\,(h/D)^2$$

$$+ 6336\,(h/D)^3]\, \phi^{\circ}\, EXP(-.1V_F)$$

for $.5 \le h/D \le 1.4$

else $\mathcal{L}_{GEF} = 0$

WING ON ROTOR INTERFERENCE

AVERAGE NACELLE INCIDENCE

$$\bar{i}_N = 0.5\ (i_{NL} + i_{NR})$$

AVERAGE LIFT COEFFICIENT

$$C_{LW} = 0.5\ (C_{LSRW} + C_{LSLW})/(q/\bar{q}_S)$$

WING ON ROTOR UPWASH

$$\varepsilon_{WRR} \text{ and } \varepsilon_{WRL} = f_7\ (\bar{i}_N\ ,\ C_{LW})$$

ROTOR/ROTOR INTERFERENCE

POSITIVE SIDESLIP, I.E., V > 0.0

$$\chi = \varepsilon_{PRR}$$

$$\left(\frac{\delta v^*_{RL}}{v^*_{RR}}\right) = \left[T_1 + T_2\chi + T_3\chi^2\right]\chi$$

$$\delta v_{RL} = \left(\frac{\delta v^*_{RL}}{v^*_{RR}}\right) v_{*R}\sqrt{\frac{R_{RR}}{2\rho\pi R^2}}$$

$$\varepsilon'_{iRL} = -\tan^{-1}\left[\frac{\delta v_{RL}}{V_{LR} + 1.0}\right]$$

$$\varepsilon_{iRL} = (|\beta_F|)\quad(.40528\ i_{NL})\quad\delta v_{RL}$$

$$\varepsilon_{iLR} = 0.0$$

NEGATIVE SIDESLIP, I.E., V < 0.0

$$\chi = \varepsilon_{PLR}$$

$$\left(\frac{\delta v^*_{LR}}{v^*_{LR}}\right) = \left[T_1 + T_2\chi + T_3\chi^2\right]\chi$$

$$\delta v_{LR} = \left(\frac{\delta v^*_{LR}}{v^*_{RR}}\right) v_{*L}\sqrt{\frac{R_{LR}}{2\rho\pi R^2}}$$

$$\varepsilon'_{iLR} = -\tan^{-1}\left[\frac{\delta v_{LR}}{V_{RR} + 1.0}\right]$$

$$\varepsilon_{iLR} = (|\beta_F|)\quad(.40528\ i_{NR})\quad\delta v_{RL}$$

$$\varepsilon_{iRL} = 0.0$$

NOTE: v_{*R} & v_{*L} FROM WING EQUATIONS.

ROTOR EQUATIONS

RIGHT ROTOR

$$\alpha_{RR} = \tan^{-1}\left\{\frac{\sqrt{V_{RR}^2 + (W_{RR} + U_{RR}\,\varepsilon_{WRR})^2}}{U_{RR} + \varepsilon_{i_{LR}}}\right\}$$

$$V_{RR} = \sqrt{(U_{RR}+\varepsilon_{iLR})^2+V_{RR}^2+W_{RR}^2}\ ; \quad \mu_{RR} = \frac{V_{RR}}{|\Omega_R|R}$$

LEFT ROTOR

$$\alpha_{LR} = \tan^{-1}\left\{\frac{\sqrt{V_{RL}^2 + (W_{RL} + U_{RL}\,\varepsilon_{WRL})^2}}{U_{RL} + \varepsilon_{iRL}}\right\}$$

$$V_{LR} = \sqrt{(U_{RR}+\varepsilon_{iLR})^2+V_{RR}^2+W_{RR}^2}\ ; \quad \mu_{LR} = \frac{V_{LR}}{|\Omega_L|R}$$

ROTOR ANGULAR RATE TRANSFORMS

RIGHT-NACELLE AXES

$$P_{NR}^N = -p\cos i_{NR} + r\sin i_{NR}$$

$$Q_{NR}^N = q + \dot{i}_{NR}$$

$$R_{NR}^N = -\,r\cos i_{NR} - p\sin i_{NR}$$

LEFT-NACELLE AXES

$$P_{NL}^N = p\cos i_{NL} - r\sin i_{NL}$$

$$Q_{NL}^N = q + \dot{i}_{NL}$$

$$R_{NL}^N = r\cos i_{NL} + p\sin i_{NL}$$

RIGHT WIND AXES

$$P_{NR}^R = P_{NR}^N$$

$$Q_{NR}^R = Q_{NR}^N\cos\xi_{HR} + R_{NR}^N\sin\xi_{HR}$$

$$R_{NR}^R = R_{NR}^N\cos\xi_{HR} - Q_{NR}^N\sin\xi_{HR}$$

LEFT WIND AXES

$$P_{NL}^R = P_{NL}^N$$

$$Q_{NL}^R = Q_{NL}^N\cos\xi_{HL} - R_{NL}^N\sin\xi_{HL}$$

$$R_{NL}^R = R_{NL}^N\cos\xi_{HL} + Q_{NL}^N\sin\xi_{HL}$$

NOTE: USE WIND AXIS RATES IN ROTOR ROUTINE.

RIGHT ROTOR

THRUST

$$C'_{TRR} = \left[\frac{\tau_1 S+1}{\tau_2 S+1}\right]\left[C_{T_{ORR}} \text{ Cos } A_{1_{C_R}} \text{ Cos } B_{1_{C_R}}\right]$$

WHERE: $C_{T_O} = 0.000679\ \phi + 0.000015\ \phi^2 + 0.0022\ \mu\phi + 0.000211\ \mu^2\phi$

and

$$\phi = \theta^\circ_{75} - \tan^{-1}\left[\frac{\mu \cos \alpha}{0.75}\right] - 6.3015\mu + 5.5816\mu^2 - 8\ \mu \sin \alpha + 1.8$$

GROUND EFFECT

$$h_{RR} = -Z_{DOWN} + (L_S \text{ Cos } i_{NR} - X_{CG}) \text{ Sin } \theta + \left[(L_S \text{ Sin } i_{NR} + Z_{CG}) \text{ Cos } \phi - Y_N \text{ Sin } \phi\right] \text{ Cos } \theta$$

$$\left(\frac{h}{D}\right)_{\substack{EFF\\RR}} = \frac{h_{RR}}{2R\left[\left|\text{Sin}(\theta + i_{NR}) \text{ Cos } \phi\right| + .0174\right]}$$

$$\left(\frac{T_{IGE}}{T_{OGE}}\right)_{RR} = \left[\left(\frac{h}{D}\right)^2_{\substack{EFF\\RR}} (.1741 - .6216\ \mu_{RR}) + \left(\frac{h}{D}\right)_{\substack{EFF\\RR}} (1.4779\ \mu_{RR} - .4143) + 1.2479 - .8806\ \mu_{RR}\right]$$

$$C_{T_{RR}} = C'_{T_{RR}} \left(\frac{T_{IGE}}{T_{OGE}}\right)_{RR}$$

SPECIAL CONDITIONS: IF $\mu_{RR} \geq 0.283$; $\left(\frac{T_{IGE}}{T_{OGE}}\right)_{RR} = 1.0$

or IF $\left(\frac{h}{D}\right)_{\substack{EFF\\RR}} \geq 1.3$; $\left(\frac{T_{IGE}}{T_{OGE}}\right)_{RR} = 1.0$

POWER

$$C_{P_{RR}} = C_{P_{ORR}} = .00015 + .795\, C_T^{3/2} + \mu\, (.00005 + .000843\, \mu + .910\, C_T)$$

$$+ \mu\, [.00674 - .0146\mu - (3.4 - 8\mu)C_T]\, \frac{|\dot{\alpha}|}{180}$$

$$+ [(.08756 - 2.18\mu)\, C_T' - .00043488]\, \mu \sin \alpha$$

NORMAL FORCE

$$C_{NF_{RR}} = C_{NFO_{RR}} + \frac{dC_{NF_{RR}}}{dA_{1C_R}} A_{1CR} + \frac{dC_{NF_{RR}}}{dB_{1C_R}} B_{1C_R}$$

WHERE: $$C_{NF_O} = C_{NF_1} = 0.089\mu^3 \sin 2\alpha + [0.172753\mu C_T$$

$$+ 73.444\, \mu C_T^2 (1-\mu)]K \qquad 0 \le \mu \le 0.6$$

where $K = \sin \alpha$ for $\alpha > 20°$

and $K = \sin \alpha (10 - 0.45\alpha°)$ for $0 \le \alpha \le 20$

For $0.6 < \mu$

$$C_{NF} = (C_{NF_1})\ (1-0.8(\mu-0.6))$$

$$\frac{dC_{NF_{RR}}}{dA_{1CR}} = D_{NF_1} C_{T_{RR}} + D_{NF_2} \mu_{RR}^2 + D_{NF_3} \mu_{RR} + D_{NF_4}$$

$$+ D_{NF_5} \mu_{RR} \sin 2\, \alpha_{RR}$$

$$\frac{dC_{NF_{RR}}}{dB_{1CR}} = E_{NF_1} C_{T_{RR}} + E_{NF_2} \mu_{RR}^2 + E_{NF_3} \mu_{RR} + E_{NF_4}$$

$$+ E_{NF_5} \mu_{RR} \sin \alpha_{RR}$$

SIDE FORCE

$$C_{SF_{RR}} = C_{SF_{ORR}} + \frac{dC_{SF_{RR}}}{dA_{1CR}} A_{1CR} + \frac{dC_{SF_{RR}}}{dB_{1CR}} B_{1CR}$$

WHERE: $C_{SF_O} = \mu \sin \alpha \; (.00566 + 2.830 \; \mu^2 C_T + .016 \; C_T \psi) - .0037249 \mu \alpha^2$

if $\alpha > \pi/2$ use $\pi - \alpha$

where $\psi^\circ = \tan^{-1} \left[\frac{\mu - \mu_i \cos \alpha}{\mu_i \sin \alpha} \right]$

and $\mu_i = \left[\left((\mu^4 + C_T{}^2)^{1/2} - \mu^2 \right) / 2 \right]^{0.5}$

$$\frac{dC_{SF_{RR}}}{dA_{1CR}} = D_{SF_1} C_{T_{RR}} + D_{SF_2} \mu_{RR}^2 + D_{SF_3} \mu_{RR} + D_{SF_4} + D_{SF_5} \mu_{RR} \sin \alpha_{RR}$$

$$\frac{dC_{SF_{RR}}}{dB_{1CR}} = E_{SF_1} C_{T_{RR}} + E_{SF_2} \mu_{RR}^2 + E_{SF_3} \mu_{RR} + E_{SF_4} + E_{SF_5} \mu_{RR} \sin 2 \alpha_{RR}$$

HUB PITCHING MOMENT

$$C_{PM_{RR}} = C_{PM_{ORR}} + \frac{dC_{PM_{RR}}}{dA_{1CR}} A_{1CR} + \frac{dC_{PM_{RR}}}{dB_{1CR}} B_{1CR} + \frac{dC_{PM_{RR}}}{dQ} Q^{R}_{NR}$$

WHERE:

$$C_{PM_O} = 0.012857\ \mu \sin\alpha - 0.014163\mu^2 \sin\alpha$$

$$+ 0.0036344\ \mu \sin 2\alpha - 0.0074613\ \mu \sin\alpha \left[\frac{RPM}{386}\right] + \frac{\partial C_{PM}}{\partial C_T} C_T$$

$$-1000 \frac{dC_{PM}}{dQ} = 1.5 + \mu \qquad 0 \leq \mu \leq .2$$

$$= 0.25 + 7.26\ \mu \qquad .2 < \mu \leq .39$$

$$= 4.1681 - 2.79\ \mu \qquad \mu > .39$$

$$\frac{\partial C_{PM}}{\partial C_T} = \mu\ (-.393141 \times 10^{-2} + .201377 \times 10^{-2}\alpha - .220903 \times 10^{-4}\alpha^2)$$

$$+ \mu^2\ (.120036 + .634542 \times 10^{-2}\alpha + .799823 \times 10^{-3}\ \alpha^2)$$

$$+ \mu^3\ (-.141322 - .170706 \times 10^{-1}\alpha - .61104 \times 10^{-3}\ \alpha^2)$$

$$\frac{dC_{PM_{RR}}}{dA_{1CR}} = D_{PM_1} C_{T_{RR}} + D_{PM_2} \mu^2_{RR} + D_{PM_3} \mu_{RR} + D_{PM_4}$$

$$+ D_{PM_5} \mu_{RR} \sin 2\ \alpha_{RR} + D_{PM_6} \mu_{RR} (|\Omega_R| - \Omega_o)$$

HUB PITCHING MOMENT (CONTINUED)

$$\frac{dC_{PMRR}}{dB_{1CR}} = E_{PM_1} C_{TRR} + E_{PM_2} \mu^2_{RR} + E_{PM_3} \mu + E_{PM_4}$$

$$+ E_{PM_5} \mu_{RR} \sin\alpha_{RR} + E_{PM_6} \mu_{RR} (|\Omega_R| - \Omega_o)$$

HUB YAWING MOMENT

$$C_{YM_{RR}} = C_{YM_{ORR}} + \frac{dC_{YM_{RR}}}{dA_{1CR}} A_{1CR} + \frac{dC_{YM_{RR}}}{dB_{1CR}} B_{1CR} + \frac{dC_{YM_{RR}}}{dR} R^R_{NR} f_{YM}$$

Where:

For $0 \leq \mu \leq 0.37$

$$C_{YM} = (0.023736 \mu - 0.0010)\mu\sin\alpha - 1.6 \mu^2 C_T \sin \alpha$$

$$+ \left[0.00816 - 0.003366\mu - 0.006303 \left(\frac{RPM}{386} - 1\right)\right] \left(\frac{RPM}{386} - 1\right) \mu \sin \alpha$$

and for $\mu > 0.37$

$$C_{YM} = (0.02476 - 0.19798 (\mu - 0.7024)^2) \sin \alpha$$

$$-1.6 \mu^2 C_T \sin \alpha + \mu \left[.00816 - .003366\mu - .006303 \left(\frac{RPM}{386} - 1\right)\right] \left(\frac{RPM}{386} - 1\right)$$

$$\frac{dC_{YM}}{dR} = - \frac{dC_{PM}}{dQ}$$

HUB YAWING MOMENT (CONTINUED)

$$\frac{dC_{YM_{RR}}}{dA_{1CR}} = D_{YM_1} C_{T_{RR}} + D_{YM_2} \mu_{RR}^2 + D_{YM_3} \mu_{RR} + D_{YM_4}$$

$$+ D_{YM_5} \mu_{RR} \sin \alpha_{RR} + E_{YM_6} \mu_{RR} (|\Omega_R| - \Omega_o)$$

$$\frac{dC_{YM_{RR}}}{dB_{1CR}} = E_{YM_1} C_{T_{RR}} + E_{YM_2} \mu_{RR}^2 + E_{YM_3} \mu_{RR} + E_{YM_4}$$

$$+ E_{YM_5} \mu_{RR} \sin 2\alpha_{RR} + E_{YM_6} \mu_{RR} (|\Omega_R| - \Omega_o)$$

ENGINE TAIL PIPE THRUST AND MOMENT

$$\Delta T_{E_R} = 26 + .080\ SHP_R - 350M$$

$$\Delta T_{E_L} = 26 + .080\ SHP_L - 350M$$

$$\Delta M_{E_L} = 1.92\ \Delta T_{E_L} \cos \xi_{HL}$$

$$\Delta M_{E_R} = 1.92\ \Delta T_{E_R} \cos \xi_{HR}$$

$$\Delta N_{E_L} = 1.92\ \Delta T_{E_L} \sin \xi_{HL}$$

$$\Delta N_{E_R} = 1.92\ \Delta T_{E_R} \sin \xi_{HR}$$

SPINNER DRAG AND NORMAL FORCE

$$\Delta C_{T_{SPIN_R}} = - \frac{\mu^2 S_W}{2A} (.001866 + .019039 \sin \alpha_{RR}) \cos \alpha_{RR}$$

$$\Delta C_{T_{SPIN_L}} = - \frac{\mu^2 S_W}{2A} (.001866 + .019039 \sin \alpha_{LR}) \cos \alpha_{LR}$$

$$\Delta C_{NF_{SPIN_R}} = - \frac{\mu^2 S_W}{2A} (.001866 + .019039 \sin \alpha_{RR}) \sin \alpha_{RR}$$

$$\Delta C_{NF_{SPIN_L}} = - \frac{\mu^2 S_W}{2A} (.001866 + .019039 \sin \alpha_{LR}) \sin \alpha_{LR}$$

ROTOR FORCE & MOMENT CALCULATION

$$T_R = f_{T_R} C'_{TRR} \rho \pi R^4 \Omega_R^2 + \Delta T_{E_R} \quad ; \quad C'_{T_{RR}} = C_{T_{RR}} + \Delta C_{T_{SPINR}}$$

$$NF_R = f_{NF_R} C'_{NFRR} \rho \pi R^4 \Omega_R^2 \quad ; \quad C'_{N_{FRR}} = C_{N_{FRR}} + \Delta C_{NF_{SPINR}}$$

$$SF_R = f_{SF_R} C_{SFRR} \rho \pi R^4 \Omega_R^2$$

$$M_R = f_{PM_R} C_{PMRR} \rho \pi R^5 \Omega_R^2 + \Delta M_{ER}$$

$$N_R = f_{YM_R} C_{YMRR} \rho \pi R^5 \Omega_R^2 + \Delta N_{ER}$$

$$Q_{RREQ} = f_{Q_R} C_{PRR} \rho \pi R^5 \Omega_R^2$$

$$RHP_{RR} = \left| Q_{RREQ} \frac{\Omega_R}{550} \right|$$

LEFT ROTOR FOLLOWS SIMILAR FORMAT WITH SUBSCRIPTS CHANGED.

THE LEFT ROTOR ALTITUDE EQUATION IS AS FOLLOWS:

$$h_{LR} = -Z_{DOWN} + (L_S \cos i_{NL} - X_{CG}) \sin \theta$$
$$+ [(L_S \sin i_{NL} + Z_{CG}) \cos \phi + Y_N \sin \phi] \cos \theta$$

or;

$$h_{LR} = h_{RR} + 2 Y_N \sin \phi \cos \theta$$

ROTOR FORCE & MOMENT RESOLUTION

HUB MOMENTS - NACELLE AXES

LEFT

$$\mathcal{L}_{LRH} = - Q_{LREQ} - I_P \dot{\Omega}_L \kappa$$

$$M_{LRH} = M_L \cos \xi_{HL} - N_L \sin \xi_{HL}$$

$$- (p \sin i_{NL} + r \cos i_{NL}) (KI_p\Omega_L + N_{EL} K_1 I_E \Omega_{EL})$$

$$N_{LRH} = -N_L \cos \xi_{HL} - M_L \sin \xi_{HL} + (KI_p\Omega_L + N_{EL} K_1 I_E\Omega_{EL}) (q+\dot{i}_{NL})$$

RIGHT

$$\mathcal{L}_{RRH} = Q_{RREQ} + I_P \dot{\Omega}_R \kappa$$

$$M_{RRH} = M_R \cos \xi_{HR} + N_R \sin \xi_{HR}$$

$$+ (p \sin i_{NR} + r \cos i_{NR}) (KI_p\Omega_R - N_{ER} K_1 I_E\Omega_{ER})$$

$$N_{RRH} = N_R \cos \xi_{HR} - M_R \sin \xi_{HR} - (KI_p\Omega_R - N_{ER} K_1 I_E\Omega_{ER}) (q + \dot{i}_{NR})$$

NOTE: NACELLE AXES ARE RIGHT HANDED SYSTEMS

$K_1 = 0$ if non-tilting engines

$= 1$ if tilting engines

RESOLUTION OF ROTOR/NACELLE FORCES TO BODY AXES AT PIVOTS

LEFT ROTOR

$$i'_{NL} = i'_{NL} + \theta_{tLW}$$

$$X^{NL}_{AERO} = (T_L + \Delta X'_{LN}) \cos i'_{NL} - \sin i'_{NL} (NF_L \cos \xi_{HL} + SF_L \sin \xi_{HL} - \Delta Z'_{LN})$$

$$Y^{NL}_{AERO} = SF_L \cos \xi_{HL} - NF_L \sin \xi_{HL} + \Delta Y'_{LN}$$

$$Z^{NL'}_{AERO} = -(T_L + \Delta X'_{LN}) \sin i'_{NL} - \cos i'_{NL} (NF_L \cos \xi_{HL} + SF_L \sin \xi_{HL} - \Delta Z'_{LN})$$

$$\mathcal{L}^{NL'}_{AERO} = (\mathcal{L}_{LRH} + \Delta\mathcal{L}'_{LN}) \cos i'_{NL} + \sin i'_{NL} (N_{LRH} + \Delta N'_{LN} + L_s Y^{NL}_{AERO})$$

$$M^{NL}_{AERO} = M_{LRH} + \Delta M'_{LN} + NF_L L_s \cos \xi_{HL} + SF_L L_s \sin \xi_{HL} - L_s \Delta Z'_{LN} - I_E \Omega_{EL} r N_{EL} K_2$$

$$N^{NL}_{AERO} = \cos i'_{NL} (N_{LRH} + \Delta N'_{LN} + L_s Y^{NL}_{AERO}) - \sin i'_{NL} (\mathcal{L}_{LRH} + \Delta\mathcal{L}'_{LN}) + I_E \Omega_{EL} q N_{EL} K_2$$

$K_2 = 0$ if tilting engines

$= 1$ if non-tilting

RIGHT ROTOR

$$i'_{NR} = i_{NR} + \theta_{tRW}$$

$$X^{NR}_{AERO} = (T_R + \Delta X'_{RN}) \cos i'_{NR} + \sin i'_{NR} (-NF_R \cos \xi_{HR} + SF_R \sin \xi_{HR} + \Delta Z'_{RN})$$

$$Y^{NR}_{AERO} = -SF_R \cos \xi_{HR} - NF_R \sin \xi_{HR} + \Delta Y'_{RN}$$

$$Z^{NR'}_{AERO} = -(T_R + \Delta X'_{RN}) \sin i'_{NR} + \cos i'_{NR} (-NF_R \cos \xi_{HR} + SF_R \sin \xi_{HR} + \Delta Z'_{RN})$$

$$\mathcal{L}^{NR'}_{AERO} = (\mathcal{L}_{RRH} + \Delta\mathcal{L}'_{RN}) \cos i'_{NR} + \sin i'_{NR} (N_{RRH} + L_s Y^{NR}_{AERO} + \Delta N'_{RN})$$

$$M^{NR}_{AERO} = M_{RRH} + \Delta M'_{RN} + NF_R L_s \cos \xi_{HR} - SF_R L_s \sin \xi_{HR} - L_s \Delta Z'_{RN} - I_E \Omega_{ER} r N_{ER} K_2$$

$$N^{NR}_{AERO} = \cos i'_{NR} (N_{RRH} + \Delta N'_{RN} + L_s Y^{NR}_{AERO}) - \sin i'_{NR} (\mathcal{L}_{RRH} + \Delta\mathcal{L}'_{RN}) + I_E \Omega_{ER} q N_{ER} K_2$$

WING VERTICAL BENDING

LEFT WING TIP DEFLECTION: -

$$\ddot{h}_{1_L} = \omega_W^2 (F_L - h_{1_L}) - 2\xi_W \omega_W \dot{h}_{1_L}$$

$$F_L = -K_{W1} Z_{AERO}^{NL'} - K_{W2} Z_{AERO}^{LW'} - K_{W3} \mathcal{L}_{AERO}^{NL'} + K_{W4} \frac{Z_{AERO}}{m} - K_{W5} \dot{p}$$

$$h_{1_{LWAC}} = K_{W6} h_{1_L} \quad \text{deflection at left wing a.c.}$$

RIGHT WING TIP DEFLECTION: -

$$\ddot{h}_{1_R} = \omega_W^2 (F_R - h_{1_R}) - 2\xi_W \omega_W \dot{h}_{1_R}$$

$$F_R = -K_{W_1} Z^{NR'} - K_{W_2} Z_{AERO}^{RW'} + K_{W_3} \mathcal{L}_{AERO}^{NR'} + K_{W_4} \frac{Z_{AERO}}{m} + K_{W_5} \dot{p}$$

$$h_{1_{R_{WAC}}} = K_{W_6} h_{1_R}$$

WING TORSION

Left wing twist at tip:

$$K_{\theta_t} \theta_{t_{LW}} = M_{N_{LACT}} - N_{EL} I_E \Omega_{EL} [(r \cos i_{N_L} + p \sin i_{N_L}) K_1 + K_2 r]$$
$$+ M_{AERO}^{LW} - Z_{AERO}^{LW} X_{WAC}$$

Right wing twist at tip:

$$K_{\theta_t} \theta_{t_{RW}} = M_{N_{RACT}} - N_{ER} I_E \Omega_{ER} [(r \cos i_{N_R} + p \sin i_{N_R}) K_1 + K_2 r]$$

Left wing twist at a.c.

$$\theta_{t_{LWAC}} = (Y_{WAC}/Y_N) \theta_{t_{LW}}$$

Right wing twist at a.c.

$$\theta_{t_{RWAC}} = (Y_{WAC}/Y_N) \theta_{t_{RW}}$$

TOTAL FORCE AND MOMENT SUMMATION ABOUT C.G.

$$X_{AERO} = X^{NL}_{AERO} + X^{NR}_{AERO} + X^{F}_{AERO} + X^{LW}_{AERO} + X^{RW}_{AERO} + X^{T}_{AERO}$$

$$Y_{AERO} = Y^{NL}_{AERO} + Y^{NR}_{AERO} + Y^{F}_{AERO} + Y^{LW}_{AERO} + Y^{RW}_{AERO} + Y^{T}_{AERO}$$

$$Z_{AERO} = Z^{NL}_{AERO} + Z^{NR}_{AERO} + Z^{F}_{AERO} + Z^{LW}_{AERO} + Z^{RW}_{AERO} + Z^{T}_{AERO}$$

$$\mathcal{L}_{AERO} = \mathcal{L}^{NL}_{AERO} + \mathcal{L}^{NR}_{AERO} + \mathcal{L}^{F}_{AERO} + \mathcal{L}^{W}_{AERO} + \mathcal{L}^{T}_{AERO}$$
$$+ Y_N \,(Z^{NR}_{AERO} - Z^{NL}_{AERO}) + Z_{CG}\,(Y^{NL}_{AERO} + Y^{NR}_{AERO})$$

$$M_{AERO} = M^{NL}_{AERO} + M^{NR}_{AERO} + M^{F}_{AERO} + M^{W}_{AERO} + M^{T}_{AERO}$$
$$+ X_{CG}(Z^{NL}_{AERO} + Z^{NR}_{AERO}) - Z_{CG}\,(X^{NL}_{AERO} + X^{NR}_{AERO})$$

$$N_{AERO} = N^{NL}_{AERO} + N^{NR}_{AERO} + N^{F}_{AERO} + N^{W}_{AERO} + N^{T}_{AERO}$$
$$+ Y_N \,(X^{NL}_{AERO} - X^{NR}_{AERO}) - X_{CG}\,(Y^{NL}_{AERO} + Y^{NR}_{AERO})$$

BASIC EQUATIONS OF MOTION

INERTIAS:

$$I_{XX} = I_{XXO} + K_{I_1} i_N$$

$$I_{YY} = I_{YYO} + K_{I_2} i_N$$

$$I_{ZZ} = I_{ZZO} + K_{I_3} i_N$$

$$I_{XZ} = I_{XZO} + K_{I_4} i_N$$

$$J_{XX} = I_{ZZ} - I_{YY}$$

$$J_{YY} = I_{XX} - I_{ZZ}$$

$$J_{ZZ} = I_{YY} - I_{XX}$$

ROLL EQUATION

$$I_{xx}\dot{p} = -J_{xx}\,rq + I_{xz}\,(\dot{r} + pq)$$

$$+ \ell m_N\, Y_N \left\{ \ddot{i}_{NR} \cos(i_{NR} - \lambda) - \ddot{i}_{NL} \cos(i_{NL} - \lambda) \right\}$$

$$+ \mathcal{L}_{AERO}$$

PITCH EQUATION

$$I_{yy}\dot{q} = -J_{yy}\,pr - I_{xz}\,(p^2 - r^2)$$

$$- \ddot{i}_{NR} \left\{ I'_{yy} + \ell m_N [-Z_R \sin(i_{NR} - \lambda) + X_R \cos(i_{NR} - \lambda)] \right\}$$

$$- \ddot{i}_{NL} \left\{ I'_{yy} + \ell m_N [-Z_L \sin(i_{NL} - \lambda) + X_L \cos(i_{NL} - \lambda)] \right\}$$

$$+ M_{AERO}$$

YAW EQUATION

$$I_{zz}\dot{r} = -J_{zz}\,pq - (rq - \dot{p})\,I_{xz}$$

$$- \ell m_N\, Y_N \left\{ \ddot{i}_{NR} \sin(i_{NR} - \lambda) - \ddot{i}_{NL} \sin(i_{NL} - \lambda) \right\}$$

$$+ N_{AERO}$$

RIGHT NACELLE ACTUATOR PITCHING MOMENT EQUATION

$$
\begin{aligned}
M_{NRACT} = & - \ddot{i}_{NR} \left[I'_{yy} + \ell^2 m_N \left(1 - \frac{m_N}{m}\right) \right] \\
& - \ell^2 m_N \left(1 - \frac{m_N}{m}\right) \Big[- pr \cos 2 (i_{NR} - \lambda) + \dot{q} \\
& + (r^2 - p^2) \sin (i_{NR} - \lambda) \cos (i_{NR} - \lambda) \Big] \\
& - (r^2 - p^2) \left[I'_{zz} \sin i_{NR} \cos i_{NR} \right] - I'_{yy} \dot{q} \\
& + \ell \frac{m_N}{m} \left[X_{AERO} \sin (i_{NR} - \lambda) + Z_{AERO} \cos (i_{NR} - \lambda) \right] \\
& - \ell m_N Y_N \Big\{ (\dot{r} - pq) \left[\sin (i_{NR} - \lambda) \right] \\
& \qquad - (\dot{p} + rq) \left[\cos (i_{NR} - \lambda) \right] \Big\} \\
& + M_{NRAERO}
\end{aligned}
$$

LEFT NACELLE PITCHING MOMENT EQUATION OBTAINED BY CHANGING SIGN OF Y_N AND CHANGING SUBSCRIPT FROM R TO L.

<u>NOTE</u>: THE ABOVE EQUATION MUST BE CALCULATED FOR WING TORSION CALCULATION ONLY.

MOTION OF A.C. MASS CENTER

$$\dot{U} = \frac{X_{AERO}}{m} - g \sin \theta - qW + rV$$

$$\dot{V} = \frac{Y_{AERO}}{m} + g \cos \theta \sin \phi - rU + pW$$

$$\dot{W} = \frac{Z_{AERO}}{m} + g \cos \theta \cos \phi + qU - pV$$

EULER ANGLE CALCULATION

$$\dot{\psi} = (r \cos \phi + q \sin \phi)/\cos \theta$$

$$\dot{\theta} = q \cos \phi - r \sin \phi$$

$$\dot{\phi} = p + \dot{\psi} \sin \theta$$

AIRCRAFT CONDITION CALCULATIONS

GROUND TRACK

NORTHWARD VELOCITY

$$\dot{X}_{NORTH} = U \cos\theta \cos\psi + V (\sin\phi \sin\theta \cos\psi - \cos\phi \sin\psi) + W (\cos\phi \sin\theta \cos\psi + \sin\phi \sin\psi)$$

EASTWARD VELOCITY

$$\dot{Y}_{EAST} = U \cos\theta \sin\psi + V (\sin\phi \sin\theta \sin\psi + \cos\phi \cos\psi) + W (\cos\phi \sin\theta \sin\psi - \sin\phi \cos\psi)$$

DOWNWARD VELOCITY

$$\dot{Z}_{DOWN} = - U \sin\theta + V \sin\phi \cos\theta + W \cos\phi \cos\theta$$

PILOT STATION ACCELERATIONS (BODY AXES)

$$a_{XPA} = \frac{X_{AERO}}{m} + (\dot{q} + pr)\ (Z_{PA} - Z_{CG})$$

$$+ (q^2 + r^2)\ (X_{CG} - \ell_{PA}) + Y_{PA}\ (pq - \dot{r})$$

$$- 2\ q\ \dot{Z}_{CG} - \ddot{X}_{CG}$$

$$a_{YPA} = \frac{Y_{AERO}}{m} + (\dot{p} - qr)\ (Z_{CG} - Z_{PA}) + (\dot{r} + pq)(\ell_{PA} - X_{CG})$$

$$- Y_{PA}\ (r^2 + p^2) + 2\ (p\dot{Z}_{CG} - r\dot{X}_{CG})$$

$$a_{ZPA} = \frac{Z_{AERO}}{m} + (\dot{q} - pr)\ (X_{CG} - \ell_{PA}) + (p^2 + q^2)\ (Z_{CG} - Z_{PA})$$

$$+ Y_{PA}\ (\dot{p} + qr) + 2q\dot{X}_{CG} - \ddot{Z}_{CG}$$

PILOT STATION VELOCITIES (BODY AXES)

$$U_{PA} = U_P + qZ_{PA} - rY_{PA}$$

$$V_{PA} = V_P + r\ell_{PA} - pZ_{PA}$$

$$W_{PA} = W_P + pY_{PA} - q\ell_{PA}$$

GUST MODEL

The gust model will be that represented by NASA-AMES program NAPS-80. The output of this program, in the form of gust velocity components U_g, V_g, W_g, p_g, q_g, r_g will be added to the aircraft velocity components in clear air as follows:

$$U = U' + U_g \qquad p = p' + p_g$$

$$V = V' + V_g \qquad q = q' + q_g$$

$$W = W' + W_g \qquad r = r' + r_g$$

APPENDIX F

Appendix F

This appendix contains the numerical constants and functions required by the equations presented in Appendix E.

The data is listed by reference to the page number in Appendix E where the numerical constant or function first appears.

INPUT DATA

PAGE NO.	QUANTITY	VALUE	UNITS
E-7	$K_{\delta_{STEER}}$	0.0	deg/cm (deg/in)
	$K_{\delta_{RUD}}$	-3.15 (-8.0)	"
	K_{δ_r}	1.0	-
	ω_A	20.0	rad/sec
	ζ	1.0	-
	K_{δ_S}	1.0	-
	ω_L	35.5	rad/sec
	ζ'	0.18	-
	K_{δ_B}	1.0	-
	$K'_{\delta S}$	0.0	-
	K_{δ_e}	-1.638(-4.16)	deg/cm (deg/in)
	Schedule A	Figure F-1	
	Schedule B	set to zero	
	Schedule C	Figure F-1	
	Schedule D	Figure F-1	
	Schedule E	Figure F-2	
	Schedule H	Figure F-2	
	Schedule I	Figure F-2a	
	Schedule J	Figure F-2a	
	Schedule K	Figure F-2b	
E-8	Schedule A	Figure F-3	
	Schedule B	Figure F-4	
	Schedule C	Figure F-4	
E-9	Schedule FPR	Figure F-5	
E-13	Engine data	Tables F-1 through F-4, Figures F-6 through F-9	

INPUT DATA

PAGE NO.	QUANTITY	VALUE	UNITS
	WDTIND	1.0	-
	SHP*	1156.3 (1550.0)	kw (SHP)
	$\dot{w}_{MAX}/\dot{w}^*$	1.11	-
	N1IND	1.0	-
	$N_{I_{MAX}}/N_I^*$	1.04	-
	N1θIND	0.0	-
	$(N1/\sqrt{\theta_1}/N_I^*)_{MAX}$	0.0	-
	QIND	1.0	-
	QMAX/Q*	1.446	-
E-15	$N_{II_{MAX}}/N_{II}^*$	1.128	-
	N_I^*	2662.5 (25425.0)	rad/sec (RPM)
E-16	$(N_{II}/N_{II_{MAX}})_{REF}$	0.8865	-
	Ω_{REF}	57.6923	rad/sec
	G_1	2.5	deg/sec/rad/sec
	G_2	2.66	deg/rad/sec
	G_3	0.0	deg/sec/deg
	I_p	764.8 (564.0)	$kg\ m^2$ ($slugs\ ft^2$)
	κ	-1.0	-
	η_{tr}	0.97	-
	Schedule A	Figure F-10	
	Schedule B	Figure F-11	
	Schedule C	Figure F-11	
	Schedule D	Figure F-11	
	Schedule G	Figure F-12	
	Schedule K	set to zero	

INPUT DATA

PAGE NO.	QUANTITY	VALUE	UNITS
E-17	ϕ_p	-30.0	deg
	m_f	-1443.28(-125.947)	kg (slugs)
	ℓ_f	0.304(1.0)	m (ft)
	m_w	0	kg (slugs)
	ℓ_w	0	m (ft)
	m	5895.94(404)	kg (slugs)
	ℓ	0.502(1.65)	m (ft)
	m_N	903.95(61.94)	kg (slugs)
	λ	24.75	deg
	h_f	-1.943(-6.376)	m (ft)
	h_w	0.0	m (ft)
E-20	Z_{WAC}	.105(0.346)	m (ft)
	Y_{WAC}	3.048(10.0)	m (ft)
	X_{WAC}	0.224(0.736)	m (ft)
	Y_N	4.902 (16.083)	m (ft)
	L_S	1.423 (4.667)	m (ft)
E-21	i_W	0.0	deg
E-22	Z_{HT}	-0.076 (-0.25)	m (ft)
	X_{HT}	-6.605 (-21.67)	m (ft)
	Z_{VT}	-0.399 (-1.308)	m (ft)
	X_{VT}	-6.858 (-22.5)	m (ft)
	Y_{VT}	1.956 (6.417)	m (ft)

INPUT DATA

PAGE NO.	QUANTITY	VALUE		UNITS
E-23	Solutions to Quartic	Table F-5		
	A	49.325 (530.93)		$m^2 (ft^2)$
	K_s	1.6		-
E-24	ε_{WRR}	set to zero		rad
	ε_{WLR}	set to zero		rad
	PC	0.884 (2.9)		m (ft)
	h_p	0.0		m (ft)
	D	7.925 (26.0)		m (ft)
	c_w	1.6 (5.25)		m (ft)
E-25	S_w	16.815 (181.0)		$m^2 (ft^2)$
	$C_{L_{\alpha_w}}$	4.393 (1)	3.281 (2)	rad^{-1}
E-28	a_7	0.010845	.00869	deg^{-1}
	δ_2	65.0	65.0	deg
	a_8	0.397	0.3366	-
	a_9	0.00474	0.00351	deg^{-1}
	a_{10}	0.0	0.0	deg^{-2}
	δ_3	180.	180.	deg
	a_{11}	0.0	0.0	-

(1) @ $i_N = 0°$

(2) @ $i_N = 90°$

INPUT DATA

PAGE NO.	QUANTITY	VALUE		UNITS
	a_{12}	0.0	0.0	deg^{-1}
	a_{13}	0.0	0.0	deg^{-2}
	a_{29}	-0.7648×10^{-3}	-0.7648×10^{-3}	deg^{-1}
	a_{30}	0.2135×10^{-4}	0.2135×10^{-4}	deg^{-2}
	δ_5	180.0	180.0	deg
	a_{31}	0.0	0.0	-
	a_{32}	0.0	0.0	deg^{-1}
E-29	a_0	16.5	16.5	deg
	a_1	-.058	-.047	-
	δ_1	122.0	122.0	deg
	a_2	9.42	10.766	deg
	a_3	-21.0	-21.0	deg
	a_4	0.0	0.0	-
	a_5	-21.0	-21.0	deg
	a_6	0.255	0.180	-
	$C'_{L_{\alpha_W}}$	4.4192	3.3015	rad^{-1}
	C_{DO_W}	0.0175	0.212	-
	a_{26}	0.0	0.0	-
	a_{27}	0.057	0.1175	-
	a_{28}	0.0	0.0	-

INPUT DATA

PAGE NO.	QUANTITY		VALUE		UNITS
E-30	a_{18}		0.0	0.0	deg
	a_{20}		0.0	0.0	-
	a_{21}		0.0	0.0	deg^{-1}
	a_{22}		0.0	0.0	deg^{-2}
E-31	a_{19}		0.0	0.0	deg
E-33	b_2		0.0	0.0	-
	b_3		0.0	0.0	deg^{-1}
	$i_N \leq 60°$	b_4	-0.025	-0.025	-
	$i_N > 60°$	b_4	0.21994	0.21994	-
	b_5		-.003231	-.003231	deg^{-1}
	b_6		0.154×10^{-4}	0.154×10^{-4}	deg^{-2}
	$i_N \leq 60°$	b_7	0.0019166	0.0019166	deg^{-1}
	$i_N > 60°$	b_7	-0.002166	-0.002166	deg^{-1}
E-34	$C_{L_{MAX}}$		1.625		-
	f_1		Figure F-13		-
E-38	K_{20}		0.04	0.04	rad^{-1}
	K_{21}		-0.05	0.09	rad^{-1}
	b_W		9.805	(32.17)	m (ft)
	$K_{\mathcal{L}}$			1.0	-
	$\bar{Y}_{AC}$		3.048	(10.0)	m (ft)
	K_{22}			-0.0315	rad^{-1}

INPUT DATA

PAGE NO.	QUANTITY	VALUE	UNITS
E-39	f_2	Table F-6	
	f_3	Table F-7	
E-40	i_{HT}	0	deg
	τ_{HT}	0.5565	-
	$\alpha_{HT_{STALL}}$	16.0	deg
	$C_{L_{\alpha_{HT}}}$	0.071	deg
	f_6	Figure F-13	
	S_{HT}	4.67 (50.25)	m^2 (ft^2)
E-44	f_{10}	Table F-8	
E-47	η_{HT}	Table F-9	
	S_{VT}	2.35 (25.25)	m^2 (ft^2)
E-49	C_{DON}	0.0	-
	K_{30}	0.0	-
	K_{31}	0.0	-
	K_{32}	0.0	-
	C_{MON}	0.0	-
	K_{34}	0.0	-
	K_{35}	0.0	-
E-50	K_{36}	0.0	-
	K_{37}	0.0	-
	K'_{36}	0.0	-

INPUT DATA

PAGE NO.	QUANTITY	VALUE		UNITS
	K'_{37}	0.0		-
	C_{NORN}	0.0		-
	K_{38}	0.0		-
	K_{39}	0.0		-
	C_{NOLN}	0.0		-
	K_{40}	0.0		-
	K_{41}	0.0		-
E-51	X_{G1}	-0.661	(-2.17)	m (ft)
	X_{G2}	-0.661	(-2.17)	m (ft)
	X_{G3}	4.090	(13.42)	m (ft)
	Y_{G1}	-1.301	(-4.27)	m (ft)
	Y_{G2}	1.301	(4.27)	m (ft)
	Y_{G3}	0.0		m (ft)
	Z_{G1}	2.057	(6.75)	m (ft)
	Z_{G2}	2.057	(6.75)	m (ft)
	Z_{G3}	2.128	(6.98)	m (ft)
	γ_1	0.026	(0.855)	m (ft)
	γ_2	0.026	(0.855)	m (ft)
	γ_3	0.165	(0.54)	m (ft)
	K_{ST1}	56040	(3840)	N/m (lb/ft)
	K_{ST2}	56040	(3840)	N/m (lb/ft)

INPUT DATA

PAGE NO.	QUANTITY	VALUE	UNITS
	K_{ST3}	56040 (3840)	N/m (lb/ft)
	D_{ST1}	8756 (600)	N/m/s(lb/ft/sec)
	D_{ST2}	8756 (600)	N/m/s(lb/ft/sec)
	D_{ST3}	8756 (600)	N/m/s(lb/ft/sec)
E-52	μ_o	0.03	-
	μ_1	0.005	-
	μ_s	0.5	-
E-54	C_{DOF}	0.01219	-
	K_o	27.89	
$\alpha \geq 0$	K_2	0.28363	rad^{-2}
$\alpha < 0$	K_2	0.58237	rad^{-2}
	K_1	0.0	rad^{-1}
	ΔC_{DLG}	0.0221	-
	K_3	0.302	-
	K_4	0.0	-
	K_{42}	0.04	-
	K_7	-0.46	-
	K_8	-0.225	-
	C_{MOF}	-0.00455	-
	K_5	0.0	-
	K_6	0.0	rad^{-2}

INPUT DATA

PAGE NO.	QUANTITY	VALUE	UNITS
	ΔC_{MLG}	-0.00233	-
	t_G	8.0	sec
	C_{NOF}	0.0	-
	K_9	-0.2	-
	K_{10}	-0.092	-
	K_{13}	-0.075	-
E-55	Z_{PAC}	0.405 (1.33)	m (ft)
	X_{PAC}	0.177 (0.58)	m (ft)
E-56	f_7	set to zero	-
E-57	T_1	0.2434	rad^{-1}
	T_2	-0.483	rad^{-2}
	T_3	0.5208	rad^{-3}
E-59	τ_1	0.1	sec
	τ_2	0.1	sec
E-60	D_{NF1}	0.00425	deg^{-1}
	D_{NF2}	0.0014483	deg^{-1}
	D_{NF3}	-0.0000734	deg^{-1}
	D_{NF4}	0.00002175	deg^{-1}
	D_{NF5}	-0.0006	deg^{-1}
	E_{NF1}	-0.0245	deg^{-1}
	E_{NF2}	-0.0017028	deg^{-1}

INPUT DATA

PAGE NO.	QUANTITY	VALUE	UNITS
	E_{NF3}	-0.0010492	deg^{-1}
	E_{NF4}	-0.0000425	deg^{-1}
	E_{NF5}	0.0017892	deg^{-1}
E-61	D_{SF1}	0.0245	deg^{-1}
	D_{SF2}	0.0017028	deg^{-1}
	D_{SF3}	0.0010492	deg^{-1}
	D_{SF4}	-0.0000425	deg^{-1}
	D_{SF5}	-0.001735	deg^{-1}
	E_{SF1}	0.00425	deg^{-1}
	E_{SF2}	0.0014483	deg^{-1}
	E_{SF3}	-0.0000734	deg^{-1}
	E_{SF4}	0.00002175	deg^{-1}
	E_{SF5}	-0.0067758	deg^{-1}
E-62	D_{PM1}	0.002	deg^{-1}
	D_{PM2}	-0.00072556	deg^{-1}
	D_{PM3}	0.00111967	deg^{-1}
	D_{PM4}	0.0002094	deg^{-1}
	D_{PM5}	0.00036524	deg^{-1}
	D_{PM6}	-0.00007296	deg^{-1}/rad/sec
	Ω_o	40.422	rad/sec

INPUT DATA

PAGE NO.	QUANTITY	VALUE	UNITS
E-63	E_{PM1}	-0.0025	deg^{-1}
	E_{PM2}	0.0004375	deg^{-1}
	E_{PM3}	0.0000729	deg^{-1}
	E_{PM4}	-0.000111245	deg^{-1}
	E_{PM5}	0.00063045	deg^{-1}
	E_{PM6}	-0.00006809	deg^{-1}/rad/sec
	f_{YM}	-1.0	-
E-64	D_{YM1}	-0.0025	deg^{-1}
	D_{YM2}	0.0004375	deg^{-1}
	D_{YM3}	0.0000792	deg^{-1}
	D_{YM4}	-0.000111245	deg^{-1}
	D_{YM5}	0.0005	deg^{-1}
	D_{YM6}	-0.00007296	deg^{-1}/rad/sec
	E_{YM1}	-0.002	deg^{-1}
	E_{YM2}	0.00072556	deg^{-1}
	E_{YM3}	-0.00111967	deg^{-1}
	E_{YM4}	-0.0002094	deg^{-1}
	E_{YM5}	-0.0004702	deg^{-1}
	E_{YM6}	0.00007296	deg^{-1}/rad/sec
E-65	f_{TR}	1.0	-
	f_{TL}	1.0	-
	f_{NFR}	1.0	-

INPUT DATA

PAGE NO.	QUANTITY	VALUE	UNITS
	f_{NFL}	1.0	-
	f_{SFR}	-1.0	-
	f_{SFL}	-1.0	-
	f_{PMR}	1.0	-
	f_{PML}	1.0	-
	f_{YMR}	-1.0	-
	f_{YML}	-1.0	-
	f_{QR}	-1.0	-
	f_{QL}	-1.0	-
E-66	I_E	0.248 (0.22)	$kg \cdot m^2$ (slug ft^2)
	K	-1.0	-
E-69	K_{W1}	$4.8x10^{-6}$ ($.596x10^{-4}$)	m/N(ft/lb)
	K_{W2}	$1.12x10^{-6}$ ($.1637x10^{-4}$)	m/N(ft/lb)
	K_{W3}	$4x10^{-7}$ ($.5836x10^{-5}$)	m/N(ft/lb)
	K_{W4}	$.2599x10^{-2}$	sec^2
	K_{W5}	$.1656x10^{-2}$	sec^2
	K_{W6}	$1.17x10^{-6}$ ($.1709.x10^{-4}$)	m/N(ft/lb)
	ξ_W	0.5	-
	ω_W	20.0	rad/sec
	$K_{\theta t}$	$.1096x10^{-6}$ ($1.6x10^6$)	Nm/rad(ft lb/rad)

INPUT DATA

PAGE NO.	QUANTITY	VALUE		UNITS
	I_{xxo}	54965	(40535)	kg.m^2(slug ft^2)
	I_{yyo}	17924	(13218)	kg.m^2(slug ft^2)
	I_{zzo}	68196	(50292)	kg.m^2(slug ft^2)
	I_{xzo}	327.6	(241.6)	kg.m^2(slug ft^2)
E-71	K_{I1}	27.783	(20.489)	kg.m^2/deg(slug ft^2/deg)
	K_{I2}	15.247	(11.244)	kg.m^2/deg(slug ft^2/deg)
	K_{I3}	-12.551	(-9.256)	kg.m^2/deg(slug ft^2/deg)
	K_{I4}	2.387	(1.76)	kg.m^2/deg(slug ft^2/deg)
E-72	I'_{yy}	584.4	(431.0)	kg.m^2(slug ft^2)
	I'_{xx}	110.4	(81.4)	kg.m^2(slug ft^2)
	I'_{zz}	515.3	(380.0)	kg.m^2(slug ft^2)
E-76	Z_{PA}	1.28	(4.2)	m (ft)
	Y_{PA}	0.427	(1.4)	m (ft)
	ℓ_{PA}	2.155	(7.07)	m (ft)

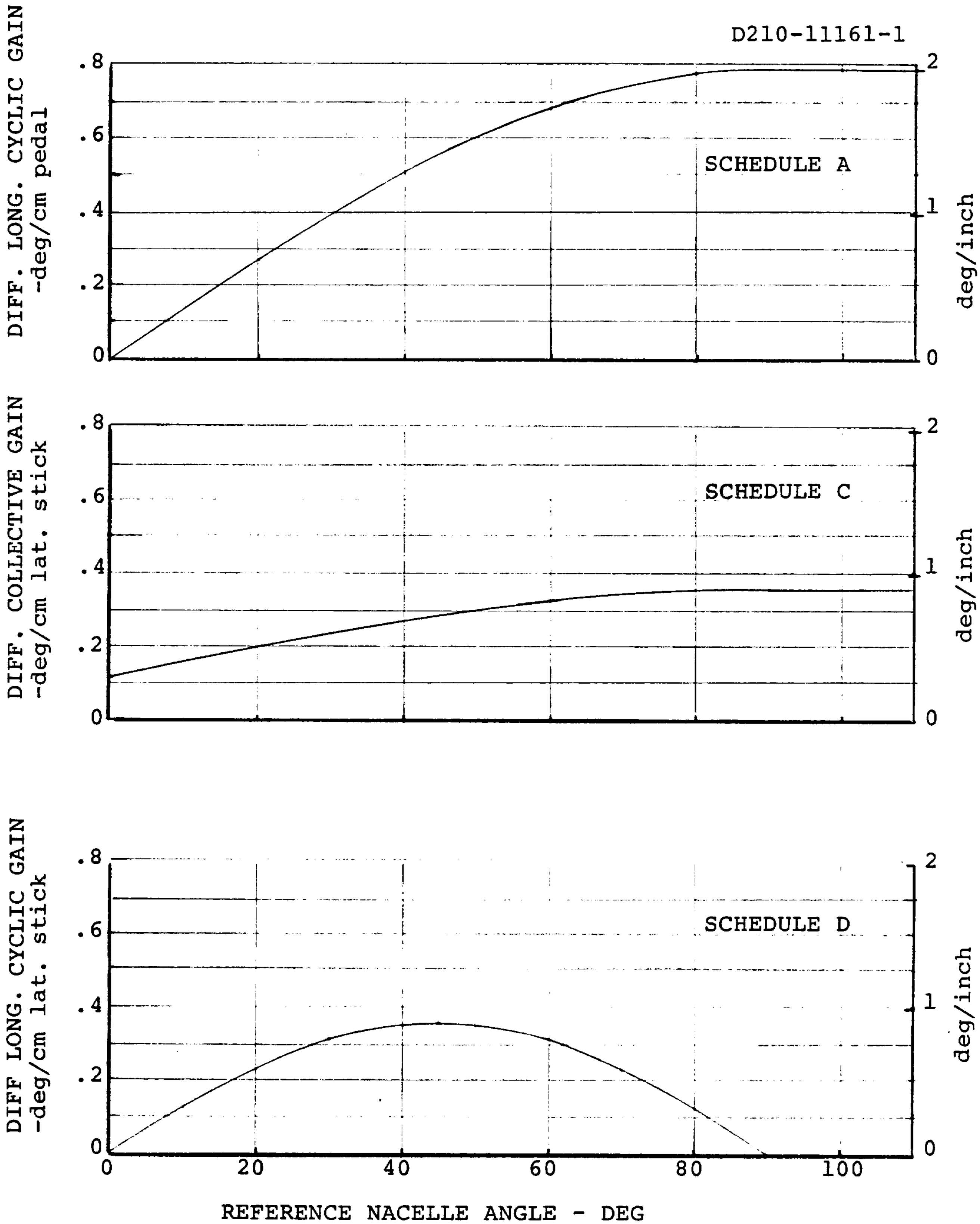

FIGURE F.1. CONTROL SYSTEM GAIN SCHEDULES

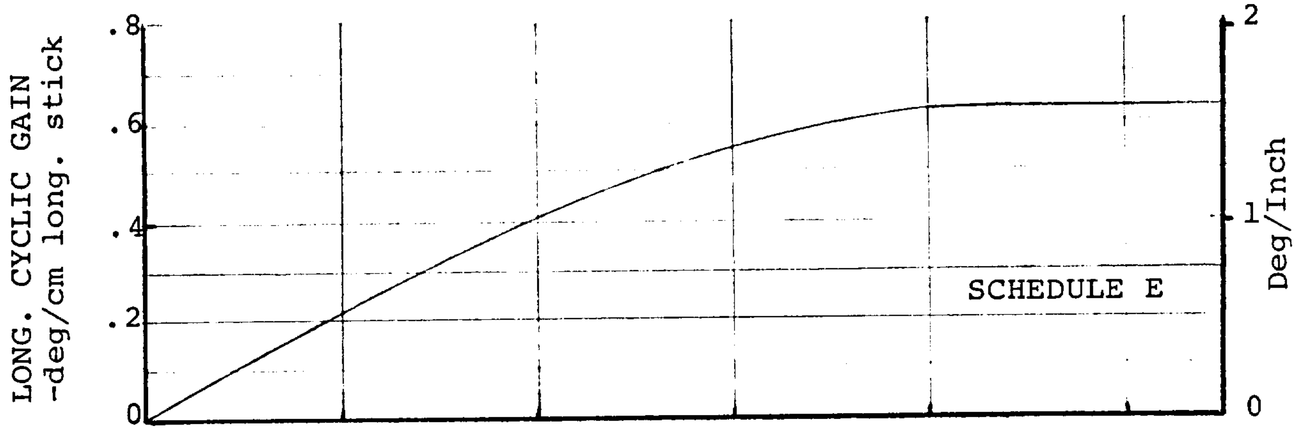

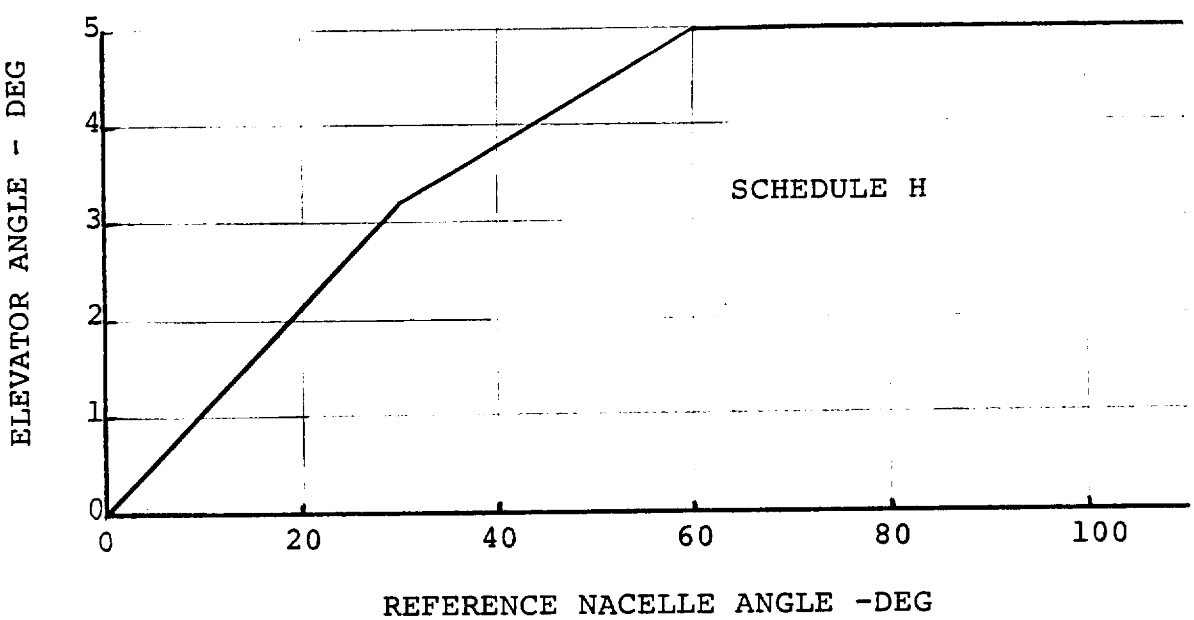

FIGURE F.2. CONTROL SYSTEM GAIN SCHEDULES

CONTROL AXIS CYCLIC PITCH INPUT AS A FUNCTION OF LONGITUDINAL STICK AT $i_N = 0°$

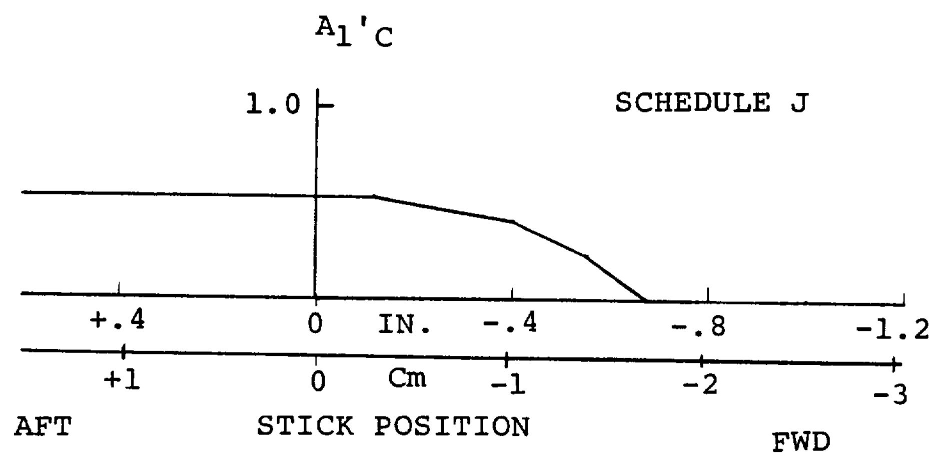

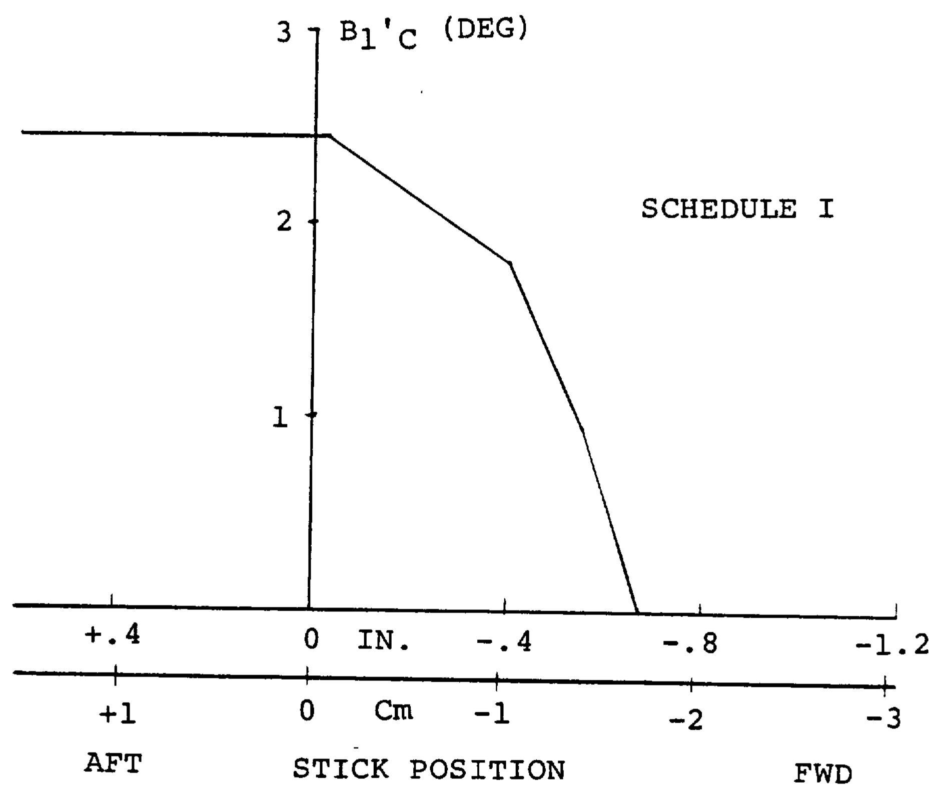

FIGURE F.2a. CYCLIC PITCH CONTROL ON THE STICK AT $i_N = 0°$

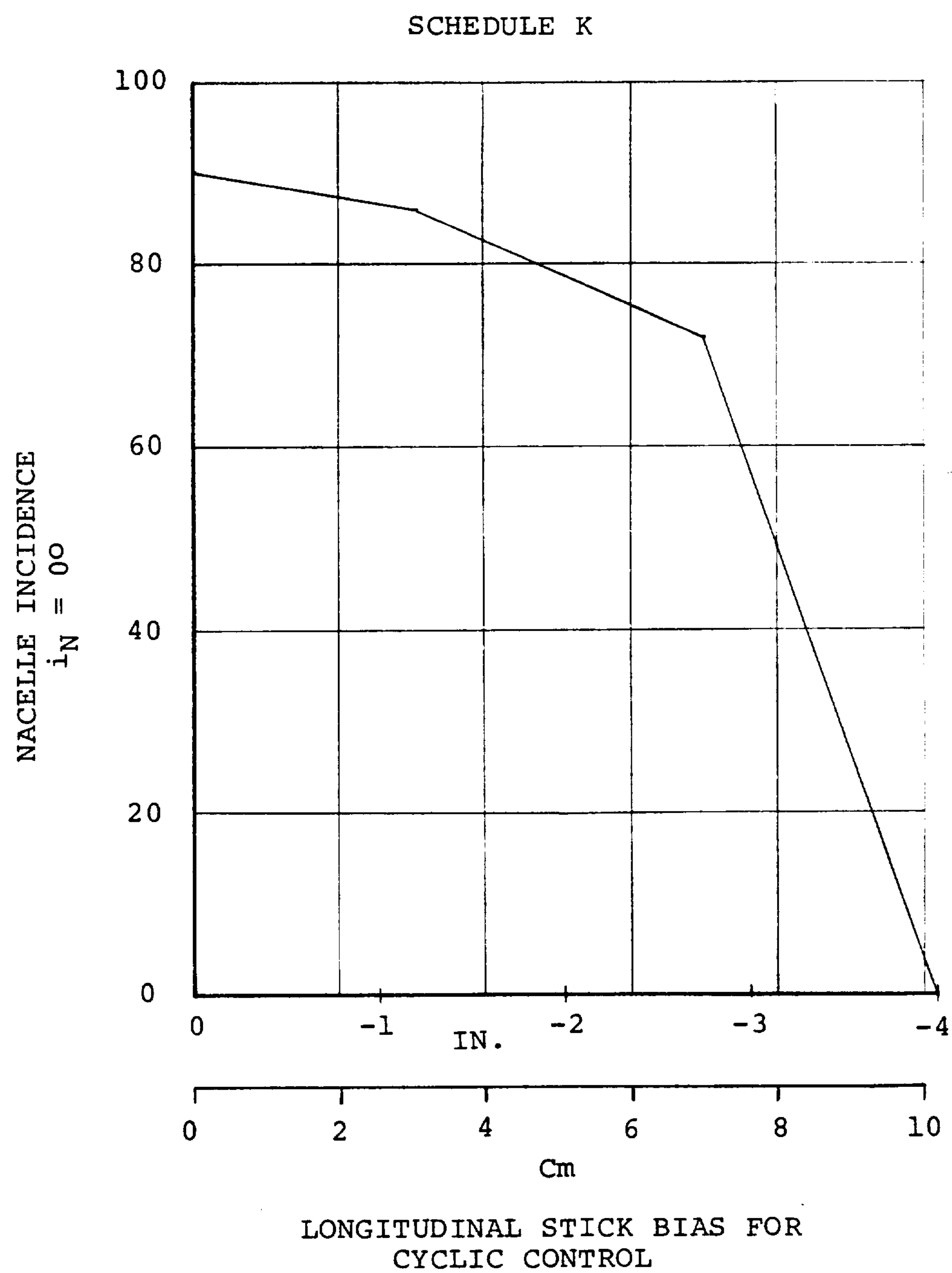

FIGURE F-2b. CONTROL SYSTEM LONGITUDINAL STICK BIAS - SCHEDULE K

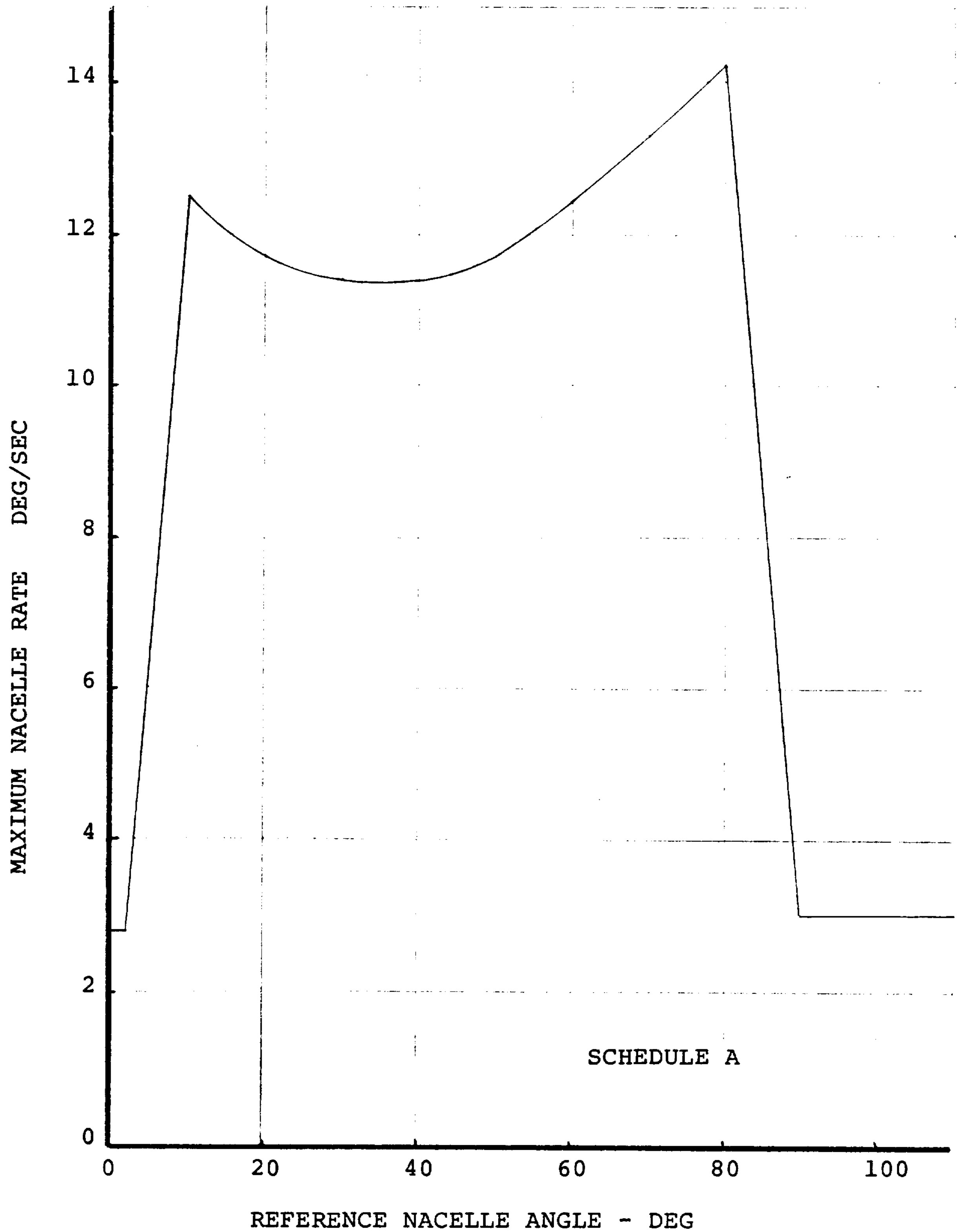

FIGURE F.3. FLAP, NACELLE, AILERON CONTROLS - SCHEDULE A

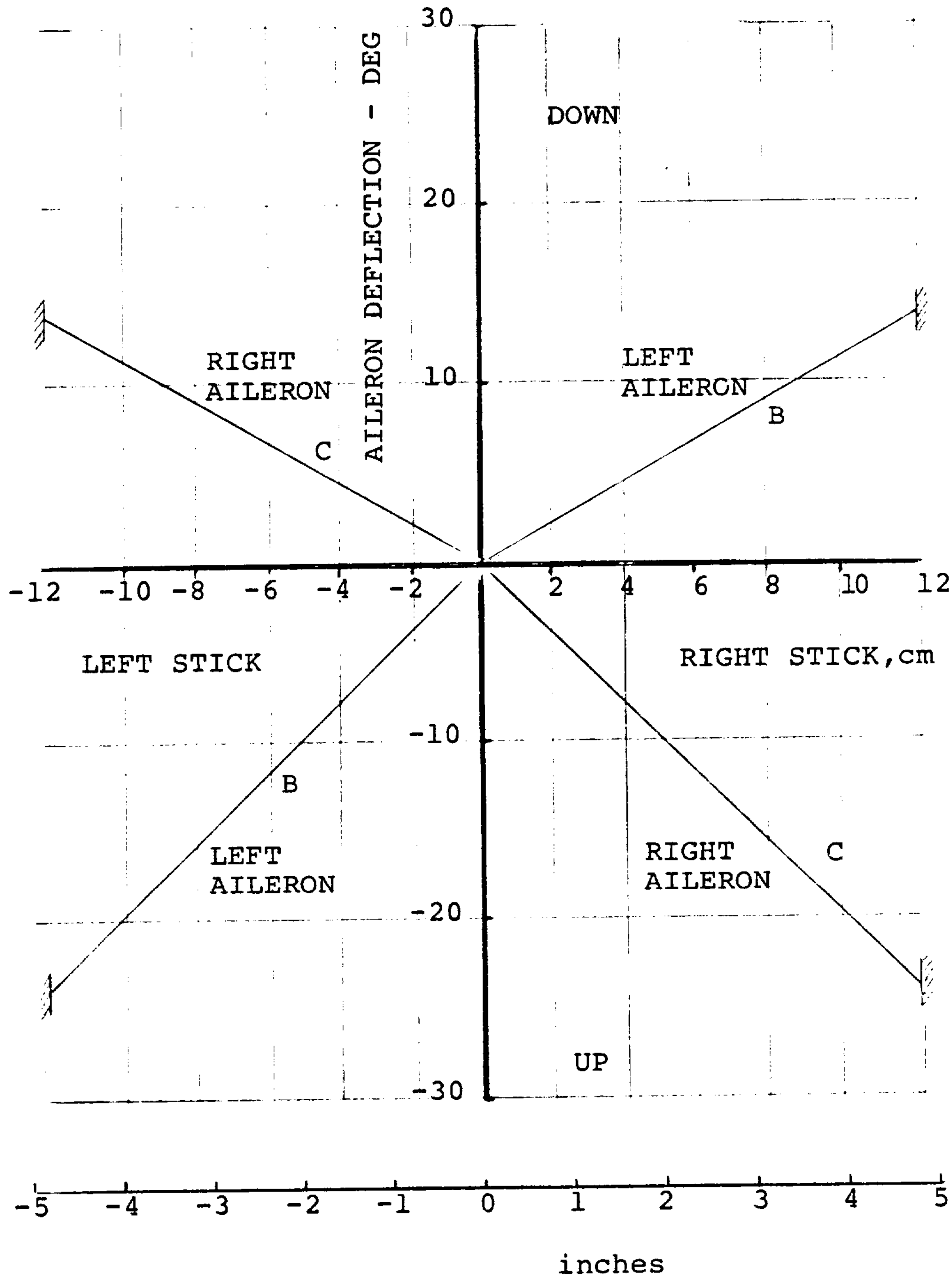

FIGURE F.4. FLAP, AILERON, NACELLE CONTROLS - SCHEDULES B & C

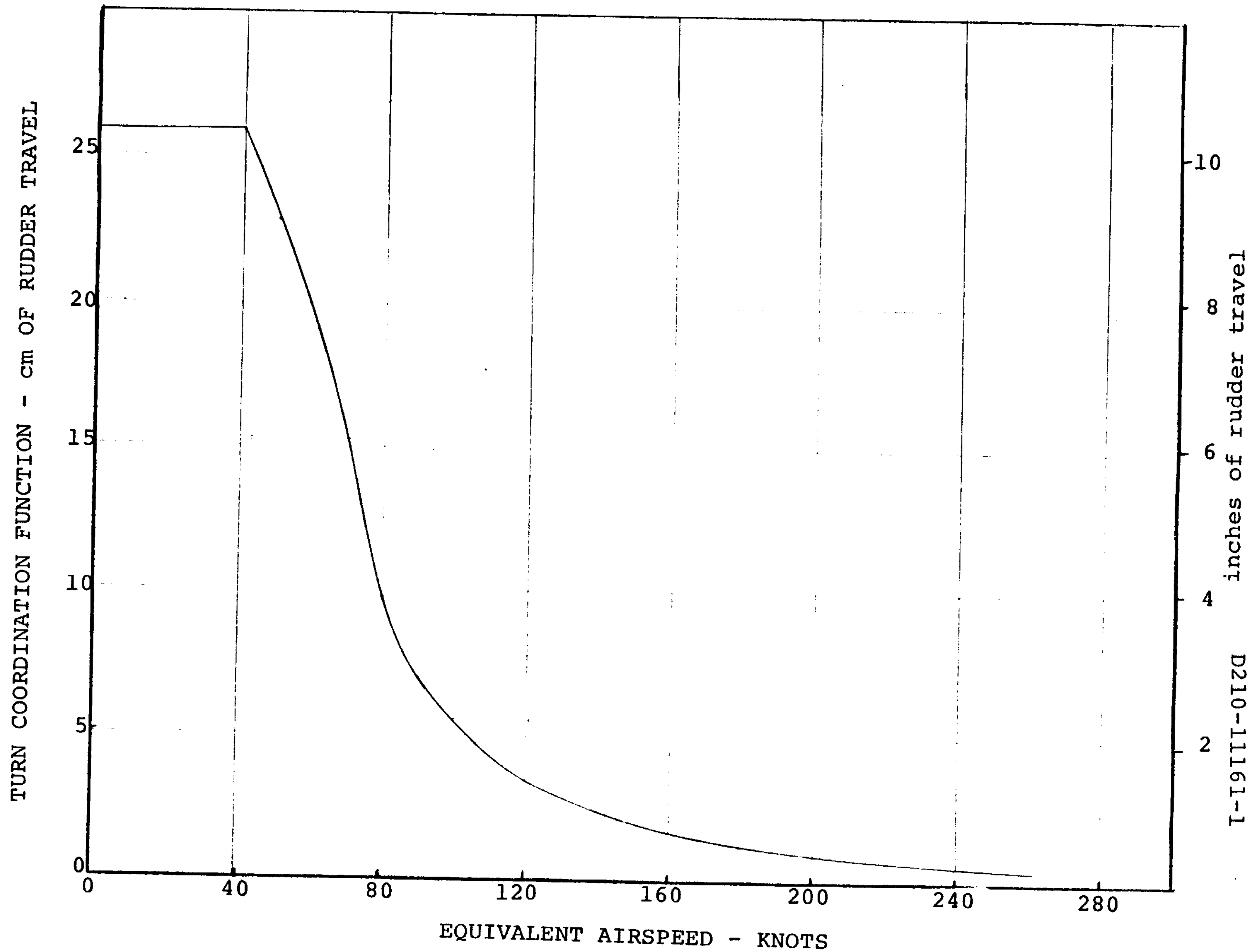

FIGURE F.5. LATERAL DIRECTIONAL SAS FUNCTION FPR

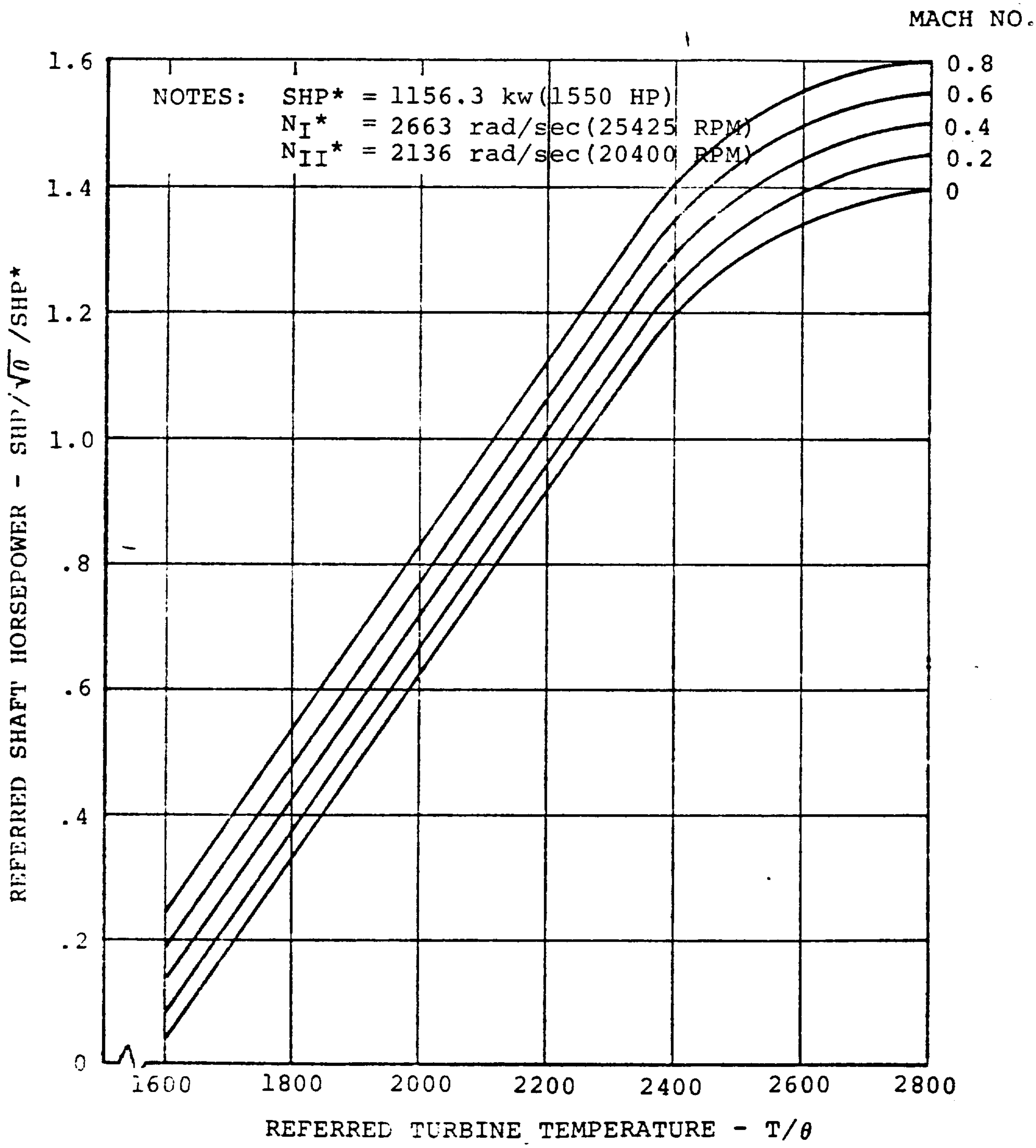

Figure F.6 . Turbine Engine Performance - Engine Cycle 1.78

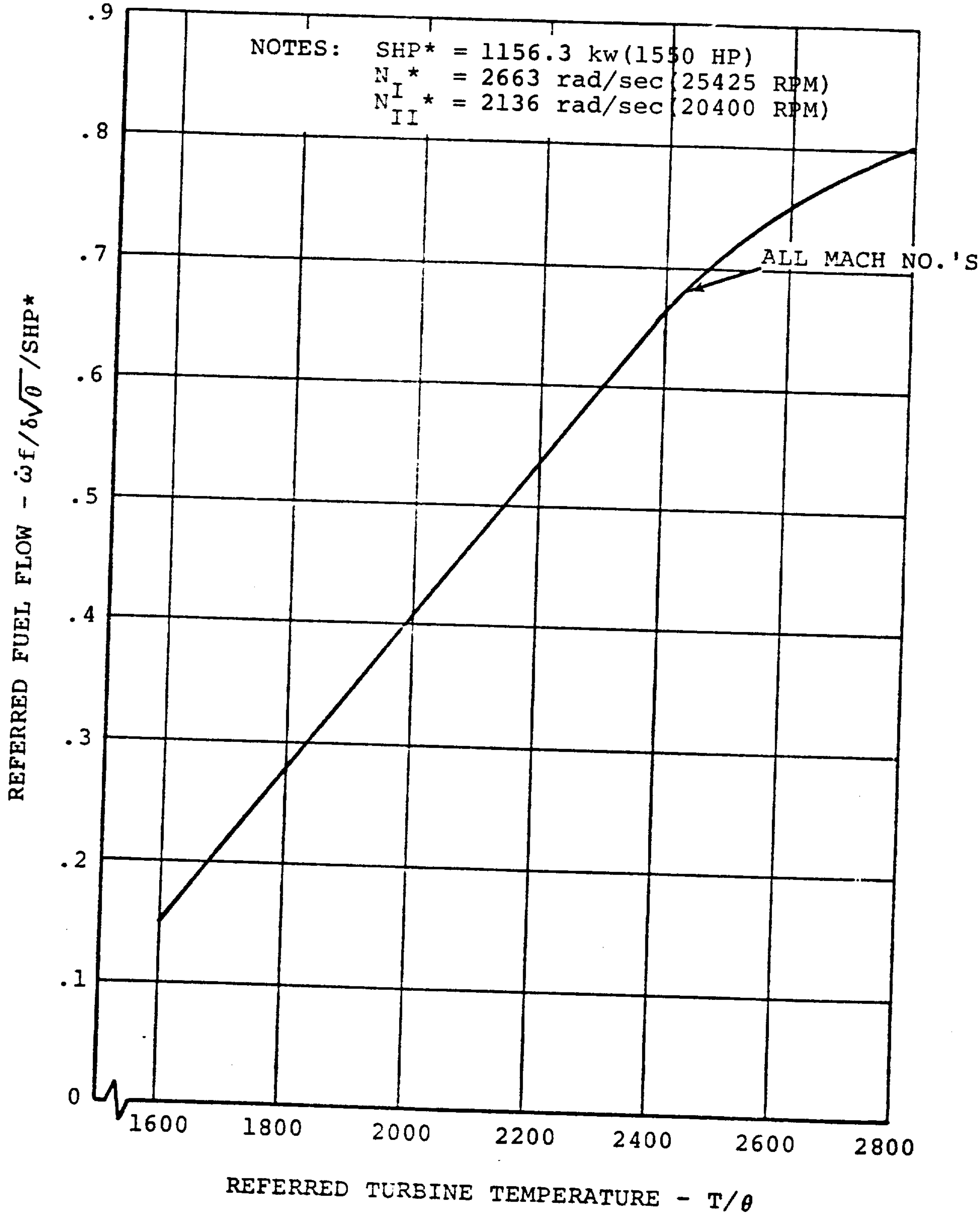

Figure F. 7 . Turbine Engine Performance - Engine Cycle 1.78

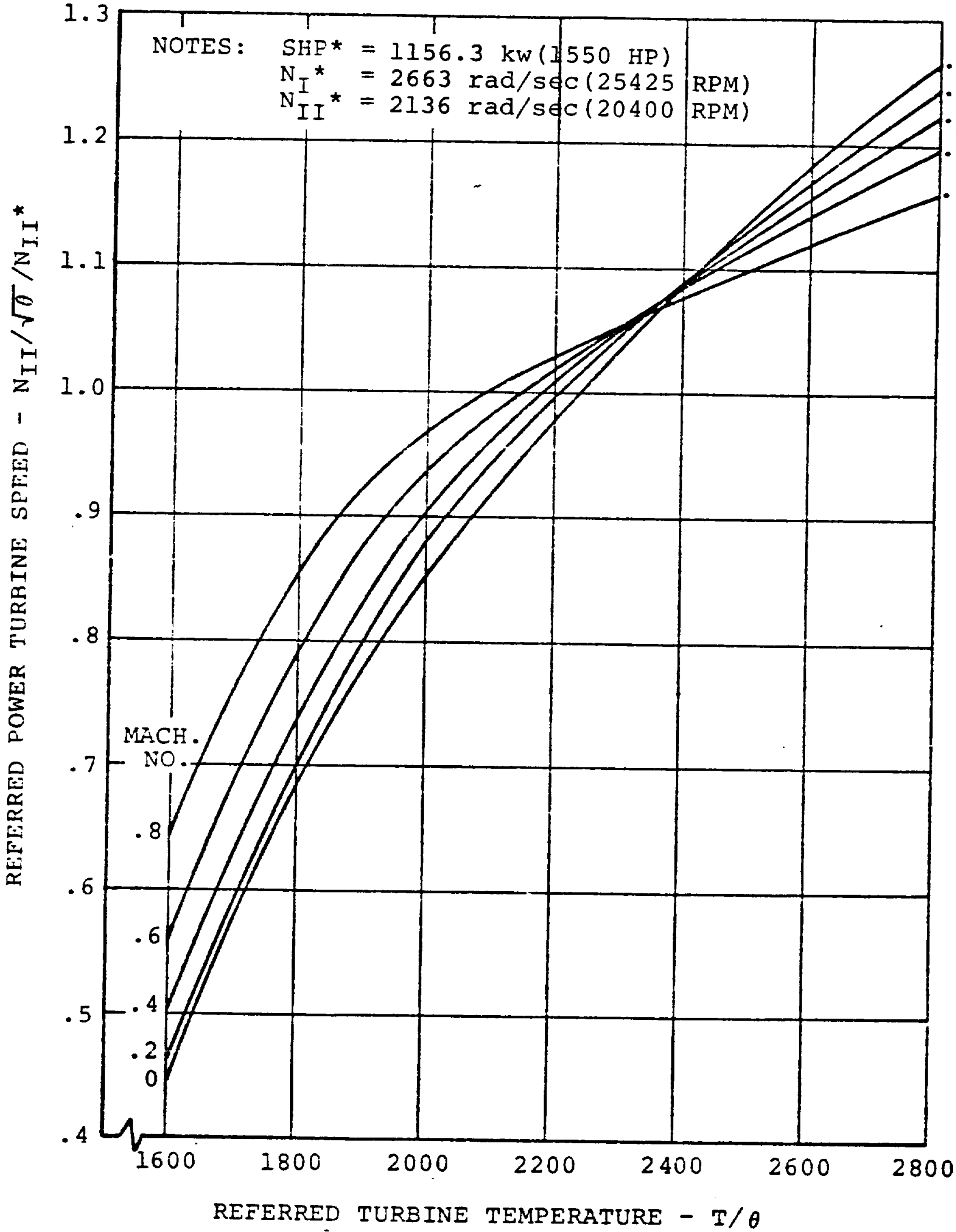

Figure F. 8 . Turbine Engine Performance - Engine Cycle 1.78

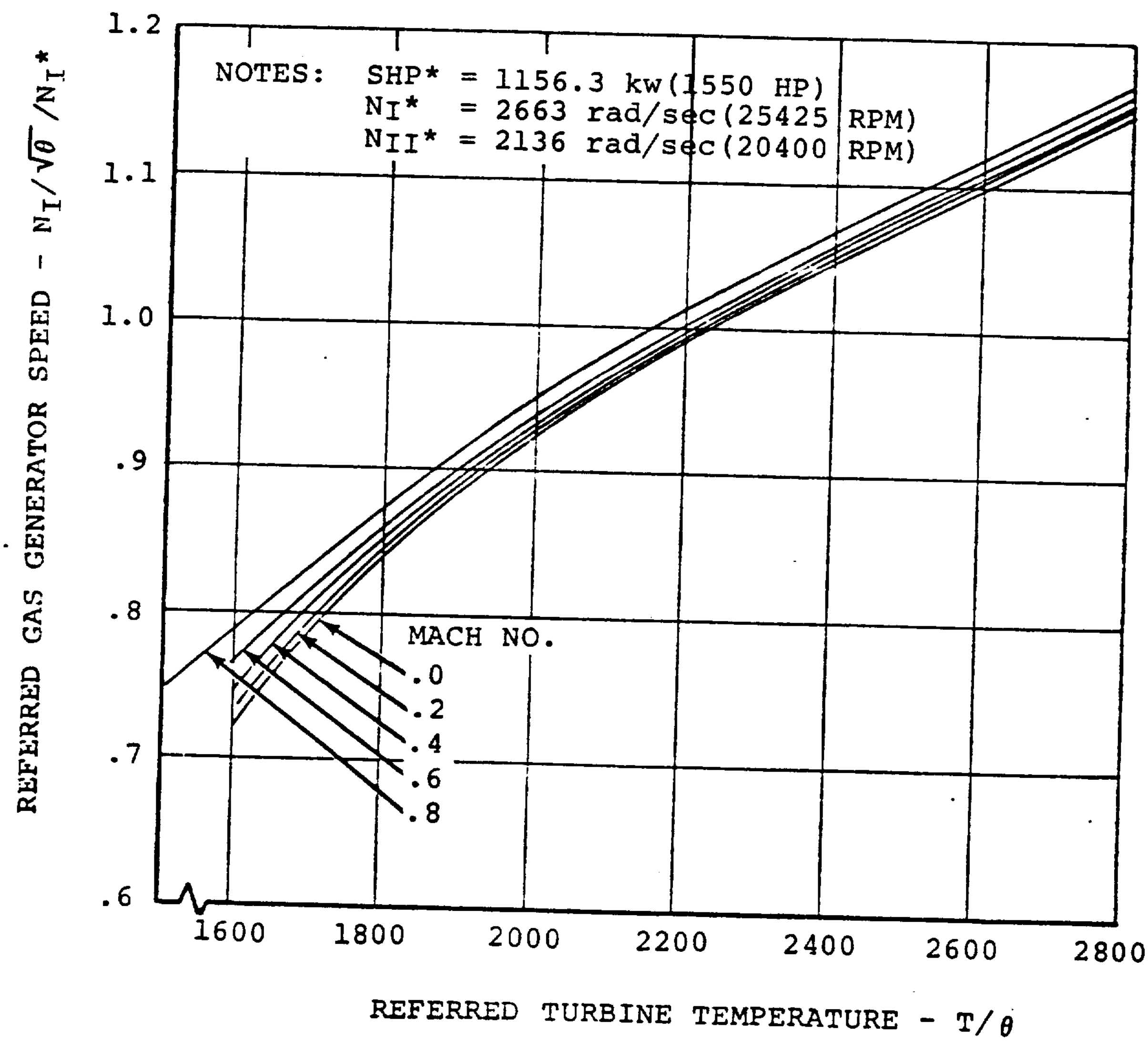

Figure F. 9. Turbine Engine Performance - Engine Cycle 1.78

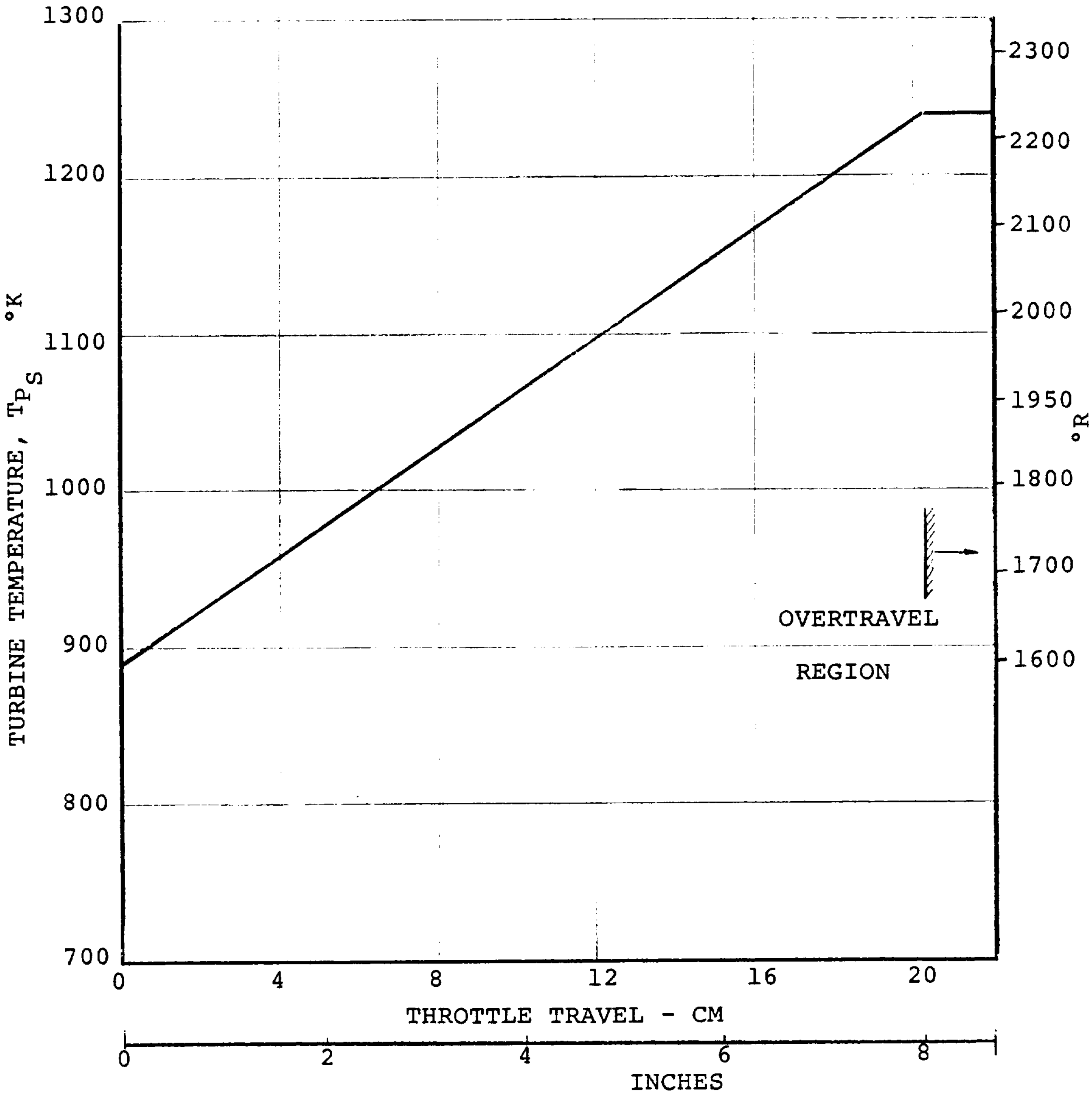

FIGURE F.10. THRUST MANAGEMENT SYSTEM - SCHEDULE A

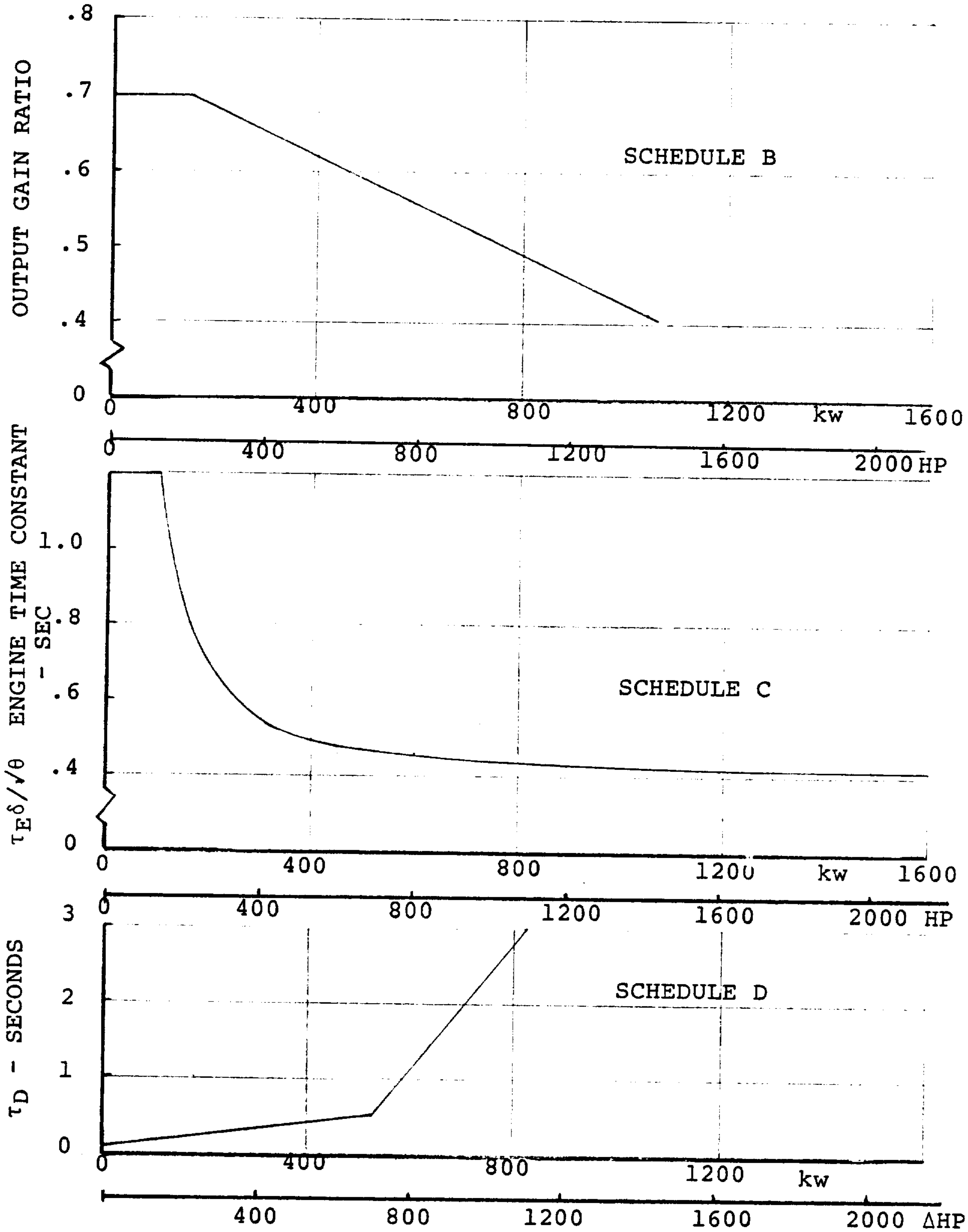

FIGURE F. 11. ENGINE RESPONSE CHARACTERISTICS

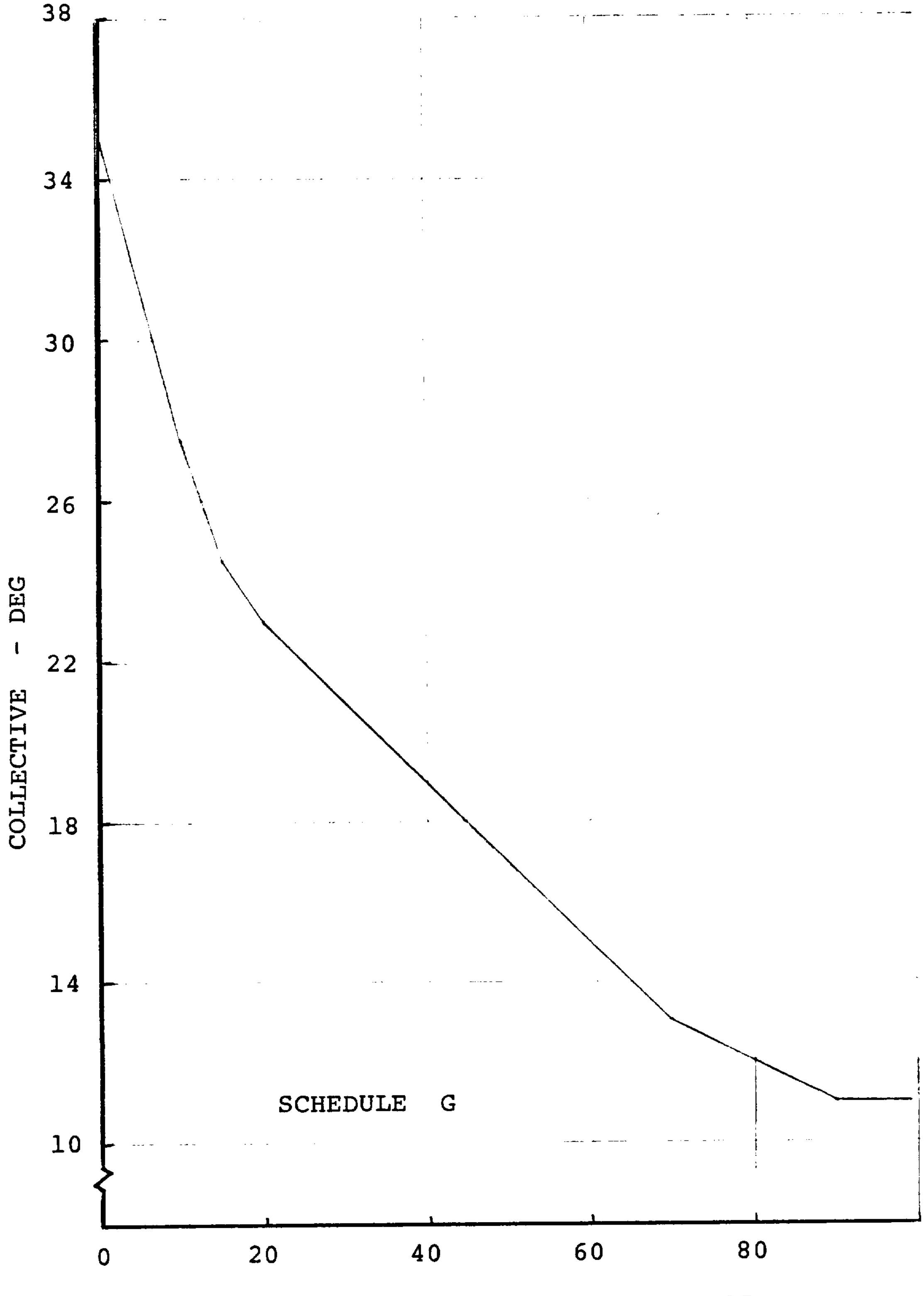

FIGURE F.12. INCREMENTAL COLLECTIVE SCHEDULE

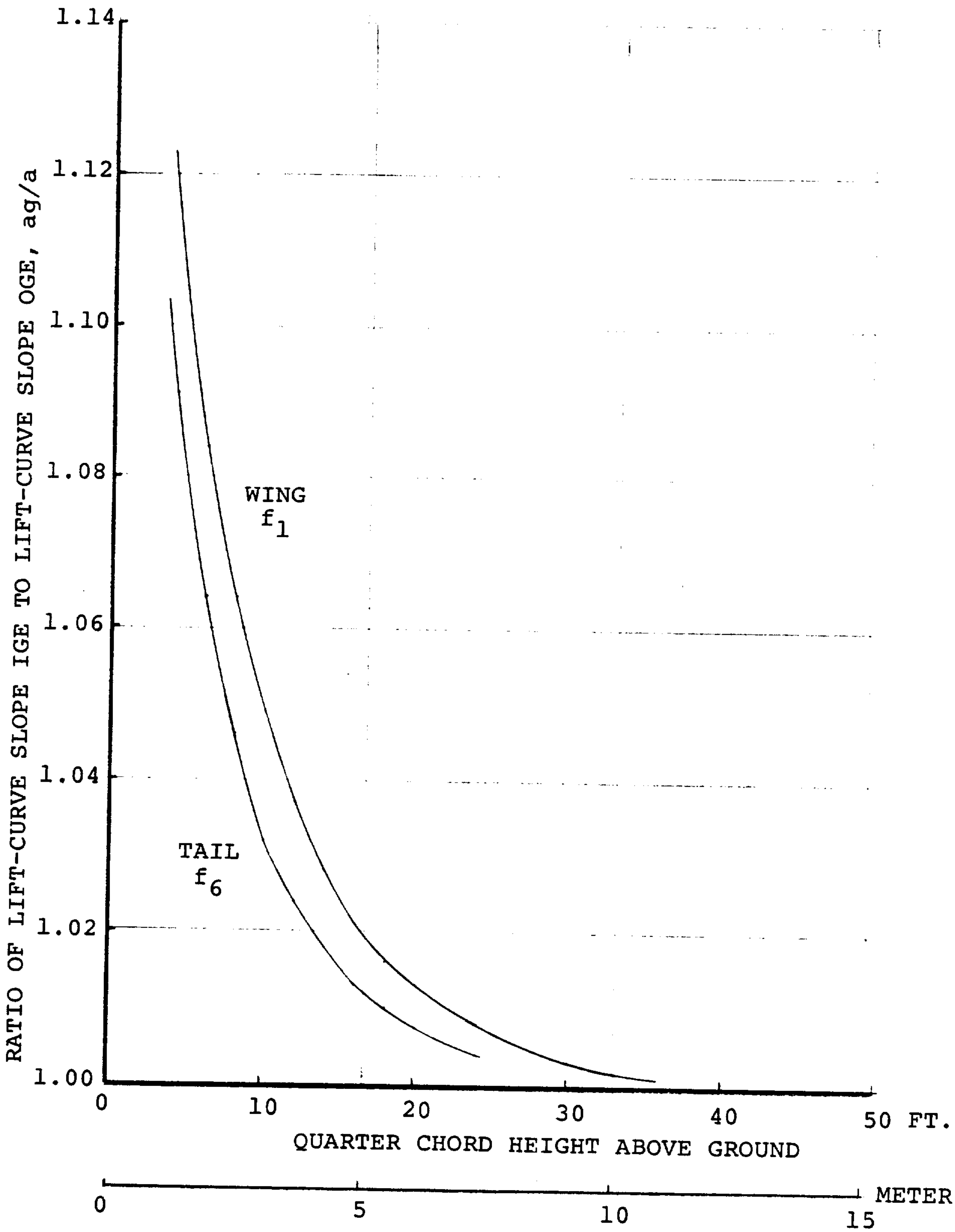

FIGURE F.13. WING AND HOR. TAIL GROUND EFFECT FUNCTIONS

1. VALUES OF REFERRED HORSEPOWER $SHP/\delta\sqrt{\theta}/SHP^*$

MACH NO.	T/θ=1600	T/θ=1800	T/θ=2000	T/θ=2200	T/θ=2400	T/θ=2600	T/θ=2800
0	.035	.330	.630	.920	1.200	1.340	1.400
.2	.075	.375	.670	.960	1.245	1.390	1.450
.4	.125	.425	.720	1.010	1.295	1.440	1.500
.6	.180	.480	.775	1.065	1.350	1.495	1.550
.8	.240	.534	.835	1.125	1.410	1.550	1.600

2. VALUES OF REFERRED FUEL FLOW $\dot{W}/\delta\sqrt{\theta}/SHP^*$

MACH NO.	T/θ=1600	T/θ=1800	T/θ=2000	T/θ=2200	T/θ=2400	T/θ=2600	T/θ=2800
0	.150	.278	.407	.535	.662	.750	.802
.2	.150	.278	.407	.535	.662	.750	.802
.4	.150	.278	.407	.535	.662	.750	.802
.6	.150	.278	.407	.535	.662	.750	.802
.8	.150	.278	.407	.535	.662	.750	.802

TABLE F.1 AND F.2 ENGINE PERFORMANCE DATA

3. VALUES OF REFERRED GAS GENERATOR SPEED $N_I/\sqrt{\theta}/N_I^*$

MACH NO.	T/θ=1600	T/θ=1800	T/θ=2000	T/θ=2200	T/θ=2400	T/θ=2600	T/θ=2800
0	.722	.840	.925	.990	1.045	1.097	1.150
.2	.735	.846	.927	.992	1.048	1.100	1.154
.4	.748	.853	.933	.997	1.052	1.105	1.158
.6	.766	.860	.939	1.004	1.059	1.111	1.162
.8	.789	.871	.950	1.015	1.068	1.119	1.170

4. VALUES OF REFERRED POWER TURBINE SPEED $N_{II}/\sqrt{\theta}/N_{II}^*$

MACH NO.	T/θ=1600	T/θ=1800	T/θ=2000	T/θ=2200	T/θ=2400	T/θ=2600	T/θ=2800
0	.445	.685	.856	.983	1.084	1.178	1.264
.2	.461	.699	.880	.997	1.088	1.169	1.246
.4	.500	.734	.908	1.009	1.089	1.158	1.224
.6	.557	.789	.940	1.023	1.086	1.145	1.197
.8	.640	.858	.973	1.029	1.076	1.123	1.161

TABLE F.3 AND F.4 ENGINE PERFORMANCE DATA

V_* \ τ	0°	±15°	±30°	±45°	±60°	±75°	±90°	105°	120°
50	.01999	.01999	.01999	.01999	.02000	.02000	.02000	.02000	.02000
40	.02498	.02498	.02499	.02499	.02499	.02500	.02500	.02500	.02501
30	.03330	.03330	.03330	.03331	.03331	.03332	.03333	.03334	.03335
20	.04988	.04988	.04989	.04991	.04994	.04997	.05000	.05003	.05006
15	.06637	.06638	.06641	.06646	.06652	.06659	.06667	.06674	.06681
10	.09902	.09905	.09915	.09930	.09950	.09974	.10000	.10026	.10050
9	.10977	.10982	.10995	.11015	.11043	.11075	.11117	.11146	.11180
8	.12311	.12317	.12335	.12364	.12403	.12448	.12498	.12550	.12598
7	.14005	.14015	.14041	.14084	.14141	.14208	.14283	.14359	.14432
6	.16228	.16242	.16283	.16349	.16437	.16543	.16660	.16782	.16900
5	.19258	.19281	.19348	.19457	.19605	.19783	.19984	.20196	.20403
4	.23607	.23647	.23767	.23964	.24234	.24567	.24952	.25368	.25790
3.5	.26556	.26612	.26779	.27054	.27435	.27914	.28477	.29102	.29752
3.0	.30278	.30357	.30595	.30992	.31550	.32266	.33132	.34126	.35207
2.5	.35078	.35194	.35544	.36136	.36983	.38102	.39510	.41217	.43208
2.0	.41421	.41594	.42121	.43025	.44352	.46170	.48587	.51764	.55954
1.5	.5000	.50258	.51051	.52434	.54515	.57480	.61660	.67688	.76971
1.0	.61803	.62167	.63287	.65252	.68233	.72522	.78615	.87344	1.0000
.9	.64659	.65041	.66217	.68276	.71389	.75842	.82091	.90836	1.02956
.8	.67703	.68101	.69320	.71449	.74650	.79183	.85437	.93933	1.05150
.7	.70948	.71355	.72599	.74763	.77989	.82494	.88576	.96560	1.06595
.6	.74403	.74810	.76055	.78203	.81370	.85718	.91437	.98670	1.07333
.5	.78078	.78475	.79682	.81749	.84755	.88796	.93956	1.00236	1.07414
.4	.81980	.82352	.83475	.85377	.88097	.91667	.96083	1.01249	1.06897
.35	.84020	.84371	.85429	.87212	.89736	.93007	.96986	1.01549	1.06433
.30	.86119	.86444	.87421	.89055	.91346	.94274	.97776	1.01713	1.05840
.25	.88278	.88571	.89447	.90902	.92920	.95462	.98450	1.01744	1.05127
.20	.90499	.90751	.91505	.92747	.94450	.96564	.99005	1.01644	1.0430
.15	.92781	.92985	.93592	.94585	.95930	.97574	.99439	1.01416	1.03367
.10	.95125	.95272	.95706	.96411	.97353	.98487	.99750	1.01063	1.02334
.05	.97531	.97610	.97843	.98218	.98712	.99298	.99938	1.00590	1.01210
0	1.00000	1.00000	1.00000	1.00000	1.00000	1.00000	1.00000	1.00000	1.00000

TABLE F.5 SOLUTIONS TO INDUCED VELOCITY QUARTIC Values of v_* at V_* and τ

V_F, KTS / α_F, DEG	0	20	40	60	80	100	120	≥ 140
-180	0.0	0.0	0.0	0.0	0.0	0.0	0.0	0.0
- 30	0.0	0.0	0.0	0.0	0.0	0.0	0.0	0.0
- 28	0.0	-.02	-.06	-.10	-.15	-.12	-.02	0.0
- 24	0.0	-.05	-.15	-.30	-.60	-.37	-.05	0.0
- 20	0.0	-.06	-.25	-.50	-.92	-.65	-.06	0.0
- 16	0.0	-.07	-.40	-.70	-1.10	-.85	-.07	0.0
- 12	0.0	-.07	-.46	-.85	-1.13	-.90	-.08	0.0
- 8	0.0	-.087	-.46	-.692	-1.05	-.80	-.10	0.0
- 4	0.0	-.0945	-.33	-.623	-.98	-.67	-.09	0.0
0	0.0	-.072	-.154	-.560	-.725	-.57	-.07	0.0
4	0.0	-.0314	-.095	-.392	-.55	-.45	-.03	0.0
8	0.0	-.075	-.127	-.290	-.44	-.34	-.07	0.0
12	0.0	-.06	-.10	-.250	-.38	-.27	-.06	0.0
16	0.0	-.04	-.045	-.160	-.20	-.15	-.04	0.0
20	0.0	0.0	0.0	0.0	0.0	0.0	0.0	0.0
180	0.0	0.0	0.0	0.0	0.0	0.0	0.0	0.0

$i_N = 90°$

V_F, KTS / α_F, DEG	0	20	40	60	80	100	120	≥ 140
-180	0.0	0.0	0.0	0.0	0.0	0.0	0.0	0.0
- 30	0.0	0.0	0.0	0.0	0.0	0.0	0.0	0.0
- 28	0.0	-.05	-.10	-.15	-.25	-.22	-.05	0.0
- 24	0.0	-.10	-.25	-.40	-.55	-.50	-.10	0.0
- 20	0.0	-.15	-.40	-.65	-.90	-.75	-.15	0.0
- 16	0.0	-.20	-.50	-.78	-1.05	-.90	-.20	0.0
- 12	0.0	-.20	-.60	-.85	-1.03	-.95	-.20	0.0
- 8	0.0	-.16	-.55	-.80	-1.04	-.92	-.16	0.0
- 4	0.0	-.10	-.45	-.75	-.92	-.85	-.10	0.0
- 0	0.0	-.09	-.30	-.61	-.75	-.65	-.09	0.0

$i_N = 75°$

TABLE F-6 ROTOR ON HORIZONTAL TAIL INTERFERENCE = $v_{i_{HT}}/\bar{v}_i$

V_T, KTS / α_F, DEG	0	20	40	60	80	100	120	≥140
4	0.0	-.10	-.17	-.48	-.56	-.52	-.10	0.0
8	0.0	-.08	-.27	-.34	-.36	-.35	-.08	0.0
12	0.0	-.07	-.22	-.25	-.27	-.26	-.07	0.0
16	0.0	-.05	-.15	-.15	-.15	-.15	-.05	0.0
20	0.0	0.0	0.0	0.0	0.0	0.0	0.0	0.0
180	0.0	0.0	0.0	0.0	0.0	0.0	0.0	0.0

$i_N = 75°$ (cont'd)

V_T, KTS / α_F, DEG	0	20	40	60	80	100	120	≥140
-180	0.0	0.0	0.0	0.0	0.0	0.0	0.0	0.0
- 30	0.0	0.0	0.0	0.0	0.0	0.0	0.0	0.0
- 28	0.0	-.02	-.03	-.04	-.05	-.05	-.02	0.0
- 24	0.0	-.04	-.06	-.06	-.10	-.10	-.04	0.0
- 20	0.0	-.05	-.08	-.14	-.15	-.15	-.05	0.0
- 16	0.0	-.07	-.15	-.20	-.26	-.26	-.07	0.0
- 12	0.0	-.08	-.20	-.25	-.38	-.38	-.08	0.0
- 8	0.0	-.08	-.22	-.35	-.44	-.44	-.08	0.0
- 4	0.0	-.08	-.26	-.43	-.48	-.48	-.08	0.0
0	0.0	-.08	-.30	-.45	-.52	-.52	-.08	0.0
4	0.0	-.07	-.30	-.45	-.60	-.60	-.07	0.0
8	0.0	-.06	-.24	-.30	-.44	-.44	-.06	0.0
12	0.0	-.06	-.15	-.24	-.28	-.28	-.06	0.0
16	0.0	-.04	-.06	-.10	-.14	-.14	-.04	0.0
20	0.0	0.0	0.0	0.0	0.0	0.0	0.0	0.0
180	0.0	0.0	0.0	0.0	0.0	0.0	0.0	0.0

$i_N = 60°$

VALUES ARE ZERO FOR $i_N \leq 30°$

TABLE F. 6 ROTOR ON HORIZONTAL TAIL INTERFERENCE = $v_{i_{HT}}/\bar{v}_i$ cont'd

NACELLE ANGLE - DEG

β_F deg	90	75	60	30	0
0	1.0	1.0	1.0	1.0	1.0
± 4	.9	.99	1.1	1.0	1.0
± 8	.625	.96	1.3	1.0	1.0
±12	.30	.89	1.4	1.0	1.0
±16	.05	.70	.8	1.0	1.0
±20	-.17	.15	.45	1.0	1.0
± 24	-.28	0.0	.225	.5	.5
± 28	-.17	0.0	.07	.25	.25
± 32	0.0	0.0	0.0	0.0	0.0
±180	0.0	0.0	0.0	0.0	0.0

TABLE F. 7 VALUES OF K_{H_β}

SIDESLIP ANGLE, β_V	0	±5	±10	±15	±20	±25	±30
Velocity, V_F KTS							
0	1.0	1.0	1.0	1.0	1.0	1.0	1.0
20	1.0	1.0	1.0	1.0	1.0	1.0	1.0
40	-.5	.25	.80	1.25	1.5	1.0	1.0
60	.2	.40	.80	1.1	1.4	1.0	1.0
80	.5	.60	.80	1.0	1.2	1.0	1.0
100	.75	.80	.80	1.0	1.0	1.0	1.0
120	1.0	1.0	1.0	1.0	1.0	1.0	1.0
350	1.0	1.0	1.0	1.0	1.0	1.0	1.0

TABLE F.8 VALUES OF K_β

V_F, KTS / α_F, deg	0	20	40	60	80	≥ 100
-180	1.0	1.0	1.0	1.0	1.0	1.0
- 40	1.0	1.0	1.0	1.0	1.0	1.0
- 30	1.0	1.17	1.08	1.0	.92	.935
- 28	1.0	1.20	1.12	1.0	.92	.935
- 24	1.0	1.40	1.21	1.0	.92	.935
- 20	1.0	1.70	1.43	1.05	.93	.935
- 16	1.0	1.90	1.67	1.18	.96	.935
- 12	1.0	2.08	1.80	1.37	1.0	.935
- 8	1.0	2.20	1.88	1.54	1.25	.935
- 4	1.0	2.20	1.80	1.52	1.23	.935
0	1.0	2.07	1.70	1.35	1.05	.935
4	1.0	1.90	1.60	1.10	1.0	.935
8	1.0	1.70	1.46	1.00	.93	.935
12	1.0	1.55	1.30	.90	.86	.86
16	1.0	1.37	1.05	.82	.80	.80
20	1.0	1.20	.93	.80	.80	.72
30	1.0	1.0	1.0	1.0	1.0	1.0
180	1.0	1.0	1.0	1.0	1.0	1.0

$i_N = 90°$

V_F, KTS / α_F, deg	0	20	40	60	80	≥ 100
-180	1.0	1.0	1.0	1.0	1.0	1.0
- 40	1.0	1.0	1.0	1.0	1.0	1.0
- 30	1.0	1.24	1.1	.97	.92	.935
- 28	1.0	1.37	1.14	.98	.90	.935
- 24	1.0	1.54	1.24	.99	.88	.935
- 20	1.0	1.80	1.35	1.0	.87	.935
- 16	1.0	2.0	1.52	1.03	.87	.935
- 12	1.0	2.2	1.63	1.08	.92	.935
- 8	1.0	2.38	2.04	1.15	.97	.935
- 4	1.0	2.44	2.24	1.25	1.0	.935

$i_N = 75°$

TABLE F-9 TAIL EFFICIENCY FACTOR - η_{HT}

V_F, KTS / α_F, deg	0	20	40	60	80	≥100
0	1.0	2.42	2.25	1.3	1.05	.935
4	1.0	2.36	2.0	1.23	1.06	.935
8	1.0	2.23	1.8	1.15	1.05	.935
12	1.0	2.0	1.6	1.06	1.03	.935
16	1.0	1.8	1.4	1.0	.97	.935
20	1.0	1.6	1.2	.92	.9	.80
30	1.0	1.0	1.0	1.0	1.0	1.0
180	1.0	1.0	1.0	1.0	1.0	1.0

$i_N = 75°$ cont'd

in deg / α_F, deg	60	30	0
-180	1.0	1.0	1.0
- 40	1.0	1.0	1.0
- 30	1.0	1.0	1.0
- 28	1.0	1.0	1.0
- 24	1.0	1.0	1.0
- 20	1.0	1.0	1.0
- 16	1.0	1.0	1.0
- 12	1.0	1.05	1.0
- 8	1.0	1.05	1.0
- 4	1.0	1.05	1.0
0	1.0	1.05	1.0
4	1.0	1.05	1.0
8	1.0	1.05	1.0
12	1.0	1.05	1.0
16	1.0	1.05	1.0
20	.8	.8	.8
30	1.0	1.0	1.0
180	1.0	1.0	1.0

TABLE F. 9 TAIL EFFICIENCY FACTOR - η_{HT}

APPENDIX G

APPENDIX G - ROTOR LOADS AND CONTROLS PARAMETRIC STUDY

INTRODUCTION

The key to a successful tilt rotor vehicle is in the design compromises in the control system which provides trimmed sustained flight conditions with low blade fatigue loads and acceptable control variations and vehicle response characteristics. At a given nacelle incidence, a tradeoff can be made between elevator and rotor cyclic control to trim the aircraft. Ideally the cyclic control used should be that value which minimizes blade bending loads and the rest of the airplane trimmed on the elevator. Obviously as airspeed decreases elevator effectiveness diminishes with dynamic pressure requiring non-optimum rotor inputs to be made in order to trim. In addition, the desirability of using a simple control system with no primary controls driven by flight parameters (e.g., q' sensed) further complicates the ideal situation. The control system studies contained in this appendix are a preliminary try at a good compromise.

Loads Model:

In order to perform control system parametric variations and assess their impact on the blade fatigue loads, a fast (on-line) method of evaluating blade bending loads is necessary. The more rigorous analyses and manual interpretation of test data for the many combinations of velocity, angle of attack, cyclic pitch, collective pitch and RPM are much to cumbersome to be used in this type of application. This problem was surmounted by using a simple empirical equation to define the loads

Alternating bending moment at 12.5% R (ABM)

$$= 2000 + 8753.6\mu + 24829\mu\ (\alpha rad) + 3.35066\left(1 + \frac{\mu C_{P_M}}{.0005}\right)\left(P_M^{\ 2} + Y_M^{\ 2}\right)^{1/2}$$

This equation was derived under IR&D funding during analysis of the test data of Reference 4 in 1976 and was used in this contractual work to provide a quick estimate of blade loads. Correlation of this equation with the full scale data of Reference 4 is shown in Figure G-1 and the symbol key is provided as Table G-1.

The equation provides a reasonable estimate of loads for most of the cases shown, however, in some transition cases correlation becomes erratic though in general in these cases the calculation is conservative as indicated by $i_N = 85$, $\mu = .111$ data. This procedure needs further refinement and should be

*NOTES: 1. TEST DATE INTERPOLATED OR EXTRAPOLATED FROM MEASURED POINTS IN SOME CASES
2. SYMBOL KEY - SEE TABLE
3. SOURCE REFERENCE: 4

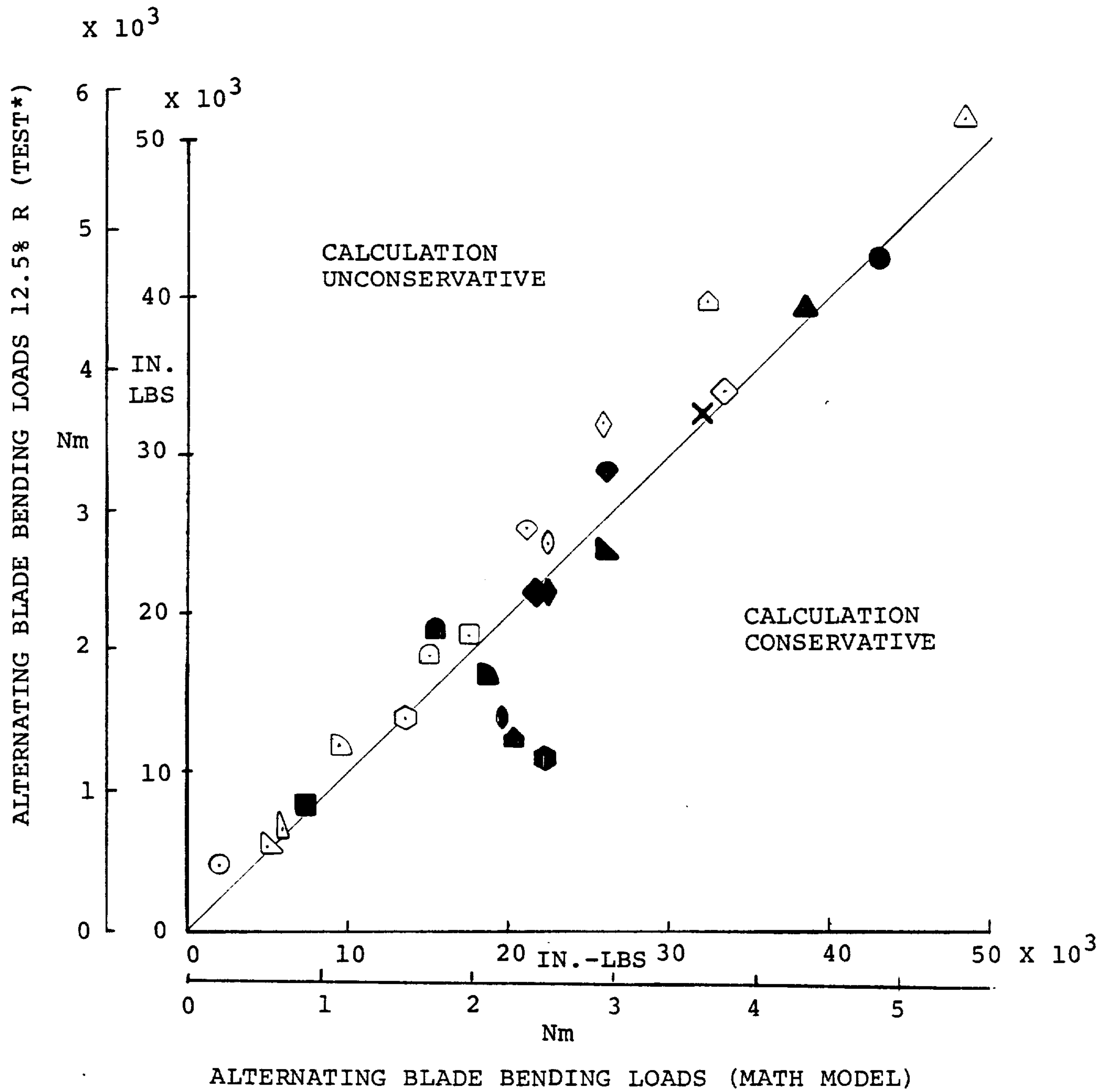

FIGURE G.1. BLADE BENDING MOMENT DATA CORRELATION

SYMBOL	α/i_N	μ	C_T	$A_1{}^{\circ}$	$B_1{}^{\circ}$
⊙	90	0	.0054	0	0
⊡	90	0	.0054	0	2
	90	0	.0054	0	4
	90	0	.0054	0	6
	0	.321	W*	0	0
	2	.321	W	0	0
	4	.321	W	0	0
	6	.321	W	0	0
	8	.321	W	0	0
	10	.321	W	0	0
	0	.450	W	0	0
	2	.450	W	0	0
	4	.450	W	0	0
×	6	.450	W	0	0
●	8	.450	W	0	0
■	0	.617	W	0	0
◆	2	.617	W	0	0
▲	4	.617	W	0	0
	66	.180	.0009	-1.77	3.35
	66	.180	.00387	-1.77	3.35
	66	.180	.00634	-1.77	3.35
	66	.180	.00881	-1.77	3.35
◆	15	.236	.0004	-1.15	3.14
	20	.236	.00129	-1.15	3.14
	85	.111	.0059	-4.24	3.05
⬢	85	.111	.0083	-4.24	3.05
	85	.111	.011	-4.24	3.05

(*WINDMILLING CASES)

TABLE G.1. SYMBOL KEY FOR FIGURE G-1.

expanded to include the newly acquired data from NASA Contract NAS2-9015 as well as the rest of the available data in Reference 4.

The basic premise of the equation is that 1/rev alternating bending loads primarily produce out-of-plane hub moments or at least the in-plane loads will remain roughly proportional to the out-of-plane loads. This is, of course, an approximation because the variations of the per rev frequencies of the first two blade bending modes with collective and RPM will change the relative magnitudes of the out-of-plane and in-plane blade deflections.

No blade loads data were measured at 12.5% radius in the tests of Reference 4, however, measured radial distributions of bending moments were used to provide the data points shown in Figure G-1.

Though the method is approximate (i.e., ±20% for most cases) it provides a means of evaluating the blade fatigue loads with little or no effect on the simulation time frame.

Parametric Studies

As described in Section 12.0 of this report the control system design commenced with setting the hover control phasing and gains to give adequate control in hover. The cyclic pitch gains were then washed out according to a sine law of nacelle incidence.

Azimuthal Location:

An initial trade study was made varying the azimuthal location at which the cyclic control inputs were made for various levels of elevator. Figure G-2 shows the estimated rotor loads for various azimuthal locations with the elevator fixed at 10°. The definition of ϕ_p in Figure G-2 is the azimuthal location at which the resultant cyclic vector acts, and is depicted in Figure G-3. The data in Figure G-2 are for i_N = 90° and clearly show a blade loads minimum between ϕ_p = 25 to 30°. The minimum loads occur at higher ϕ_p at low speed, but this is of little significance since the load levels are low anyway.

Figures G-4 and G-5 show similar data with elevator settings varied. The level of the resultant loads changes, but the azimuthal angle at which minimum loads are achieved remains essentially the same. Since ϕ_p = 30° was close to optimum hover and near optimum for a loads reduction standpoint at high i_N and velocity it was decided to use a constant value of ϕ_p = 30° for the remainder of the studies.

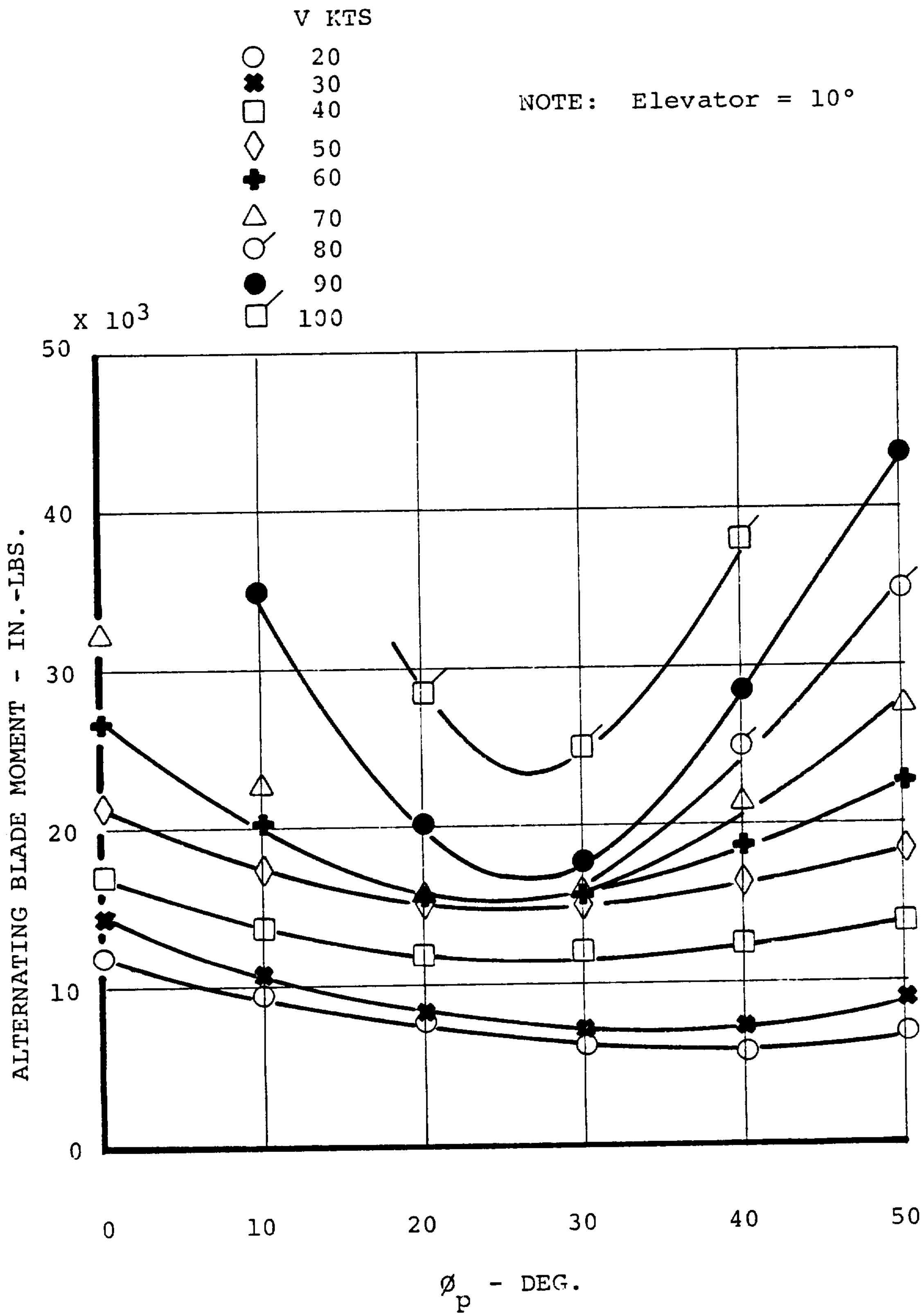

FIGURE G.2. INFLUENCE OF AZIMUTHAL LOACATION OF CYCLIC INPUTS ON BLADE FATIGUE LOADS $i_H = 90°$, $\delta_F = 40°$ GW = 5896.7 Kg (13000 LBS) SL STD DAY

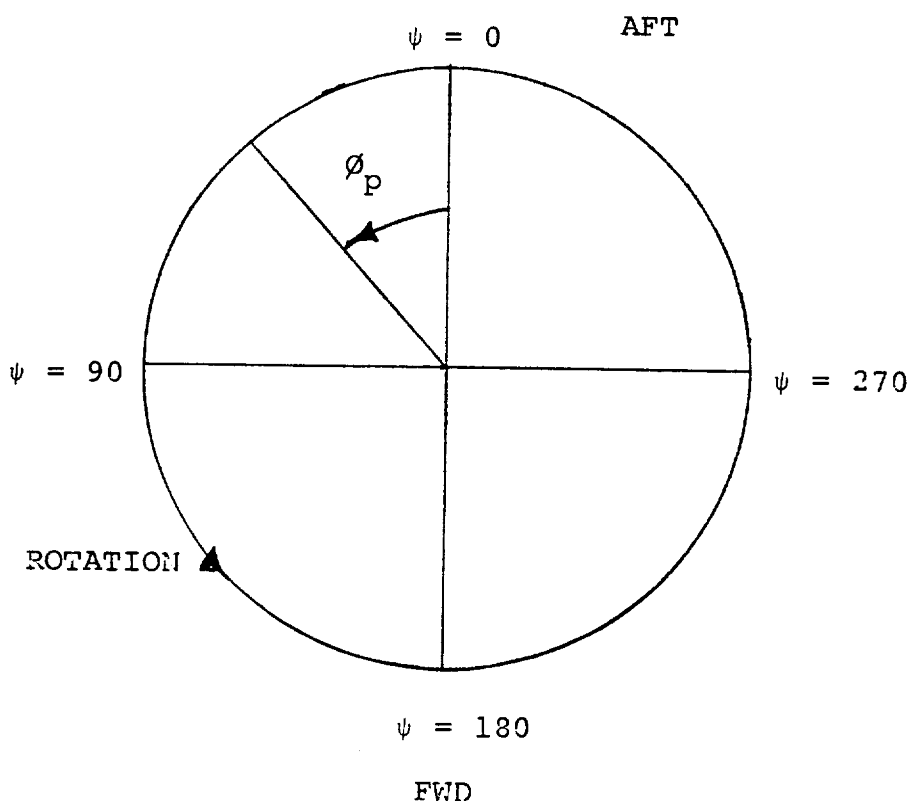

PLAN VIEW OF ROTOR WHEN $i_N = 90°$

$$\Delta\theta = -A_1 \sin \phi_p - B_1 \cos \phi_p$$

where A_1 and B_1 are cyclic inputs relative to classical axes

FIGURE G.3. DEFINITION OF ϕ_p

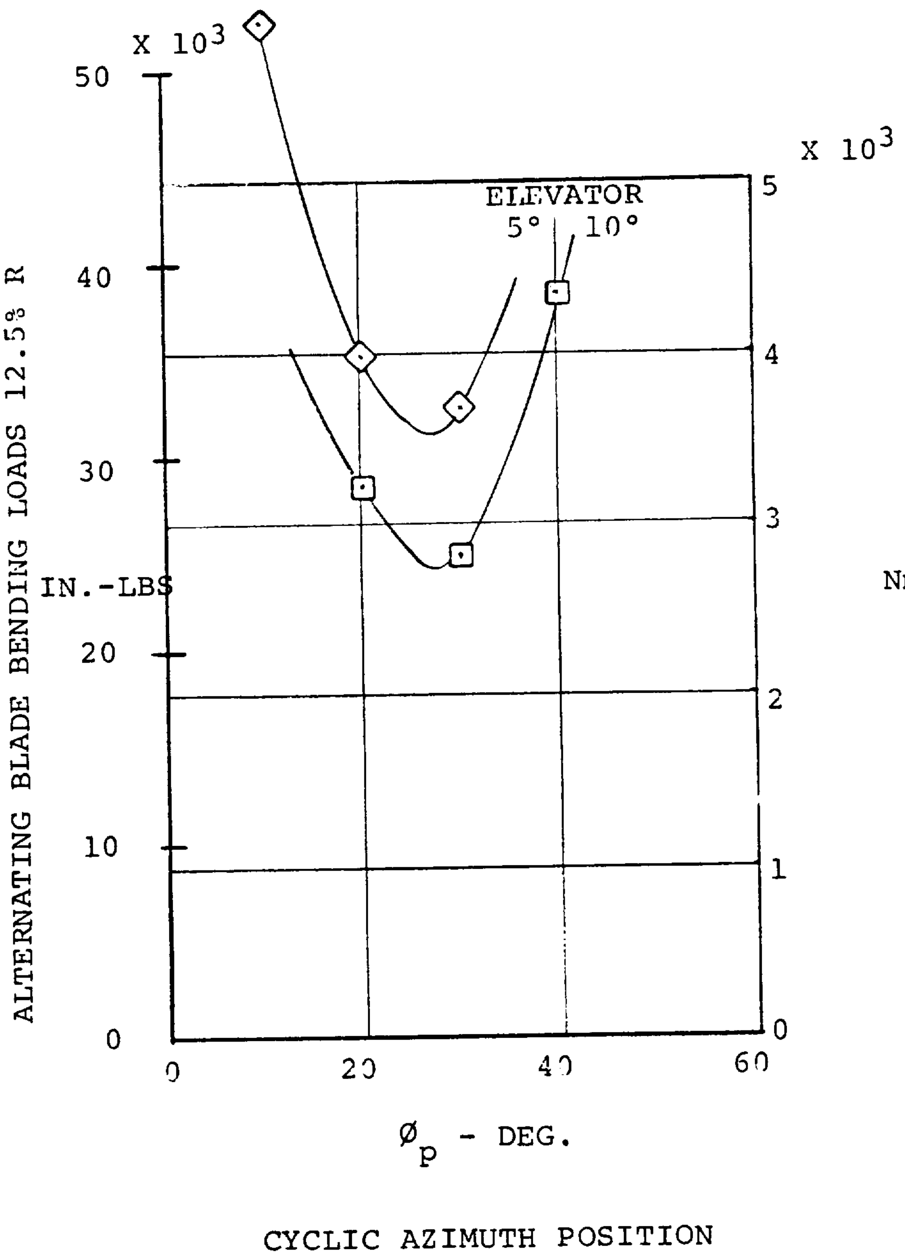

FIGURE G.4. INFLUENCE OF ELEVATOR ON BLADE LOADS AT 100 KTS
$i_N = 90°$ $\delta_F = 40°$ GW = 5896.7 Kg (13000 LBS)

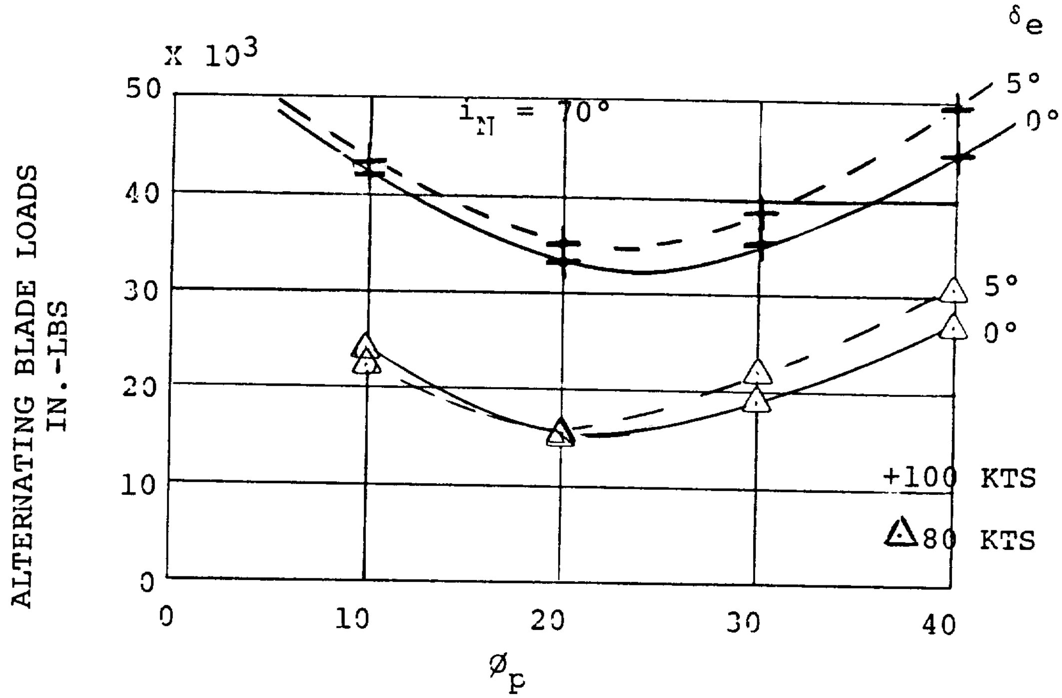

FIGURE G.5. ALTERNATING BLADE LOADS $i_N = 70°$ AT 80 AND 100 KTS FOR VARIOUS VALUES OF ϕ_p

Thus far the cyclic pitch inputs were defined by the hover gain °/inch stick at $\phi_p = 30°$ and washed out as nacelle incidence decreased by sin i_N. This of course implies no cyclic pitch in cruise.

The next step was to determine the cruise cyclic requirements.

Cruise Flight - Cyclic Control Design

The primary area of concern in cruise flight arises at low airspeeds where the angle of attack to trim the aircraft in 1g steady flight is high. The rotor loads, with no cyclic pitch, approach the blade endurance limit leaving little room for maneuver within the blade fatigue allowable. This problem is corrected by the introduction of 2.5° cyclic pitch for aft stick positions and washing this out as the stick moves forward. A series of different washout schedules were tried with varying results in terms of blade loads.

Figure G-6 shows four schedules of cyclic as functions of longitudinal stick. The alternating blade loads calculated by the simulation loads model are shown for the "no cyclic" case in Figure G-7 and indicate alternating bending moments at the blade 12.5% radial station of about 36,000 in.-lbs at 140 KTS. This load level is expected to be the infinite life level for the blade fiberglass spar (10^8 cyclies, $M-3\sigma$). The design procedure adopted aimed at minimizing the bending loads such that,at all sustained flight conditions the loads remain less than or equal to the infinite life value.

The alternating loads corresponding to schedules 1, 2 and 3 are also shown for the aft cg case at sea level standard day conditions. Schedule 1 produced a drastic reduction in loads at the low speed end of the spectrum, but caused an increase at high speeds. This was due to the washout being to far forward resulting in cyclic being used at high speed and agravating the loads. Schedule 2 is the same as Schedule 1, but pulled back so that it washes out 0.2" earlier. The trims resulting from this provided loads less than 53% of the fatigue allowable at all speeds. Schedule 3 provides a straight line washout and results in the loads increasing in the 180 knot to 200 knot range.

Schedule 4 was finally selected and the alternating blade loads for both forward and aft cg are shown in Figure G-8. The aft cg case gives 1g loads less than 46% of the infinite life allowable with the aft cg case. For the forward cg case the loads increase at high speed due to too much cyclic pitch at these conditions. Even so the 1g loads are within the allowable and the cyclic will cause the loads to decrease when maneuvers are pulled in coordinated turns.

At the low speed end of the cruise flight regime, it must be possible for the pilot to select any flap setting without causing unacceptable loads on the rotor. The alternating loads for both forward and aft cg with flaps at 80° and 40° are shown in Figure G-9. These data show acceptable loads from stall speed up to 200 knots. The flap q limit is at 170 knots.

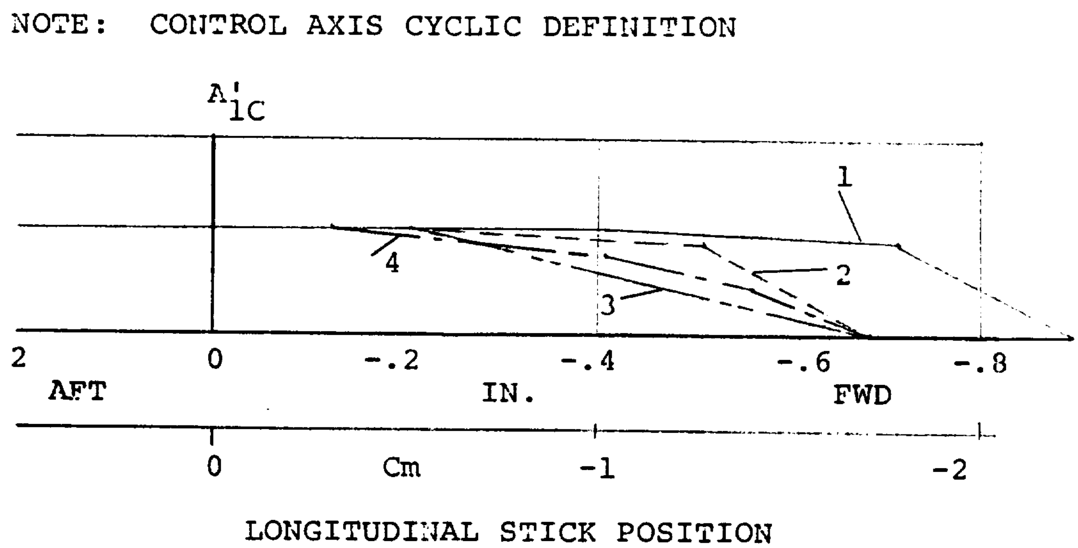

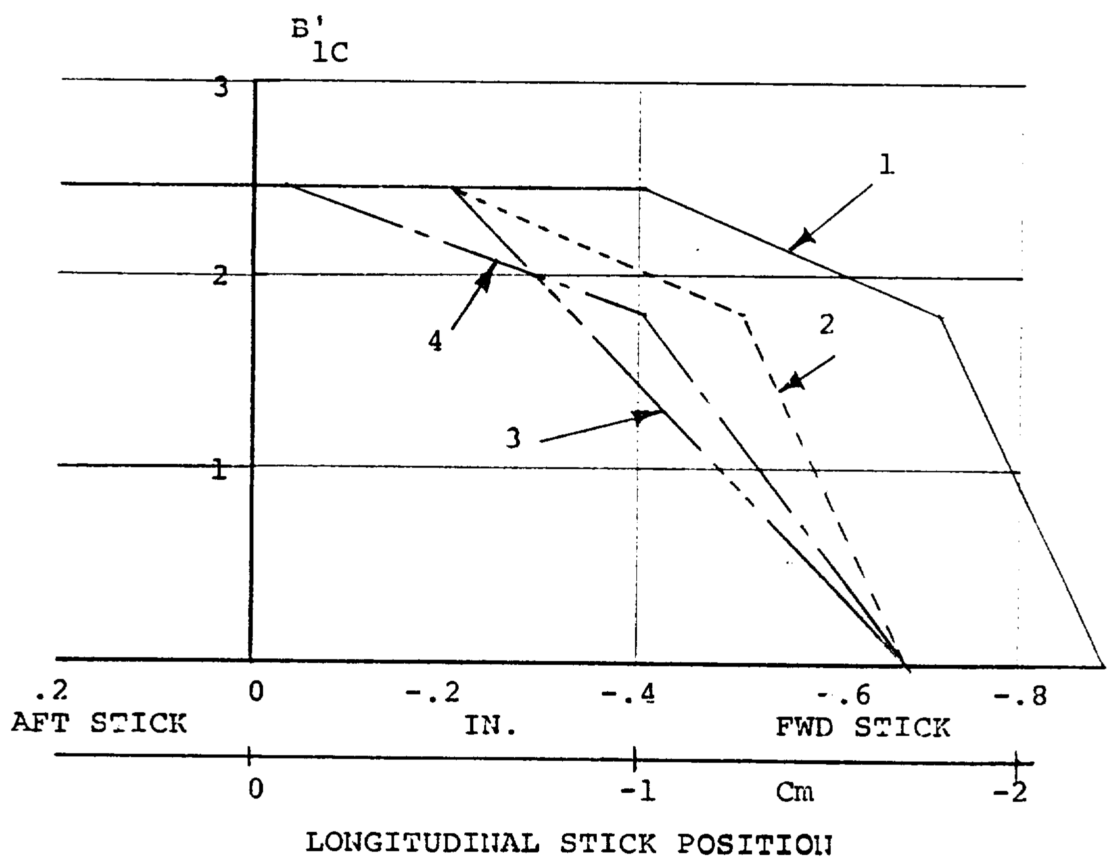

FIGURE G.6. "CYCLIC ON STICK" SCHEDULES

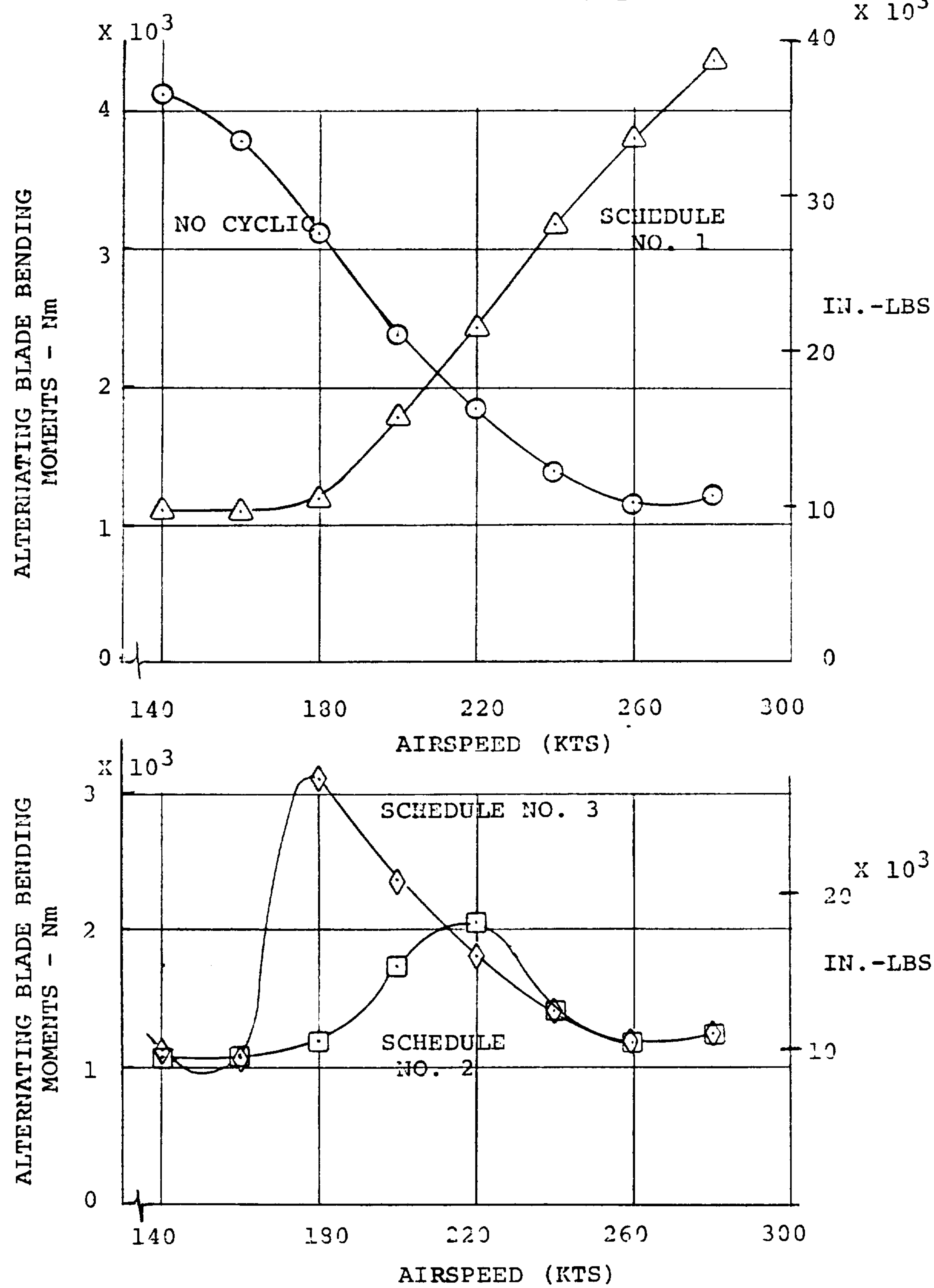

FIGURE G.7. ALTERNATING BLADE BENDING LOADS IN CRUISE WITH VARIOUS CYCLIC SCHEDULES

NOTE: GW = 5896.7 (Kg) - 13000 LBS
SL STD DAY
$i_N = 0°$

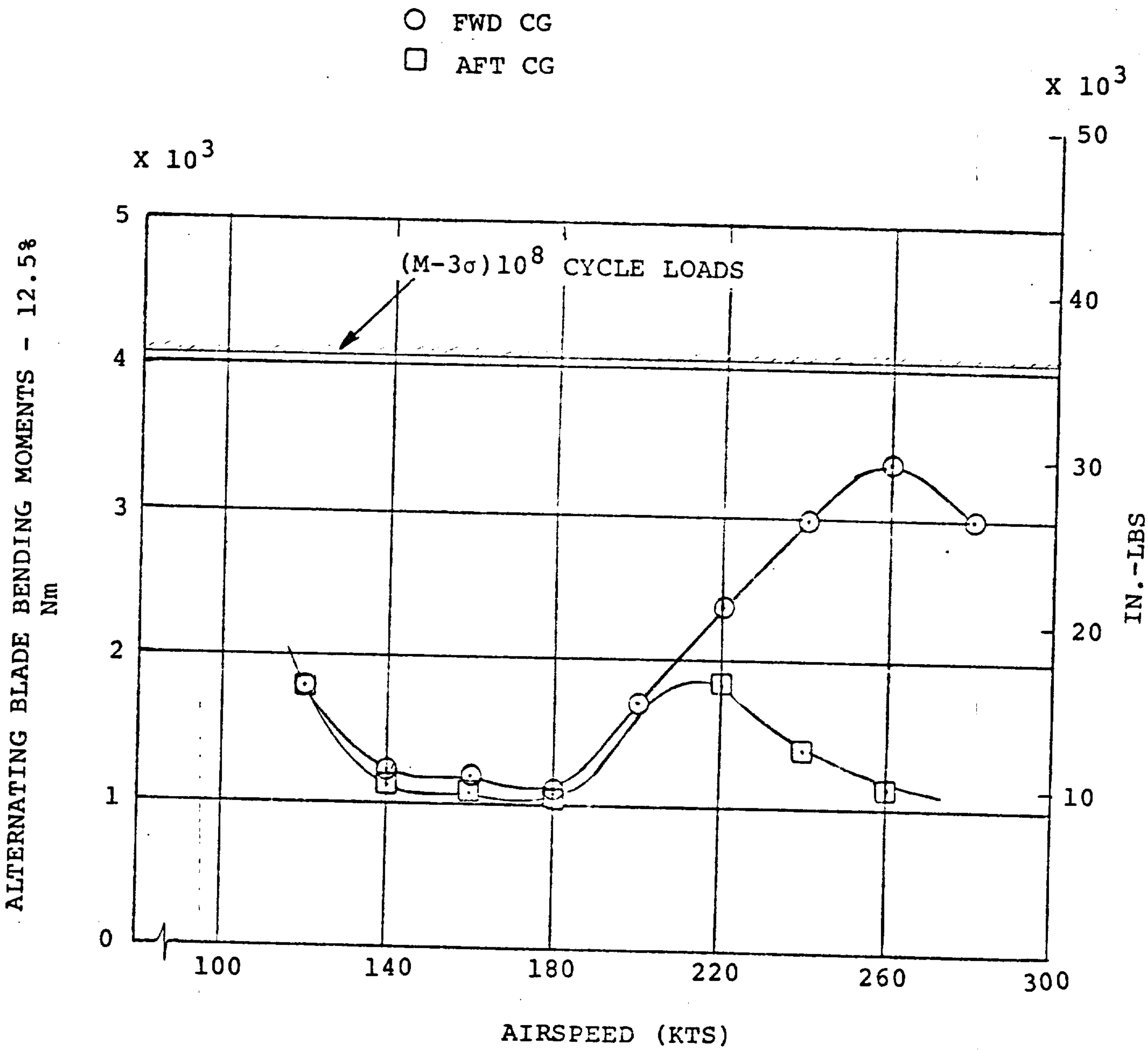

FIGURE G. 8. ESTIMATED BLADE BENDING LOADS IN STEADY CRUISE FLIGHT - FLAPS UP

NOTE: GW = 5896.7 Kg (13000 LBS)
SL STD DAY
$i_N = 0^\circ$

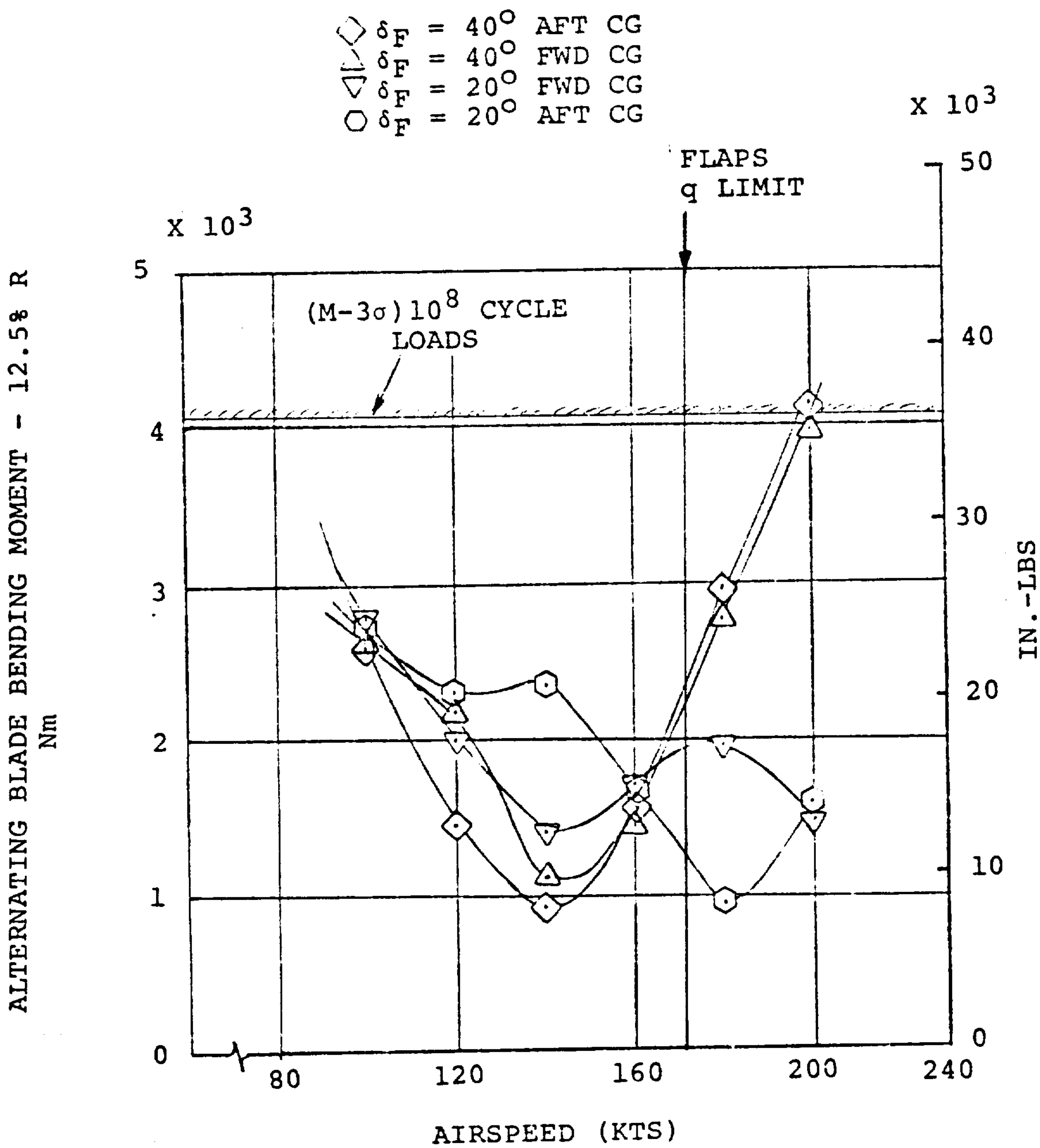

FIGURE G.9. ESTIMATED BLADE BENDING LOADS 12.5% R IN CRUISE FLIGHT - FLAPS DOWN

The rotor loads were also obtained in coordinated turns at sea level with no flaps. As expected, the low speed cases were the most critical. However, with the scheduled cyclic on the stick a bank angle of 58° is possible at 140 KTS with a forward cg. This represents a sustained load factor of 1.89g's with no fatigue damage to the blades.

At 180 KTS the load factor at which fatigue allowable loads were achieved was 2.3g's (64° bank) and at 220 KTS and higher the loads limit was in excess of 3g's, and the aircraft sustained flight envelope is limited by the power train torque limit.

The cruise cyclic is obviously not required or useful when $i_N = 90°$ and must be washed out as i_N increases. Initially a cosine i_N law was used such that the cruise cyclic

$$\gamma = f(\delta_B) \cos i_N°$$

where $f(\delta_B)$ is the Schedule 4 shown in Figure G-6. It should be pointed out that this cyclic is independant of SAS inputs and is totally separate from the cyclic pitch resulting from the stick travel times the cyclic gain.

The estimated rotor loads were investigated back into transition using the hover cyclic control washed out as sin i_N and the cruise cyclic washed in as cos i_N. These cases are labelled (Bias = 0) in Figures G-10 through G-15 and shows that the loads are reasonable with respect to the sustained flight allowable (406A Nm, 36000 in.-lbs) except near the middle of the i_N range (see $i_N = 45°$, Figure G-11).

A study was performed to determine the effect of a stick bias on the cyclic input. This bias is only applied to the cyclic gain and is defined by

$$\text{cyclic} = G\ (\delta_B - \text{Bias}) \sin i_N°$$

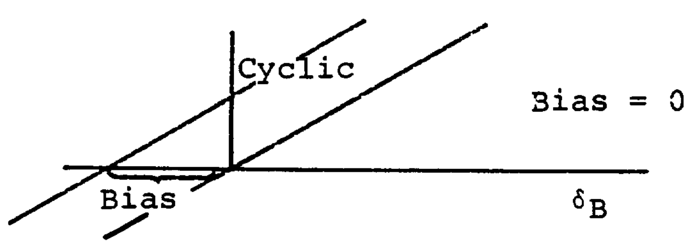

Figures G-10 through G-15 show estimated blade loads in transition for forward and aft cg cases with varying amounts of bias. The effect of cyclic stick bias was to reduce the rotor loads and widen the fatigue envelope at all conditions.

Clearly zero bias is necessary in hover ($i_N = 90°$) since any other value would produce assymetry in available control power whereas any value of bias is acceptable in cruise ($i_N = 0°$) since the gain multiplier is reduced to zero at this condition.

At $i_N = 85°$ the forward cg case is the most critical and a bias of at least -1" is desirable to maintain alternating bending loads less than 4064 Nm (36000 in.-lbs). At $i_N = 75°$ a value of -2" is required for acceptable loads. At 60° a bias of -2" is needed. At 40° a bias of -2" provides adequate loads and -3" provides about the same loads picture. At 30° and 15" i_N a bias of -2" is acceptable and -4" pushes the loads boundary to a little higher speed.

These findings are summarized in Figure G-16 and Schedule K used in the control system is shown superimposed.

The preceeding study was performed with an elevator offset of 5° held between $i_N = 90°$ and $i_N = 45°$ and then reduced linearly to zero as $i_N \rightarrow 0°$. The cruise cyclic was also washed out as a cosine law during this work.

During final assessment of the transition trims these two schedules were modified in an attempt to smooth the control travel variations and resulted in an elevator offset defined by Schedule H and the cruise cyclic washout changed to a $(1 - i_N/90°)$ function instead of a cosine law. The parametrics were not rerun, however, the final loads were computed and found to be acceptable. The loads with this system are included with the simulation results in Section 11 of this report.

The system will provide a reasonably wide transition corridor with room to maneuver within it in most cases. This first examination of the problem for the hingeless rotor XV-15 is not, however, necessarily the optimal answer or necessarily the simplest useable system.

This work needs to be continued with the updated rotor force and moment and loads model and should examine the effects of azimuthal input variation at low values of i_N and the practicality of separating trim and control cyclic inputs to provide minimum loads at trim and maximum available control power. The cyclic schedule used to provide load alleviation in cruise brings with it some attendant difficulties from a handling qualities point of view since the introduction of a cyclic pitch step in the longitudinal stick travel produces a discontinuity in the control power available. This is discussed in Section 12 and currently handled by rate limiting the cruise cyclic input. Another way of achieving good handling qualities is to tailor the elevator schedule in cruise to match the moment-producing capability of the cruise cyclic. This provides a further avenue of exploration which should be examined as the development of the control system continues.

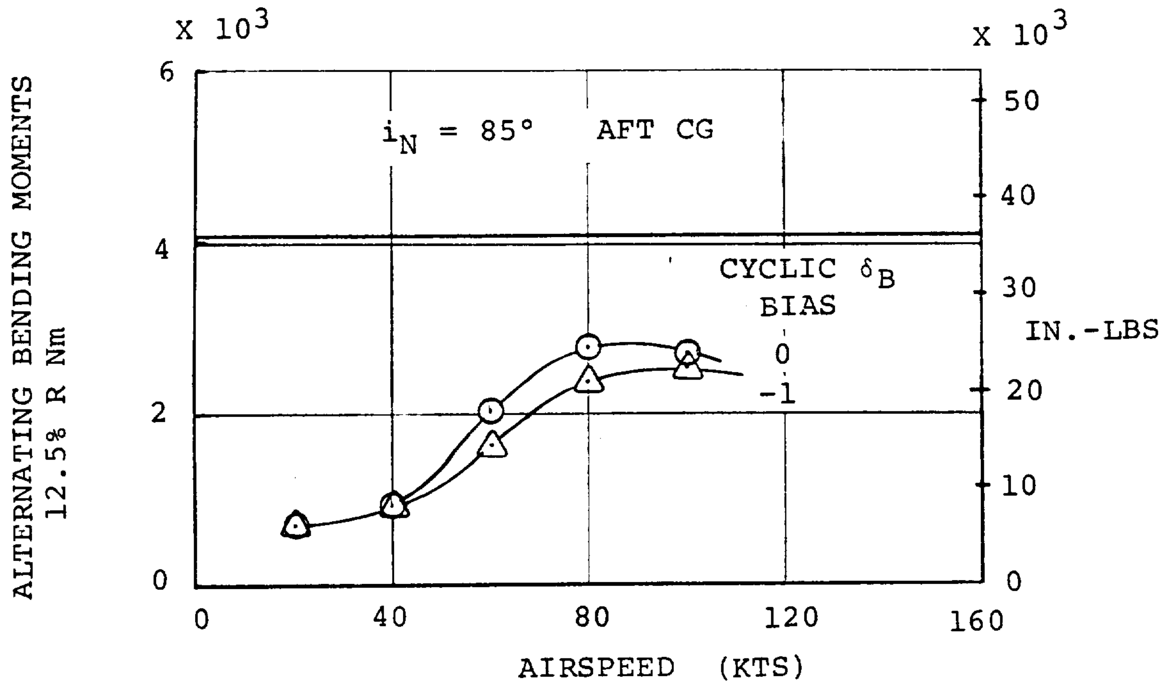

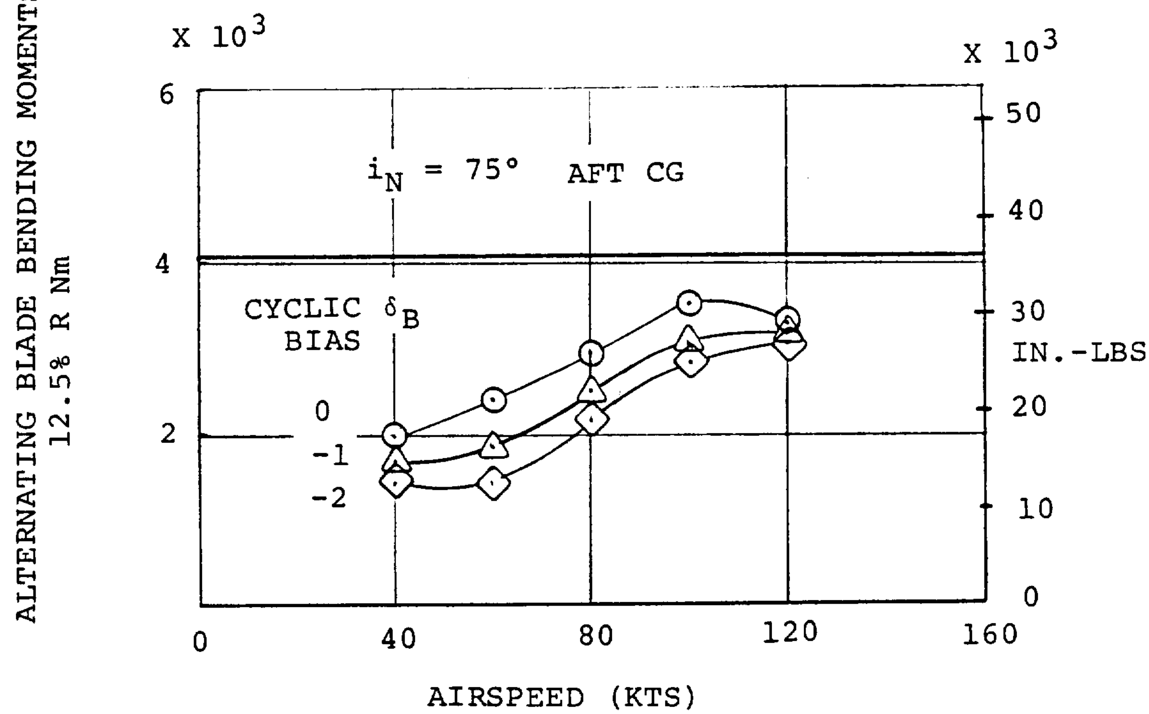

FIGURE G.10. CYCLIC STICK BIAS, LOADS DATA i_N = 85°, 75° AFT CG

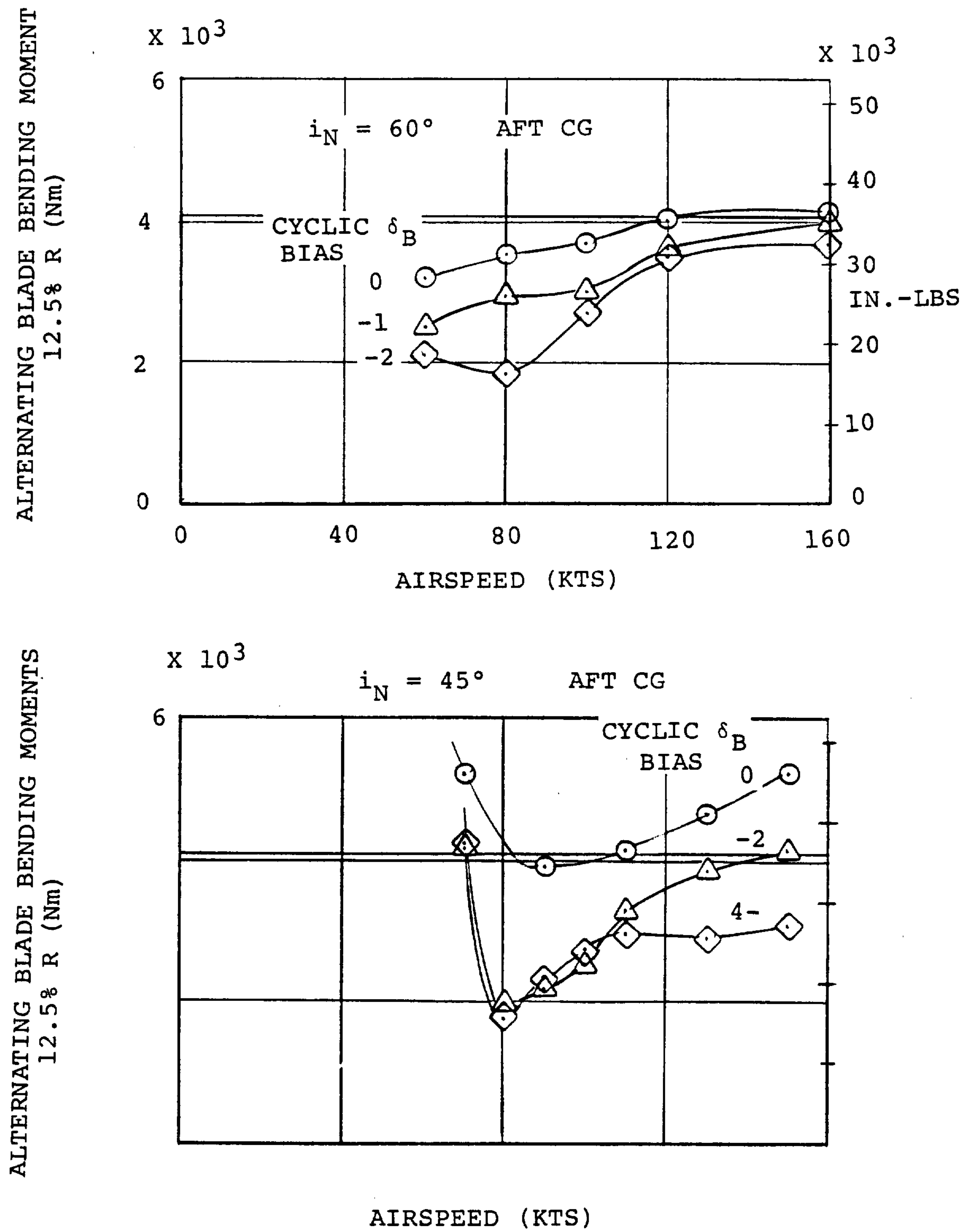

FIGURE G.11. CYCLIC STICK BIAS, LOADS DATA i_N = 60°, 45° AFT CG

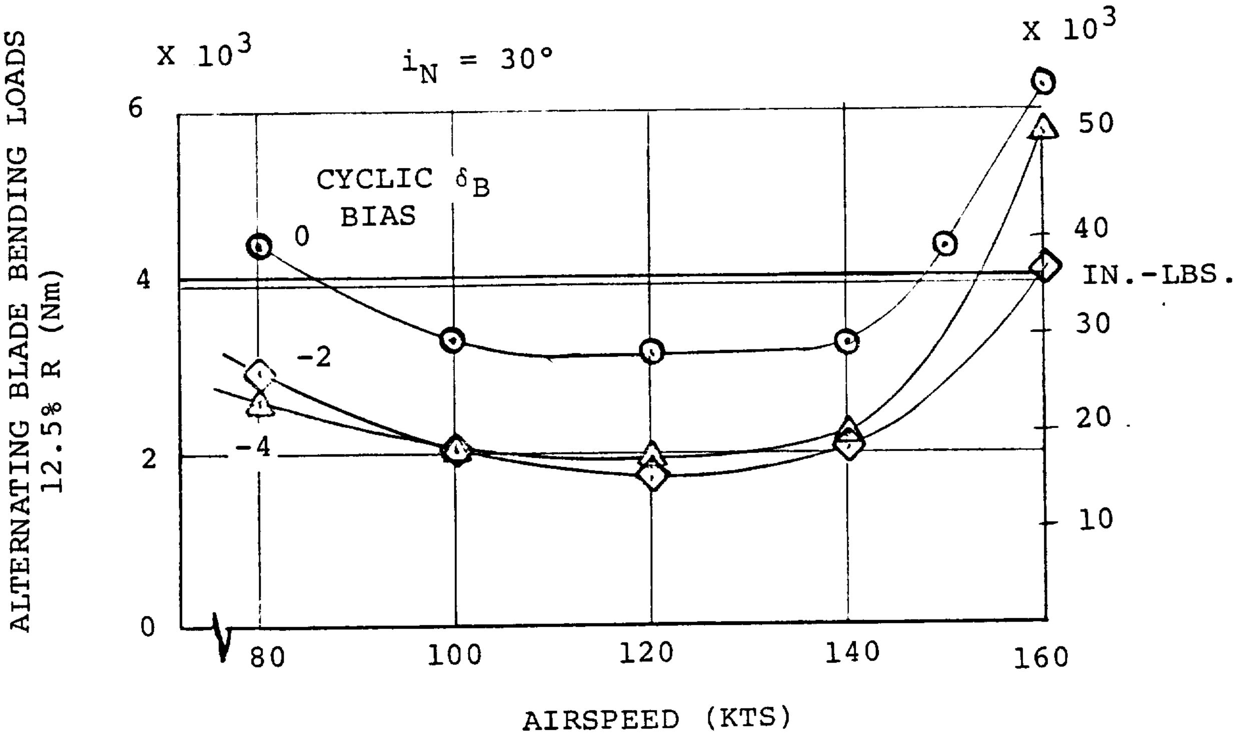

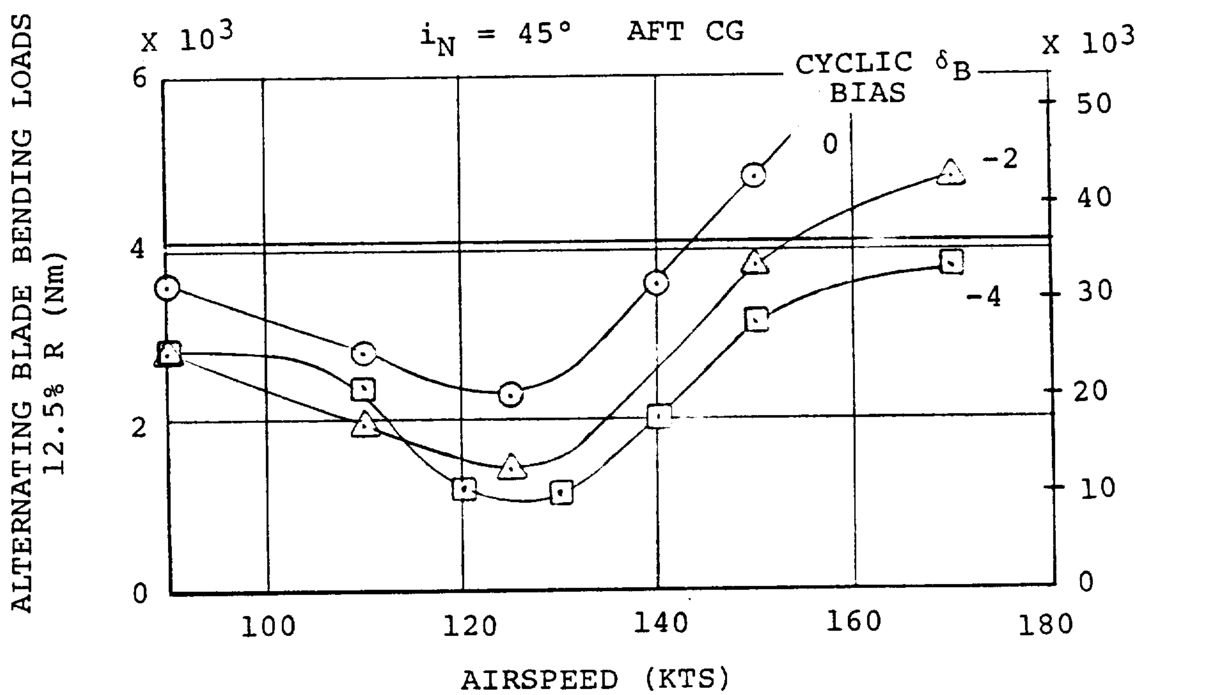

FIGURE G.12. CYCLIC STICK BIAS - LOADS DATA
i_N = 30°, 45° AFT CG

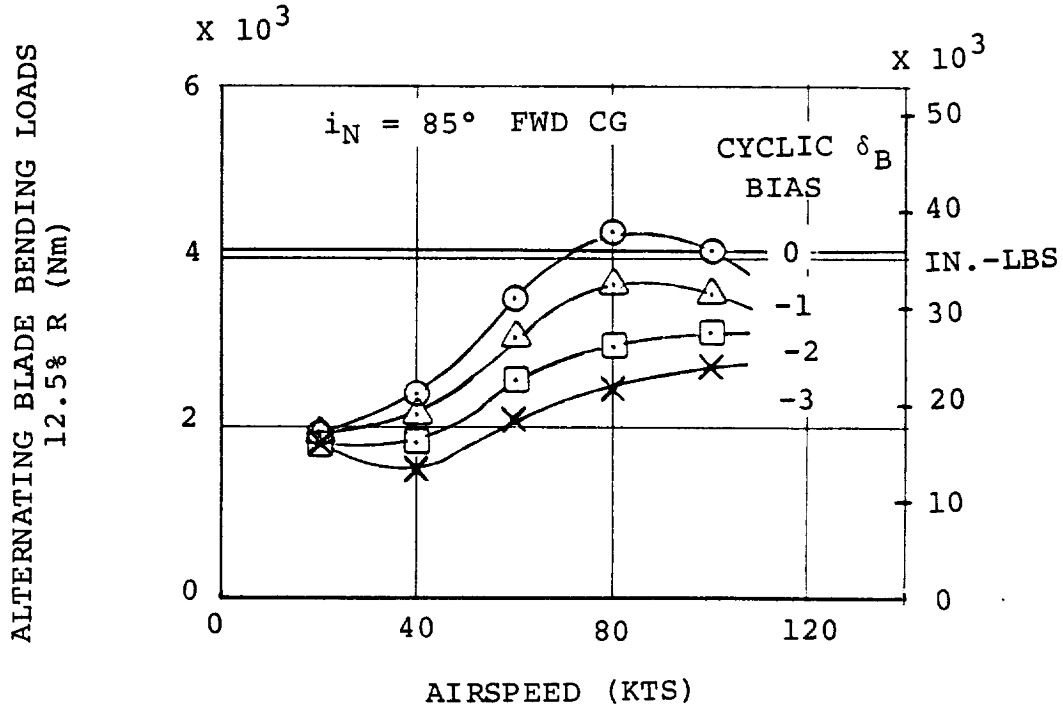

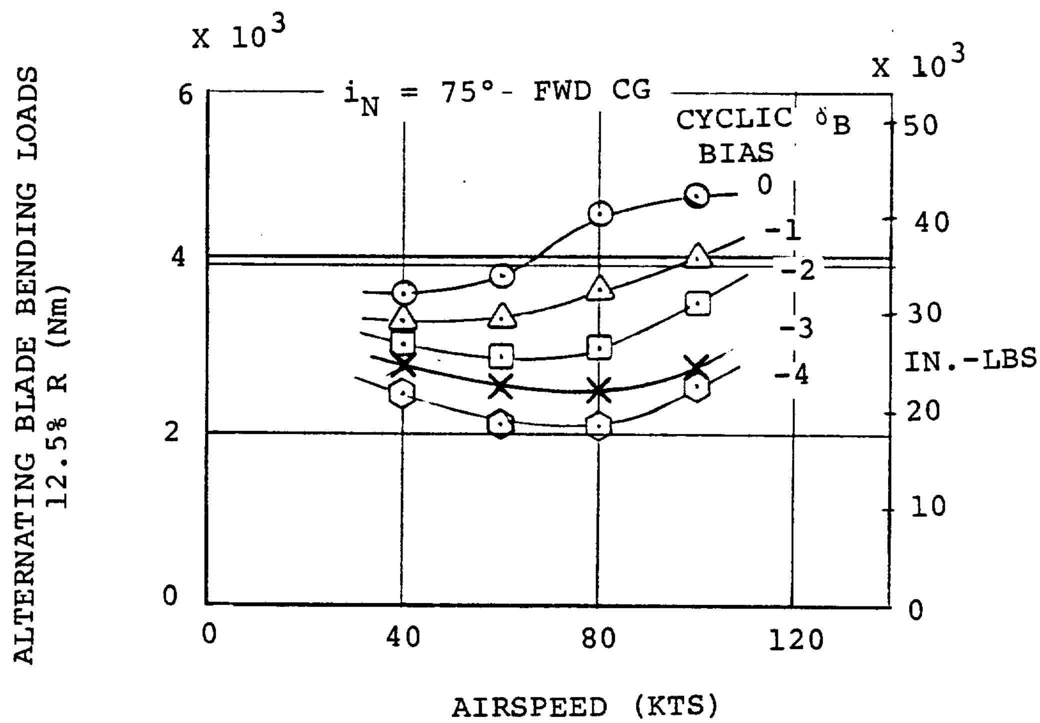

FIGURE G.13. CYCLIC STICK BIAS - LOADS DATA
i_N = 85°, 75° - FWD CG

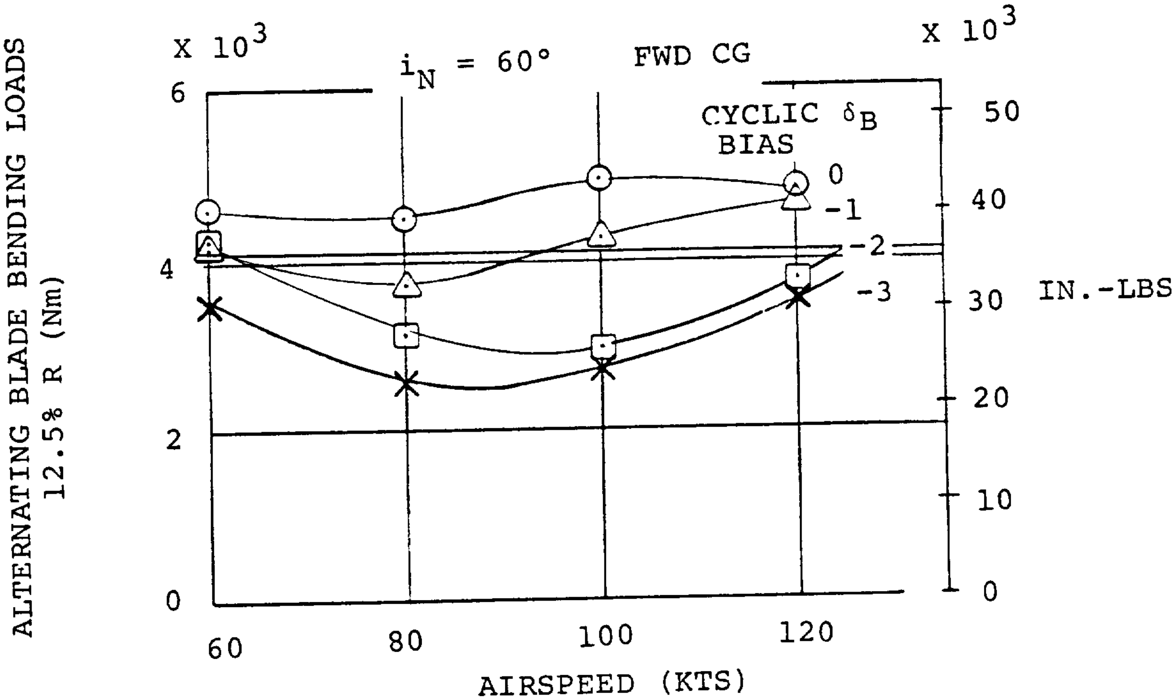

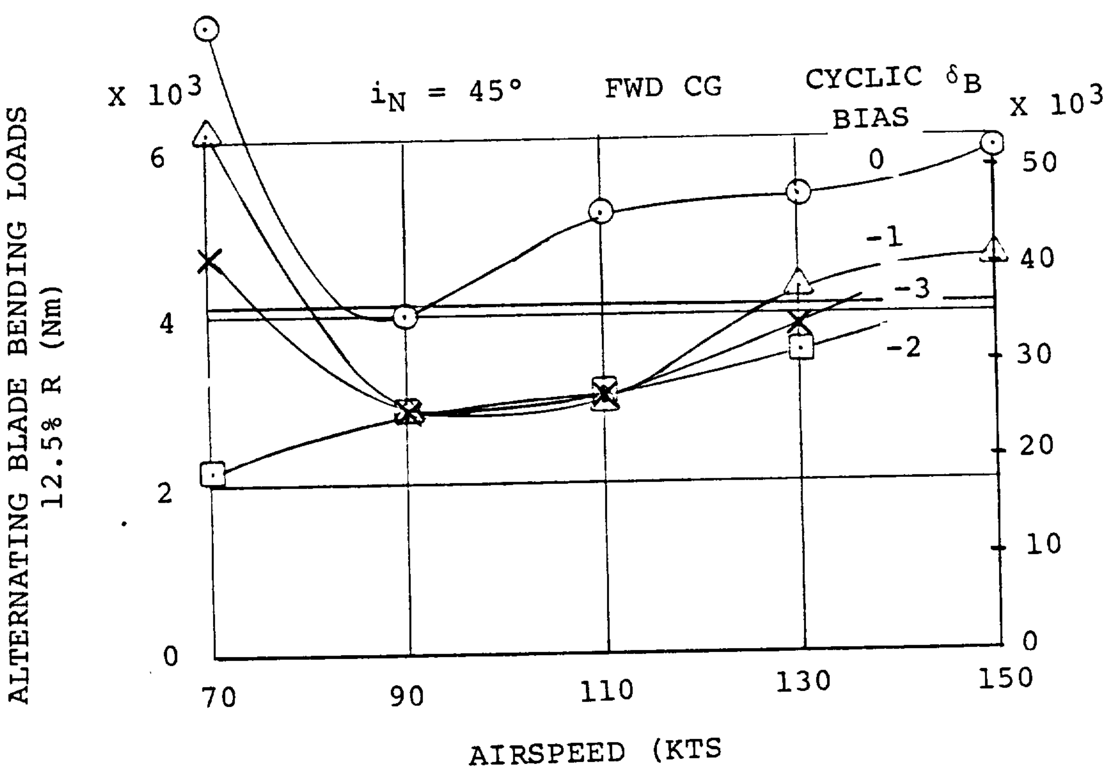

FIGURE G.14. CYCLIC STICK BIAS - LOADS DATA
i_N = 60°, 45° FWD CG

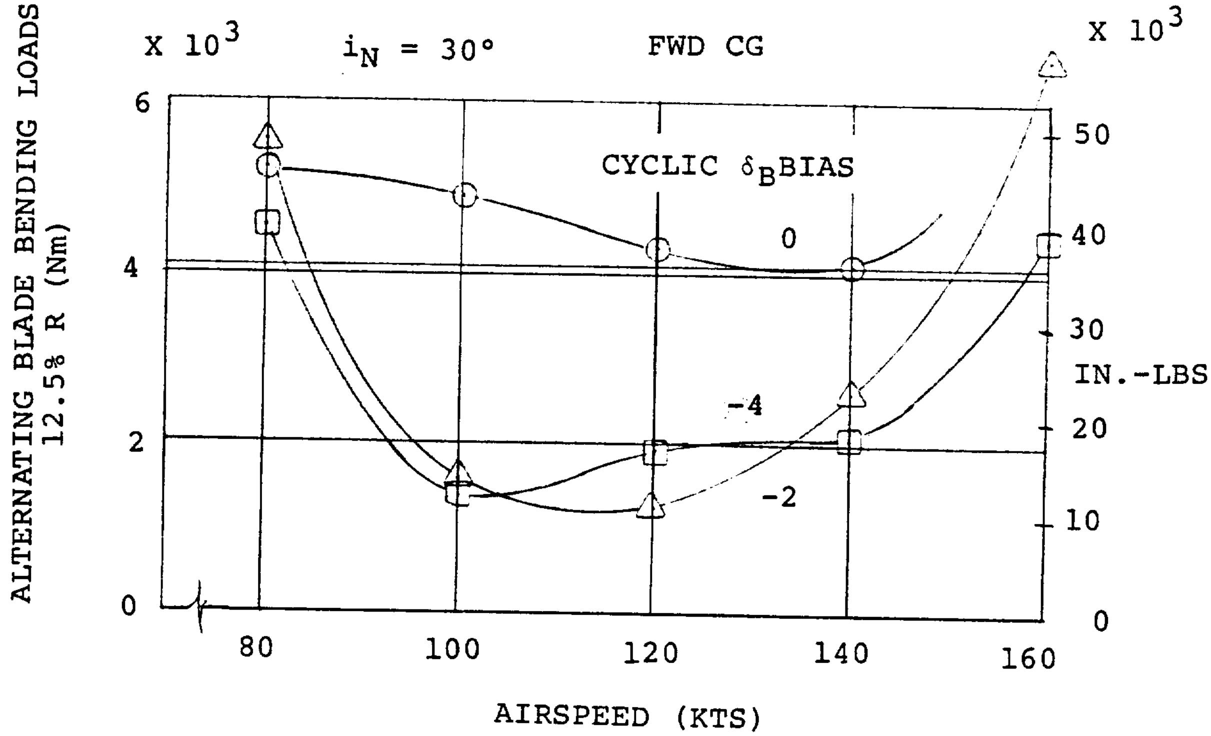

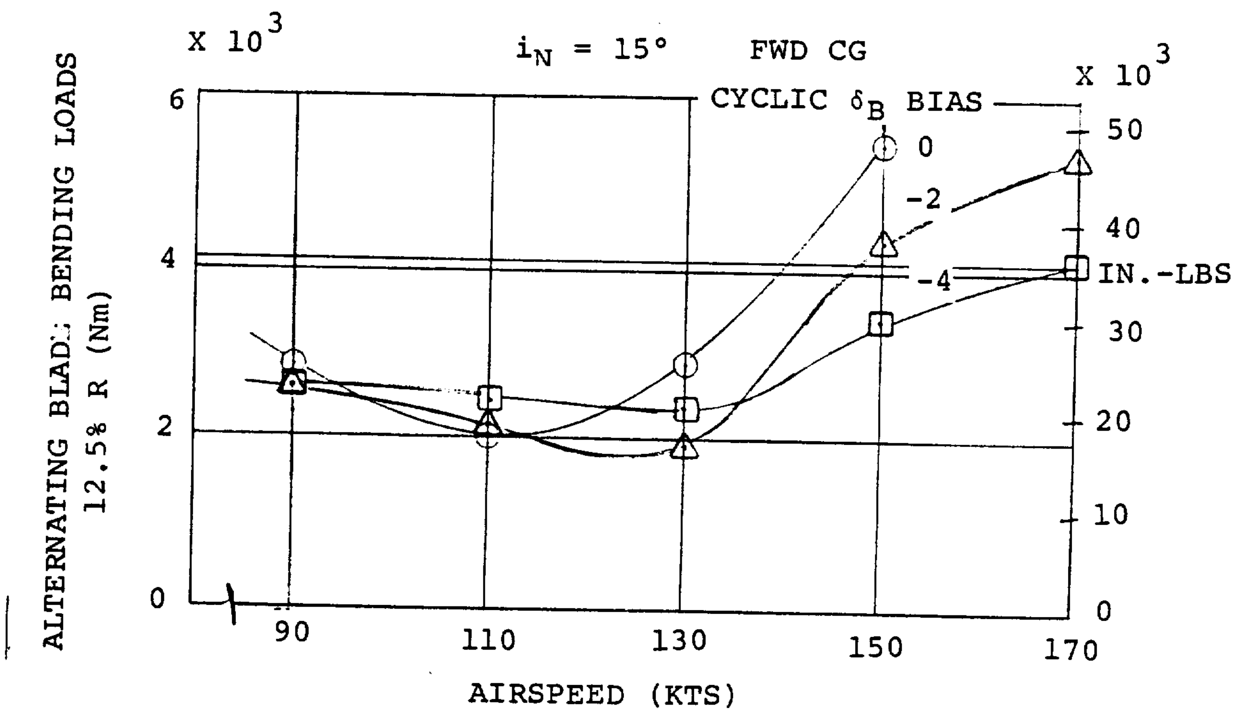

FIGURE G·15. CYCLIC STICK BIAS - LOADS DATA i_N = 30°, 15° FWD CG

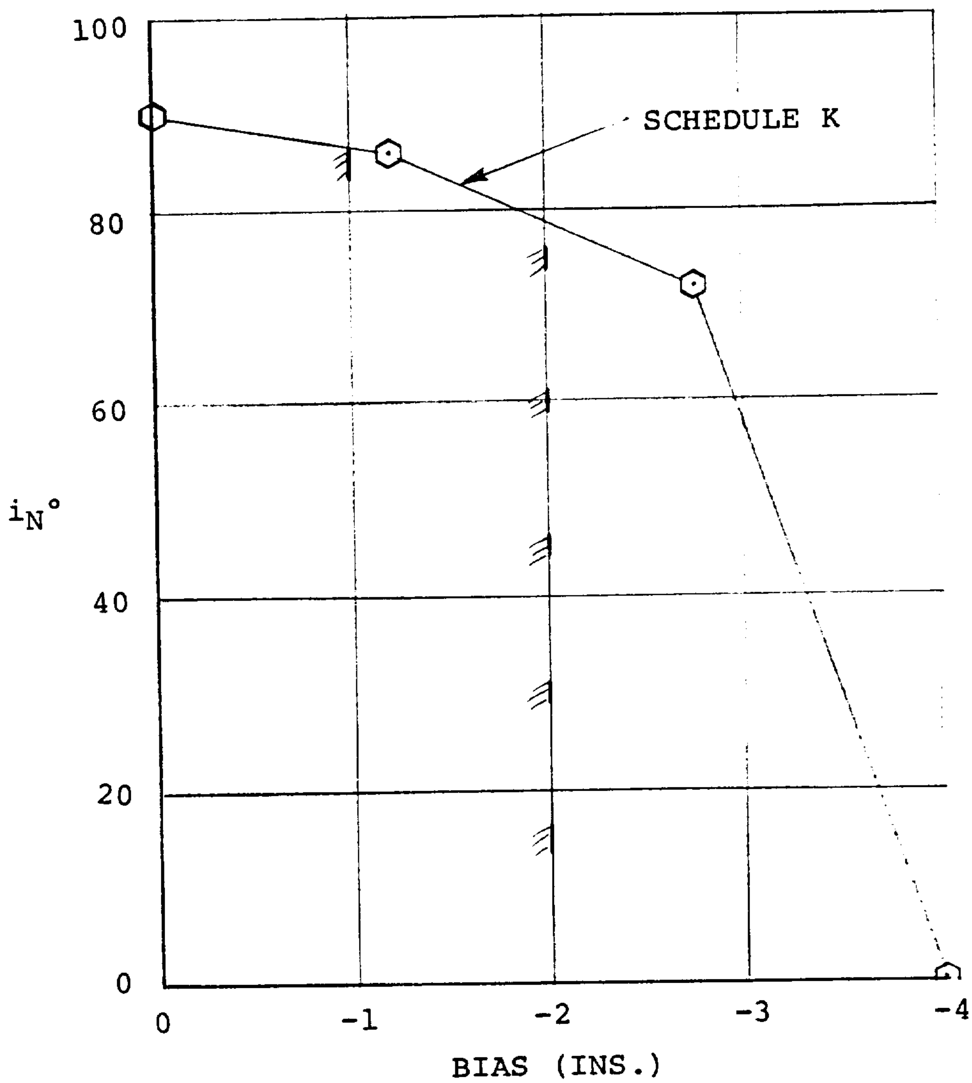

FIGURE G.16. CYCLIC STICK BIAS SCHEDULE

APPENDIX H

APPENDIX H - IN-HOUSE REAL TIME DIGITAL SIMULATION

Simulation Facilities

The math model described in this report was mechanized as a real-time digital simulation using a subset of the total resources that form the digital computer facility called the STAR system (Simulation and Test Analysis in Real Time). The STAR system supports either real time flight test or real time simulation while concurrently providing batch and Terminal Job Entry (TJE) operation.

The STAR Lab resources required to provide real time simulation are:

Xerox Sigma 9 computer

160K words core

CP-R Operating System

2 - 800 bpi tapes

2 - 1600 bpi

86 - megabyte disks

1 - line printer

1 - card reader

1 - BC-100 scope device/software

1 - console typewriter

6 - 8 channel brush strip chart recorders

1 - DMS-12 direct memory system for D/A and A/D operation

128 channels digital to analog (D/A) converters

60 channels analog to digital (A/D) converters

In addition to the hardware, the software used to provide real time simulation consists of the following elements:

Xerox CP-R operation system and utilities

Xerox BC-100 slope software

Xerox assembly language

Xerox Extended Fortran IV

An in-house software package for control system implementation called VECEX (VECtor EXecution)

Other special simulation oriented programs

Simulation Architecture

The real time digital simulation used to provide data for this report was generated by extensively modifying an existing tilt rotor digital simulation.

The real time simulation model provides capability to analyze the tilt rotor aircraft in three simulation modes:

1. Basic aircraft - non-piloted
2. Basic aircraft - piloted
3. Basic aircraft with rotor perturbation dynamic model - non-piloted

The non-piloted simulation is used to take static trim and stability derivative data, via the line printer and dynamic data, stick pulses and steps, via the strip chart recorders. The math model is separated into two groups, those equations (fast) that require a small time increment, and those equations (slow) that can be calculated at a slower rate. An external clock is used to schedule the execution of the math model such that the fast equations are executed every time the timer requests, but only half the slow equations are executed. The fast equations are updated every 45 ms. and the slow equations every 90 ms.

The piloted simulation is used to evaluate the flying qualities of the aircraft. To provide this, the normal simulation is interfaced with the nudge-base simulator lab through a trunking station. In addition to the normal model, additional signals must be input on digital to analog convertors (DAC's) and signals must be received from analog to digital convertors (ADC's). Due to the increase in processing of the additional inputs and outputs, the piloted simulation cycle time is 55 ms. using the same fast/slow approach. Strip chart printout and pilot comment is the primary form of output.

Subroutine Outline

The content of the main program subroutines is described below.

Subroutine RTFAST

- o Simulator tie-in analog to digital signal processing
- o Stick input section controlled via secondary task
- o Execute fast portion of math model via calls to routines for

Equations of Motion	-	Subroutine EOM
Control System	-	Entry VELOC
Velocity Equations	-	Subroutine VELOC
Rotor Equations	-	Entry Rotor
Wing Equations	-	Subroutine Wing
Tail Equations	-	Entry Tail

- o Execute slow portion of math model via calls to

Slow Equations Part 1 - Entry RTSLOW1)
) in Sub. RTSLOW
Slow Equations Part 2 - Entry RTSLOW2)

- o Execute final portion of simulation via call to Subroutine Final
- o Execute digital to analog real outputs via Subroutine SIMDAC
- o Discrete output processing section
- o Function keyboard lights

Subroutine EOM

- o Basic Equations of Motion
- o Trim Loops
- o Trim Check Section
- o EOM Integrations
- o Simulator Tie-in Section for correction of Visual/Motion System

Subroutine EOM (continued)

- o Gust Model Section

  Test Section for W Gust Forcing Functions

- o Final Summation of A/C Velocities/Rates
- o Fuselage Angles and Total Velocity

Entry VEXSUB

- o Real Inputs to VECEX Defined
- o Logical Inputs to VECEX Defined
- o Execute Control System Portion via call to VECEX
  - o Mechanical Controls
  - o SCAS
  - o Thrust Management System
- o Real Outputs from VECEX Defined
- o Stall Flasher for Function Keyboard
- o Logical Outputs from VECEX Defined

Subroutine VELOC

- o Velocity and acceleration of left and right nacelle incidence angles with rate limit
- o CG velocity and acceleration w.r.t. pivot
- o Pilot station accelerations - body axes
- o Fuselage pivot velocities/rates

  For normal A/C treatment

  For rotor dynamic model

- o Pilot station velocities

Subroutine VELOC (continued)

- o Rotor velocity calculations - left and right rotor

    Hub body axes

    Hub shaft axes

    Free stream

- o Left and right wing velocity calculations

    Body axes

    Chord axes

    Free stream

Entry ROTOR

<u>Left and Right</u>

- o Rotor angle of attack and sideslip calculations - bypassed when rotor dynamic option chosen and simulation in fly

- o Rotor angular rate transforms

    Nacelle axes

    Wind axes

- o Rotor speed, tip speed, advance ratio

- o Rotor control coordinate axis transform

- o Rotor equations for power, thrust, normal force, side force, pitching moment, yawing moment coefficients, the forces and moments from the coefficients; bypassed when rotor dynamic option chosen and simulation in fly.

- o Execute rotor dynamic perturbation model if selected

- o Rotor force and moment resolution to body axes

Subroutine WING

- o Aero equations for left and right wing

    Angle of attack and sideslip

Subroutine WING (continued)

Contribution due to totally downwashed wing

Contributions due to totally unwashed wing

Total CL, CD, CM coefficients

Aero forces calculations in body axes

Aero moment calculations in body axes

Wing/rotor interference section

Entry TAIL

- o Horizontal tail

    Horizontal tail downwash equations

    Rotor-on-horizontal tail interference effects

    Horizontal tail velocities

    Angle of attack

    CL, CD calc.

    Dynamic pressure

  Horizontal tail efficiency function

    Forces and moments in body axes

- o Vertical tail

    Velocity calcs, dynamic pressure

    Angle of attack and sideslip

    Rotor sidewash effect

    CY, CD calculation

    Force and moment resolution

Subroutine RTSLOW

Entry RTSLOW1

- o Nacelle Velocity - Resultant
- o CG Location w.r.t. pivot
- o Air Density Model
- o Engine Model (minus thrust management system) provision for failures
- o Wing Stall Calculation
- o Fuselage Aerodynamics

    Wind axes coefficients

    Body Axes Forces and Moments

- o Ground effect section for wing, tail, rotor-if selected
- o Nacelle Aerodynamics

    Angle of attack and sideslip

    Wind axes coefficients

    Body axes forces and moments

- o Unstable rolling moment induced by ground effect

Entry RTSLOW2

- o Wing Aerodynamic Section for Submersed Surface Area Calcs.
- o Variable Inertia Calculations
- o Steady Wind Model
- o Wind Ramp Model
- o Integration Logic Control Calculation

Subroutine FINAL

- Landing gear executed via subroutine gear, if selected
- Final summation of A/C forces and moments
- Wing vertical bending equations
- Wing twist equations
- Stability derivative section

Entry SIMDAC

- DACS for 6 brush recorders
- DACS for simulator tie-in
- DACS for rotor dynamic option, plus

    RMS calculations

    Phase angle calculation

    Rotor blade modes

Program Listing

A listing of the program is available on request.